Model Name: Mass-Balance Compartment Model

Functional Area: Eco-Hydrology

Model Proponents: Coastal Protection and Restoration Authority

Model Developer(s): Ehab Meselhe, University of Louisiana at Lafayette
John A McCorquodale, University of New Orleans
Jeff Shelden, Moffatt & Nichol
Mark Dortch, Moffatt & Nichol
Stokka Brown, Fenstermaker
Mallory Davis, Fenstermaker
Zhanxian Wang, Moffatt & Nichol
Peter Elkan, Moffatt & Nichol
Jennifer Schindler, University of New Orleans

Table of Contents

Table of Contents ii

1. Background 1

a. **Purpose of Model** 1

b. **Model Description and Depiction** 5

c. **Contribution to Planning Effort** 9

d. **Description of Input Data** 10

e. **Description of Output Data** 47

f. **Statement on the Capabilities and Limitations of the Model** 50

g. **Description of Model Development Process including Documentation on Testing Conducted (Alpha and Beta Tests)** 52

2. Technical Quality 78

a. **Theory** 78

b. **Description of System Being Represented by the Model** 106

c. **Analytical Requirements** 112

d. **Assumptions** 113

e. **Identification of Formulas Used in the Model and Proof that the Computations are Appropriate and Done Correctly** 115

3. System Quality 116

a. **Description and Rationale for Selection of Supporting Software Tool/Programming Language and Hardware Platform** 116

b. **Proof that the Programming was Done Correctly** 117

c. **Availability of Software and Hardware Required by Model** 128

d. **Description of Process Used to Test and Validate Model** 129

e. **Discussion of the Ability to Import Data into Other Software Analysis Tools (Interoperability Issue)** 183

4. Usability 184

a. **Availability of Input Data Necessary to Support the Model** 184

b. **Formatting of Output in an Understandable Manner** 186

c. **Usefulness of Results to Support Project Analysis** 187

d. **Ability to Export Results into Project Reports** 188

e. **Training Availability** 189

f. **Users Documentation Availability and Whether it is User Friendly and Complete** 190

g. **Technical Support Availability** 191

h. **Software/Hardware Platform Availability to All or Most Users** 192

i. **Accessibility of the Model** 193

j. Transparency of Model and How it Allows for Easy Verification of Calculations and Outputs 194
5. Sources of Model Uncertainty 195
6. Suggested Model Improvements 196
7. Quality Review 197
8. Uncertainty Analysis 199
9. References 205
Attachment A 208
Attachment B 233
Attachment C 488

1. *Background*

a. Purpose of Model

The 2012 Coastal Master Plan (master plan) was based upon an extensive numerical modeling effort initiated by the Coastal Protection and Restoration Authority (CPRA). The goal of the master plan was to evaluate the performance of potential protection and restoration projects on the Louisiana Coast for the next 50 years. This numerical modeling effort was unprecedented in that it attempted to create an intricate chain of model outputs that could be used as input for additional models, where the final stage presented an overall "outlook" of the Coast after implementing proposed projects for 50 years. This project "outlook" would then be compared to a similar undisturbed "outlook" that represents nature being left to its own devices, a.k.a. a future without action (FWOA).

Before the model simulations could begin, CPRA provided several "scenarios" to test the most optimistic, moderate, and least optimistic natural conditions possible. For example, a less optimistic situation could be a drought, where the amount of rainfall, or precipitation, would be set relatively low compared to average annual conditions. Other examples of parameters that could be changed to alter the natural conditions included the tributary discharge, estimated sea level rise, and evapotranspiration, among others. These parameters were manipulated individually and were then grouped to create a future "scenario". For example, this less optimistic scenario of a drought could include low precipitation, high evapotranspiration, and low tributary discharge. The combination of these conditions constituted a "scenario". These scenarios provided yearly future conditions for the 50-year period, and they needed to be adjusted to produce daily inputs for the models. For example, let's say an estimated sea level rise of 0.5 m was designated in one of the future scenarios. Therefore, that 0.5 m would have to be divided by the number of days within the 50-year period to create an incremental daily estimated sea level rise input.

The modeling teams of the master plan modeling effort consisted of members from a range of scientific industries including the United States Geological Survey (USGS), CPRA, Brown and Caldwell, C.H. Fenstermaker & Associates, Moffatt & Nichol, several Louisiana universities, and more. The modeling teams were separated into models for Eco-Hydrology, Wetland Morphology, Barrier Shoreline Morphology, Vegetation, Storm Surge and Waves, Ecosystem Services (e.g. habitat suitability indices), and Risk Assessment. **Figure 1** below demonstrates the complex cooperative modeling structure of these models, where the output from one model was used as input for one or more other models.

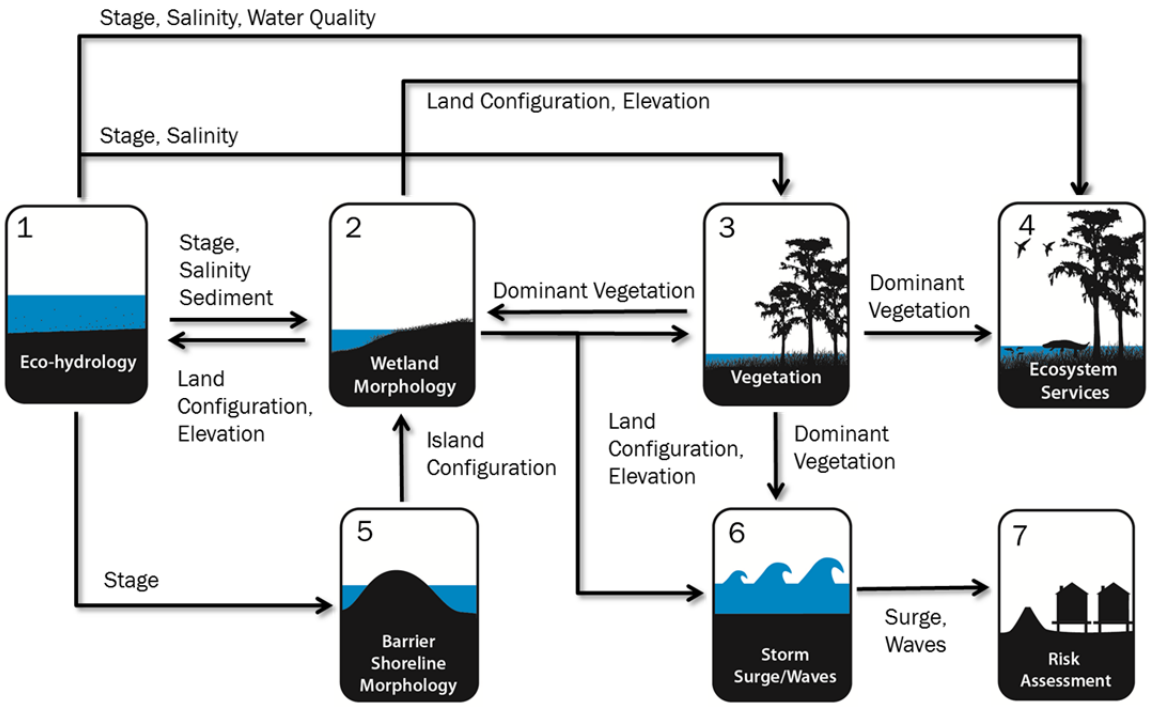

Figure 1 2012 Louisiana Coastal Master Plan Predictive Modeling Structure

The remainder of this report describes the modeling efforts of the Eco-Hydrology team. The Eco-Hydrology model provided essential outputs needed to complete the simulations of the majority of the models mentioned above. This model allowed its users to simulate the future hydrodynamic and water quality conditions of the Louisiana Coast based on a specific set of initial conditions and boundary driven data. In order to create the 50-year outlook of the Louisiana Coast, the Eco-Hydrology model was run for two 25-year simulations. These two simulations were termed year-set one and year-set two.

The Eco-Hydrology team was divided into three main regions along the Louisiana Coast: Lake Pontchartrain/Barataria Basin (PB), Atchafalaya Basin (AA), and Chenier Plain (CP) (**Figure 2**). The PB region[1] (blue) extended from Bayou Lafourche to Gulf Shores and as far north as Simmesport to offshore in the Gulf of Mexico. The AA region (red) extended from West Cote Blanche Bay to Bayou Lafourche and from just north of I-10 to offshore in the Gulf of Mexico. The CP region (yellow) extended from Sabine Lake on the Louisiana-Texas border to West Cote Blanche Bay and from just north of the Gulf Intracoastal Waterway (GIWW) to offshore in the Gulf of Mexico. Each of these regions had its own compartment model that was developed specifically for that region. The description below details the development history of these models.

[1] It should be noted that the PB region overlaps the east portion (Terrebonne) of the AA region. However, these compartments in Terrebonne are only included to improve the PB boundary conditions, and their results are not reported.

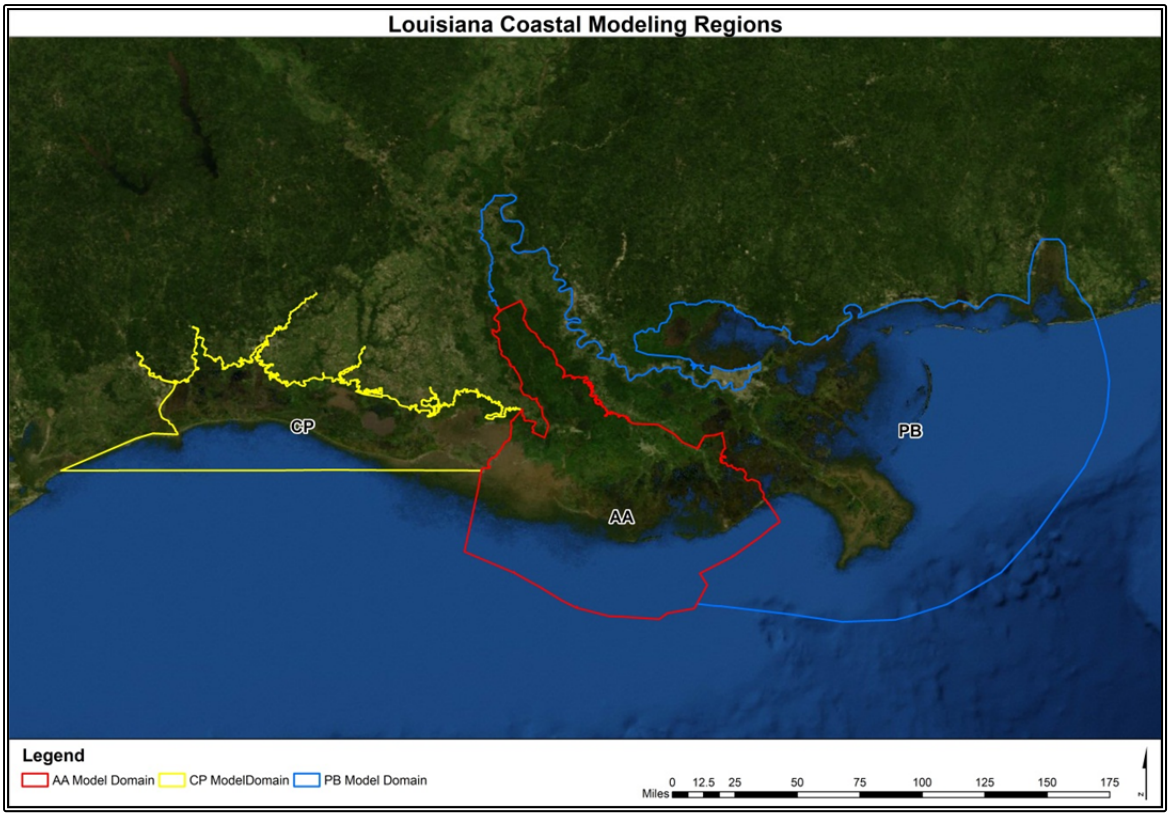

Figure 2 Eco-Hydrology Modeling Regions

A mass-balance compartment model was developed in the Fortran programming language by the University of New Orleans (UNO) for the Coastal Restoration Enhancement through Science and Technology (CREST) Program project: "Hydrologic Modeling and Budget Analysis of the Southwestern Louisiana Chenier Plain" (Meselhe et al., 2008)[2]. The model has been used in multiple projects since that time, including the Coastal Louisiana Ecosystem Assessment & Restoration's (CLEAR) Water Quality Modeling of the Pontchartrain Estuary project (McCorquodale et al., 2008[3]; Roblin, 2008), the National Oceanic and Atmospheric Administration's (NOAA) Mississippi River Gulf Outlet (MRGO) Violet Optimization Study (Georgiou et al., 2009), and the joint project for the Environmental Protection Agency (EPA), NOAA, CLEAR, and Lake Pontchartrain Basin Foundation (LPBF) to study Pontchartrain Estuary Salinity, Nutrients, and Sediment Dynamics (McCorquodale et al., 2009). This Pontchartrain/Barataria Basin Fortran model was used as the basis for developing the models for the AA and CP regions. For these two regions, the Berkeley Madonna (Macey, 2001) modeling environment was used. Both the Fortran and Madonna models used the mass-balance approach to treating state variables, and the governing equations and assumptions were similar across all three regions. However, the calibration parameters differed between the three regions. One of the reasons for selecting Madonna was its simplified user interface which made for easier model implementation, update, and maintenance. Another reason for using Madonna was that the AA and CP models needed to be developed in a relatively short time frame in order to start screening projects for the master plan modeling effort. Since the PB

[2] http://www.mvd.usace.army.mil/lcast/pdfs/Chenier%20Plain%20-%20Report%20III.pdf
[3] http://www.clear.lsu.edu/pdfs/clear_report_20081023154426.pdf

model had already been tested and partially calibrated for the Pontchartrain and Barataria Estuaries, the decision was made to keep the existing code and modify it so that processes were similar for both the Fortran and Madonna models. Also, the PB system required significantly different treatment from the AA and CP regions because of the Mississippi River and Mississippi River Delta. Therefore, a formal programming language like Fortran was needed to provide more flexibility for describing complex system dynamics. It should be noted that since both the Fortran and Madonna codes had to be developed in a short amount of time, the simplified mass-balance approach was used instead of the full suite of hydrodynamics equations, and, as a result, the calibrations and validations were not "perfect." Also, the simplified mass-balance approach was used so that long simulation periods for a large domain could be run with a reasonable amount of execution time.

Coordination and data exchange across models was important in the success of this master plan modeling effort. Other models such as Wetland Morphology used the first 25 years of Eco-Hydrology output to execute their model for the first 25 years. The Wetland Morphology outputs from the last year of the first 25 years were used to update the compartment average elevations and percent land values for the second year-set of the Eco-Hydrology models. The year-set two output was then used by Wetland Morphology to execute their model for the second 25 years. The combination of the two 25-year simulations resulted in the master plan desired 50 years of output used by the planning tool. From **Figure 1** the other teams that utilized the Eco-Hydrology output were Barrier Shoreline Morphology, Vegetation, and Ecosystem Services.

The table in Attachment C provides a list of the acronyms used in this report.

b. Model Description and Depiction

A mass-balance compartment model is a 0-dimensional grid, where the compartment centroids are connected with one another and with the boundary by way of links. The links typically run from centroid to centroid or mid-point to mid-point, depending on the compartments being connected.

The models were designed to calculate hydrodynamic and water quality processes. They took into account water and constituents entering and exiting the domains, exchange between the compartments, and atmospheric processes, such as precipitation and evapotranspiration. In addition to the hydrodynamics (stage, flow rate, and velocities), the following constituents were included in the models: total suspended solids (TSS), salinity (SAL), water temperature (TMP), nitrate + nitrite nitrogen (NO3), ammonium nitrogen (NH4), dissolved organic nitrogen (DON), phytoplankton as chlorophyll-a (ALG), detritus (DET), and residence time or age (AGE). These parameters were computed using a hybrid upwinding and central difference numerical integration scheme in the PB model and using the UPWIND scheme in the AA and CP models. The dynamics of the PB model are displayed in **Figures 3a** and **3b**, whereas **Figures 4a** and **4b** show the dynamics of the AA and CP models.

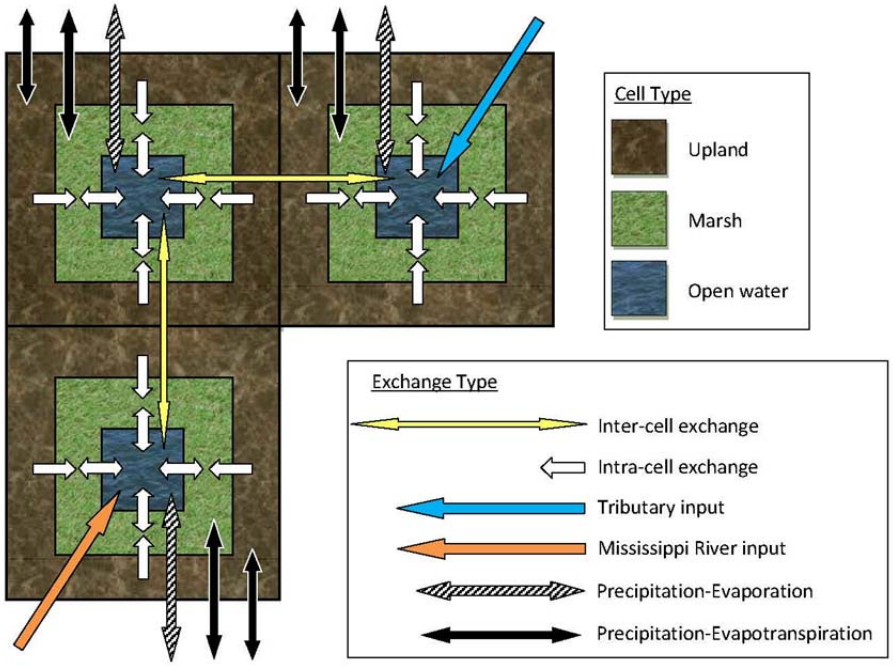

a. Plan view of PB model dynamics

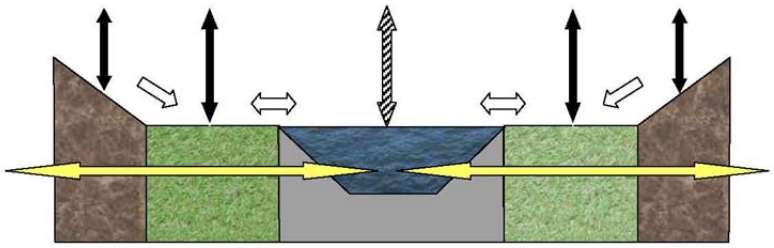

b. Cross-section view of PB model dynamics for a generalized interior cell

Figures 3a and 3b Model Dynamics for the PB Model

As shown in **Figures 3a** and **3b,** the PB modelers separated the areas inside each compartment into upland, marsh, and open water sub-compartments with links providing the exchanges between the open water sub-compartments. These open water sub-compartments consisted of the bays, lakes, and any other water bodies located within the PB domain, and the links consisted of the channels, passes, and waterways that connect the larger water bodies. Local tributaries, including the Mississippi River, supplied fresh water to the open water sub-compartments. Upland sub-compartments exchanged with the marsh sub-compartments via runoff. It should be noted that there were no compartments in the offshore boundary, but in fact it actually comprised of individual nodes with no geometric features. These nodes were given compartment ID numbers so that they would be properly applied in the model.

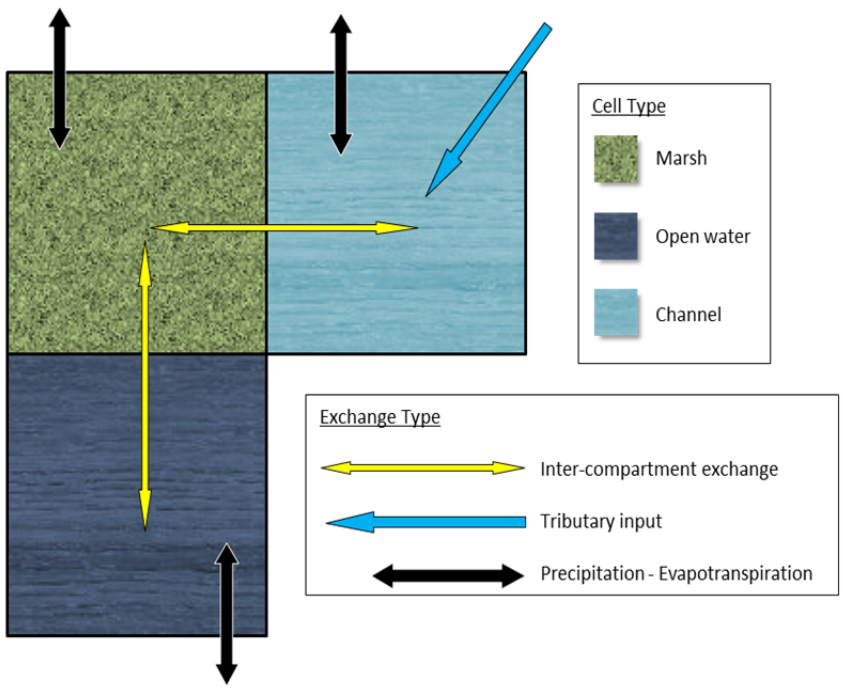

a. Plan view of AA and CP model dynamics

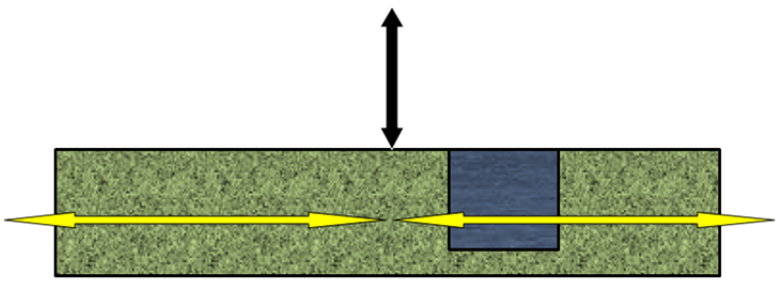

b. Cross-section view of AA and CP model dynamics for a generalized interior marsh compartment

Figures 4a and 4b Model Dynamics for the AA and CP Models

As shown in **Figures 4a** and **4b**, the AA and CP compartments were explicitly separated into three types: channel, open water, and marsh, where either compartment type could exchange with the other two types via links. Local tributaries provided fresh water to any of the compartment types. Unlike the PB model, the AA model included compartments for the offshore boundary. However, the CP model contained theoretical nodes for the offshore boundary, similar to the PB model. The CP nodes were also given compartment ID numbers for modeling purposes. It should be noted that the use of theoretical nodes instead of compartments for the offshore boundary was at the discretion of the modeling team and had no effect on the outputs of the internal compartments because the equations were not applied to the boundary in either of the regions.

As mentioned above, the channels and passes of the PB region constituted the links of the model rather than compartments, and the open water bodies, e.g. bays and lakes, were designed as sub-compartments of a whole compartment. The marsh areas of the PB region

were also designed as sub-compartments of a whole. In the AA and CP regions, however, channels were given their own compartment, where a channel compartment encompassed a certain length of an existing channel or river in the region and contained links that connect to adjacent compartments. Also, an open water compartment in the AA and CP regions encompassed an entire bay or lake. The last compartment type of the AA and CP regions, marsh, behaved differently from the rest because a marsh compartment could contain patches of open water, depending on the productivity of the marsh. To account for the water inside a marsh compartment, a percentage of land was applied to each compartment, where 100% corresponded to all land/marsh and 0% corresponded to all water. Consequently, all channel, water, and offshore compartments had a percent land of 0 (zero). **Table 1** shows the number of compartments and surface types for each Eco-Hydrology model region. The size of the compartments across the three regions was on the order of several square kilometers. The ranges and averages of surface areas of the compartments for each region are also included in **Table 1**.

Table 1 Number of Compartments and Surface Types in the Eco-Hydrology Regions

Region	Channel[4]	Open Water	Marsh	Upland	Offshore[5]	Total	Surface Area Ranges in km^2 (Average)
PB	-	89[6]			7 Nodes	89	2.2 – 5844 (716)
AA	73	21	67	-	4	165	0.04 – 3361 (121)
CP	28	19	102	-	6 Nodes	149	0.6 – 1844 (86)

As seen in **Figures 3a** and **3b** and **Figures 4a** and **4b**, the compartments experienced exchange with the atmosphere through precipitation, *P*, and evapotranspiration/evaporation, *ET*, and with one another via exchange flows, *Q*. It should be noted that the modelers acknowledge that evaporation occurs over water and evapotranspiration occurs over land, however, for simplification purposes, evapotranspiration is used synonymously with evaporation for the remainder of this report. The PB region included runoff from upland and marsh areas into open water compartments, and the AA region included runoff from upland areas into the marsh and open water compartments. The CP region included local runoff since local rainfall and ET are modeled. The PB model included discharges and nutrient loads from wastewater that is pumped into the Mississippi River. The AA and CP models included discharges and nutrient loads from local wastewater treatment plants that are pumped into the local tributaries.

[4] The PB model does not contain channel compartments because the channels in the domain are represented by links. There are 183 links in the PB domain.
[5] The AA model consists of 4 offshore compartments, which contribute to the total number of compartments, whereas, the PB and CP models contains 7 and 6 offshore nodes, respectively, with no physical attributes. Because the PB and CP offshore nodes are ones that do not contain actual geometric features, they do not contribute to the total number of compartments in the models.
[6] As mentioned above, the PB compartments are divided into marsh, open water, and upland; whereas, the AA and CP models designate a compartment for each surface type.

c. Contribution to Planning Effort

As a contribution to the 2012 Coastal Master Plan modeling effort, the Eco-Hydrology models provided essential information on the hydrodynamics and quality of water in the coastal regions of Louisiana. The Fortran and Madonna models are capable of simulating long periods of time (25 years maximum for this modeling effort), which created a "foresight" of the future effects on the system. When both year-sets were completed, this 50-year "foresight" allowed for adequate planning-level screening of proposed projects, which can assist decision-makers in their chore of selecting the most efficient methods to achieve their near and long-term goals of protection and restoration.

d. Description of Input Data

The data required for the model setup and boundary conditions of the Eco-Hydrology models included geometry (bathymetry, topography, dimensions of hydraulic structures, etc.), boundary conditions (riverine inflows, open water tide and salinity time-series records, rainfall records, and ET records), initial conditions (initial water depth and concentrations of the various water constituents), structure operation schedules, and system parameters (roughness, diffusion coefficients, and other physical and numerical parameters). Further details about the calibration parameters are provided in Section 3.d. of this report. It should be noted that the modelers attempted to acquire the best available data from appropriate observation stations that would accurately correspond to their respective modeling regions, as well as to use that given data in order to fill empty records to the best of their ability.

Geometric Data

The geometry of the link-node/mass-balance compartment model consisted of compartments connected to each other by links. The attributes of a compartment included surface area, average bed elevation, percentage of land (mentioned previously), bed roughness, and the flood fraction[7]. Each link needed an average width, length of connection inside each compartment, loss coefficient, and roughness coefficient. These link and compartment attributes were estimated with the help of the Advanced Circulation Model (ADCIRC) Bathymetry, National Oceanic and Atmospheric Administration (NOAA) Navigation Maps, and Google Earth Pro® for the PB model and with the help of ArcGIS for the AA and CP models. The Wetland Morphology team provided Digital Elevation Model (DEM) and Land and Water (LNW) maps (**Figure 5** and **Figure 6**, respectively) at a 30x30 m resolution to create the compartment bed elevation and percent land files for both year-sets. However, these maps were not used directly for the compartment bed elevations of each region. In general, the elevations used in the Eco-Hydrology models for marsh areas were lower than the arithmetic average of the area encompassed within each compartment. This can be attributed to several factors. Initially, the compartment elevations were lowered to accurately capture their hydraulic capacity. Furthermore, when channels and deep areas were not considered substantial features they were excluded when determining the representative elevations of some compartments. It should be noted that major channels were modeled explicitly as a link among the neighboring compartments. Finally, the compartments' elevations were fine-tuned during the calibration process to best mimic the temporal and spatial patterns observed in the field measurements. It should also be mentioned that there are areas of uncertain bathymetry throughout the coastal zone. These uncertainties could be as large as 1 m.

[7] The flood fraction refers to the fraction of time that a marsh sub-compartment is flooded. This was only used in the PB model.

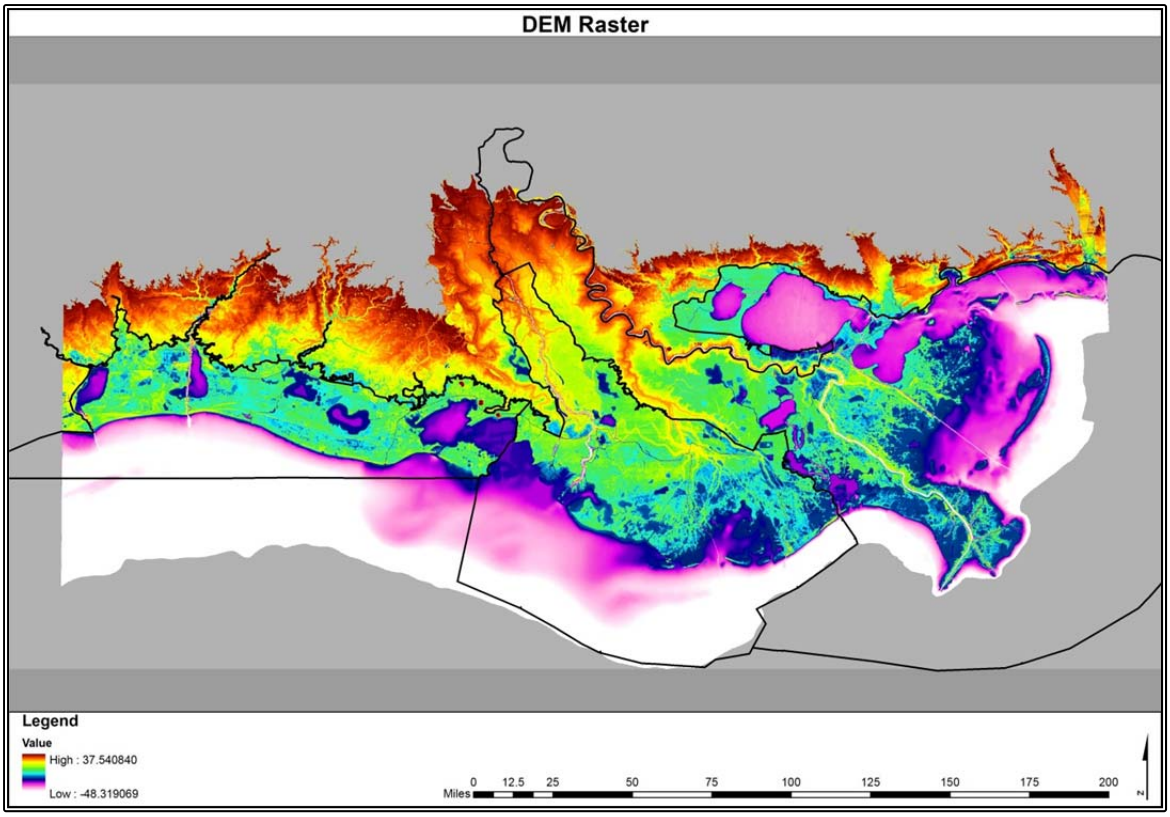

Figure 5 Example of Wetland Morphology 30x30 m DEM

The PB model required separate elevations for the open water and marsh sub-compartments in order to accurately calculate exchange between marsh and open water areas of the compartments. Therefore, open water bathymetry and marsh topography had to be used to establish initial conditions instead of using the DEM from the Wetland Morphology team. As a result, an ADCIRC composite LiDAR[8]/bathymetry dataset was initially chosen for use in the Barataria Basin model. This was the same file used for post-Katrina simulations by the U.S. Army Corps of Engineers (USACE) district office in New Orleans for the Louisiana Coastal Protection and Restoration (LaCPR) plan. The ADCIRC grid available at the time this study was initiated was the SL15v06r09 (Georgiou et al., 2010). However, there were issues of quality with the bathymetry coverage in this region. For instance, Bayou Perot/Rigolettes exhibited deeper bathymetry near the shoreline banks than within the channel thalweg. This feature appeared to be the result of a gap in coverage between the modern LiDAR data and the older bathymetric data. Within this coverage gap, the depths were incorrectly extrapolated. Similar patterns were identified in other portions of the basin. In addition, transects surveyed in 2002 and 2003 illustrated that the bayous and tidal passes connecting the major lakes are significantly deeper than the depth soundings within the ADCIRC bathymetry (SL15v06r09). It was decided that the LiDAR data above mean sea level (MSL) (~0.08 m NAVD[9] 88) would be retained due to their more recent acquisition, while the bathymetry would be replaced with other sources of available data, such as channel design specifications. In areas where no other data were available, the ADCIRC grid SL15v06r09 was used for the bathymetry. All bathymetry data were

[8] Light Detection and Ranging (LiDAR)
[9] North American Vertical Datum (NAVD)

converted into a common horizontal and vertical datum (UTM[10] zone 15 meters, NAVD 88 meters) and interpolated onto the mesh. It should be noted that even though the SL18 ADCIRC grid had become available during this modeling effort, it would have been too time costly for the modelers to perform a similar QA/QC[11] check and then manually manipulate any inconsistent data. Therefore, the older SL15 grid was used because it has already been through a rigorous QA/QC check as well as having been manually adjusted to known dimensions. For the Pontchartrain Basin the bathymetry was taken from the NOAA Office of Coast Survey (OCS) Navigational Charts[12].

For the AA region, the elevations from the Wetland Morphology DEM for the channel and open water compartments were replaced with higher resolution data from other sources. The bathymetry in the Atchafalaya River compartments was developed from the USACE Atchafalaya Hydrobook 1997-1998 cross-section surveys. For the offshore compartments, the bathymetry was based on the NOAA Estuarine Bathymetry[13] in Terrebonne/Timbalier Bays and Atchafalaya Bay, and the National Geophysical Data Center (NGDC) 3 arc-second Coastal Relief Model[14]. For other channel compartments, such as those in the Gulf Intracoastal Waterway (GIWW), the bathymetry was taken from the NOAA OCS Navigational Charts. The topography for the marsh/swamp compartments was initially based on the DEM provided by the Wetland Morphology Group. Elevations in the compartments for the first year-set were modified during the model calibration process in order to obtain fair agreement on water stages.

For the CP region, the initial average elevations for the first year-set came from the Louisiana State University (LSU) Atlas[15] 5x5 m DEM which was a higher resolution than the Wetland Morphology DEM (30x30 m). The marsh compartment elevations were altered during the model calibration to obtain fair agreement on water stages. Bathymetry from the NOAA OCS Navigational Charts, Wetland Morphology year-set 1 DEM, and physical surveys were used for creating lake bed elevations and channel depth-relationship curves. These relationship curves are described further in Section 2.a.

For the second year-set, the Wetland Morphology DEM maps were used for updating the compartment elevations. ArcGIS was used to calculate the average elevation in each compartment from these maps for each region. These year-set 2 average elevations were then subtracted by the year-set 1 elevations from the Wetland Morphology team to obtain a difference in elevation. This elevation difference was added to the calibrated elevations mentioned above for each region. The resulting elevations were then used for the second year-set. The following formulation describes this process:

$$EL2_{EH} = EL1_{EH} + (EL2_{WM} - EL1_{WM}) \quad \textbf{(1)}$$

where,

[10] Universal Transverse Mercator (UTM)
[11] Quality Assurance and Quality Control
[12] http://www.nauticalcharts.noaa.gov/mcd/enc/
[13] http://estuarinebathymetry.noaa.gov/
[14] http://www.ngdc.noaa.gov/mgg/coastal/crm.html
[15] http://atlas.lsu.edu/lidar/

$EL2_{EH}$ = Eco-Hydrology compartment elevation for year-set 2 (m)
$EL1_{EH}$ = calibrated Eco-Hydrology compartment elevation for year-set 1 (m)
$EL2_{WM}$ = Wetland Morphology compartment elevation for year-set 2 (m)
$EL1_{WM}$ = Wetland Morphology compartment elevation for year-set 1 (m)

The LNW maps (**Figure 6**), provided by the Wetland Morphology group, were used to designate the amount of land and water present in the model domains. The maps contained two values: 1 (land) and 2 (water). ArcGIS was used to calculate the average amount of land and water within each compartment of the model domains, where a compartment of 100% land had a value of 1, a compartment of 100% water had a value of 2, and a compartment containing both land and water had a value between 1 and 2. The percentage of land (PCL) was calculated according to the following equation:

$$PCL = [1 - (LNW - 1)] * 100\% \quad \textbf{(2)}$$

where,

PCL = percentage of land in the compartment, %
LNW = average land and water value calculated in ArcGIS (1 - 2), unitless

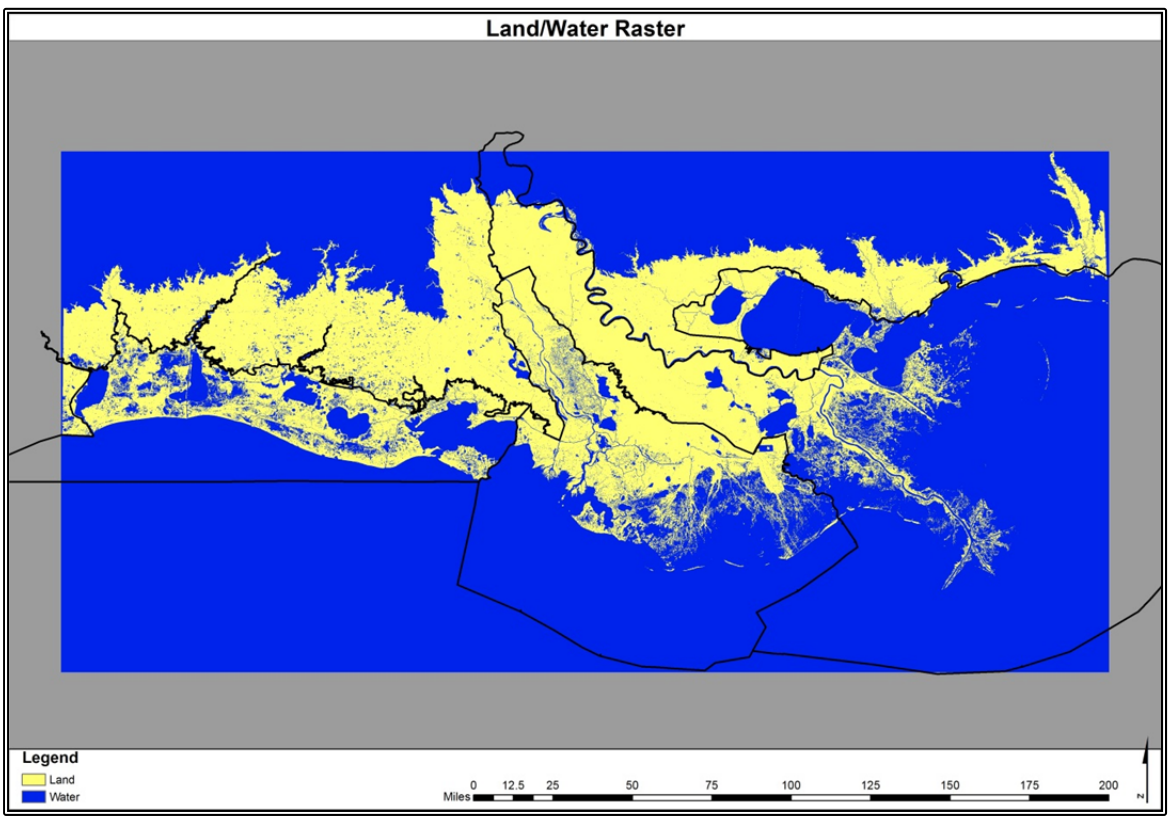

Figure 6 Example of Wetland Morphology LNW Map

For the PB model, the compartments were separated into sub-compartments for marsh, open water, and upland and therefore, the code required a surface area for each sub-compartment. However, the Wetland Morphology's LNW values were averaged over the entire compartment.

As a result, the initial surface area of each sub-compartment was determined using Google Earth Pro®, and the percentage of land for each compartment was estimated from these sub-compartment areas. Keeping the surface areas of the upland sub-compartments constant for year-set 2, the areas of the marsh and open water sub-compartments for year-set 2 were determined from the percentage of land values provided by the Wetland Morphology team. The change in marsh area from year-set 1 to year-set 2 was then inputted into the PB model. The percentage of land values provided by Wetland Morphology were used directly for the AA and CP regions for both year-sets.

Boundary Conditions

The boundary conditions of the model included atmospheric, tributary, distributary/diversion, offshore, wastewater, and runoff data from several observation stations throughout each of the model domains. The atmospheric boundary conditions came from observed precipitation, evapotranspiration/evaporation, and wind data. The tributary, distributary/diversion, wastewater, and runoff boundary conditions came from observed discharge, water quality, and/or temperature and salinity[16] data. The offshore boundary conditions came from observed tidal stage, salinity, water quality, and temperature data. It should be noted that the PB model applied a temperature boundary for the offshore boundary nodes, the Mississippi River and its distributaries/diversions, and the entire onshore domain rather than having a temperature boundary for each tributary. All available data were collected across the three Eco-Hydrology regions to create a 25-year dataset for the model boundaries. Where data records were incomplete or unavailable, the modeling teams performed standard filling techniques, which are described below for each boundary condition type. It should be mentioned that the three teams worked independently and followed similar procedures as best as possible, but they also used different approaches based on previous work each had done in their respective basin. Also, the availability of data varied across the three regions, and some teams already had data that would take another team too long to obtain so they took a different, timelier approach given the schedule necessary to complete the modeling effort for the 2012 Coastal Master Plan.

Atmospheric

Each of the models was considered open to the atmosphere, which means they were subjected to the natural meteorological processes of evapotranspiration/evaporation, precipitation, and wind. These weather conditions were measured by several agencies across the three domains. In order to efficiently model the hydrodynamic and ecological processes occurring in each of the model domains, these measured values needed to be applied as boundary conditions. Below is a description of each of these boundary conditions. It should be noted that meteorological data also consisted of air temperature, dew point temperature, and cloud cover, which were used along with wind speed to compute water temperature in the AA and CP models. This is further explained in the water temperature theory portion of Section 2.a.

Precipitation

Daily accumulated precipitation data from the National Climatic Data Center (NCDC)[17] was used to create the precipitation boundary condition. The NCDC stations shown in **Figure 7** contained daily Surface Data (SOD data) from years 1990 to 2009. The years of 1990 – 1994 were repeated after 2009 to create the 25-year precipitation dataset. These 5 years were chosen because they

[16] Temperature and salinity data are not included in the wastewater and runoff boundary conditions.
[17] http://www.ncdc.noaa.gov/oa/climate/climateinventories.html

were representative of average conditions. **Table 53** in Attachment A shows the ID numbers, names, sample intervals, and model regions for each station. All models used these records obtained from NCDC.

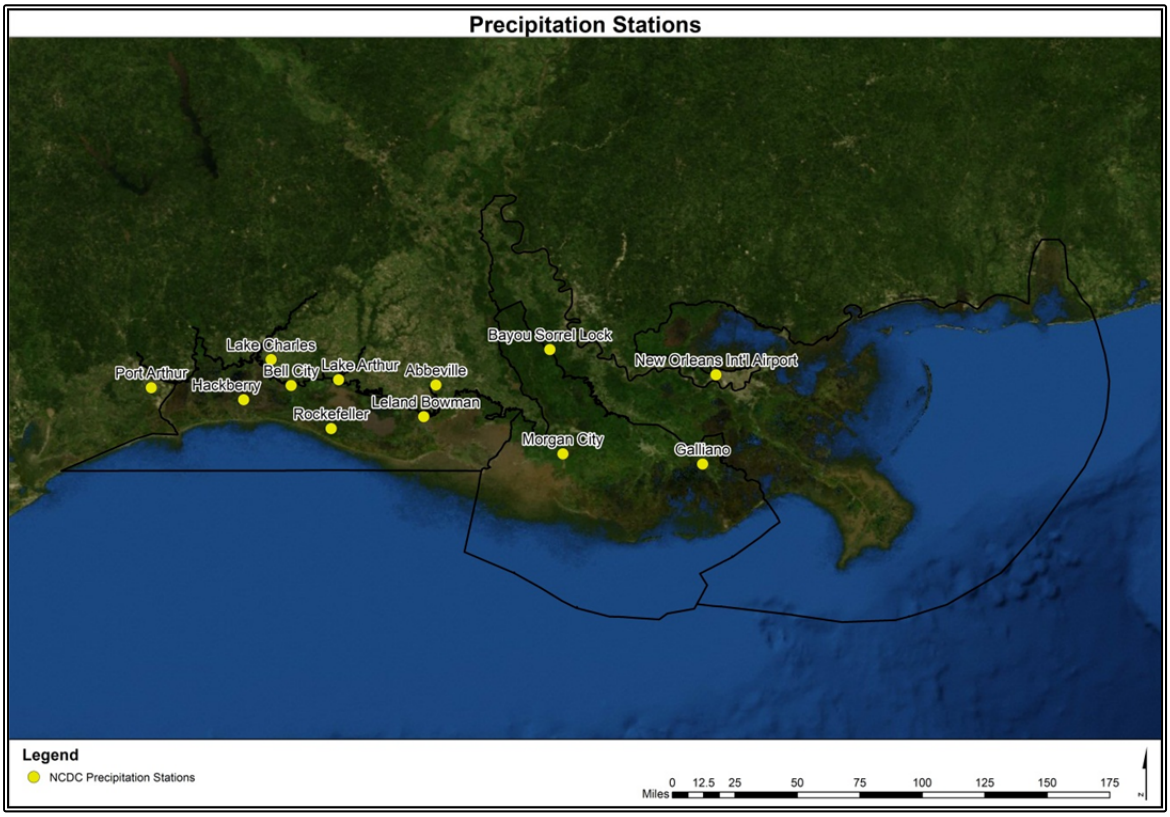

Figure 7 Precipitation Stations for the Eco-Hydrology Models

Missing precipitation records were filled using the arithmetic mean of neighboring stations. According to Ponce, the location of a compartment's centroid to the Thiessen polygons created from the stations in each region determines the rainfall record used in each compartment (1989).

Spatially distributed 2007 rainfall data downloaded from the Lake Charles NEXRAD[18] radar[19] were aggregated to hourly totals on a 4x4 km resolution grid. These hourly totals were aggregated into daily accumulation values and used only for the CP model calibration. The precipitation for each compartment was the average of the data point values inside and within 2 km of the compartment. Since the spacing of the point values was 4 km, points within 2 km, or half the spacing, were assumed to represent part of the compartment and were therefore included in the average.

[18] Next-Generation Radar (NEXRAD)
[19] http://www.ncdc.noaa.gov/oa/radar/radarresources.html#welcome

Evapotranspiration/Evaporation[20]

The PB model used daily evapotranspiration values projected from Fontenot's (2004) composite coastal monthly dataset. This dataset was based on results from the Food and Agriculture Organization (FAO) Penman-Monteith model, which used data between December 2002 and November 2003 from five LSU AgCenter[21] sites: Ben Hur, Hammond, Houma, Rice, and Southeast Louisiana**.** The stations used for *ET* data are shown in **Figure 8** for all three regions.

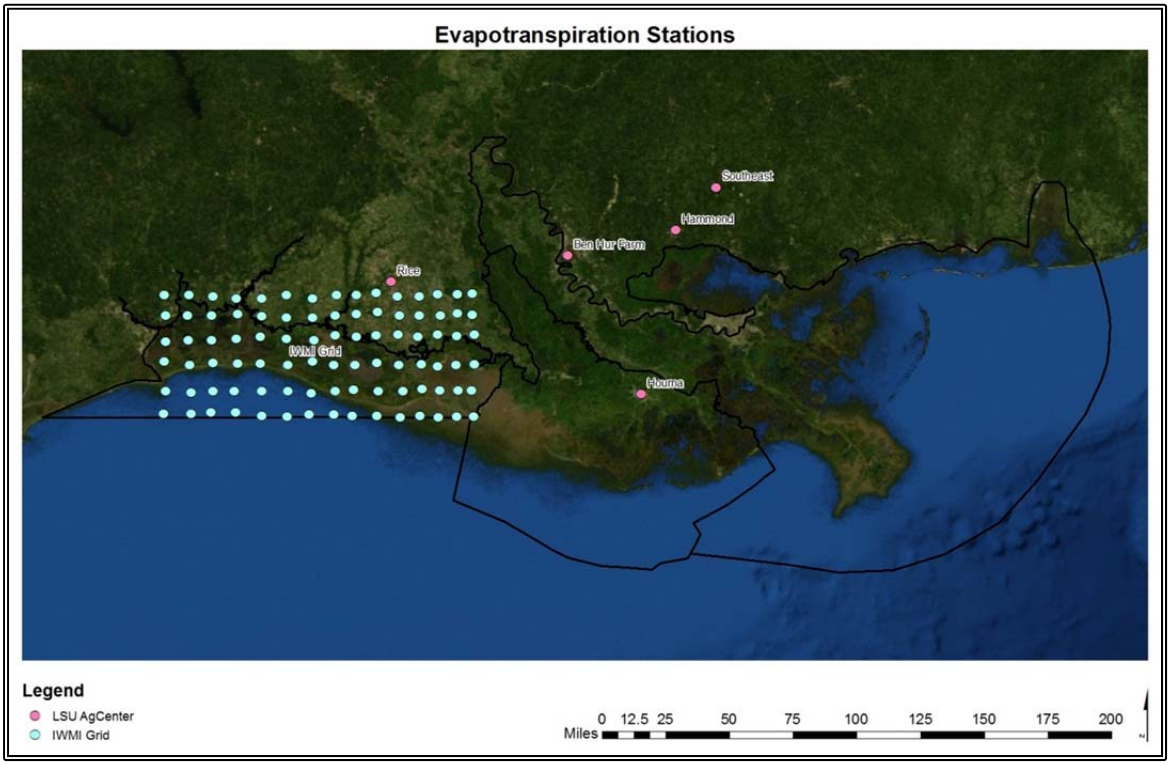

Figure 8 Evapotranspiration Stations for the Eco-Hydrology Models

Evapotranspiration pan data from the NCDC station in Houma Louisiana was assumed uniformly applicable to the entire AA model area. In order to more accurately represent existing conditions, a reduction factor was applied to the marsh compartments to account for the limited sunlight penetration in the marsh due to plant coverage. This will be discussed further in Section 2.

A 4x4 km grid of mean monthly evapotranspiration data obtained from the International Water Management Institute (IWMI) World Water and Climate Atlas[22] is used in the CP model domain. The value for each compartment is the average of the values inside and within 2 km of each compartment. Again, since the spacing of the point values is 4 km, points within 2 km, or half the spacing, are assumed to represent part of the compartment and are therefore included in the average. In order to more accurately represent existing conditions, a reduction factor is applied to the marsh compartments, similar to the AA model, to account for the limited sunlight penetration in the marsh due to plant coverage. This will be discussed further in Section 2.a.

[20] Evapotranspiration is over land and evaporation is over water. In this report, they are referred to as the same thing.
[21] http://weather.lsuagcenter.com/
[22] http://www.iwmi.cgiar.org/WAtlas/Default.aspx

Wind Speed

In the PB model, wind speed data for 1990-2009 were calculated by averaging the available daily values at the Louisiana Universities Marine Consortium (LUMCON) Lake Pontchartrain station and three NCDC sites (New Orleans International Airport, New Orleans Lakefront Airport, and Slidell). The years of 1990 – 1994 were repeated to complete the last 5 years of the first 25-year dataset. These years were used because they are representative of average conditions, with no extreme conditions. The entire 25 years is repeated for the second year-set.

The AA and CP models used daily average wind speed data from the Lafayette Regional Airport from 1945 – 2010. Since the sediment sub-model uses wind speed only, wind direction was not specified. **Table 54** in Attachment A describes the stations used to generate the wind speed input files, including the operating agency, station ID number, location, and period of downloaded data.

Tributary

For each of the models, there are one or more rivers, canals, and/or waterways that supply additional fresh water into the domains. These tributaries have specified discharge, water quality, temperature, and salinity values that were measured by state and federal agencies. In order to efficiently model the hydrodynamic and ecological processes occurring in each of the model domains, these measured values needed to be applied as boundary conditions. Below is a brief description of each of these boundary conditions. One special case that should be mentioned was the reflective boundary at the GIWW for the AA model, which is described below.

Discharge

Tributary discharge data were obtained from existing USGS stations for the rivers or channels entering the model domains. For the larger rivers, such as the Mississippi and Atchafalaya, the USACE stations were used. **Figure 9** shows the locations of these stations.

Table 55 in Attachment A lists the numbers, names, and region(s) for the stations.

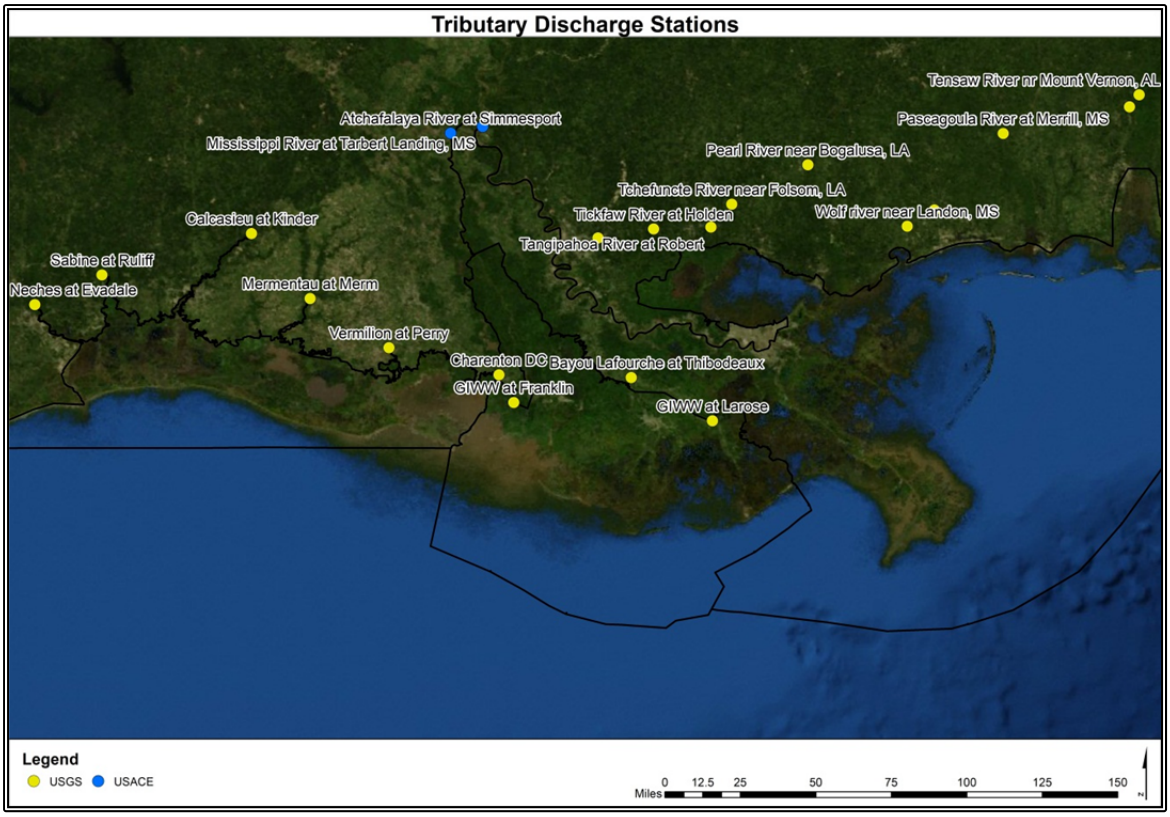

Figure 9 Tributary Discharge Stations for the Eco-Hydrology Models

To accurately fill missing discharge records, the measured discharge in the PB model was analyzed over a long-term period. First, a relationship between consecutive gauges located along each tributary was determined. On six rivers in this region, the average annual daily discharge per unit area was compared between upstream and downstream gauges to analyze changes in flow as one travels downstream along each individual river. For example, a relationship between average annual daily discharge per unit area at the upstream gauge near Darlington and the downstream gauge near Denham Springs was established for the Amite River. The resulting relationship was nearly linear, and similar results were found for the other five rivers (Roblin, 2008). These linear relationships indicated that discharge per unit area was relatively independent of location along the tributary (Roblin, 2008). **Table 2** identifies the upstream and downstream gauges used for the six rivers, as well as the relationship between the gauges and the R^2 value associated with each relationship. As seen in the table, the Tangipahoa River showed a slight drop in the relationship as compared to the other rivers. This was thought to be the cause of inaccurate data measurements and/or calibration to the smaller Osyka gauge, and the unusual relationship was likely the cause of the poor R^2 value. Since this Tangipahoa River relationship was only used to fill in minimal missing data, it was believed that the correlation was acceptable.

Table 2 Discharge Correlations for PB Tributaries (Roblin, 2008)

River	Downstream	Upstream	Downstream = f(Upstream)	R^2
Amite	Denham Springs	Darlington	$Q_{downstream} = 1.0166*Q_{upstream}$	0.8978
Tangipahoa	Robert	Osyka	$Q_{downstream} = 0.9165*Q_{upstream}$	0.7893
Bogue Chitto	Bush	Tylertown	$Q_{downstream} = 1.026*Q_{upstream}$	0.9212
Pearl	Bogalusa	Jackson	$Q_{downstream} = 1.1119*Q_{upstream}$	0.8577
Tickfaw	Holden	Liverpool	$Q_{downstream} = 1.0723*Q_{upstream}$	0.9450
Comite	Comite	Olive Branch	$Q_{downstream} = 1.0468*Q_{upstream}$	0.9383

Further analysis of the individual gauges confirmed that the average annual daily discharge per unit area did not vary significantly between locations in the watershed (**Figure 10**). Therefore, a conclusion was made that the discharge per unit area remained constant around the Pontchartrain Estuary basin (Roblin, 2008). This was likely due to the relatively uniform topography and climate throughout the watershed. It should be noted that the poor R^2 value shown in **Figure 10** was a result of the lack in correlation of the discharge per unit area and drainage basin area, which reinforced the use of the relationships in **Table 2** to fill in missing records.

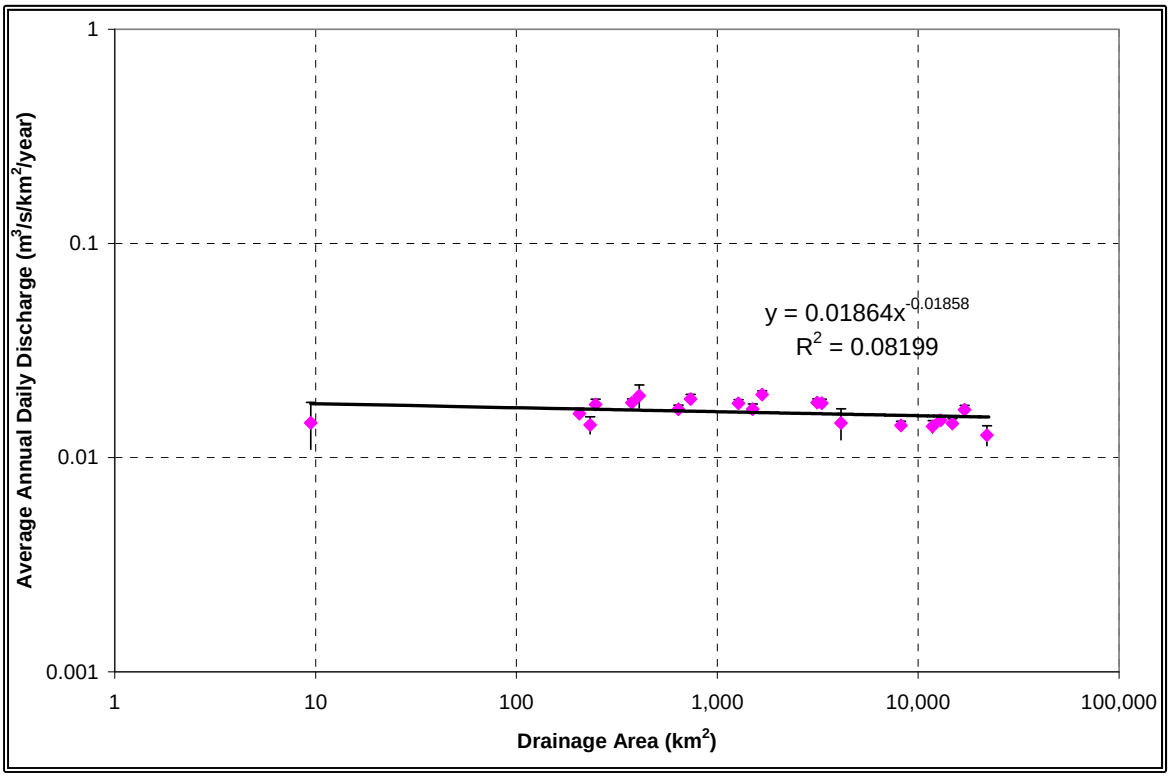

Figure 10 Average Annual Discharge Relationship for PB Tributaries (Roblin, 2008)

Mean daily discharge data for ungauged tributaries in the PB model were generated using the long-term daily discharge relationship shown above (**Figure 10**). The mean ungauged river discharge was varied throughout the year by multiplying it by the normalized discharge values for the Tangipahoa River at Robert, LA (Roblin, 2008).

In the AA and CP models, missing discharge data was filled by applying the equation developed from a correlation to another station. **Table 3** gives the stations with missing data, the percentage of the record complete, the station to which it was correlated, the correlation frequency, and the R^2value. **Figure 11** shows a plot of the correlation between the GIWW at Franklin and the Atchafalaya River.

Table 3 Tributary Discharge Station Correlations for Data Filling Across all Eco-Hydrology Models

Station	Complete	Correlation	Frequency	R^2
Neches at Evadale	32%	Neches at Beaumont	Daily	0.825
Vinton Waterway	0%	Calcasieu at Kinder	Daily	--
Lacassine River	0%	Mermentau at Mermentau	Daily	--
Mermentau at Mermentau	90%	Calcasieu at Kinder	Monthly	0.619
Vermilion at Perry	64%	Mermentau at Mermentau	Monthly	0.391
Charenton DC	46%	Mermentau at Mermentau	Monthly	0.508
GIWW Franklin	47%	Atchafalaya at Simmesport	Daily	0.898
GIWW Larose	50%	Atchafalaya at Simmesport	Daily	0.264

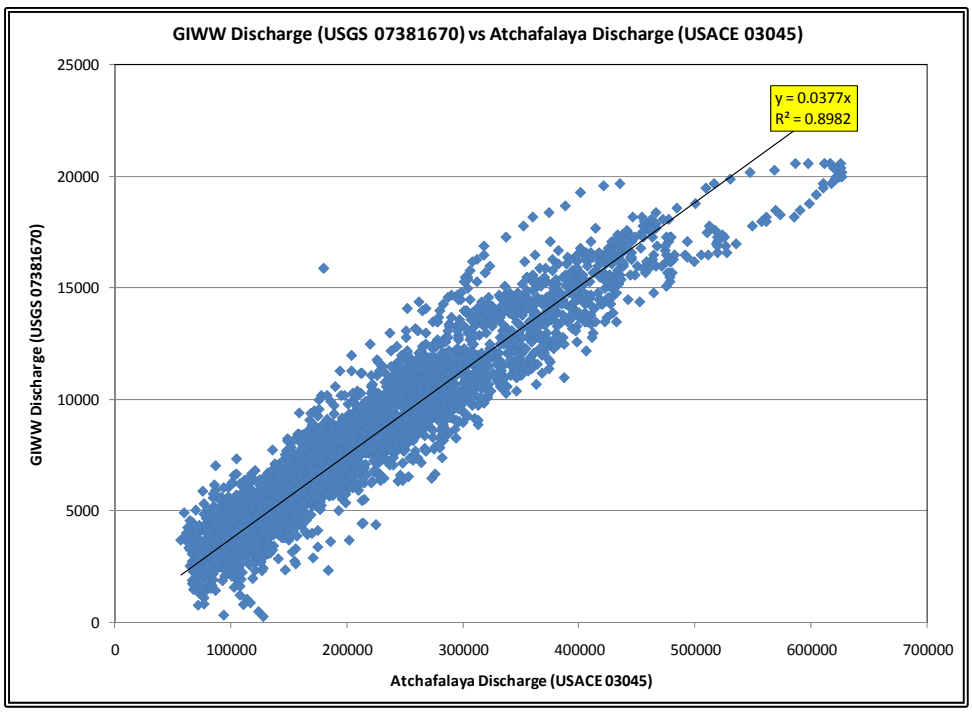

Figure 11 Discharge Regression Relationship between GIWW West and Atchafalaya River for the AA Model

A constant flow of 300 cfs was assumed for Bayou Lafourche in the AA model based on anticipated operations as stated by the CPRA for modeling this project in the future without action (FWOA) landscape.

Water Quality

Table 4 illustrates the parameters and their respective symbols that are discussed in this section.

Table 4 Water Quality Parameters and Symbols for the Eco-Hydrology Boundary Conditions

Water Quality Parameter	Symbol
Algae (Chlorophyll-a)	ALG
Ammonium Nitrogen	NH4
Detritus	DET
Discharge	Q
Dissolved Organic Nitrogen	DON
Dissolved Organic Phosphorus	DOP
Nitrate + Nitrite Nitrogen	NO3
Salinity	SAL
Suspended Sediment Concentration	SSC
Water Temperature	TMP
Total Kjeldahl Nitrogen	TKN
Total Organic Carbon	TOC
Total Organic Nitrogen	TON
Total Phosphorus	TPH
Total Suspended Solids	TSS
Turbidity	TUR
Water Age	AGE

In the PB model, water quality concentrations were collected from several Louisiana Department of Environmental Quality (LDEQ) and USGS stations along eight water bodies. **Table 56** in Attachment A shows these stations and their corresponding measured constituents and **Figure 12** shows their locations in the PB domain. Several of these stations had missing records, and in order to fill these gaps, Roblin (2008) proposed using discharge relationships for each tributary. Roblin (2008) determined from a long-term discharge analysis that the tributary discharges per unit area were nearly independent of the watershed drainage areas for each tributary. Therefore, daily discharge from the nearest gauge could be applied to the measured concentrations to create a relationship without introducing significant errors. As a result, Roblin (2008) developed relationships between the measured concentrations (mg/L) and the discharges divided by the drainage areas ($m^3/s/km^2$). Analysis of observed data showed that TPH, NH4, and TON were relatively insensitive to the tributary discharge. For these constituents, long-term averages were used (see below for additional TON description). The concentrations of TPH and NH4 in the PB tributaries can be found in **Table 57** in Attachment A. Water quality concentrations for the ungauged drainage areas were created using long-term loading relationships of adjacent drainage areas.

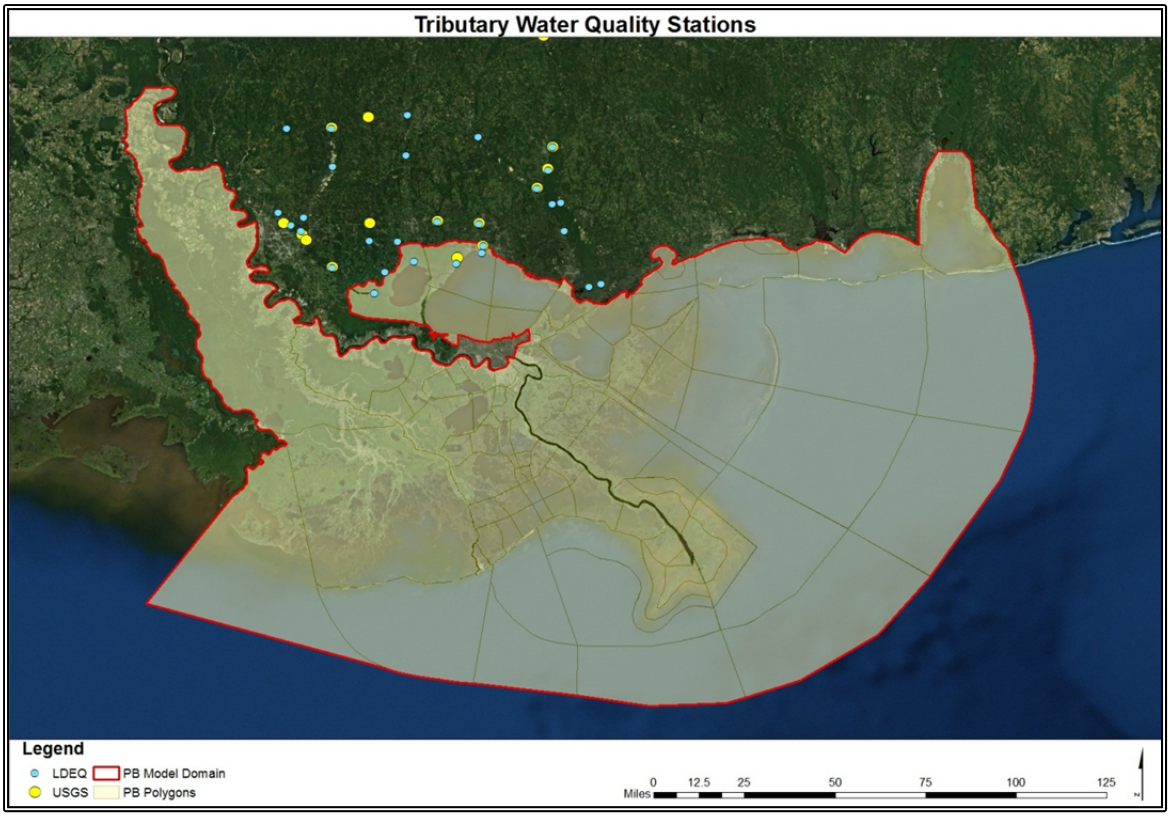

Figure 12 Tributary Water Quality Sites for the PB Model

For the NO3 loadings in the PB model, the concentration-discharge/area relationships were shown in **Table 5** (Roblin, 2008). As presented in the table, several of the tributaries had two relationships, which were separated by a single splitting value (a flow per unit area at which the relationships below and above this value were different). Other tributaries had a single relationship and no splitting value, which represented a direct relationship. The Tickfaw River was a special case which had two splitting values and three relationships. It should be noted that DA stands for drainage area and Q represents discharge.

Table 5 NO3 Relationships for PB Tributaries (Roblin, 2008)

River	NO3 (mg/L) for Q/DA < Splitting Value	Splitting Value ($m^3/s/km^2$)	NO3 (mg/L) for Q/DA > Splitting Value
Amite	$-637673*Q^6 + 514426*Q^5 - 150380*Q^4 + 20231*Q^3 - 1280.5*Q^2 + 33.093*Q - 0.0478$	0.03	$0.0565*Q^{-0.4}$
Tangipahoa	$-8752700*Q^6 + 1190100*Q^5 - 1225500*Q^4 + 352260*Q^3 - 5621.6*Q^2 + 93.372*Q - 0.27777$	0.0252	$0.1298*Q^{-0.343}$
Bogue Chitto	$-5171400*Q^6 + 2928600*Q^5 - 609660*Q^4 + 58800*Q^3 - 2794.9*Q^2 + 61.067*Q - 0.14389$	0.02	$0.127*Q^{-0.2525}$
Pearl	$-24171000*Q^6 + 9579300*Q^5 -$	0.014	$0.0377*Q^{-0.437}$

River	NO3 (mg/L) for Q/DA < Splitting Value	Splitting Value ($m^3/s/km^2$)	NO3 (mg/L) for Q/DA > Splitting Value
	$1452100*Q^4 + 105550*Q^3 - 3774.2*Q^2 + 59.312*Q - 0.081608$		
Tickfaw	$21{,}000*Q^3 – 2{,}550*Q^2 + 86*Q - 0.225$	0.008	$0.15*Q^{-0.15}$
		0.027	$0.0251*Q^{-0.65}$
Natalbany	$0.25*Q^{0.07}$		
Comite	$0.4247*Q^{0.2398}$		
Tchefuncte	$0.093*Q^{-0.085}$		

In the PB model, TON was measured at several of the USGS stations, but it was not measured at the LDEQ stations. The LDEQ stations, however, did have an extensive dataset of TKN, where TKN is a measurement derived from the summation of NH4 and TON. Since NH4 concentrations in the tributaries were known, TON concentrations were inferred from the LDEQ's TKN measurements. This approach to calculating TON was preferred since the LDEQ dataset was more robust than that of the USGS. Consequently, the USGS dataset was used to determine the percent errors between datasets (Roblin, 2008). Average TKN concentrations and the predicted and measured concentrations of TON are shown in

Table 58 in Attachment A, along with the percent errors from the predictions.

The USGS periodically measures both suspended sediment concentration (SSC) and turbidity while the LDEQ only measures turbidity on a regular basis. Uhrich (2002) showed that regression equations between TSS concentrations and turbidity measurements can accurately predict TSS concentrations with site-specific calibration. It should be noted that while the methods for determining SSC and TSS differed, the terms were often used interchangeably in literature[23]. The quantity of available turbidity measurements was much greater than that of SSC data in the PB region. Therefore, relationships between these two parameters were developed and used to complete the datasets for each tributary (**Table 6**). SSC data were not available for the Natalbany, Tickfaw, or Comite Rivers and were instead transferred from the Tchefuncte River since their drainage areas are similar.

Table 6 SSC Relationships for PB Tributaries (Roblin, 2008)

River	Suspended Sediment Concentration (mg/L) vs. Turbidity (JTU, NTU, mg/L as SiO2)	Suspended Sediment Concentration (mg/L) vs. Discharge ($m^3/s/km^2$)
Amite	$SSC = 4.4137*T^{0.8082}$	$SSC = 454.6143*Q^{0.4605}$
Bogue Chitto	$SSC = 12.9710*T^{0.4772}$	$SSC = 176.8691*Q^{0.3070}$
Comite	$SSC = 7.4201*T^{0.5175}$	$SSC = 152.1685*Q^{0.2710}$
Natalbany	$SSC = 7.4201*T^{0.5175}$	$SSC = 74.7192*Q^{0.1334}$
Pearl	$SSC = 18.7612*T^{0.4013}$	$SSC = 127.9681*Q^{0.1455}$
Tangipahoa	$SSC = 9.9394*T^{0.6300}$	$SSC = 384.6485*Q^{0.4753}$
Tchefuncte	$SSC = 7.4201*T^{0.5175}$	$SSC = 95.8189*Q^{0.2678}$
Tickfaw	$SSC = 7.4201*T^{0.5175}$	$SSC = 96.2056*Q^{0.2403}$

In the AA model, the water quality concentrations were collected from one LDEQ and two USGS stations. **Table 59** in Attachment A shows these stations and their corresponding measured constituents and **Figure 13** shows their locations in the AA domain. Stoichiometric relations were used to estimate concentrations of the water quality variables that were not measured, i.e. DOP, DET, DON, etc. Long-term monthly averages were computed for each tributary, and a step-wise concentration boundary condition was created by assigning the calculated value to the first and last day of the corresponding month. This stepped boundary was repeated for every year of the simulations. Also, the AGE for all tributary inflows was set to zero.

[23] http://www.jlakes.org/web/wrir00-4191.pdf

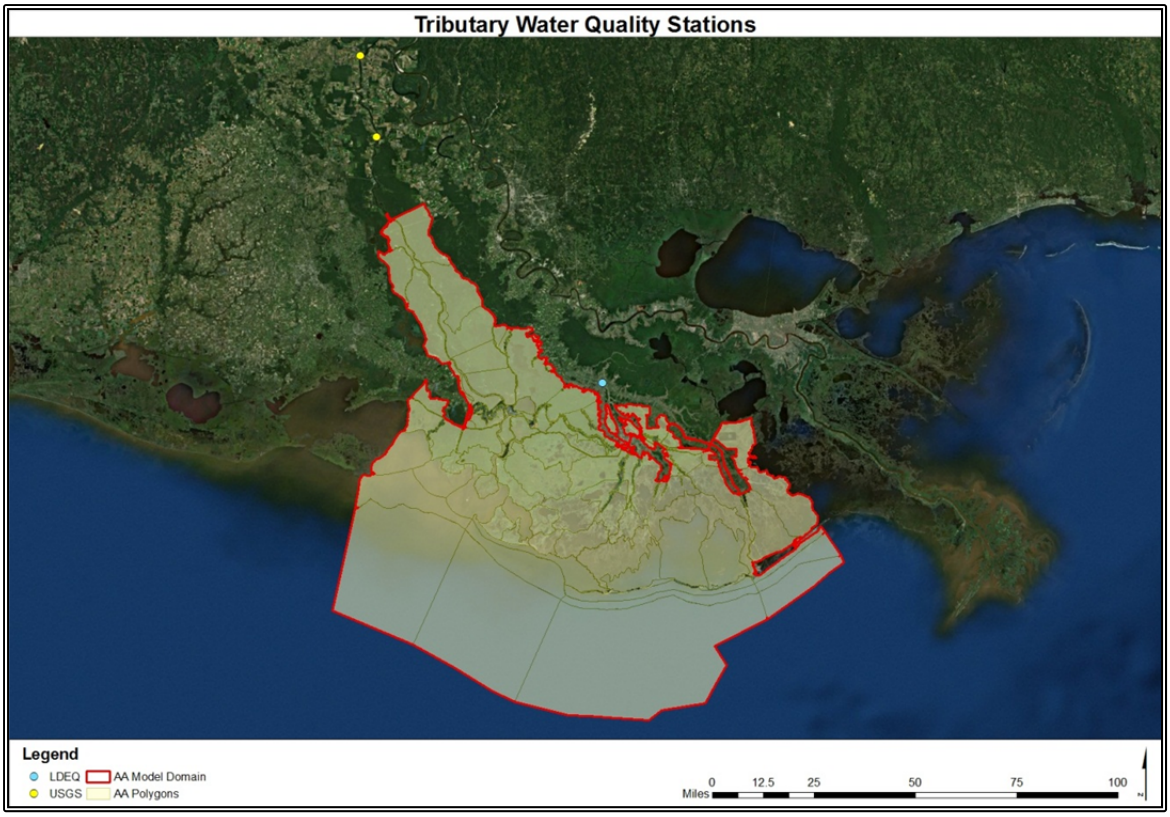

Figure 13 Tributary Water Quality Sites for the AA Model

TSS was estimated as a function of the Atchafalaya River discharge. A regression of suspended sediment as related to stream flow was developed for the Atchafalaya River so that a daily boundary concentration for TSS could be provided based on daily river discharge. Observed suspended sediment and discharge at Simmesport on the Atchafalaya River were used to develop the regression relationship shown in **Figure 14**.

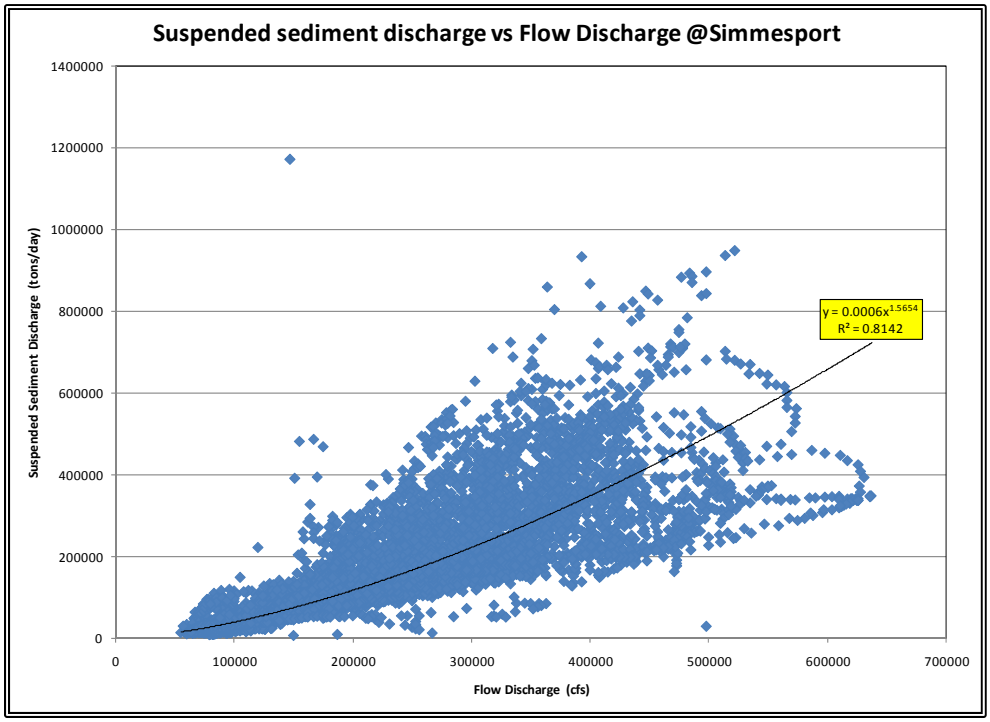

Figure 14 TSS Regression Relationship for Atchafalaya River in the AA Model

In the CP model, the concentrations of water quality constituents were specified for entering flows of nine water bodies to provide loading boundary conditions. Data were collected from the USGS, the LDEQ, and the Texas Commission on Environmental Quality (TCEQ). **Table 60** in Attachment A shows these stations and their corresponding measured constituents and **Figure 15** shows their locations in the CP domain. Stoichiometric relations were used to estimate concentrations for water quality variables that were not measured, i.e. DOP, DET, DON, etc. Long-term monthly averages were computed for each tributary, and a step-wise concentration boundary condition was created by assigning the calculated value to the first and last day of the corresponding month. This stepped boundary was repeated for every year of the simulations. Also, the AGE for all tributary inflows was set to zero.

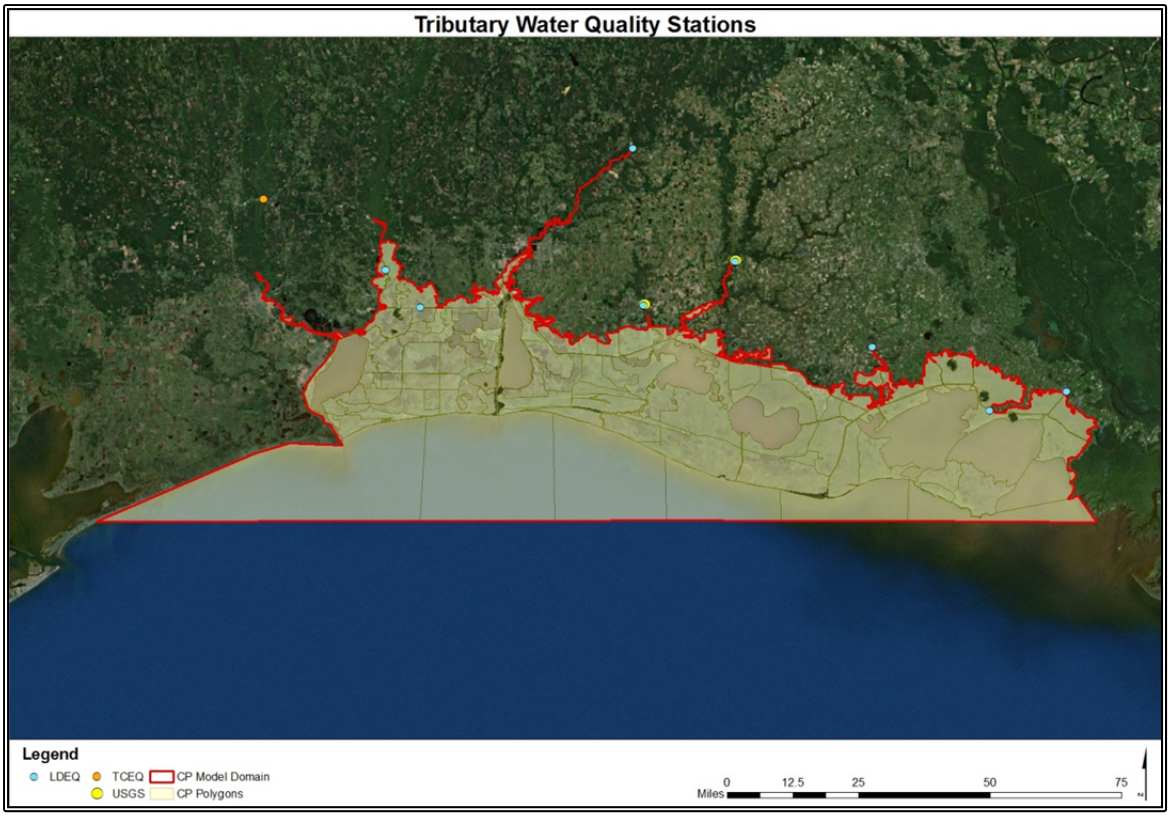

Figure 15 Tributary Water Quality Sites for the CP Model

The LDEQ stations did not provide ALG records. Therefore, a constant value of 5 µg/L was used for all of the freshwater inflows in the CP (excluding the Mermentau River and Bayou Lacassine as ALG data were provided from the USGS stations). The TCEQ station for the Neches River did provide ALG data, but it did not provide TSS concentrations. As a result, a constant value of 10 g/m^3 was used for TSS.

Temperature

As mentioned previously, the PB model did not include a temperature boundary for the tributaries, but instead applied a boundary across the entire onshore domain. The method for developing the temperature boundary for the onshore domain is described here. Both air temperature and water temperature were used to create the water temperature boundary condition. The air temperature was spatially averaged from the actual mean daily values of stations in the Pontchartrain and Barataria Basins to create a daily record. **Figure 16** shows the locations of the air temperature stations. **Table 61** in Attachment A shows the station ID (or COOP ID) numbers and the periods of record supplied by each station. **Table 62**, also in Attachment A, shows the average, maximum, and minimum monthly air temperatures from 1990 – 2006 (Roblin, 2008).

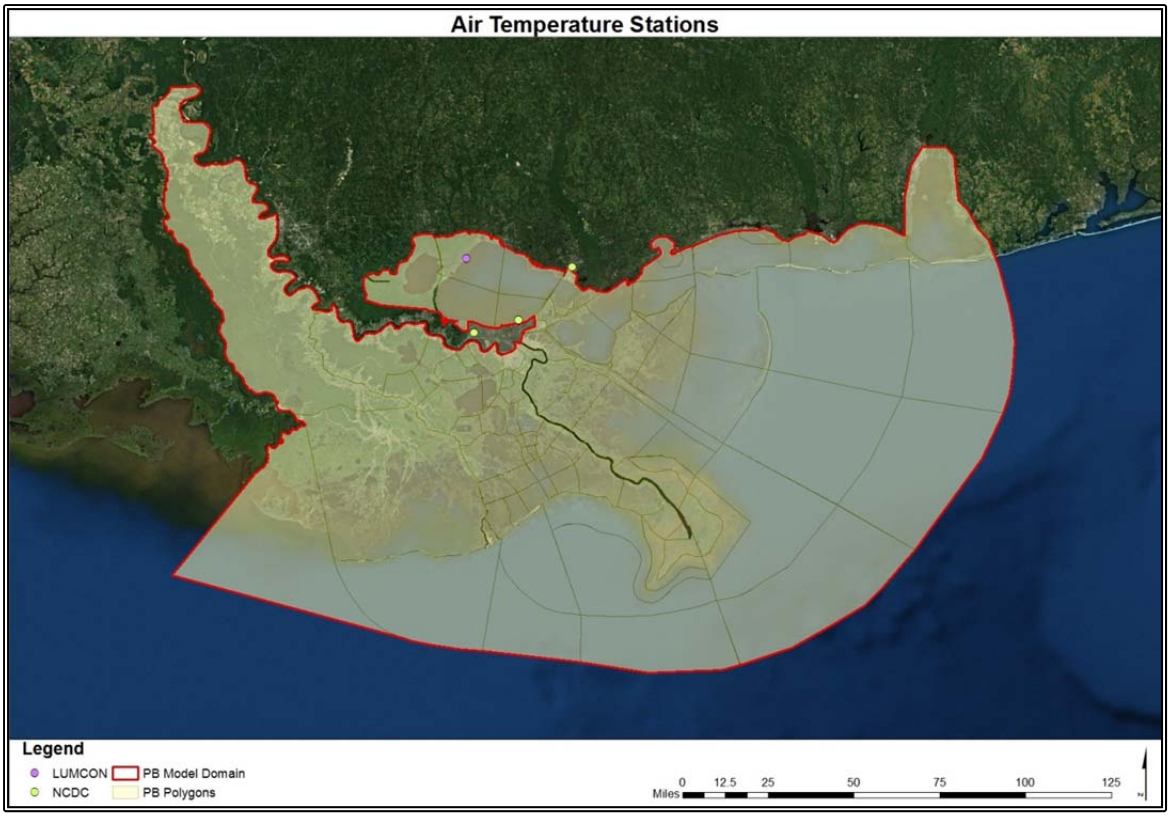

Figure 16 Air Temperature Sites for the PB Model

There were no stations that continuously monitored water temperature in the PB domain for the entire period of simulation. Therefore, all available daily data were averaged (1 LUMCON station, 4 USGS stations, and 95 LDEQ sites) from 1990 to 2008 (**Figure 17**). This spatially averaged water temperature was again averaged over fourteen days to smooth out any irregularities. In order to create a continuous daily record, Roblin (2008) developed a correlation between daily observed air temperature (mentioned above) and this spatially averaged water temperature. **Figure 18** shows the correlation between the observed air temperatures and the 14-day averaged water temperatures.

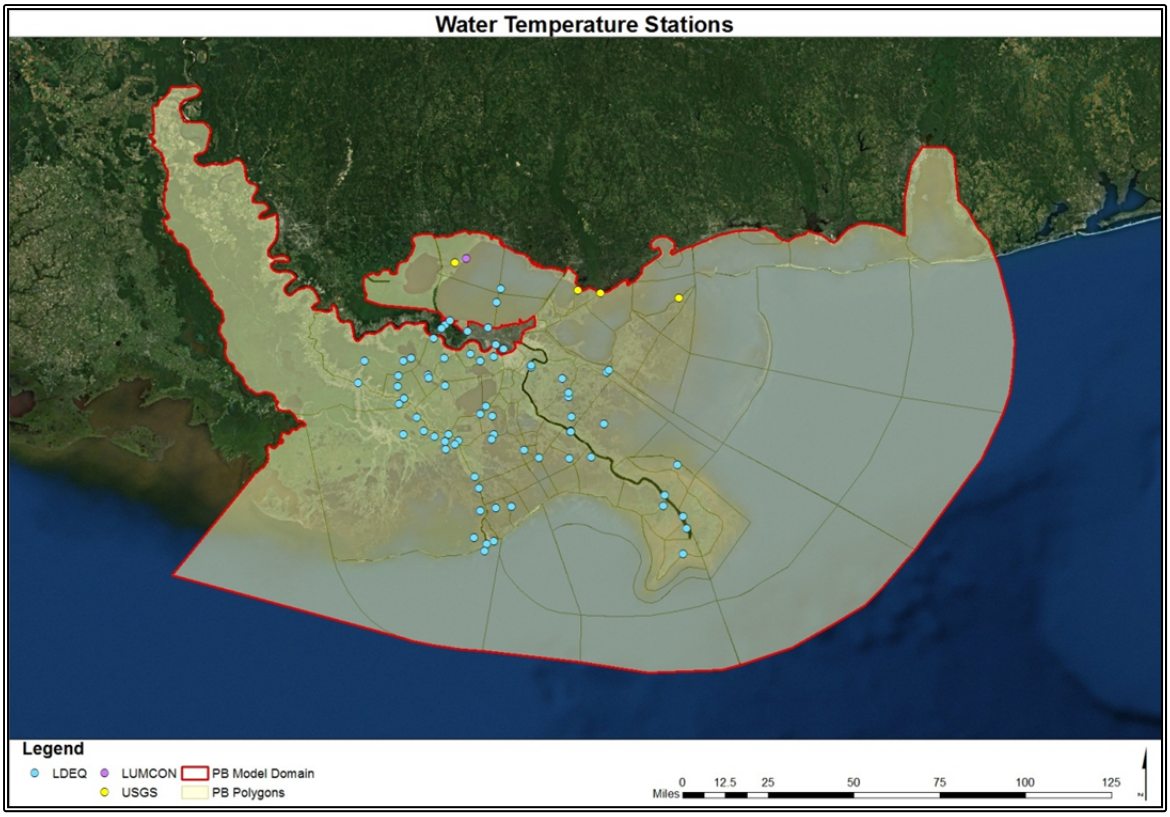

Figure 17 Water Temperature Sites for the PB Model

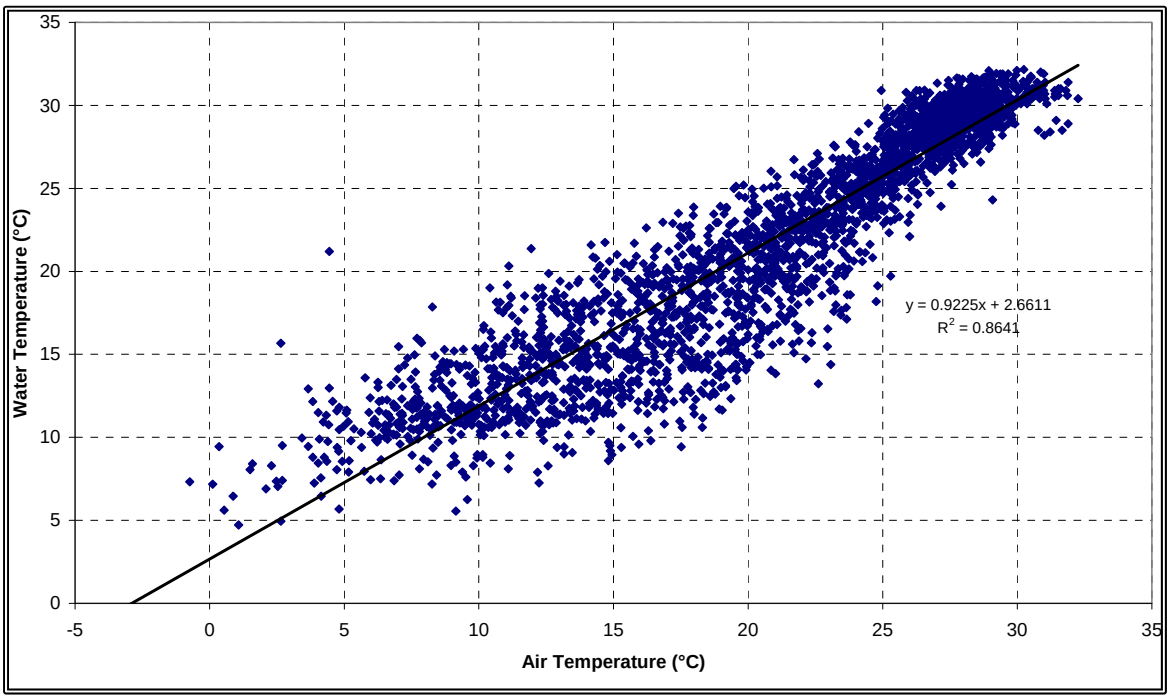

Figure 18 Correlation between Observed Air Temperature and 14-Day Averaged Water Temperature for the PB Model (Roblin, 2008)

Another correlation was created using a 9-day backward running average of the mean daily air temperature versus the spatially averaged water temperature. **Figure 19** illustrates this new relationship. As shown in the figure, the R^2 value (0.9566) was better than the previous correlation's value (0.8641) shown in **Figure 18** (a value of 1 is best). Therefore, the 9-day running average correlation was used to create the water temperature boundary condition for the entire onshore PB domain.

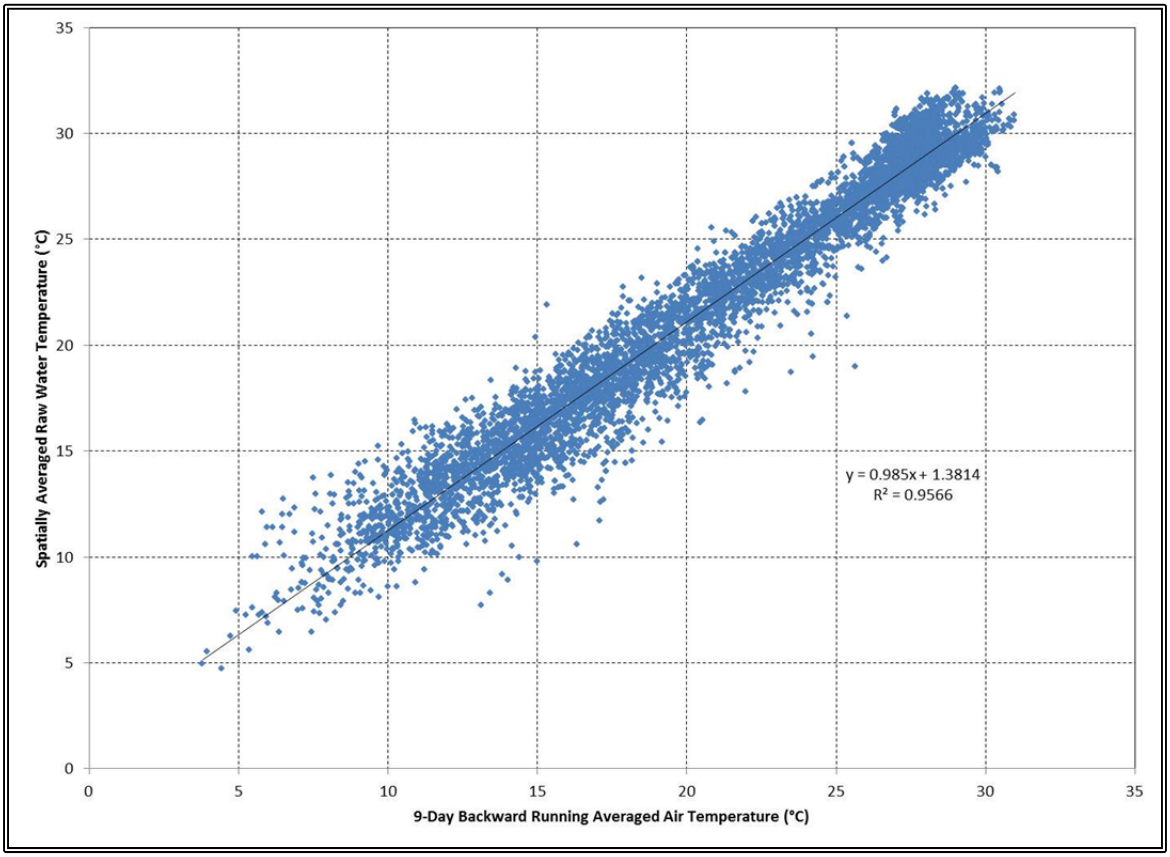

Figure 19 Correlation between 9-Day Backward Running Averaged Air Temperature and Spatially Averaged Water Temperature for the PB Model

For the AA and CP models, observed water temperatures for the tributaries were collected from the same USGS and LDEQ stations mentioned previously (**Table 59** and **Table 60** in Attachment A). These stations did not provide continuous daily temperature records. Therefore, a regression for TMP (°C) as a sine function of Julian day (*JD*) was used. The sine function has the form:

$$TMP = A * sin[f(JD - p)] + k \quad \textbf{(3)}$$

where, *A, f, p,* and *k* were fitted parameters representing amplitude, frequency, phase shift, and mean, respectively. The parameters were adjusted manually to obtain a good fit visually. The final fitted values are shown in **Table 63** in Attachment A. The sine function was used to generate daily tributary water temperatures for the calibrations, validations, and simulations of the AA and CP models.

Salinity

For the PB model, the salinity of all the tributaries was set at a constant 0.205 ppt, which was a nominal value based on a typical minimum in fresh water portions of Pontchartrain and Barataria Estuaries (i.e. Lake Maurepas). In the AA model, the salinity of the Atchafalaya River and Bayou Lafourche were set to 0 (zero) ppt, which represented a completely fresh water body. In the CP model, the salinity of all the tributaries was set constant at 0.1 ppt. Initially, the tributary salinity was set to zero, i.e. completely fresh, but it was changed to 0.1 ppt to prevent instability.

Reflective Boundary for the Gulf Intracoastal Waterway

The loadings along the east and west boundaries associated with the Gulf Intracoastal Waterway (GIWW) were handled in a special manner. There were few if any observed data available to establish inflow loading concentrations associated with the GIWW near the AA model boundaries. Rather than specifying a tributary concentration, it was necessary to use a reflective boundary condition for the GIWW. A reflective boundary is one where the boundary concentration is set equal to the most recently computed concentration of the model compartment adjacent to the boundary within the AA domain. Thus, a reflective boundary condition varies over time. This boundary condition resulted in a zero gradient condition causing no diffusion across the boundary. The reflective boundary condition was reasonable for boundaries that were tidally influenced, like the GIWW boundaries of the AA model, since the inflowing concentration can often be approximated as the most recent outflowing concentration.

Distributary/Diversion

The PB model included several distributaries and diversions that distribute Mississippi River water to areas around the PB domain. The distributaries included existing passes at or near the mouth of the River, as well as natural cuts or crevasses along the River's length. The diversions included existing natural and man-made structures. A complete list of the diversions and siphons modeled for current conditions (FWOA) in the PB domain follows: Caernarvon Freshwater Diversion, Naomi Siphon, West Point à la Hache Diversion Siphon, Bohemia Spillway, Bayou Lamoque Diversion, Davis Pond Freshwater Diversion, Violet Siphon, and Bonnet Carré Spillway. The domain also included outflow through locks on the Inner Harbor Navigational Canal (IHNC), as well as two Westbank Intracoastal Waterway (ICWW) locks. White Ditch Siphon was not included in the model as per the request of the CPRA. West Bay was open for calibration. Natural distributaries included in the PB model domain were Baptiste Collette, Fort St. Philip, Grand Pass, Main Pass, Pass a Loutré, Southwest Pass, and South Pass. Several of the distributaries and most of the diversions were monitored by local or state agencies. These agencies typically only supplied discharge data, whereas, water quality, temperature, and salinity data were assumed to be the same as the source, which was the Mississippi River. In order to efficiently model the hydrodynamic and ecological processes occurring in the PB model domain, the measured discharge values from the diversions and distributaries and the measured water quality, temperature, and salinity values of the Mississippi River needed to be applied as boundary conditions. Below is a brief description of each of these boundary conditions. It should be noted that the AA and CP models did not include distributaries or diversions.

Discharge

The amount of Mississippi River discharge available for distributaries and diversions into the PB region was calculated by subtracting the flow through the Bonnet Carré Spillway, Caernarvon Diversion, and Davis Pond Freshwater Diversion from the Mississippi River flow at Tarbert Landing. A HEC-RAS model (Davis, 2010) calibrated to 2008 data was used to distribute the flow to the distributaries where the flow was not specified previously. Also, the HEC-RAS model gradually ramped up to the maximum master plan-specified diversion flow. Therefore, the peak diversion flow corresponded to the peak Mississippi River flow.

Bonnet Carré Spillway

Roblin (2008) formulated a method for producing daily inputs from the Bonnet Carré Spillway, which were required to reproduce the increased Mississippi River flow into Lake Pontchartrain and surrounding areas when the spillway was open. Flow was not continuously monitored at the Bonnet Carré Spillway, as it was only opened intermittently. However, during opening events, flow was monitored in the spillway by the USGS. Recorded flows during the 1994[24], 1997, and 2008 openings are listed below. A daily discharge record was developed by linearly interpolating between the days with recorded measurements. Measured flows during the 2008 spillway opening were obtained from the USACE (**Table 64** in Attachment A).

Leakage events can occur when the Mississippi River stage reaches a critical height by flowing over the Spillway weir. Cruise et al. (2007) presented the following equation for calculating flow over a spillway:

$$Q = 2.19LH_d^{3/2} \tag{4}$$

where, Q was flow in m^3/s, L was the length of the spillway, and H_d was the head above the spillway crest. This equation was used to calculate flow over the Bonnet Carré Spillway during high river stages. USACE gauge 1280 at the Spillway was used to determine when the river stage exceeded the height of the weir. The head above the Spillway was calculated by subtracting the height of the weir from the river stage. The calculated flow was then reduced by 95% since the water only flows through the spaces between the creosote timbers, which make up the bays of the Spillway.

Davis Pond Freshwater Diversion

Mississippi River flow entering the Davis Pond Freshwater Diversion was monitored by USGS (Station 295501090190400 Davis Pond Freshwater Diversion near Boutte, LA). The daily discharge record from 2002 - 2010 at Davis Pond had many missing days of data, so the following procedure was used to generate a continuous dataset:

1. If there were velocity data available, use the correlation between velocity (v) and discharge (Q) to determine discharge. The velocity correlation equation follows: $Q = 266.08v^2 + 3747.4v - 134.13$
2. If there were no velocity data available, use the correlation between water elevation (WL) and discharge. The water elevation correlation equation follows:

[24] In 1994, the Bonnet Carré Spillway was opened for twelve days to test the effects of opening the Spillway for purposes other than flood control (Roblin, 2008).

$$Q = 155.94WL^3 - 369.7WL^2 + 866.57WL - 834.47$$

3. If no stage or velocity data were available and there were limited consecutive blanks (less than 15), use a linear trend to fill data.
4. If no stage or velocity data were available and there were more than 15 consecutive blanks, use a monthly average of the years before and after. Example: If 2008 was missing all of January, use the average of the January 2007 average discharge and the January 2009 average discharge.
5. Replace all negative discharges with zero.

Caernarvon Freshwater Diversion

Mississippi River flow entering the Caernarvon Freshwater Diversion was monitored by USGS (Station 295124089542100 Caernarvon Outfall Channel at Caernarvon, LA). Daily discharge data from 1990 to 2009 were collected to create the discharge boundary condition. A linear trend was used to fill in missing data.

Other Diversions and Distributaries

A 1-D unsteady hydrodynamic HEC-RAS model, developed by Davis (2010), was used to estimate the discharges of the remaining diversions and distributaries along the Lower Mississippi River. **Figure 20** shows the schematic of the HEC-RAS model (Davis, 2010). This hydrodynamic model was run in the steady-state mode, which calls for a constant discharge at the upstream boundary (Tarbert Landing, MS) for a specific amount of time or until equilibrium is achieved. Once equilibrium was reached, the final discharge value for each distributary and diversion was recorded and input into the PB model as a constant discharge into the domain.

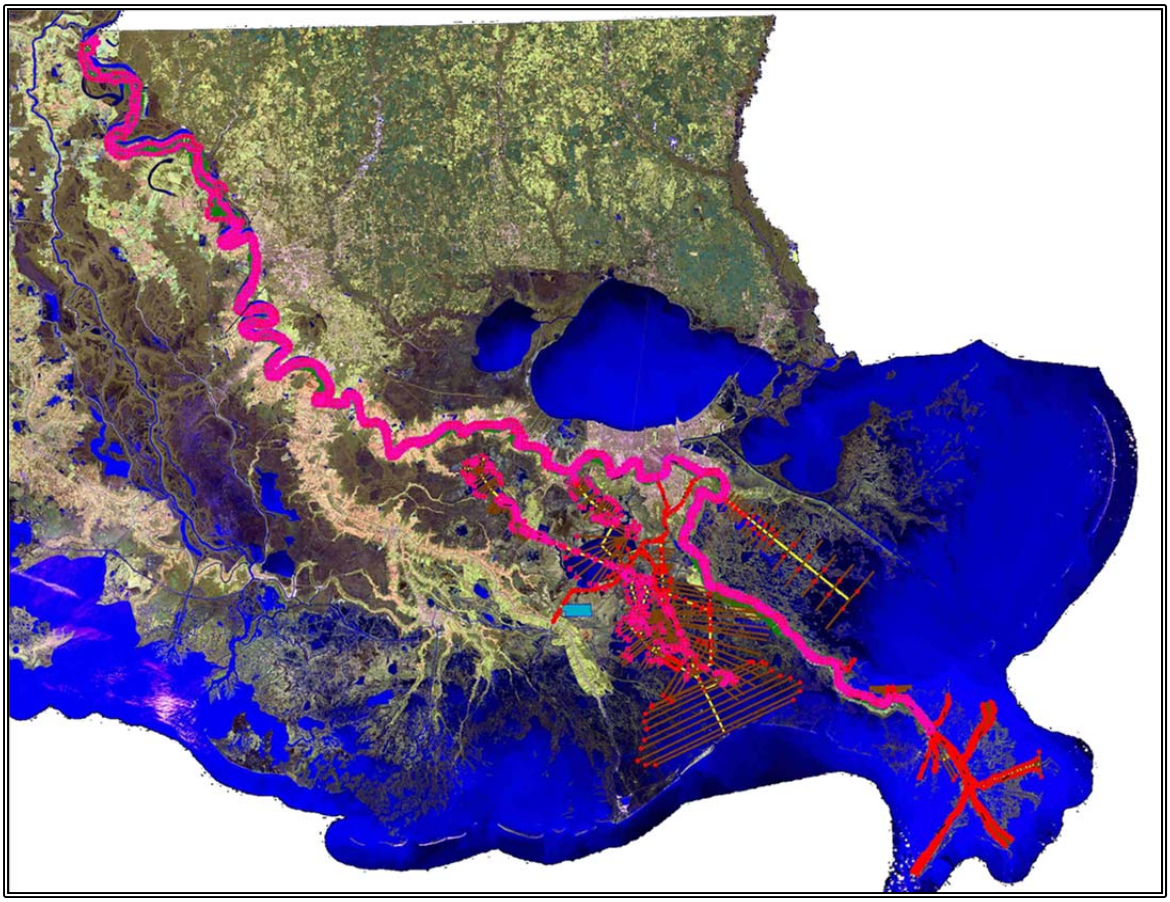

Figure 20 HEC-RAS Model Schematic for Distributary and Diversion Discharges for the PB Model (Davis, 2010)

Water Quality, Temperature, & Salinity

The USGS Mississippi River near St. Francisville, LA station (07373420) was used to create the water quality, temperature, and salinity boundary conditions for all diversions and distributaries. The Bonnet Carré Spillway was different in that the USGS Mississippi River at Luling, LA station (07374400) was also used to develop the water quality boundary condition at that diversion (see below). **Figure 21** shows the USGS stations used to create the water quality, temperature, and salinity boundary conditions for the distributaries and diversions in the PB model. Missing daily values were replaced by averages developed by Roblin (2008). These average monthly water quality concentrations are shown in **Table 65** of Attachment A.

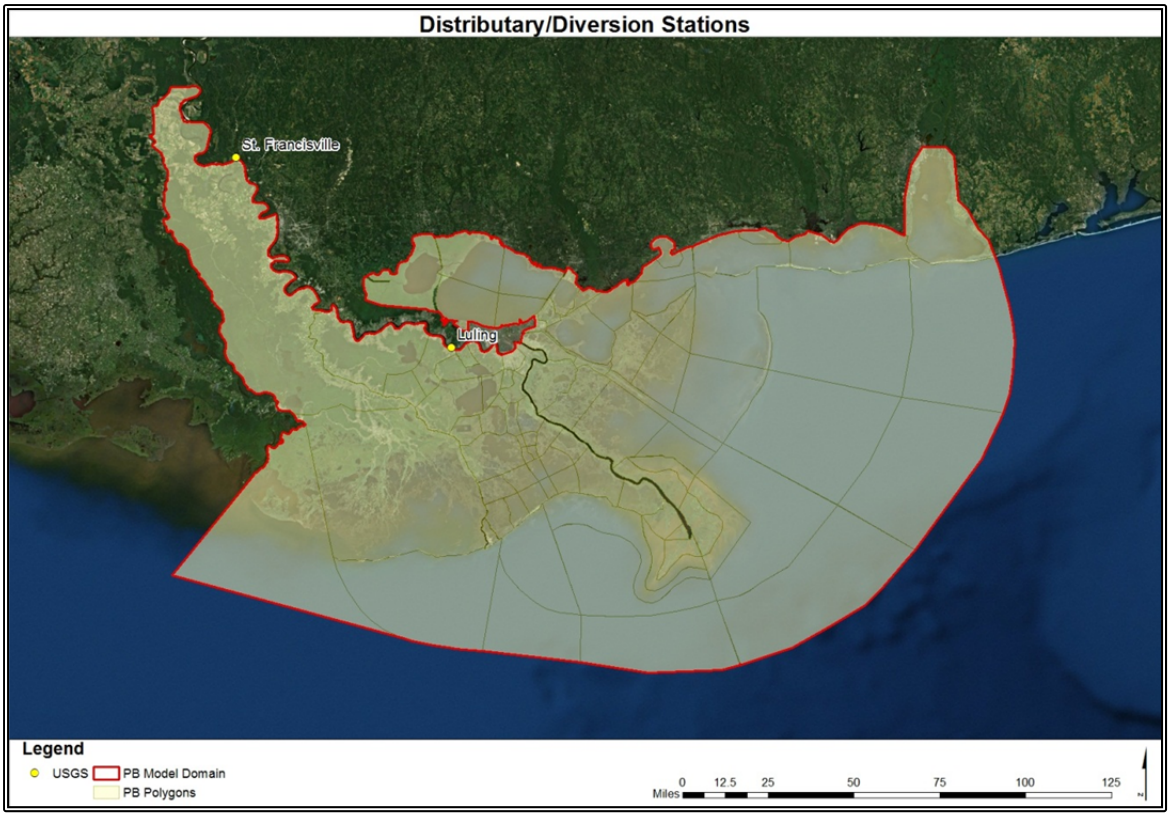

Figure 21 Distributary/Diversion Water Quality, Temperature, and Salinity Stations for the PB Model

Bonnet Carré Spillway

Monthly averages of NO3, NH4, TPH, TON, and TSS were estimated for both the St. Francisville and Luling datasets mentioned above. These monthly averages were then spatially averaged between the two stations and repeated to establish a long-term monthly concentration for each nutrient. The Luling dataset had limited TSS data. Therefore, concentrations at the St. Francisville station were used for this parameter. Resulting concentrations were used to develop the loadings entering the Bonnet Carré Spillway (Roblin, 2008).

Offshore

For each of the models, the Gulf of Mexico acted as a physical boundary where excess water from the domains was released. Several agencies monitored the stage, salinity, water quality, and temperature of the Gulf along the Louisiana coast. In order to efficiently model the hydrodynamic and ecological processes occurring in each of the model domains, these measured values needed to be applied as boundary conditions. Below is a brief description of each of these boundary conditions. The stations used to create the offshore stage boundary for each region are shown in **Figure 22** and the station information can be found in **Table 66** in Attachment A.

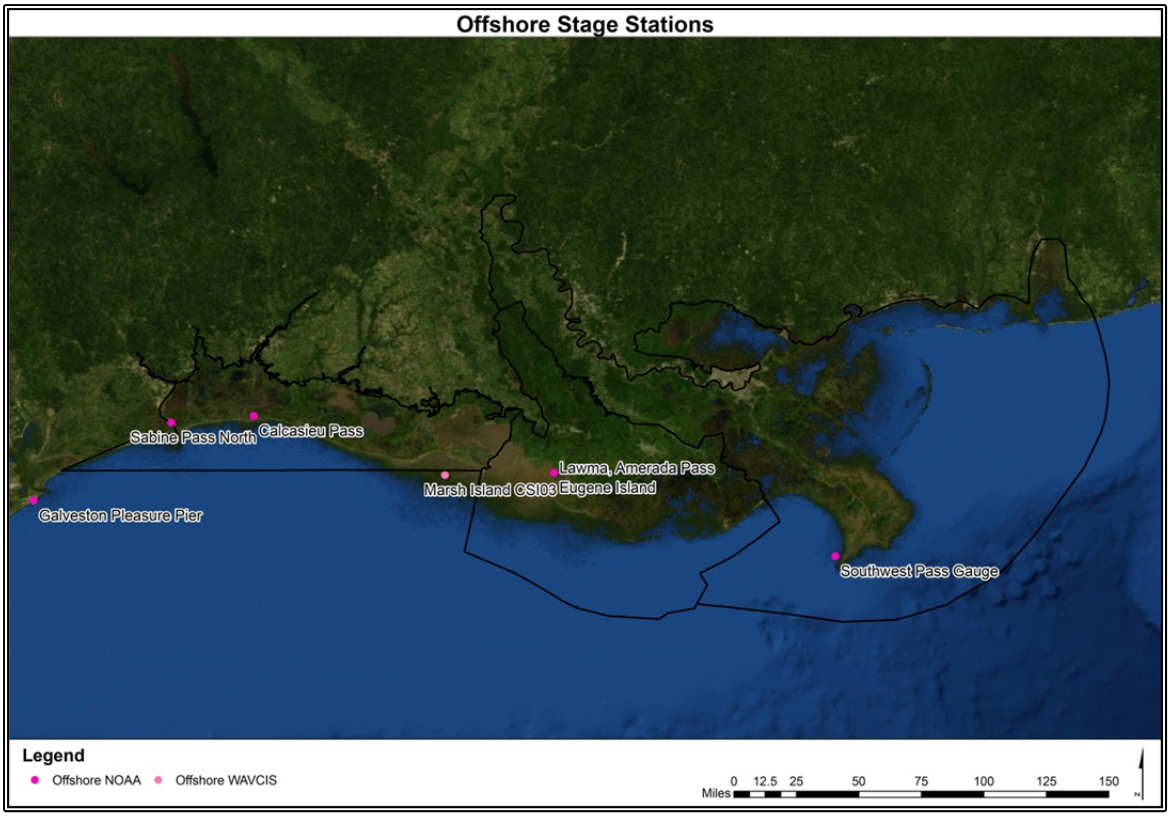

Figure 22 Offshore Stage Stations

Stage

The offshore stage boundary of the PB model was calculated by adjusting the USACE Southwest (SW) Pass Gauge at East Jetty (Station 01670) water level. From Station 01670's observed data for 1999 through 2003, a polynomial fit of mean annual Gulf stage was formulated ($y = 1.00482E\text{-}22x^6 - 2.83698E\text{-}18x^5 + 2.99401E\text{-}14x^4 - 1.46371E\text{-}10x^3 + 3.26479E\text{-}07x^2 - 2.33005E\text{-}04x - 0.07$). This polynomial equation (with a correlation coefficient of $R^2 = 0.98$) was used to estimate offshore water level for the entire 25-year simulation period. A graphical comparison of the measured data, calculated average data, and the polynomial trendline can be found in **Figure 23**. This figure also illustrates the seasonal effects represented through this polynomial expression. To develop the stage record used as model input, a diurnal lunar tide calculation and a mean daily surge record were then added to the mean seasonal Gulf stage.

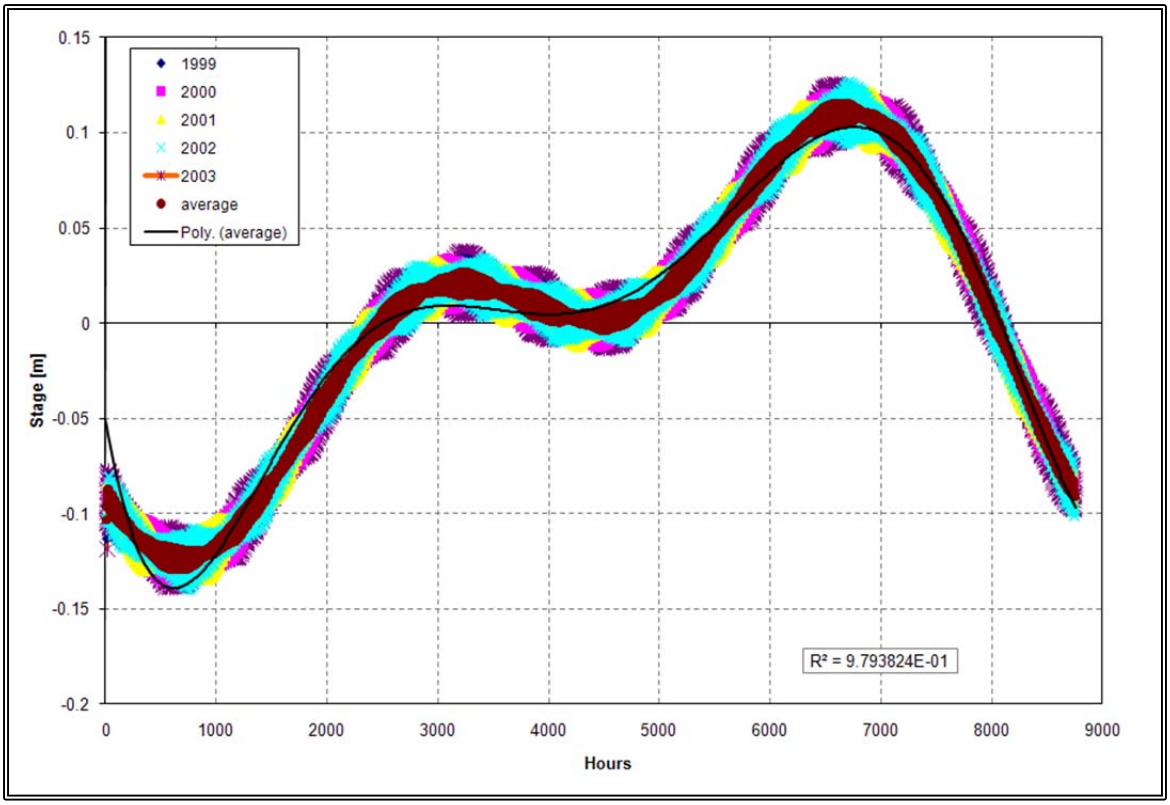

Figure 23 Southwest Pass Stage Correlation in the PB Model

The daily surge record reflected tropical storm and hurricane activity from 1990 through 2009. **Table 67** in Attachment A describes the tropical event, date of impact, and surge in meters applied at the offshore boundary nodes. Dates not listed in this table had no significant tropical activity and therefore had a surge of zero meters.

The tidal boundary condition for the PB model was based on the mean spring and neap tidal amplitudes at Station 01670. A typical tidal record for 1999 at this gauge is given in **Figure 24**. The offshore tidal input for the model was developed by transferring this tidal signal to the offshore nodes and then calibrating its amplitudes until the model reproduced the observed mean spring and neap tides at the compartment containing the Southwest Pass gauge (PB031).

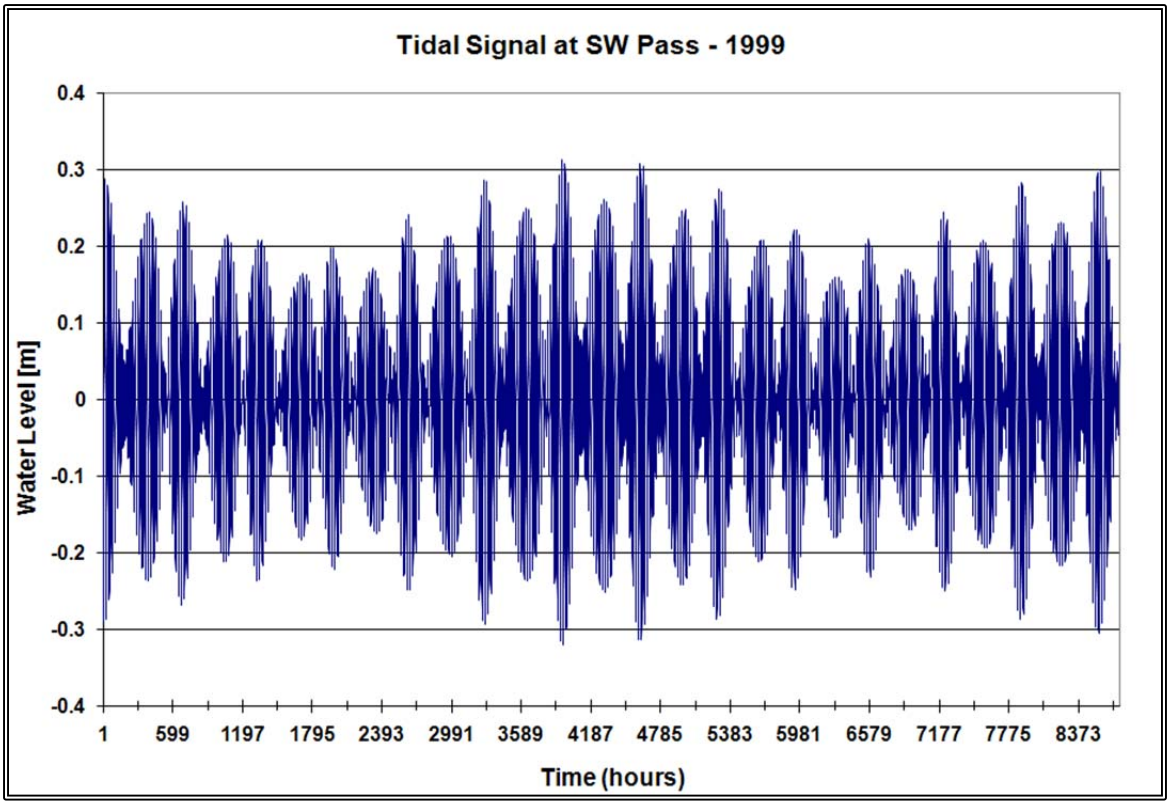

Figure 24 Southwest Pass Tidal Signal in the PB Model

The offshore stage boundary of the AA model was mainly based on observations from the Sabine Pass North NOAA station (8770570). Small gaps in the stage data (on the order of a couple of hours) were filled using linear interpolation. Data from the USACE gauge 88550 at Eugene Island and NOAA gauge 8768094 at Calcasieu Pass were used to fill the large gaps in the Sabine Pass dataset. The input interval for each of the datasets was 1 hour. In order to capture the differences in both amplitude and phase, the offshore boundary conditions were developed by extracting tidal constituents from the ADCIRC East Coast 2001 model. It should be mentioned that the Eco-Hydrology teams did not use the master plan ADCIRC model because it was not available when the boundary conditions were being developed. Because there was no direct interaction between the Eco-Hydrology and ADCIRC model as part of the master plan analysis, this should not affect model outcomes.

ADCIRC East Coast 2001 was a high resolution, finite-element tidal model of the Western North Atlantic Tidal (WNAT) domain developed by the USACE (Mukai et al., 2002). The WNAT domain encompassed the Western North Atlantic Ocean, the Gulf of Mexico, and the Caribbean Sea. The ADCIRC model computed amplitude and phase for the M2, N2, S2, O1, K1, Q1, and K2 tidal constituents as well as the M4 and M6 overtides. In general, the computed amplitude of the seven major tidal constituents was within 6-13% of the measured amplitude and the computed phase was within 7-13° of the measured phase. These clearances were acceptable and therefore, the ADCIRC-modeled constituents were used to construct the predicted tides at the offshore boundary compartments.

On subtidal timescales, meteorological effects are important, especially along the Gulf Coast where storm winds blowing over the shallow continental shelf pile water against the coast. This wind-induced sea level rise is called Ekman transport, and in order to accurately simulate this transport, a very large, three-dimensional offshore domain over which the along-shelf currents could develop was required, along with an extensive meteorological dataset. This type of model was not necessary to assess the potential environmental consequences of the proposed projects and was therefore beyond the scope of this study. Instead, an estimate of the meteorological component of the offshore water level was added to the tidal boundaries.

This offshore meteorological component (also referred herein as the "residual") was obtained by subtracting the predicted harmonic water levels from their corresponding measured water levels at the boundary stations and combing them temporally. The combined residuals were filtered with a 26-hour low-pass filter to eliminate any of the high frequency (daily) variability. The filtered residuals were then added to the predicted tidal signal at each boundary compartment's centroid.

The CP offshore stage boundary was developed using the following procedure. Residuals were calculated as the difference between the hourly predicted tides, a calculation based on harmonic constituents[25], and observed tides obtained from the Galveston Pleasure Pier NOAA station from 1990 to 2010 (Tides & Currents, 2011). Hourly predicted tides were also obtained for 2007 from the Calcasieu Pass and Lawma, Amerada Pass NOAA stations. The Calcasieu Pass station was projected off the coast to assist in creating the offshore boundary. Using observed data from 2007, the Calcasieu Pass time-series was shifted backwards by one hour based on a comparison to the Marsh Island time-series. This shift accounted for the difference in location of the station to the boundary, which was approximately thirty-five (35) kilometers offshore.

The three stations were then connected by imaginary lines (**Figure 25**), where points, placed 500 m apart on the lines, contained a tide time-series that was weighted based on the points' proximity to the two nearest stations. For example, a point closer to the Galveston station had a time-series that was more heavily weighted towards the Galveston station than the modified Calcasieu station. However, points within twelve (12) km east and ten (10) km west of the projected Calcasieu Pass station solely used this station's time-series. The east/west bounds of the 6 open water compartments that lie off the coast in the CP domain were projected to the imaginary lines. The points on the lines that fall within the east/west bounds of those 6 compartments were averaged together to create the tidal boundary for the respective offshore node.

[25] Harmonic constituents are used in a mathematical expression to estimate the tide-producing force and they are also used in corresponding formulas for estimating the tide or tidal current. Each constituent represents a periodic change or variation in the relative positions of the earth, moon, and sun (Tides, 2011).

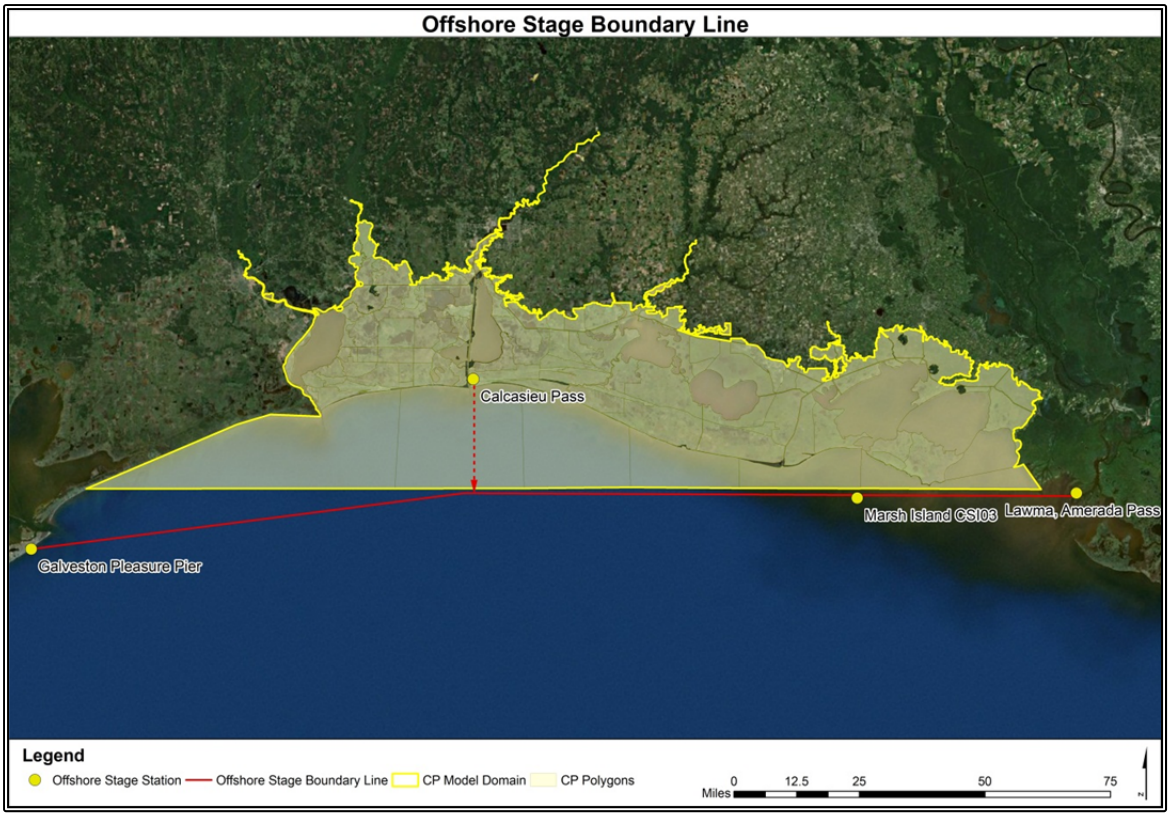

Figure 25 Offshore Stage Boundary Line for the CP Model

Since the predicted tides do not vary greatly from year to year, these time-series were repeated twenty (20) times to create a 20-year offshore predicted tide time-series. The residuals (calculated from earlier) were added to each of the time-series and the first five years (1990 – 1994) were repeated at the end of the series to create a 25 year offshore tide record, excluding sea-level-rise (SLR). These 5 years were chosen because they represent average conditions.

SLR was included in the tide time-series using the estimated sea-level-rise (ESLR) provided by the CPRA. The ESLR gave the estimated end-of-year accumulated rise starting from day zero in meters. The yearly incremental rise (m/year) was calculated by subtracting the accumulated rise of the previous year from the accumulated rise of the year of concern. This yearly incremental rise was then broken down to estimate the hourly incremental rise, assuming the rise occurs uniformly and consistently throughout the year. The resulting hourly incremental rise time-series was added to each of the 25-year offshore time-series to create the offshore stage boundary used in the CP model.

The observed tides from the NOAA stations and the LSU Wave-Current-Surge Information System[26] (WAVCIS) Marsh Island Station CSI03 were used for the development of the 2007 calibration and 2010 validation offshore stage boundaries. The same procedure described above was used for the calibration and validation tide boundaries except for the inclusion of SLR because the observed tides were used instead.

[26] http://wavcis.csi.lsu.edu/index.asp

Salinity

In the PB model, the offshore salinity boundary values were based on "A Bathymetric and Hydrographic Climatological Atlas for the Gulf of Mexico" (Herring, 1993)[27]. This atlas provided maps with annual salinity isohalines at various locations in the Gulf of Mexico. These isohalines were used to determine average salinity values at the corresponding offshore boundary nodes (**Figure 26**). Again, the PB model used nodes to define the offshore boundary, rather than using compartments like the AA model. For modeling purposes, these nodes were given compartment ID numbers (PB101 through PB107). It should also be mentioned that compartment PB107 was actually onshore in Terrebonne (**Figure 26**), but it was included as an offshore node to enforce the salinity boundary there. **Table 68** found in Attachment A describes the offshore compartment number and corresponding salinity value.

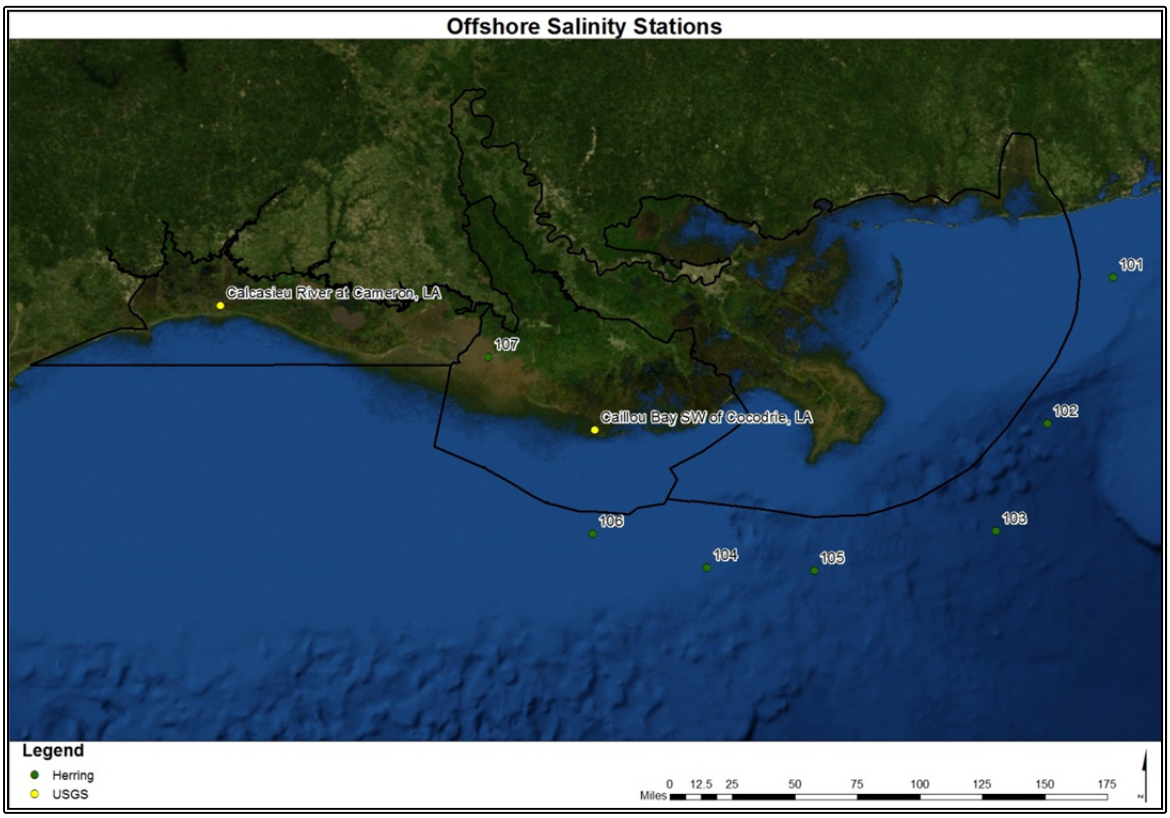

Figure 26 Offshore Salinity Stations for the Eco-Hydrology Models

For the offshore salinity boundary conditions in the AA model, monthly average salinity values were developed based on records from USGS gauge 073813498 (Caillou Bay SW of Cocodrie) from 1999 to 2002 and were repeated every year. This USGS station is shown in **Figure 26**. **Table 69** in Attachment A lists the monthly average offshore salinities.

[27] The Herring atlas was used for the offshore boundary because this report was comprehensive and the modelers did not anticipate significant changes in these boundary conditions in terms of relative response of the estuaries to proposed projects.

For the CP model, salinity measurements in Calcasieu Pass just inshore of the Gulf of Mexico (USGS station 08017118, **Figure 26**) from 1998 to 2009 were used to construct a 25-year record. **Table 7** illustrates how the 25-year record was established for the CP region.

Table 7 Comparison between Measured and Model Years

Model Year	Model Calendar Year	Measured Data Year
1-7	1990-1996	2001-2007
8	1997	2008
9-18	1998-2007	1998-2007
19	2008	2008
20-24	2009-2013	1998-2002
25	2014	2003

Since the location of the USGS station was inside Calcasieu Pass (**Figure 26**), a 24-hour moving maximum was calculated to estimate the salinity at the model boundary, which was approximately 35 km offshore. These values were extrapolated along the boundary line using the Gulf of Mexico salinity distribution from the SHELF model simulations (Meselhe et. al., 2008). This distribution was further lowered offshore of Vermilion Bay based on observed data in the bay and at the Marsh Island station CSI03. This distribution can be seen in **Table 70** in Attachment A. Again, the CP model used nodes to define the offshore boundary, and the offshore salinities described here were applied to those nodes. Also, the nodes were given compartment ID numbers so that they could be included in the model.

Water Quality & Temperature

Water quality concentrations and temperature observations were collected from the stations shown in **Figure 27**. The data from these stations were used to create the offshore water quality and temperature boundary conditions for each of the model regions. The information for each station is listed in **Table 71** in Attachment A.

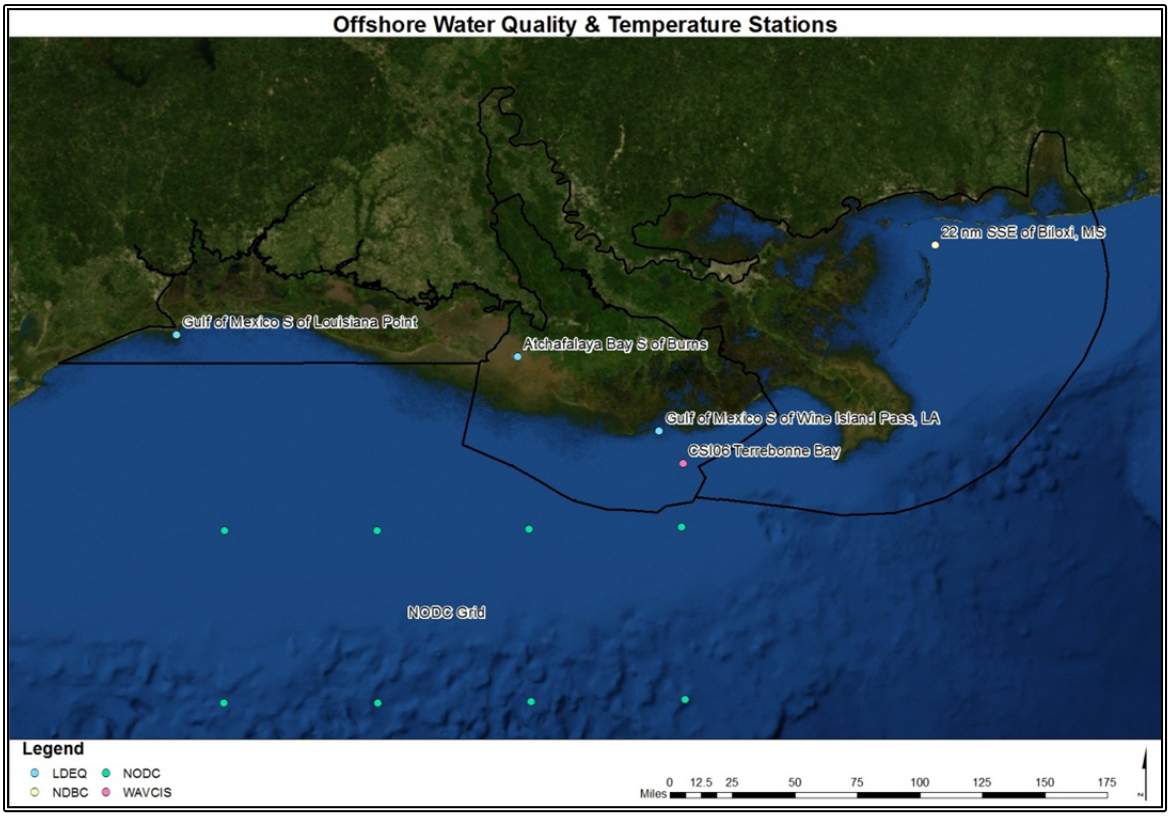

Figure 27 Offshore Water Quality and Temperature Boundary Stations for the Eco-Hydrology Models

In the PB model, the water temperature boundary condition for the offshore nodes was estimated using the 14-day correlation from Roblin (2008) (**Figure 17**). The air temperature inputs for the correlation were based on mean monthly air temperature calculations from the National Data Buoy Center (NDBC) Station 42007 (LLNR 345) climatic summary table[28]. This station was used because of its continuous record during the simulation period and because of its proximity to the PB domain (**Figure 27**). Water quality parameters were specified at the boundary nodes based on estimates from various research publications on the Gulf of Mexico dead zone. **Table 72** in Attachment A lists these PB offshore boundary values assigned for TSS, NO3, NH4, TON, and TPH. Additionally, the AGE was set to zero for these boundary nodes. All offshore boundary nodes had a default concentration of 0.03 mg/L for ALG and 1.0 mg/L for DET, with the exception of PB105, which had a DET concentration of 1.5 mg/L.

For the AA model, data stored in the National Oceanographic Data Center (NODC) were retrieved from the World Ocean Atlas using the WOA select tool[29] for the offshore boundary. The following data grid was chosen in the Gulf of Mexico: 90.5° to 93.5° west longitude and 27.5° to 28.5° north latitude. The data in this grid were retrieved in the comma separated value (CSV) file format. Only data for TMP, NO3, and SPH were available. The temperature data were monthly averages for the period of record, and the nutrients were seasonally averaged for the

[28] http://www.ndbc.noaa.gov/data/climatic/42007.txt
[29] http://www.nodc.noaa.gov/OC5/SELECT/woaselect/woaselect.html

period of record. After the data files were retrieved, surface values were averaged spatially for the region. The final processed data used for the AA model offshore boundary condition are shown in Table 73 in Attachment A. However, a constant value of 0.054 mg/L, the highest observed value, was used for the seaward boundary concentration for SPH, because it was difficult to maintain enough SPH in the model near the coast. Also, AGE was set to zero along the offshore boundary.

The WAVCIS had one offshore Gulf station (Terrebonne Bay) with chlorophyll-a (ALG) data. These data were for July of the years 1999 through 2007. The average of these data, 0.75 µg/L, was applied along the AA offshore boundary.

Data from the LDEQ station 0962 located at Wine Island Pass was used to obtain the AA offshore boundary estimates for NH4, DON, and DOP. DON was estimated from other measured variables and stoichiometry. The offshore boundary values that were applied are 0.0, 0.33, and 0.0 mg/L for NH4, DON, and DOP, respectively. It was assumed that DET and TSS are zero along the offshore boundary. All offshore boundary water quality concentrations were applied uniformly along the coastal AA boundary compartments and were constant in time (i.e. they were not computed in the model simulations).

For the CP model, LDEQ stations 1170 (Gulf of Mexico S of Louisiana Point) and 1204 (Atchafalaya Bay S of Burns, LA) were used to define the offshore water quality boundary (**Figure 27**). In order to account for the Atchafalaya River plume that swings westward along the CP coast, linear interpolation was performed between these two stations and was applied to the offshore nodes. TSS, TMP, and ALG concentrations were set to the same values as AA for the offshore boundary. None of the measured data contained continuous daily records. Therefore, long-term monthly averages were estimated. The final processed monthly averages used for the CP model offshore boundary condition are shown in **Table 74** in Attachment A. For each constituent, the averaged concentrations were assigned to the first and last day of the corresponding month. This created a step-wise concentration boundary condition for an average year which was then repeated to create the full 25-year dataset. Also, AGE was set to zero along the offshore boundary.

Wastewater

In the PB model, the wastewater from the New Orleans Metropolitan Area is pumped to the Mississippi River. Several wastewater treatment plants (WWTP) were identified in the AA and CP model domains that were thought to provide additional nitrogen and phosphorus loads to each of the regions. In order to efficiently model the hydrodynamic and ecological processes occurring in the model domains, measured discharge and water quality values needed to be applied as boundary conditions. Below is a brief description of each of these boundary conditions.

Discharge

The wastewater discharges for the PB model were estimated from McCorquodale et al., 2001. Wastewater discharge data were obtained from the following WWTP's in the AA model: Morgan City WWTP, Thibodaux WWTP, and Houma North and South WWTP's. The annual mean discharge for each of these plants is shown in **Table 75** in Attachment A.

In the CP model, wastewater discharges were estimated for residential areas along Calcasieu River (Lake Charles[30] and Sulphur[31], LA), Neches River (Beaumont[32], TX), and Sabine Lake (Port Neches[33], Groves[34], and Port Arthur[35], TX). These discharges were estimated from the average daily residential discharge per capita presented by Metcalf and Eddy (1972), 0.28 m^3/c/day, and the population of each city (Wikipedia). **Table 75** in Attachment A shows the populations and wastewater discharges for the CP model.

Water Quality

In the PB region, there are high nutrient levels in the stormwater that enters Lake Pontchartrain from the Mississippi River. The concentrations of NO3 and TPH have been measured at the drainage canals flowing from the River (McCorquodale et al., 2001) and were used for these inputs. The nutrient concentrations for the water quality loadings in the AA and CP models were based on values from Thomann and Mueller (1987). These nutrient concentrations are shown in **Table 75** in Attachment A and were considered constant in time.

Runoff

All regions included runoff loadings in their models. Runoff loadings flowing into the GIWW from the north where no compartments were present were included in the CP model during calibration in order to calibrate the water quality constituents. However, it was determined that the loadings had very little effect on the concentrations (± 10^{-4} g/m^3), and they were therefore, removed from the model. In order to efficiently model the hydrodynamic and ecological processes occurring in the PB and AA model domains, measured discharge, water quality, and temperature values needed to be applied as boundary conditions. Below is a brief description of each of these boundary conditions.

Discharge

In the PB model, discharge for runoff loadings was calculated on a daily basis from water balance equations (rainfall minus evapotranspiration). In the AA model, discharge for runoff loadings was calculated as the drainage area multiplied by the net precipitation, where the net precipitation is the precipitation minus the evapotranspiration. If the precipitation was less than the evapotranspiration then the net precipitation was set to zero. In the CP model, discharge for runoff loadings was incorporated by a proration of the Calcasieu and Mermentau Rivers based on the drainage area and net precipitation.

Water Quality & Temperature

In the PB model, input representing local agricultural runoff was assumed to have the same nutrient concentrations, temperatures, and salinities as that of the nearest tributary. If the local drainage area was not adjacent to a measured tributary, a default value of 0.36 mg/L was applied as a NO3 concentration, which was determined by Roblin (2008) from observations in the drainage tributaries of the Pontchartrain Estuary. Additional NO3 loads (kg/d) were defined for specific compartments to account for urban stormwater build-up (**Figure 28**). All other

[30] http://en.wikipedia.org/wiki/Lake_Charles,_Louisiana
[31] http://en.wikipedia.org/wiki/Sulphur,_Louisiana
[32] http://en.wikipedia.org/wiki/Beaumont,_Texas
[33] http://en.wikipedia.org/wiki/Port_Neches
[34] http://en.wikipedia.org/wiki/Groves,_Texas
[35] http://en.wikipedia.org/wiki/Port_Arthur,_Texas

compartments had an initial urban stormwater input value of zero. These specified values shown in **Table 76** in Attachment A were established through calibration with LDEQ and USGS stations. Additionally, the stormwater loading from Jefferson and Orleans Parishes were included in the tributary load inputs.

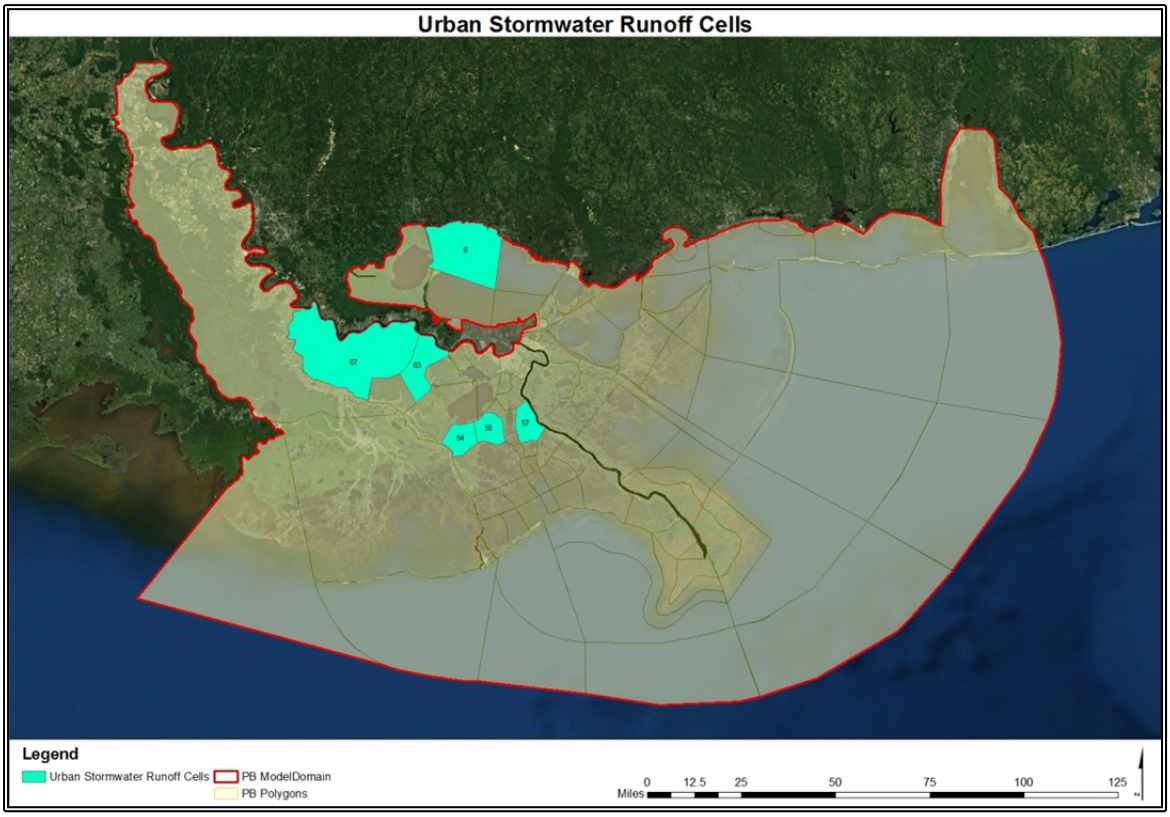

Figure 28 Urban Stormwater Runoff Compartments

For the AA model, water quality concentration data from CP tributaries originating mostly in Louisiana were averaged together to develop local runoff loading estimates. These tributaries included the Vermilion River at Perry, Mermentau River at Mermentau, Bayou Lacassine at Lake Arthur, Charenton Canal at Baldwin, Sabine River at Toomey, and Bayou Blue at North Bend and GIWW (LDEQ 1209) (**Figure 15** for tributary station locations). The spatial averages of NO3, NH4, DON, DIP, DOP, ALG, DET, and TSS were averaged monthly to develop the local runoff concentrations of the AA model. These monthly averages are shown in **Table 77** in Attachment A and were repeated for each year of the simulations. The concentrations were multiplied by the local runoff flows mentioned above to provide the local runoff loadings. The daily TMP records (developed using the sine curve fit mentioned earlier) of each of the CP tributaries mentioned previously were averaged spatially to create an average daily TMP estimate for the local runoff.

Initial Conditions

The initial conditions of the model were determined based on the best temporal and spatial data available. For the PB model, a ramp-up of 1 day was used in the simulations to assimilate to acceptable values for initial conditions. For the AA model, the initial conditions for all parameters were set to zero, thus the first month of the simulation acted as a spin-up period.

For the CP region, a model spin-up was used for determining initial conditions, where values were set to zero and were run for a month. Then the resulting month was averaged (except for the first day) to acquire a new initial value. The required initial conditions for each compartment included the values for TSS, NO3, NH4, DON, DOP, SPH, DET, ALG, SAL, STG, and AGE.

Structure Schedules

Locks and control structures were modeled using the open and closed schedules recorded by the United States Army Corps of Engineers Team New Orleans[36]. These lock and control structure schedules provided the number of hours open and closed each day for the locks. Structures without recorded schedules were given a documented, assumed schedule.

System Parameters

In the PB model, a central difference/upwinding calibration factor was used for the advection terms to determine the weighting between each solution method where 1.0 represented pure upwinding and 0.5 represented pure central differencing. A factor of 0.5001 was used in all calibrations, validations, and simulations. Therefore, the PB model was essentially a second order accurate central difference model. The AA and CP models used upwinding for the advection terms. Therefore, no additional weighting factors were required to run those models. The Euler Method was used as the time integration method for all three models.

The computational time step for the PB model was 60 seconds while the time step for the AA and CP models was 0.0005 days (43.2 seconds). The model outputs were post-processed to provide monthly averages except for stage where the output was daily. The metric system was adopted for the units, and the acceleration due to gravity was set to 9.81 m/s^2.

For the project group simulations, the models started on January 1, 2010 and were run for 25 years (including leap years) ending on December 31, 2034 for year-set 1. For the second year-set, the models started on January 1, 2035 and were run for 25 years (including leap years) ending on December 31, 2059.

For numerical stability during the wetting and drying process, the CP model required specifying wet and dry depths. The dry and wet depths were numerical flags to declare a location (compartment) to be fully dry or wet. To avoid a division by zero, water depths were not allowed (numerically) to reach an exact zero. Further explanation is given on the use of these depths in Section 2.a.

e. Description of Output Data

As mentioned in Section 1.a., the output of the Eco-Hydrology models was used as input for several other models. These models included Wetland Morphology, Barrier Shoreline Morphology, Vegetation, and Ecosystem Services.

Table 8 presents the Eco-Hydrology output data that were used by these models. The table also includes the abbreviation, or symbol, used to represent each parameter, as well as the units and frequency of the data.

[36] http://www.mvn.usace.army.mil/od/lockupdates/mermentaubasin/displayindex.asp

Table 8 Eco-Hydrology Output Parameters

Parameter	Symbol	Units	Frequency
Stage	STG	m (NAVD88)	Daily
Sediment Retention (Total Suspended Solids)	TSS	mg/L	Monthly
Accretion (from Inorganic TSS)	ACC	$g/m^2/yr$	Yearly
Salinity	SAL	ppt	Monthly
Tidal Range	TRG	m (NAVD88)	Monthly
Total Kjeldahl Nitrogen	TKN	mg/L	Monthly
Water Temperature	TMP	°C	Monthly
Nitrate + Nitrite Nitrogen	NO3	mg/L	Monthly
Ammonium Nitrogen	NH4	mg/L	Monthly
Dissolved Organic Nitrogen	DON	mg/L	Monthly
Total Phosphorus	TPH	mg/L	Monthly
Soluble Phosphorus	SPH	mg/L	Monthly
Phytoplankton as Chlorophyll-a	ALG	$\mu g/L$	Monthly
Detritus	DET	mg/L	Monthly
Water Age	AGE	days	Monthly
Nitrogen Removal (Denitrification)	NRM	$g/m^2/yr$	Yearly
Compartment Configuration Shapefile	SHP	-	-

The models calculated a value in each compartment for all of the output parameters at every computational time step. Due to the number of compartments and the size of the computational time steps, the outputs would have become very large and would not be able to be executed by the programs. As a result, the model output frequency was set to one day. Also, the nature of the difference equations provided accumulated outputs for each of the parameters. Therefore, after each time step, the models were programmed to calculate the daily average for each parameter, excluding ACC and NRM which were accumulations and should not be averaged.

Even with the outputs averaged on a daily basis, they were still quite large because the simulations were large. For instance, a 25-year simulation corresponded to approximately 9,131 days. That time period, combined with the number of compartments in each of the Eco-Hydrology models, created a very large output file. As a result, the outputs were post-processed at a specific frequency to reduce the number of results. A daily frequency corresponded to the output of the model without post-processing, and it was only used for STG. A monthly frequency corresponded to the average of the values in a given month. A yearly frequency was used for the accumulated parameters, ACC and NRM, and it corresponded to a value at the end of each year with respect to the start of the model.

The output from Madonna is a text file which was processed into a tab delimited file. The header of the first column of the tab delimited file indicated the frequency of the data in the file (i.e. “MONTH” for monthly). The numbers in the first column represented a monotonic increase based on the frequency (i.e. “1” for the first month, “2” for the second month, etc.). The first row contained an alpha-numeric code indicating the model region and compartment number

(i.e. AA008 for Atchafalaya Basin compartment number 8, CP135 for Chenier Plain compartment number 135, etc.) for the data in each column.

One type of output that was not actually a result of the models was a shapefile. A shapefile is an ArcGIS file that provides compartment delineation data. Shapefiles for all three models were provided for each group of project runs.

Combining the attributes of the shapefiles with the model output, spatial maps of the models output were created using the Louisiana Applied Coastal Engineering and Science (LACES) Data Converter and EverVIEW (a USGS software). **Figure 29** and **Figure 30**).

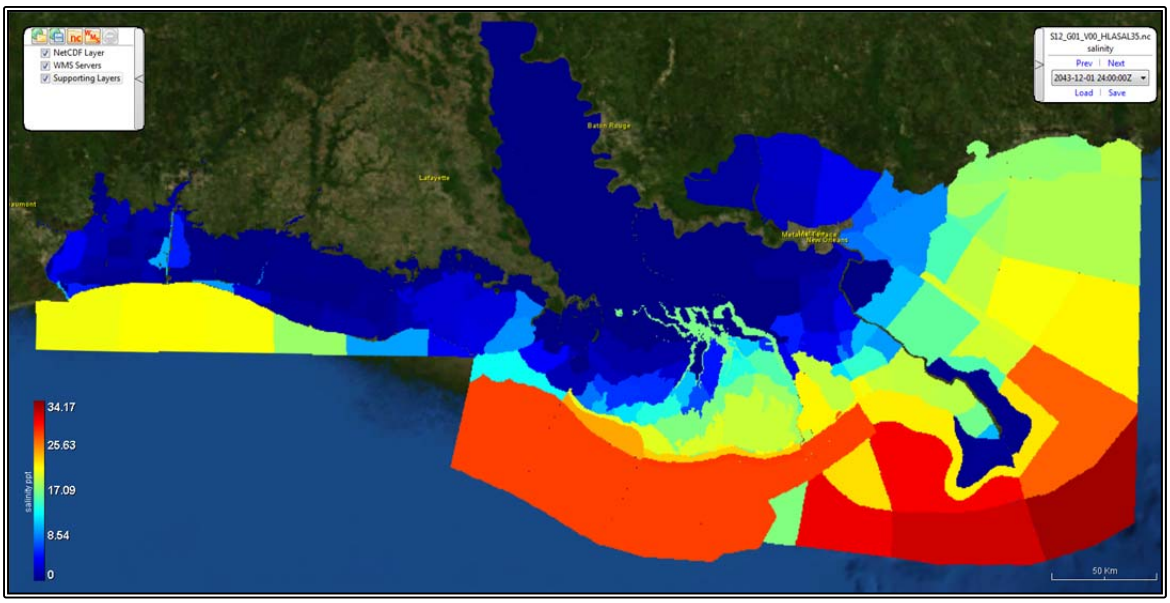

Figure 29 Sample EverVIEW Spatial Map of Salinity

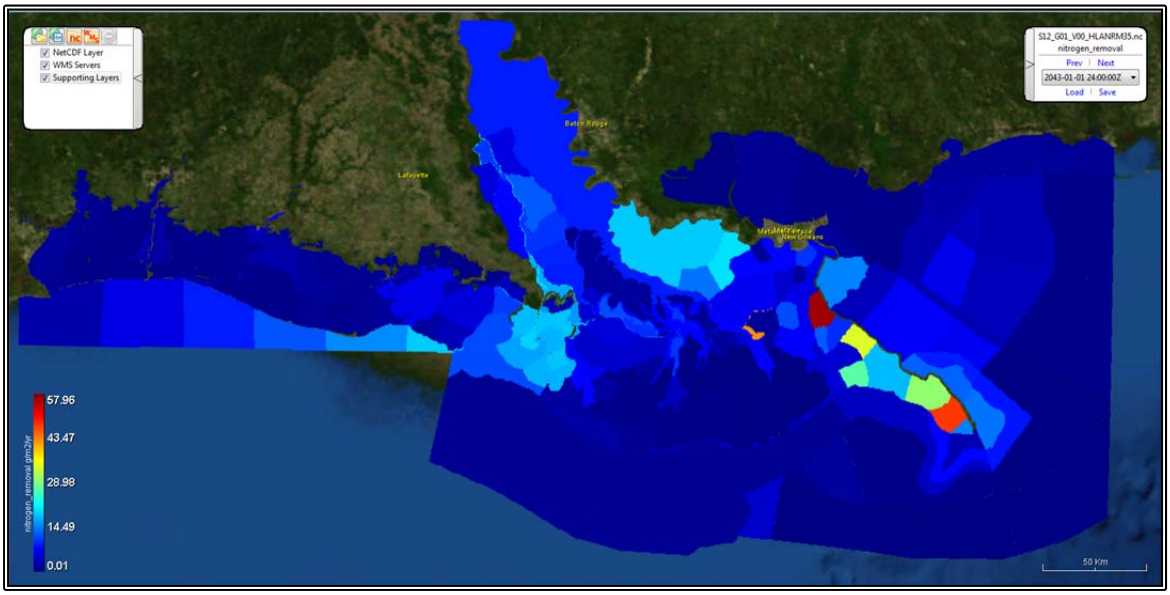

Figure 30 Sample EverVIEW Spatial Map of NRM

f. Statement on the Capabilities and Limitations of the Model

Model Capabilities

The Eco-Hydrology models are capable of simulating long-term hydrodynamic and water quality processes, where the maximum simulation period was 25 years. They can also cover large spatial domains, e.g. the entire Louisiana coast. The models can simulate complex systems such as the nutrient cycles of nitrogen and phosphorus, which involve multiple chemical processes occurring simultaneously. The models provide an estimate of average daily water surface elevations, salinity, total suspended solids, and several other water quality constituent concentrations, as well as accumulated accretion (i.e. sediment accumulation; actual wetland accretion is calculated in the Wetland Morphology model) values at the resolution of the compartment design.

Model Limitations

The Fortran and Madonna models' performances are mainly limited by the adequacy of the boundary conditions and the physical processes incorporated into the formulations. Several observation stations are missing continuous data and most stations only provide discrete measurements once a month. As a result, approximations and regression relationships are created to fill in these gaps of data. Also, due to the lack of data in certain locations, nearby stations are used to create boundaries and sometimes a single station is used to represent the entire offshore boundary. The main issues with using approximated data are that the natural irregularities of the area will not be adequately represented in the model and the relationships between neighboring areas may not be fully understood and thus applied incorrectly.

The nature of the mass-balance compartment models is that they are dimensionless, and are therefore, limited from simulating the horizontal flow patterns or vertical mixing patterns normally found in water bodies. As a result, the water quality in all of the models is very primitive since there is no explicit benthic compartment. The benthic reactions, e.g. denitrification, are approximated using a calibrated denitrification rate. However, nitrogen uptake potential in the water, sediment, and vegetation is considered in the Nitrogen Uptake Potential model. Similarly there is neither a complete marsh water quality model nor a complete sediment accumulation/accretion model. For example, the sediment accretion formulations do not account for grain size, which is important for determining the settling ability of the suspended solids. There is also no accountability in the PB and CP models once the sediment gets deposited onto the bed. It should be noted that in the AA model the elevation change caused by deposited sediments is being accounted for in order to restrict the future deposition amount to prevent building a mountain of sediment.

The models are limited to an output resolution of the compartment design. However, it should be realized that finer or smaller compartments force a smaller computational time step to maintain numerical stability. Since the run time is a critical factor in this effort, a balance is found to optimize both of these indirectly related criteria for each model. In the PB model, a 25-year simulation takes approximately an hour to an hour and a half to compute in Fortran, whereas, the Madonna codes of the AA and CP models take approximately ten hours to compute a 25-year simulation. The disparity in the run time is directly related to the platform used to perform the calculations. Fortran is more efficient computationally, but it requires high level of technical knowledge. Madonna on the other hand is much more user friendly despite

the fact that it computationally more demanding. In the future, the intent is to unify the platform used in all regions. However, due to time limitations for this analysis, we used the PB Fortran platform as is since it was already setup and calibrated.

In the PB model only, stage can be aggregated hourly for tides and storm surges but not for wind shear effects. Typically, salinity and nutrients should not be aggregated at less than a weekly level. One of the simplifications in the PB model is that wind stresses on the open water compartments are neglected. For long-term mean responses, this is not a serious problem but it does limit the simulation of wind related fluctuations in stage, i.e. wind setup in Lake Pontchartrain.

The Fortran and Madonna models generate output on the order of seconds. However, the codes are written to provide mean daily values due to the limitations of the models and the reliability of the results and the requirements of the subsequent master plan modeling teams, e.g. Wetland Morphology and Vegetation.

Despite these limitations, the Eco-Hydrology modeling team feels that the current models will provide a good assessment of relative project effects on the ecosystem hydrology, where these models are primarily intended to be used as planning-level screening tools for the ranking of proposed projects.

g. Description of Model Development Process including Documentation on Testing Conducted (Alpha and Beta Tests)

Since the PB model separated the areas inside each compartment into upland, marsh, and open water, the PB model setup differed slightly from the AA and CP models. Compartment areas were defined based on knowledge of drainage area boundaries and the presence of hydraulic blockages or barriers (e.g. levees, elevated highways, etc.). Compartment geometric inputs included the surface area (estimated through Google Earth Pro®), open water hydrologically connected area (estimated through Google Earth Pro®), and percent open water of each compartment. The depth of open water was estimated from a study by Georgiou et al. (2010) in which the ADCIRC Storm Surge Bathymetry was corrected for updated field data collected by UNO as well as NOAA maps. Additionally, each compartment had a defined flood fraction and elevation for marsh areas. All open water compartments exchanged flow, sediment, and nutrients via links with the surrounding compartments. These links were based on the actual channels, passes, and canals in the system. The links were depicted as rectangular channels with a defined roughness coefficient, width, and depth, as well as minor loss and diffusion coefficients. The PB model consisted of 89 open water/marsh/upland compartments, 7 offshore nodes, and 183 links.

The AA and CP model area delineations originated from the Louisiana Coastal Area Polygons modified by USGS. Alterations were made to the USGS delineation in terms of the hydraulic conditions associated with the system:

- The rivers and canals within the AA and CP systems were depicted as channel compartments. These channel compartments were defined as volumetric compartments, where the AA model assumed the channels were rectangular in cross-section due to a lack in available bathymetric data. The CP model used depth-storage curves where bathymetric data (cross-sections) were available to incorporate higher accuracy in channel water levels and stages.
- Compartments were further delineated based on the presence of structural hydraulic blockages (e.g. levees, elevated highways, etc.).
- Further modification was made based on land cover, where there were clear changes in vegetation type.

The AA model consisted of 73 channel compartments, 21 open water compartments, 67 marsh compartments, 4 offshore compartments, and 291 links. The CP model consisted of 28 channel compartments, 19 open water compartments, 102 marsh compartments, 6 offshore nodes, and 388 links. These numbers correspond to the compartment configurations used for most of the project simulations. For example, compartments were added as needed to better capture the effects of a certain project.

After the compartment layout was set up, the linkage between compartments was defined. The links between compartments were connected from:

- Centroid to centroid between marsh/open water compartments
- Midpoint to midpoint between channel compartments
- Midpoint to centroid between channel compartments and marsh/open water compartments

The geometry for the AA and CP compartments included surface area, average bottom elevation, and average roughness coefficient. The geometry for the links included average width and the connection length extending into each of the two exchanging compartments. All of these attributes were calculated with the help of ArcGIS. Since the link width, which was calculated by ArcGIS, was the common boundary between two compartments and was not necessarily the hydraulically connected width, the width for each link was adjusted based on measured cross-sections, elevation data, aerial data, and engineering judgment.

The PB model code was developed in Fortran (McCorquodale et al., 2009; Roblin, 2008). The model code had been modified over the years and was used as a basis for developing the AA and CP models in Berkeley Madonna. Internal compartment concentrations and properties were computed from the boundary conditions based on a hybrid upwinding and central differencing numerical integration scheme which was used to solve the advective transport of salinity, suspended sediment, and chemical equations in the PB model. The UPWIND scheme was used to compute concentrations and properties in the AA and CP models. The dynamics of the PB model are displayed in **Figures 3a** and **3b,** while **Figures 4a** and **4b** show the dynamics of the AA and CP models. **Figures 3** and **4** provide a graphical representation of how the compartments interacted with each other, as well as with the various boundaries.

Calibration/validation was achieved for each region by adjusting flow parameters, reaction parameters, and boundary conditions. The PB model was calibrated and validated to measured data from the years of 1990 – 2009. The AA model was calibrated using observed field values for the calendar year of 2007. It was then validated with observed field values for the calendar years of 2008 and 2009. The CP model was calibrated using observed field values for the calendar year of 2007. It was then validated with observed field values for the calendar year of 2010. It should be noted that several observation stations across the Louisiana coast only provided discrete measurements with large gaps as opposed to consistent daily values. As a result, the years chosen for calibration and validation were based on the availability of data and estimates were made to fill the missing data using standard techniques. More detailed descriptions of the filling methods are presented in the "Boundary Condition" Section above (1.d.). Also, the stations and parameters used for the calibrations and validations in each region are presented in tables in Attachment A. (**Table 78** for the PB model, **Table 79** for the AA model, and **Table 80** for the CP model). Attachment B presents the plots of the calibrations and validations with the appropriate years used for each modeled parameter and constituent.

Once the models were calibrated and validated based on the best available data, they were used to analyze the various proposed projects designated by CPRA. The projects were organized by region and assembled into groups. Creating these project groups reduced the total number of simulations that were needed, as opposed to simulating them individually. Care was taken by CPRA to only combine projects in a group that were assumed to be independent of each other with respect to potential outcomes. The various types of proposed projects included hydrologic restoration, shoreline protection, marsh creation, ridge restoration, oyster reef development, diversions, bank stabilization, barrier island/headland restoration, channel re-alignment, and complex. The complex type refers to any combination of the other project types. Once the 50 years were modeled, CPRA then compared the impacts of each of the project Groups against a 50-year future without action (FWOA). It should be noted that several of the project groups were designated for only one region; therefore, the group numbers skipped around between

regions. The following section describes how each of the projects was incorporated into each model.

Pontchartrain and Barataria Basins

All flow distributions of the Mississippi River were determined using a HEC-RAS model (Davis, 2010). Unless otherwise specified, it was assumed that the Old River Control Structure maintained its existing operation with 70% to the Mississippi River and 30% to the Atchafalaya River.

Group 1 – Future without Action (FWOA)

Projects that are constructed or have received construction funding were included in this group. The MRGO was closed for the FWOA, but was open for the calibration runs since the MRGO was open for the Pontchartrain calibration/validation years. West Bay was closed for Groups 1 – 49, but was open for calibration.

Table 81 in Attachment A provides the properties specified for each link in Group 1. For projects in Groups 2-49, if link properties were varied from that of Group 1, a table is provided listing the links changed and the modified properties of those links. In these tables, *Link ID* represents the PB link number, *U/S Compartment* describes the upstream compartment number, *D/S Compartment* describes the downstream compartment number, *Depth* represents the link depth in meters, *Length* represents the link length in meters, *Width* represents the mean link width in meters, *Manning's n* represents the link's Manning's *n* value, K_m represents the minor loss coefficient in the link due to structures, K_{en} represents the entrance loss coefficient in the link, K_{ex} represents the exit loss coefficient in the link, and E_{xy} (m^2/s) represents the diffusion coefficient through the link. Links were adjusted to maintain a stage less than that of the Mississippi River and to reach a velocity near 4 ft/s. The exception to this rule was the storm surge stage which could exceed the neighboring River stage. The Manning's *n* and E_{xy} values were derived by calibration. It should be noted that a Manning's *n* value of 999 or higher represents a blocked link.

Group 2

001.HR.01 – Amite River Diversion Canal Hydrologic Restoration

Amite River Diversion Canal Hydrologic Restoration was modeled by increasing the percent marsh in PB007 by 20% (or from 68.69% to 82.06%) to account for marsh flooding. No changes were made to the links because connecting links already had adequate capacity.

002.RC.01 – Bayou Long Ridge Restoration

The Manning's *n* roughness factor in link 75 was increased by a factor of 10 to simulate the ridge restoration and thereby limit the exchange between PB039 and PB040 (**Table 9**).

Table 9 Changes to Links in Group 2 to Implement 002.RC.01

Link ID	Manning's *n*
75	0.205

002.RC.03 – Bayou Grand Chenier Ridge Restoration

This project does not affect the links in the model. Therefore, it was not modeled by the Eco-Hydrology team. It was included in the Wetland Morphology model as a landscape feature.

Group 3

001.DI.25 – Benney's Bay Diversion (20,000 cfs)

Outflow from the 20,000 cfs Benney's Bay Diversion (River Mile (RM) 7) was placed entirely in PB088. The links were adequately sized, and therefore were not adjusted.

Group 4

001.DI.04 – Lower Breton Diversion (250,000 cfs)

PB012, PB015, PB030, and PB088 were given 50%, 25%, 12.5%, and 12.5% of the 250,000 cfs Lower Breton Diversion outflow, respectively. Link 42 was adjusted as per **Table 10** to allow for increased flow. This distribution was intended to represent the distributary system that would develop as the sedimentation occured.

Table 10 Changes to Links in Group 4 to Implement 001.DI.04

Link ID	Manning's *n*
42	0.03

002.DI.05 – Northwest Barataria Diversion (5,000 cfs)

Outflow from the 5,000 cfs Northwest Barataria Diversion (RM 157) was placed entirely in PB067. The links were adequately sized, and therefore were not adjusted.

Group 5

002.HR.02 – Bayou Rigolettes Hydrologic Restoration

Link 97 was adjusted as per **Table 11** to produce results according to project specifications. The reduction in width and depth of this link simulated the construction of sheet pile walls with boat bays and thereby restricted tidal flow.

Table 11 Changes to Links in Group 5 to Implement 002.HR.02

Link ID	Depth (m)	Width (m)
97	3.6	167.64

Group 6

002.RC.02 – Spanish Pass Ridge Restoration

This project does not affect the links in the model. Therefore, it was not modeled by the Eco-Hydrology team. It was included in the Wetland Morphology model as a landscape feature.

Group 7

001.OR.01 – Biloxi Marsh Oyster Barrier Reef

This project does not affect the links in the model. Therefore, it was not modeled by the Eco-Hydrology team. It was included in the Wetland Morphology model as a landscape feature.

002.CO.01 – Grand Liard Marsh/Ridge Restoration

This project was implemented using DEM changes provided by the Wetland Morphology team.

Group 8

001.RC.01 – Bayou LaLoutré Ridge Restoration

This project does not affect the links in the model. Therefore, it was not modeled by the Eco-Hydrology team. It was included in the Wetland Morphology model as a landscape feature.

Group 9

001.DI.22 – East Maurepas Diversion (25,000 cfs)

Outflow from the 25,000 cfs East Maurepas Diversion was placed entirely in PB007. The links were adequately sized, and therefore were not adjusted.

002.DI.04 – Mid-Barataria Diversion (250,000 cfs)

PB047, PB057, PB051, PB053, PB046, PB050, and PB045 were given 25%, 10%, 10%, 10%, 25%, 10%, and 10% of the 250,000 cfs Mid-Barataria Diversion outflow, respectively. Links were adjusted as per **Table 12** to allow for increased flow.

Table 12 Changes to Links in Group 9 to Implement 002.DI.04

Link ID	Depth (m)	Width (m)	Manning's *n*
92	2.0	3000	
93	2.0	4000	
94	3.0		
99	3.0		
102	2.0		
106	2.5	2000	0.03
107	3.0	2000	0.03

Group 10

001.DI.20 – Central Wetlands Diversion

PB001, PB002, PB008, PB073, and PB075 were given 30%, 30%, 15%, 15%, and 10% of the 250,000 cfs Central Wetlands diversion (RM 85) outflow, respectively. Links were adjusted as per **Table 13** to allow for increased flow. Preliminary model runs indicated significant impacts

from excessive water impoundment; therefore, the project was eliminated from further consideration. Diversions at this same location but with lower flow regimes were modeled in other groups.

Table 13 Changes to Links in Group 10 to Implement 001.DI.20

Link ID	Depth (m)	Width (m)	Manning's *n*
13		1000	
135	2.25	1000	0.05
145	6.0	1700	0.02

002.DI.02 – Mid-Barataria Diversion (5,000 cfs)

Outflow from the 5,000 cfs Mid-Barataria Diversion (RM 59) was placed entirely in PB057. The links were adequately sized, and therefore were not adjusted.

Group 11

001.DI.15 – Upper-Breton Diversion (50,000 cfs)

Outflow from the 50,000 cfs Upper-Breton Diversion was placed entirely in PB011. Links were adjusted as per Table 14 to allow for increased flow.

Table 14 Changes to Links in Group 11 to Implement 001.DI.15

Link ID	Depth (m)	Width (m)	Manning's n
41	2.0	6000	0.03
140	2.0	6000	0.03

002.DI.03 – Mid-Barataria Diversion (50,000 cfs)

PB057, PB051, and PB053 were given 50%, 25%, and 25% of the 50,000 cfs Mid-Barataria Diversion outflow, respectively. Links were adjusted as per **Table 15** to allow for increased flow.

Table 15 Changes to Links in Group 11 to Implement 002.DI.03

Link ID	Depth (m)	Width (m)	Manning's *n*
107	3.0	600	0.03

Group 12

001.DI.29 – West Maurepas Diversion (5,000 cfs)

The West Maurepas Diversion flow extraction (assumed 5,000 cfs at RM 161) was placed entirely in PB007. The links were adequately sized, and therefore were not adjusted.

002.DI.07 – West Point a la Hache Diversion (50,000 cfs)

PB047, PB046, and PB039 were given 50%, 25%, and 25% of the 50,000 cfs West Point a la Hache Diversion outflow, respectively. Links were adjusted as per **Table 16** to allow for increased flow.

Table 16 Changes to Links in Group 12 to Implement 002.DI.07

Link ID	Depth (m)	Width (m)
85	4.0	500
89	4.0	500

Group 13

001.DI.24 – Mid-Breton Sound Diversion (50,000 cfs)

PB012 and PB079 each were given 50% of the 50,000 cfs Mid-Breton Sound Diversion outflow (RM 59). Links were adjusted as per **Table 17** to allow for increased flow.

Table 17 Changes to Links in Group 13 to Implement 001.DI.24

Link ID	Depth (m)	Width (m)
140	1.5	23000

002.DI.18 – Hermitage Diversion (5,000 cfs)

Outflow from the 5,000 cfs Hermitage Diversion (RM 55) was placed entirely in PB051. The links were adequately sized, and therefore were not adjusted.

Group 14

001.DI.19 – Central Wetlands Diversion (50,000 cfs)

PB075, PB002, and PB001 were given 50%, 25%, and 25% of the 50,000 cfs Central Wetlands Diversion (RM 85) outflow, respectively. The links were adequately sized, and therefore were not adjusted.

002.DI.15 – Lower Barataria Diversion (50,000 cfs)

Outflow from the 50,000 cfs Lower Barataria Diversion (RM 30) was placed entirely in PB039. The links were adequately sized, and therefore were not adjusted.

Group 15

001.DI.09 – Bayou Lamoque Diversion (4,500 cfs)

Outflow from the 4,500 cfs Bayou Lamoque Diversion (RM 33) was placed entirely in PB012. The links were adequately sized, and therefore were not adjusted. This project was removed from further consideration following project-level evaluation.

001.DI.21 – East Maurepas Diversion (5,000 cfs)

Outflow from the 5,000 cfs East Maurepas Diversion (RM 136) was placed entirely in PB007. The links were adequately sized, and therefore were not adjusted.

002.DI.06 – West Point a la Hache Diversion (5,000 cfs)

Outflow from the 5,000 cfs West Point a la Hache Diversion (RM 49) was placed entirely in PB047. The links were adequately sized, and therefore were not adjusted.

Group 16

001.DI.05 – Bonnet Carré Diversion (5,000 cfs)

The Bonnet Carré Diversion flow input was adjusted to increase the base Bonnet Carré flow by a constant 141.58 m^3/s (5,000 cfs). The links were adequately sized, and therefore were not adjusted.

002.DI.09 – West Point a la Hache Diversion (250,000 cfs)

PB047, PB046, PB038, and PB039 were given 20%, 30%, 20%, and 30% of the 250,000 cfs West Point a la Hache Diversion outflow, respectively. Links were adjusted as per **Table 18** to allow for increased flow.

Table 18 Changes to Links in Group 16 to Implement 002.DI.09

Link ID	Depth (m)	Width (m)
85	2.0	1000
89	2.0	2600

Group 17

001.DI.14 – Upper Breton Diversion (5,000 cfs)

Outflow from the 5,000 cfs Upper-Breton Diversion was placed entirely in PB011. The links were adequately sized, and therefore were not adjusted.

002.DI.16 – Lower Barataria Diversion (250,000 cfs)

PB040, PB039, and PB031 were given 25%, 50%, and 25% of the 250,000 cfs Lower Barataria Diversion (RM 30) outflow, respectively. The links were adequately sized, and therefore were not adjusted.

Group 18

001.DI.02 – Lower Breton Diversion (50,000 cfs)

PB012, PB030, PB088, and PB015 were given 50%, 12.5%, 12.5%, and 25% of the 50,000 cfs Lower Breton Diversion outflow, respectively. The links were adequately sized, and therefore were not adjusted.

002.DI.17 – Hahnville Diversion (5,000 cfs)

Outflow from the 5,000 cfs Hahnville Diversion (RM 127.2) was placed entirely in PB063. The links were adequately sized, and therefore were not adjusted.

Group 19

001.DI.01 – Lower Breton Diversion (5,000 cfs)

Outflow from the 5,000 cfs Lower Breton Diversion (RM 46.9) was placed entirely in PB012. The links were adequately sized, and therefore were not adjusted.

002.DI.14 – Lower Barataria Diversion (5,000 cfs)

Outflow from the 5,000 cfs Lower Barataria Diversion (RM 30.1) was placed entirely in PB039. The links were adequately sized, and therefore were not adjusted.

Group 20

001.DI.17 – Upper Breton Diversion (250,000 cfs)

PB011 and PB079 were given 60% and 40% of the 250,000 cfs Upper Breton Diversion outflow, respectively. Link 140 was adjusted and Link 184 was added as per **Table 19** to allow for increased flow.

Table 19 Changes to Links in Group 20 to Implement 001.DI.17

Link ID	U/S Compart-ment	D/S Compart-ment	Depth (m)	Length (m)	Width (m)	Manning's *n*	K_m	K_{en}	K_{ex}	E_{xy} (m^2/s)
140			2.0		23000	0.035				
184	11	79	3.0	10000	23000	0.025	0	0.02	0.25	12.551

Group 21

001.DI.23 – Mid-Breton Sound Diversion (5,000 cfs)

Outflow from the 5,000 cfs Mid-Breton Sound Diversion was placed entirely in PB079. The links were adequately sized, and therefore were not adjusted.

002.DI.08 – West Point a la Hache Diversion

PB047, PB046, PB038, and PB039 were given 20%, 30%, 20%, and 30% of the 250,000 cfs West Point a la Hache Diversion outflow, respectively. Links were adjusted as per **Table 20** to allow for increased flow. This project was modeled with a Mississippi River/Atchafalaya River flow distribution of 60/40 at the Old River Control Structure rather than the current 70/30 distribution. Additional evaluations of modifying the flow distribution at the Old River Control Structure will be included in the Mississippi River Hydrodynamic and Delta Management Study. This project was removed from further consideration following project-level evaluation.

Table 20 Changes to Links in Group 21 to Implement 002.DI.08

Link ID	Depth (m)	Width (m)
85	2.0	1000
89	2.0	2600

Group 22

001.DI.18 – Central Wetlands Diversion (5,000 cfs)

Outflow from the 5,000 cfs Central Wetlands Diversion (RM 85) was placed entirely in PB075. The links were adequately sized, and therefore were not adjusted.

001.DI.28 – East Maurepas Diversion (5,000 cfs)

Outflow from the 5,000 cfs East Maurepas Diversion (RM 142) was placed entirely in PB007. The links were adequately sized, and therefore were not adjusted. This project was removed from further consideration following project-level evaluation.

Group 23

001.DI.03 – Lower Breton Diversion (250,000 cfs)

PB012, PB015, PB030, and PB088 were given 50%, 25%, 12.5%, and 12.5% of the 250,000 cfs Lower Breton Diversion outflow, respectively. Link 42 was adjusted as per **Table 21** to allow for increased flow. This project was modeled with a Mississippi River/Atchafalaya River flow distribution of 60/40 at the Old River Control Structure rather than the current 70/30 distribution. Additional evaluations of modifying the flow distribution at the Old River Control Structure will be included in the Mississippi River Hydrodynamic and Delta Management Study. This project was removed from further consideration following project-level evaluation.

Table 21 Changes to Links in Group 23 to Implement 001.DI.03

Link ID	Manning's *n*
42	0.03

Group 24

001.DI.16 – Upper Breton Diversion (250,000 cfs)

PB011, PB012, and PB079 were. Link 140 was adjusted and Link 184 was added as per **Table 22** to allow for increased flow. This project was modeled with a Mississippi River/Atchafalaya River flow distribution of 60/40 at the Old River Control Structure rather than the current 70/30 distribution. Additional evaluations of modifying the flow distribution at the Old River Control Structure will be included in the Mississippi River Hydrodynamic and Delta Management Study. This project was removed from further consideration following project-level evaluation.

Table 22 Changes to Links in Group 24 to Implement 001.DI.16

Link ID	Compartment U/S	D/S	Depth (m)	Length (m)	Width (m)	Manning's *n*	K_m	K_{en}	K_{ex}	E_{xy} (m^2/s)
140			2.0		23000	0.035				
184	11	79	3.0	10000	23000	0.025	0	0.02	0.25	12.551

Group 25

001.DI.30 – Pontchartrain-Barataria Multi-Diversion Plan

Outflow from the 5,000 cfs Maurepas Diversion (RM 136.1) was placed entirely in PB007. Outflow from the 5,000 cfs Myrtle Grove Diversion (RM 58.4) was placed entirely in PB057. Outflow from the 5,000 cfs Northwest Barataria Diversion (RM 157.2) was placed entirely in PB067. Outflow from the 5,000 cfs Hahnville Diversion (RM 126.5) was placed entirely in PB063. Outflow from the 5,000 cfs Central Wetlands Diversion (RM 85.1) was placed entirely in PB075. Outflow from the 5,000 cfs Mid-Breton Sound Diversion (RM 59.1) was placed entirely in PB079. Outflow from the 5,000 cfs Hermitage Diversion (RM 55) was placed entirely in PB051. Outflow from the 10,000 cfs Empire Diversion (RM 30.1) was placed entirely in PB039. Outflow from the 5,000 cfs Black Bay Diversion (RM 47.2) was placed entirely in PB012. Outflow from the 10,000 cfs Venice Diversion (RM 11.1) was placed entirely in PB040. Outflow from the 5,000 cfs Caernarvon Diversion was placed entirely in PB011. Outflow from the 10,000 cfs Baptiste Collette Diversion (RM 12) was placed in PB030 and PB088 (50% each). The Bonnet Carré flow input was adjusted to increase the base Bonnet Carré flow by a constant 141.58 m^3/s (5,000 cfs). The links were adequately sized, and therefore were not adjusted.

Group 26

002.DI.19 – Hermitage Diversion (250,000 cfs Seasonally Operated)

PB047, PB051, PB046, and PB038 were given 25%, 30%, 25%, and 20% of the 250,000 cfs Hermitage Diversion (RM 55) outflow, respectively. Links were adjusted as per **Table 23** to allow for increased flow.

Table 23 Changes to Links in Group 26 to Implement 002.DI.19

Link ID	Depth (m)	Width (m)	Manning's *n*
89	2.5	500	

Link ID	Depth (m)	Width (m)	Manning's *n*
92	2.0	1000	0.025
93	2.0		
94	2.0		
126	2.0		

Group 29

03a.DI.08 – Bayou Lafourche Diversion (5,000 cfs)

Outflow from the 5,000 cfs Bayou Lafourche Diversion (RM 85) was placed in PB067 and PB071 (50% each). The links were adequately sized, and therefore were not adjusted.

Group 31

03b.DI.06 – Violet, Davis Pond, and Bayou Lafourche Diversions (100,000 cfs each)

PB067, PB062, PB058, PB055, PB048, and PB054 were given 5%, 5%, 35%, 20%, 15%, and 20% of the 100,000 cfs Bayou Lafourche Diversion (RM 175) outflow, respectively. PB068, PB064, PB058, PB059, and PB055 were given 5%, 25%, 40%, 25%, and 5% of the 100,000 cfs Davis Pond Diversion (RM 117) outflow, respectively. PB075, PB002, PB008, and PB073 were given 10%, 35%, 5%, and 50% of the 100,000 cfs MRGO/Violet Diversion (RM 85) outflow, respectively. Links were adjusted as per **Table 24** to allow for increased flow.

Table 24 Changes to Links in Group 31 to Implement 03b.DI.06

Link ID	Depth (m)	Width (m)	Manning's *n*
13		1200	
21	2.0		0.03
28			0.03
47	2.0	3000	0.03
61		2000	0.035
62		2000	
63		2000	
67	3.0	3000	0.03
70	2.0		
77	2.5	2600	
80	2.0		
82	2.0	10000	
86	3.0	3000	
90		10000	
96	3.0	2000	
97	8.0	2000	
108	10.0	1550	
109		1200	
118		1000	
119		1000	

Link ID	Depth (m)	Width (m)	Manning's *n*
120		3000	
121		1000	
122	3.0		
123	2.5	3000	
131		3000	0.03
135	2.5	1500	0.03
145		1700	
150		1200	0.035
152		1500	
153		1000	
170		1000	
171		600	

Group 34

03a.DI.01 – Bayou Lafourche Diversion (2,000 cfs)

Outflow from the 2,000 cfs Bayou Lafourche Diversion was placed in PB067 and PB071 (50% each). The links were adequately sized, and therefore were not adjusted. Since the time this project was modeled, the flow has been reduced to 1,000 cfs for future model runs.

Group 38

001.DI.26 – Benney's Bay Diversion (50,000 cfs)

Outflow from the 50,000 cfs Benney's Bay Diversion (RM 7) was placed in PB030 and PB088 (25% and 75%, respectively). The links were adequately sized, and therefore were not adjusted. This project was removed from further consideration following project-level evaluation.

Group 40

001.DI.06 – Fort St. Phillip Diversion (5,000 cfs)

Outflow from the 5,000 cfs Fort St. Phillip Diversion (RM 21.7) was placed entirely in PB088. The links were adequately sized, and therefore were not adjusted.

002.DI.01– Spanish Pass Diversion (7,000 cfs)

Outflow from the 5,000 cfs Spanish Pass Diversion (RM 12) was placed entirely in PB040. The links were adequately sized, and therefore were not adjusted.

Group 42

002.DI.20 – Pass a Loutré Channel Re-alignment with Up-River Diversions

Up-River Diversions: PB007 was given all of the 5,000 cfs Bayou Manchac/ Bayou Braud (Maurepas) Diversion (RM 143.7) outflow. PB007 was given all of the 5,000 cfs Convent/Blind River Diversion (RM 162.3) outflow. PB007 was given the entire 3,000 cfs Garyville/Hope Canal Diversion (RM 143.3) outflow. The Bonnet Carré flow input into PB010 was adjusted to increase the base Bonnet Carré flow by a constant 283.17 m^3/s (10,000 cfs). PB075 and PB008 were given 85% and 15% of the 20,000 cfs MRGO/Violet Diversion (RM 83.9) outflow, respectively. PB011 was given the entire 1,000 cfs White's Ditch Diversion (RM 64.5) outflow. PB030 and PB088 were given 25% and 75% of the 50,000 cfs Benney's Bay Diversion (RM 5.8) outflow, respectively. PB011 and PB079 were given 60% and 40% of the 200,000 cfs Belair (Black Bay) Diversion (RM 64.9) outflow, respectively. PB012, PB030, PB015, PB088, and PB028 were given 75%, 5%, 10%, 5%, and 5% of the 200,000 cfs Bohemia Diversion (RM 38) outflow, respectively.

Channel modifications: PB033 and PB087 were given 60.7% and 39.3% of the 200,000 cfs Pass-a-Loutré (RM 0) outflow, respectively. PB067 was given the entire 1,000 cfs Lagan (NW Barataria) (RM 156.1) outflow. PB063 was given the entire 1,000 cfs Johnson (Hahnville) (RM 126.3) outflow. PB061 was given the entire 5,000 cfs Jesuit Bend (RM 68) outflow. PB057 was given the entire 20,000 cfs Myrtle Grove (RM 60.4) outflow. PB051 was given the entire 10,000 cfs Deer Range (Hermitage) (RM 53.9) outflow. PB040, PB089, PB041, and PB031 were given 70%, 10%, 10%, and 10% of the 60,000 cfs Buras (Venice) (RM 24.9) outflow, respectively.

Links were adjusted as per **Table 25** to allow for the channel re-alignment.

Table 25 Changes to Links in Group 42 to Implement 002.DI.20

Link ID	Depth (m)	Width (m)	Manning's *n*
21			0.03
28			0.03
41	4.5	10000	0.02
42	4.0		0.025
47			0.03
65		1500	
69			0.03
93	3.0	2000	
112	1.5		0.03
131			0.03
135			0.03
140	4.5	10000	0.02
143	3.0		0.03
144		5000	0.03
145		300	
181	3.0	3000	0.03
182	3.0	2000	
183	3.0		

Group 43

001.DI.32 – Down-River Reallocation (50/50)

Down-River Reallocation: PB012, PB030, PB088, PB015, and PB028 were given 75%, 5%, 5%, 10%, and 5% of the Black Bay (RM 47) flow, respectively (percentages of 50% of the main channel flow). PB040, PB031, and PB039 were given 12.5%, 12.5%, and 75% of the Empire (RM 30.1) flow, respectively (percentages of 50% of the main channel flow). Links were adjusted as per **Table 26** to allow for the channel re-alignment.

Table 26 Changes to Links in Group 43 to Implement 001.DI.32

Link ID	Depth (m)	Width (m)	Manning's *n*
65	6.5	1000	
66	7.5	1740	0.03
69			0.03
143	2.0		0.03
144		3800	0.03
181	2.0	3000	0.03
182		2000	

Group 44

001.DI.33 – Down-River Reallocation (90/10)

Down-River Reallocation: PB012, PB030, PB088, PB015, and PB028 were given 75%, 5%, 5%, 10%, and 5% of the Black Bay (RM 47) flow, respectively (percentages of 90% of the main channel flow). PB040, PB031, and PB039 were given 12.5%, 12.5%, and 75% of the Empire (RM 30.1) flow, respectively (percentages of 10% of the main channel flow). Links were adjusted as per **Table 27** to allow for the channel re-alignment.

Table 27 Changes to Links in Group 44 to Implement 001.DI.33

Link ID	Depth (m)	Width (m)	Manning's *n*
42	10.0		
43	8.0		
65	6.5	1000	
66	5.0	1740	0.03
69			0.03
143	4.0		0.03
144	5.0	5000	0.03
177	3.5		
181	4.0	3000	0.03
182	8.0		

Group 45

001.DI.34 – Down-River Reallocation (10/90)

Down-River Reallocation: PB012, PB030, PB088, PB015, and PB028 were given 75%, 5%, 5%, 10%, and 5% of the Black Bay (RM 47) flow, respectively (percentages of 10% of the main channel flow). PB040, PB031, and PB039 were given 12.5%, 12.5%, and 75% of the Empire (RM 30.1) flow, respectively (percentages of 90% of the main channel flow). Links were adjusted as per **Table 28** to allow for the channel re-alignment.

Table 28 Changes to Links in Group 45 to Implement 001.DI.34

Link ID	Depth (m)	Width (m)	Manning's *n*
65	8.0	2000	
66	10.0	3000	0.03
69	8.0		0.03
74	4.0		
75	4.0		
78	4.5		
144		3800	0.03
160	4.0		
172	10.0		
176	8.0		

Group 46

001.DI.35 – Up-River Reallocation (50/50)

Up-River Reallocation: PB012 and PB079 each were given 50% of the Mid-Breton Sound (RM 59) flow (percentages of 50% of the main channel flow). PB047, PB051, PB046, and PB038 were given 25%, 30%, 25%, and 20% of the Hermitage (RM 55) flow, respectively (percentages of 50% of the main channel flow). Links were adjusted as per
Table 29 to allow for the channel re-alignment.

Table 29 Changes to Links in Group 46 to Implement 001.DI.35

Link ID	Depth (m)	Width (m)	Manning's *n*
41		10500	0.03
42	5.0		
65	10.0	1000	
66	7.5	1500	0.03
85	2.5	2500	
89	2.0	2000	
93	3.0	2500	
94	3.0	2500	
140	3.0	23000	0.03

Link ID	Depth (m)	Width (m)	Manning's *n*
144		2500	0.03
182	4.0		

Group 47

001.DI.36 – Up-River Reallocation (90/10)

Up-River Reallocation: PB079, PB088, PB030, PB012, PB015, and PB028 were given 15%, 10%, 10%, 50%, 10%, and 5% of the Mid-Breton Sound (RM 59) flow, respectively (percentages of 90% of the main channel flow). PB047, PB051, PB046, and PB038 were given 25%, 30%, 25%, and 20% of the Hermitage (RM 55) flow, respectively (percentages of 10% of the main channel flow). Links were adjusted as per **Table 30** to allow for the channel re-alignment.

Table 30 Changes to Links in Group 47 to Implement 001.DI.36

Link ID	Depth (m)	Width (m)	Manning's *n*
36	6.0		
41		10500	0.04
42	10.0		
43	8.0		
51	6.0		
65	6.5	1000	
66	5.0	1740	0.03
85		2000	
89		2000	
93	2.0	2500	
94	2.0	2500	
140	6.0	23000	0.03
143	2.0		0.03
144	4.5	5000	0.03
181	2.0		0.03
182	8.0		

Group 48

001.DI.37 – Up-River Reallocation (10/90)

Up-River Reallocation: PB012 and PB079 each were given 50% of the Mid-Breton Sound (RM 59) flow (percentages of 10% of the main channel flow). PB047, PB031, PB051, PB046, PB038, and PB039 were given 3%, 54%, 3%, 10%, 15%, and 15% of the Hermitage (RM 55) flow, respectively (percentages of 90% of the main channel flow). Links were adjusted as per Table 31 to allow for the channel re-alignment.

Table 31 Changes to Links in Group 48 to Implement 001.DI.37

Link ID	Depth (m)	Width (m)	Manning's *n*
41			0.04
65	10.0	3000	
66	6.0	5000	0.03
68	3.0	3000	0.03
85	4.0	10000	
88	2.5		
89	3.0	10000	
92	2.0	1000	
93	5.0	5000	
94	5.0	5000	
126	2.0		0.035
140	2.5	5000	0.03
144		1000	0.03
172	10.0		

Group 49

001.DI.38 – Up-River Reallocation (80/20)

Up-River Reallocation: PB012 and PB079 each were given 50% of the Mid-Breton Sound (RM 59) flow (percentages of 80% of the main channel flow). PB047, PB051, PB046, and PB038 are given 25%, 30%, 25%, and 20% of the Hermitage (RM 55) flow, respectively (percentages of 20% of the main channel flow). Links were adjusted as per **Table 32** to allow for the channel re-alignment.

Table 32 Changes to Links in Group 49 to Implement 001.DI.38

Link ID	Depth (m)	Width (m)	Manning's *n*
36	5.5		
41		10500	0.03
42	10.0		
43	8.0		
51	6.0		
65	6.5	1000	
66	5.0	1740	0.03
68	1.0		0.045
85	2.5	2500	
89	2.0	2000	
92		500	
93	2.0	2500	
94	2.5	2500	
140	6.0	23000	0.03
143	2.0		0.03

Link ID	Depth (m)	Width (m)	Manning's *n*
144	4.5	5000	0.03
181	2.0		0.03
182	8.0		

Atchafalaya Basin

Group 1 – Future without Action (FWOA)

This group represented projects that are currently built, currently under construction, or receiving funds for construction.

Group 2

03a.RC.04 – Mauvais Bois Ridge Restoration
The ridge restoration project would block flows from compartment AA036 to both AA037 and AA044. The flow exchanges across the links between these compartments were set to 0.

03a.RC.06 – Bayou Pointe au Chene Ridge Restoration

The ridge restoration project would block flows from compartment AA033 to AA054, AA049 and AA110. The flow exchanges across the links between these compartments were set to 0.

03a.HR.03 – GIWW Bypass South of Houma

A new by-pass channel would be dredged to replace the existing GIWW channel through Houma. Two new links were added: one connecting AA084 to AA097, the other connecting AA097 to AA092. AA097 was the compartment containing the Houma Navigation Canal (HNC). The dimensions of the new channel links were 25 ft deep x 425 ft wide. The existing GIWW channel links through Houma were blocked. In addition, the GIWW east boundary flows were assumed to be doubled due to the efficiency of the new by-pass channel.

Group 3

03a.HR.02 – Central Terrebonne Hydrologic Restoration

A new channel link between marsh compartments AA037 and AA038 was added to simulate this project. The size of the link iswas depth = 15 ft and width = 150 ft.

Group 4

03a.RC.03 – Small Bayou LaPointe Ridge Restoration

Part of the restored ridge was located on the boundary of AA038 with no connection to other compartments, and the other part of the ridge was within AA036. The ridge was considered to have no effect on the hydrology per the current compartment design, and thus it was not simulated.

Group 5

03a.RC.01 – Bayou DeCade Ridge Restoration

The ridge was cut across compartment AA036. The flows from AA036 to AA037 and AA044 would be blocked by the ridge. The flow exchanges across the links between these compartments were set to 0.

03a.HR.01 – North Lake Boudreaux Basin Hydrologic Restoration

A new connection channel would be cut to introduce freshwater from Houma Navigation Canal to North Lake Boudreaux Basin. The added channel link size was depth = 10 ft and width = 74 ft. It was assumed that a gate would not allow reverse flow from marsh compartment AA026 to HNC. Although this project was modeled, it is already funded for construction and is moving forward; as such it was not considered for inclusion in the 2012 Coastal Master Plan.

Group 6

03a.RC.02 – Restore the Bayou DuLarge Ridge Restoration

The ridge was located right at the boundary between AA028 and AA036, and the flow between these two compartments would be completely blocked. The flow exchanges across the links between these compartments were set to 0.

03b.HR.01 – Freshwater Introduction to GIWW Toward Highway 82

The project was outfall management to convey freshwater east through GIWW widening. The additional channel was assumed to be 5 ft deep and 100 ft wide with dredging along GIWW. The resulted area increase in AA086 was about 450,000 m^2 and the average depth became 3.4 m. The outflow boundary at GIWW west side to Chenier Plain was also increased by 6.3% based on the percentage of channel area changes.

03a.HR.04 – Chacahoula Basin Hydrologic Restoration

The width of the links between marsh compartments and channel compartments within the project area were increased to 14 m with link depth = 0.6 m.

Group 7

03a.RC.05 – Bayou Terrebonne Ridge Restoration

The ridge would block the flow between AA049 and AA043. The flow exchanges across the links between these compartments were set to 0.

Group 8

03b.RC.01 – Bayou Sale Ridge Restoration

The ridge would block part of the flow exchange between AA018 and AA019, thus the link width was reduced.

Group 27

03a.DI.02 – Wax Lake Delta Diversion (150,000 cfs)

The minimum flow to Wax Lake Outlet was set at 150,000 cfs when the upstream Atchafalaya River flow before the split at the Old River Control Structure was greater than 200,000 cfs. The Atchafalaya River inflow boundary was increased by 1/3 to simulate the 60% Mississippi and 40% Atchafalaya split at the Old River Control Structure rather than the current 70/30 distribution. Additional evaluations of modifying the flow distribution at the Old River Control Structure will be included in the Mississippi River Hydrodynamic and Delta Management Study. This project was removed from further consideration following project-level evaluation.

Group 28

03a.DI.03 – Upper Penchant Diversion (20,000 cfs)

The water was diverted from the Lower Atchafalaya River compartment AA005 to the Upper Penchant Basin compartment AA050. The diversion was simulated in the model by adding an additional link between these two compartments. The diverted flow was assumed to be 20,000 cfs whenever the southward Atchafalaya River flow was exceeding 70,000 cfs.

Group 29

03a.DI.08 – Bayou Lafourche Diversion (5,000 cfs)

A fixed diversion flow of 5,000 cfs was input to the Bayou Lafourche compartment AA108 whenever the flow in the Mississippi River was above 200,000 cfs. The diverted sediment concentration as assumed to be the same as in the Mississippi River. The water quality concentrations were assumed to be the same as the ones used in Group 1 (FWOA), not the Mississippi River Water Quality (WQ) concentrations. The reason for this was that the inputs for the WQ variables were much different between the AA model and the PB model. Although the diversion would change the flow magnitude to the Barataria Basin through GIWW, the quantitative change was uncertain and therefore the GIWW east flow boundary condition was assumed the same as during Group 1 (FWOA).

Group 34

03a.DI.01 – Bayou Lafourche Diversion (2,000 cfs)

Assumptions were the same as in 03a.DI.08 (Group 29) except the diversion flow magnitude became 2,000 cfs. Since the time this project was modeled, the flow has been reduced to 1,000 cfs for future model runs.

Group 35

03a.DI.05 – Upper Penchant Diversion (150,000 cfs)

Water was diverted from the Lower Atchafalaya River compartment AA005 to the Upper Penchant Basin compartment A050. The diversion was simulated in the model by adding an additional link between these two compartments. The diverted flow was assumed to be 60% of the southward Atchafalaya flow exceeding 50,000 cfs.

Group 36

03b.DI.04 – Increase Atchafalaya Flow to Eastern Terrebonne

Eastward flows from the Atchafalaya River compartment AA076 to AA077 were set to a minimum of 20,000 cfs. The flows from AA077 to AA078 through the Bayou Boeuf Lock were also set to a minimum of 20,000cfs. In Group 1 (FWOA), most of the flows would be going south through Bayou Shaffer because of the restriction of the Bayou Boeuf Lock.

Group 37

03b.DI.05 – Wax Lake Delta Reallocation

This project called for diverting 20% of the latitudinal flow or 20% of the combined flow of the Mississippi River and the Red River. The normal flow split was considered to be 70% Mississippi and 30% Atchafalaya. Therefore 2/3 of the Atchafalaya flow would be diverted to Wax Lake Outlet.

Group 38

03a.DI.04 – Upper Penchant Diversion (150,000 cfs)

Water was diverted from the Lower Atchafalaya River compartment AA005 to the Upper Penchant Basin compartment A050. The diversion was simulated in the model by adding an additional link between these two compartments. The diverted flow was assumed to be 50% of the southward Atchafalaya River flow exceeding 50,000 cfs. The inflow boundary from the Atchafalaya River was also increased by 1/3 to simulate the 60% Mississippi and 40% Atchafalaya split at the Old River Control Structure rather than the current 70/30 distribution. Additional evaluations of modifying the flow distribution at the Old River Control Structure will

be included in the Mississippi River Hydrodynamic and Delta Management Study. This project was removed from further consideration following project-level evaluation.

Group 41

002a.DI.21 – Third Delta Diversion (West Fork)

This diversion flow was defined as a function of the available flow in the Mississippi River – 40% of excess flow above 200,000 cfs in the Mississippi River would be diverted with the maximum flow capped at 250,000 cfs and the minimum flow of 60,000 cfs. The receiving compartment of the diversion was AA161. The sediment concentration was assumed to be the same as the Mississippi River. WQ concentrations were assumed to be the same as the Atchafalaya River[37].

<u>Chenier Plain</u>

Group 1 – Future without Action (FWOA)

Projects currently built, receiving funds, or scheduled to receive funds were included in this group.

Group 2

004.HR.12 – Tom's Bayou Hydrologic Restoration

Tom's Bayou was located in the interior of CP128. Since no link represented this bayou alone, the link connecting the compartment to CP039 (Vermilion Bay) was adjusted. The width of the link used in the model was 750 m, which was five times the measured (150 m) width of the two canals combined. Using this factor, a width of 325 m was used in the model to incorporate a project area of 150 ft^2, or 13.9 m^2.

004.HR.19 – Mermentau Basin Hydrologic Restoration (South of Grand Lake)

Even though the project was located in CP104, the compartment was skinny enough to where the project's hydraulic improvement would increase connection between CP108 (marsh south of Highway 82) and CP109 (marsh north of Highway 82). The project's open area of 503 ft^2, or 46.7 m^2, was assumed to be an increase in link width of 20 m. This brought the original width of 200 m to 220 m.

[37] The PB model used different water quality input parameters from the AA and CP models because it was an older model. As a result, the AA team could not use the Mississippi River scenario spreadsheet from CPRA because it was designed for the PB model inputs. Instead the AA used the Atchafalaya River for the water quality concentrations of the third delta. This is acceptable because the Atchafalaya River receives 30% of the Mississippi River at the Old River Control Structure.

Group 3

004.HR.05 – Little Pecan Bayou Hydrologic Restoration

A link of width 15 m was added to convey freshwater from CP105 (marsh north of Highway 82 and east of the Mermentau River) to CP100 (marsh south of Highway 82 and east of the Mermentau River).

004.HR.08 – Sabine Pass Hydrologic Restoration

The connection width between CP003 (Sabine Pass) and CP029 (Sabine Lake) was reduced from 600 m to 0 m to represent a complete cutoff of exchange.

004.HR.14 – Alkali Ditch Area Hydrologic Restoration

Black Lake Bayou connected CP081 (Brown Lake and Portie Lakes) and CP009 (GIWW). Alkali Ditch and Crab Gully connected CP081 and CP012 (Calcasieu Ship Channel). The link width to the GIWW was reduced from 60 m to 48.8 m to incorporate a project design width of one 60 ft wide barge gate and two 50 ft wide sheetpile weirs. The link width to the Calcasieu Ship Channel was reduced from 10 m to 5 m to incorporate the reduction in connection.

03b.OR.03 – West Vermilion Bay Oyster Reef Restoration

The oyster reef was located on the boundary between CP039 (Vermilion Bay) and CP040 (West Cote Blanche Bay). To represent it in the model, the invert elevation of the connection between the compartments was fixed to the project specified 1.5 ft, or 0.46 m, NAVD88.

Group 4

004.HR.03 – Mermentau River Hydrologic Restoration

CP016 (Mermentau River) was routed to its original connection to the Gulf by adding a new compartment. In the absence of channel data for this new compartment, the cross-section of the chainage furthest south was used and kept constant from its location to the Gulf. The new compartment CP029 (Mermentau Ship Channel) retained its cross-section as it was larger than the authorized dimension. The extension of CP016 cut through marsh compartment, CP093. The area to the west remains CP093 while the new area to the east was CP145. Links between these compartments were added and/or updated where necessary.

004.HR.20 – Mermentau Basin Hydrologic Restoration (South of White Lake)

To facilitate freshwater flow from CP039 (White Lake) to CP117 (marsh south of Highway 82), a 20 m wide link was added connecting the two compartments.

004.HR.23 – Humble Canal Hydrologic Restoration

The spillway at Humble Canal connected CP016 (Lower Mermentau River) to CP104 (compartment Humble Canal was located in). The width of the connection was increased from 0 m to a project design width of 150 ft, or 45.7 m.

03b.OR.02 – East Vermilion Bay Oyster Reef Restoration

The oyster reef was located on the boundary between CP041 (West Cote Blanche Bay) and CP042 (East Cote Blanche Bay). To represent it in the model, the invert elevation of the connection between the compartments was fixed to the project specified 1.5 ft, or 0.46 m, NAVD88.

Group 5

004.HR.10 – Gum Cove Ridge Hydrologic Restoration

CP009 (GIWW between Sabine Lake and Calcasieu Lake) was split at Gum Cove Ridge. The west portion remained CP009 while the east portion became a new compartment, CP029. A link between the two was added with a connection width of 18.3 m for the project barge gate width of 60 ft. The connections from the surrounding marshes to the respective GIWW compartment were updated.

004.HR.18 – Mermentau Basin Hydrologic Restoration (East of Calcasieu Lake)

The connection width between CP092 (area west of Highway 27) and CP096 (area east of Highway 27) was increased from 0 to 20 m representing the project designated open area of 503 ft^2, or 46.7 m^2.

004.HR.22 – East Calcasieu Lake Hydrologic Restoration

The link representing this spillway connected CP036 (Calcasieu Lake) to CP087 (marsh southeast of Calcasieu Lake). Its width was increased from 22 m to the project design width of 200 ft, or 61 m.

Group 6

004.HR.07 – Little Pecan Bayou Sill

The measured width of Little Pecan Bayou was 100 m while the model width of the link representing this connection was five times less (20 m). Using this relationship, the new model connection width was 4 m, five times less than the project design width of 60 ft, or about 20 m.

004.HR.17 – Oyster Bayou Hydrologic Restoration

The measured width of Oyster Bayou was 35 m. The model width of the link representing this connection was 14.6 m. Using this relationship, the new model connection width was 10.5 m representing the project design open area of 480 ft^2, or about 25 m wide.

004.HR.21 – Southwest Pass Hydrologic Restoration

The connection between CP039 (Vermilion Bay) and CP149 (offshore of Marsh Island) represented the Southwest Pass. The area of the connection link was reduced to 50% of the original area and the width of the link was reduced from 1501 m to 1067 m to represent the project specifications.

004.HR.24 – Sabine River Hydrologic Restoration (5,000 cfs)

Water was diverted from CP005 (Sabine River) into CP057 (wetland south of GIWW). The amount of water exchanged was calculated based on the head differential between the water stage of the two compartments and a connection width of 100 m.

03b.HR.01 – Freshwater Introduction to GIWW Toward Highway 82

An additional 500 ft^2, or 46.5 m^2, was added to the GIWW cross-sections used to calculate the depth-volume relationship curve for CP026 (GIWW north of Vermilion Bay).

Group 7

004.HR.06 – Calcasieu Ship Channel Gulf Salinity Control Structure

The connection between CP145 (offshore of Calcasieu Ship Channel) and CP011 (Calcasieu Ship Channel) was treated as a lock using the schedule from the Calcasieu Lock east of the Calcasieu Ship Channel with a minimum of at least 2 hours open per day to represent a higher traffic pattern through this lock. The width of the link was 175 m, the width of similar sized locks in the model.

Group 8

004.HR.02 – GIWW Lock West of Calcasieu Ship Channel

The connection between CP009 (GIWW) and CP014 (Calcasieu River/ Ship Channel) was treated as a lock using the schedule and size from the Calcasieu Lock east of the Calcasieu Ship Channel.

2. *Technical Quality*

a. Theory

The equations used in the Eco-Hydrology models were based on theoretical concepts found in literature for the hydrodynamic processes (including discharge, evapotranspiration, precipitation, volume, stage, depth, and structure schedules) and the water quality (including nutrient cycles and nitrogen removal, salinity, total suspended solids and accretion, chlorophyll-a as algae, and water age) processes found in nature. In order to efficiently model the hydrodynamic and ecological processes occurring in each of the model domains, these governing equations and theories needed to be applied. It should be noted that all of these equations were computed sequentially at each time step for each state variable in each compartment.

Hydrodynamic Equations

The hydrodynamic theory used in the models included equations for discharge, volume, stage, and depth. The implementation of locks and other structures was also included in the hydrodynamic theory.

Discharge

It was assumed that the flows throughout the models were governed by gravity and friction force. The different discharges[38] used in the models included exchange flows, tributary flows, distributary/diversion flows, atmospheric contributions, and runoff contributions. The tributary, distributary/diversion, atmospheric, and runoff discharges were supplied by the boundary conditions (Section 1) and were repeated for every year of the model simulations. The exchange flows between compartments were estimated in the models at every time step and they are described below. It should be mentioned that evapotranspiration was reduced because of external stimuli, such as sunlight and depth fluctuations. These reductions are also described in this section.

Exchange Flows

The exchange flows of the links, Q_i, between compartments were calculated using a variation of the Manning's equation (Chow, 1959):

$$Q_i = A_i \left\{ \frac{2g \left| \left(E_j + \frac{d_i SAL_j}{1000} \right) - \left(E_{j+1} + \frac{d_i SAL_{j+1}}{1000} \right) \right|}{\left(\sum k_{im} + 2g n_i^2 \frac{L_i}{R_i^{4/3}} \right)} \right\}^{\frac{1}{2}} (3600 \cdot 24) \quad \textbf{(5)}$$

where,

i	=	link identifier
j	=	upstream compartment identifier
$j+1$	=	downstream compartment identifier
Q_i	=	water flow rate in link i, m^3/day

[38] Wastewater discharges are excluded from this list because the hydrodynamics of the models are calibrated before wastewater flows are included. The wastewater inflows are only included to improve the calibration of the water quality of the models.

A_i	=	cross-sectional water flow area for link *i*, m^2
g	=	gravitational constant, 9.81 m/s^2
E_j	=	water surface elevation of compartment *j*, m
d_i	=	centroidal water depth for link *i*, m
SAL_j	=	concentration of salinity in compartment *j*, ppt or kg/m^3
k_{im}	=	minor loss coefficient for link *i*, $1/s^2m^{2/3}$
n_i	=	Manning's roughness coefficient
L_i	=	length for link *i*, m
R_i	=	hydraulic radius for link *i*, m

The cross-sectional water flow area for link *i*, A_i, was the product of the flow width for link *i*, w_i, and the flow depth of link *i*, H_i. The flow width was obtained by approximating the width in which water can pass between two compartments. In the CP and AA models, the flow depth was defined as the minimum depth of the two connecting compartments. The PB model used the average depth of flow in each link at every time step rather than the minimum depth. For links connecting to offshore[39] compartments (AA) or nodes (PB and CP), the depth was defined as the depth of the upstream or near-shore compartment (assuming that the boundary compartment or node was always downstream).

The centroidal depth was the depth to the centroid, or middle of the water column, and it was defined as the flow depth for the link divided by 2. The minor loss coefficient was a calibration parameter to account for link geometry that cannot be captured using the standard attributes. The Manning's roughness coefficient for a link, *n*, was the average of the roughness values of the two compartments connected by the link. The roughness of the offshore links in the CP and PB models was designated as the roughness of the upstream or near-shore compartment. The length of a link was defined as the approximated travel distance between the centroids of the two connected compartments. The hydraulic radius was defined as the average of the water depth weighted by the length of the link in each of the compartments. The direction of flow was based on the defined upstream and downstream compartments and the resulting sign of **Equation (5)**. For example, compartments *A* and *B* are defined as the upstream and downstream of a link, respectively. If the exchange flow is calculated to be positive, the flow is from *A* to *B*. If for the same link, the exchange flow is calculated to be negative, the flow is from *B* to *A*.

When water depth was equal to zero, the exchange flow equation becomes undefined. Therefore, a minimum depth was defined in the models to avoid division by zero. The PB and AA models apply a minimum depth of 0.01 m. The CP model behaves a little differently in that it applies minimum depths for both wetting and drying. The minimum depth for the drying, or emptying, of a compartment was called the *dry* depth, H_{dry}, and was equal to 0.01 m. A compartment was considered *dry*, i.e. have no water, when it reaches this depth. This was simulated in the model by restricting the outflows in the compartments whose depth was equal to H_{dry}. Sometimes small amounts of additional water were added to a compartment and cause it to become *wet* or have a depth above 0.01 m. In the next time step the compartment releases this small amount of water, and if the compartment does not receive any additional

[39] Again, the AA model uses offshore compartments for the offshore boundary, whereas, the PB and CP models use theoretical nodes for the offshore boundary. These offshore nodes do not have physical properties. Therefore, the minimum depth of the links is defined as the depth of the upstream or near-shore compartments.

water, the compartment will become *dry* again. This creates instability in the CP model. Therefore, to alleviate this instability, the CP model applies a *wet* depth, H_{wet}, during the wetting of the compartments at a value of 0.02 m, where a compartment was not allowed to release water until reaching H_{wet} and above. Again, the PB and AA models do not use a *wet* depth because their codes do not go unstable during the wetting and drying processes.

The inclusion of both the dry and wet depths was simulated in the CP model as follows:

A compartment was allowed to receive and release water when its depth was above H_{dry} regardless of the relation to H_{wet}. Flow was not altered until the depth reaches H_{dry} at which the compartment was restricted from releasing water. However, it was still allowed to receive water. As water was received, it was not released until the depth reaches H_{wet} and above. Once above H_{wet}, the compartment was again operating under normal conditions – both receiving and releasing water. It is important to note that if the initial depth originates above H_{wet}, drops below H_{wet}, and then starts rising again before it reaches H_{dry}, there were no flow restrictions. Again, flow restrictions do not start until H_{dry} is reached. **Figure 31** is a diagram of water depth over time showing flow restrictions in relation to the *wet* and *dry* depths.

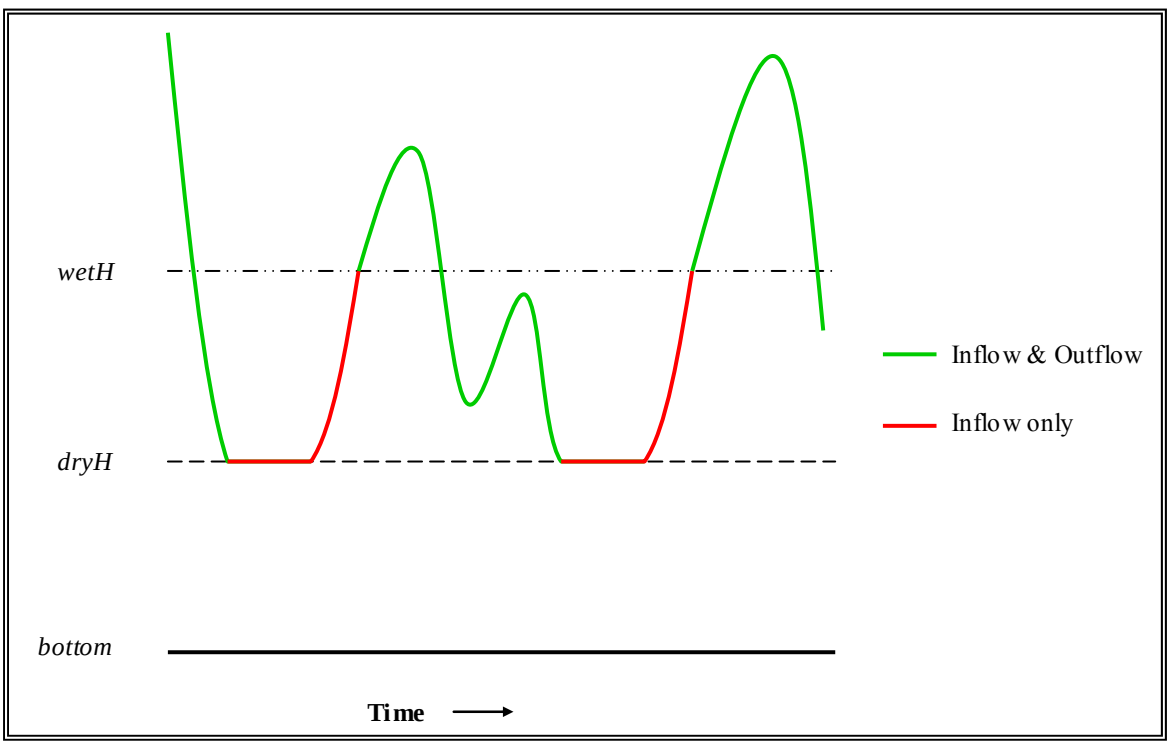

Figure 31 Wet and Dry Depth Flow Conditions for the CP Model

Evapotranspiration

Evapotranspiration (*ET*) was defined as an outflow in the models because it removes water from the compartments. Therefore, *ET* must be included in the flow and volume equations in order to accurately simulate existing conditions.

As mentioned in Section 1, evapotranspiration is used synonymously with evaporation in this report. However, for modeling purposes, the PB team separates evaporation from evapotranspiration because that region's compartments were segmented into marsh, upland, and open water sub-compartments, where the open water sub-compartments undergo evaporation and the marsh and upland sub-compartments undergo evapotranspiration. In the AA and CP models, however, the marsh was not separated from the open water in a given compartment and therefore, evapotranspiration was applied over the entire compartment. In order to more accurately represent existing conditions, the AA and CP models apply a reduction factor to the marsh compartments to account for the limited sunlight penetration in the marsh due to plant coverage. **Equation (6)** below illustrates the calculation of this sunlight-limited reduction factor.

$$f_{ET\,j} = max\left[ET_{min}, min\left[1, \frac{H_j}{H_{ET}}\right]\right] \tag{6}$$

where,

$f_{ET,j}$	=	reduction factor for reduced sunlight through marsh
ET_{min}	=	minimum reduction factor, 0.20
H_{ET}	=	depth below which *ET* is reduced, m, 0.25
H_j	=	water depth in compartment *j*, m

The AA model introduces an additional reduction to the marsh compartments, f_{HETj}, which takes into account the reduction in available surface area as the depth decreases. **Equation (7)** below illustrates how the depth-limited reduction factor was estimated.

$$f_{HET\,j} = \frac{\left(min\left[H_j, H_{max\,j}\right] - H_{dry}\right)}{H_{max\,j} - H_{dry}} \tag{7}$$

where,

$f_{HET,j}$	=	reduction factor for reduced water surface area as depth decreases for marsh compartments
H_{max}	=	depth below which *ET* is reduced for a reduction in water surface area, m, ($E_{max} - E_{avg}$)
H_{dry}	=	dry depth, 0.01 m, (used to prevent division by zero)

Equation (8) below shows how the sunlight-limited reduction factor was applied in the CP model, and **Equation (9)** shows how both the sunlight-limited and the depth-limited reduction factors were applied in the AA model. Again, the PB model does not include reduction factors for evaporation or evapotranspiration.

$$ET_{marsh\,j} = f_{ET\,j} \cdot ET_j \tag{8}$$

$$ET_{marsh\,j} = f_{ET\,j} \cdot f_{HET\,j} \cdot ET_j \tag{9}$$

where,

$ET_{marsh,j}$	=	reduced *ET* in marsh compartment *j*, m/day
ET_j	=	original *ET* in marsh compartment *j* from boundary conditions, m/day

In the PB region, *ET* was always active and was always used in calculations. In the AA region, *ET* was only affected by the minimum depth rule. In the CP region, *ET* was affected by both the *wet* and *dry* depth rules.

Stage and Depth

Stage and depth were inherently dependent on each other, as well as on the change in volume of the water within each compartment, V_j (m^3). The volume was estimated from the discharges mentioned above and the atmospheric exchange of precipitation and evapotranspiration. **Equation (10)** below presents the formulation for the change in depth as a function of exchange flows and atmospheric exchanges.

$$\frac{dH_j}{dt} = \left(\frac{\sum Q_{j,i} + \sum Q_{j,trib} + \sum Q_{j,div} + \sum Q_{j,run}}{As_j}\right) + \left(P_j - ET_j\right) \tag{10}$$

where,

dH_j/dt	=	rate of change in water depth for compartment *j*, m/day
$Q_{j,i}$	=	flow to compartment *j* from all links *i*, m^3/day
$Q_{j,trib}$	=	flow to compartment *j* from all tributaries, m^3/day
$Q_{j,div}$	=	flow to compartment *j* from all diversions and distributaries, m^3/day
$Q_{j,run}$	=	flow to compartment *j* from all runoff contributions, m^3/day[40]
P_j	=	precipitation on compartment *j*, m/day
ET_j	=	evapotranspiration from compartment *j*, m/day
As_j	=	water surface area of compartment *j*, m^2

The depth equation above **(10)** was defined as a differential equation which was calculated at every time step. The equation represents an accumulation with a known starting point, the initial depth. The initial depth was estimated from the boundary conditions for the initial stage and bed elevations of the compartments. **Equation (11)** below illustrates how the initial depth was calculated, and **Equation (12)** below shows how the successive depths were calculated from **Equation (10)** and **Equation (11)**. **Figure 32** shows a diagram of how these equations were calculated in the models.

$$H_{j,0} = E_{j,0} - E_{j,bed} \tag{11}$$

[40] Only the AA and PB models include runoff discharges.

where,

$H_{j,0}$	=	initial depth of compartment *j*, m
$E_{j,0}$	=	initial stage of compartment *j*, m, from initial conditions
$E_{j,bed}$	=	bed elevation of compartment *j*, m, from bathymetric inputs

$$H_{j,t} = H_{j,t-1} + \frac{dH_j}{dt} \tag{12}$$

where,

$H_{j,t}$	=	depth of compartment *j* at time step *t*, m
$H_{j,t-1}$	=	depth of compartment *j* at previous time step *t-1*, m[41]

[41] For time step $t = 1$, $H_{j,t-1} = H_{j,0}$ which corresponds to the initial depth for each compartment *j*.

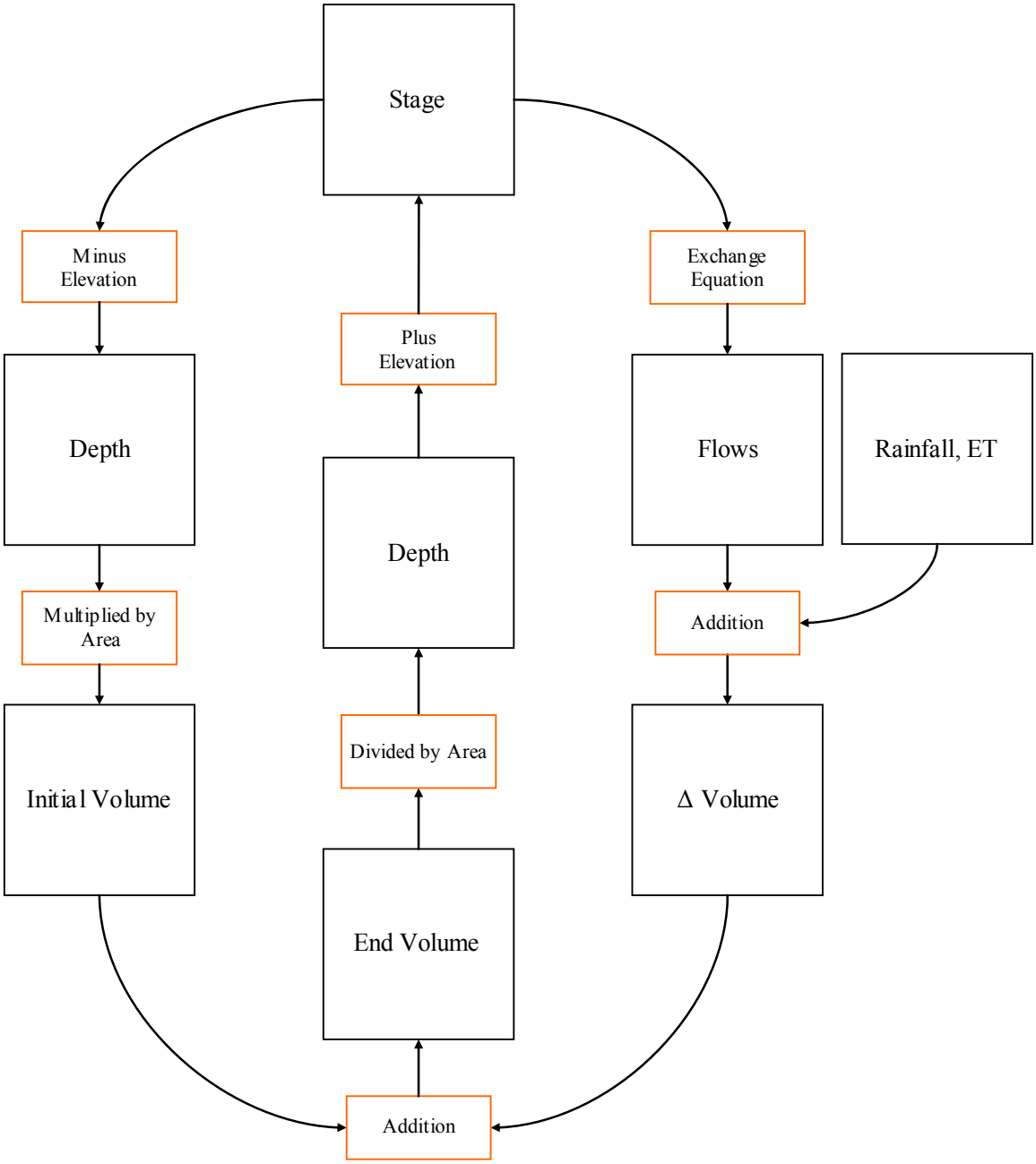

Figure 32 Change in Stage Calculations for the Eco-Hydrology Models

It should be noted that the stage in the channel compartments of the CP model were calculated differently than the rest of the compartments. For these compartments, the volume of water in each compartment was calculated and referenced to a depth-volume relationship curve to find the corresponding depth. The curves were constructed using channel cross-section data in MIKE11 from the Center for Louisiana Inland Water Studies (CLIWS). The following describes how a curve was developed for a channel. The MIKE11 data provide cross-sections at non-uniform chainages along the channel. MIKE11 processes the data to give the area of water in the channel at specified depths for each of the cross-sections. Linear interpolation between the depths given and extrapolation above the largest depth given were used to estimate the water

depth to water area (depth-area) relationship for each cross-section at water depths ranging from 0 m to 20 m (in 1 m intervals). Each cross-section's depth-area relationship was assumed to be uniform from the cross-section's location on the channel to the cross-section downstream. Using this assumption, the length to the downstream cross-section was multiplied with the areas for each of the depths to produce a depth-volume relationship for each segment of the channel. ArcGIS was used to determine which channel chainages were associated with the channel compartment in the model. The average of the volumes at each of the depth was taken among the chainages and the resulting relationship was used in the model as the depth-volume curve for the compartment.

To use the depth-volume curves, the volume of a compartment was calculated using a variation on **Equation (10)**. **Equations (13)** and **(14)** below illustrate how the volume was estimated in the models. This calculated volume was used with the curves to find the corresponding depth of the channel compartment. **Figure 33** below shows how the stage was calculated for the channel compartments of the CP model.

$$\Delta V_{j,t} = \sum Q_{j,t,i,trib,div,run} + \left(P_{j,t} - ET_{j,t}\right) * As_{j,t} \tag{13}$$

$$V_{j,t} = V_{j,t-1} + \Delta V_{j,t} * DT \tag{14}$$

where,

$\Delta V_{j,t}$	=	rate of change in volume in compartment *j* at time step *t*, m^3/day
$V_{j,t-1}$	=	volume in compartment *j* at previous time step *t-1*, m^3
$V_{j,t}$	=	volume in compartment *j* at time step *t*, m^3
DT	=	computational time step, day

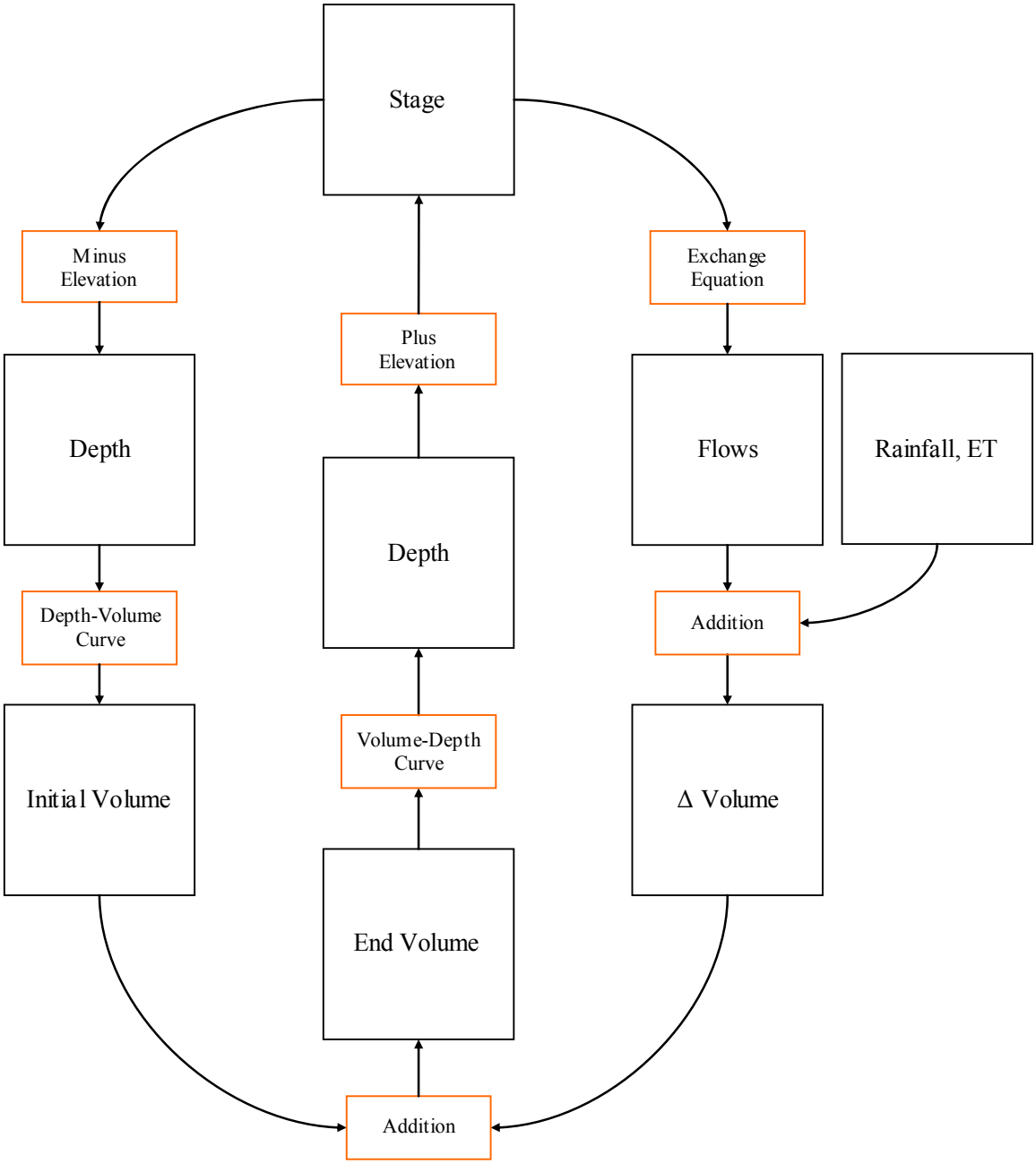

Figure 33 Change in Stage Calculations for the Channel Compartments of the CP Model

Structures

There were several types of structures in the models including levees, locks, gates, and saltwater barriers. Levees were modeled by restricting flow from one compartment to the other when the levee was located at the boundary between them. Saltwater barriers were modeled by allowing flow from the upstream (freshwater) to downstream (saltwater), but restricting flow from downstream to upstream. Locks and control structures were modeled using the daily operational schedules recorded by the USACE Team New Orleans[42]. These lock and control

structure schedules provide the number of hours open and closed for each lock. The percentage of hours open per day was calculated and multiplied by the calculated exchange flow to give the adjusted exchange flow used to represent the structure in the model.

Water Quality

The water quality theory used in the models includes a general approach to water quality modeling, the source/sink terms used for computing mass transfers due to kinetic processes, and any other supporting formulations. The formulations include equations for salinity, temperature, the nitrogen and phosphorus cycles, algae as chlorophyll-a, detritus, deposition and resuspension of suspended solids, and water age. The formulations are presented below and were coded into the AA and CP models. Similar formulations were coded into the PB model. The documentation of those formulations can be found in McCorquodale et al. (2008) and Meselhe et al. (2008).

General Approach

The water quality portions of the models include transport and reactions which affect conventional water quality variables that were dissolved or were in particulate form in the water column. The models include processes that deposit or transfer material onto the sediment bed, but they do not predict the fate of those constituents once they were in the bed. The water column was assumed to be fully mixed and aerobic at all locations and times. Thus, there were no transfers of nutrients from the bed to the water column that can occur when the water column was anoxic, or oxygen-deprived.

The mass-balance-based, reactive transport equation for each water quality constituent solved within each computational compartment can be stated as follows:

$$\frac{dC_{k,j}}{dt} = -\frac{C_{k,j}V_j'}{V_j} + \frac{\sum C_{k,j,s}Q_{j,s}}{V_j} - \frac{k_{dis}}{V_j}\sum_i \frac{A_i}{L_i}\left(C_{k,j} - C_{k,jn}\right) + \frac{\sum Ss_{k,j,l}}{V_j} + \frac{1000L_k As_j}{V_j} \quad \textbf{(15)}$$

where,

$dC_{k,j}/dt$	=	rate of change of concentration of constituent *k* in compartment *j*, g/m^3 or mg/L
s	=	water source via a tributary, a diversion/distributary, or runoff
$C_{k,j,i,s}$	=	concentration of constituent *k* flowing into or out of compartment *j* via link *i* or a source *s*, g/m^3 or mg/L
$Q_{i,s}$	=	water flow rate entering or exiting compartment *j* via link *i* or a source *s*, m^3/day
A_i	=	cross-sectional water flow area for link *i*, m^2
V_j	=	water volume of compartment *j*, m^3
V_j'	=	change in water volume with respect to time for compartment *j*, m^3/day
t	=	time, days
k_{dis}	=	dispersion coefficient, m^2/day
L_i	=	length of link *i*, m

$C_{k,jn}$	=	concentration of constituent *k* in compartment *jn* adjacent to compartment *j*, g/m^3 or mg/L
$Ss_{k,j,l}$	=	rate of change of mass of constituent *k* in compartment *j* due to source/sink *l* associated with kinetic processes including transformations/reactions and settling, g/day
As_j	=	water surface area for compartment *j*, m^2
L_k	=	regional atmospheric deposition rate (for water compartments) or local loading flux (such as marsh/wetland delivery) for constituent *k*, kg/m^2/day

The above equation can be used for all compartments, regardless if they were open water, such as lakes and bays, marsh, or channels and canals. However, an alternative form of **Equation (15)** was used for the PB compartments which have vertical side walls, i.e. $V_j = y_j As_j$. This alternate equation is shown below:

$$\frac{dC_{k,j}}{dt} = -\frac{C_{k,j}E_j'}{y_j} + \frac{\sum C_{k,j,s}Q_{j,s}}{y_j As_j} - \frac{k_{dis}}{y_j As_j}\sum_i \frac{A_i}{L_i}\left(C_{k,j} - C_{k,jn}\right) + \frac{\sum Ss_{k,j,l}}{y_j As_j} + \frac{1000L_k}{y_j} \quad \textbf{(16)}$$

where, E_j' *was* the change in water surface elevation with respect to time (m/day), and y_j was water depth in compartment *j*, m. For compartments that do not have vertical side walls, volume versus depth tables based on bathymetric or channel cross-section data must be provided to the model.

There were two types of model compartments, river/channel and open water/marsh. The open water/marsh compartments each have a fraction of marsh specified so that sediment resuspension and available light can be reduced for vegetation effects.

The water quality constituents or state variables that were simulated in the models include the following:

- Salinity, *SAL*, parts per thousand (ppt)
- Temperature, *TMP*, °C
- Total suspended solids, *TSS*, mg/L (or g/m^3)
- Nitrate + nitrite nitrogen (NO_3+NO_2), referred to as simply nitrate (*NO3*) for short, mg/L (or g/m^3)
- Ammonium nitrogen, *NH4*, mg/L (or g/m^3)
- Dissolved organic nitrogen, *DON*, mg/L (or g/m^3)
- Total inorganic phosphorus, *TIP*, includes phosphates as phosphorus, mg/L (or g/m^3)
- Dissolved organic phosphorus, *DOP*, mg/L (or g/m^3)
- Phytoplankton as chlorophyll a (Chl-a), *ALG*, µg /L (or mg/m^3)
- Detritus as dry weight mass, *DET*, mg /L (or g/m^3)
- Water age, *AGE*, or contact time within each compartment, days

Ammonia was assumed to exist solely as the cation ammonium (NH_4), which was a reasonable assumption for the relatively neutral pH range experienced in estuarine waters. Dissolved oxygen (DO), biochemical oxygen demand (BOD), organic carbon, and related DO source/sink

processes were not included since these models assume that the water column was always aerobic and DO was not a concern. However, it should be noted that this was a general assumption and there were most probably several areas within the model regions that were not aerobic. Only nitrogen and phosphorus experience atmospheric deposition. The mass transfer pathways for the above state variables are shown in **Figure 34**.

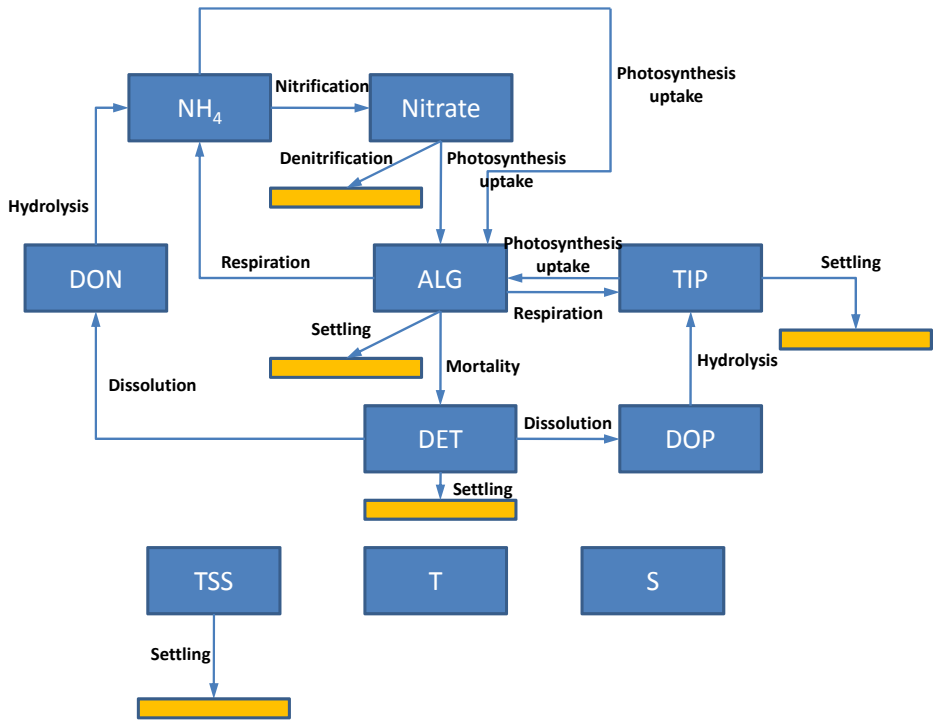

Figure 34 Mass Transfer Diagram of the Water Quality State Variables for the Eco-Hydrology Models

It is noted that the hydrolysis process shown in **Figure 34** is also referred to as mineralization in some water quality models. It is the process that transforms dissolved organic matter into inorganic forms, such as DON transformed into NH_4. Also, dissolution is referred to as hydrolysis in some water quality models, but it is the process that transforms particulate organic matter into dissolved organic matter, such as DET transformed into DON.

Only one phytoplankton group was modeled, and this group will represent a mix of algal species of predominantly the green and blue-green types, which occur during the warmer months. Blue-green algae were the most problematic and can be a nuisance by resulting in harmful algal blooms (HAB's). They were prone to occur in late spring through early fall and were usually found in fresh to slightly brackish waters. Although only one algal group was modeled, consideration was given to a portion of the algae within this group that can fix nitrogen from the atmosphere as some species of blue-green algae do.

Water quality variables that can be derived or determined from the above list of state variables include:

- Particulate organic nitrogen, PON; determined from (DET + ALG) and stoichiometry

- Total nitrogen, TN; sum of NO3, NH4, DON, and PON
- Particulate organic phosphorus, POP; determined from (DET + ALG) and stoichiometry
- Total phosphorus, TP; sum of TIP, DOP, and POP
- Total Kjeldahl nitrogen, TKN; sum of NH4, DON, and PON
- Particulate organic carbon, POC; determined from (DET + ALG) and stoichiometry
- Dissolved organic carbon, DOC; determined from DON and stoichiometry

The derived value of DOC does not account for any inflowing DOC since it was simply proportioned to the amount of DON.

Source/Sink Terms

The sources/sinks and reaction terms ($Ss_{k,j,l}$) for each of the above state variables are discussed in this section and were based primarily on the formulations used in the QUAL2K water quality model (Chapra and Pelletier, 2003). The source/sink terms were written as the derivative of concentration with respect to time for the left side of each equation below, but it should be understood, that this was the change in concentration with respect to time due to sources and sinks without the contributions from transport and loadings. Therefore, the right-hand side of several of the source/sink equations include values from the previous time step of the parameter being calculated. All source/sink terms were turned off, i.e. set to 0 (zero), when a compartment was *dry* (**Figure 31**).

To simplify the equations that follow, the subscript *j* will be omitted for the remainder of the kinetic formulations. It should be understood that the source/sinks terms apply to each compartment *j*.

Salinity

There were no reactions or source/sink terms for salinity, thus *Ss* was zero for simulating salinity.

Temperature

Temperature was modeled using the equilibrium temperature concept (Edinger et al., 1974). Equilibrium temperature TMP_E is a site-location and time dependent reference water temperature at which no heat exchange occurs. It can be computed independently of the temperature simulation using standard meteorological data, including air temperature, wet bulb or dew point temperature, wind speed, cloud cover, and incident short wave solar radiation. A benthic sediment heat flux term was also included in the models.

The source/sink term for temperature (Ss_T), i.e., the change in water temperature *TMP* for compartment *j* with respect to time due to heat exchange at the water surface and at the sediment-water interface, was computed as follows:

$$\frac{dTMP}{dt} = \frac{Ss_{TMP}}{V} = \frac{K_E}{\rho c_p y}(TMP_E - TMP) + \frac{\rho_s c_{ps} \alpha_s}{\rho c_p H_s y}(TMP_{sed} - TMP) \quad \textbf{(17)}$$

where,

K_E	=	heat exchange coefficient for a site, W/m^2/ °C
ρ	=	density of water, 1.0 g/cm^3
ρ_s	=	density of sediments, g/cm^3
c_p	=	specific heat of water, 1.0 cal/g/°C
c_{ps}	=	specific heat of sediments, cal/g/°C
α_s	=	sediment thermal diffusivity, m^2/day
H_s	=	effective thickness of the sediment layer, m
TMP_{sed}	=	temperature of the sediments, °C
TMP_E	=	equilibrium temperature, °C

The terms of **Equation (17)** were divided by water depth y_j. This is because in their original forms the numerators of each term were multiplied by the water surface area which cancels out the surface area in the volume terms of the denominators. It was assumed that water volume is the product of depth and water surface area even for channel compartments that do not have vertical walls. This approximation was used for all other water quality processes that involve surface area, depth, and water volume.

K_E from **Equation (17) was** multiplied by a conversion factor of 0.02066 to convert the units from W/m^2/ ^{o}C to units of (cal · m) / (cm^3 · ^{o}C · day). This simplifies the division by ρc_p (1.0 g/cm^3 · 1.0 cal/g/^{o}C = 1.0 cal/cm^3/^{o}C), resulting in units of m/day. These units were consistent with division by the depth to obtain the time rate of change in temperature. An existing heat exchange computer program was used to compute TMP_E and K_E from climate data consisting of air temperature, dew point temperature, wind speed, and sky cover. Meteorological data from the Lafayette, LA, Regional Airport were used to compute daily average values of TMP_E, K_E, and solar radiation, $I_{da}(0)$, (W/m^2) for each day of the year for all three regions. The use of solar radiation is described later.

Chapra and Pelletier (2003) have provided values for α_s with a recommended value of 0.005 cm^2/sec or 0.0432 m^2/day, which was used in the models. They also provide values of the product $\rho_s c_{ps}$ for various types of bed substrates. The value for beds with a mix of mud and sand was approximately 0.8 cal/cm^3/^{o}C. The value of $H_{s\ was}$ 0.1 m, which is consistent with recommendations by Chapra and Pelletier (2003).

The only variable that remains undefined in the two temperature source/sink terms is the sediment temperature. Annual average surficial soil temperatures can be approximated by the annual average air temperature. The annual average air temperature measured at the Lafayette Regional Airport for 2007 (the year used for model calibration in the AA and CP models) was about 20 ^{o}C. It was assumed that the sediment temperature closely correlates to annual average air temperature as soil is closely correlated to annual average air temperature. Thus, a value of 20 ^{o}C was recommended for the sediment temperature. Sediment temperature was assumed to be spatially uniform throughout the domain.

Total Suspended Solids

Total suspended solids (TSS) are mostly composed of inorganic suspended solids, so this state variable should be considered as mineral sediment. The measured TSS entering the system includes organic solids, but since its contribution was small there was no correction to separate organic suspended solids from TSS.

TSS is lost due to deposition and can be gained by bottom sediment resuspension. In calculating TSS, it was assumed that there is an infinite source of bed sediment for resuspension. Since the models do not include the vertical dimension, the settling rate and the deposition rate were the same. The rate of change of TSS in a compartment was stated as:

$$\frac{dTSS}{dt} = \frac{Ss_{TSS}}{V} = \frac{E_{res}}{y} - \frac{v_s TSS}{y} \tag{18}$$

where, v_s *was* the TSS deposition rate (m/day), E_{res} was the resuspension flux (g/m^2/day), and all other variables have been previously defined. The resuspension flux and the deposition rate were calculated from a sediment sub-model based on ambient conditions and wind.

Nitrate + Nitrite

The source of NO3 is nitrification from NH4, and the sinks were photosynthetic uptake and sediment denitrification. Water column denitrification was not included since it was assumed that the water column would always be aerobic. (For additional nitrogen uptake calculations, see the Nitrogen Uptake model in Appendix D-22). The rate of change in NO3 concentration due to these source and sinks is stated as:

$$\frac{dNO3}{dt} = k_n(TMP)NH4 - \frac{k_{dn}(TMP)}{y}NO3 - r_{na}(1 - P_{ap})\mu_p \frac{(1 - f_{Nfix})ALG}{1000} \tag{19}$$

where,

$k_n(TMP)$	=	temperature dependent nitrification rate, day^{-1}
$k_{dn}(TMP)$	=	temperature dependent sediment denitrification rate, m/day
r_{na}	=	stoichiometric ratio of mass of nitrogen to mass of Chl-a
P_{ap}	=	phytoplankton preference for ammonium uptake, dimensionless
μ_p	=	phytoplankton photosynthesis or growth rate, day^{-1}
f_{Nfix}	=	fraction of ALG that fix nitrogen

The division of ALG by 1000 in the last term of **Equation (19) was** required to convert ALG in units of µg/L of Chl-a to mg/L Chl-a. Calculation of the phytoplankton growth rate, ammonium preference, and stoichiometric ratios are described in the "Supporting Formulations" section below. The sediment denitrification rate actually includes the nitrate mass transfer rate from the water column to the bed where denitrification occurs. Some species of cyanobacteria or glue-green algae fix nitrogen from the atmosphere, but most blue-green algae cannot tolerate much salinity. Thus, if the salinity was greater than 2.0 ppt, f_{Nfix} was set to zero.

Ammonium

Sources of NH4 are DON hydrolysis and algal respiration. Sinks include algal uptake for growth and nitrification. The rate of change of NH4 concentration due to these sources and sinks is stated as:

$$\frac{dNH4}{dt} = k_{hn}(TMP)DON + r_{na}k_{rp}(TMP)\frac{ALG}{1000} - k_n(TMP)NH4 - r_{na}P_{ap}\mu_p\frac{(1-f_{Nfix})ALG}{1000} \quad \textbf{(20)}$$

where,

$k_{hn}(TMP)$ = temperature dependent DON hydrolysis rate, day^{-1}
$k_{rp}(TMP)$ = temperature dependent phytoplankton respiration rate, day^{-1}

All other variables have been previously defined.

Dissolved Organic Nitrogen
The one source of DON is dissolution of particulate organic nitrogen (PON) within DET, and the one sink is hydrolysis to NH4. The rate of change of DON concentration due to this source and sink is stated as:

$$\frac{dDON}{dt} = r_{na}k_{dt}(TMP)DET - k_{hn}(TMP)DON \quad \textbf{(21)}$$

where,

$k_{dt}(TMP)$ = temperature-dependent DET dissolution rate, day^{-1}
r_{nd} = stoichiometric ratio of mass of nitrogen to mass of DET

All other variables have been previously defined.

Total Inorganic Phosphorus
The sources of TIP were algal respiration, hydrolysis of DOP, and release of orthophosphate from marsh sediments, and the sinks were settling and phytoplankton uptake during growth. The rate of change of TIP concentration due to these sources and sinks is stated as:

$$\frac{dTIP}{dt} = k_{hp}(TMP)DOP + r_{pa}k_{rp}(TMP)\frac{ALG}{1000} - r_{pa}\mu_p\frac{ALG}{1000} - \frac{v_s}{y}F_{pp}TIP + f_{marsh}\frac{R_p(TMP)}{y} \quad \textbf{(22)}$$

where,

$k_{hp}(TMP)$ = temperature-dependent DOP hydrolysis rate, day^{-1}
r_{pa} = stoichiometric ratio of mass of phosphorus to mass of Chl-a
F_{pp} = fraction of TIP that is adsorbed to TSS in the water column
$R_p(TMP)$ = temperature-dependent orthophosphate P release from marsh sediments, g/m^2/day
f_{marsh} = fraction of marsh compartment surface area that is covered with marsh

All other variables have been previously defined. The formulation for estimating F_{pp} will be discussed in a later section below on supporting formulations. Saltwater marsh sediments can be a source of phosphorus release (Reddy et al., 1999) due to the presence of sulfates that are reduced to sulfide in the anaerobic sediments. Sulfides bind and precipitate with reduced iron (ferrous iron), thus, freeing phosphates to pore water that can diffuse into the water column. Therefore, the last term on the right hand side of **Equation (22)** was applied only for marsh

compartments that were saltwater marsh, or where the salinity was greater than 1.0 ppt. The release rate increases as water temperatures increase. The phosphorus release rate must be calibrated.

Dissolved Organic Phosphorus

The one source of DOP is dissolution of particulate organic phosphorus (POP) within DET, and the one sink is hydrolysis to TIP. The rate of change of DOP concentration due to this source and sink is stated as:

$$\frac{dDOP}{dt} = r_{pd} k_{dt}(TMP) DET - k_{hp}(TMP) DOP \tag{23}$$

where,

r_{pd} = stoichiometric ratio of mass of phosphorus to mass of DET

All other variables have been previously defined.

Detritus

The source of DET is algal mortality, and the sinks are settling and dissolution to dissolved organic matter. The rate of change of DET concentration due to this source and sinks is stated as:

$$\frac{dDET}{dt} = r_{da} k_{mp}(TMP) \frac{ALG}{1000} - \frac{v_d}{y} DET - k_{dt}(TMP) DET \tag{24}$$

where,

r_{da} = stoichiometric ratio of mass of DET to mass of Chl-a
$k_{mp}(TMP)$ = temperature-dependent phytoplankton mortality rate, day^{-1}
v_d = settling rate of DET, m/day

All other variables have been previously defined. It was assumed that the algal mortality rate includes predation and that predation ultimately results in formation of DET.

Algae

The source of phytoplankton (algae) biomass is photosynthesis or growth and the sinks are respiration, mortality, and settling. The rate of change of ALG concentration (as Chl-a) due to this source and sinks is stated as:

$$\frac{dALG}{dt} = \mu_p ALG - k_{rp}(TMP) ALG - k_{mp}(TMP) ALG - \frac{v_a}{y} ALG \tag{25}$$

where,

v_a = algal settling rate (m/day)

All other variables have been previously defined.

Water Age

Other teams working on modeling higher trophic levels required information regarding water contact time or transit time through various marshes and bays. This information was provided by modeling water age, which is an additional transported state variable. Water age was accounted for by including a source term of unity. Thus, the time rate of change of water age (AGE) due to this source term became:

$$\frac{dAGE}{dt} = \frac{Ss_{AGE}}{V} = 1.0 \tag{26}$$

The other terms in **Equation (16)** still apply as stated previously except there was no atmospheric deposition term. The initial condition at time 0 for AGE was 0.0 throughout the domains. The boundary conditions for AGE were also 0.0 on all inflowing boundaries at all times. Thus, as **Equation (16)** was integrated over time with the source of 1.0, the AGE of water in each compartment advances according to how long water has been in that compartment. If a compartment was never flushed or dispersed by water from adjacent compartments, then the AGE in that compartment would equal the length of the simulation period. Water age can vary over space and time. Thus, to provide a water contact time for a bay or marsh, it would be necessary to drive the model to a dynamic (repeating) steady-state condition and average AGE over the repetitive cycling time and over all compartments within the bay or marsh of interest, thus providing a bay-wide average contact time over the long-term (i.e., at dynamic steady-state). Since the models included only water level fluctuations to drive the hydrodynamics along the coastal boundary, it could take an unrealistically long time to flush large computational compartments located on the coastal boundary, which could lead to inaccurate water age in the interior of the model domain. Therefore, it was recommended that the water age for coastal boundary compartments be set to zero throughout the simulation.

Other Supporting Formulations

Other formulations were used in the model to support the source/sink terms discussed above. These formulations included stoichiometric relations, photosynthesis rates, temperature dependencies, phosphorus partitioning, ammonium preference, and others.

Stoichiometric Ratios

Stoichiometry is based on the Redfield ratios (Redfield et al., 1963), which state that the number of carbon (C), nitrogen (N) and phosphorus (P) molecules in aquatic plant and DET organic matter are:

106 C : 16 N : 1 P

Implementing the molecular weights of C, N, and P, changes the above relation to gram mass units or

41 g C : 7.2 g N : 1 g P

Carbon is approximately 40 percent of the dry weight of aquatic plant and DET organic matter. Also, the ratio of carbon mass to algal Chl-a mass is typically between about 50 and 100. With this information, the ratio relation can be extended to state:

100 g DET : 41 g C : 7.2 g N : 1.0 g P : 0.4 to 1.0 g Chl-a

Given this stoichiometric relation, the stoichiometric ratios presented in the previous sections can be derived. Since the mass of Chl-a is variable, r_{ca} (i.e., g carbon to g Chl-a) was used as an input calibration parameter. The stoichiometric derivations are shown below:

$$r_{na} = \frac{r_{ca}}{r_{cn}} = \frac{7.2}{41} r_{ca} = 0.176\, r_{ca}$$

$$r_{nd} = r_{nc} r_{cd} = \frac{7.2}{41}\frac{41}{100} = 0.072$$

$$r_{pa} = r_{pc} r_{ca} = \frac{1}{41} r_{ca} = 0.0244\, r_{ca}$$

$$r_{pd} = r_{pc} r_{cd} = \frac{1}{41}\frac{41}{100} = 0.01$$

$$r_{da} = r_{dc} r_{ca} = \frac{100}{41} r_{ca} = 2.44\, r_{ca}$$

Photosynthesis Rate

The photosynthesis rate, μ_p, was used in the formulations of ALG, TIP, NH4, and NO3 to estimate the amount of algal growth through photosynthesis. The PB model used the Michaelis-Menten formulations adopted by Thomann and Mueller (1987) and applied calibrated nutrient, salinity, and suspended sediment limitations to estimate the amount of algae growth (Roblin, 2008). The calibrated constants were KnSal = 1 ppt, KnSS = 50 mg/L, KnN = 20 µg/L, and KnP = 3 µg/L, where KnSal was the salinity limitation constant, KnSS was the suspended sediment limitation constant, KnN was the DIN limitation constant, and KnP was the phosphorus limitation constant. For more detail on these parameters and their use in the formulations of the PB model see Roblin (2008). The following photosynthesis equations were used only in the AA and CP models. The total (N fixing and non-N fixing) algal photosynthesis rate was calculated as:

$$\mu_p = k_{gp}(TMP)\varphi_{Np}\varphi_{Lp}\varphi_S \qquad \textbf{(27)}$$

where,

$k_{gp}(TMP)$	=	temperature-dependent maximum photosynthetic rate, day^{-1}
φ_{Np}	=	nutrient limitation factor, 0 – 1
φ_{Lp}	=	light limitation factor, 0 – 1
φ_S	=	salinity toxicity limitation factor, 0 – 1

The nutrient limitation factor was determined using the minimization approach with Michaelis-Menten kinetics and considers N fixation. The formulation for the nutrient limitation factor is as follows:

$$\varphi_{Np} = min\left[\frac{(1-f_{Nfix})DIN}{KHn+DIN} + f_{Nfix}, \frac{(1-F_{pp})TIP}{KHp+(1-F_{pp})TIP}\right] \quad \textbf{(28)}$$

where,

DIN	=	dissolved inorganic nitrogen, NH4 + NO3, mg/L
KHn	=	half saturation concentration for algal uptake of N, mg/L
KHp	=	half saturation concentration for algal uptake of P, mg/L

All other variables have been previously defined. The quantity $(1 - F_{pp})$ is the fraction of TIP in dissolved form (DIP) and is readily available for uptake.

The light limitation function requires determination of light attenuation in the water which follows the Beer-Lambert law shown below:

$$PAR(H) = PAR(0)e^{-k_e H} \quad \textbf{(29)}$$

where,

k_e	=	light extinction coefficient, m^{-1}
PAR(H)	=	photosynthetically available radiation (PAR) at depth H below the water surface, ly/day

The PAR at the water surface, *PAR(0)*, is a portion of the visible spectrum and thus was assumed to be a fixed fraction of the incident solar radiation at the water surface, *I(0)* (ly/day). This relation of surface water PAR and incident solar radiation is illustrated in **Equation (30)** below. A langley (ly) is equal to 1.0 calorie (cal)/cm^2, and 1 ly/day = 0.484 W/m^2.

$$PAR(0) = 0.47 * I(0) \quad \textbf{(30)}$$

Light extinction is related to material concentrations in the water by the following formulation:

$$k_e = k_{eb} + \alpha_i ISS + \alpha_0 DET + \alpha_p ALG + \alpha_{pn} ALG^{0.667} \quad \textbf{(31)}$$

where,

k_{eb}	=	background light extinction coefficient due to water and color, m^{-1}
ISS	=	inorganic suspended solids concentration, mg/L
α_i	=	light extinction coefficient due to inorganic suspended solids, L/mg/m
α_o	=	light extinction coefficient due to detritus, L/mg/m
α_p	=	light extinction coefficient due to Chl-a, L/µg/m
α_{pn}	=	light extinction coefficient due to Chl-a, $(L/\mu g)^{0.667}/m$

For these models, it was assumed that *ISS = TSS*. Suggested values for the extinction coefficients as provided in the QUAL2K documentation (Chapra and Pelletier, 2003) are listed in **Table 33**. It

is noted that the background coefficient k_{eb} was specified during calibration, but values typically fall within a given range.

Table 33 Suggested Values of Light Extinction Coefficients due to Material Concentrations

Extinction Coefficient	α_i	α_o	α_p	α_{pn}
Value	0.052	0.174	0.0088	0.054

Steele's equation, shown below, was used for algal growth due to PAR with photo-inhibition.

$$F_{Lp} = \frac{PAR(H)}{K_{Lp}} exp\left[1 - \frac{PAR(H)}{K_{Lp}}\right] \quad \textbf{(32)}$$

where, F_{Lp} was the normalized algal growth relationship as dependent on light, and K_{Lp} was the light or PAR (ly/day) at which phytoplankton growth is optimal. The variable F_{Lp} increases from 0 for no light to a maximum of 1.0 when *PAR(H)* equals K_{Lp}, and then decreases back towards 0 as light increases above the optimal light. **Equation (29)** can be combined with **Equation (32)** and integrated over water depth and over a day to yield the algal light limitation factor shown below.

$$\varphi_{Lp} = \frac{2.718f}{k_e H}\left[exp\left(\frac{-PAR_a(0)e^{-k_e H}}{K_{Lp}}\right) - exp\left(\frac{-PAR_a(0)}{K_{Lp}}\right)\right] \quad \textbf{(33)}$$

where, $PAR_a(0)$ was the average photosynthetic light intensity over the daylight hours at the water surface, H was the water depth integrated over, f was the fraction of a day that is daylight, and all other variables have been defined previously.

Blue-green algae can form large blooms even in fairly turbid water due to their floatation abilities. However, it is noted that the computed Chl-a concentrations were depth-averaged quantities, not surface concentrations.

The fraction of daylight f varies from about 0.42 to 0.58 and was output by the heat exchange program that computes K_E and TMP_E for temperature modeling and solar radiation. Incident short wave solar radiation is often measured directly at meteorological stations. It can also be calculated from the site location, time of year, and cloud cover, which was the case with the heat exchange program mentioned above. The heat exchange program outputted daily average incident short wave radiation $I_{da}(0)$ (W/m^2) and the fraction of day that is daylight (f). Thus, it was necessary to calculate $I_a(0)$ for estimating $PAR_a(0)$ for use in **Equation (33)** with the relation shown in **Equation (34),** where the constant 0.484 has units of (W/m^2)/(ly/day) and was needed to convert $I_{da}(0)$ from W/m^2 to ly/day (units of $I_a(0)$).

$$I_a(0) = \frac{I_{da}(0)}{0.484f} \quad \textbf{(34)}$$

Emergent vegetation in the marshes essentially shuts out most light incident on the water surface, thus, greatly limiting algal growth in the marshes. For marsh compartments, it was necessary to multiply φ_{Lp} by the fraction of open water since it was assumed that marsh vegetation would shade out all light. Thus, for a marsh compartment that was 100 percent marsh, the light limitation function was 0.

Salinity toxicity limitation on growth was included since some blue-green algae cannot tolerate salt. *Anabaena and Microcystis sp.* are two fairly common blue-green algae that are found in freshwater and in estuaries with low salinity. The growth of these algae has been found to be limited by salinity as low as 1 to 2 ppt. In the AA and CP regions, the following salinity limitation function φ_S was adopted from the CE-QUAL-ICM model (Cerco and Cole, 1993).

$$\varphi_S = \frac{SAL_{tox}^2}{SAL_{tox}^2 + SAL^2} \tag{35}$$

where, SAL was salinity (ppt) and SAL_{tox} was the salinity at which algal growth was halved. A value for SAL_{tox} = 2 ppt was suggested. The square function causes the limitation factor to decrease more sharply with increasing salinity than does the usual Michaelis-Menten function.

Temperature Dependencies

The temperature effect for all first-order reactions used in these models is represented by **Equation (36)** below.

$$k(TMP) = k(20)\theta^{(TMP-20)} \tag{36}$$

where, $k(TMP)$ was the reaction rate (day^{-1}) at ambient water temperature TMP (^{o}C), and Θ was the temperature coefficient for the reaction. The input rate parameter $k(20)$ is the reaction rate at 20 ^{o}C. The temperature coefficients required by the model and their recommended values are shown in **Table 34**. These values were set in the model code and were not part of the input files.

Table 34 Temperature Rate Coefficients for the Eco-Hydrology Models

Coefficient	Rate Process	Recommended Value
Θ_n	Nitrification	1.085
Θ_{dn}	Denitrification	1.05
Θ_{hn}	DON hydrolysis	1.047
Θ_{gp}	Algal growth	1.066
Θ_{rp}	Algal respiration	1.08
Θ_{dt}	Detritus dissolution	1.02
Θ_{hp}	DOP hydrolysis	1.047
Θ_{mp}	Algal mortality	1.047

Coefficient	Rate Process	Recommended Value
Θ_{RPO4}	Marsh sediment release of PO_4	1.085

Phosphorus Partitioning

It was assumed that the distribution of TIP between suspended solids and water due to adsorption could be adequately described through linear, reversible, equilibrium partitioning. Inorganic P actually is best described with a Langmuir partitioning relationship, but such a relationship would require iterative solutions. Linear partitioning is reasonable for low concentrations of dissolved inorganic P (DIP).

The adsorption distribution coefficient K_d (L/kg) is defined as the ratio of chemical concentration adsorbed onto solids (mass chemical per mass solids) to concentration of chemical dissolved in water (mass chemical per volume of water). Linear, reversible, equilibrium partitioning assumes that the value of K_d is constant regardless of the dissolved chemical concentration.

The fraction of TIP that is in particulate form in the water column, F_{pp}, can be computed from K_d and the TSS concentration as shown in **Equation (37)**.

$$F_{pp} = \left(\frac{K_d}{1.0E6}TSS\right) \Big/ \left(1 + \frac{K_d}{1.0E6}TSS\right) \tag{37}$$

The value of K_d for phosphate (both dissolved and adsorbed) was an input parameter for the models. The distribution coefficient for phosphate can vary widely, but a value of about 1000 L/kg is in the range of values that have been measured. With this value and a TSS concentration of 100 mg/L, the value of F_{pp} was 0.09. Much higher values of K_d, such as 80,000 L/kg, have been measured. This value with 100 mg/L TSS would result in an F_{pp} of 0.89. Thus, the value of K_d can have a profound effect on the amount of particulate inorganic phosphorus in the water column, which greatly affects the amount settled on the bottom.

Ammonium Preference

The formulation used for determining the preference for algal uptake of NH4 over NO3 is illustrated in **Equation (38)**.

$$P_{ap} = \frac{NH4 * NO3}{(KHn + NH4) * (KHn + NO3)} + \frac{NH4 * KHn}{(NH4 + NO3 + 0.001) * (KHn + NO3)} \tag{38}$$

All variables have been previously defined. A small number (0.001) has been added to the denominator of the second term of **Equation (38)** so that there would not be division by zero for any case where both NH4 and NO3 were zero.

Deposition and Resuspension

The sediment in the models was either in the water column as TSS and could be deposited or it was on the bed and could be resuspended. The supporting formulations for sediment deposition and resuspension are presented in this section. The baseline deposition rate, v_{s0}

(m/s), was estimated with the Krone (1962) formulation, which is based on the concentration of TSS in the water column. This formulation is shown in **Equation (39)**.

$$v_{s0} = Kr_c \left(\frac{TSS}{1000}\right)^{1.33} \tag{39}$$

where, Kr_c was Krone's coefficient and all other variables have been previously defined. A recommended value of the Krone's coefficient was 0.0003. The deposition rate increases due to flocculation associated with salinity. An empirical formulation including salinity based on the modeling of TSS in Lake Pontchartrain by McCorquodale et al (2009) was used to define a salinity factor f_{sal} (dimensionless). **Equation (40)** illustrates the salinity factor formulation.

$$f_{sal} = min\left[\frac{\left(1 + 2\frac{SAL^2}{SAL_{cr}^2}\right)}{2}, 1.5\right] \tag{40}$$

where SAL_{cr} was a critical value of salinity above which there was no increase in flocculation. A value of 5 ppt was recommended for the critical salinity based on the Lake Pontchartrain modeling. The resulting deposition rate including the salinity effects that was used in the TSS source/sink term was calculated using **Equation (41)**.

$$v_s = v_{s0} f_{sal} \tag{41}$$

where, v_s was the resulting deposition rate in m/s that took into account salinity flocculation effects.

To limit deposition and prevent compartments from completely filling up in the Wax Lake Outlet and Atchafalaya Delta of the AA model, a deposition reduction factor was applied. This factor is described in **Equation (42)**, and it was a function of the minimum depth, H_{min}, which is the smallest depth that will allow water conveyance. The formulation for the minimum conveyance depth is illustrated in **Equation (43)** and cannot drop below the dry depth.

$$RFS = max\left[0\,, min\left[1\,, \frac{H - H_{min}}{3 * H_{min}}\right]\right] \tag{42}$$

$$H_{min} = \frac{\sum Q_{in}}{V_{cr} * \sqrt{As}} \tag{43}$$

where,

RFS	=	reduction factor for sediment deposition
H_{min}	=	minimum depth required to keep room for water conveyance, m

$\sum Q_{in}$	=	sum of all inflows to a compartment, m^3/sec
V_{cr}	=	critical velocity above which no deposition occurs, m/sec

The critical velocity, V_{cr}, was a calibration parameter based on historical accretion in deltas. It was set at 1 m/sec in the AA model. The deposition rate in the AA model was calculated as v_s * RFS for each compartment. The dynamic water depth at each time step was computed as the water depth at the previous time step minus the net sediment accretion depth. However, the dynamic depth as affected by accretion was used only for computing the RFS, and it was not used in the hydrodynamic solutions for compartment advective flows and water stage.

The formulation for the resuspension flux E_{res} (g/m^2/day) was based on other similar models for resuspension except that the square of the wind speed was used as a surrogate for bottom shear stress. The two formulations for estimating the resuspension flux as a function of wind speed are shown in **Equations (44)** and **(45)** below.

$$E_{res} = \rho_b v_{r0} \left(\frac{W^2}{W_{cr}^2} - 1 \right)^n (1 - f_{marsh}) \quad \text{for } W > W_{cr} \tag{44}$$

$$E_{res} = \rho_b v_{r0} (1 - f_{marsh}) \quad \text{for } W < W_{cr} \tag{45}$$

where,

ρ_b	=	bed sediment dry bulk density, g/m^3
v_{r0}	=	base resuspension rate, m/day
W	=	wind speed, m/sec
W_{cr}	=	critical wind speed for resuspension above base resuspension, m/sec
n	=	empirical exponent

The product of the bulk density and base resuspension rate results in a calibration parameter C_r (g/m^2/day) for resuspension. The critical wind speed was also a calibration parameter. A value of 1.75 was suggested for n based on other models. The resuspension flux was multiplied by the fraction of compartment open water since resuspension was assumed to be nearly zero for the part that was marsh. The above resuspension and deposition formulations were used only for the marsh compartments. The TSS source/sink terms were assumed to be zero in the channel compartments, where deposition and resuspension were assumed to be in balance.

Variable Nitrification Rate

The nitrification rates varied with ambient conditions, particularly water depth. Shallow water allows more frequent contact of the water column with the benthic sediments, which serves as a substrate for nitrifying bacteria. Dortch et al. (1992) developed a nitrification rate relationship based on water flow velocity and depth. That relationship was adapted for the present model, where the nitrification rate at 20 degrees C, $k_n(20)$ (day^{-1}), was computed from **Equation (46)**.

$$k_n(20) = \frac{0.4}{H}$$

(46)

where, H was the water depth in meters. A lower and upper bound of $k_n(min)$ and $k_n(max)$, respectively, were placed on the computed nitrification rate.

Variable Detrital Settling Rate

A variable settling rate for detritus v_d (m/day) was applied to account for the amount of marsh present in each compartment. This variable settling rate was used as follows,

$$v_d = v_{d0} f_{marsh}$$

(47)

where, v_{do} was the input value of v_d for full marsh or swamp and f_{marsh} was the fraction of compartment surface area that was either marsh or swamp. Thus, if a compartment was 100 percent open water (i.e., $f_{marsh} = 0$), the detrital settling rate was zero. The detrital settling rate is actually a net deposition rate, and when it is zero, it means that deposition is balanced by resuspension. For channels, a single settling rate was applied even when there was no marsh or swamp.

Derived Variables

After solving for the state variables discussed above, the following derived variables were easy to estimate:

$PON = r_{na} ALG/1000 + r_{nd} DET = 0.176\ r_{ca}\ ALG/1000 + 0.072\ DET$
$TN = NO3 + NH4 + DON + PON$
$POP = r_{pa} ALG/1000 + r_{pd} DET = 0.0244\ r_{ca}\ ALG/1000 + 0.01\ DET$
$TP = TIP + DOP + POP$
Dissolved inorganic phosphorus (*DIP*) = $(1 - F_{pp})TIP$
$TKN = NH4 + DON + PON$
Filtered $TKN = NH4 + DON$
$POC = r_{ca} ALG/1000 + r_{cd} DET = r_{ca} ALG/1000 + 0.41\ DET$
$DOC = r_{cn}\ DON = r_{cd}\ r_{dn}\ DON = 41/100 \times 100/7.2\ DON = 41/7.2\ DON = 5.69\ DON$

Additionally, the amount of nitrogen fixed (N_{fixed}, mg/L/day) from the atmosphere was determined from **Equation (48)**.

$$N_{fixed} = f_{Nfix} \mu_p r_{na} \frac{ALG}{1000}$$

(48)

where, all variables were previously defined.

The rate of change of the mass of nitrogen removed per unit area via sediment denitrification, *NRM*, was calculated for each model compartment and for each time step from **Equation (49)**.

$$\frac{dNRM}{dt} = k_{dn}(TMP) * NO3$$

(49)

The rate of change of the mass of *TSS* accreted per unit area, *ACC*, was computed for each model compartment and for each time step from **Equation (50)**.

$$\frac{dACC}{dt} = v_s TSS - E_{res}$$

(50)

All variables in **Equations (49) – (50)** were previously defined, and the water quality state variable on the right–hand side of each of these equations took the value from the previous time step to compute the variable on the left-hand side for the present time step. It should be noted that *ACC* was turned off (i.e. set to zero) when a compartment was *dry* (**Figure 31**) because there was theoretically no water present in the compartment for sediment to be accreted.

It is emphasized that the nitrogen fixation flux defined by **Equation (48)** provided values at any given time step; thus, these values varied over time and were not annual averages. The other two fluxes, *NRM* and *ACC*, were integrated over time to become cumulative fluxes (e.g., accreted mass per unit area per year) that provided the total mass accumulated up to that point in time.

All boundary concentrations from observed measurements were in the proper form for direct input for water quality state variable loadings except for *TIP*. Stations typically measure phosphate or *DIP*, thus, this boundary condition input was converted to *TIP* to be consistent with the modeled state variable. The conversion to *DIP* is shown in **Equation (51)** below.

$$TIP = \frac{DIP}{(1 - F_{pp})}$$

(51)

where, all variables were previously defined. The boundary concentration of *TSS* was used to compute F_{pp} when computing boundary *TIP*.

Additional Information

During model calibration the AA model tended to under-predict *TPH* for the coastal marsh compartments. Variations in calibration parameters could not correct this problem. It was believed that a refractory form of particulate inorganic phosphorus (*PIP*) in benthic sediments was re-suspended along the coast. Total phosphorus includes inorganic and organic forms, each with phases of particulate and dissolved. For these models, inorganic P was assumed to be PO_4 (or *DIP*) which is a transported state variable and could adsorb to *TSS*, thus partitioning between particulate and dissolved phosphate. Phosphate is considered labile and readily available for plant uptake. However, there are other mineral forms of inorganic P that are refractory and generally remain in a particulate or rock-like form. It was suspected that some of the *TPH* measured within the modeled domain could contain refractory, inorganic, particulate P. Such a

form of P would correlate to *TSS* values. As a result, the calculation of *TPH* was performed as follows:

$$TPH = TIP + DOP + 0.0244 r_{ca} \frac{ALG}{1000} + 0.01 DET + f_{rp} TSS \quad \textbf{(52)}$$

where, *TIP* was the total concentration (particulate and dissolved) for the labile form of inorganic P (phosphate), and f_{rp} was the fraction of *TSS* that was refractory, inorganic, particulate P. The addition of the last term in the above equation for deriving *TPH* had no effect on any of the reacting state variables. The value of f_{rp} was set to 0.002 for open water and marsh compartments, and f_{rp} was set to 0.0005 for channel compartments.

b. Description of System Being Represented by the Model

The domain for the PB model encompassed both the Pontchartrain and Barataria Basins. The Terrebonne Basin was included but only to provide a boundary condition for the Barataria Basin; thereby enabling exchange between the Barataria and Terrebonne Basins, as well as between the Terrebonne Basin and the Atchafalaya River. It included the Northern Gulf of Mexico (NGOM) from Point Au Fer Island, LA, to Gulf Shores, AL. The northernmost border stretched from Lake Pontchartrain in Louisiana and along the coastlines of Mississippi and Alabama; the southernmost boundary extended offshore to the Continental Shelf in the Gulf. Multiple rivers discharge into the domain including : the Amite, Tangipahoa, Tickfaw, Pearl, Tchefuncte, and Mississippi Rivers in LA; the Wolf, Pascagoula, and Biloxi Rivers in MS; the Tensaw and Mobile Rivers in AL; and multiple smaller, ungauged rivers within the domain. All of the existing diversions from the Mississippi River to the Barataria and Pontchartrain Basins were included. **Figure 35** defines the compartment boundaries and identifies the compartment numbers.

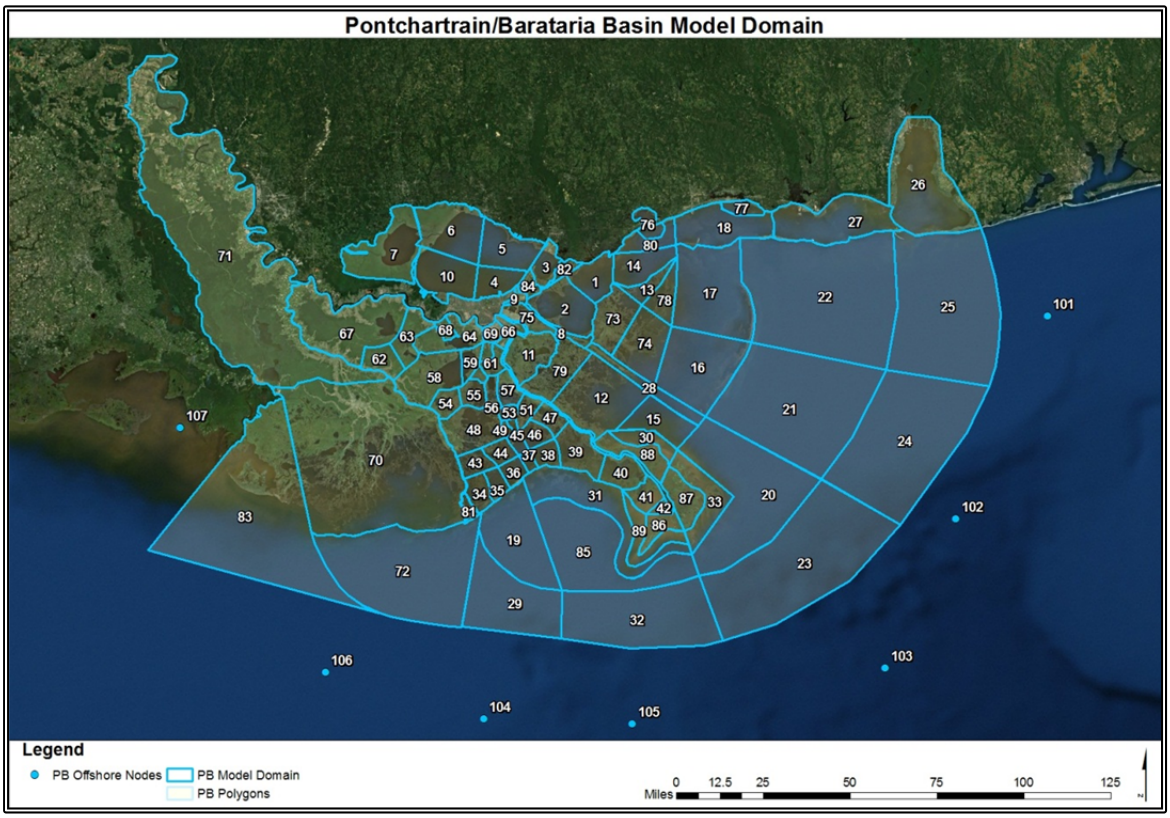

Figure 35 Pontchartrain/Barataria Basin Model Domain

The Pontchartrain Basin stretched over the Florida Parishes[43] of Louisiana in the Gulf Coast Plain and the entire Mississippi Delta Plain (**Figure 36**). As one of the largest estuaries in the NGOM, the Pontchartrain Estuary includes more than 12,000 km^2 of southeast Louisiana (Georgiou, et al., 2009). The upper Pontchartrain Estuary is composed of three lakes (from west to east - Maurepas, Pontchartrain, and Borgne). Natural tidal channels and artificial navigation

[43] The Florida Parishes consist of any parish north of Lake Pontchartrain and east of the Mississippi River in Louisiana. These parishes were part of West Florida in the 18th and early 19th centuries. They include East Baton Rouge, East Feliciana, Livingston, St. Helena, St. Tammany, Tangipahoa, Washington, and West Feliciana.

complexes connect these lakes and they were all represented in the model. The estuary occupies a shallow depression between the alluvial ridge of the Mississippi River to the west, the sloping uplands to the north, the Pearl River basin to the east, and the Mississippi Sound to the southeast (Kindinger, 1988; USACE NOD, 1982). Two natural tidal passes connect these lakes to the Breton, Chandeleur, and Mississippi Sounds: the Rigolets (opening into Lake Borgne/Western Mississippi Sound) and the Chef Menteur (opening into Lake Borgne).

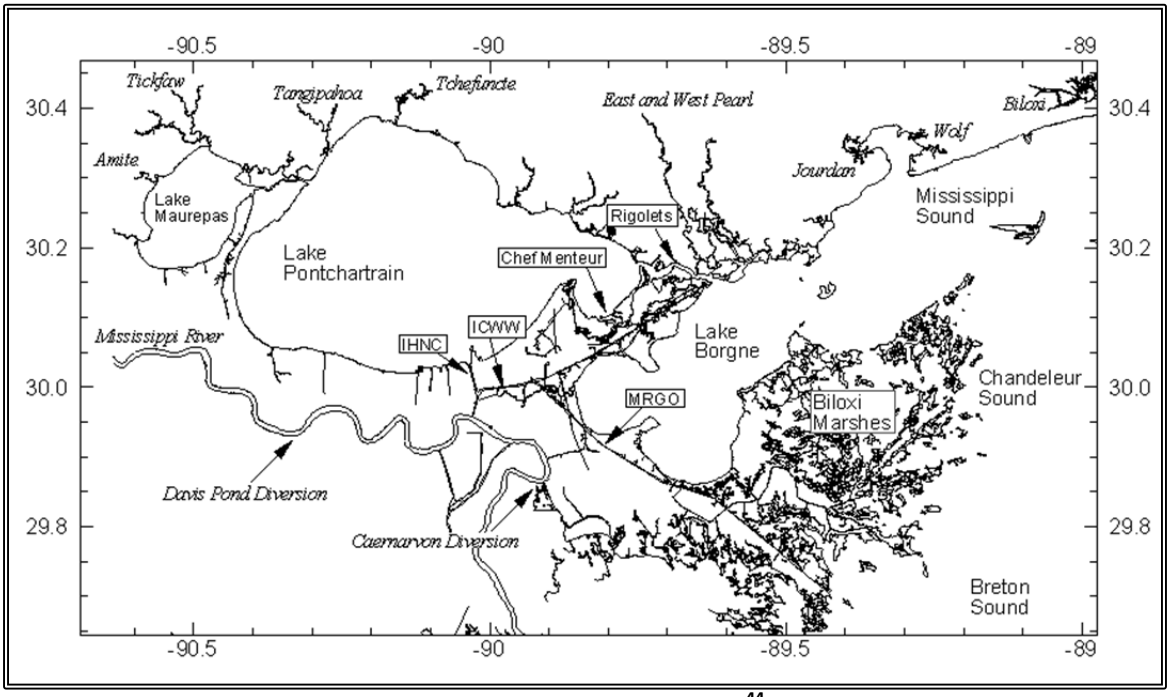

Figure 36 Map of Upper and Central Pontchartrain Estuary[44] (Figure from Schindler, 2010; Adapted from Georgiou et al., 2009)

Additionally, an artificial navigation canal, the Inner Harbor Navigation Canal (IHNC), is located on the south of Lake Pontchartrain and opens into the Intracoastal Waterway (ICWW) and the Gulf of Mexico through the Mississippi River Gulf Outlet (MRGO). The MRGO, authorized by the River and Harbor Act of 1956 as an alternate navigation route to the port of New Orleans, was constructed from 1958 through 1968. It was de-authorized in 2009 due to a number of channel enlargements caused by factors such as shoreline erosion by tidal currents and vessel wakes, saltwater intrusion, increased conveyance during storms, and other negative effects (LPBF, 2006). Prior to the MRGO closure, flow distribution among the three main passes during spring tides (IHNC, Chef Menteur, and the Rigolets) was approximately 6%, 30%, and 64% respectively (Haralampides, 2000).

The Barataria Basin was bordered by Bayou Lafourche on the west and the Plaquemines delta lobe to the east (**Figure 37**). The sediment transported through these distributary headlands formed the barrier islands between Barataria Bay and the Gulf as well as the area's beach ridge/Chenier systems (FitzGerald et al., 2007; Georgiou et al., 2010). Caminada Pass, Barataria Pass, Pass Abel, and Quatre Bayou are the principal tidal inlets that control the flux of water and

[44] River names are shown in italics.

nutrients between Barataria Bay and the Gulf. Additionally, tidal channels connect Barataria Bay to a series of oligohaline lakes by way of tidal channels known as bayous. The region is comprised of extensive wetlands that transition from saltwater to freshwater marsh along the modern salinity gradient.

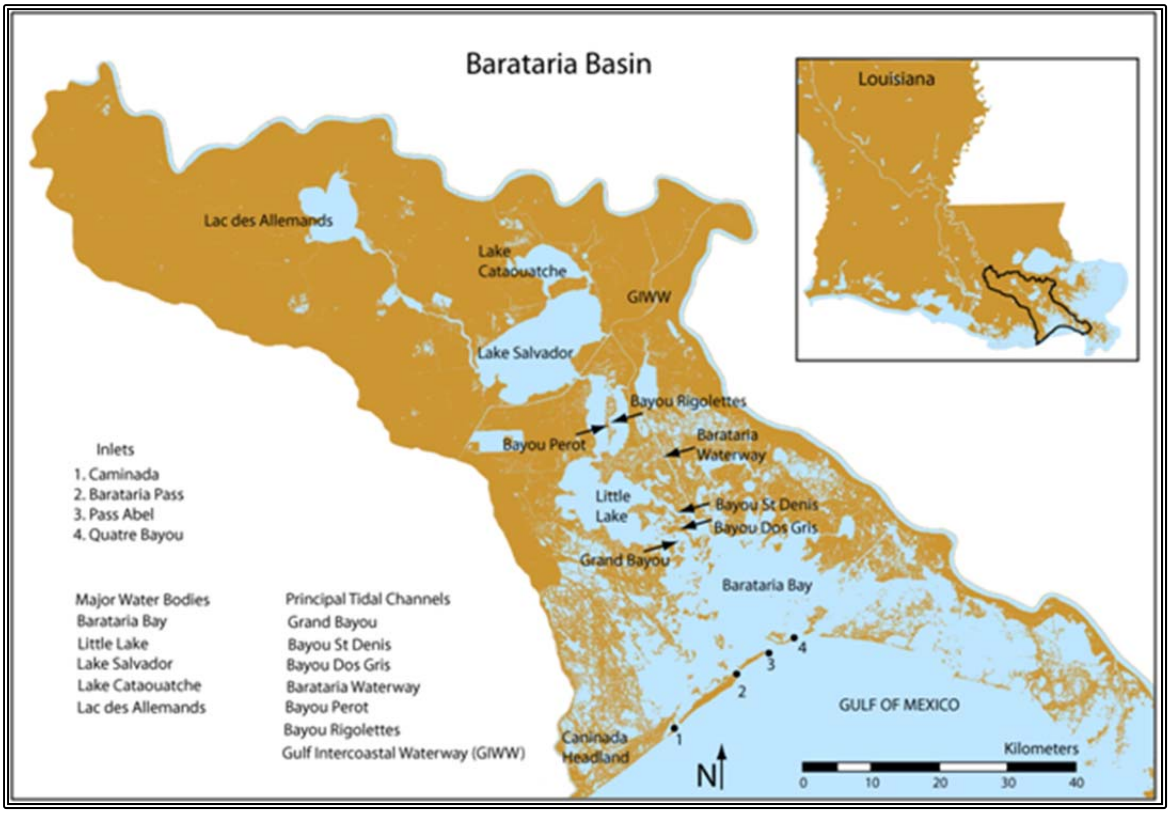

Figure 37 Principal Hydrodynamic Features within the Barataria Basin for the PB Model (Georgiou, et al., 2010)

The Atchafalaya Basin model was situated between the Pontchartrain/Barataria and Chenier Plain Basins. The AA model domain extended from West Cote Blanche Bay to Bayou Lafourche and from just north of I-10 to offshore in the Gulf of Mexico spanning a total of approximately 7,700 square miles. The Atchafalaya River extended a total of approximately 100 miles from the north end of the model domain to the Gulf of Mexico. **Figure 38** illustrates the domain of the AA model.

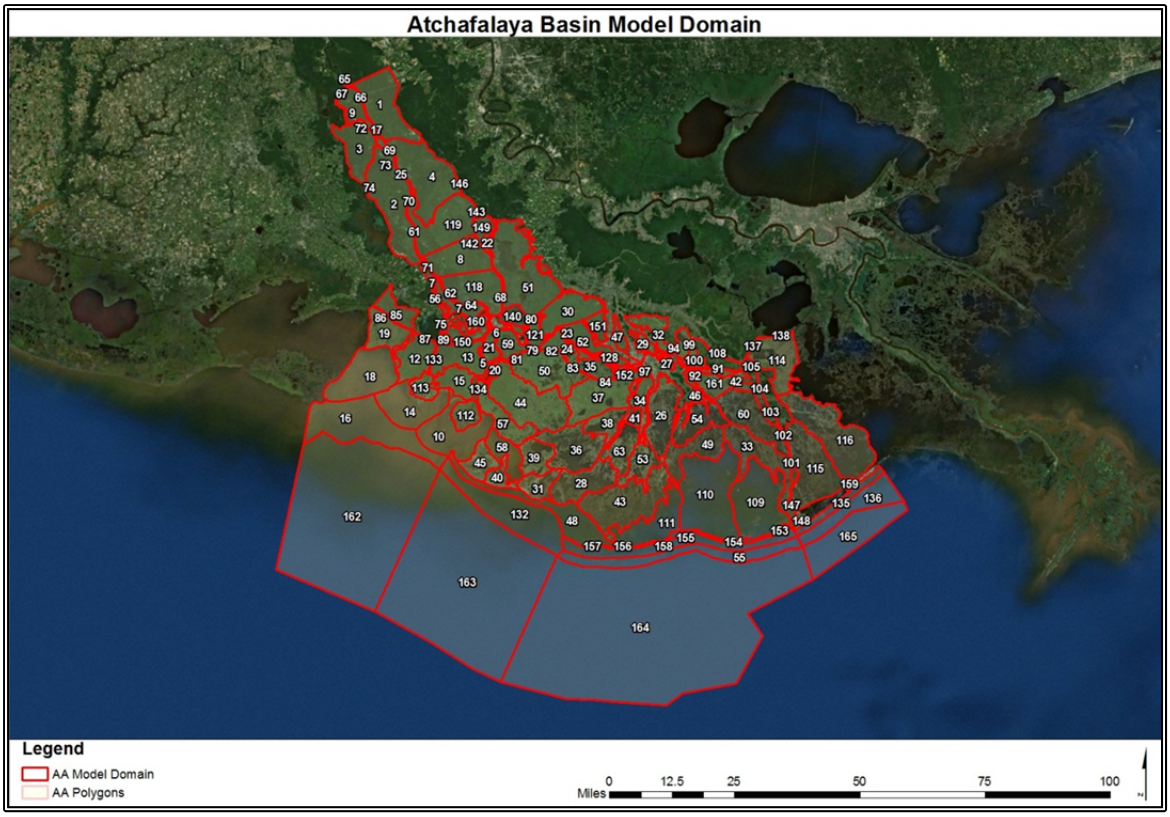

Figure 38 Atchafalaya Basin Model Domain

Hydrology throughout the basin is strongly influenced by the flow of the Atchafalaya River. The River begins approximately 57 miles north of the model boundary at the confluence of the Red River and the outlet channel from the Old River Control Structure (ORCS). Diversion of water from the Mississippi River to the Atchafalaya is regulated by the USACE using the ORCS.

The Upper part of the Atchafalaya River Basin is delineated by flood protection levees; the levees are set back approximately 6 miles from and run parallel to the Atchafalaya River. There is also a natural levee system adjacent to the main stem of the Atchafalaya River. The main stem is also connected to an intricate network of bayous and channels that run throughout the floodplain. Land use in the upper basin is characterized predominantly by forested swamplands. The model domain also included a portion of the Terrebonne Basin, east of the Atchafalaya River East levee and north of the GIWW. This region includes Lake Verret and Lake Palourde. The lower part of the model domain was comprised predominantly of low lying marsh and open water areas susceptible to inundation and flooding. At Six Mile Lake a portion of the Atchafalaya River is diverted directly to the Gulf via Wax Lake Outlet. Given the tremendous sediment load in the Atchafalaya River system to the areas, the Lower Atchafalaya River Delta and Wax Lake Outlet Delta were two areas in the AA model domain with the highest potential for land building.

The Atchafalaya River as well as other major channels (Wax Lake Outlet, the GIWW, Bayou Lafourche) were represented by a combination of compartments and links in the model. Links were used to simulate the connectivity from the major channels to adjacent floodways and

wetlands areas. A single link was used to represent cumulative connectivity of several smaller channels.

A number of flood control and navigation structures were situated within the AA model. The structures of the upper basin included: Bayou Sorrel Lock which is located in the northeast and is operated for both flood control and navigation; Bayou Courtableau Control Structure which is a drainage structure in the northwest portion of the basin; and Bayou Charenton Control Structure which is a local floodgate. The following structures were located in the lower part of the basin: the West and East Calumet floodgates which control the flow of water from Wax Lake Outlet to Bayou Teche (target elevation with Bayou Teche is 2.7 ft NGVD); Berwick lock which allows control of water levels on the Bayou Teche as well as provides for navigation to the Atchafalaya River; and Bayou Boeuf Lock situated in Morgan City which regulates flow and allows for navigation along the GIWW to the East. Additionally, there are control structures at Bayou Terrebonne and Bayou Petit Caillou near Lapeyrouse. However, given the limited knowledge of the operation of the structures and the coarse size of the hydrologic units, although the structures were included in the model, the operational controls of them were not simulated.

The Chenier Plain region extended about 240 km (150 mi) from just west of the Louisiana-Texas border and Sabine Lake to West Cote Blanche Bay (**Figure 39**). The GIWW running from east to west was included just south of the model's northern boundary. The Gulf of Mexico formed the southern boundary.

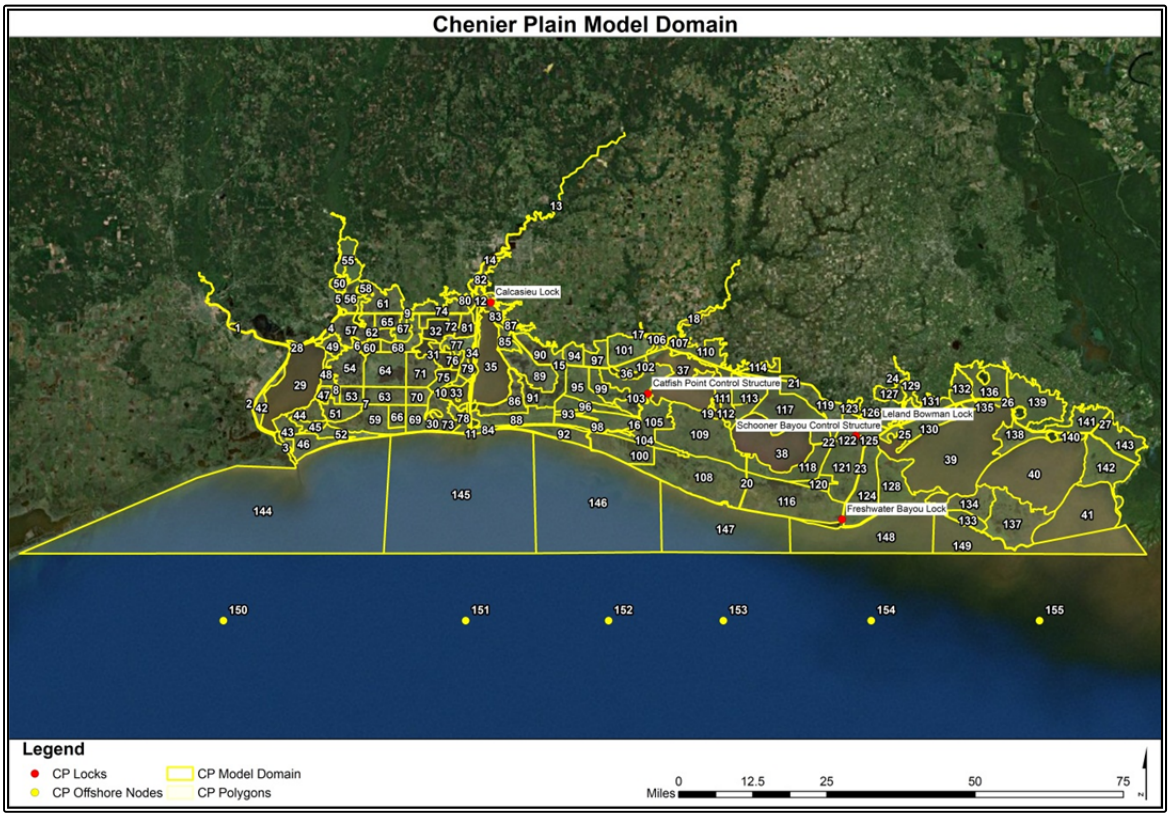

Figure 39 Chenier Plain Model Domain

The Calcasieu/Sabine, Mermentau, and Teche/Vermilion Basins made up the CP domain. The region contains six (6) large bodies of water: Sabine Lake, Calcasieu Lake, Grand Lake, White Lake, Vermilion Bay, and East and West Cote Blanche Bay; six (6) major river systems flowing into the system from the north: Neches River in Texas, Sabine River on the Louisiana-Texas border, Calcasieu River, Lacassine River, Mermentau River, and the Vermilion River; and an intricate network of channels and canals. The Sabine Ship Channel, Calcasieu Ship Channel, GIWW, and Freshwater Bayou are major waterways used for navigation. The Sabine Pass, Calcasieu Pass, Mermentau River, Freshwater Bayou, Southwest Pass of Marsh Island, and East Cote Blanche Bay connected the inland model area to the Gulf of Mexico.

The Calcasieu/Sabine basins are mainly north-south flowing basins influenced by the Calcasieu, Sabine, and Neches Rivers and the Gulf of Mexico tide with the GIWW allowing some east-west movement. When the riverine flows are low, the deep Sabine Navigation Water Way (SNWW) and the Calcasieu Ship Channel (CSC) allow the saline water of the Gulf to intrude well inland into the lakes and marshes. When the river flows are high, the sediment mainly travels south straight into the Gulf due to the deep channels.

The Mermentau basin is protected from saltwater and tidal intrusion by the natural chenier ridges and the operation of five USACE locks and control structures: Calcasieu Lock on the GIWW east of the Calcasieu River, Catfish Point Control Structure south of Grand Lake on the Mermentau River, Leland Bowman Lock on the GIWW west of Freshwater Bayou, Schooner Bayou Control Structure on Schooner Bayou west of Freshwater Bayou, and Freshwater Bayou Canal Lock on Freshwater Bayou just north of its connection to the Gulf. The operation of the locks on the GIWW is heavily influenced by barge traffic. Since the water in this basin remains relatively fresh, farmers pump large amounts of it into their crops and return it throughout the year.

The Teche/Vermilion basin is comprised mainly of Vermilion Bay and East and West Cote Blanche Bay. The Vermilion River, Bayou Teche via Charenton Drainage Canal, and the Atchafalaya River via GIWW and the Gulf contribute freshwater to the area. The tide of the Gulf is mostly blocked by Marsh Island although it flows into Vermilion Bay through a rather deep Southwest Pass and into East Cote Blanche Bay passing through the Atchafalaya River plume (Meselhe et al., 2008).

c. Analytical Requirements

ArcGIS and Google Earth Pro were used to identify surface features of the model domains so that they could be appropriately accounted for in the models. For example, the models designated which compartments were lakes or bays by giving them a percent land of zero.

Light Detection and Ranging (LiDAR) data was used to capture the marsh and land elevations. LiDAR is a complex system of airborne instruments which employ an airborne/ground-based GPS in inertial measurement units (IMU), and an active laser sensor as the source to measure distances (ranging) and angles to specific and densely-spaced points (between 2 to 6 m) on the ground (Cunningham et. al, 2004). In addition, Cunningham et al. (2004) state that the laser ranging device is sensitive to 0.3 ft elevation change, which would support its use in the present case. LiDAR vertical data used in the model were given in NAVD 88 feet with the horizontal coordinates given in meters relative to the North American Datum (NAD 1983) horizontal datum under the UTM-15 projection system. The laser does not penetrate through water surfaces and therefore does not capture lake and riverbed elevations.

Bathymetry data was used to capture the elevations of land covered with water for the lakes (bed elevations) and channels (cross-sections). Bathymetry data were obtained through physical surveys, National Geophysical Data Center's U.S. Coastal Relief Model, NOAA Estuarine Bathymetry, NOAA OCS Navigational Charts, and the ADCIRC Grid.

Hydraulic structures were modeled using the existing physical dimensions and attributes. The operation schedules of the locks were captured in the model using the number of hours per day the lock was open. Dividing the number of hours open per day by the total hours per day yields the percentage the lock is open per day. This percentage was multiplied by the calculated flow across the lock assuming 100% open. The resulting flow represented the amount of flow across the lock for the given operation.

The models were based on the mass-balance concept. They also emulated the process of flow exchange between lakes, channels, open water, and marsh. The physical processes captured in the models along with the geometrical details of the physical system, allowed the models to be a realistic representation of the real world system.

d. Assumptions

Several assumptions were required in order to successfully model the hydrodynamics and water quality of the coastal domains. Below is a brief description of the assumptions made:

- All variables changed with respect to time, but they were all uniform in space within a compartment.
- The models were run on a long-term basis (decadal runs) instead of a hydrologic event basis (e.g. hours or months). Further, the results were integrated spatially over large compartments. Under these circumstances, the momentum exchange did not play a primary role. Even if it had been taken into account, its impact would be lost for these temporal and spatial averaging. Therefore, the momentum exchange between channels and open water, lakes or marshes was assumed negligible.
- Sediment accretion in channels was assumed to be zero because it was difficult to represent the narrow canals in the 30 mx30 m DEM. Therefore, it was difficult to calculate the change in bed elevation for the 25-year update. This assumption would not affect the capacity of the channels and their ability to convey flow.
- A deposition reduction factor was applied to limit deposition and prevent compartments from completely filling up (AA model only).

One of the tasks of the 2012 Coastal Master Plan was to create planning-level models that could implement multiple proposed projects in order to estimate their general effects on the ecosystem. The types of projects proposed for the master plan were geared towards protection and restoration of the Louisiana coast. These restoration and protection projects included marsh creation, hydrologic restoration (locks and saltwater barriers), ridge restoration, barrier island restoration, diversions, channel re-alignments, oyster barrier reefs, and hurricane protection. Below is a description of how each of these projects was incorporated into the Eco-Hydrology models for the model simulations:

Marsh Creation projects – updated compartment elevations and percentage of land based on Wetland Morphology outputs.

Hydrologic Restoration projects – added additional linkage with proposed channel depth and width, modified existing linkage depth and width, adjusted flow based on control structure operation, and/or increased land areas.

Ridge Restoration projects – cut off flow linkages between affected compartments when the ridge falls along the compartment boundary, cut off flow linkages between affected compartments when the ridge falls inside the compartment boundary, increased Manning's *n* for linkages between affected compartments when the ridge falls inside a compartment, or adjusted compartment elevations and percentage of land based on Wetland Morphology outputs.

Barrier Island Restoration projects (PB and AA only) – adjusted flow linkages in the vicinity of barrier islands and updated compartment elevations and percentage of land based on Wetland Morphology outputs.

Diversion projects (PB and AA only) – added additional inflows at boundaries, added additional linkages between diversion intake and release compartments, or redistributed flows on existing linkages. Linkage capacities affected by diversions were increased to tolerate the larger flow conditions. In the PB model, the percent flow was based on HEC-RAS modeling of the Mississippi River (Davis, 2010) and the percent sediment was prorated to the river flow squared. For large diversions, it was assumed that the water will flow in a fan-like or deltaic pattern towards the Gulf. In the AA model, the diverted flow was based on the flow condition in the water source location and the diverted sediment concentration was assumed to be the same as the concentration of the source. Unless specified, it was assumed that the Old River Control Structure would maintain its existing operation with 70% to the Mississippi River and 30% to the Atchafalaya River.

Channel Re-alignment projects (PB and CP only) – For the PB model, Mississippi River flow was distributed to nearby compartments similar to diversion projects; linkages connecting the nearby compartments and linkages connecting to downstream compartments were increased to permit the additional flow and to allow it to move towards the Gulf; and the flow distribution in the River downstream of the re-alignment was zeroed out to simulate closure of the River. It was assumed that the water would flow in a deltaic pattern towards the Gulf. For the CP model, the channel compartment was re-delineated to include the new alignment of the channel. The old channel segment became a new channel compartment, and two marsh compartments were created from one where the newly delineated channel split the old marsh compartment.

Oyster Barrier Reef projects – increased the bed elevation of affected compartment links.

Hurricane Protection projects – cut off or reduced flow linkages between affected compartments when the levee falls along the compartment boundary. Linkages were also reduced based on the number of gates and their dimensions.

e. Identification of Formulas Used in the Model and Proof that the Computations are Appropriate and Done Correctly

This Section and 3.b. are nearly identical.

3. System Quality

a. Description and Rationale for Selection of Supporting Software Tool/Programming Language and Hardware Platform

The modeling approach adopted was mass balance for constituents, but it was also balance of gravity and bottom friction for flow, or a simplified conservation of momentum, a.k.a. the diffusion wave equation. The approach was selected for its computational efficiency. The spatial coverage of the Louisiana Coastal Area is quite large and the temporal scale needed for the 2012 Coastal Master Plan was 50 years. As such, it was critical to select a modeling approach with a reasonable run time. The Fortran code for the PB model (previously existing) and the Berkeley Madonna equation solver for the AA and CP models provided appropriate platforms to perform these long-term simulations.

b. Proof that the Programming was Done Correctly

It was not possible to prove that there were no coding or logical errors in either of the Eco-Hydrology models. However, during the model development, a series of tests were performed. These tests were intended to verify that:

- The models responded properly to the boundary conditions
- The models were mass conserving
- The models reproduced spatial and temporal trends observed in the field measurements (calibration and validation in Section 3.d.)

In order to prove that the models were responding to the boundary conditions properly, six tests were performed that applied a simplistic approach to the hydrodynamic boundary. These tests also included manipulation of the tributary inflows and atmospheric boundary conditions. **Table 35** below describes the six tests as well as the parameters that were affected. It should be noted that the PB model had a limit on the tidal range, where the stage could not drop below -0.5 m. Therefore, for tests 3 and 6, the maximum and minimum stages for the PB model were 0.5 and -0.5 m, respectively.

Table 35 Stage[45] and Parameter Values for Hydrodynamic Tests[46] for the Eco-Hydrology Models

Test #	Stage 1	Stage 2	Stage 3	Stage 4	Stage 5	Stage 6	Inflows	P	ET
1	5	5	5	5	5	5	0	0	0
2	5	6	5	4	5	5	0	0	0
3	0	1 (0.5)	0	-1 (-0.5)	0	0	0	0	0
4	5	5	5	5	5	5	0	ET	ET
5	5	6	5	4	5	5	0	ET	ET
6	0	1 (0.5)	0	-1 (-0.5)	0	0	0	ET	ET

As shown in the table, each compartment was provided an initial uniform stage (Stage 1) that was then altered after a short time-interval, depending on the test number. Once the end of the tidal signal reached the starting point (Stage 5 = Stage 1), the compartments were kept at the same stage until equilibrium was achieved. The tributary inflows were set to zero to prevent the compartments' stages from elevating due to additional flow. The same was done for P and ET in tests 1 – 3. However, tests 4 – 6 set P equal to ET to prove that the atmospheric loads were being accounted for accurately.

For test-1, all compartments in the models were given a constant stage of 5.0 m. The model domains were essentially submerged by standing water with no external influences and should remain level throughout the simulations. The results of test-1 for each model region can be seen in **Figure 40**, **Figure 41**, and **Figure 42**. The models passed the test as all stages were level at 5.0 m throughout the simulations.

[45] It should be noted that all tests used stage values corresponding to the NAVD 88 datum.
[46] The parentheses in the table denotes the different stages that are used in the PB model due to the limitation on tidal range.

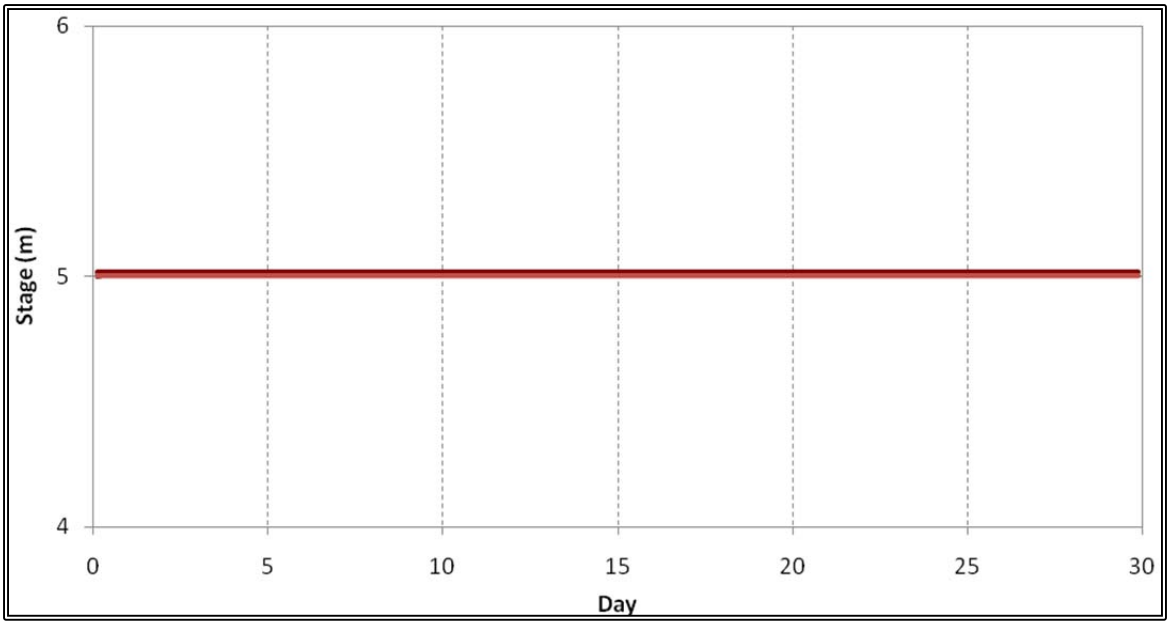

Figure 40 Test-1 Stage Results for the PB Model

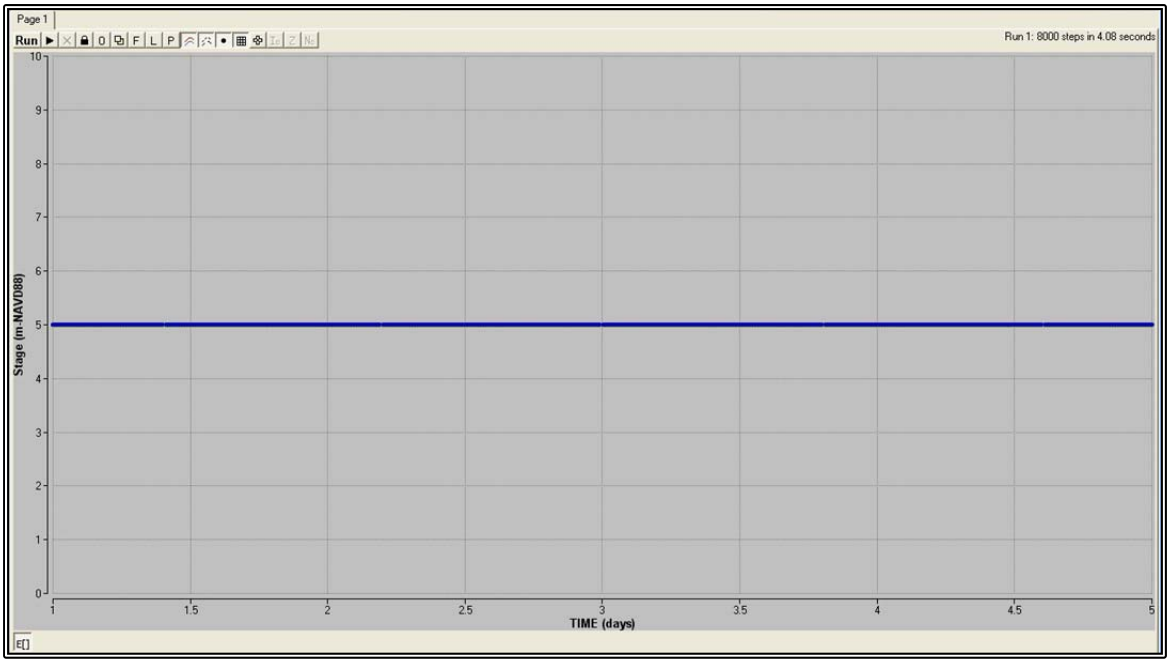

Figure 41 Test-1 Stage Results for the AA Model

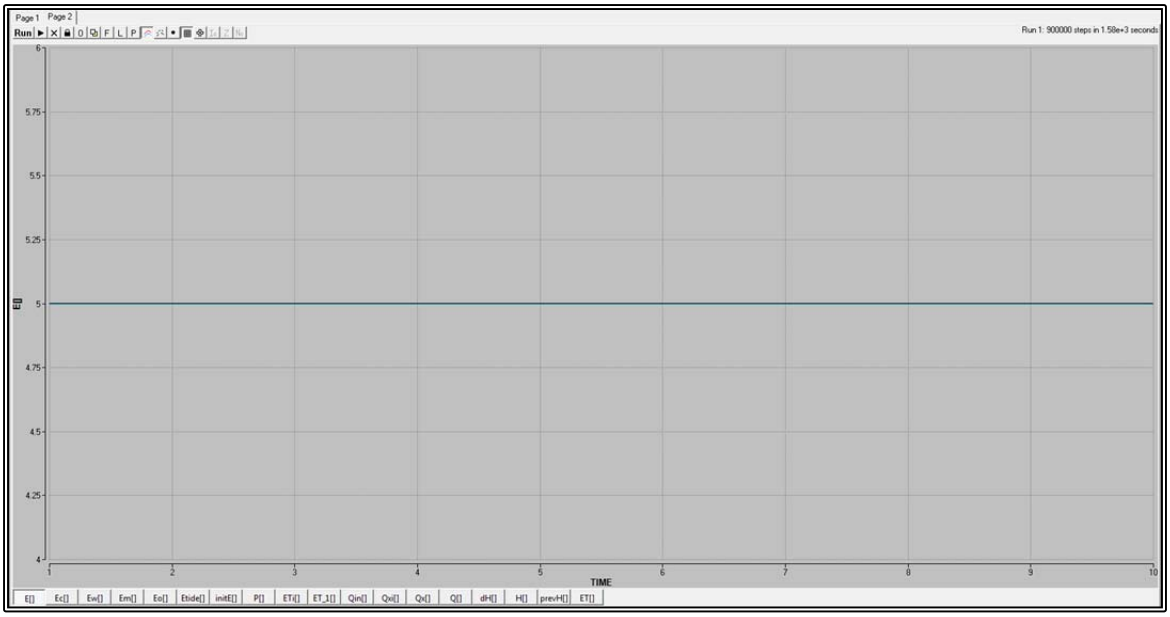

Figure 42 Test-1 Stage Results for the CP Model

For test-2, all compartments in the models were given an initial stage of 5.0 m and were then subjected to a tidal signal going from 5.0 m to 6.0 m, back to 5.0 m, then to 4.0 m, and back to 5.0 m where it remained constant until equilibrium was achieved. There were again no tributary inflows, no P, and no ET. The results of test-2 for all three regions can be seen in **Figure 43**, **Figure 44**, and **Figure 45**. The models all passed the test as the compartment stages increased and decreased with the boundary signal (inland compartments reacting more slowly as it took time for the wave to propagate inland), and finally leveled back off at 5.0 m.

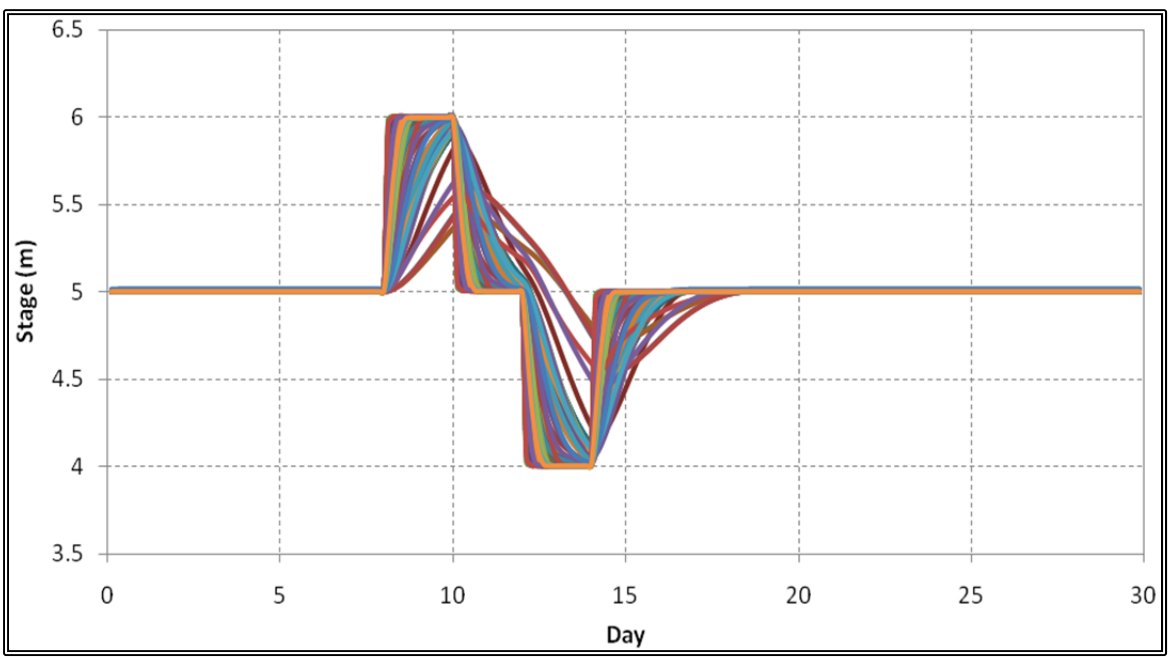

Figure 43 Test-2 Stage Results for the PB Model

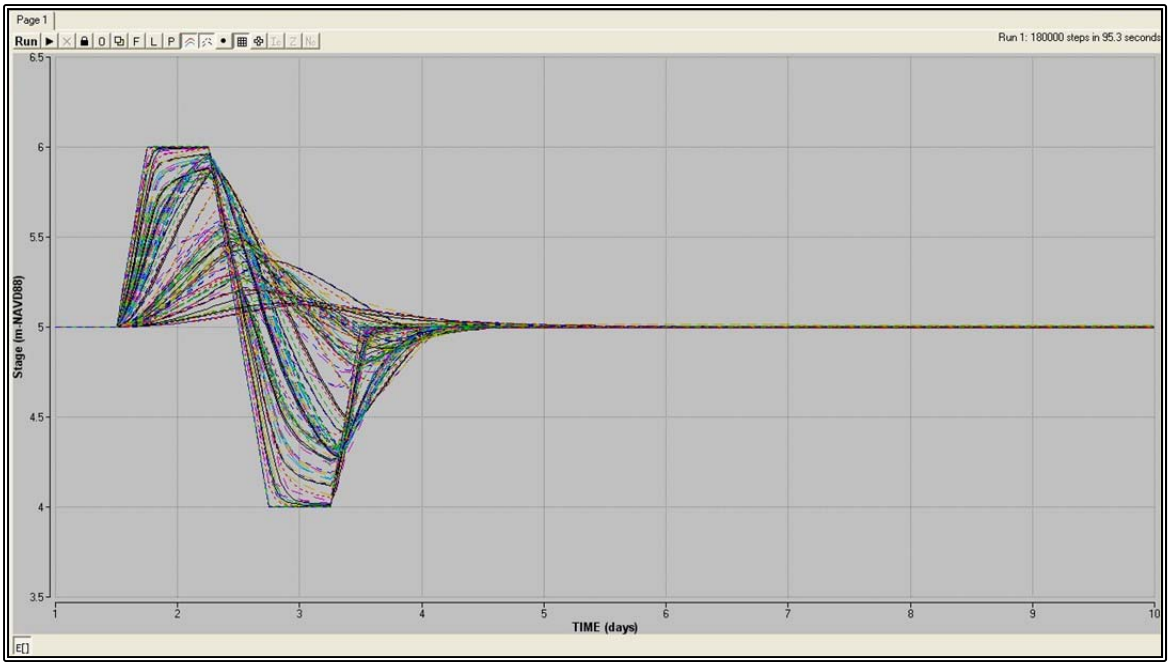

Figure 44 Test-2 Stage Results for the AA Model

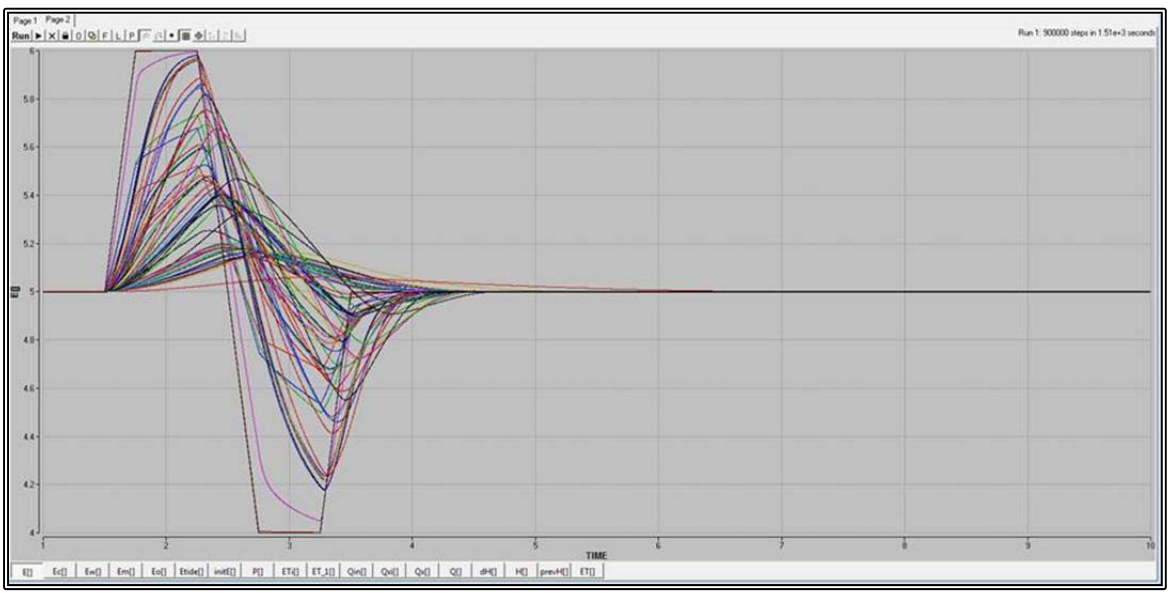

Figure 45 Test-2 Stage Results for the CP Model

For test-3, all compartments in the models were given an initial stage of 0.0 m (forcing some compartments to be *dry*) and were then subjected to a tidal signal going from 0.0 m to 1.0 m (0.5 m for PB), back to 0.0 m, then to -1.0 m (-0.5 m for PB), and back to 0.0 m where it remained constant until equilibrium was achieved. There were again no tributary inflows, no P, and no ET. The results of test-3 for each region can be seen in **Figure 46**, **Figure 47**, and **Figure 48**. The models all passed the test as the compartment stages increased and decreased with the boundary signal (inland compartments reacting more slowly as it took time for the wave to propagate inland), and finally leveled back off at 0.0 m. As seen in the figures, some compartments had a constant stage above the tidal signal, which indicated that their bed

elevation was above the water stage. Therefore, the *drying* rule took effect and set the stage to the minimum depth of 0.01 m above the bed elevation.

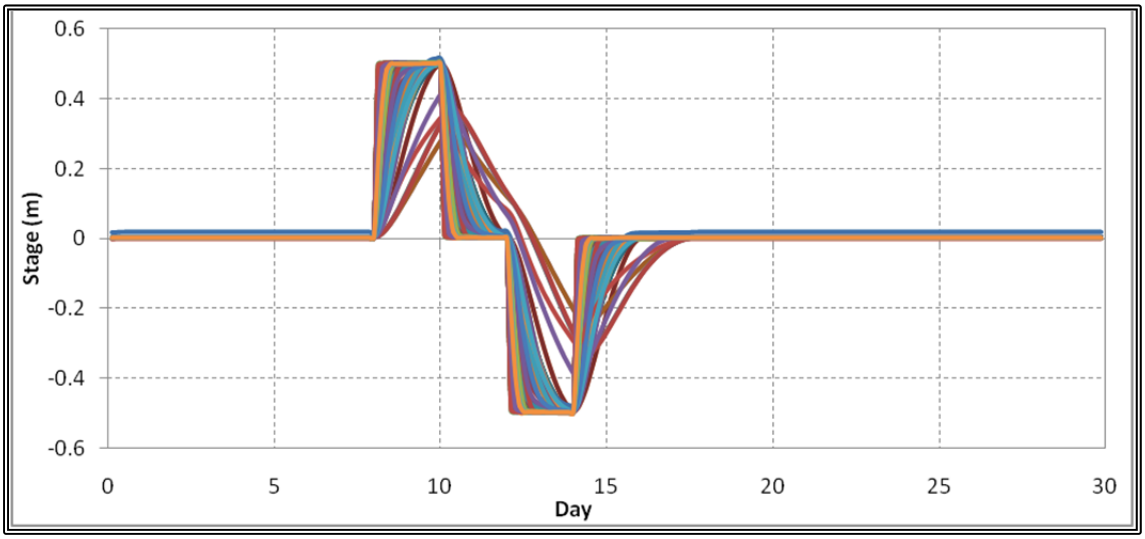

Figure 46 Test-3 Stage Results for the PB Model

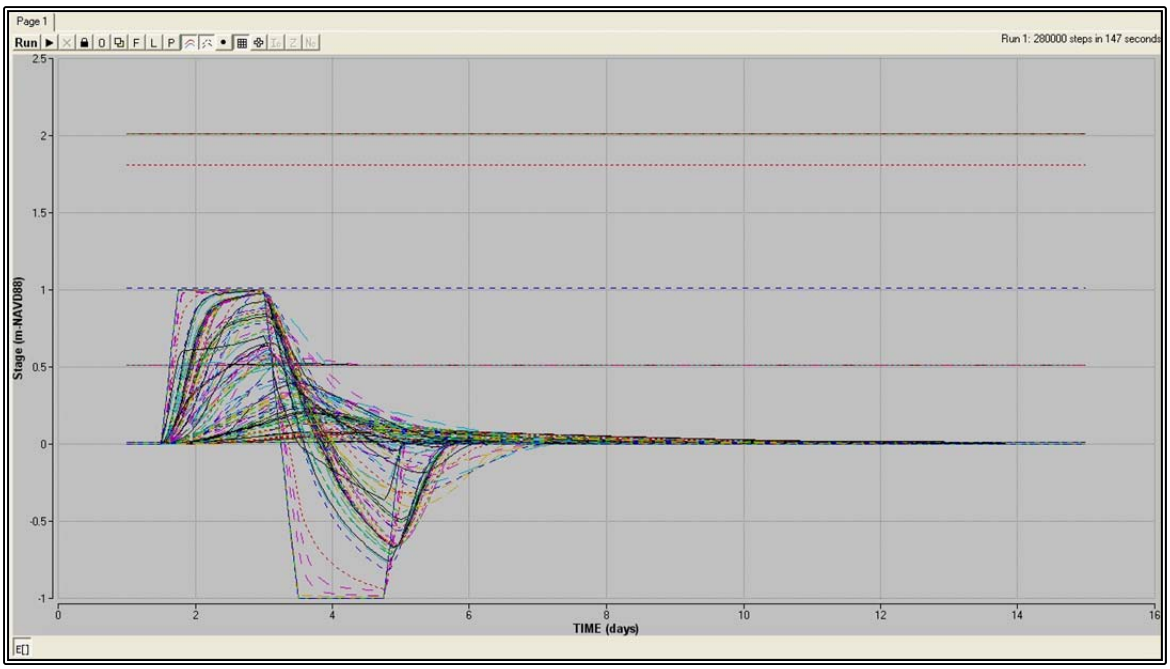

Figure 47 Test-3 Stage Results for the AA Model

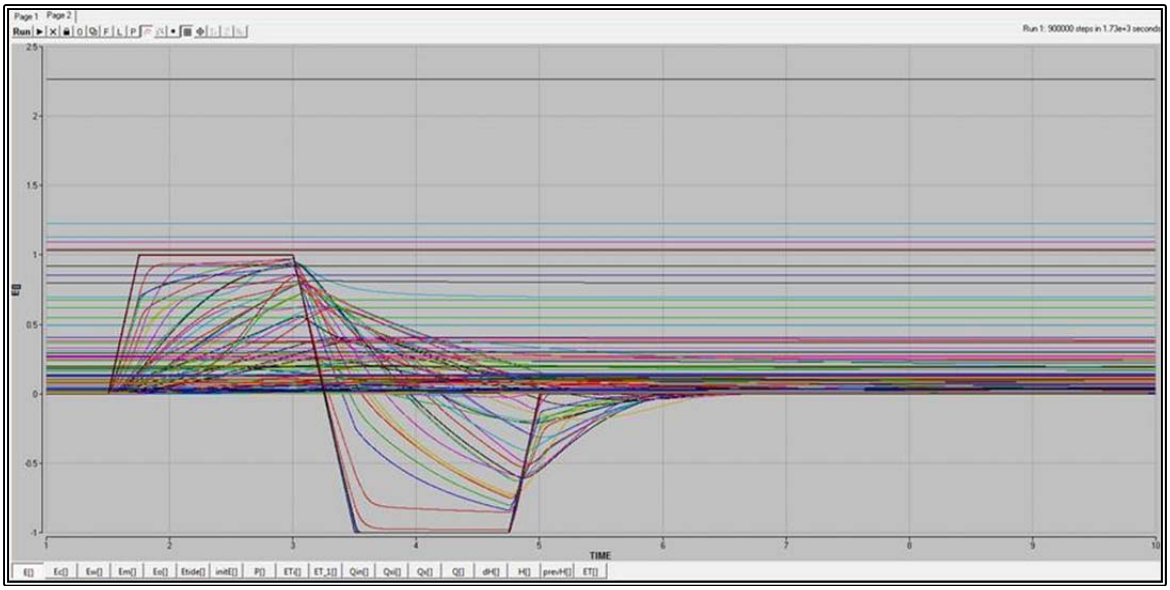

Figure 48 Test-3 Stage Results for the CP Model

For test-4, all compartments in the models were given a constant stage of 5.0 m and no tributary inflows. The ET was set equal to the P which would introduce a change in stage of zero to the models. The results of test-4 for the three regions can be seen in **Figure 49**, **Figure 50**, and **Figure 51**. The models passed the test as all stages were level at 5.0 m throughout the simulations.

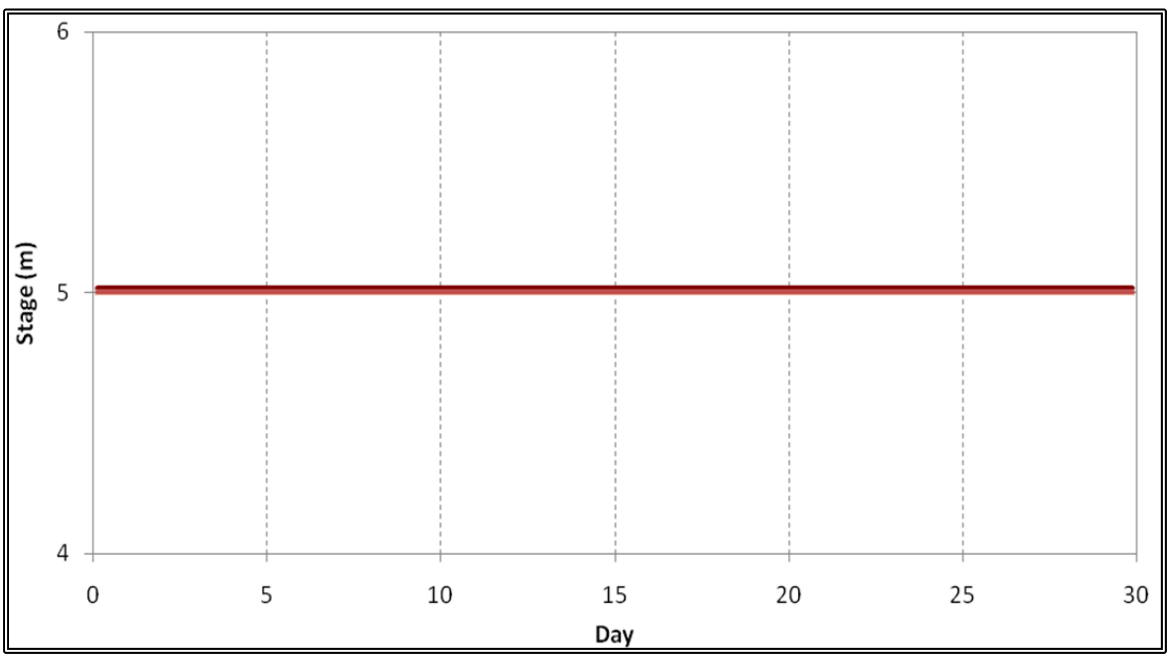

Figure 49 Test-4 Stage Results for the PB Model

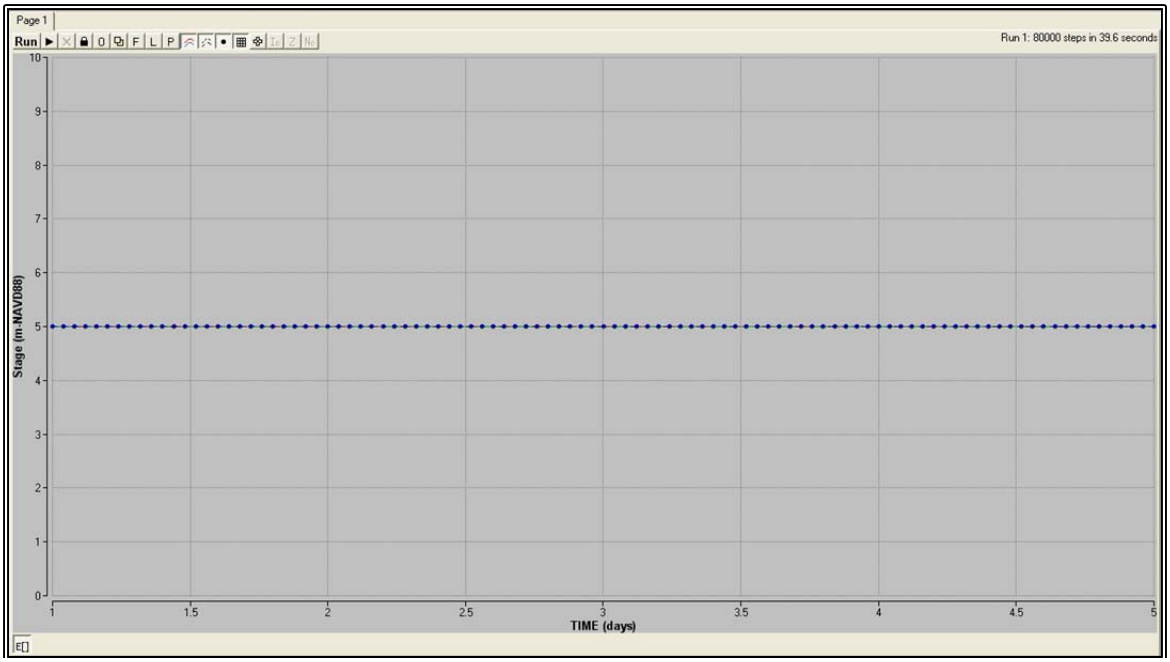

Figure 50 Test-4 Stage Results for the AA Model

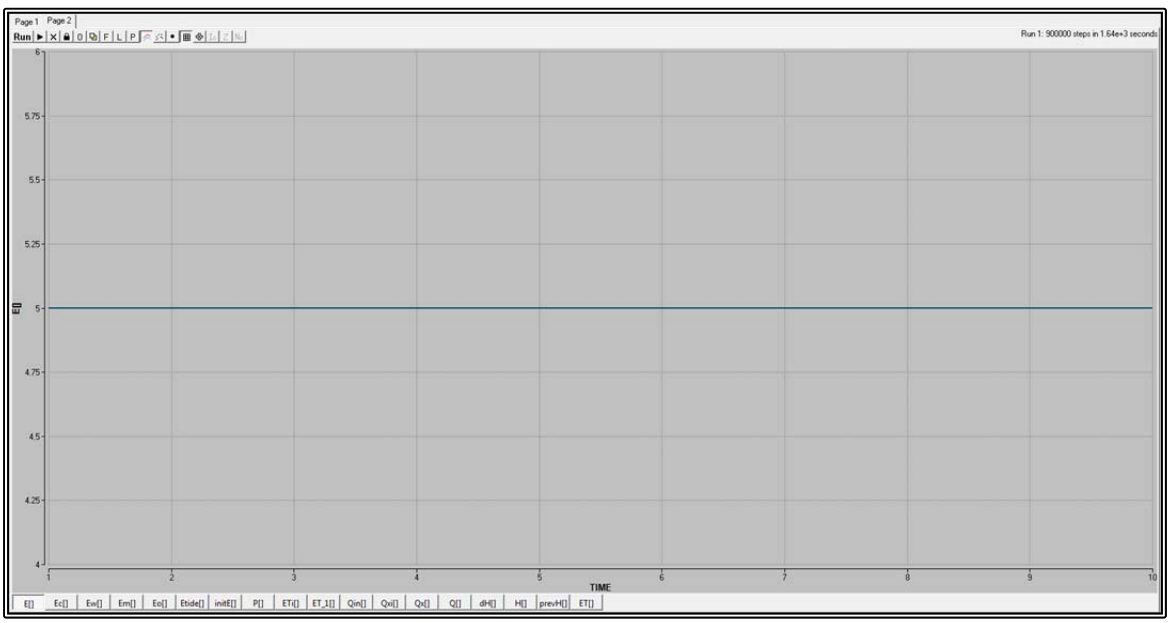

Figure 51 Test-4 Stage Results for the CP Model

For test-5, all compartments in the model were given an initial stage of 5.0 m and were then subjected to a tidal signal going from 5.0 m to 6.0 m, back to 5.0 m, then to 4.0 m, and back to 5.0 m where it remained constant until equilibrium was achieved. The ET was set equal to the P, and there were no tributary inflows. The results of test-5 for each region can be seen in **Figure 52**, **Figure 53**, and **Figure 54**. The models all passed the test as the compartment stages increased and decreased with the boundary signal (inland compartments reacting more slowly as it took time for the wave to propagate inland), and finally leveled back off at 5.0 m.

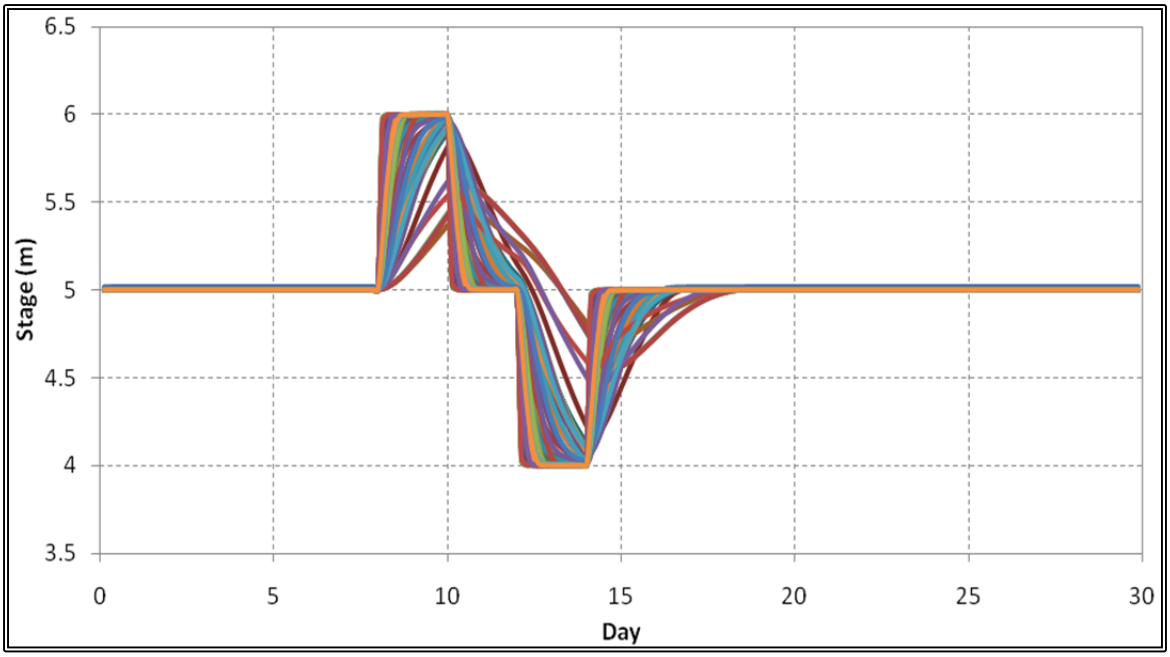

Figure 52 Test-5 Stage Results for the PB Model

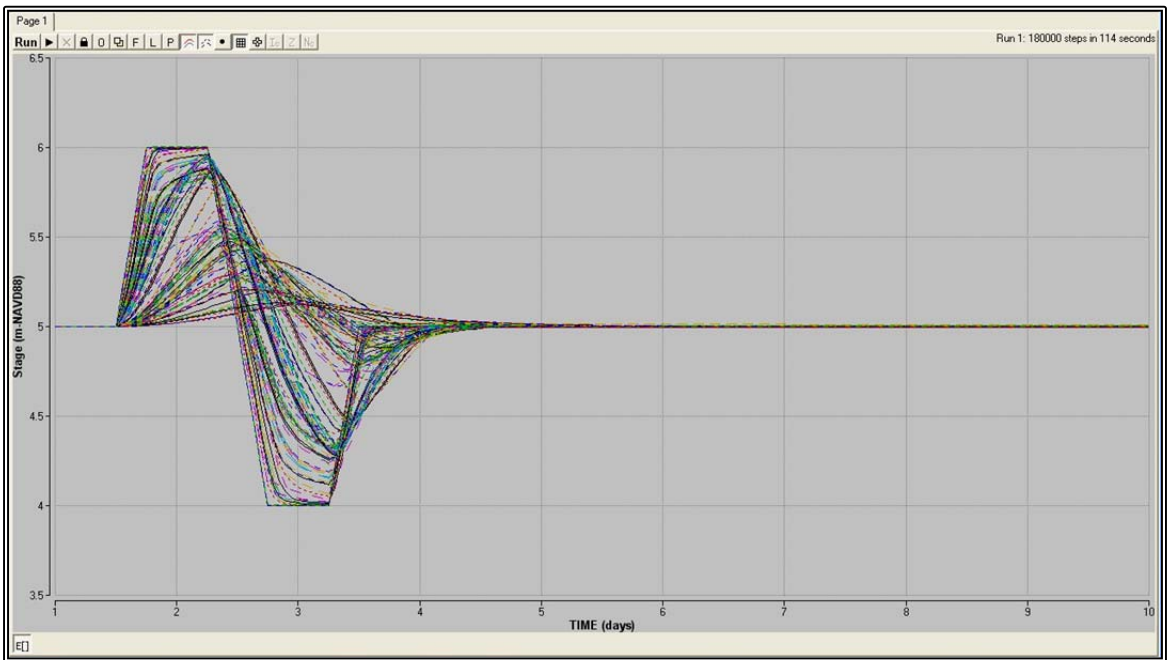

Figure 53 Test-5 Stage Results for the AA Model

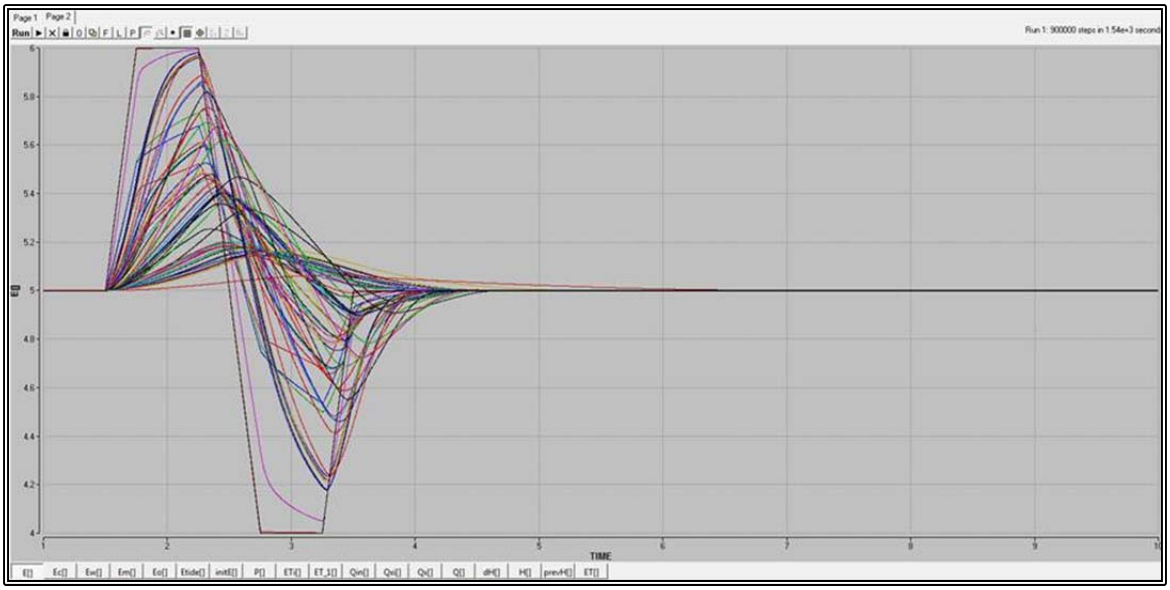

Figure 54 Test-5 Stage Results for the CP Model

For test-6, all compartments in the models were given an initial stage of 0.0 m (forcing some compartments to be *dry*) and were then subjected to a tidal signal going from 0.0 m to 1.0 m (0.5 m for PB), back to 0.0 m, then to -1.0 m (-0.5 m for PB), and back to 0.0 m where it remained constant until equilibrium was achieved. The ET was set equal to the P, and there were no tributary inflows. The results of test-6 for all three regions can be seen in **Figure 55**, **Figure 56**, and **Figure 57**. The models all passed the test as the compartment stages increased and decreased with the boundary signal (inland compartments reacting more slowly as it took time for the wave to propagate inland), and finally leveled back off at 0.0 m. As seen in the figures, some compartments had a constant stage above the tidal signal, which indicated that their bed elevation was above the water stage. Therefore, the *drying* rule took effect and set the stage to the minimum depth of 0.01 m above the bed elevation.

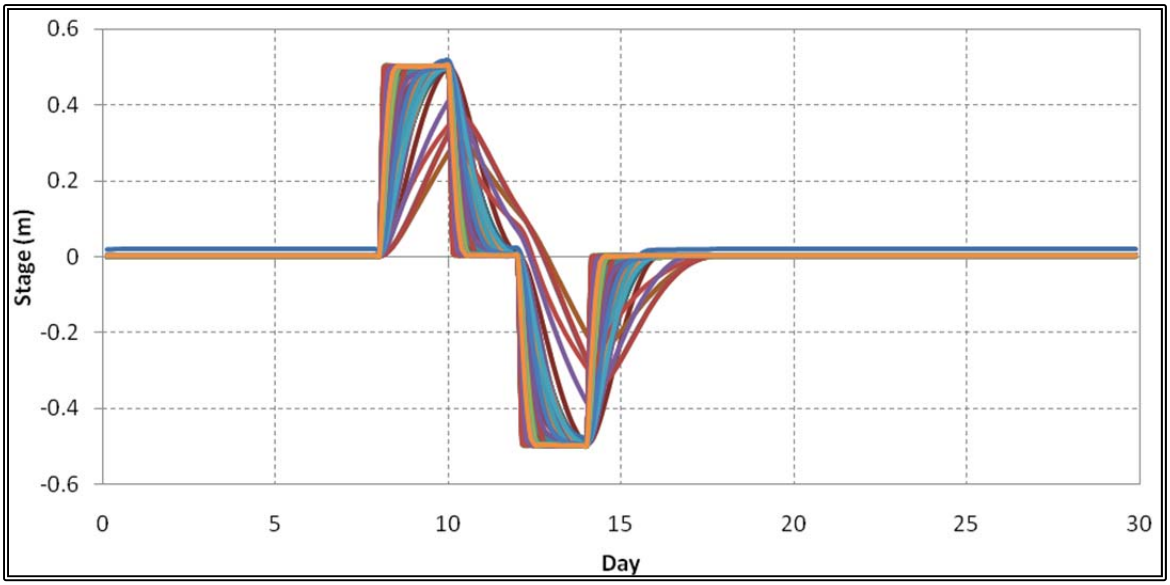

Figure 55 Test-6 Stage Results for the PB Model

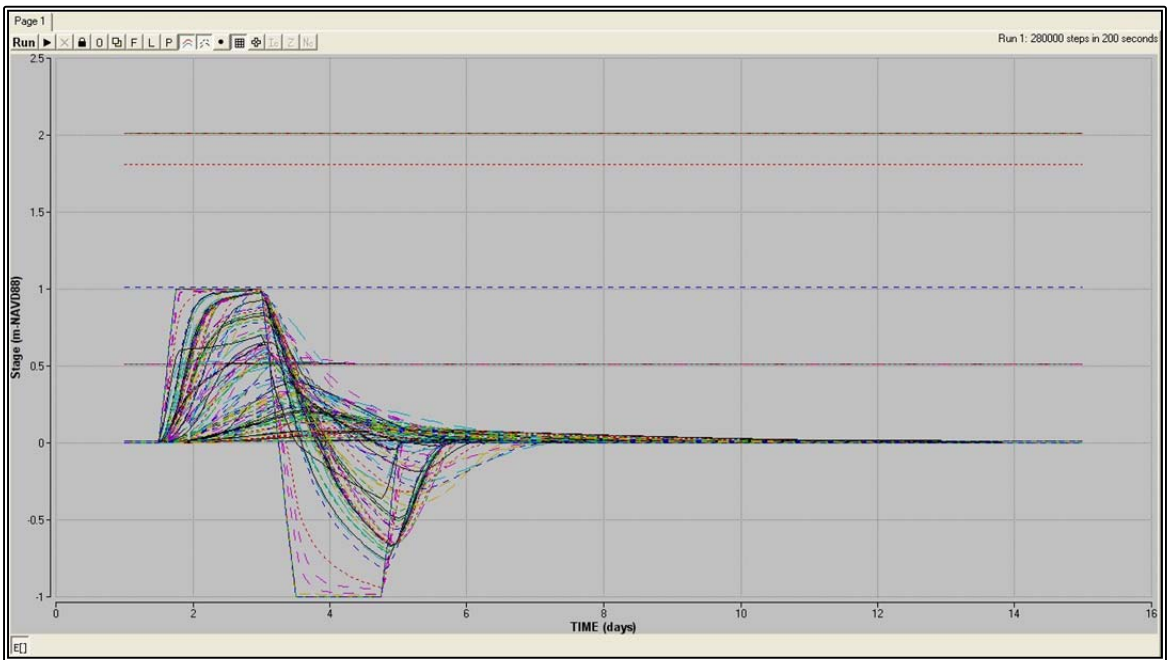

Figure 56 Test-6 Stage Results for the AA Model

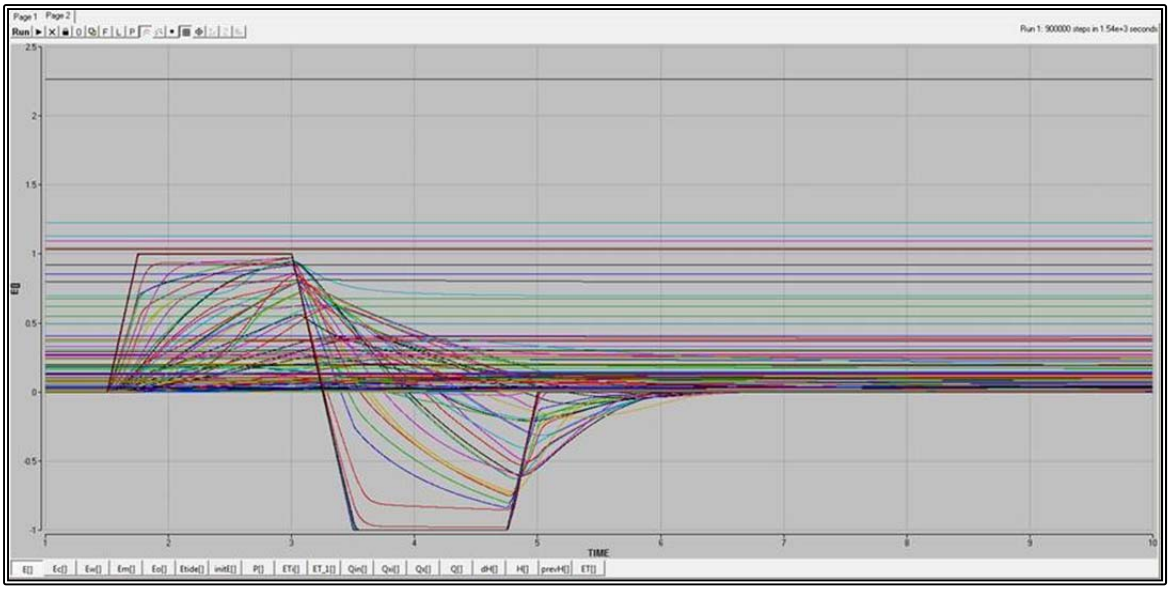

Figure 57 Test-6 Stage Results for the CP Model

In order to prove that the models were mass-conserving, two tests were performed to verify the constituent transport equation as programmed in the AA and CP models. These mass-balance verifications consisted of modeling the domain with an initial concentration of zero and 100 mg/L, applying boundary conditions of 100 mg/L, and running the model to equilibrium for the two initial conditions. For both simulations, there were no source/sink terms. In both cases, the equilibrium concentration reached 100 mg/L throughout the domain, which indicated mass conservation.

Additional testing planned as part of this modeling effort is to apply these models to simple systems where analytical solutions exist. This would provide additional verification that the models conform to the basic physical laws.

c. Availability of Software and Hardware Required by Model

Originally released by IBM in 1957, the Fortran System (FORmula TRANslating System[47]) is especially suited for numeric computation and scientific computing (Backus, 1998). Fortran quickly became the dominant system of science and engineering programming due to its wide scope of applicability, conciseness and convenience (comparatively short amount of time required to write, compile, debug, and execute the program), ease of use, built-in debugging facilities, and ability to accurately translate algebraic expressions to machine language (Backus, et al., 1957). Fortran codes are often used in computationally intensive areas such as numerical weather prediction, finite element analysis, computational fluid dynamics, storm surge modeling, computational physics, and computational chemistry. As an additional benefit, Fortran can be combined with C++ to incorporate graphical interfaces.

The PB model was coded in Fortran 90 and compiled with Compact Visual Fortran 6.6 for 32-bit machines. For 64-bit machines, the code has been compiled using the INTEL Fortran compiler, which operates much faster. The compiled code runs on all Windows operating systems. The code can be written to accept input in free format (e.g. comma separated variables) or fixed format. The output can be provided in any of these formats.

Berkeley Madonna™ is a closed-source differential equation solver developed by a team at the University of California at Berkeley, and it is a modified version of the STELLA®[48] model. The solver software is written in the C programming language and can be run on Windows or Mac computers. Its flowchart editor requires the installation of the latest Java™ Runtime Environment. However, the actual model formulation is open and can be viewed, verified, and customized. Berkeley Madonna for Windows runs on personal computers with Intel x86 or compatible processors under Microsoft Windows 95, Windows 98, Windows NT 4.0, Windows XP, and later versions of these operating systems.[49] Berkeley Madonna for Macintosh runs on Apple Power Macintosh and 100% compatible computers with a PowerPC CPU (601, 604, G3, etc.). It will also run on the new Intel-based Macintosh under the Rosetta emulator. Older machines with 68K CPUs are not supported.[7]

[47] Fortran was all caps prior to 1977 (e.g. FORTRAN), then when Fortran 77 came out it was switched to lower case so people would know which version is being used.
[48] http://www.iseesystems.com/softwares/Education/StellaSoftware.aspx
[49] http://www.berkeleymadonna.com/download.html

d. Description of Process Used to Test and Validate Model

To verify that the Eco-Hydrology models were applicable for modeling hydrodynamic and water quality at a screening level for the 2012 Coastal Master Plan modeling effort, the models were calibrated for a specific period of record and then validated for a separate period of record. Calibration/validation was achieved for each region by adjusting flow parameters and reaction parameters, as well as boundary conditions. The PB model was calibrated and validated to measured data from the years of 1990 – 2009. Attachment B presents the plots of the calibration and validation with the appropriate years used for each modeled parameter and constituent. The AA model was calibrated using observed field values for the calendar year of 2007. It was then validated with observed field values for the calendar years of 2008 and 2009. The CP model was calibrated using observed field values for the calendar year of 2007. It was then validated with observed field values for the calendar year of 2010. It should be noted that several observation stations across the Louisiana coast only provide discrete measurements with large gaps as opposed to consistent daily values. As a result, the years chosen for calibration and validation were based on the availability of data and estimates were made to fill the missing data using standard techniques. Also, the stations and parameters used for the calibrations and validations in each region are presented in tables in Attachment A. (**Table 78** for the PB model, **Table 79** for the AA model, and **Table 80** for the CP model).

Pontchartrain and Barataria Basin Model

The PB model originated as the Pontchartrain Basin model (Roblin, 2008). Subsequently, the Barataria Basin was included to establish the PB model domain used today. As a result, the calibration and validation of the model was performed separately for each basin. The following sections include the stations used in each PB basin for the calibrations and validations, as well as a sample of the comparison plots for each basin. It should be noted that due to a limited amount of observed data, the model was run for 20 years (1990 – 2009) and the calibrations and validations for each parameter were achieved by comparing observed values to two specific periods of record where abundant data were available during that 20-year period. Therefore, the calibrations and validations for the two PB basins did not always use the same calendar years.

<u>Calibration & Validation</u>

Tidal Range & Discharge

Initially, the PB model was calibrated/validated using both observed stage and tidal range data. However, the tidal range is more efficient because some of the stage measurements have incorrect or disagreeing values for their datums. Also, the stage variation due to wind shear is very high for the large open water areas, like Lake Pontchartrain. Therefore, tidal range was used to calibrate water level in the PB model. The stations used for calibrating/validating tidal range are shown in **Figure 58**. Average annual discharges from water bodies around Lake Pontchartrain, which were estimated in a Mississippi River Gulf Outlet (MRGO) study (Georgiou et al., 2009), were used to visually calibrate/validate the average discharges for those specific water bodies.

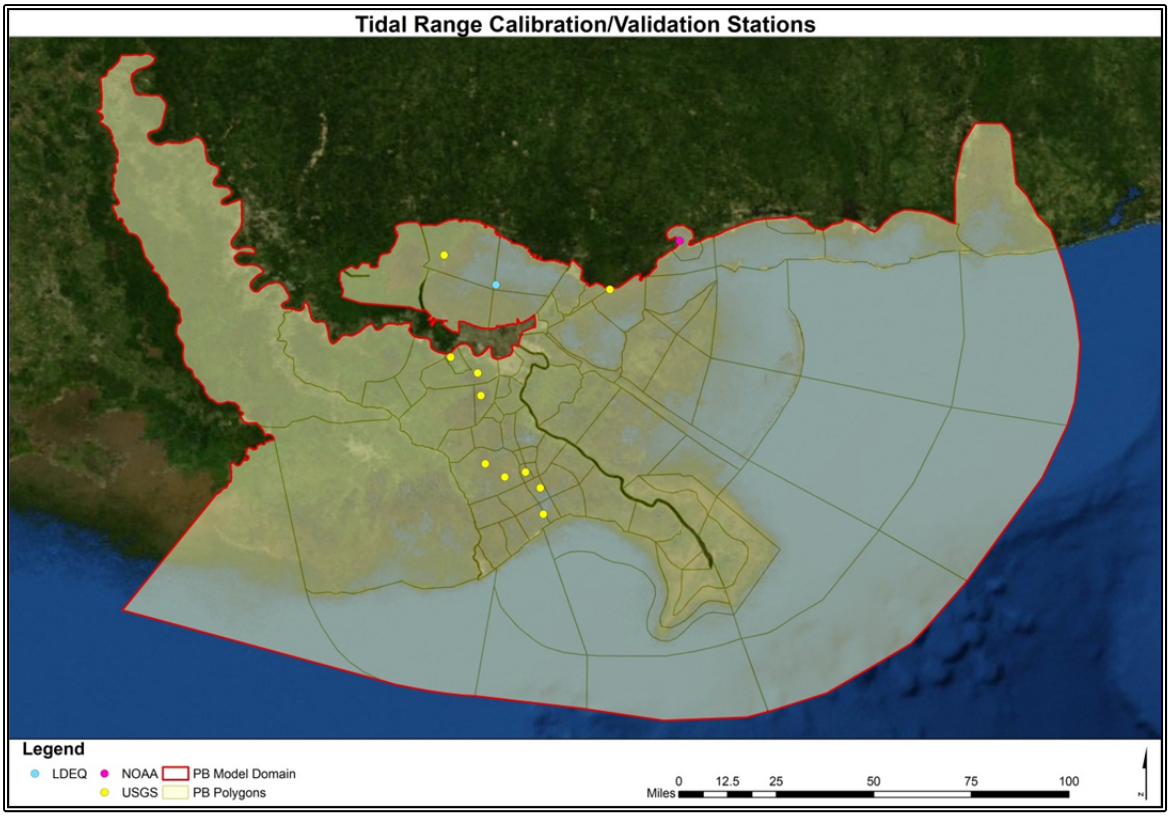

Figure 58 Tidal Range Calibration/Validation Sites for the PB Model

The model calibration/validation input coefficients for tidal range and flow were the Manning's roughness factors. Manning's roughness was assigned based on the channel bed material (ranging from 0.01 to 0.04), and then adjusted to obtain the observed tidal range and/or stage. If structures were present, minor loss coefficients were used to adjust the head loss through these structures.

Figure 59 shows plots of the tidal range calibration/validation at several locations in the PB domain. These plots along with the rest of the tidal range calibration/validation plots are included in Attachment B.

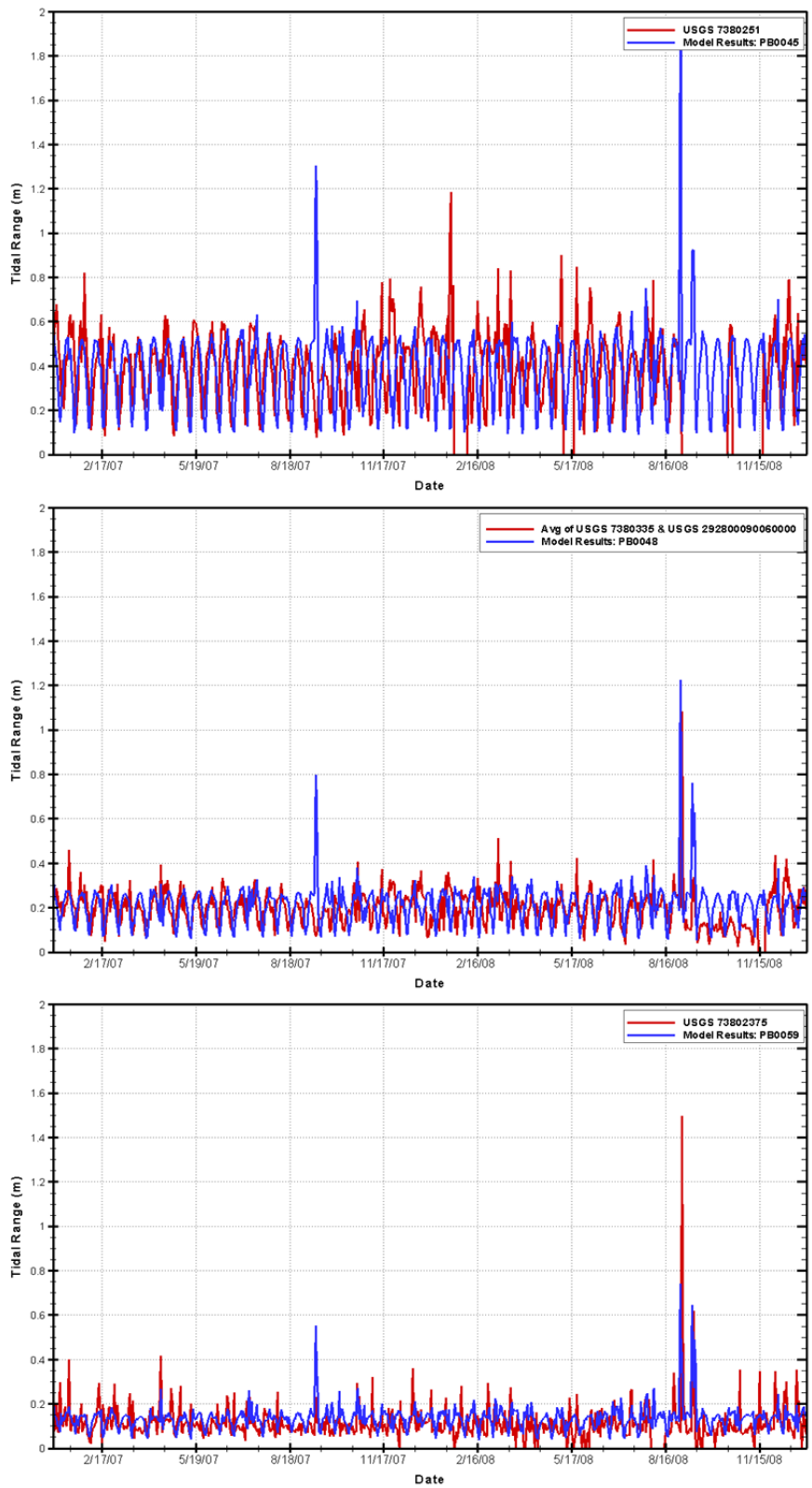

Figure 59 Sample Tidal Range Calibration (2008) & Validation (2007) Results for: Barataria Bay North of Grand Isle, Little Lake, and Lake Salvador in the PB Model

Overall, the model results agreed quite well with the tidal range measurements. The tidal range and discharge were also compared to observed values near Lake Pontchartrain from Retana (2008), Haralampides (2000), and Georgiou et al. (2009) as illustrated in **Table 36** and **Table 37**, respectively. The primary reasons for discrepancies between the measurements and simulated results were: (1) the lack of wind forcing on interior open water compartments and (2) uncertainty and inaccuracy of bathymetry in the region (for instance, much of the Pontchartrain and Maurepas bathymetry was published in 1898). Additionally, the model neglected inertial forces (acceleration effects) in the passes, which could cause slight discrepancies. Due to a lack of measured data, discharge calibration/validation was not conducted for the Barataria Basin region.

Table 36 Observed and Modeled Spring Tidal Ranges near Lake Pontchartrain (Retana, 2008)

Location	Tidal Range (m)	
	Observed	Modeled
Waveland, MS	0.53	0.58
Pass Rigolets	0.25	0.28
Lake Pontchartrain	0.16	0.17
Pass Manchac (Turtle Cove)	0.11	0.11

Table 37 Observed and Modeled Spring Flood/Ebb Discharges near Lake Pontchartrain (Georgiou et al., 2009)

Location	Discharge (cfs)	
	Observed	Modeled
Pass Manchac	35,000	30,000
IHNC	13,000 – 15,000	12,000
Chef Menteur	85,000	80,000
Pass Rigolets	180,000	200,000

Salinity

The stations used for calibrating salinity are shown in **Figure 60** and the stations used for validating salinity are shown in **Figure 61**. Several of the stations are repeated in the calibration and validation maps below, which allows the comparisons to be plotted on the same graphs.

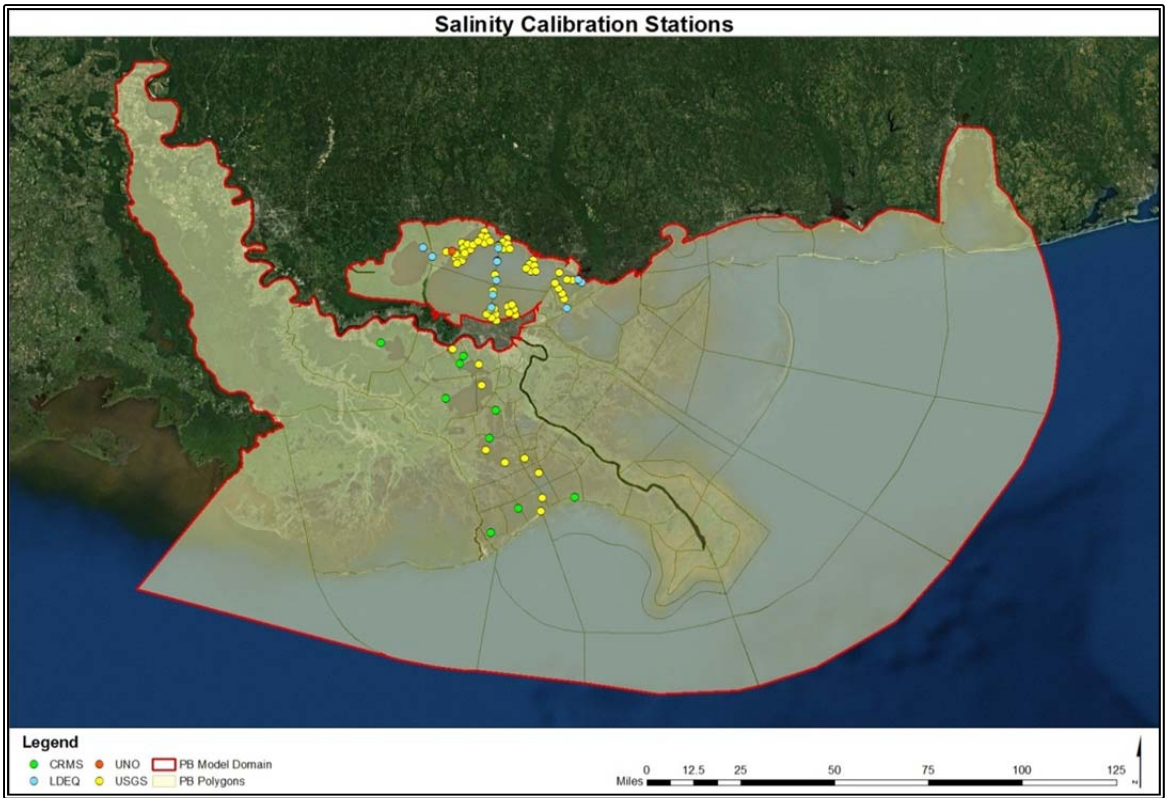

Figure 60 Salinity Calibration Sites for the PB Model

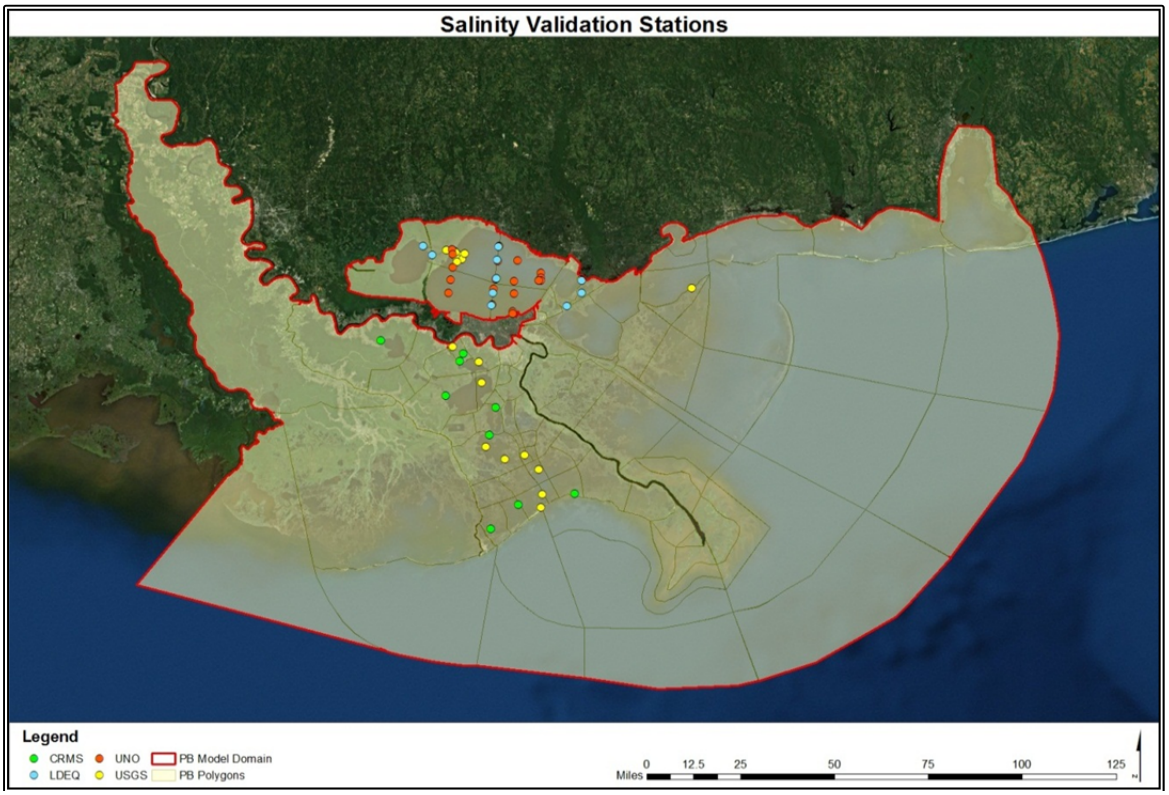

Figure 61 Salinity Validation Sites for the PB Model

The model calibration input coefficient for salinity was diffusivity. The initial diffusivities were set to 10.0 m^2/s and were then adjusted to replicate observed salinity values. The actual diffusivity included both hydraulics and wind shear effects.

Overall, the model results agreed quite well with the salinity measurements as illustrated in **Figure 62**. These plots along with the rest of the salinity calibration/validation plots are presented in Attachment B. The primary reasons for discrepancies between measurements and simulated results were: (1) the lack of wind forcing on interior open water compartments, (2) uncertainty and inaccuracy of bathymetry in the region, and (3) the inability of the model to reproduce salinity stratification.

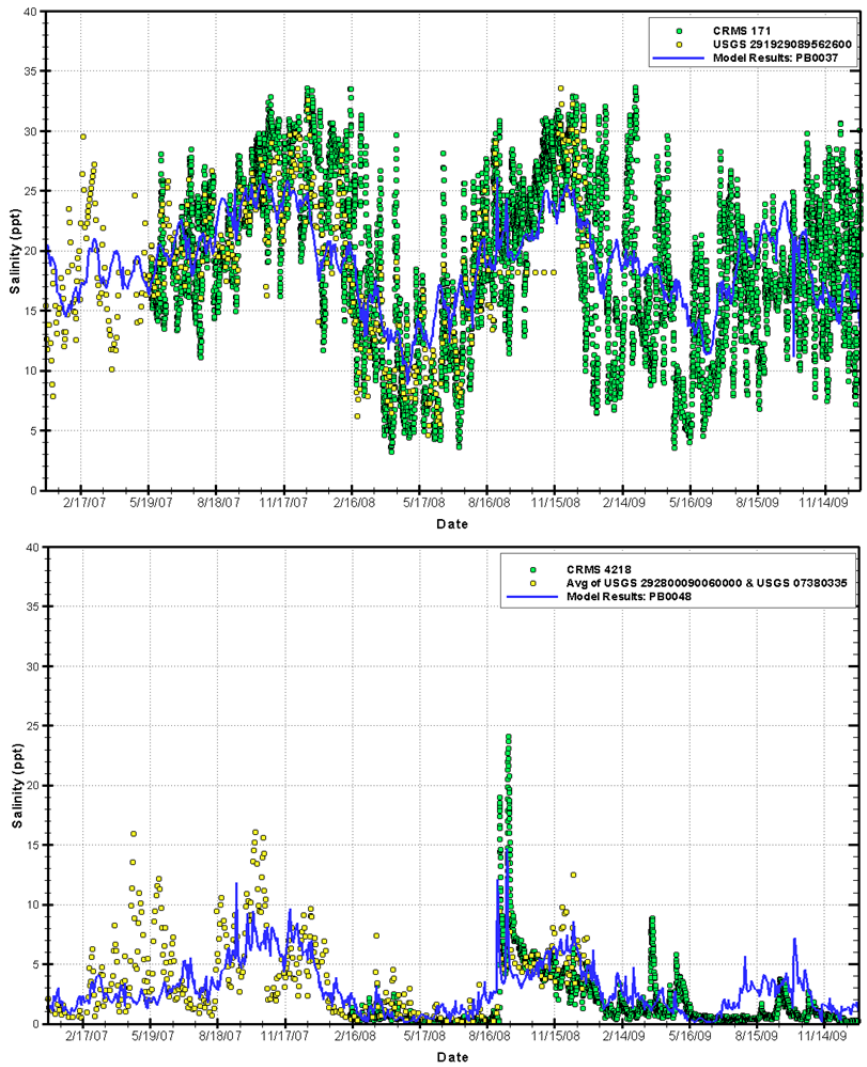

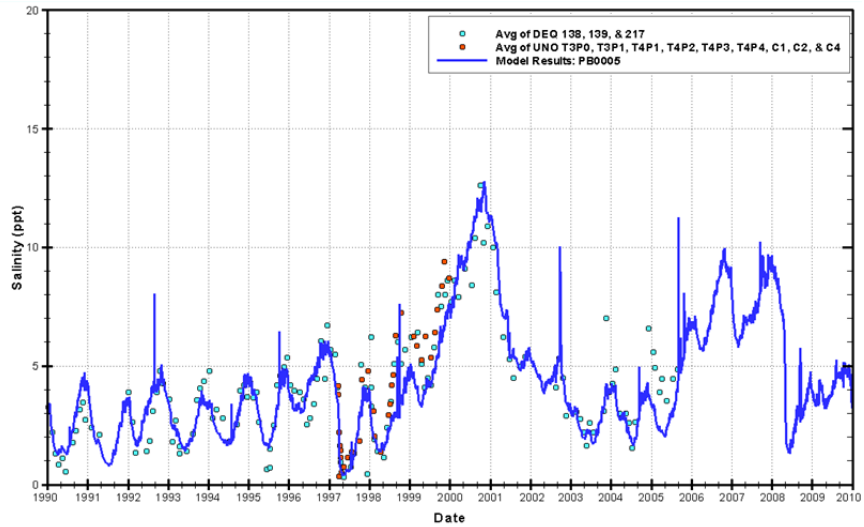

Figure 62 Sample SAL Calibration (2008 – 2009) & Validation (2007) Results for Barataria Bay North of Grand Isle, Little Lake, and Northeast Lake Pontchartrain in the PB Model

Temperature

The stations used for calibrating temperature and the other water quality constituents are shown in **Figure 63**. The stations used for validating temperature and the other water quality constituents are shown in **Figure 64**. Several of the stations are repeated in the calibration and validation maps below, which allows the comparisons to be plotted on the same graphs.

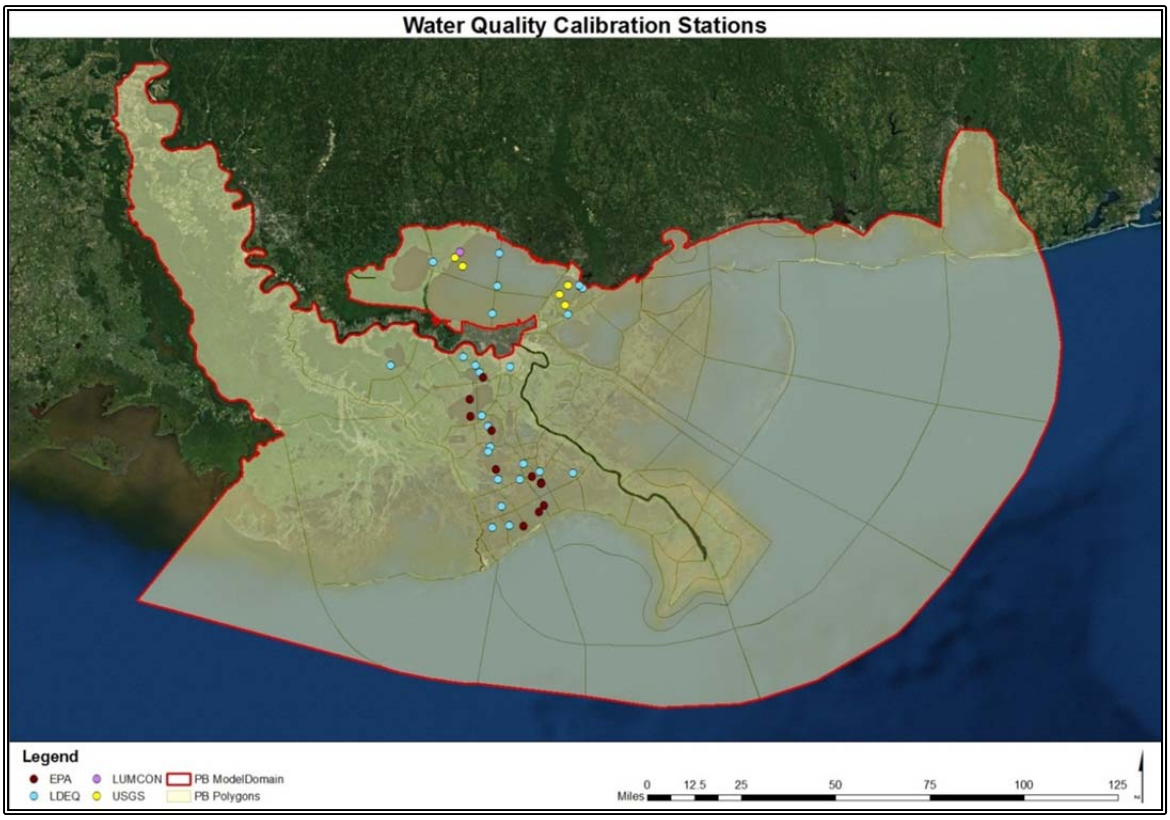

Figure 63 Water Quality Calibration Sites for the PB Model

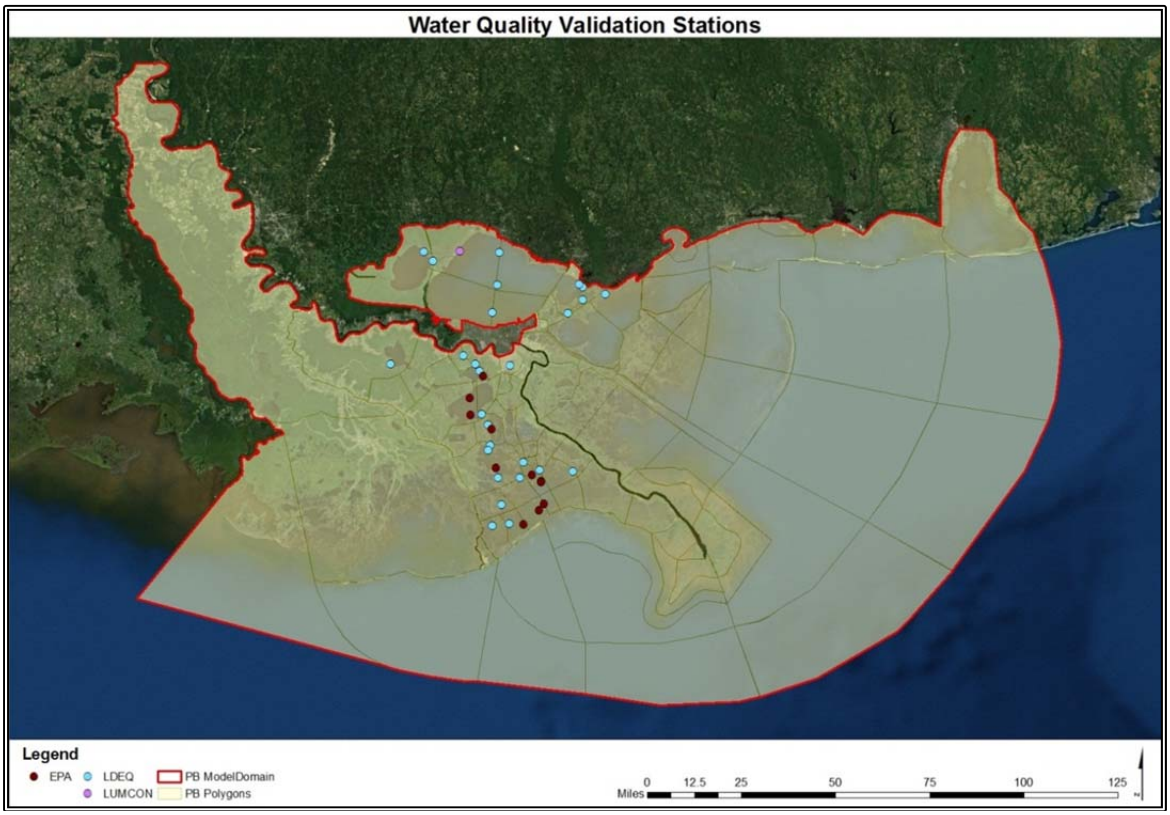

Figure 64 Water Quality Validation Sites for the PB Model

The model calibration input coefficient for the equilibrium temperature was a heat exchange coefficient used to adjust perturbations from the equilibrium temperatures. The equilibrium temperature was based on the previously mentioned correlation with air temperature.

Overall, the model results agreed quite well with the temperature measurements as illustrated in **Figure 65**. These plots along with the rest of the temperature calibration/validation plots are shown in Attachment B. The primary reasons for discrepancies between measurements and simulated results were: (1) the lack of wind forcing on interior open water compartments, (2) lack of daily inputs of explicit meteorological conditions such as humidity and cloud cover, and (3) the model's inability to reproduce temperature stratification (most temperature measurements are taken near the surface of the water column).

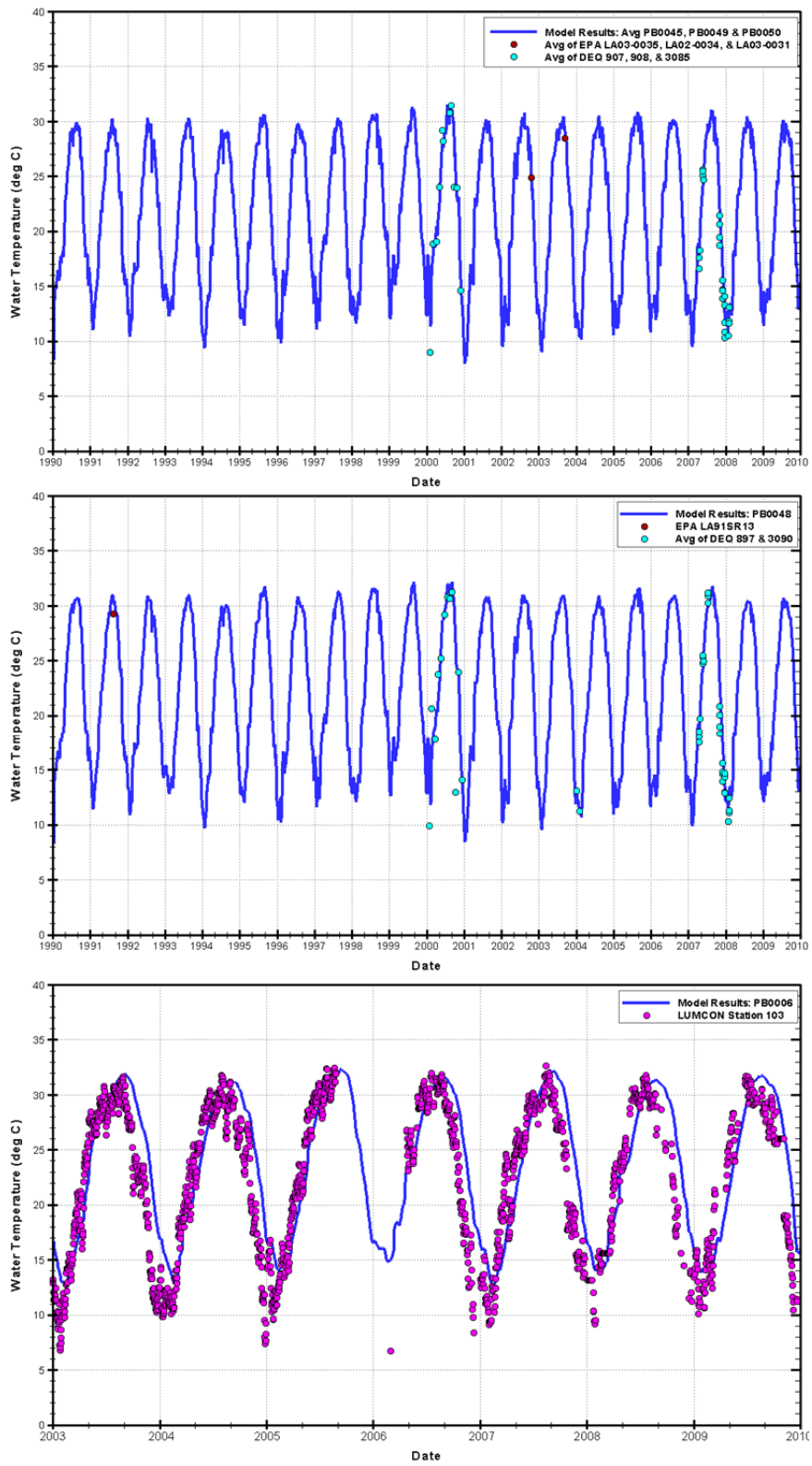

Figure 65 Sample TMP Calibration & Validation Results for Barataria Waterway South of Lafitte, Little Lake, and Northeast Lake Pontchartrain in the PB Model

Water Quality

Again, the stations used for calibrating the water quality are shown in **Figure 63** and the stations used for validating the water quality are shown in **Figure 64**. Several of the stations are repeated in the calibration and validation maps, which allows the comparisons to be plotted on the same graphs. **Figure 66** and **Figure 67** below illustrate some of the calibration and validation results for TN and TPH, respectively, for the PB model. These and the rest of the water quality calibration/validation plots are presented in Attachment B.

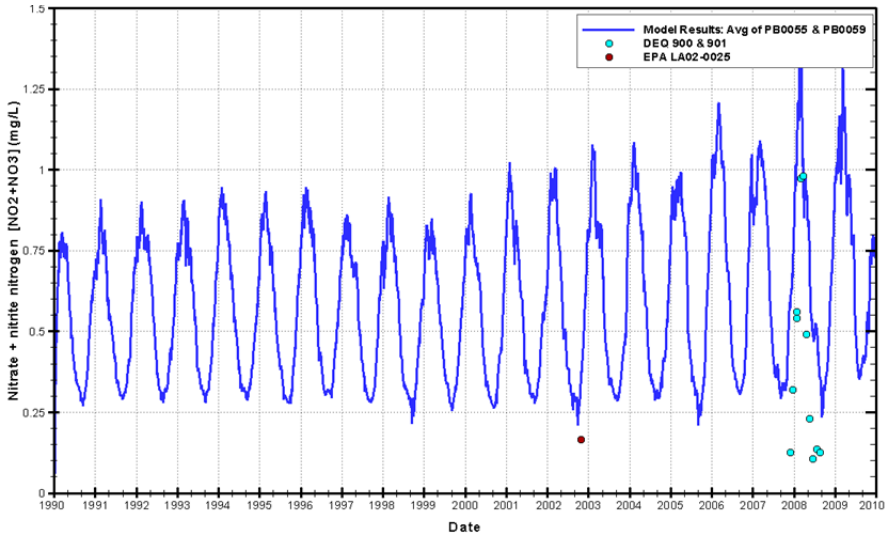

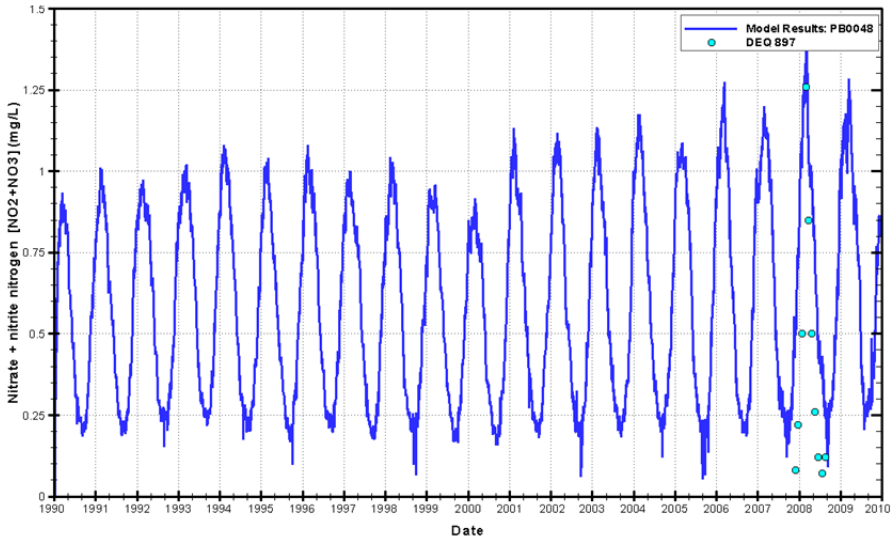

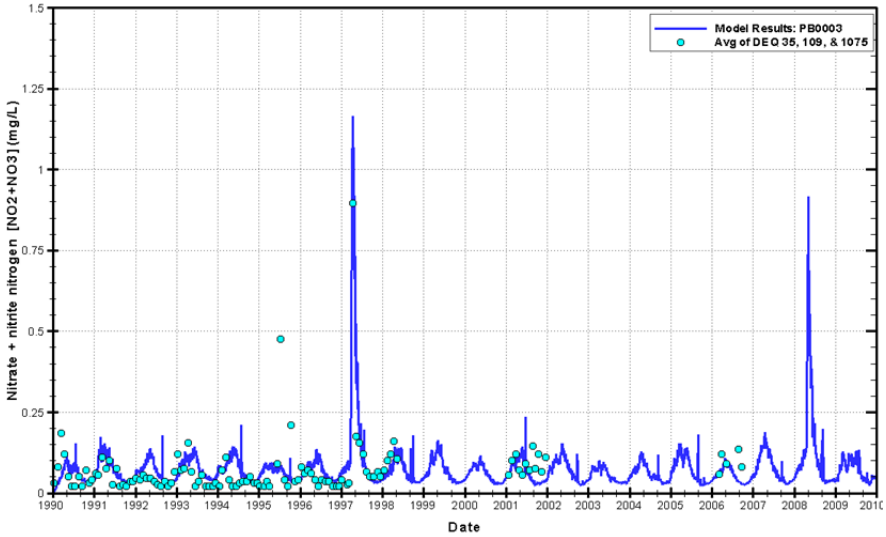

Figure 66 Sample NO3 Calibration Results for Bayou Perot, Little Lake, and East Lake Pontchartrain in the PB Model

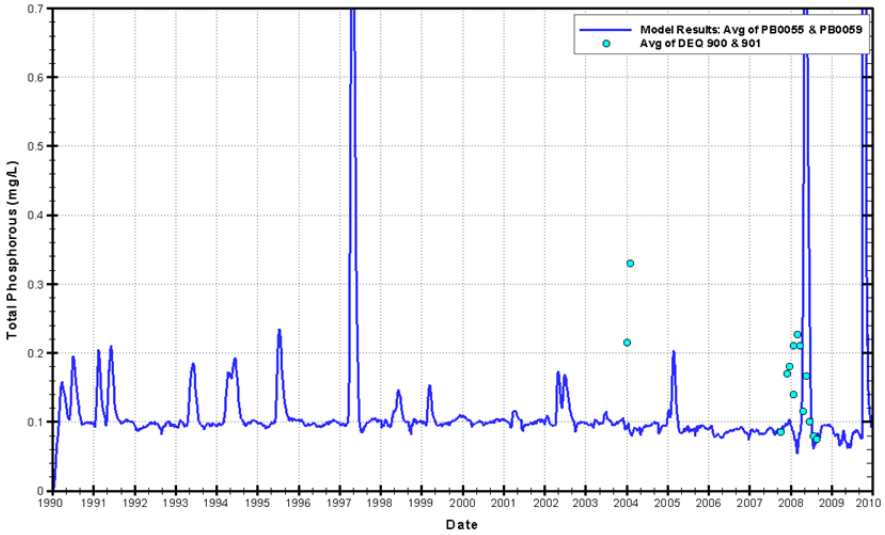

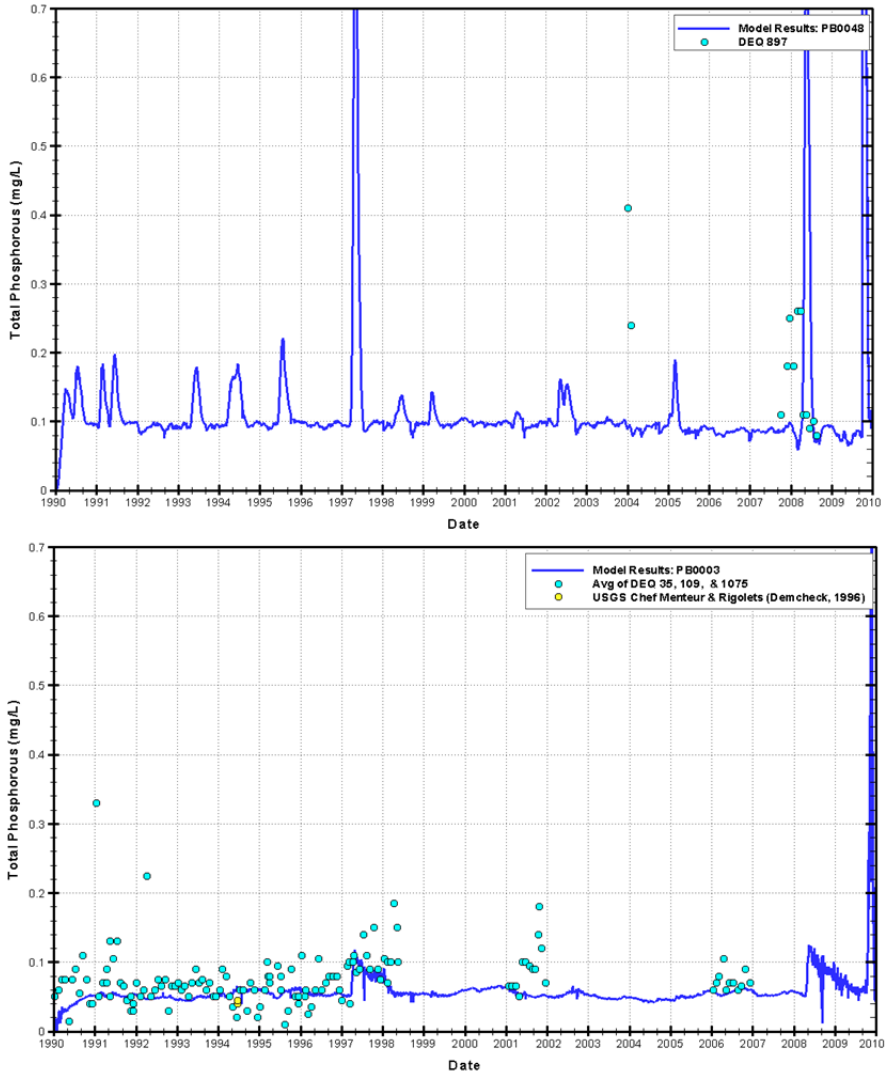

Figure 67 Sample TPH Calibration Results for Bayou Perot, Little Lake, and East Lake Pontchartrain in the PB Model

Atchafalaya Basin Model

Calibration

The AA model was calibrated to observed measurements for the calendar year of 2007.

Stage and Discharge

The model calibration input coefficients for stage and flow were the Manning's roughness and minor loss coefficients. In the model setup, the Manning's roughness coefficient was calibrated based on vegetation/surface types. There were eight different vegetation/surface types; **Table 38** lists the calibrated Manning's roughness for each type. The master plan Vegetation team had compiled a list of 19 vegetation types for the Louisiana Coast. This list was not used, however, because of the nature of the AA compartment grid. The compartment grid was very coarse (i.e. large compartment sizes), and therefore a more generalized classification scheme was used to assign Manning's *n* values. A minor loss coefficient was applied to adjust the flow resistance in individual links.

Table 38 Calibrated Manning's Roughness Coefficients for the AA Model

Vegetation/Surface Type	Manning's *n*
Deep open water	0.02
Intermediate open water	0.03
Shallow open water	0.05
Deep Channel	0.026
Intermediate Channel	0.04
Shallow Channel	0.05
Marsh	0.15
Swamp	0.25

Figure 68 presents the gauge locations for the stage calibration, and the gauges used for discharge calibration are illustrated in **Figure 69**. Stage measurements were taken from the LDNR, NOAA's National Ocean Service (NOS), USACE, and USGS, while the flow measurements were from the USGS. It should be noted that the Coastwide Reference Monitoring System Sites[50] (CRMS) sites shown in **Figure 68** were from the LDNR. **Figure 70** and **Figure 71** show the calibration results at select locations for stage and discharge, respectively. These and the remaining stage and discharge calibration plots are shown in Attachment B.

[50] http://sonris.com/

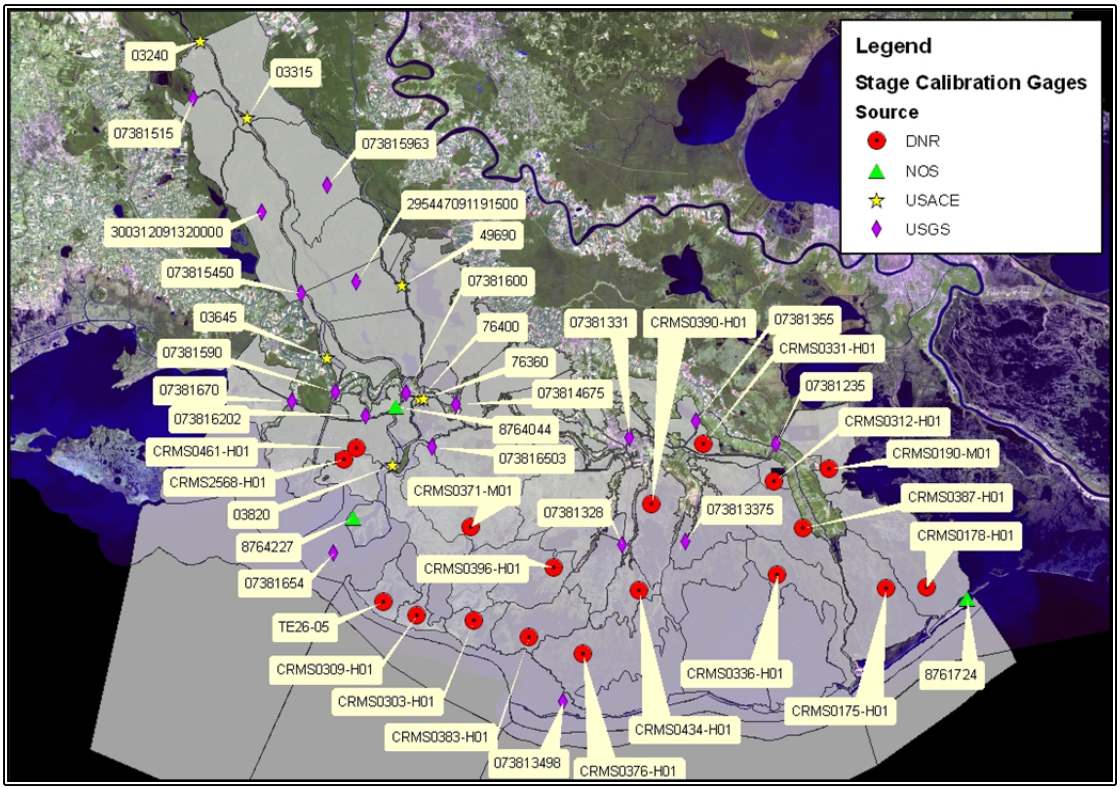

Figure 68 Stage Calibration Sites in the AA Model

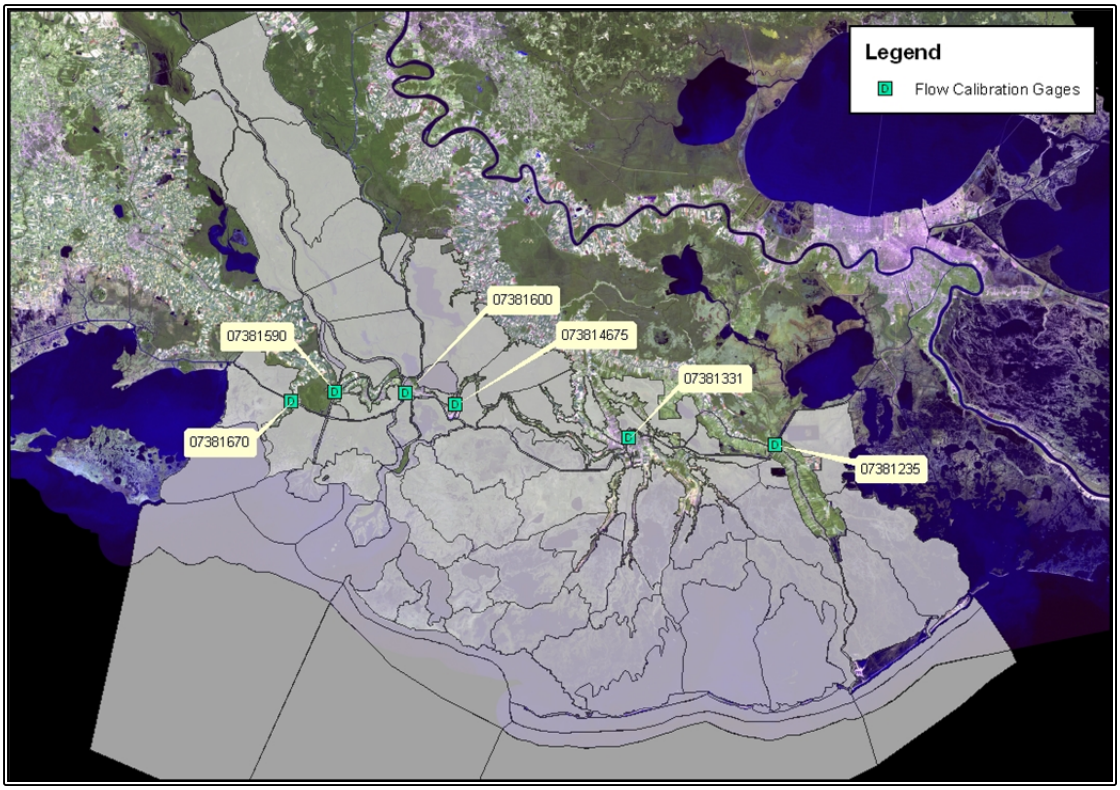

Figure 69 Discharge Calibration Sites in the AA Model

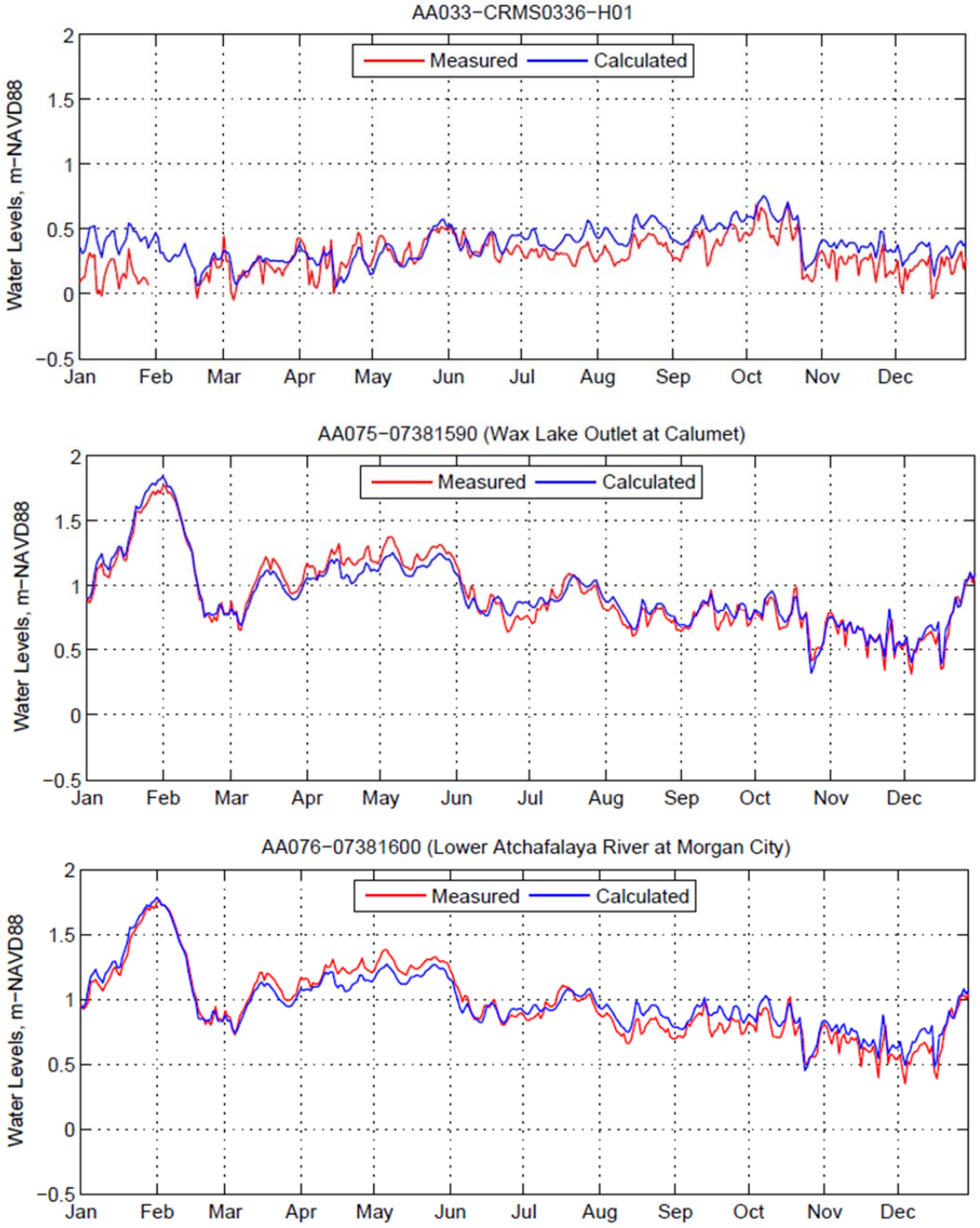

Figure 70 Sample Stage Calibration Results for the AA Model

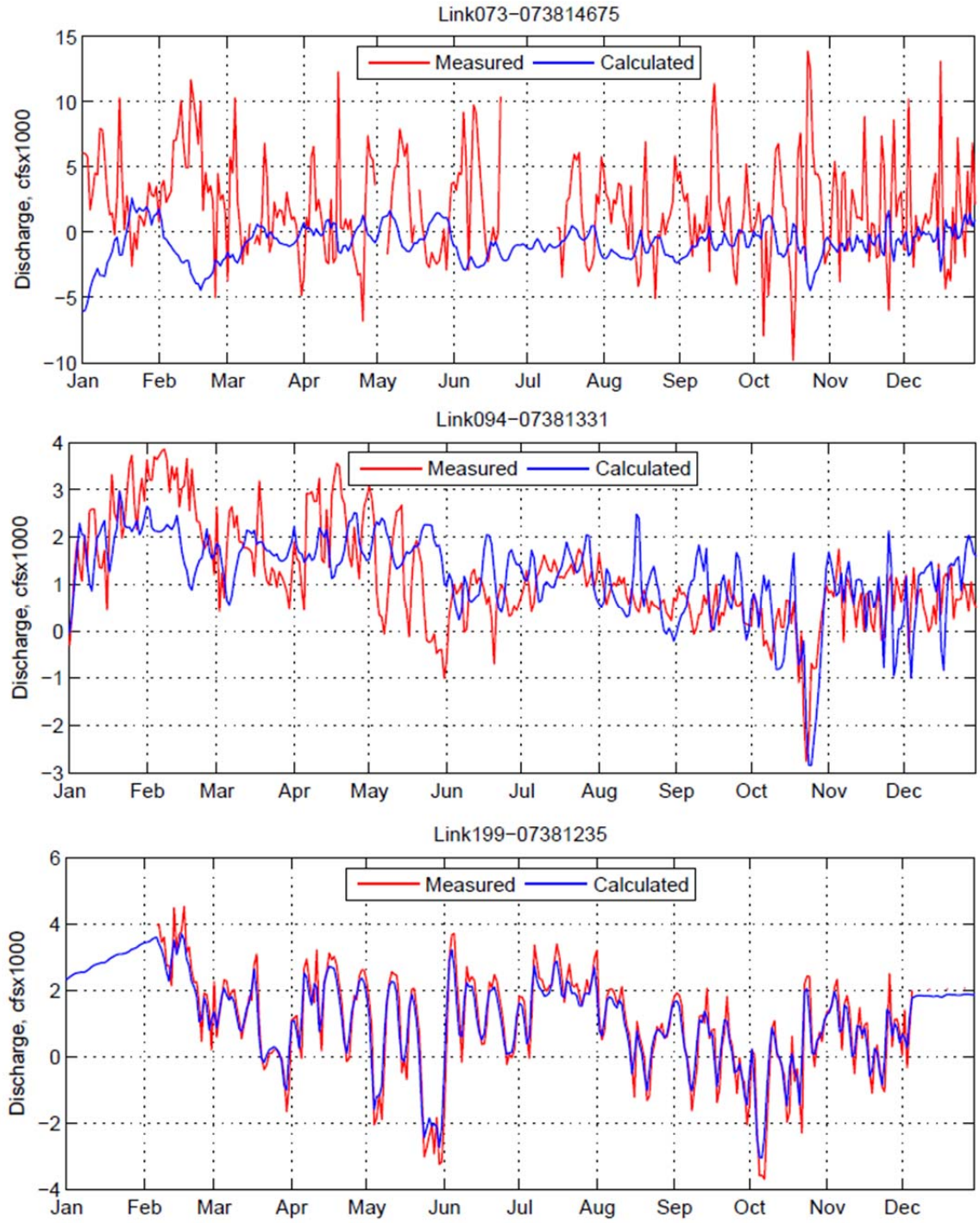

Figure 71 Sample Discharge Calibration Results for the AA Model

Overall, the model results agreed fairly well with the stage and flow measurements as illustrated in **Figure 70** and **Figure 71**, respectively. Potential reasons for the discrepancies between modeled and measured data included: (1) the model was calculating mean representative values of variables for large compartments and was being compared to a measured gauge data value from a specific location; (2) the datum for some of the stage gauges was not known and

therefore an approximation was made based on the best available information; (3) in a large scale link-node model such as this, the hydro connections were not fully represented in detail but instead a general approximation of the connectivity was utilized.

Salinity

Figure 72 presents the gauge locations used for the salinity calibration. The sources of the salinity measurements were the LDNR, LUMCON, and USGS. Due to the lack of salinity measurements offshore, the salinity data at USGS gauge 073813498 was used as the offshore salinity boundary input and was adjusted during calibration. **Figure 73** shows some examples of the calibration results. These and the rest of the salinity calibration plots are shown in Attachment B.

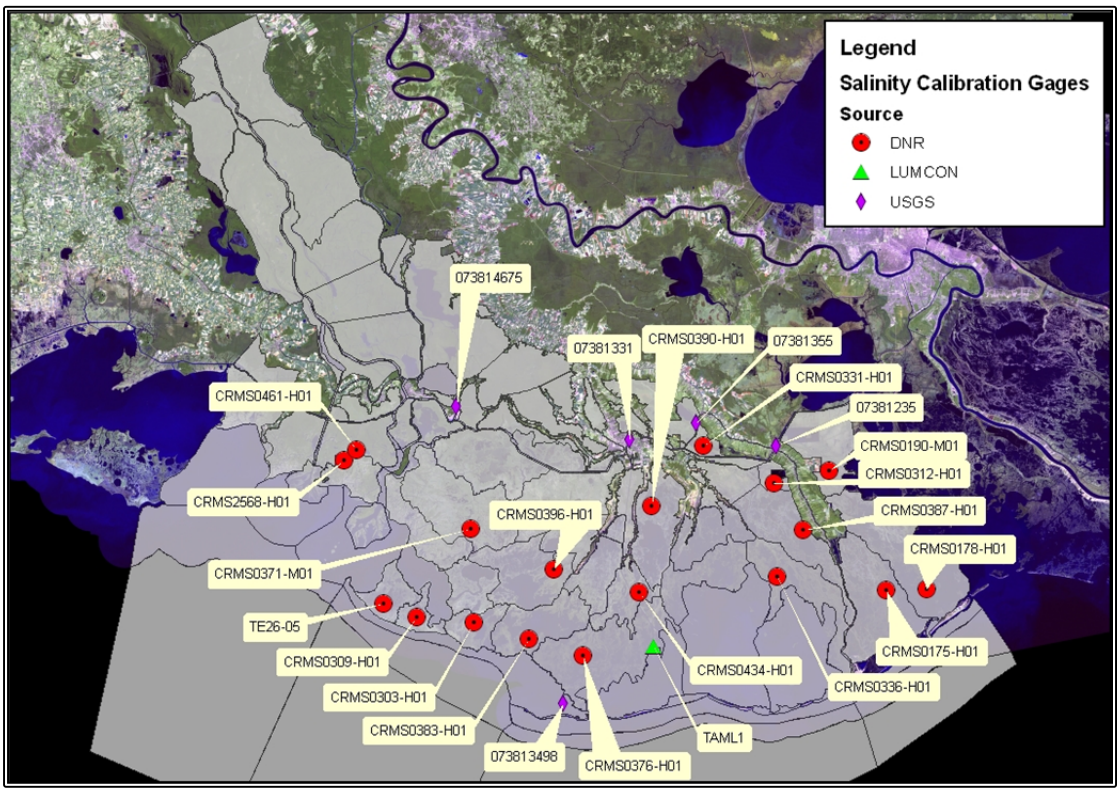

Figure 72 Salinity Calibration Sites in the AA Model

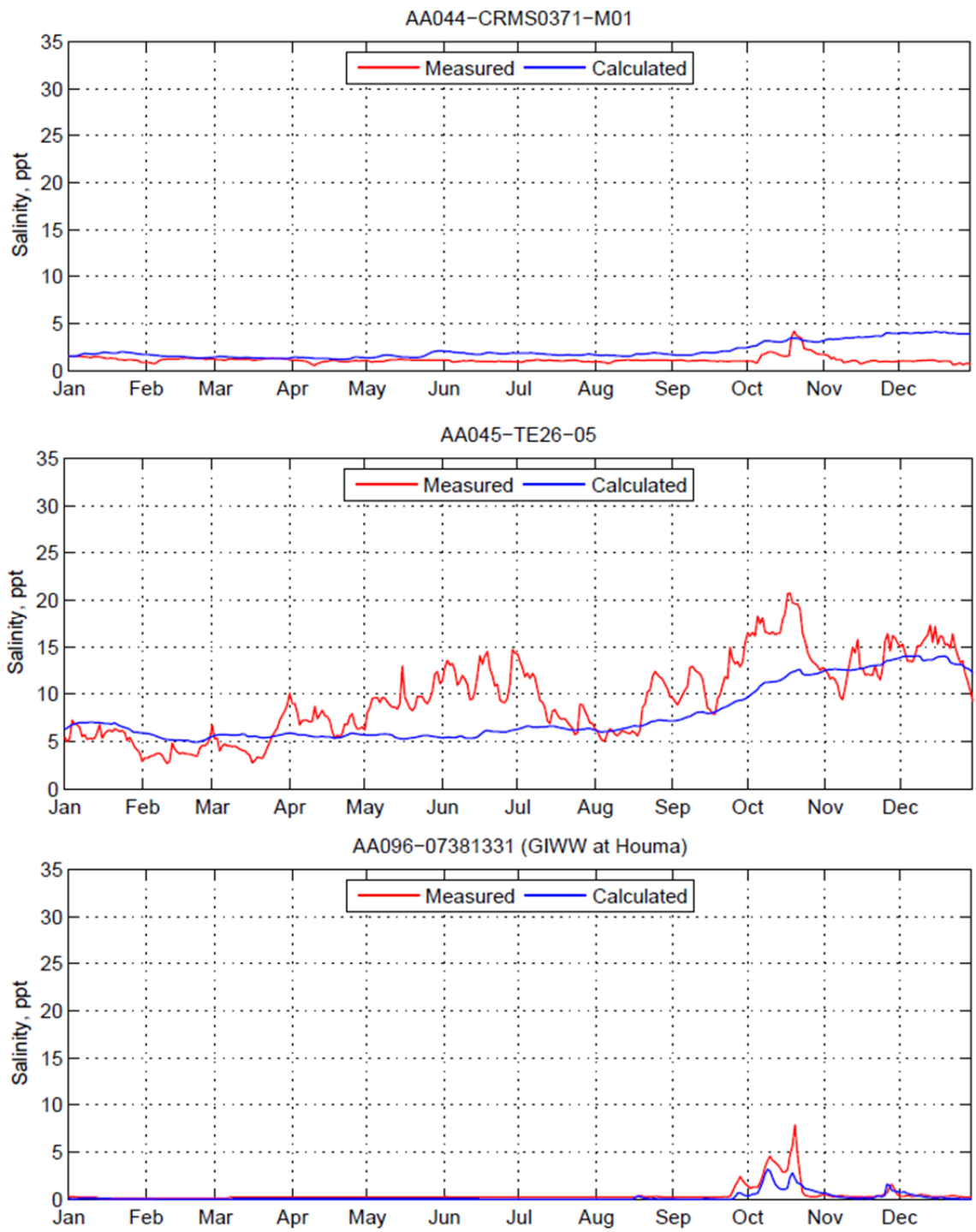

Figure 73 Sample Salinity Calibration Results for the AA Model

Temperature

The calibration parameter for temperature was the sediment temperature and it was set to 20°C, which was equivalent to the daily average air temperature. The computed water temperatures agreed relatively well with those observed when using 20°C for sediment temperature. **Figure 74** presents the temperature calibration results at selective locations.

These and the rest of the temperature calibration plots are shown in Attachment B. The gauge locations are shown in **Figure 68**.

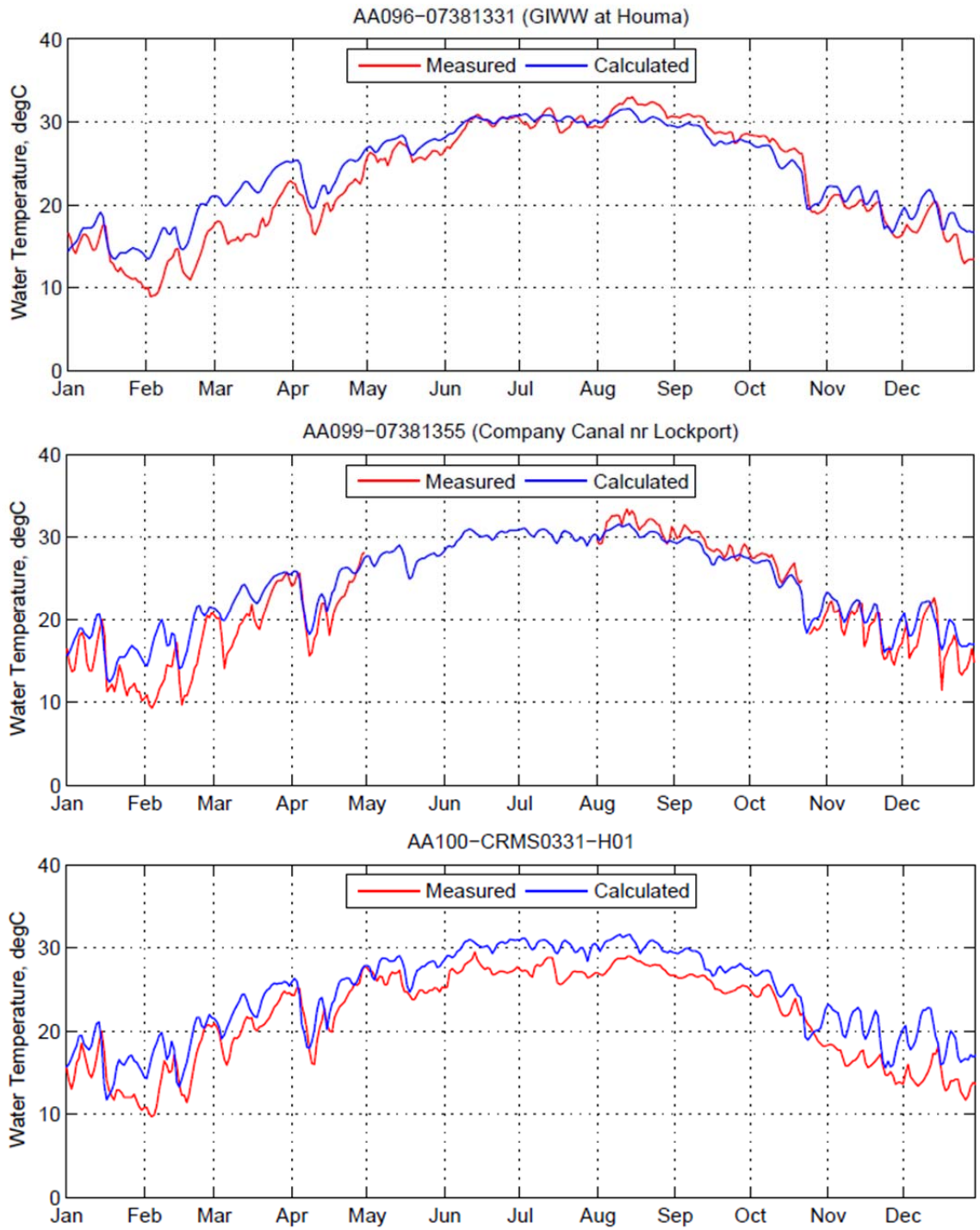

Figure 74 Sample Temperature Calibration Results for the AA Model

Water Quality

Available water quality measurement data were collected by the LDEQ and USGS. **Figure 75** shows the stations that had the 2007 water quality data. Final water quality calibration parameter inputs for the AA model are identified in **Table 39**.

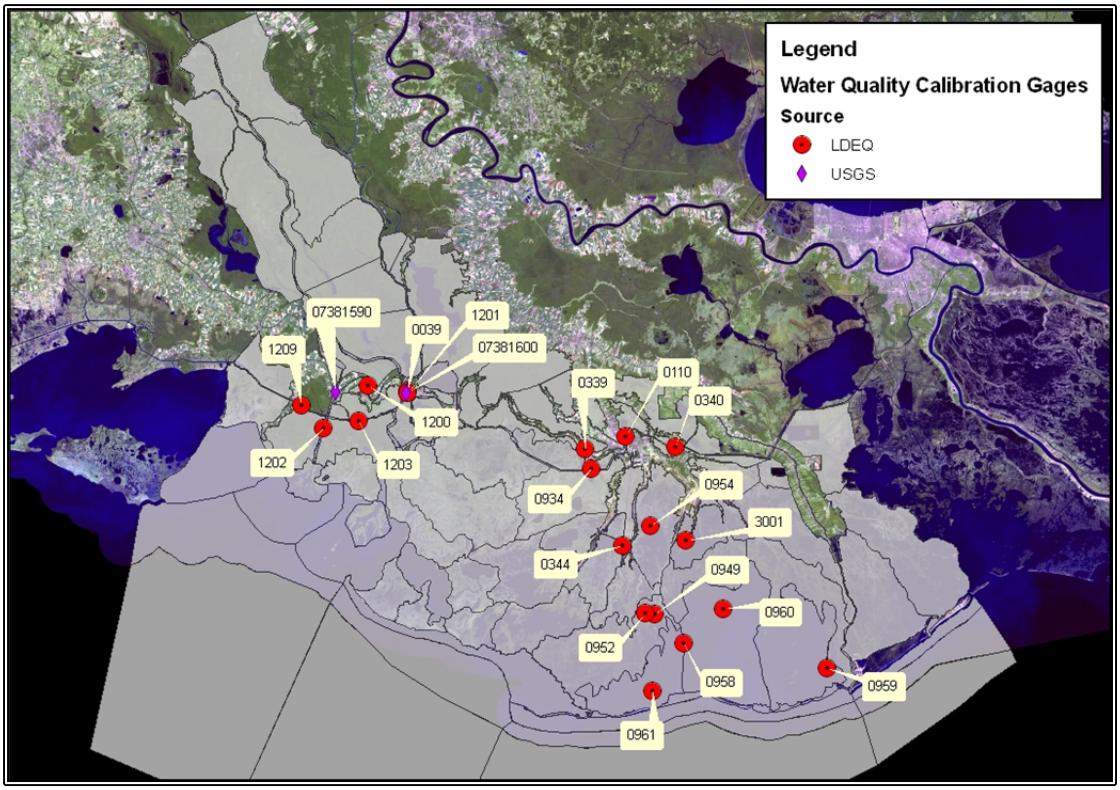

Figure 75 Water Quality Calibration Sites in the AA Model

Table 39 Final Water Quality Calibration Input Parameters for the AA Model

Parameter	Definition	Recommended Values and Ranges
$k_n(20)$	nitrification rate at 20 °C, day^{-1}	computed
$k_n(min)$	lower bound on computed nitrification rate, day^{-1}	0.4
$k_n(max)$	upper bound on computed nitrification rate, day^{-1}	4.0
$k_{dn}(20)$	sediment denitrification rate at 20 °C, m/day	0.05
$k_{hn}(20)$	DON hydrolysis rate at 20 °C, day^{-1}	0.015
$k_{rp}(20)$	phytoplankton respiration rate at 20 °C, day^{-1}	0.05
$k_{dt}(20)$	detritus dissolution rate at 20 °C, day^{-1}	0.05
$k_{hp}(20)$	DOP hydrolysis rate at 20 °C, day^{-1}	0.1
$k_{mp}(20)$	phytoplankton mortality rate at 20 °C, day^{-1}	0.02
v_{d0}	settling rate of detritus for marsh, m/day	0.05 with 0.01 for channels

Parameter	Definition	Recommended Values and Ranges
v_a	algal settling rate, m/day	0.01
$R_P(20)$	orthophosphate P release rate at 20 °C from saltwater marsh sediments, g/m^2/day	0.001
r_{ca}	carbon to chlorophyll ratio, g/g	75
$k_{gp}(20)$	maximum photosynthetic rate at 20 °C, day^{-1}	2.0
KHn	half saturation concentrations for algal uptake of N, mg/L	0.02
KHp	half saturation concentrations for algal uptake of P, mg/L	0.001
f_{Nfix}	fraction of algal group that fixes nitrogen from the atmosphere	0.1 if SAL < 2.0 ppt, otherwise 0.0
k_{eb}	background light extinction coefficient due to water and color, m^{-1}	0.3
KLp	PAR at which phytoplankton growth is optimal, ly/day	300
H	depth of the photic zone used to estimate light limitation for algae, m	Full depth
SAL_{tox}	salinity at which algal growth is halved, ppt	40.0
SAL_{cr}	salinity threshold for flocculation and increased sediment deposition rate, ppt	5.0
K_d	TIP sorption distribution coefficient for partitioning between suspended solids and water, L/kg	500
TMP_s	sediment temperature, ^{o}C	20.0
C_r	base resuspension flux calibration parameter, g/m^2/day	50
W_{cr}	critical wind speed for resuspension above base resuspension, m/sec	2.0

Final calibration results (based on the parameters identified in **Table 39**) at select locations are illustrated in **Figure 76** – **Figure 79** for TSS, ALG, TN, and TPH. These and the rest of the water quality calibration plots are shown in Attachment B.

The computed parameters were daily average values. The observed values were assumed to be representative of the daily mean values although the samples were instantaneous (measured at a particular time on that day). Good agreements between the computed and observed water quality variables in Wax Lake Outlet (USGS 07381590) and Lower Atchafalaya River at Morgan City (USGS 07381600) indicated the proper loading input from the Atchafalaya River.

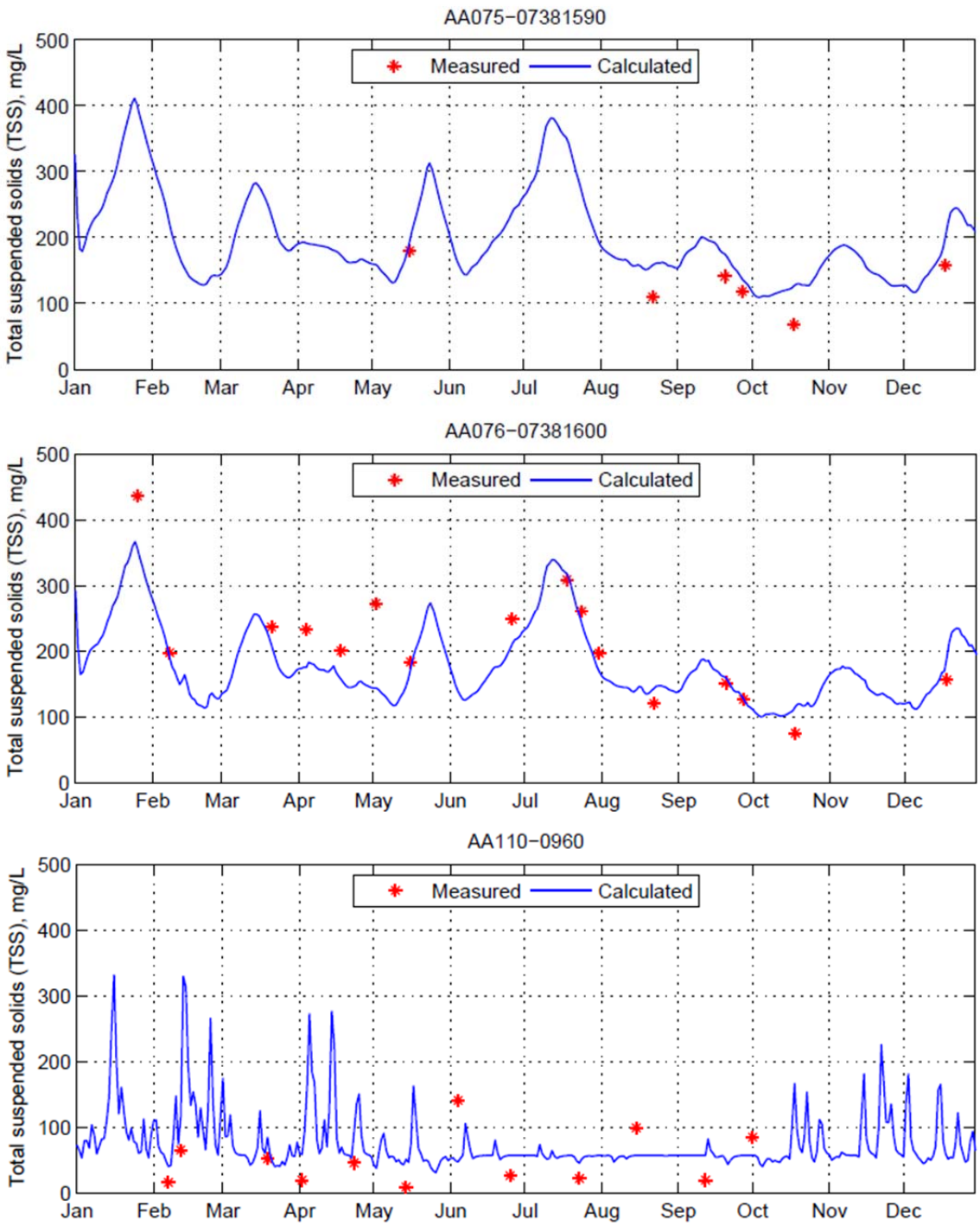

Figure 76 Sample TSS Calibration Results for the AA Model

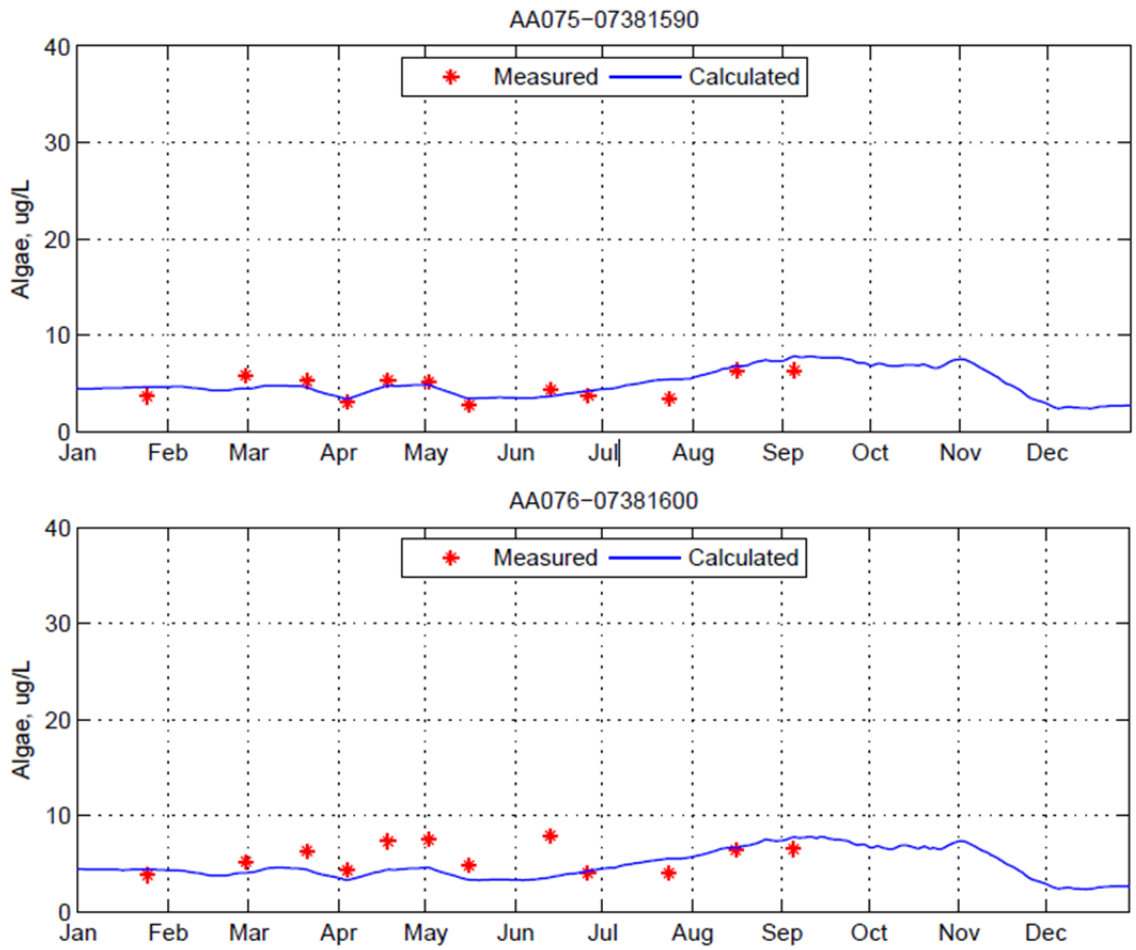

Figure 77 Sample ALG Calibration Results for the AA Model

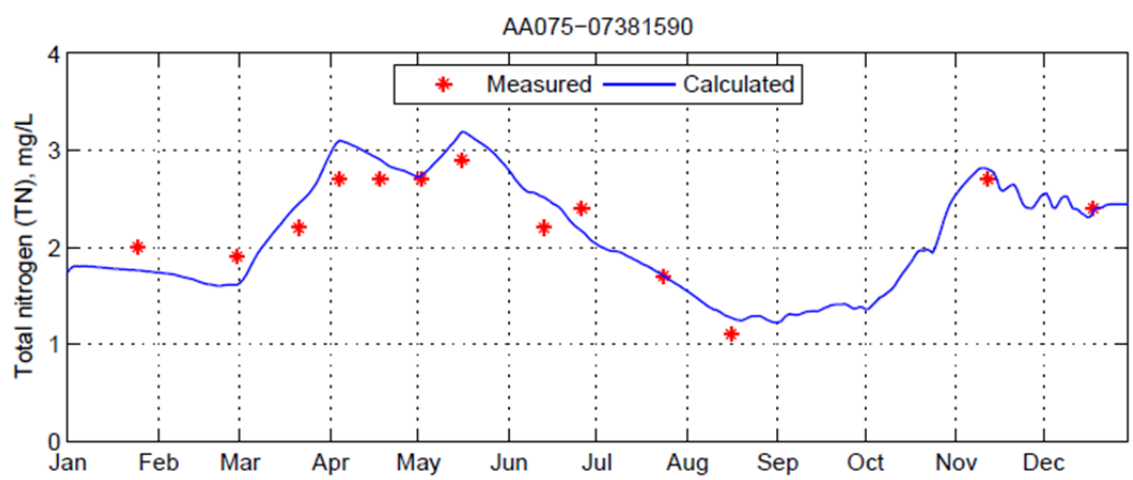

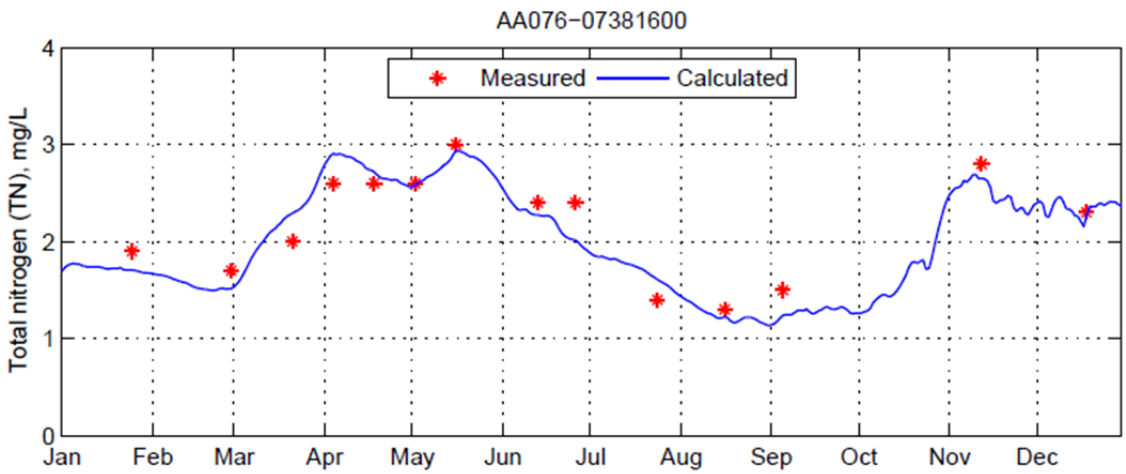

Figure 78 Sample TN Calibration Results for the AA Model

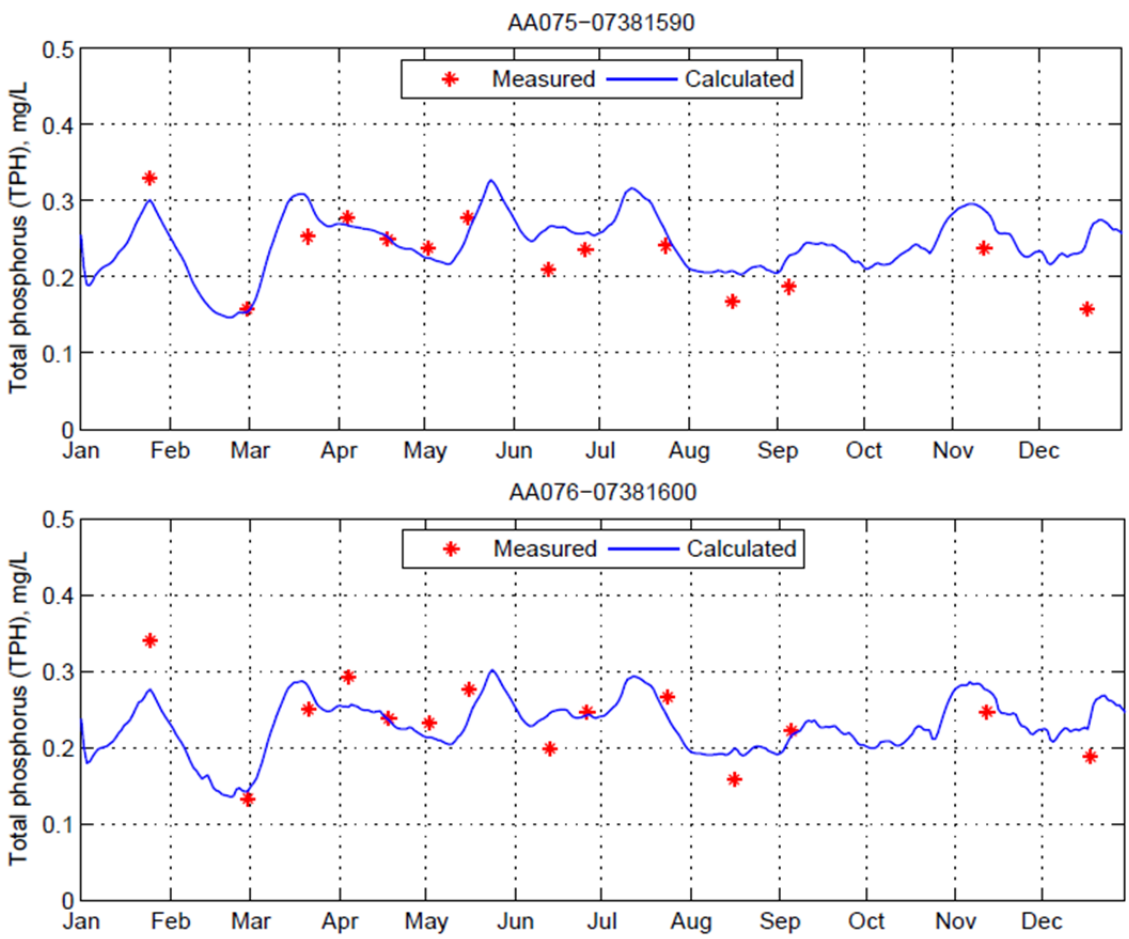

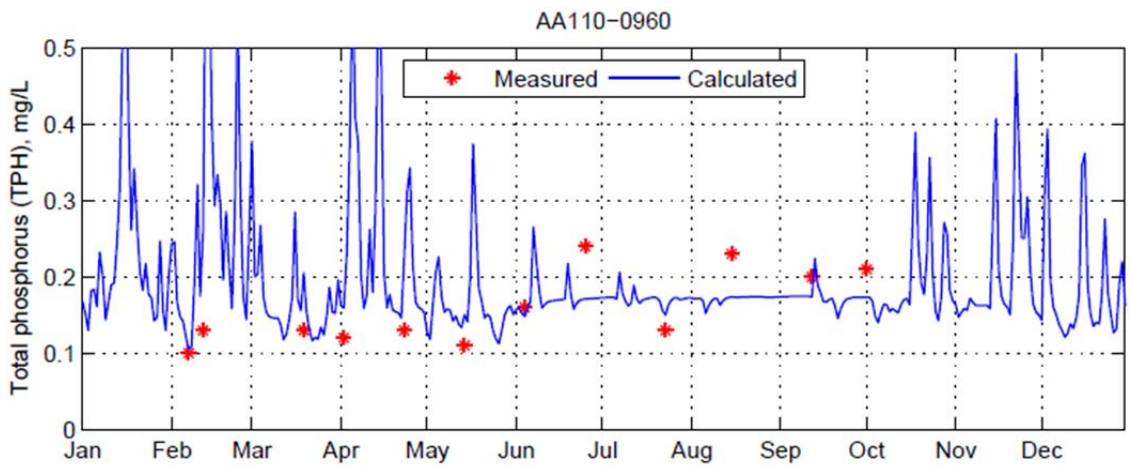

Figure 79 Sample TPH Calibration Results for the AA Model

Validation

The AA model was validated using observed measurements from the calendar years of 2008 – 2009.

Stage and Discharge

Figure 80 depicts stage validation results at representative gauges across the model domain. **Figure 81** illustrates the discharge validation results. These and the rest of the stage and discharge validation results are shown in Attachment B. Overall, with the exceptions of major flood events, the model-predicted results agreed well with the stage and flow measurements during the 2008 and 2009 periods.

During major flood events on the Atchafalaya River, the model over-predicted the stage and discharge at locations within the main stem of the Atchafalaya River. For example, during the Spring of 2008 at the Lower Atchafalaya River gauge at Morgan City (07381600) the peak estimated discharge was over-predicted by approximately 10% at that location. The difference between predicted and measured values could be attributed to limitations of the model, where the model was a simplified representation of the physical system that did not capture in full detail the floodplain hydrology and hydraulics. It appeared that during extreme floods there was overbank flow from the main stem of the Atchafalaya River as well as storage within the floodplain that the calibrated model did not capture. Given that the objective of the model application was to assess long term average conditions, it was determined that the model results were acceptable.

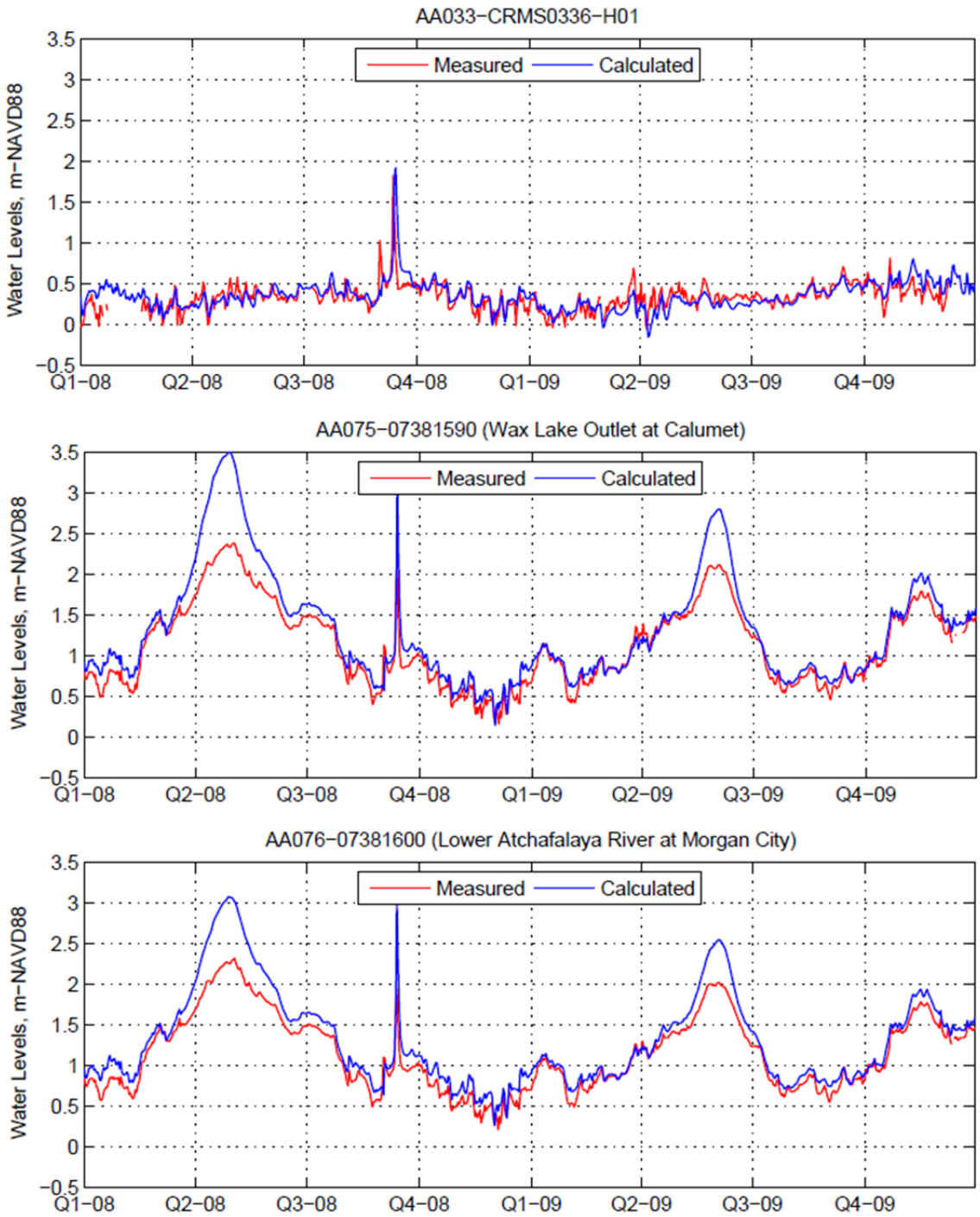

Figure 80 Sample Stage Validation Results for the AA Model

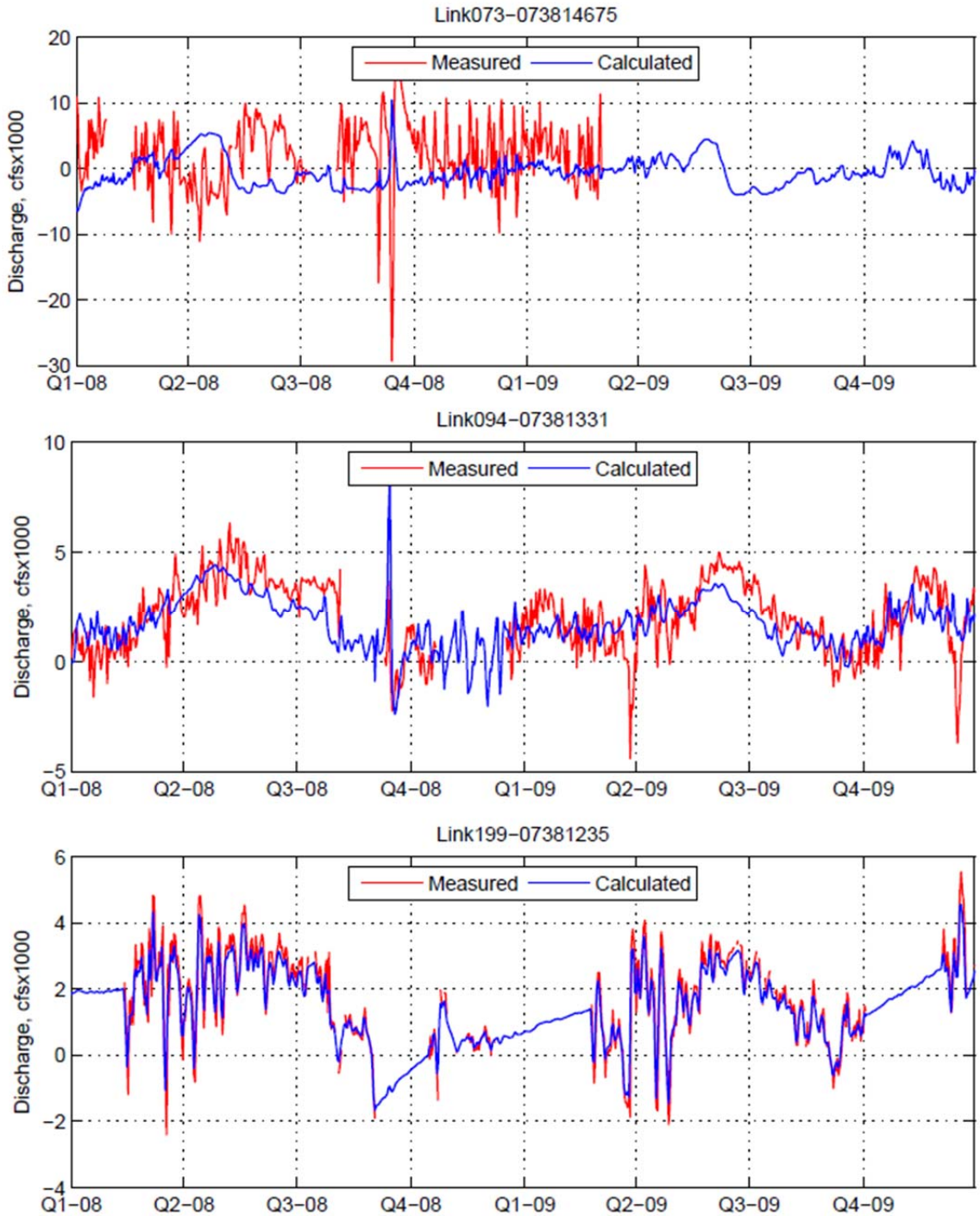

Figure 81 Sample Discharge Validation Results for the AA Model

Salinity

Figure 82 shows some examples of the salinity validation results. These and the rest of the salinity validation results are shown in Attachment B.

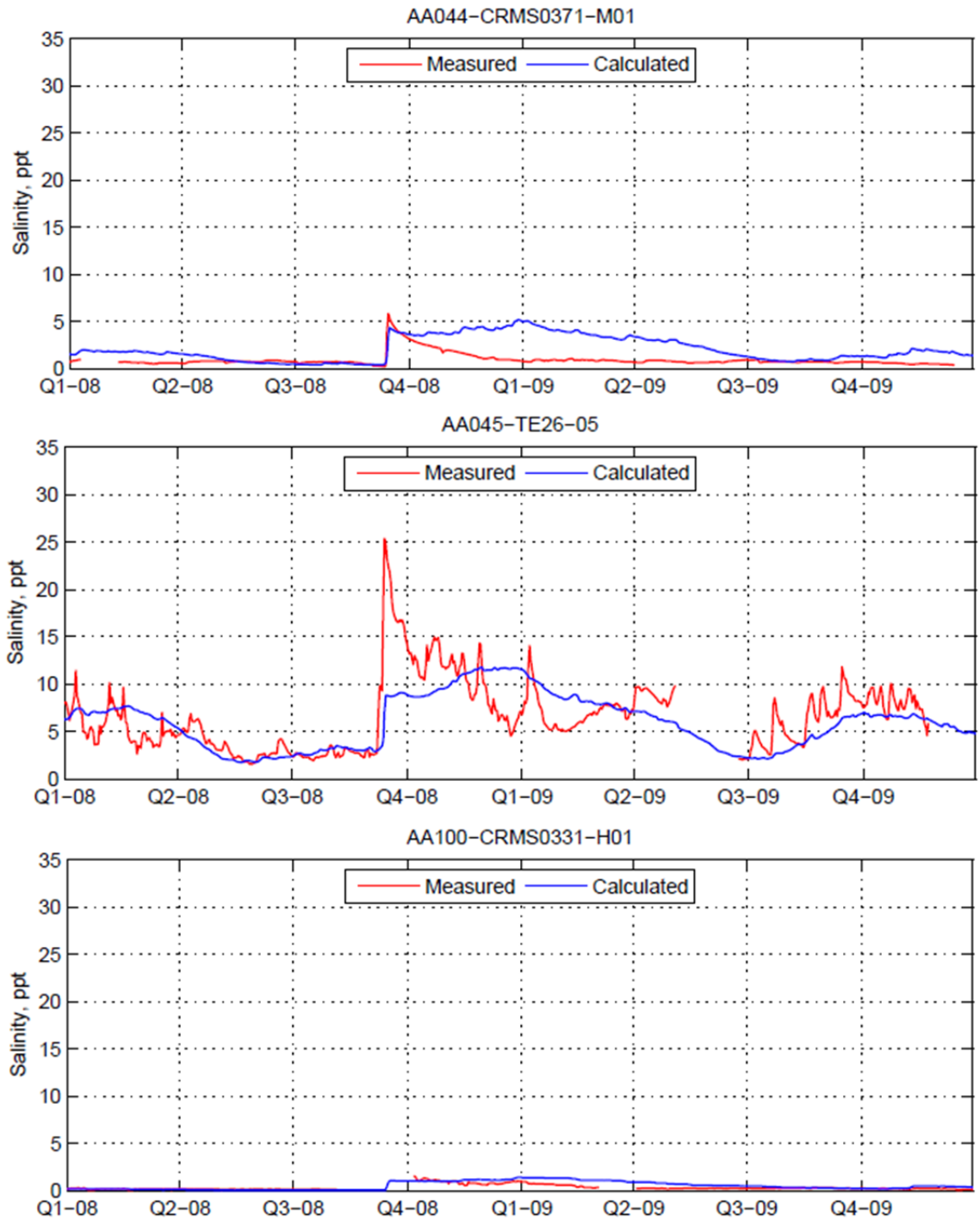

Figure 82 Sample Salinity Validation Results for the AA Model

Temperature

Figure 83 presents the temperature validation results at selective locations. These and the rest of the temperature validation results are shown in Attachment B.

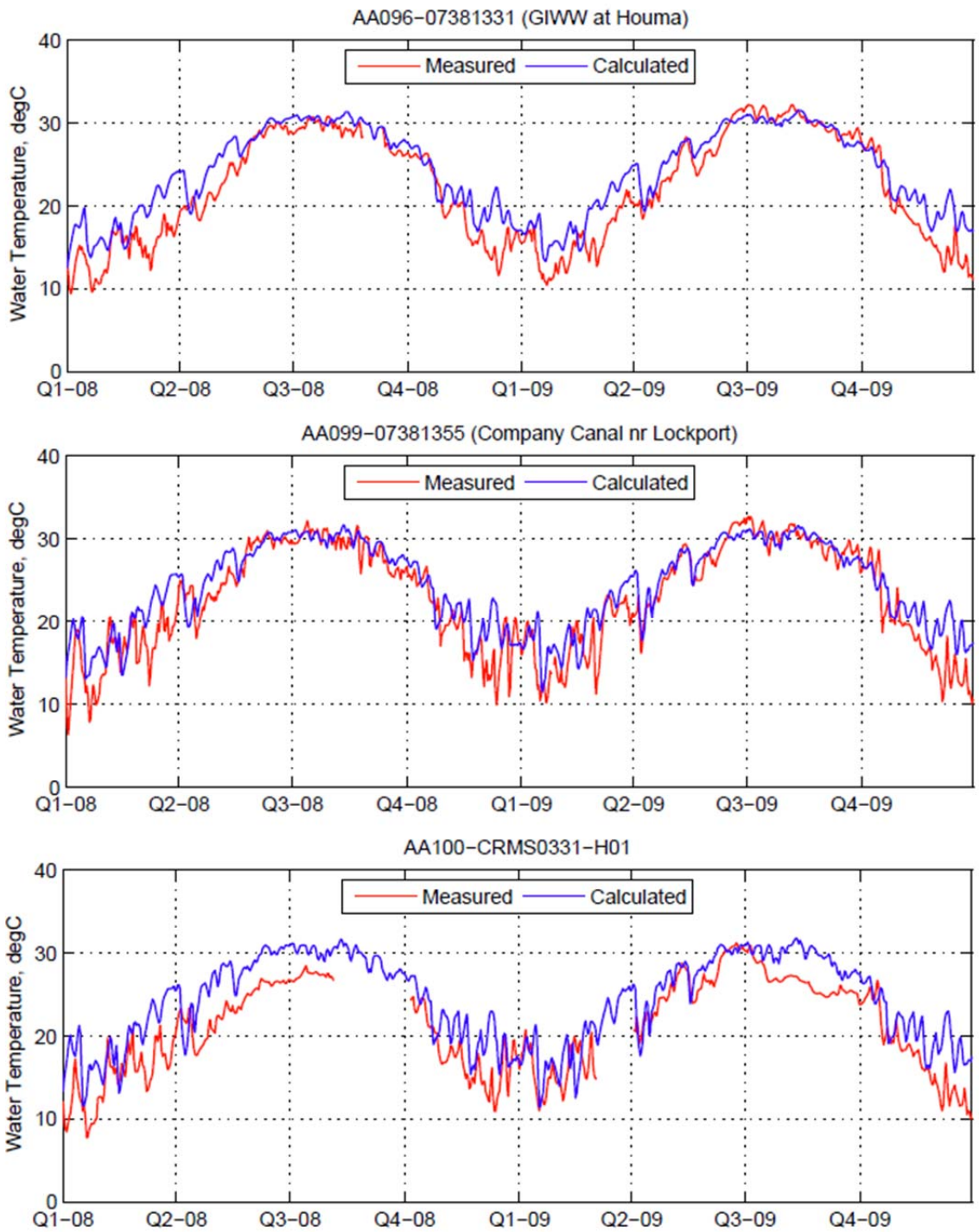

Figure 83 Sample Temperature Validation Results for the AA Model

Water Quality

Figure 84 illustrates the locations of gauges where the 2008-2009 water quality data were available for validation. Validation results are presented below for the gauges located at Wax Lake Outlet (USGS 07381590) and Lower Atchafalaya River at Morgan City (USGS 07381600). The following water quality parameters are illustrated in **Figure 85**, **Figure 86**, and **Figure 87**:

TSS, TN, and TPH. Unfortunately, there were no algae data available during the 2008-2009 periods for comparison.

The computed parameters were daily average values. The observed values were assumed to be representative of the daily mean values although the samples were taken at a particular time on that day. There was generally good agreement between the computed and observed water quality variables in Wax Lake Outlet (USGS 07381590) and Lower Atchafalaya River at Morgan City (USGS 07381600), which indicated the proper loading input from the Atchafalaya River was used.

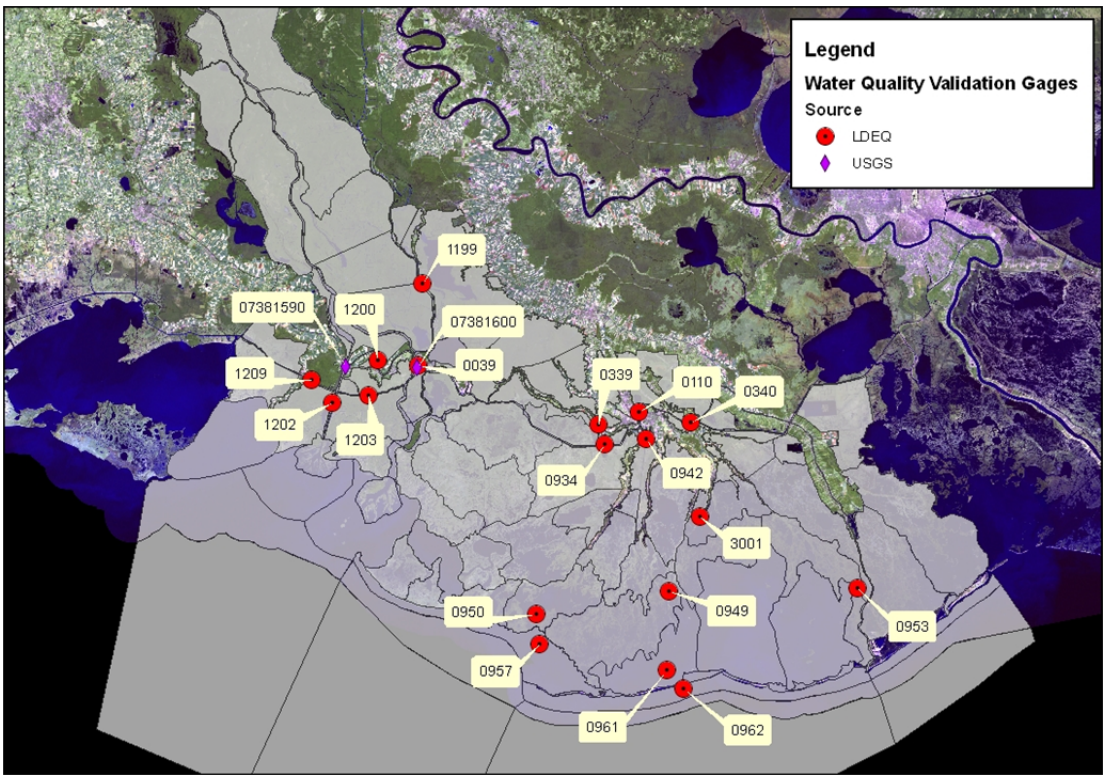

Figure 84 Water Quality Validation Sites in the AA Model

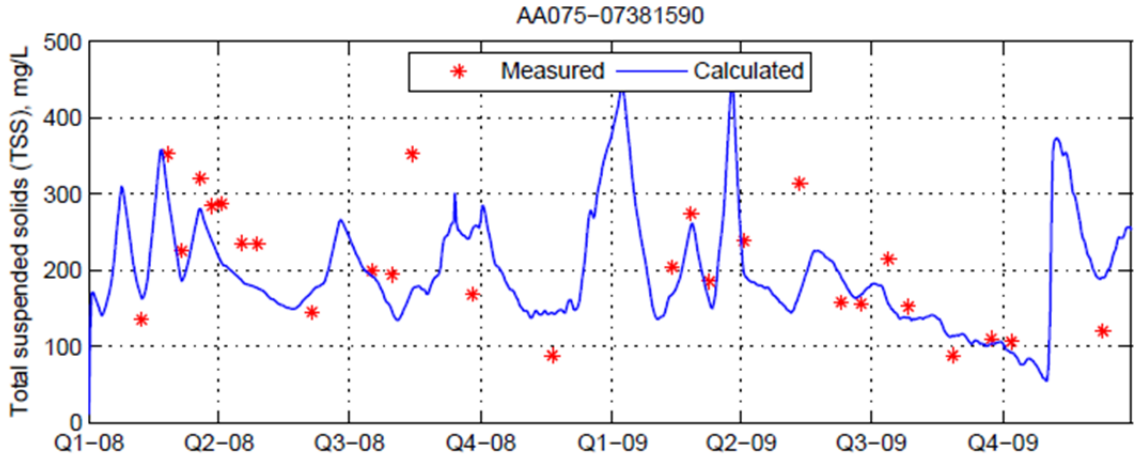

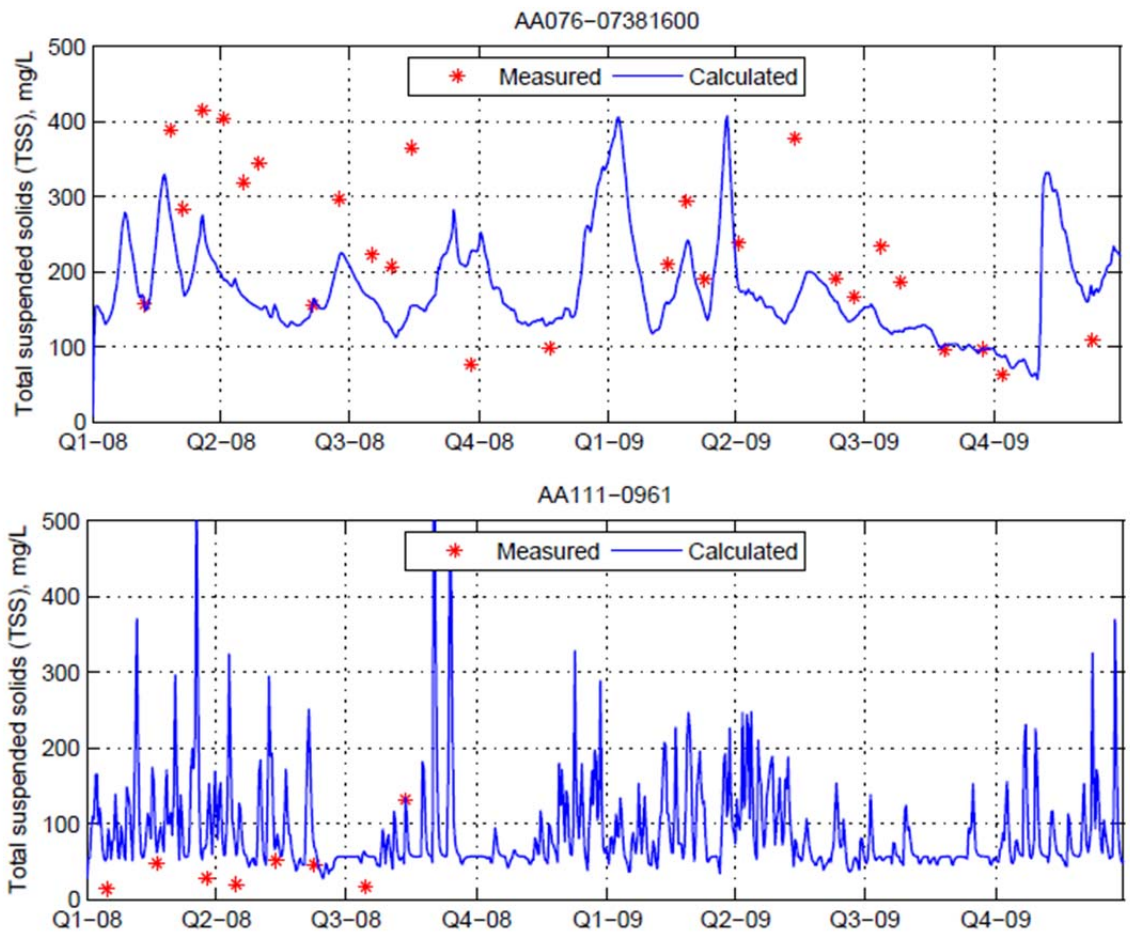

Figure 85 Sample TSS Validation Results for the AA Model

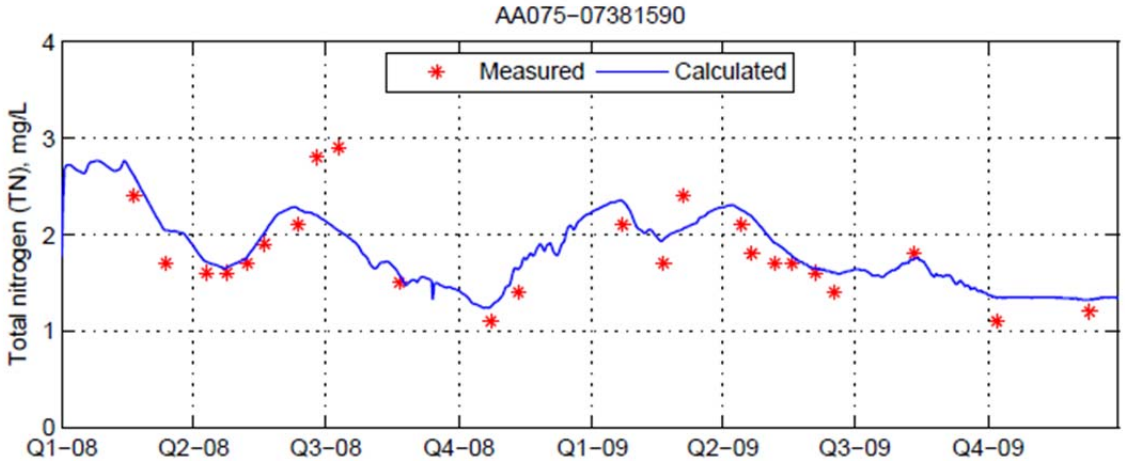

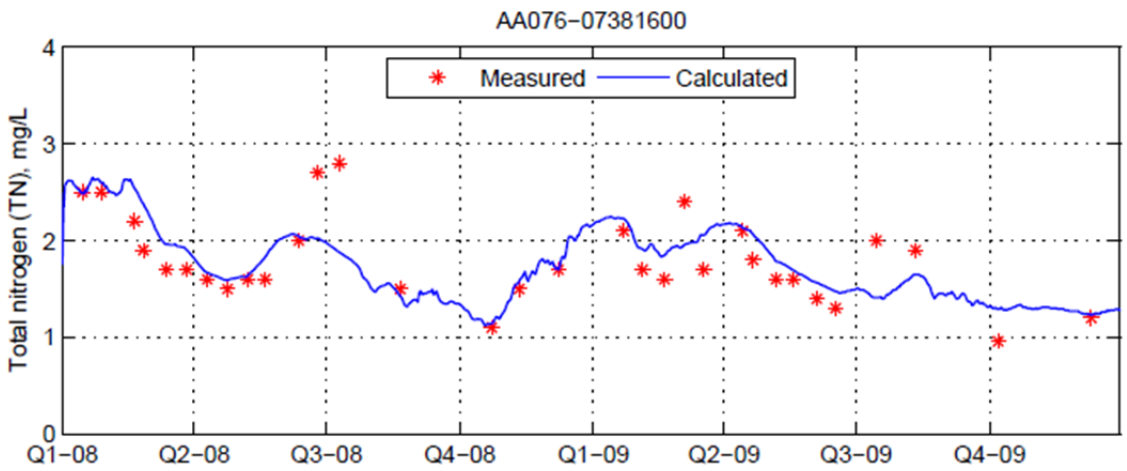

Figure 86 Sample TN Validation Results for the AA Model

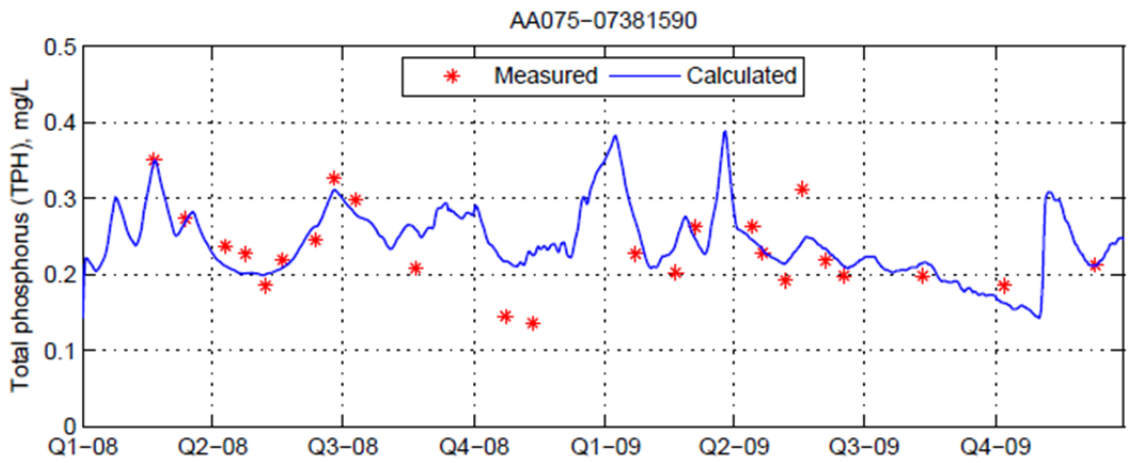

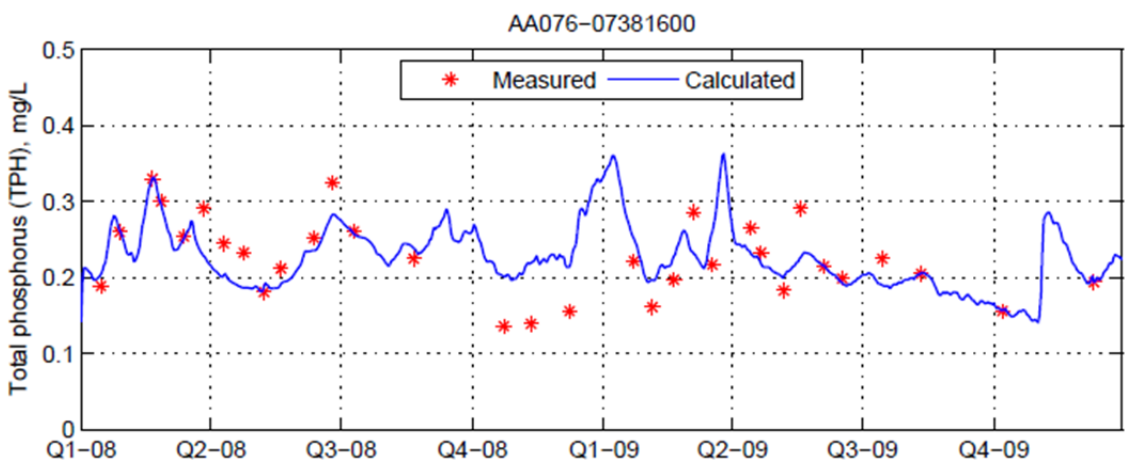

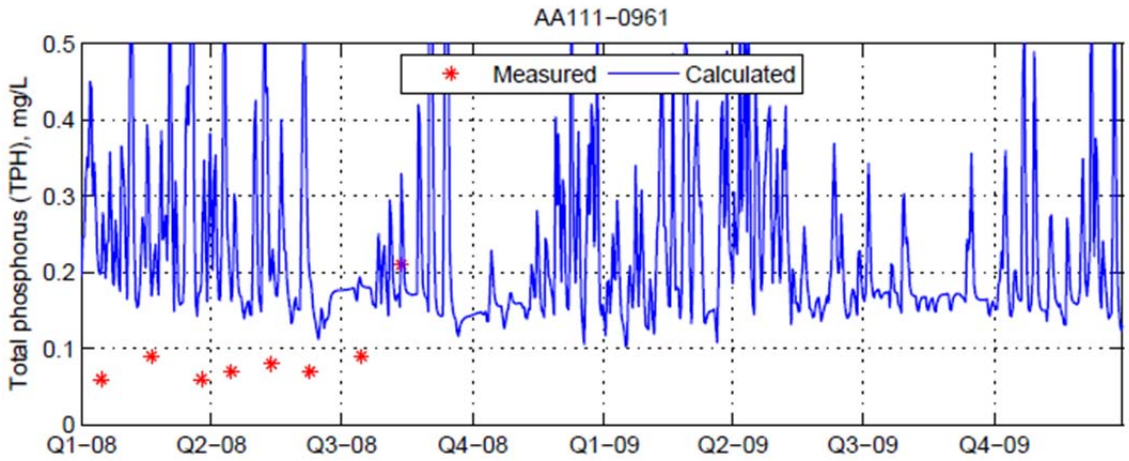

Figure 87 Sample TPH Validation Results for the AA Model

Chenier Plain Model

Calibration

The CP model was calibrated using observed measurements for the calendar year of 2007.

Stage

The stations used for stage calibration were collected from the USGS, USACE, NOAA, and CRMS and are shown in **Figure 88**. Effective compartment exchange widths were measured in ArcGIS and were updated in the model during calibration. The minor loss coefficient and further modifications to the exchange width based on LiDAR, aerials, and cross-section data were used to calibrate the stage and salinity simultaneously.

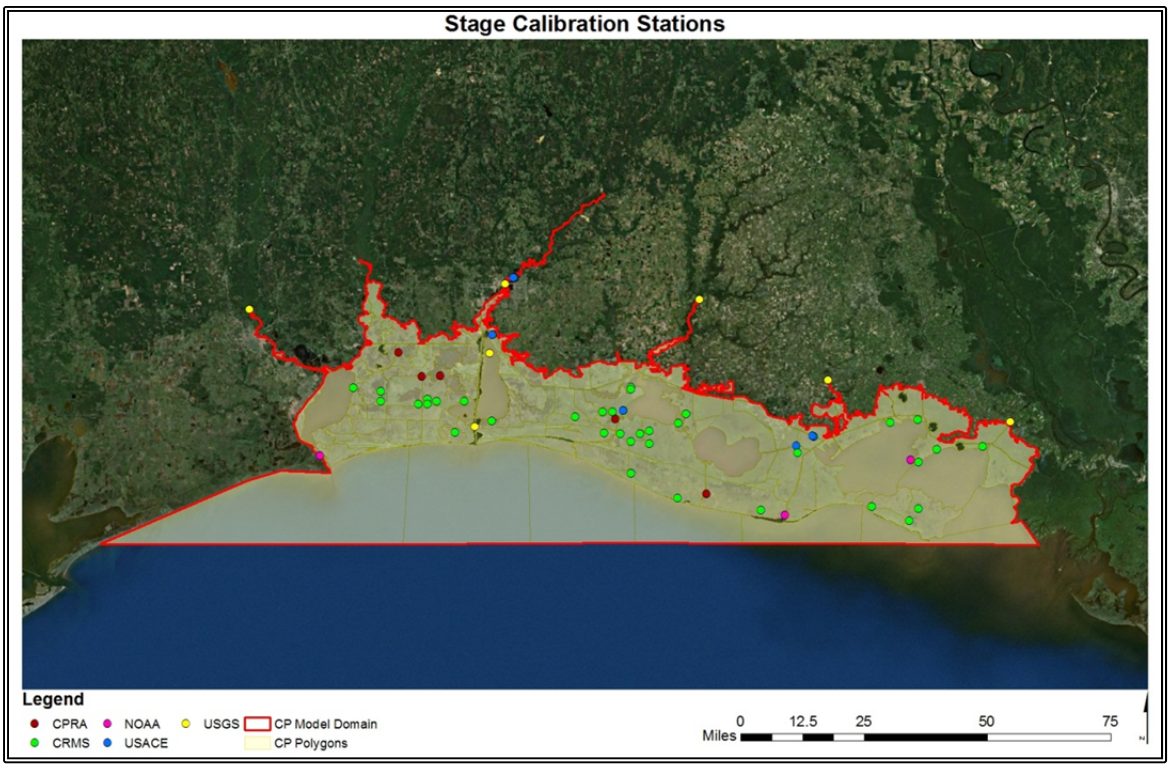

Figure 88 Stage Calibration Sites in the CP Model

Figure 89 shows some of the stage calibration results. These and the rest of the plots are included in Attachment B. The model-predicted stage agreed well with the measured data in the west (Sabine and Calcasieu Basins) while it over-predicted year round in the central portion (Mermentau Basin) and only over-predicted low stages in the east (Vermilion/Teche Basin). The Mermentau Basin was consistently over-predicting due to the lack of information regarding the amount of water pumped out of the area and into farmland. This higher water adjacent to the east was likely the culprit for over-predicting the low stages.

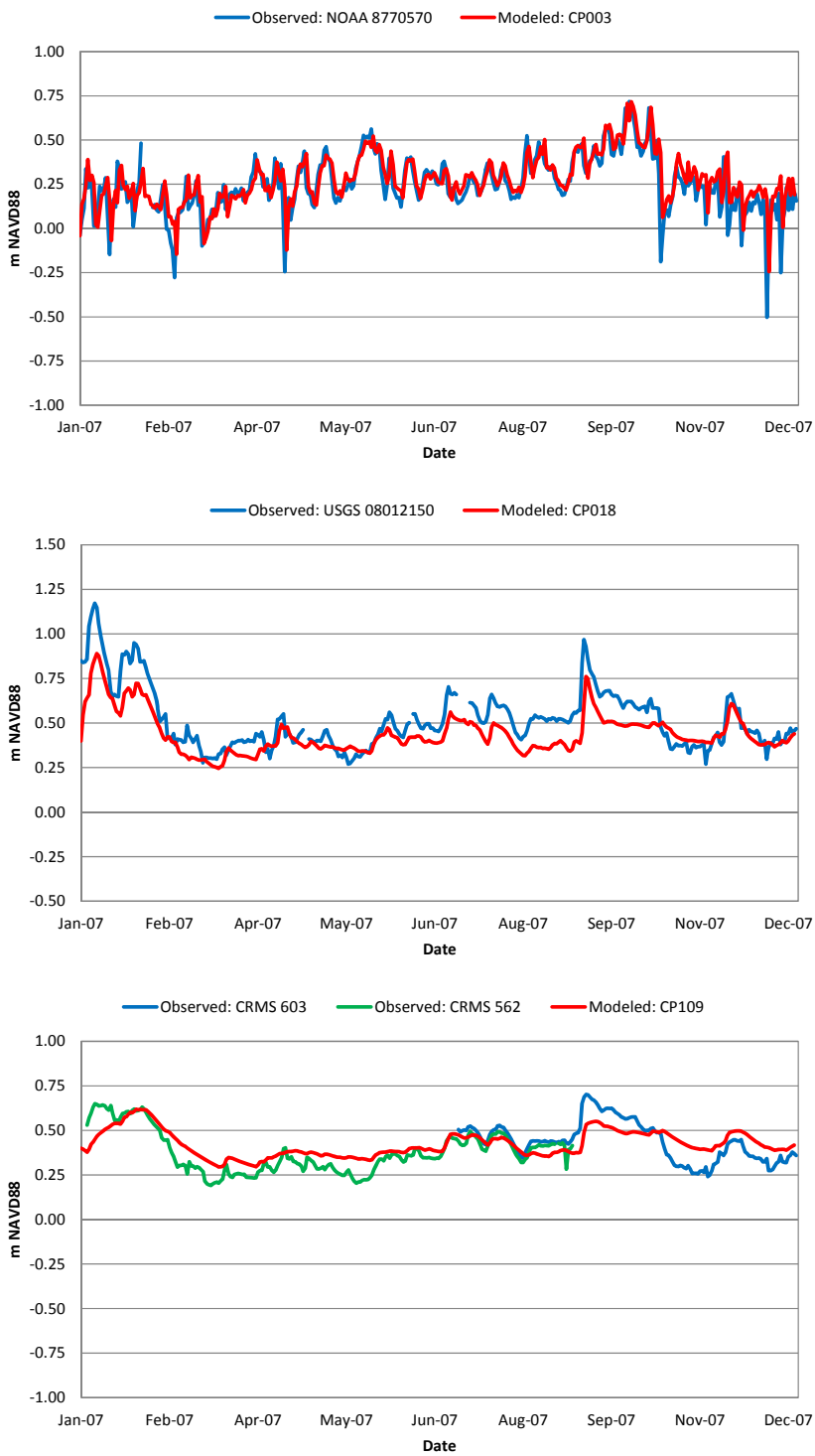

Figure 89 Sample Stage Calibration Results for the CP Model

Salinity

The stations used for calibrating salinity were collected from the CPRA, CRMS, LDEQ, NOAA, TCEQ, USACE, and USGS and are shown in **Figure 90**. As mentioned in the previous section, stage and salinity were calibrated simultaneously.

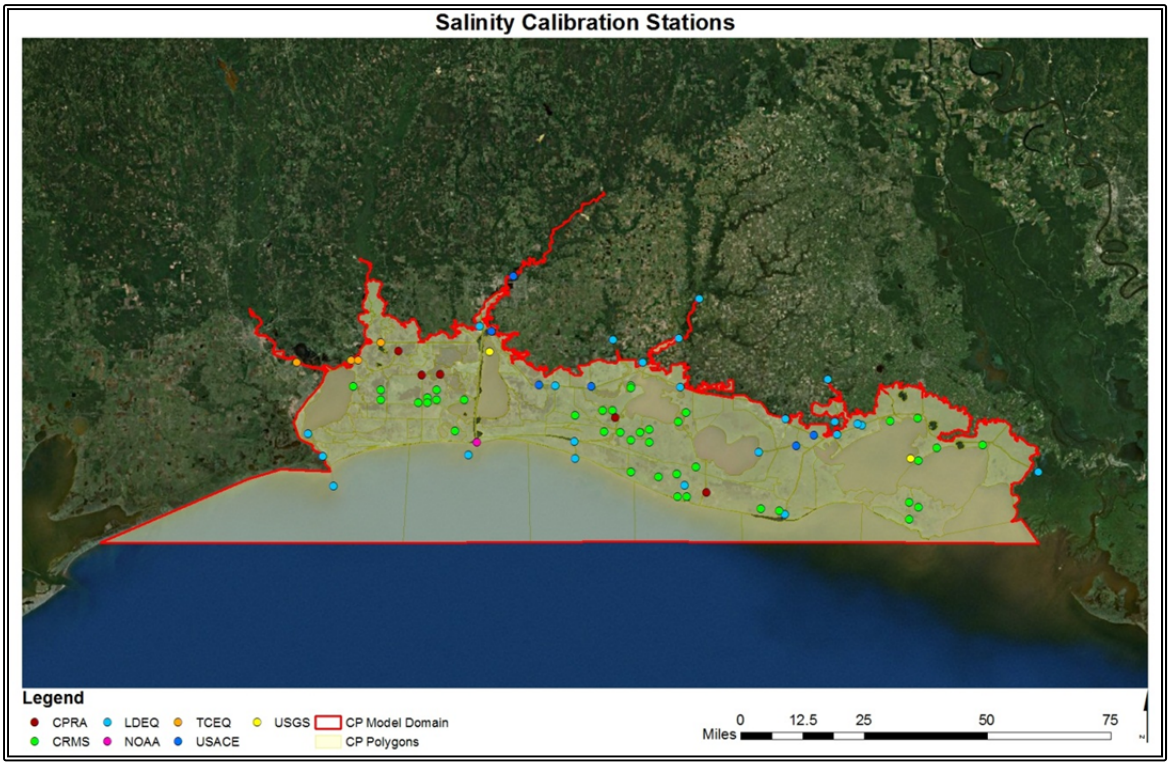

Figure 90 Salinity Calibration Sites in the CP Model

Figure 91 shows some of the salinity calibration results. These and the rest of the plots are included in Attachment B. The model salinity agreed fairly well against observed data with the exception of the GIWW east and west of the Calcasieu River. The model over-predicted the salinity directly west and under-predicted salinity directly east of the Calcasieu River. The model compartments for these two GIWW segments spanned approximately 24 miles for the west and 32 miles for the east. The model only calculated a single average value for each compartment no matter how large it was. In reality, the salinity on one side of the GIWW compartments could sometimes be 10 ppt higher or lower than the other, which could be the cause of the over-prediction in the GIWW segments.

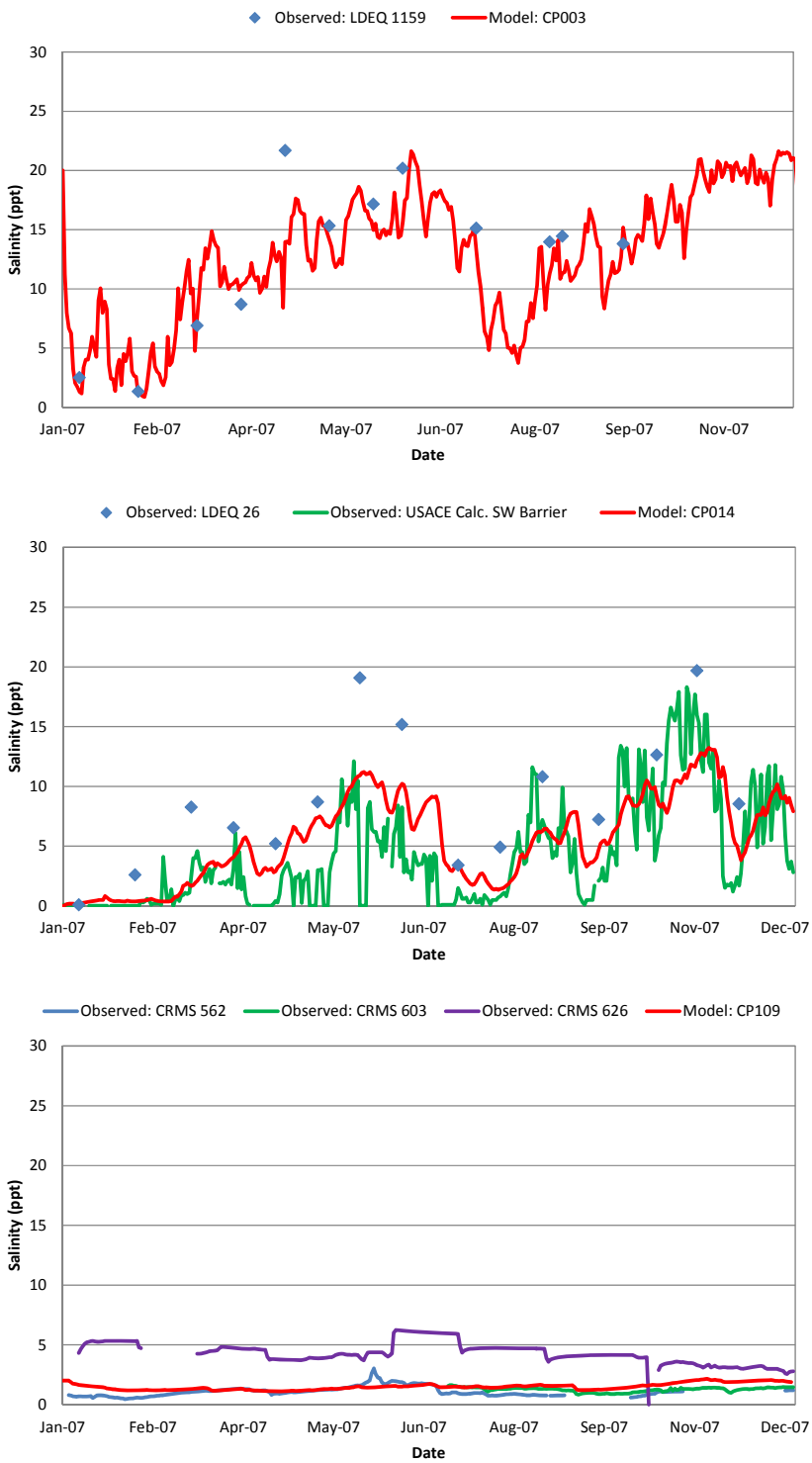

Figure 91 Sample Salinity Calibration Results for the CP Model

Temperature

The temperature and water quality data used for calibration were collected from the LDEQ website. The stations used for calibrating temperature and the other water quality constituents are shown in **Figure 92**.

Again, the only calibration parameter for temperature was the bed sediment temperature, TMP_{sed}. The sediment temperature was set to 20 °C, similar to the AA region. For the offshore boundary conditions, the surface temperatures were set to the AA values, which were taken from stations in the Gulf. These values were reduced for the winter and fall months to account for the cooler water flowing from the Atchafalaya River westward along the coast into the CP domain. The temperatures were adjusted until observed values matched measured values.

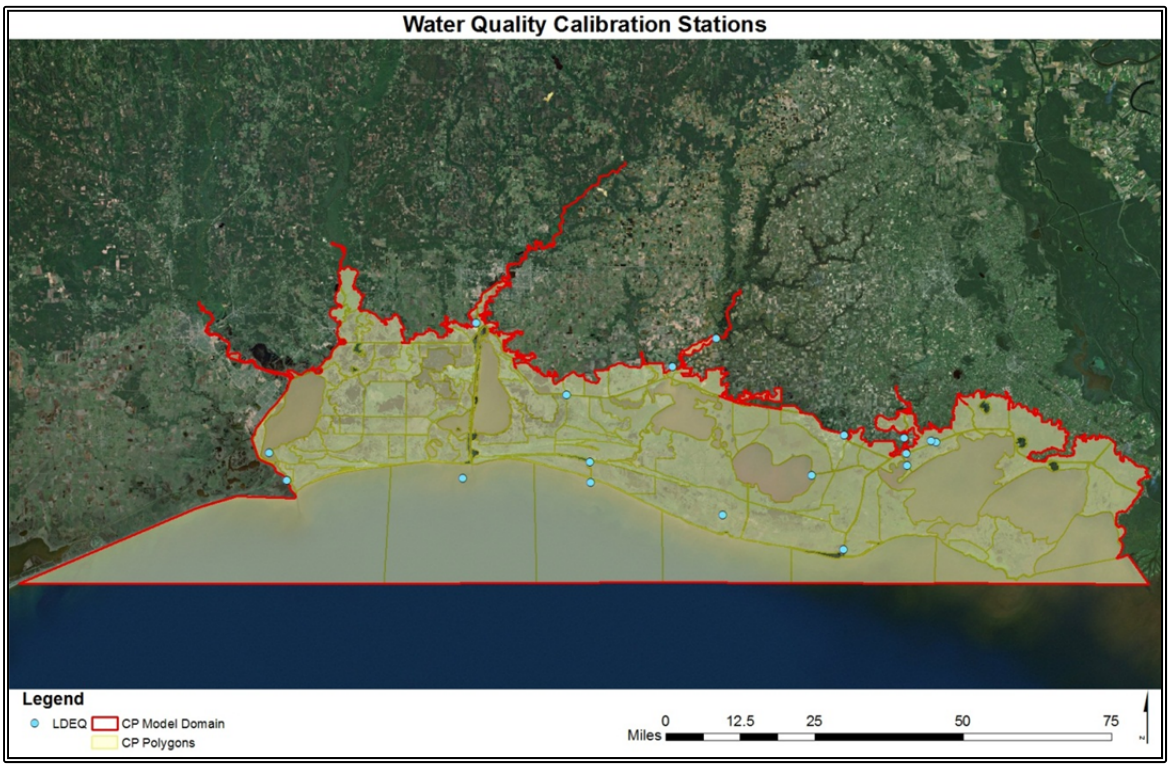

Figure 92 Water Quality Calibration Sites in the CP Model

Figure 93 presents the temperature calibration results at selective locations. These and the rest of the plots are also included in Attachment B. The temperature results compared very well to observed values. There were slight discrepancies near the end of the calibration period, which could be the result of using the sine curve fit to create the freshwater inflows.

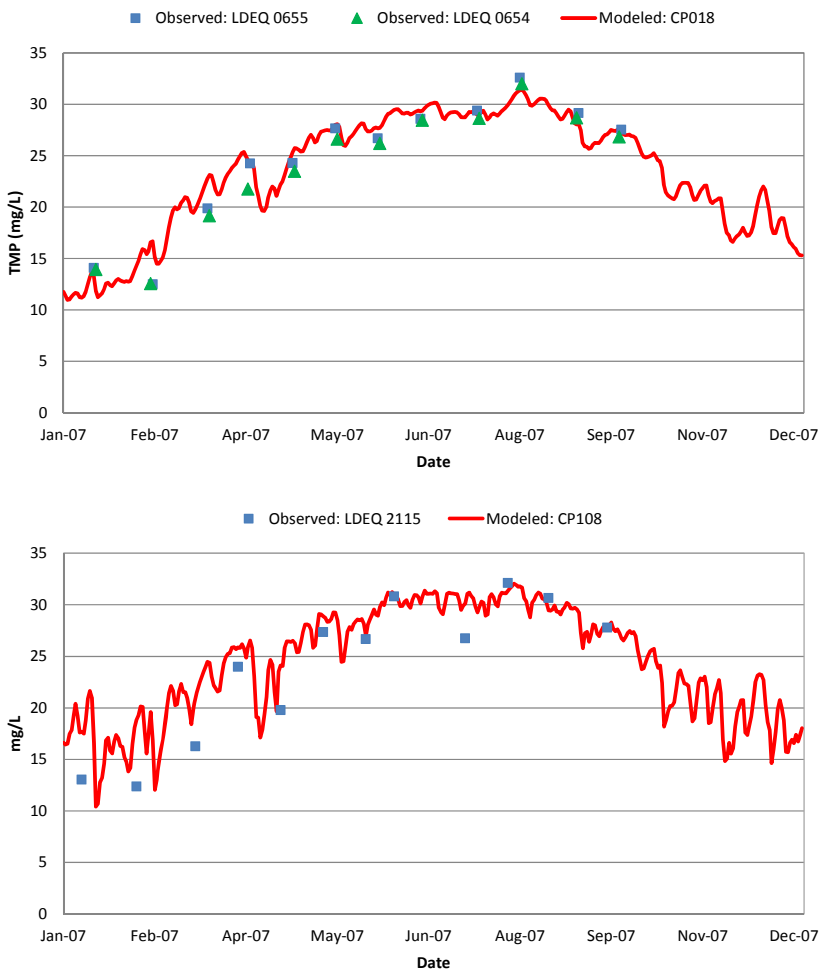

Figure 93 Sample Temperature Calibration Results for the CP Model

Water Quality

The following table lists the water quality calibration parameters used in the CP model. Most of these parameters pertain to algae and nutrients, but the table also includes parameters used for TSS and temperature.

Table 40 Water Quality Calibration Parameters for the CP Model

Parameter	Definition	Recommended Values and Ranges
$k_n(20)$	nitrification rate at 20 ° C, day^{-1}	computed
$k_n(min)$	lower bound on computed nitrification rate, day^{-1}	0.05
$k_n(max)$	upper bound on computed nitrification rate, day^{-1}	0.3
$k_{dn}(20)$	sediment denitrification rate at 20 °C, m/day	0.05
$k_{hn}(20)$	DON hydrolysis rate at 20 °C, day^{-1}	0.05

Parameter	Definition	Recommended Values and Ranges
$k_{rp}(20)$	phytoplankton respiration rate at 20 °C, day^{-1}	0.05
$k_{dt}(20)$	detritus dissolution rate at 20 °C, day^{-1}	0.02
$k_{hp}(20)$	DOP hydrolysis rate at 20 °C, day^{-1}	0.1
$k_{mp}(20)$	phytoplankton mortality rate at 20 °C, day^{-1}	0.05
v_{d0}	settling rate of detritus for marsh, m/day	0.01
v_a	algal settling rate, m/day	0.01
$R_P(20)$	orthophosphate P release rate at 20 °C from saltwater marsh sediments, g/m^2/day	0.0
r_{ca}	carbon to chlorophyll ratio, g/g	75
$k_{gp}(20)$	maximum photosynthetic rate at 20 °C, day^{-1}	1.5
KHn	half saturation concentrations for algal uptake of N, mg/L	0.1
KHp	half saturation concentrations for algal uptake of P, mg/L	0.005
f_{Nfix}	fraction of algal group that fixes nitrogen from the atmosphere	0.1 if SAL < 2.0 ppt, otherwise 0.0
k_{eb}	background light extinction coefficient due to water and color, m^{-1}	0.3
KLp	PAR at which phytoplankton growth is optimal, ly/day	300
H	depth of the photic zone used to estimate light limitation for algae, m	Full depth
SAL_{tox}	salinity at which algal growth is halved, ppt	40.0
SAL_{cr}	salinity threshold for flocculation and increased sediment deposition rate, ppt	5.0
K_d	TIP sorption distribution coefficient for partitioning between suspended solids and water, L/kg	500
T_s	sediment temperature, ^{o}C	20.0
C_r	base resuspension flux calibration parameter, g/m^2/day	50
W_{cr}	critical wind speed for resuspension above base resuspension, m/sec	2.0

It should be noted that the algal settling rate, V_a, was calibrated to 0.1 m/day for the open water compartments of the Vermilion Bay and both the West and East Cote Blanche Bays[51] because those compartments were connected directly to the Gulf. **Figure 94** shows the location of these compartments.

[51] For project Groups 4 and 5 these three compartments are numbered as 40, 41, and 42 because a channel compartment is added in those project groups, which requires re-numbering of the compartments.

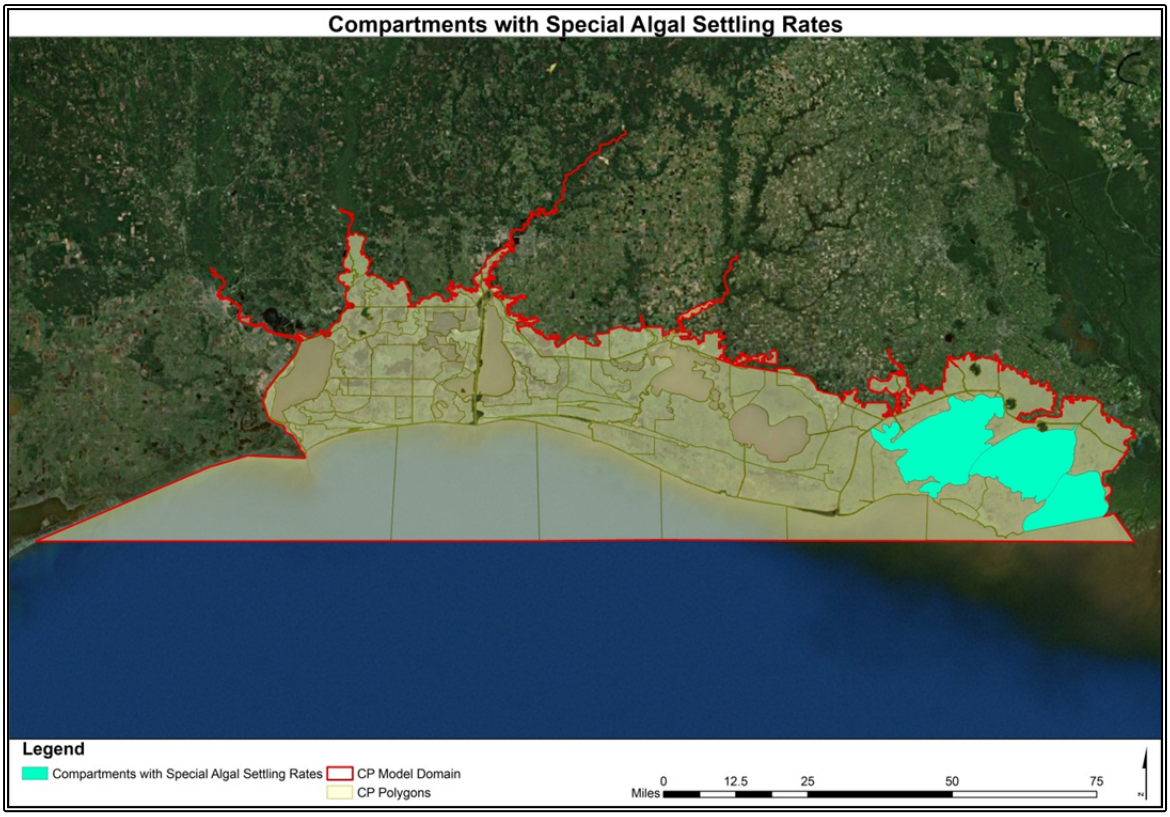

Figure 94 Lake Compartments with Special Algal Settling Rate in the CP Model

The final calibration results (based on the parameters from **Table 40**) for TSS, TN, and TPH are shown in **Figure 95**, **Figure 96**, and **Figure 97**, respectively. These and the rest of the water quality calibration plots are presented in Attachment B. Overall, the model predicted the water quality constituents fairly well in comparison to the observed values. Some spikes in the observed data were not picked up by the model because some of the boundary conditions were created from long-term monthly averages when 2007 data were unavailable. Also, the water quality constituents have an indirect relationship with the water depth. Therefore, if the water depth drops too low the constituent would spike, sometimes unrealistically. Potential reasons for the discrepancies between modeled and measured data also included: (1) the model was calculating mean representative values of variables for large compartments and was being compared to a measured gauge data value from a specific location; (2) the model computed daily average values which were being compared to instantaneous measurements.

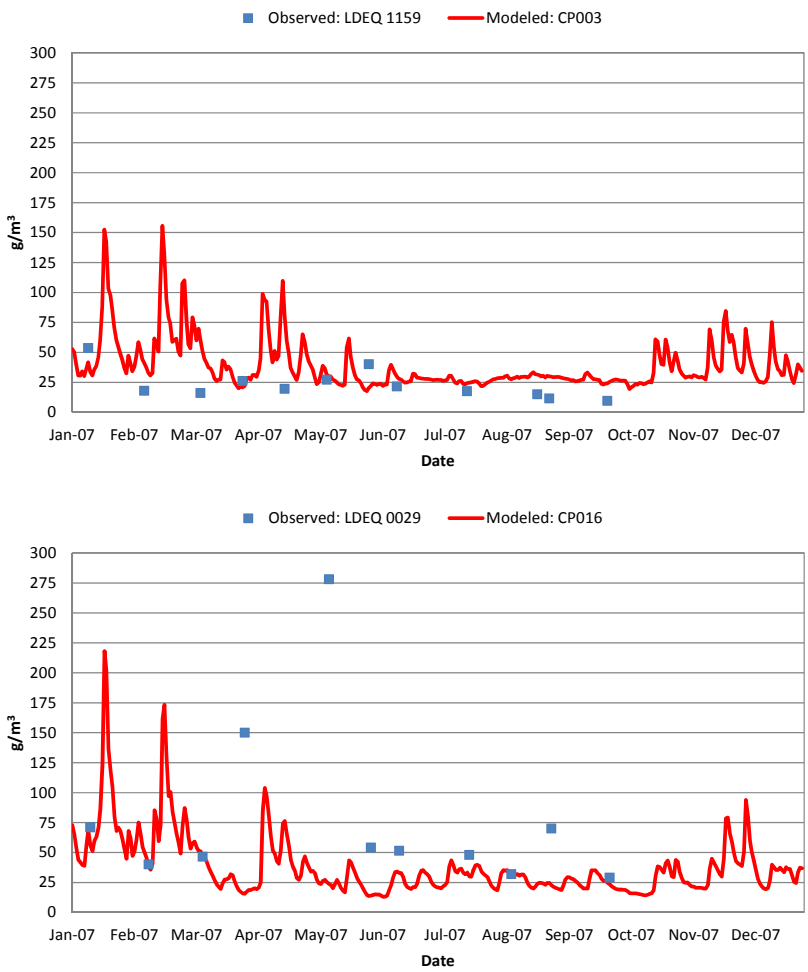

Figure 95 Sample TSS Calibration Results for the CP Model

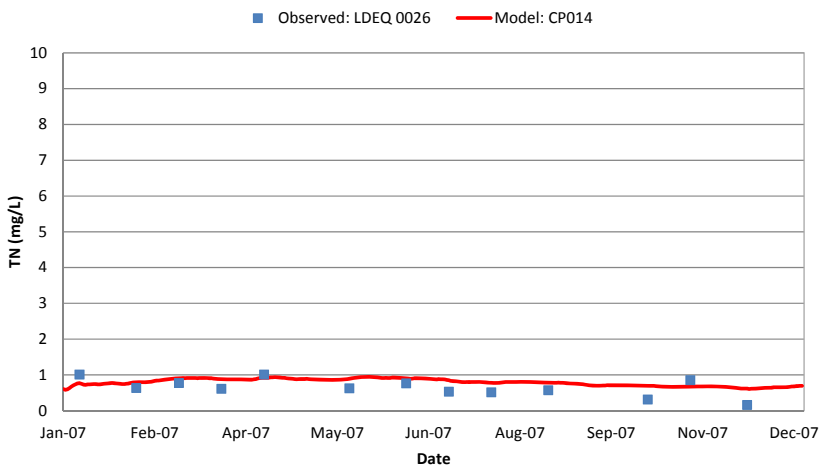

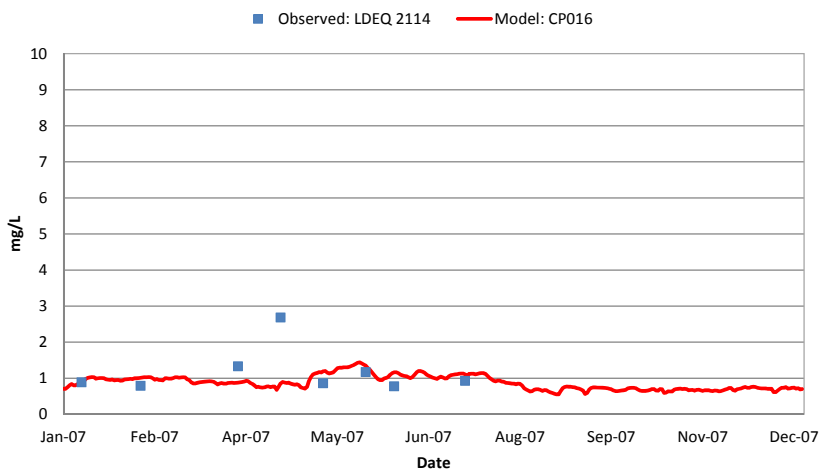

Figure 96 Sample TN Calibration Results for the CP Model

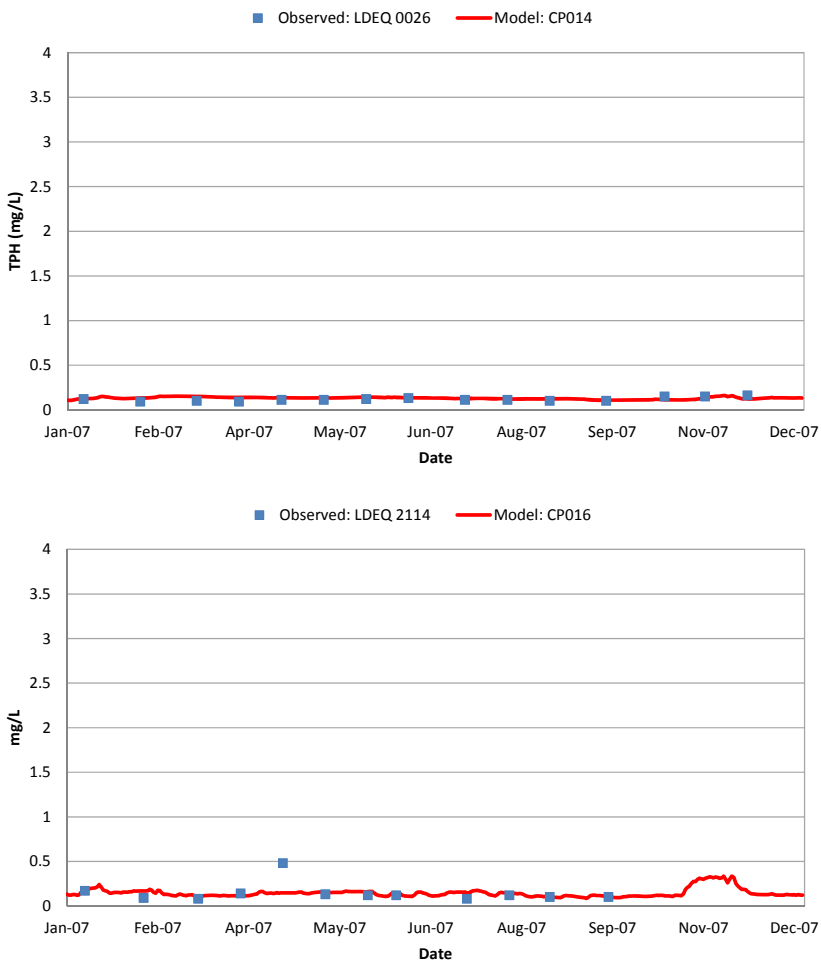

Figure 97 Sample TPH Calibration Results for the CP Model

<u>Validation</u>

The CP model was validated using observed measurements for the calendar year of 2010.

Stage

The station locations for the CP stage validation are shown in **Figure 98**. Observation data were collected from the CRMS, NOAA, USACE, and USGS.

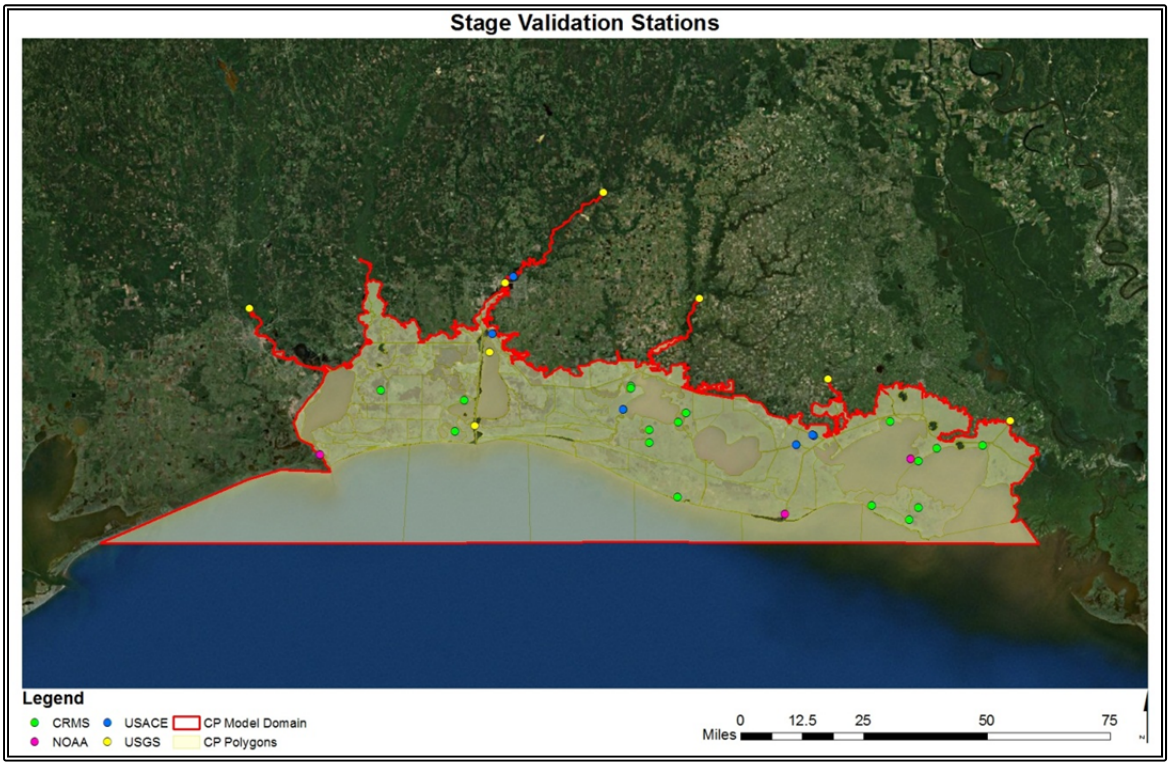

Figure 98 Stage Validation Sites in the CP Model

Figure 99 shows plots of the stage validation at several locations in the CP domain. These plots along with the rest of the stage validation plots are also included in Attachment B.

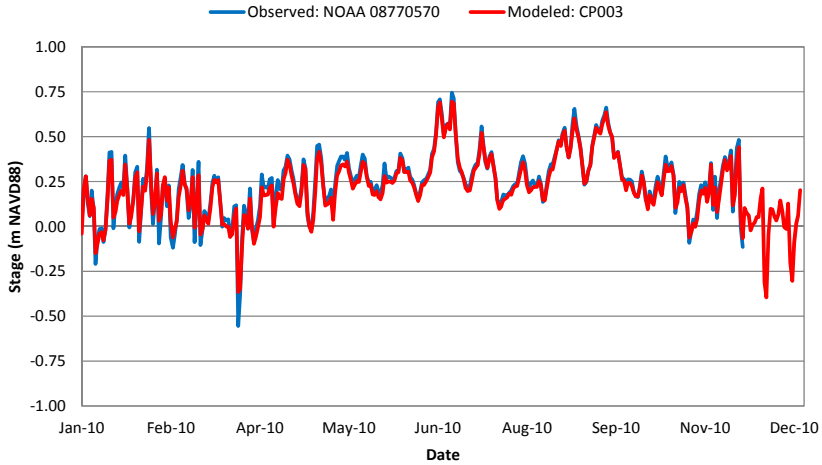

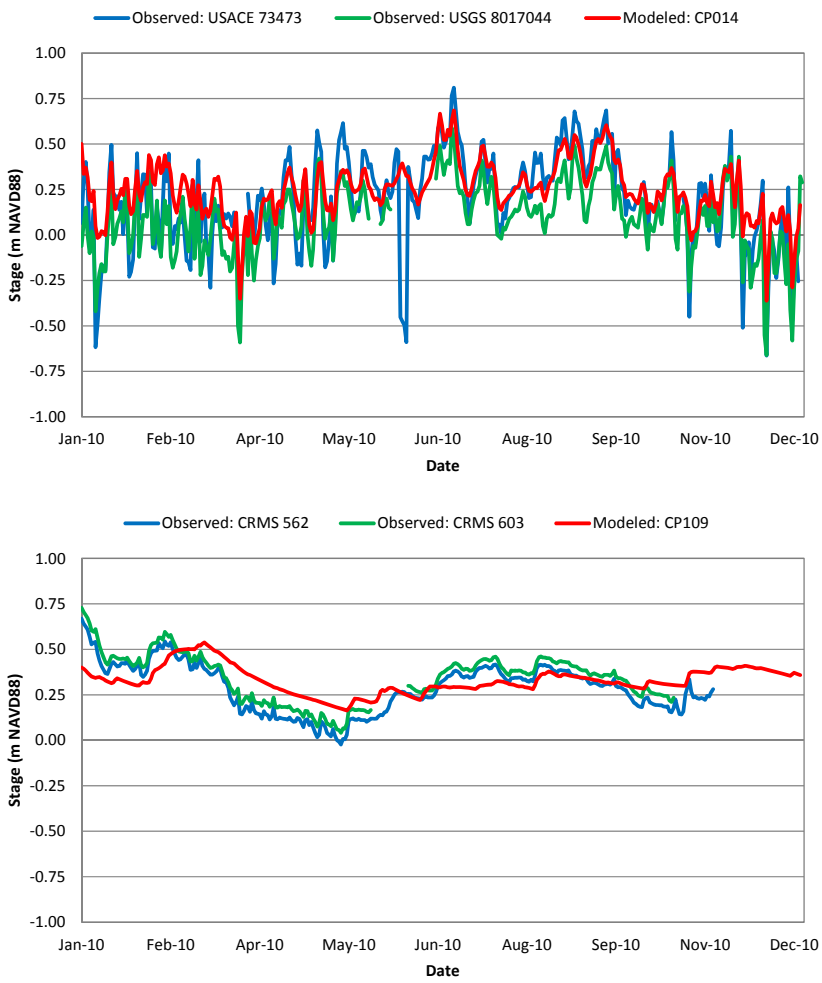

Figure 99 Sample Stage Validation Results for the CP Model

Salinity

The station locations for the salinity validation are shown in **Figure 100**. Observation data were collected from the CRMS, LDEQ, USACE, and USGS.

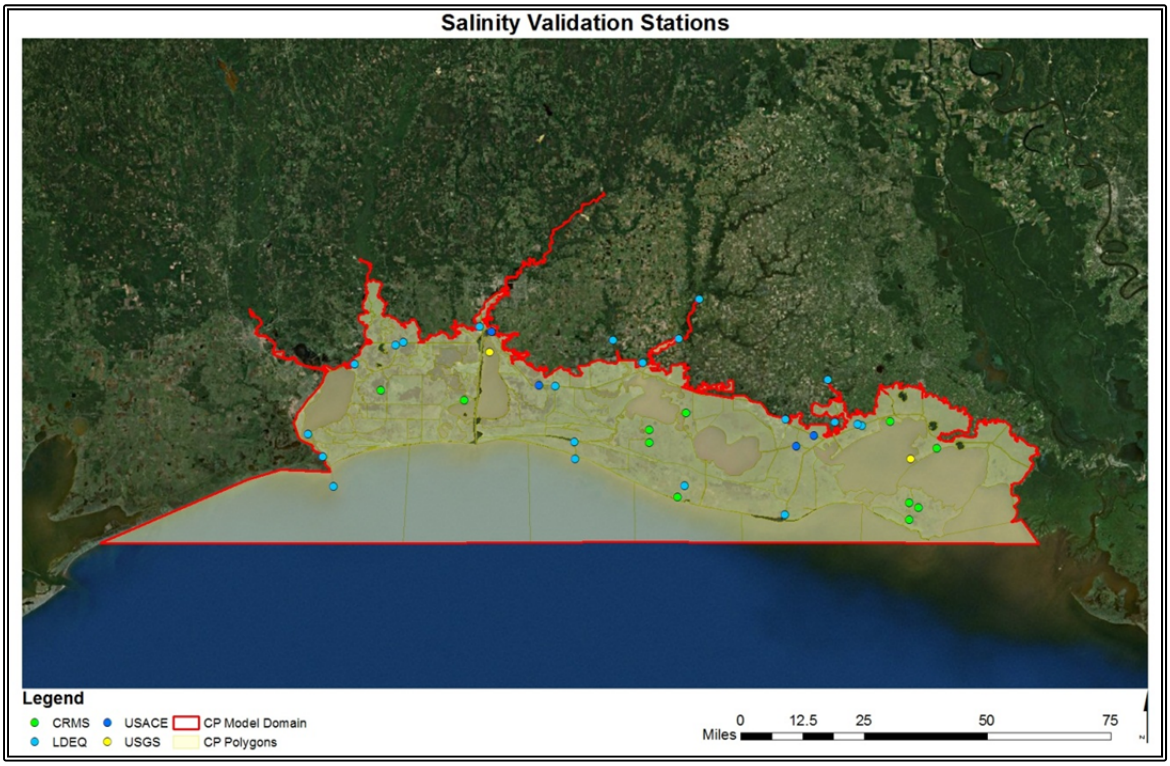

Figure 100 Salinity Validation Sites in the CP Model

Figure 101 shows plots of the salinity validation at several locations in the CP domain. These plots along with the rest of the salinity validation plots are also included in Attachment B.

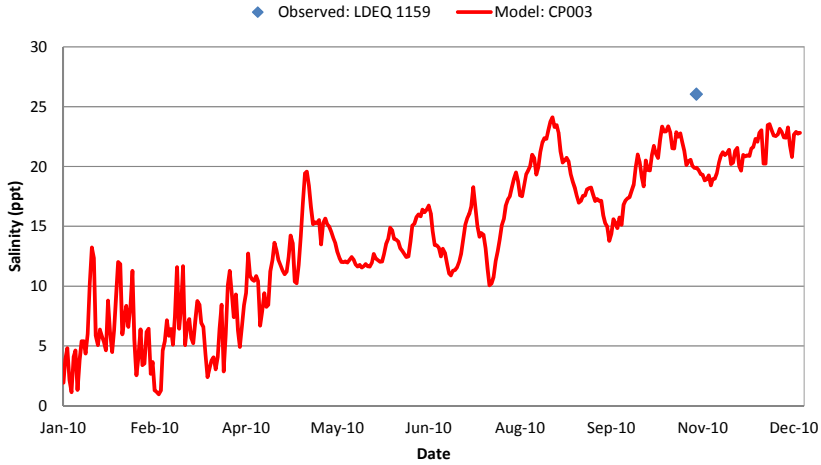

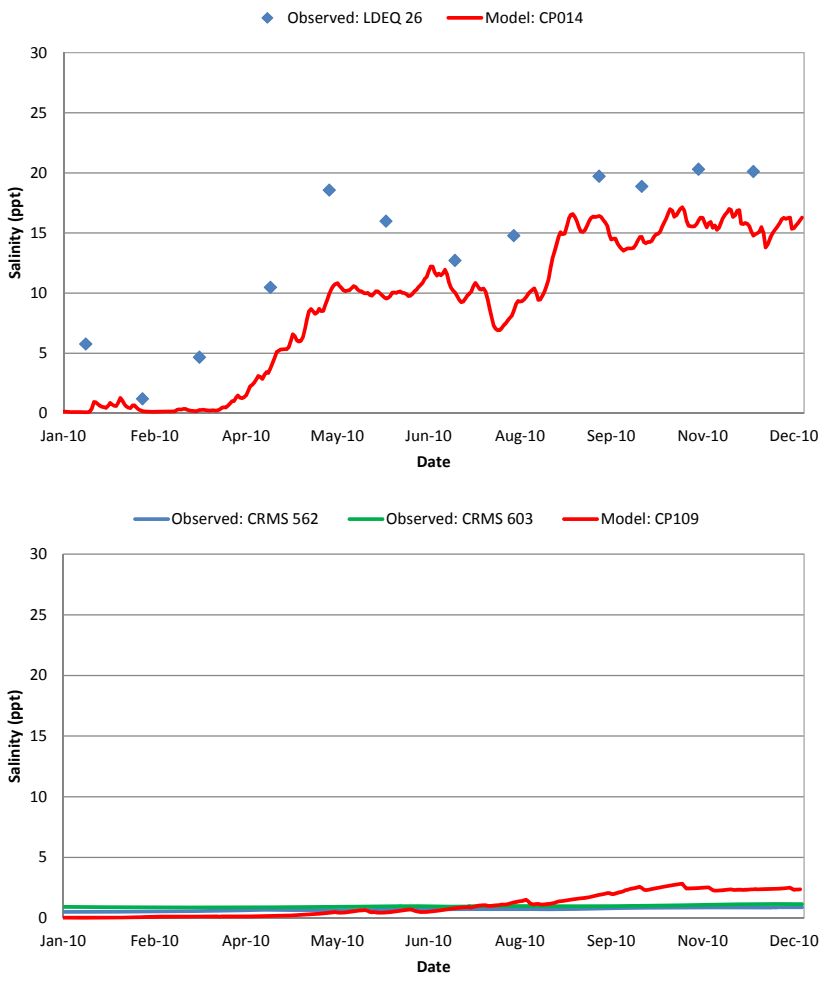

Figure 101 Sample Salinity Validation Results for the CP Model

Temperature

The stations used for validating temperature and the other water quality constituents are shown in **Figure 102**. Most of these stations are repeated from the calibration map, but some are new because they did not have 2007 data for calibration.

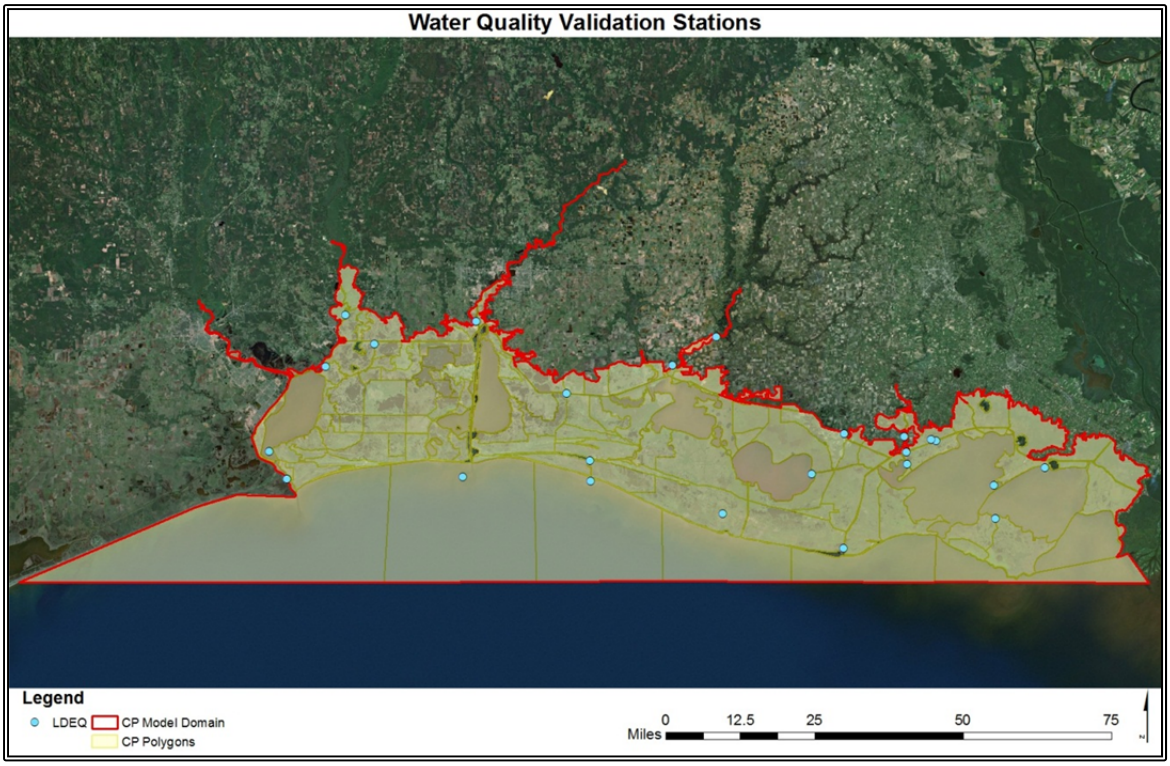

Figure 102 Water Quality Validation Sites in the CP Model

Figure 103 shows sample plots of the temperature validation at several locations in the CP domain. These plots along with the rest of the temperature validation plots are also included in Attachment B.

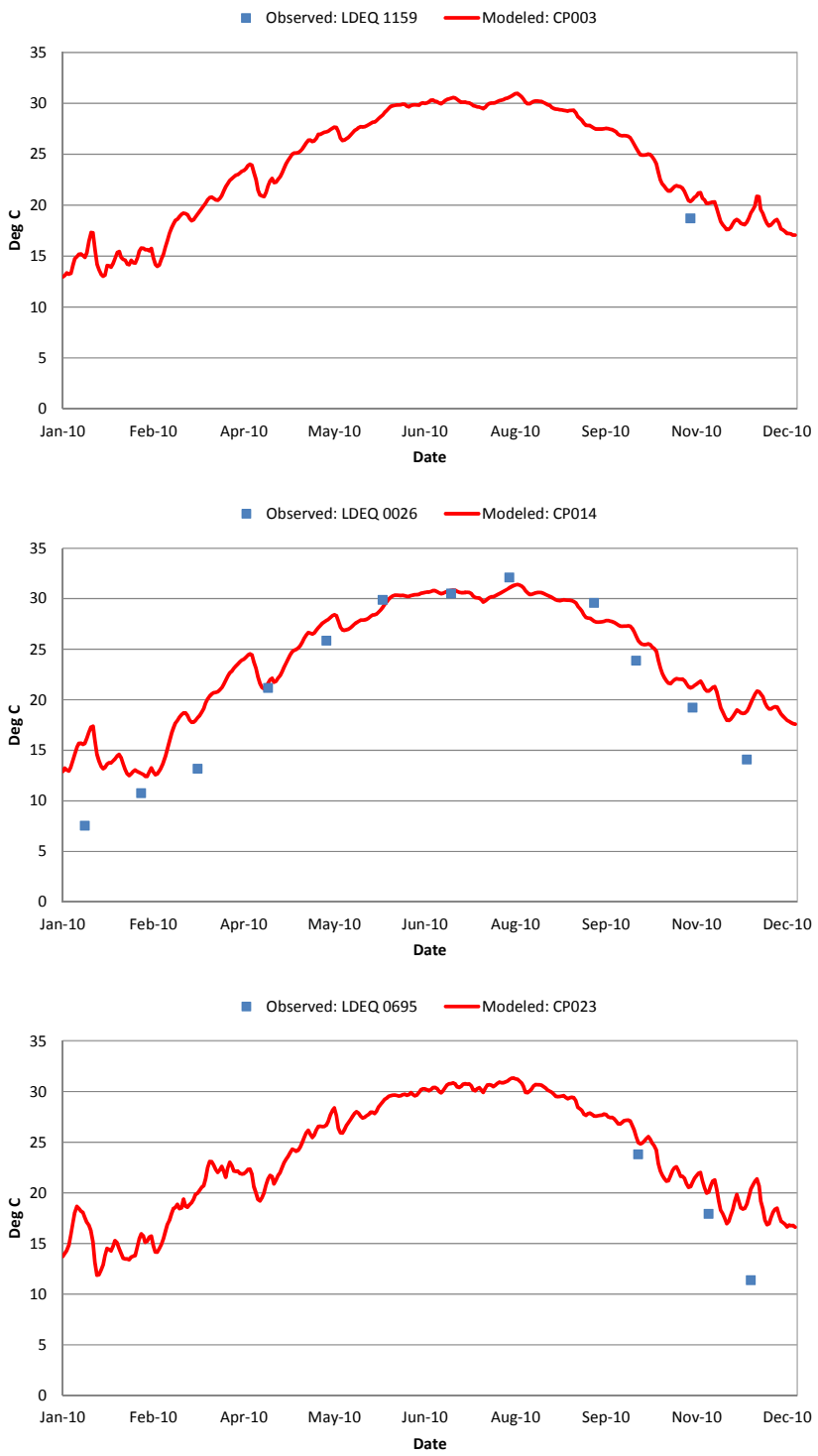

Figure 103 Sample Temperature Validation Results for the CP Model

Water Quality

Figure 104, **Figure 105**, and **Figure 106** show plots of the TSS, TN, and TPH validations at several locations in the CP domain, respectively. These plots along with the rest of the water quality validation plots are also included in Attachment B. The station locations are shown in **Figure 102**.

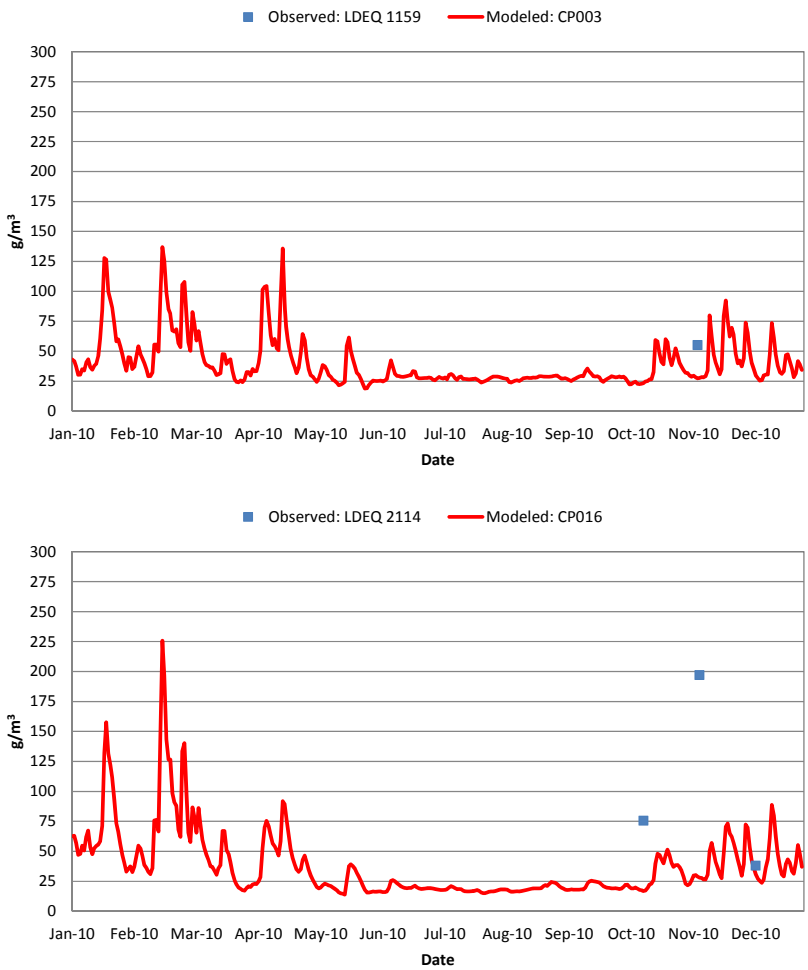

Figure 104 Sample TSS Validation Results for the CP Model

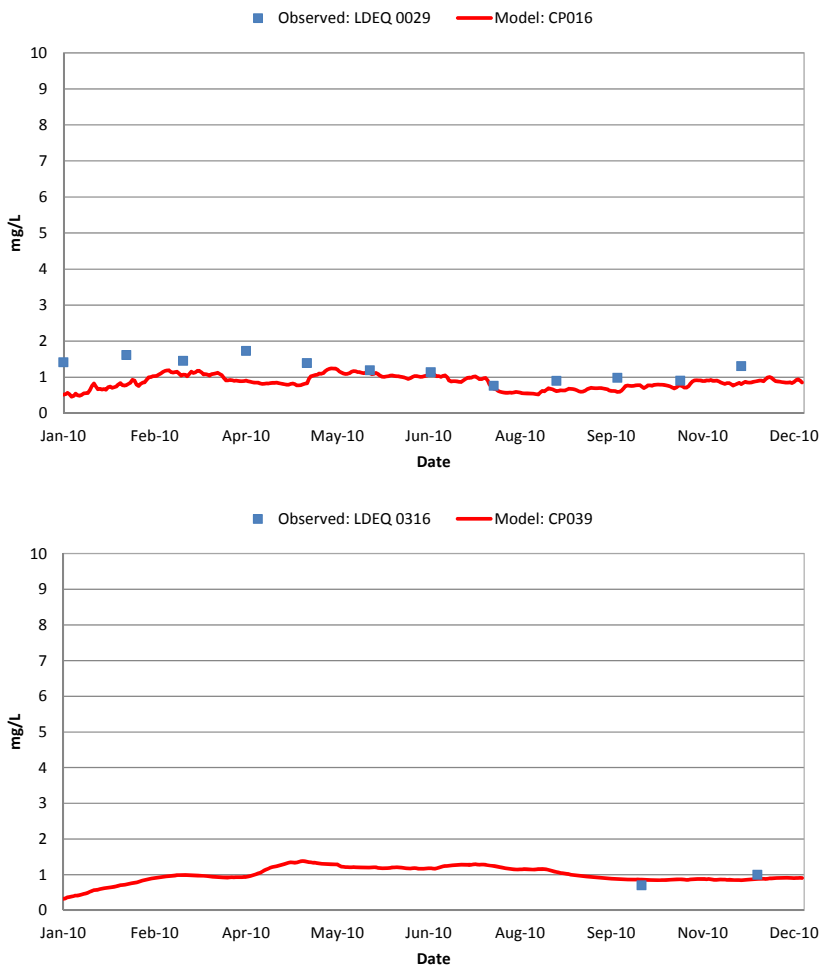

Figure 105 Sample TN Validation Results for the CP Model

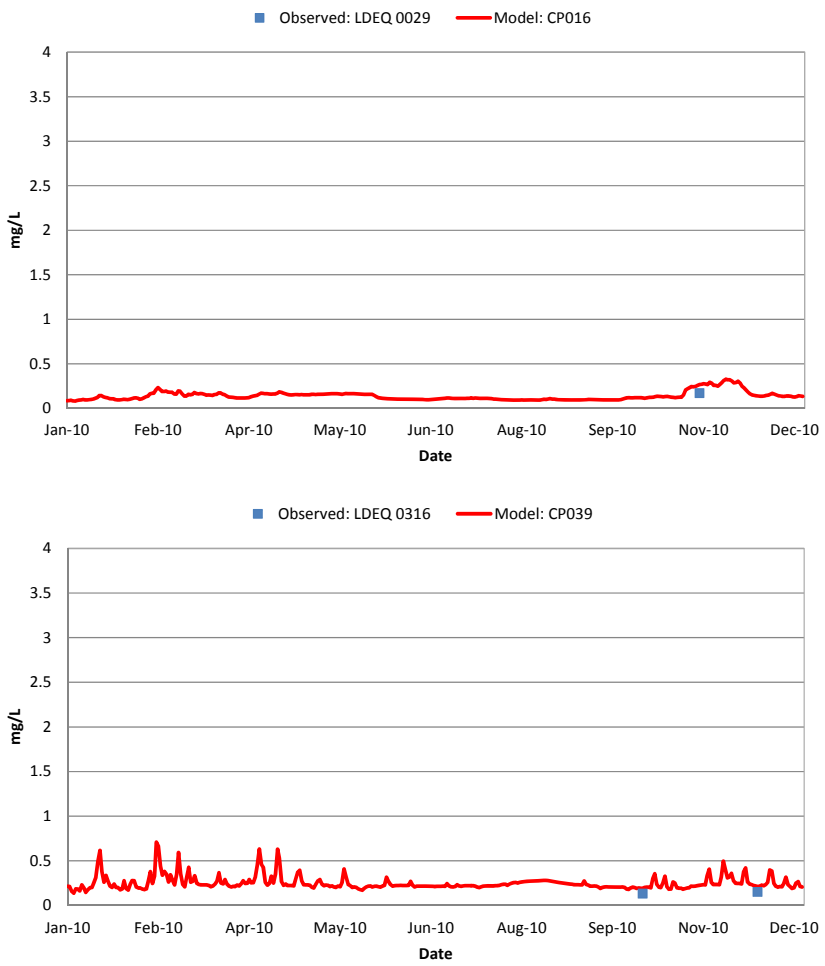

Figure 106 Sample TPH Validation Results for the CP Model

e. Discussion of the Ability to Import Data into Other Software Analysis Tools (Interoperability Issue)

The PB Fortran model produces comma delimited output (csv) or fixed format (.out) files which can be opened in Textpad, Notepad, WordPad, or Microsoft Excel. A Fortran script was written to convert the PB output to tab delimited text. The input and output data format for Berkeley Madonna files are tab delimited text. These files can be opened in Notepad, WordPad, Microsoft Excel, and MatLab.

4. Usability

a. Availability of Input Data Necessary to Support the Model

The various types of input data required to run the Eco-Hydrology models are presented in **Section 1**. The following were the sources and corresponding websites where these input data could be obtained:

Lock Schedules

US Army Corps of Engineers (USACE) New Orleans District Navigation
http://www.mvn.usace.army.mil/od/lockupdates/mermentaubasin/displayindex.asp

Elevation Profiles

LSU Atlas 5x5 Meter Resolution LIDAR
http://atlas.lsu.edu/lidar/
NOAA Nautical Charts
http://www.nauticalcharts.noaa.gov/mcd/enc/
NOAA Estuarine Bathymetry
http://estuarinebathymetry.noaa.gov/
NOAA National Geographical Data Center U.S. Coastal Relief Model
http://www.ngdc.noaa.gov/mgg/coastal/crm.html
Wetland Morphology Group

Land/Water Percentages

Aerial Maps
www.google.com/maps
www.bing.com/maps
Wetland Morphology Group

Precipitation Records

National Climatic Data Center (NCDC) Daily Surface Data (SOD)
http://www.ncdc.noaa.gov/oa/climate/climateinventories.html

Evapotranspiration Records

World Water and Climate Atlas
http://www.iwmi.cgiar.org/WAtlas/Default.aspx
Food and Agriculture Organization (FAO)
http://weather.lsuagcenter.com
National Climatic Data Center (NCDC) Daily Surface Data (SOD)
http://www.ncdc.noaa.gov/oa/climate/climateinventories.html

Tributary Discharges

United States Geological Survey (USGS) National Water Information Systems
http://water.usgs.gov/nwis/
USACE New Orleans District Water Control
http://www.mvn.usace.army.mil/eng/edhd/watercon.asp

Water Quality Records

Louisiana Department of Environmental Quality (LDEQ)
http://www.deq.louisiana.gov/portal/
United States Geological Survey (USGS) National Water Information Systems
http://water.usgs.gov/nwis/
Texas Commission on Environmental Quality
http://www.tceq.state.tx.us/
Louisiana Universities Marine Consortium
http://www.lumcon.edu/

Gulf of Mexico Stage Records

National Oceanic and Atmospheric Administration (NOAA)
http://tidesandcurrents.noaa.gov/index.shtml
USACE New Orleans District Water Control
http://www.mvn.usace.army.mil/eng/edhd/watercon.asp

Gulf of Mexico Salinity Records

United States Geological Survey (USGS) National Water Information Systems
http://water.usgs.gov/nwis/

Gulf of Mexico Water Quality Records

Louisiana University Marine Consortium (LUMCON)
http://www.lumcon.edu/
National Oceanographic Data Center (NODC) World Ocean Atlas (WOA)
http://www.nodc.noaa.gov/OC5/SELECT/woaselect/woaselect.html
Louisiana Department of Environmental Quality (LDEQ)
http://www.deq.louisiana.gov/portal/

Air and Water Temperature Records

National Climatic Data Center (NCDC) Daily Surface Data (SOD)
http://www.ncdc.noaa.gov/oa/climate/climateinventories.html
National Data Buoy Center (NDBC)
http://www.ndbc.noaa.gov/data/climatic
Louisiana University Marine Consortium (LUMCON)
http://www.lumcon.edu/
Louisiana Department of Environmental Quality (LDEQ)
http://www.deq.louisiana.gov/portal/

Wind Speed Records

National Climatic Data Center (NCDC) Daily Surface Data (SOD)
http://www.ncdc.noaa.gov/oa/climate/climateinventories.html

b. Formatting of Output in an Understandable Manner

The outputs of the Eco-Hydrology models were comma separated value (CSV) files (PB) and tabular text files (AA and CP), which could be opened and manipulated using any text editor or Excel software.

c. Usefulness of Results to Support Project Analysis

The Eco-Hydrology models provided mean daily and mean monthly values of hydrodynamic and water quality parameters for long-term simulations. As a result, the models could be used to screen the outcomes of proposed projects at a broad, planning scale. For example, the models could provide a general idea of how a marsh creation project would affect a specific area by comparing the output values of the model with the project to the output values of the model without the project. With this modeling tool, important project outcomes, such as changes in stage, salinities, algal blooms, and land area could be evaluated early in the planning phase.

d. Ability to Export Results into Project Reports

The Fortran model provided output in the form of tables and the Madonna model provided output in the form of tables and graphs. The tables gave an average value for each compartment for every day of the simulation period. The tables could be saved as text files, which could be brought into Excel to create specialized graphs to suit the user's needs. The Madonna graphs displayed the average values on the vertical axis and the time in days on the horizontal axis. These Madonna graphs could be saved as bitmap files, which could be inserted into project reports.

e. Training Availability

The PB model was written in the Fortran open source code, while the AA and CP models used the Berkley Madonna differential equation solver. Tutorials are available for training on the use and application of Fortran and Berkley Madonna (Macey, 2001). The Compact Visual Fortran has a user interface for compiling and running the Fortran model.

f. Users Documentation Availability and Whether it is User Friendly and Complete

There are several texts available for Fortran assistance, and there is a user's guide for Berkeley Madonna available for free on their website[52]. There are no in-house user manuals for the Eco-Hydrology models. However, the model codes do include brief descriptions of the parameters and equations as they are introduced. For a more thorough guide to the modeling, see the "Theory" portion of Section 2.

[52] http://www.berkeleymadonna.com/BM%20User%27s%20Guide%208.0.2.pdf

g. Technical Support Availability

The Eco-Hydrology models presented here were developed initially for research purposes at UNO and UL Lafayette. These models were further developed for the 2012 Coastal Master Plan. As such, there is no official technical support available. However, the developers are part of the master plan team and are willing to provide technical support as needed.

h. Software/Hardware Platform Availability to All or Most Users

Fortran models are run using external compilers. Compilers can be found on the internet for variable prices. The PB code was compiled using the INTEL Visual Fortran Compiler for Windows 7. Berkeley Madonna purchasing information can be found on their website under "Pricing/Purchase[53]". Individual licenses cost $299 with reduced pricing for student licenses and purchases of five (5) or more licenses.

[53] http://www.berkeleymadonna.com/pricing.html

i. Accessibility of the Model

All Fortran compilers are not the same and therefore the following procedure may differ depending on which compiler you use. Open the Fortran compiler and select "Compile" to check the code for errors in formatting and arithmetic logic. After the model is compiled, select "Execute" or "Run" in order to start the simulation. After the simulation is completed, output files are created in the project folder which contains the code and the input files. To import files, a "READ" statement is typically required followed up with the name of the file being read in and the variable name that is being assigned. Any changes made to the import file will be accounted for in the next execution of the model. Changes to the code can be made and will be checked for errors when the model is compiled.

Follow the instructions for installing Berkeley Madonna. After installation, open Berkeley Madonna and enter the registration code you received after purchasing a license. Go to "File" then click "Open". Browse to the location you saved the model file and double click it or click it, then click "Open". All input files are already imported and all parameters are set to default. If no changes are desired, click "Run" to execute the model. If changes are desired for input files, make these changes to the file, save the file as "tab delimited," and follow the import procedure found in the Berkeley Madonna User's Guide. Click "Run" to execute. If changes are desired in the model parameters, make the changes to the parameter in the code and click "Run" to execute. A window will pop up asking if you want to compile the model first; click "Yes".

j. Transparency of Model and How it Allows for Easy Verification of Calculations and Outputs

All of the Eco-Hydrology models were open source, and as such the codes are readily accessible and the formulations can be easily reviewed or changed. In order to verify the equations using the outputs, the computational time step must be set equal to the output time step. Since the computational time step is generally small, this creates a large output. As a result, a short duration is recommended for the model verification run in order to view the outputs and check the equation efficiency.

5. Sources of Model Uncertainty

The Eco-Hydrology models were designed, calibrated, and validated using the best available data in the model regions and formulations from literature. Even with the best data and formulations, uncertainty was still present in the models. The main sources of model uncertainties are listed below:

- Lack of bathymetric data for many channels and rivers in the coastal zone
- Outdated bathymetric data for many of the large lakes and other water bodies
- Large data gaps in the boundary conditions
- Insufficient information in the Gulf of Mexico (tide and salinity)
- Insufficient information about the operations of the hydraulic structures
- Insufficient water quality data
- Small scale features were muted due to such a large domain

6. Suggested Model Improvements

The Eco-Hydrology models were sufficient for the screening-level analysis of the 2012 Coastal Master Plan modeling effort. However, there is always room for improvement when it comes to numerical models, whether new data become available or new equations replace old ones. As such, below is a brief list of suggestions to improve the Eco-Hydrology models:

- Improve the TSS and ACC modeling formulations. More physical processes could be included. The inclusion of additional physical processes would highly depend on the overall approach taken in 2017. It is a process of trade off. Simple models run faster and cover larger spatial areas. The more one complicates the model the more limited the spatial and temporal coverage would be.
- Improve the coupling between the Eco-Hydrology and Wetland Morphology models in regard to the accretion and land building components.
- Improve the compartment design to better capture the spatial variability. For example, compartments could be drawn to best capture the effects of proposed projects being investigated. A detailed description of how the compartments can and will be improved is not possible at this point. We are learning from the experience of performing the simulations.
- Merge the AA and CP models into a single model. This combined model should be used for projects that fall near the interface between the two regions.
- Unify the assumptions and modeling approach across all three regions.
- Investigate the use of numerical techniques to shorten the run time.
- Validate the models using additional datasets, such as data for the calendar year of 2011.

7. Quality Review

This Section identifies the methods and procedures used to perform the quality review (QR) for the Eco-Hydrology models. Each model region's team strove to ensure that their models were designed, calibrated, and simulated to the best of their ability.

Pontchartrain and Barataria Basin Model

Specific QR procedures for the Pontchartrain-Barataria Eco-Hydrology model to support the 2012 Coastal Master Plan included the following:

1. Model calibration and validation for a 20-year period (1990 – 2009).
2. Publication of the methodology in the Journal of Coastal Research (JCR).
3. Internal vetting by the modeling team of the mass balance equations for the models.
4. Internal review of model performance via statistical and graphical media.
5. Comparison of Year 1-25 results with that of future without action (FWOA) to validate the project effects.
6. Comparison of Year 26-50 results with Year 1-25 results to validate the project implementation consistency.

Atchafalaya Basin Model

Specific QR procedures for the Atchafalaya Basin Eco-Hydrology model to support the 2012 Coastal Master Plan included the following:

1. Model calibration using the 2007 stage, salinity, and water quality data from local stations within the domain.
2. Model validation using the 2008-2009 stage, salinity, and water quality data from local stations within the domain.
3. Time series plot of model outputs and internal review of model results for all output variables.
4. Comparison of Year 1-25 results with that of future without action (FWOA) to validate the project effects.
5. Comparison of Year 26-50 results with Year 1-25 results to validate the project implementation consistency.
6. Mark Dortch and Jeff Shelden reviewed FWOA and select project group results for model parameters (e.g., sedimentation, stage and salinity).

Chenier Plain Model

Specific QR procedures for the Chenier Plain Eco-Hydrology model to support the 2012 Coastal Master Plan included the following:

1. Model calibration using the 2007 stage, salinity, and water quality data from local stations within the domain.
2. Model validation using the 2010 stage, salinity, and water quality data from local stations within the domain.
3. Incorporation of methodology from Pontchartrain-Barataria model with new methodology review by Alex McCorquodale, Ehab Meselhe, and Mark Dortch.
4. Comparison of Year 1-25 results with that of future without action (FWOA) to validate the project effects.

5. Comparison of Year 26-50 results with Year 1-25 results to validate the project implementation consistency.

8. Uncertainty Analysis

Several parameters were identified in the Eco-Hydrology models that had inherent uncertainty and would therefore cause any results/output from the model to retain this uncertainty. The uncertainty could be a result of using empirical constants or lacking information about the area of interest. The following outputs of the Eco-Hydrology models were recognized as critical inputs for the subsequent master plan models (e.g. Wetland Morphology, Vegetation, etc.): stage (STG), salinity (SAL), sediment (TSS), accretion (ACC), and algae (ALG). Below is an itemized discussion outlining the uncertainty parameters that controlled these outputs in the Eco-Hydrology models and providing the range of recommended values to analyze the effects of their uncertainty. It should be noted that in the PB model several of the parameters with the most uncertainty were varied by compartment and thus ranges of the values used are provided.

The parameters that cause the most uncertainty for stage and salinity are bed roughness and diffusion. The bed roughness is an estimate of the frictional resistance of a surface for water to pass over. Therefore, the roughness affects the advection, or forward motion, of water from compartment to compartment. Bed roughness is not a natural feature that can be measured or visually inspected, but it is typically a calibration parameter that has been extensively studied over the years. In the literature, you can find tables of recommended bed roughness factors for many different types of vegetation and structural materials. One such book is **Open-Channel Hydraulics** by Ven te Chow (1959), which presents several tables for a wide range of bed materials. In the PB domain, the roughness was originally based on vegetation type and was then altered for each compartment to calibrate the model. In the AA domain, the roughness was based on the vegetation/surface type. In the CP domain, the roughness was based on the type of compartment i.e. channel, open water, or marsh. **Table 41** shows the roughness factors most likely used in each region, along with the recommended range of values needed to analyze how changes in these parameters could lead to changes in model output. It should be noted that the PB model used multiplier factors to calibrate the roughness for each compartment. Also, the Manning's *n* in the PB model was not allowed to drop below 0.01 because that corresponds to a hydraulically smooth surface.

Table 41 Roughness Factors for Uncertainty Analysis (Unitless)

PB Compartment Type	Minimum Factor	Intermediate Minimum Factor	Most Likely Factor	Intermediate Maximum Factor	Maximum Factor
All[54]	0.3	0.7	1	1.7	2.8
AA Vegetation/ Surface Type	**Minimum**	**Intermediate Minimum**	**Most Likely Value**	**Intermediate Maximum**	**Maximum**
Deep Open Water	0.02	0.0275	0.02	0.0425	0.05
Intermediate Open Water	0.02	0.0275	0.03	0.0425	0.05
Shallow Open	0.02	0.0275	0.05	0.0425	0.05

[54] In the PB region, the actual values used were calibrated for each compartment. Therefore, the values shown in the table are multiplier factors. The Manning's *n* was not allowed to drop below 0.01 since this corresponds to a hydraulically smooth surface.

Water					
Deep Channel	0.02	0.0275	0.03	0.0425	0.05
Intermediate Channel	0.02	0.0275	0.04	0.0425	0.05
Shallow Channel	0.02	0.0275	0.05	0.0425	0.05
Marsh	0.1	0.1375	0.15	0.2125	0.25
Swamp	0.1	0.1375	0.25	0.2125	0.25
CP Compartment Type	**Minimum**	**Intermediate Minimum**	**Most Likely Value**	**Intermediate Maximum**	**Maximum**
Channel	0.02	0.0275	0.025	0.0425	0.05
Marsh	0.05	0.1375	0.08	0.2125	0.25
Open Water	0.02	0.0275	0.025	0.0425	0.05

The diffusion coefficient is the second parameter that can cause uncertainty when modeling stage and salinity. Physical diffusion is sometimes included in numerical models to help smooth out shocks and anomalies in the system which would otherwise cause the model to crash. The PB model utilized the Central Differencing scheme, which does not have as much numerical diffusion as the UPWIND scheme, and thus, a physical diffusion coefficient was introduced. The diffusion coefficient was used primarily as a calibration parameter based on compartment stage and, therefore, varies for each compartment. The diffusion coefficient can range anywhere from 1 to 1000 m^2/s. In order to calibrate the model, a multiplication factor was applied to the diffusion coefficients. The AA and CP regions already had numerical diffusion due to the UPWIND scheme used in their models; therefore, the physical diffusion coefficient was set to 0 (zero) in those two models. **Table 42** shows the recommended range of multiplier factors for the uncertainty analysis of the diffusion coefficient in the PB model.

Table 42 Diffusion Coefficient Multiplier Factors for Uncertainty Analysis (Unitless)

PB Model Compartment	Minimum Factor	Intermediate Minimum Factor	Most Likely Factor	Intermediate Maximum Factor	Maximum Factor
All	0.5	0.75	1	1.5	2

Parameters that cause uncertainty when modeling sediment and accretion are the critical wind speed, the base resuspension flux, the Krone's coefficient, the critical velocity, the percent sand, and the reference settling velocity. The critical wind speed is the minimum speed at which sediment will become resuspended into the water column. Therefore, it affects the resuspension rate of sediment, which controls the amount of TSS and ACC. The critical wind speed was calibrated to Lake Pontchartrain in the PB model, but was used across all three regions. This could introduce uncertainty into all of the regions, including the PB region, because the PB domain included the Barataria Basin as well as the Pontchartrain Basin. **Table 43** shows the recommended range of values for the uncertainty analysis of the critical wind speed in all three models.

Table 43 Critical Wind Speed Values for Uncertainty Analysis (m/s)

Region	Minimum	Intermediate Minimum	Most Likely Value	Intermediate Maximum	Maximum
PB	1.5	2	2.77	3	4
AA	1.5	2	2	3	4
CP	1.5	2	2	3	4

Base resuspension flux is another parameter that causes uncertainty when modeling sediment and accretion. The base resuspension flux is the product of the bulk density of sediment and the base resuspension rate of sediment. This parameter was used as a calibration parameter for resuspension. Uncertainty could come from using a single sediment bulk density across the entire domain or from the empirical nature of the base resuspension rate. **Table 44** shows the recommended range of values used to analyze the base resuspension flux uncertainty for all three regions.

Table 44 Base Resuspension Rates for Uncertainty Analysis ($g/m^2/d$)

Region	Minimum	Intermediate Minimum	Most Likely Value	Intermediate Maximum	Maximum
PB	25	37.5	50	62.5	75
AA	25	37.5	50	62.5	75
CP	25	37.5	50	62.5	75

The Krone's coefficient is the third parameter that can cause uncertainty when modeling sediment and accretion. The Krone's coefficient is an empirical constant used to calculate the deposition rate of sediment. Because it is empirically defined, it has inherent uncertainty. **Table 45** shows the recommended range of values used to analyze the uncertainty of the Krone's coefficient for all three regions.

Table 45 Krone's Coefficient Values for Uncertainty Analysis (Unitless)

Region	Minimum	Intermediate Minimum	Most Likely Value	Intermediate Maximum	Maximum
PB	0.00012	0.00048	0.00012	0.00083	0.001
AA	0.0003	0.00048	0.0003	0.00083	0.001
CP	0.0003	0.00048	0.001	0.00083	0.001

Critical velocity is the fourth parameter that can cause uncertainty when modeling sediment and accretion. The critical velocity is a calibration parameter and was included in the AA model to limit the amount of sediment deposited in the river deltas. For example, at higher velocities sediment is less likely to settle out than at lower velocities. Because the initial value was based on historical accretion in deltas, the uncertainty of the critical velocity comes from its empirical nature. The PB region redistributed the Mississippi River flow instead of including the critical velocity. Since the CP region did not have large rivers, the critical velocity was not included in the model. **Table 46** shows the recommended range of critical velocities for the uncertainty analysis of the AA model.

Table 46 Critical Velocities for Uncertainty Analysis (m/d)

AA Model Compartment	Minimum	Intermediate Minimum	Most Likely Value	Intermediate Maximum	Maximum
All	0.8	0.9	1	1.1	1.2

Percent sand is the fifth parameter that can cause uncertainty when modeling sediment and accretion. The PB model included the percent sand parameter to establish the settling ability of the sediment load coming from the Mississippi River. The AA and CP regions did not use the percent sand. The uncertainty of the percent sand comes from the lack of field data. In the PB model, the percent sand was calculated as a function of the River discharge and thus varied for each compartment. The percent sand can range anywhere from 3 to 35 %. In order to calibrate the model, a multiplication factor was applied to the percent sand. **Table 47** shows the recommended range of multiplier factors for the uncertainty analysis of percent sand in the PB model.

Table 47 Percent Sand Values for Uncertainty Analysis (%)

PB Model Compartment	Minimum Factor	Intermediate Minimum Factor	Most Likely Factor	Intermediate Maximum Factor	Maximum Factor
All	0.25	0.625	1	1.125	1.25

Reference settling velocity is the sixth and last parameter that can cause uncertainty when modeling sediment and accretion. For the PB model, the reference settling velocity was set to a constant and was corrected based on flocculation and salinity effects. For the AA and CP models, the reference or baseline settling velocity was calculated from the Krone's equation using TSS and the Krone's coefficient mentioned previously. The uncertainty of the reference settling velocity is due to its empirical nature. **Table 48** shows the recommended range of reference settling velocity values for the uncertainty analysis of the PB model.

Table 48 Reference Settling Velocity Values for Uncertainty Analysis (m/d)

PB Model Compartment	Minimum	Intermediate Minimum	Most Likely Value	Intermediate Maximum	Maximum
All	8	10	12	14	16

When modeling algae, uncertainty can come from the sediment denitrification rate at 20 °C, the half-saturation concentration of nitrogen, the half-saturation concentration of phosphorus, and the optimal light. The sediment denitrification rate is a reaction parameter used to determine the amount of nitrate removed from the water by bacteria in the bed sediment at 20 °C. The uncertainty of the denitrification rate comes from its empirical nature. **Table 49** shows the recommended range of denitrification rates used to analyze their uncertainty for all three regions.

Table 49 Sediment Denitrification Rates at 20 °C for Uncertainty Analysis (m/d)

Region	Minimum	Intermediate Minimum	Most Likely Value	Intermediate Maximum	Maximum
PB	0.04	0.045	0.08	0.065	0.08
AA	0.04	0.045	0.05	0.06	0.07
CP	0.04	0.045	0.05	0.06	0.07

Half-saturation concentration of nitrogen is the second parameter that can cause uncertainty when modeling algae. The half-saturation concentration of nitrogen is the nitrogen concentration at half of the maximum algal uptake rate. It is used to determine the nutrient limitation factor and the ammonium preference of algae. The uncertainty of the half-saturation concentration of nitrogen comes from its estimation for this project area. **Table 50** shows the recommended range of values used to analyze the uncertainty of the half-saturation concentration of nitrogen for all three regions. It should be noted that the PB model used a variation of the half-saturation concentration of nitrogen based on Michealis-Menten's minimization theory (McCorquodale et al., 2008; Meselhe et al., 2008).

Table 50 Half-Saturation Concentrations of Nitrogen for Uncertainty Analysis (mg/L)

Region	Minimum	Intermediate Minimum	Most Likely Value	Intermediate Maximum	Maximum
PB	0.016	0.018	0.02	0.022	0.024
AA	0.005	0.01	0.02	0.035	0.05
CP	0.01	0.055	0.1	0.55	1

Half-saturation concentration of phosphorus is the third parameter that can cause uncertainty when modeling algae. The half-saturation concentration of phosphorus is the phosphorus concentration at half of the maximum algal uptake rate. It is used to determine the nutrient limitation factor. The uncertainty of the half-saturation concentration of phosphorus comes from its estimation for this project area. **Table 51** shows the recommended range of values used to analyze the uncertainty of the half-saturation concentration of phosphorus for all three regions. It should be noted that the PB model used a variation of the half-saturation concentration of phosphorus based on Michealis-Menten's minimization theory (McCorquodale et al., 2008; Meselhe et al., 2008).

Table 51 Half-Saturation Concentrations of Phosphorus for Uncertainty Analysis (mg/L)

Region	Minimum	Intermediate Minimum	Most Likely Value	Intermediate Maximum	Maximum
PB	0.0024	0.0027	0.003	0.0033	0.0036
AA	0.0005	0.00075	0.001	0.0015	0.002
CP	0.0005	0.00275	0.005	0.0275	0.05

Optimal light is the fourth and last parameter that can cause uncertainty when modeling algae. The optimal light is the photosynthetically available radiation (PAR), or light, at which algal growth is optimal. The uncertainty of the optimal light comes from its estimation for this project area. **Table 52** shows the recommended range of values used to analyze the uncertainty

of the optimal light for all three regions. It should be noted that the PB model used a sine curve fit for the optimal light and thus used a range of values throughout each year.

Table 52 Optimal Light Values for Uncertainty Analysis (Ly/d)

Region	Minimum	Intermediate Minimum	Most Likely Value	Intermediate Maximum	Maximum
PB	200	250	225 – 375	350	400
AA	200	250	300	350	400
CP	200	250	300	350	400

9. References

Backus, J. (1998). The history of FORTRAN I, II, and III. IEEE Annals of the History of Computing, 20 (4), 68 - 78.

Backus, J. W., Beeber, R., Best, S., Goldberg, R., Haibt, L. M., Herrick, H. L., et al. (1957). The FORTRAN Automatic Coding System. Proceedings of the Western Joint Computer Conference (pp. 188 - 198). Los Angeles: ACM.

Cerco, C.F., and Cole, T. (1995). "User's Guide to the CE-QUAL-ICM Three-Dimensional Eutrophication Model," Technical Report EL-95-15, U.S. Army Engineer Waterways Experiment Station, Vicksburg, Mississippi.

Chapra, S.C, and Pelletier, G.J. (2003). "QUAL2K: A Modeling Framework for Simulating River and Stream Water Quality, Documentation and User's Manual," Civil and Environmental Engineering Deptartment, Tufts University, Medford, Massachusetts.

Chow, V.T. (1959). Open-Channel Hydraulics, McGraw-Hill Book Co., New York, New York.

Cunningham, R., Gisclair, D., and Craig, J. (2004). "The Louisiana Statewide LIDAR Project," Prepared for The Louisiana Oil Spill Coordinators Office (LOSCO), LSU, and 3001, Inc.

Davis, M. (2010). Numerical Simulation of Unsteady Hydrodynamics in the Lower Mississippi River. M.S. Thesis. University of New Orleans, New Orleans, Louisiana.

Dortch, M. S., Hamlin-Tillman, D. E., and Bunch, B. W., (1992). "Modeling Water Quality of Reservoir Tailwaters," Technical Report W-92-1, US Army Engineer Waterways Experiment Station, Vicksburg, Mississippi.

Edinger, J.E., Brady, D.K., and Geyer, J.C. (1974) "Heat Exchange and Transport in the Environment," Prepared for the Electric Power Research Institute, EPRI Publication No. 74—49-00-3, Palo Alto, California.

FitzGerald, D. M., Kulp, M. A., Huges, Z., Georgiou, I., Miner, M. D., Penland, S., and Howes, N. (2007). Impacts of Rising Sea Level to Backbarrier Wetlands, Tidal Inlets, and Barrier Islands: Barataria Coast, Louisiana. Proceedings of the Sixth International Symposium on Coastal Engineering and Science of Coastal Sediment Process, May 13-17, 2007, New Orleans, Louisiana. 1179-1192.

Georgiou, I., McCorquodale, J., Neupane, J., Howes, N., Hughes, Z., FitzGerald, D., et al. (2010). Modeling the Hydrodynamics of Diversion into Barataria Basin. Final Report submitted to the Lake Pontchartrain Basin Foundation, Pontchartrain Institute for Environmental Sciences, University of New Orleans, New Orleans, Louisiana.

Georgiou, I. Y., McCorquodale, J. A., Schindler, J., Retana, A. G., FitzGerald, D. M., Hughes, Z., and Howes, N. (2009). Impact of Multiple Freshwater Diversions on the Salinity Distribution in the Pontchartrain Estuary under Tidal Forcing. Journal of Coastal Research , vol. 54 (SI), 59-70.

Georgiou, I. Y., McCorquodale, J. A., Schindler, J., Retana, A. G., FitzGerald, D. M., Hughes, Z., Howes, N. (2009). Optimization of the Violet Diversion in the Pontchartrain Estuary along with Other Upper and Middle Estuary Diversions and MRGO Modifications. Final Report submitted to the National Oceanic and Atmospheric Administration (NOAA) Pontchartrain Restoration Program. Pontchartrain Institute for Environmental Sciences (PIES), New Orleans, Louisiana.

Haralampides, K. (2000). A Study of the Hydrodynamics and Salinity Regimes of the Lake Pontchartrain System. Ph.D. Dissertation. University of New Orleans, New Orleans, Louisiana.,

Herring, H.J. (1993). A Bathymetric and Hydrographic Climatological Atlas for the Gulf of Mexico. Dynalysis of Princeton, Princeton, NJ.

Kadlec, R.H., and Knight, R.L. (1996). Treatment Wetlands, CRC Press, Lewis Publishers.

Kindinger, J. (1988). Seismic stratigraphy of the Mississippi-Alabama shelf and upper continental slope . Marine Geology , 83 (1), 79-94.

Lake Pontchartrain Basin Foundation (LPBF). (2006, February 28). Comprehensive Habitat Management Plan for the Lake Pontchartrain Basin. Retrieved October 12, 2010, from Lake Pontchartrain Basin Foundation Save Our Lake: http://www.saveourlake.org/PDF-documents/CHMP_final_%2022706.pdf.

Macey, R. I. and George F. O. (2001). Berkeley Madonna - Modeling and Analysis of Dynamic Systems. Web. 03 Nov. 2011. <http://www.berkeleymadonna.com/>.

McCorquodale, J.A., Georgiou, I.Y., Retana, A.G., and Roblin, R. (2008). Assessment of Integrated Hydrodynamic and Transport for Long-term Predictions: FVCOM & Water Quality Modeling of the Pontchartrain Estuary Including Subprovinces 1 and 5. Chapter 11a., in R.R. Twilley (ed.), Coastal Louisiana Ecosystem Assessment & Restoration (CLEAR) Program: A Tool to Support Coastal Restoration, vol. IV. Final Report to Department of Natural Resources, Coastal Division, Baton Rouge, Louisiana. Contract No. 2512-06-02.

McCorquodale, J.A., Moulton, D., Barbe', D., Wang, Y., Haralampides, K., and Carnelos, S. (2001). "Reliability of NPDES Derived Loads in Urban Runoff". Proceedings of the Urban Drainage Modeling Symposium, American Society of Civil Engineers, Orlando, Florida, May 20-24, 2001, 10 pp.

McCorquodale, J.A., Roblin, R.J., Georgiou, I.Y., and Haralampides, K.A. (2009). "Salinity, Nutrient, and Sediment Dynamics in the Pontchartrain Estuary," Journal of Coastal Research, vol. 54, pp. 71-87.

Meselhe, E., McCorquodale, J.A., and Georgiou, I.Y. (2008). "Hydrologic Modeling and Budget Analysis of the Southwestern Louisiana Chenier Plain – Part III: Sediment Budget for the Chenier Plain" Final Report prepared for the Louisiana Coastal Area (LCA) Science and Technology Program Office, Louisiana.

Meselhe, E. and Miller, R. (2008). "Hydrologic Modeling and Budget Analysis of the Southwestern Louisiana Chenier Plain – Part I: Regional Model," Final Report prepared for the Louisiana Coastal Area (LCA) Science and Technology Program Office, Louisiana.

Metcalf & Eddy, Inc. (1972). Wastewater Engineering: Treatment, Disposal, Reuse, 2nd Edition, Revised by George Tchobanoglous, McGraw-Hill, NY.

Mukai, A.Y., Westerink, J.J., Luettich, R.A., and Mark, D. (2002). Eastcoast 2001, A Tidal Constituent Database for Western North Atlantic, Gulf of Mexico, and Caribbean Sea. ERDC/CHL TR-02-24. Engineer Research and Development Center, Coastal and Hydraulics Lab, US Army Corps of Engineers, Vicksburg, Mississippi.

Ponce, V. M. (1989). Engineering Hydrology Principles and Practices. Prentice Hall, Inc. Upper Saddle River, New Jersey.

Reddy, K. R., D'Angelo, E.M., and Harris, W.G. (1999). "Biogeochemistry of Wetland," Section G, Chapter 4, Handbook of Soil Science, Vol. 1, M.E. Sumner, Edition., Taylor and Francis, Inc.

Retana, A.G. (2008). Salinty Transport in a Finite-Volume Sigma-Layer Three Dimensional Model. Ph.D. Dissertation. University of New Orleans, New Orleans, Louisiana, 689p.

Roblin, R. (2008). Water Quality Modeling of Freshwater Diversions in the Pontchartrain Estuary. M.S. Thesis. University of New Orleans, New Orleans, Louisiana.

Schindler, J. (2010). Estuarine Dynamics as a Function of Barrier Island Transgression and Wetland Loss: Understanding the Transport and Exchange Processes. M.S. Thesis. (Reference URL: http://louisdl.louislibraries.org/u?/NOD,1089), University of New Orleans, New Orleans, Louisiana.

Thomann, R.V., and Mueller, J.A. (1987). Principles of Surface Water Quality Modeling and Control. Harper & Row, New York.

"Tides & Currents." (2011). 17 Nov. 2011. <http://tidesandcurrents.noaa.gov/products.html>

U.S. Army Corps of Engineers New Orleans District (USACE NOD). (1982). Lake Pontchartrain, Louisiana and Vicinity Hurricane Protection Project. Environmental Impact Statement, US Army Corps of Engineers, New Orleans, Louisiana.

Attachment A

Table 53 Precipitation Stations for the Eco-Hydrology Models

Station/COOP ID	Station Name	Sample Interval	Region
NCDC 166660	New Orleans International Airport	Daily	PB
NCDC 163433	Galliano	Daily	PB/AA
NCDC 160565	Bayou Sorrel Lock	Daily	AA
NCDC 166394	Morgan City	Daily	AA/CP
NCDC 160007	Abbeville	Daily	CP
NCDC 160658	Bell City 13 SW	Daily	CP
NCDC 163979	Hackberry 8 SSW	Daily	CP
NCDC 165065	Lake Arthur 10 SW	Daily	CP
NCDC 165078	Lake Charles RGNL AP	Daily	CP
NCDC 165296	Leland Bowman Lock	Daily	CP
NCDC 167932	Rockefeller Wildlife Refuge	Daily	CP
NCDC 417174	Port Arthur SE TX AP	Daily	CP

Table 54 Wind Speed Stations for the Eco-Hydrology Models

Station/COOP ID	Station Name	Record	Region
LUMCON 103	Lake Pontchartrain	2002-2009	PB
NCDC 722310	New Orleans International Airport	1990-2007	PB
NCDC 722315	New Orleans Lakefront Airport	1990-2007	PB
NCDC 722366	Slidell	1999-2007	PB
NCDC 722405	Lafayette Regional Airport	1945-2010	AA/CP

Table 55 Tributary Discharge Stations for the Eco-Hydrology Models

Station ID	Station Name	Region
USACE 01100	Mississippi River at Tarbert Landing, MS	PB
USGS 02470629	Mobile River at River Mile 31.0 at Bucks, AL	PB
USGS 02471019	Tensaw River near Mount Vernon, AL	PB
USGS 02479000	Pascagoula River at Merrill, MS	PB
USGS 02481000	Biloxi River at Wortham, MS	PB
USGS 02481510	Wolf River near Landon, MS	PB
USGS 02489500	Pearl River near Bogalusa, LA	PB
USGS 07375000	Tchefuncte River near Folsom, LA	PB
USGS 07375500	Tangipahoa River at Robert, LA	PB
USGS 07376000	Tickfaw River at Holden, LA	PB
USGS 07378500	Amite River near Denham Springs, LA	PB
USACE 03045	Atchafalaya River at Simmesport, LA	AA
USGS 07381000	Bayou Lafourche at Thibodeaux, LA	AA
USGS 07381235	GIWW West of Bayou Lafourche at Larose, LA	AA
USGS 07381670	GIWW at Bayou Sale Ridge near Franklin, LA	AA/CP
USGS 07385790	Charenton Drainage Canal at Baldwin, LA	CP

Station ID	Station Name	Region
USGS 07386980	Vermilion River at Perry, LA	CP
USGS 08012150	Mermentau River at Mermentau, LA	CP
USGS 08015500	Calcasieu River near Kinder, LA	CP
USGS 08030500	Sabine River at Ruliff, TX	CP
USGS 08041780	Neches River at Beaumont, TX	CP

Table 56 Tributary Water Quality Stations in the PB Model

Station ID	Station Name	Measured Constituents
USGS 07377000	Amite River near Darlington, LA	Q, TUR, NO3, TPH
USGS 07378500	Amite River near Denham Springs, LA	Q, TUR, TSS, TON
USGS 07380120	Amite River at Port Vincent, LA	Q, TUR, TSS, NO3, TPH, NH4, TON
USGS 07378510	Amite River at 4th Camp near Denham Springs, LA	TUR, TSS, NO3, TPH, NH4, TON
USGS 07375500	Tangipahoa River at Robert, LA	Q, TUR, TSS, NO3, TPH, NH4, TON
USGS 07375690	Tangipahoa River below Bedico Creek near Madisonville, LA	NO3, TPH
USGS 02492000	Bogue Chitto River near Bush, LA	Q, TUR, TSS, NO3, TPH, NH4, TON
USGS 07375800	Tickfaw River at Liverpool, LA	Q, TUR, NO3, TPH
USGS 07376000	Tickfaw River at Holden, LA	TUR, NO3, TPH, TKN
USGS 02488500	Pearl River near Monticello, MS	Q, TUR, TSS, NO3, TPH, NH4, TON
USGS 02489000	Pearl River near Columbia, MS	Q, TUR, TSS, NO3, TPH, NH4, TON
USGS 02489500	Pearl River near Bogalusa, LA	Q, TUR, TSS, NO3, TPH, NH4, TON
USGS 02490193	Pearl River at Pools Bluff near Bogalusa, LA	TUR, TSS, NO3, TPH
USGS 07375230	Tchefuncte River at Madisonville, LA	TSS, NO3, NH4, TON
USGS 07375050	Tchefuncte River near Covington, LA	TUR, TSS, NO3, TPH, NH4, TON
USGS 07378000	Comite River near Comite, LA	Q, NO, TPH
LDEQ 0043	Amite River at Port Vincent, LA	TUR, NO3, TPH, TKN
LDEQ 0228	Amite River at Mile 6.5 at Clio, LA	TUR, NO3, TPH, TKN
LDEQ 0268	Amite River Diversion Canal N of Gramercy, LA	TUR, NO3, TPH, TKN
LDEQ 0044	Amite River W of Darlington, LA	TUR, NO3, TPH, TKN
LDEQ 0119	Amite River at Grangeville, LA	TUR, NO3, TPH, TKN
LDEQ 0118	Amite River at Magnolia, LA	TUR, NO3, TPH, TKN
LDEQ 0108	Tangipahoa River at Arcola, LA	TUR, NO3, TPH, TKN
LDEQ 0034	Tangipahoa River near Kentwood, LA	TUR, NO3, TPH, TKN
LDEQ 0033	Tangipahoa River W of Robert, LA	TUR, NO3, TPH, TKN

Station ID	Station Name	Measured Constituents
LDEQ 1104	Tangipahoa River near Lake Pontchartrain	TUR, NO3, TPH, TKN
LDEQ 1038	Bogue Chitto River U/S from Wilson Slough	TUR, NO3, TPH, TKN
LDEQ 0065	Bogue Chitto River at Franklinton, LA	TUR, NO3, TPH, TKN
LDEQ 0064	Bogue Chitto River near Bush, LA	TUR, NO3, TPH, TKN
LDEQ 0116	Tickfaw River at Springville, LA	TUR, NO3, TPH, TKN
LDEQ 1106	Tickfaw River near Lake Maurepas	TUR, NO3, TPH, TKN
LDEQ 0032	Pearl River (E) at Pearlington, MS	TUR, NO3, TPH, TKN
LDEQ 0105	Pearl River (W) SE of Slidell, LA	TUR, NO3, TPH, TKN
LDEQ 1061	Pearl River at Walkian Bluff Boat Launch	TUR, NO3, TPH, TKN
LDEQ 1053	Pearl River Navigation Canal at Lock #1	TUR, NO3, TPH, TKN
LDEQ 0062	Pearl River at Pools Bluff, LA	TUR, NO3, TPH, TKN
LDEQ 0012	Pearl River E of Bogalusa, LA	TUR, NO3, TPH, TKN
LDEQ 0106	Tchefuncte River at Madisonville, LA	TUR, NO3, TPH, TKN
LDEQ 0107	Tchefuncta River W of Covington, LA	TUR, NO3, TPH, TKN
LDEQ 0638	Tchefuncte River S of Madisonville, LA	TUR, NO3, TPH, TKN
LDEQ 0298	Natalbany River W of Pontchatoula	TUR, NO3, TPH, TKN
LDEQ 1109	Comite River at Wilson-Clinton Road Bridge	TUR, NO3, TPH, TKN
LDEQ 0297	Comite River E of Baton Rouge, LA	TUR, NO3, TPH, TKN
LDEQ 1100	Comite River near Comite Drive Bridge	TUR, NO3, TPH, TKN
LDEQ 1099	Comite River near Stevendale Road train bridge	TUR, NO3, TPH, TKN

Table 57 TPH and NH4 Concentrations for PB Tributaries (Roblin, 2008)

River	Average TPH (mg/L)	TPH Standard Deviation	Average NH4 (mg/L)	NH4 Standard Deviation
Amite River	0.1234	0.1126	0.10976	0.07155
Bogue Chitto River	0.0887	0.0657	0.06806	0.05547
Comite River	0.1655	0.1423	0.17326	
Natalbany River	0.1981	0.0808	0.22419	
Pearl River	0.1096	0.0943	0.09625	0.11306
Tangipahoa River	0.1187	0.1043	0.08706	0.07200
Tchefuncte River	0.0992	0.0672	0.06693	0.07219
Tickfaw River	0.1076	0.0654	0.19562	

Table 58 Average LDEQ TKN, Predicted TON, Average USGS TON, and Percent Error Values for PB Tributaries (Roblin, 2008)

River	Average LDEQ TKN (mg/L)	Predicted TON (TKN-NH4) (mg/L)	Average USGS TON (mg/L)	% Error for TON (%)
Amite River	0.71037	0.60072	0.75635	20.6
Bogue Chitto River	0.59744	0.52938	0.58414	9.4
Comite River		0.59642		
Natalbany River		0.73298		
Pearl River	0.74454	0.64829	0.75051	13.6
Tangipahoa River	0.68370	0.59664	0.58524	1.9
Tchefuncte River	0.72160	0.65466	0.65254	0.3
Tickfaw River		0.66960		

Table 59 Tributary Water Quality Stations in the AA Model

Station ID	Station Name	Measured Constituents
USGS 07381495	Atchafalaya River at Melville, LA	NH4, NO3, TPH, TMP, TKN, TOC, ALG
USGS 07381490	Atchafalaya River at Simmesport, LA	TSS
LDEQ 0293	Bayou Lafourche at Thibodaux, LA	NH4, NO3, TPH, TMP, TKN, TOC, TSS

Table 60 Tributary Water Quality Stations in the CP Model

Station ID	Station Name	Measured Constituents
LDEQ 0001	Vermilion River at Perry, LA	NH4, NO3, TPH, TMP, TKN, TOC, TSS
LDEQ 0003	Mermentau River at Mermentau, LA	NH4, NO3, TPH, TMP, TKN, TOC, TSS
LDEQ 0095	Calcasieu River near Kinder, LA	NH4, NO3, TPH, TMP, TKN, TOC, TSS
LDEQ 0098	Bayou Lacassine near Lake Arthur, LA	NH4, NO3, TPH, TMP, TKN, TOC, TSS
LDEQ 0674	Charenton Canal S of Baldwin, LA	NH4, NO3, TPH, TMP, TKN, TOC, TSS
LDEQ 0685	GIWW at Cypremort Point, LA	NH4, NO3, TPH, TMP, TKN, TOC, TSS
LDEQ 1155	Sabine River NW of Toomey, LA	NH4, NO3, TPH, TMP, TKN, TOC, TSS
LDEQ 1168	Vinton Waterway S of Vinton, LA	NH4, NO3, TPH, TMP, TKN, TOC, TSS
TCEQ 10580	Neches River at US 96	NH4, TPH, TMP, TKN, TOC, ALG
USGS 08012150	Mermentau River at Mermentau, LA	ALG
USGS 08012470	Bayou Lacassine near Lake Arthur, LA	ALG

Table 61 Air Temperature Stations for the PB Model

Station	Station Name	Record
LUMCON 103	Lake Pontchartrain	2007-2010
NCDC AWS 722310/COOP-ID 166660	New Orleans International Airport	1990-2007
NCDC AWS 722315/COOP-ID 166667	New Orleans Lakefront Airport	1990-2007
NCDC AWS 722366/COOP-ID 168539	Slidell	1999-2007
NCDC AWS 722307/WBAN 53893	Golden Triangle, LA	1990-1999

Table 62 Average, Maximum, and Minimum Monthly Air Temperatures for the PB Model (1990 – 2006) (Roblin, 2008)

Month	Average Air Temperature (°C)	Maximum Air Temperature (°C)	Minimum Air Temperature (°C)
Jan	12.40	23.44	-0.74
Feb	14.09	23.46	-3.44
Mar	17.05	25.30	2.03
Apr	20.77	26.87	10.80
May	24.77	29.91	17.61
Jun	27.28	30.76	22.67
Jul	28.21	32.26	23.75
Aug	28.25	31.86	22.37
Sep	26.51	31.89	17.69
Oct	21.91	28.58	5.97
Nov	16.63	25.89	4.44
Dec	13.02	24.69	0.35

Table 63 Sine Curve Parameters for Tributary Water Temperatures for the AA and CP Models

Tributary	*A*	*f*	*p*	*k*
Vermilion River	10.25	0.014	86	19.5
Mermentau River	10	0.013	79	18
Calcasieu River	11	0.014	85	17
Bayou Lacassine	12	0.013	85	18
Charenton Canal	11	0.0135	89	20
Sabine River	11.5	0.0145	90	19
Vinton Waterway	11	0.014	93	18.5
GIWW	10	0.011	65	18
Neches River	12	0.012	70	18
Atchafalaya River	15	0.013	90	16

Table 64 Measured Flows for the 1994, 1997, and 2008 Bonnet Carré Spillway Openings

1994		1997		2008	
Date	**Flow (m^3/s)**	**Date**	**Flow (m^3/s)**	**Date**	**Flow (m^3/s)**
April 20	24.86	March 17	424.75	April 11	1025.19
May 11	247.49	March 25	6199.01	April 12	2174.26
May 15	206.71	March 31	6133.17	April 13	2156.92
May 17	247.49	April 8	4862.44	April 14	2272.85
May 18	244.37	April 14	2170.18	April 15	2330.65
May 20	238.14	April 21	141.58	April 16	2586.16
May 23	283.17			April 17	3246.20
May 25	396.44			April 18	3763.38
May 31	0.32			April 19	4376.62
				April 20	4342.28
				April 21	4537.32
				April 22	4438.61
				April 23	4456.97
				April 24	4461.28
				April 25	4434.98
				April 26	4438.61
				April 27	4360.64
				April 28	4328.45
				April 29	4186.33
				April 30	3920.63
				May 1	3475.44
				May 2	3149.75
				May 3	2667.42
				May 4	2221.35
				May 5	1680.93
				May 6	1006.15
				May 7	487.61
				May 8	453.32

Table 65 Average Monthly Water Quality Concentrations for the PB Distributaries (Roblin, 2008)

Month	NO3 (mg/L)	NH4 (mg/L)	TPH (mg/L)	TON (mg/L)	TSS [1] (mg/L)
Jan	1.2332	0.0648	0.2491	0.5932	231.7692
Feb	1.3189	0.0775	0.2584	0.7510	285.0370
Mar	1.4292	0.0657	0.2358	0.5787	239.3667
Apr	1.6365	0.0340	0.2301	0.7468	219.2667
May	1.8329	0.0356	0.2325	0.6296	202.5152
Jun	1.6459	0.0379	0.2357	0.7547	221.8378

Month	NO3 (mg/L)	NH4 (mg/L)	TPH (mg/L)	TON (mg/L)	TSS [1] (mg/L)
Jul	2.1236	0.0364	0.2560	0.8636	209.7308
Aug	1.2893	0.0390	0.2140	0.7367	172.3704
Sep	0.8984	0.0277	0.2172	0.8092	131.7917
Oct	0.9161	0.0287	0.2207	0.5233	140.0526
Nov	1.1925	0.0322	0.2112	0.7155	223.7619
Dec	1.2499	0.0518	0.2360	0.6039	242.8800

[1]TSS concentrations measured at USGS St. Francisville station only.

Table 66 Offshore Stage Stations for the Eco-Hydrology Models

Station ID	Station Name	Region
USACE 01670	Southwest Pass Gauge	PB
USACE 88550	Eugene Island	AA
NOAA 8770570	Sabine Pass North	AA
NOAA 8768094	Calcasieu Pass	AA/CP
NOAA 8771510	Galveston Pleasure Pier, Texas	CP
NOAA 8764227	Lawma, Amerada Pass	CP
WAVCIS CSI03	Marsh Island	CP

Table 67 Offshore Boundary Surge Record for the PB Model

Date	Event	Surge (m)						
		PB101	PB102	PB103	PB104	PB105	PB106	PB107
7/18/1990	Weak Pacific hurricane that crossed Mexico and entered the Gulf	0.5	0.5	0.5	0.5	0.5	0.5	0.5
8/25/1992	Hurricane Andrew	1.5	1.5	1.5	1.5	1.5	1.5	1.5
7/26/1994	Tropical Strom Alberto	1	1	1	1	1	1	1
10/3/1995	Hurricane Opal	0.8	0.8	0.8	0.8	1	1	1
7/17/1997	Hurricane Danny	0.9	0.9	0.9	0.9	0.9	0.9	0.9
9/7/1998	Tropical Strom Frances	0.8	0.8	0.8	0.8	0.5	0.5	0.5
9/27/1998	Hurricane Georges	2	2	2	1.5	2	1	1
6/20/2001	Tropical Strom Allison	1	1	1	1	1	1	1
9/20/2002	Hurricane Isidore	0.5	0.5	0.5	0.5	0.5	0.5	0.5
9/22/2002	Hurricane Isidore	0.3	0.3	0.3	0.3	0.3	0.3	0.3
9/23/2002	Hurricane Isidore	1	1.25	1	1	1	1	1.2
10/1/2002	Hurricane Lili	0.5	0.5	0.5	0.5	0.5	1	1.5
9/9/2004	Hurricane Ivan	1	1	1	1	0.5	0.5	0.5
8/28/2005	Hurricane Katrina	2.5	2.5	2.5	2	2	1	1
9/30/2005	Hurricane Rita	0.5	0.5	0.5	0.5	0.4	0.4	0.4
10/22/2005	Hurricane Wilma	1	1	1	0.75	1	0.5	0.5
9/12/2007	Hurricane Humberto	1	1	1	0.8	1	1	1.1
8/30/2008	Hurricane Gustav	1	1	1	2	1.3	2.5	2.2

Date	Event	Surge (m)						
		PB101	PB102	PB103	PB104	PB105	PB106	PB107
9/10/2008	Hurricane Ike	0.5	0.5	0.5	0.5	0.3	0.3	0.3
9/11/2008	Hurricane Ike	1.25	1.25	1.25	1	1	1	1

Table 68 Offshore Salinity Values for the PB Model (Herring, 1993)

Compartment ID[55]	PB101	PB102	PB103	PB104	PB105	PB106	PB107
Salinity (ppt)	30.0	34.0	34.6	33.2	33.0	32.28	0.2

Table 69 Average Monthly Offshore Salinity Values for the AA Model

Month	**'99**	**'00**	**'01**	**'02**	**'03**	**'04**	**'05**	**'06**	**'07**	**'08**	**'09**	**'10**	**Avg**
Jan	NA	29	28	21	18	25	20	15	24	NA	27	19	23
Feb	NA	29	27	23	20	22	22	27	21	28	27	19	24
Mar	NA	31	24	25	21	21	17	27	25	27	24	18	24
Apr	NA	27	22	22	15	22	19	29	24	21	21	20	22
May	NA	29	23	19	21	22	23	23	24	17	21	19	22
Jun	NA	28	19	20	18	24	24	29	24	19	12	18	21
Jul	NA	24	22	19	19	19	23	26	24	18	19	18	21
Aug	NA	27	22	23	21	25	24	27	23	14	21	16	22
Sep	25	26	26	24	22	26	NA	28	25	25	24	20	25
Oct	27	31	NA	24	24	24	28	28	26	25	27	NA	27
Nov	30	29	28	25	27	25	21	24	28	28	25	NA	26
Dec	29	28	25	21	23	61	11	27	30	26	18	NA	23

Table 70 Salinity Distribution from Western Boundary for the CP Model

Distance (m) from Western Boundary	**Salinity Distribution**	**Distance (m) from Western Boundary**	**Salinity Distribution**
0	0.95	150	0.99
10	0.95	160	0.96
20	0.95	170	0.92
30	0.96	180	0.85
40	0.96	190	0.70
50	0.95	200	0.57
60	0.96	210	0.46
70	0.97	220	0.37
80	0.98	230	0.30
90	0.99	240	0.23
100	1.00	250	0.16
110	1.01	260	0.11

[55] These offshore compartments are the offshore nodes of the PB model. For model labeling purposes the nodes are given compartment ID numbers.

Distance (m) from Western Boundary	Salinity Distribution	Distance (m) from Western Boundary	Salinity Distribution
120	1.01	270	0.08
130	1.02	280	0.04
140	1.01	290	0.01

Table 71 Offshore Water Quality and Temperature Stations for the Eco-Hydrology Models

Station ID	Station Name	Measured Constituents	Region
NDBC 42007	22 nautical miles SSE of Biloxi, MS	TMP	PB
NODC WOA	Grid: 90.5 – 93.5 West; 27.5 – 28.5 North	TMP, NO3, TPH	AA
WAVCIS CSI06	Chevron Platform, South Terrebonne	ALG	AA
LDEQ 0962	Wine Island Pass	NH4, DON, DOP	AA
LDEQ 1170	Gulf of Mexico S of Louisiana Point	NH4, NO3, TPH, TKN, TOC	CP
LDEQ 1204	Atchafalaya Bay S of Burns, LA	NH4, NO3, TPH, TKN, TOC	CP

Table 72 Offshore Water Quality Concentrations for the PB Model (Roblin, 2008)

Compartment ID	TSS (mg/L)	NO3 (mg/L)	NH4 (mg/L)	TON (mg/L)	TPH (mg/L)
PB101	10.0	0.051	0.05	0.4	0.08
PB102	10.0	0.051	0.05	0.4	0.08
PB103	10.0	0.051	0.05	0.5	0.1
PB104	10.0	0.15	0.05	0.5	0.1
PB105	10.0	0.15	0.05	0.5	0.1
PB106	10.0	0.1	0.05	0.5	0.1
PB107[56]	150.0	1.0	0.05	0.5	0.1

[56] This node is actually in the Terrebonne area of the PB Model. The values here are used only for boundary conditions.

Table 73 NODC Spatially Averaged Surface Recordings for Gulf of Mexico Offshore Boundary for the AA Model

Month	TMP (°C)	Season	NO3 (mg/L)	SPH (mg/L)
Jan	20.8	Winter	0.0880	0.022
Feb	19.6	Spring	0.113	0.017
Mar	19.9	Summer	0.022	0.054
Apr	22.0	Fall	0.015	0.04
May	25.0			
Jun	27.2			
Jul	29.4			
Aug	29.4			
Sep	28.9			
Oct	26.4			
Nov	24.4			
Dec	22.5			

Table 74 Linearly Interpolated, Monthly Averaged Offshore NO3 and NH4 Concentrations for the CP Model

NO3 (mg/L)	Offshore Compartment ID[57]					
Month	**CP150**	**CP151**	**CP152**	**CP153**	**CP154**	**CP155**
Jan	0.080	0.173	0.266	0.360	0.453	0.546
Feb	0.115	0.203	0.290	0.378	0.465	0.553
Mar	0.110	0.244	0.379	0.513	0.648	0.782
Apr	0.180	0.301	0.422	0.543	0.663	0.784
May	0.460	0.590	0.721	0.851	0.981	1.111
Jun	0.080	0.382	0.684	0.986	1.289	1.591
Jul	0.050	0.346	0.641	0.937	1.233	1.528
Aug	0.050	0.103	0.157	0.210	0.263	0.316
Sep	0.050	0.113	0.177	0.240	0.303	0.366
Oct	0.050	0.154	0.258	0.362	0.466	0.569
Nov	0.110	0.181	0.252	0.324	0.395	0.466
Dec	0.100	0.264	0.428	0.591	0.755	0.919
NH4 (mg/L)	**Offshore Compartment ID**					
Month	**CP150**	**CP151**	**CP152**	**CP153**	**CP154**	**CP155**
Jan	0.130	0.130	0.130	0.130	0.130	0.130
Feb	--	--	--	--	--	--
Mar	0.120	0.120	0.120	0.120	0.120	0.120
Apr	--	--	--	--	--	--
May	0.230	0.230	0.230	0.230	0.230	0.230

[57] These are the offshore nodes of the CP model. For modeling purposes, the offshore nodes are given compartment ID numbers.

NO3 (mg/L)	Offshore Compartment ID[57]					
Month	**CP150**	**CP151**	**CP152**	**CP153**	**CP154**	**CP155**
Jun	--	--	--	--	--	--
Jul	--	--	--	--	--	--
Aug	0.160	0.160	0.160	0.160	0.160	0.160
Sep	0.110	0.110	0.110	0.110	0.110	0.110
Oct	0.180	0.180	0.180	0.180	0.180	0.180
Nov	--	--	--	--	--	--
Dec	--	--	--	--	--	--

Table 75 Populations, Discharges, and Water Quality Concentrations of Wastewater for the AA and CP Models[58]

Water Body	Morgan City	Thibodeaux	Houma North	Houma South	Calcasieu River	Neches River	Sabine Lake
Population	--	--	--	--	94,500	118,300	87,100
Discharge, MGD	3.08	3.35	7.36	3.12	6.99	8.75	6.44
DON, mg/L	15	15	15	15	15	15	15
NH4, mg/L	25	25	25	25	25	25	25
DOP, mg/L	3	3	3	3	3	3	3
TIP, mg/L	5	5	5	5	5	5	5

Table 76 NO3 Urban Stormwater Runoff Loadings for the PB Model

Compartment ID	PB006	PB054	PB055	PB057	PB063	PB067
NO3 (kg/d)	0.075	0.20	0.20	0.20	0.001	0.10

Table 77 Runoff Water Quality Concentrations for the AA Model

Month	NO3 (mg/L)	NH4 (mg/L)	DON (mg/L)	SPH (mg/L)	DOP (mg/L)	ALG (µg/L)	DET (mg/L)	TSS (mg/L)
Jan	0.29	0.19	0.39	0.064	0.10	5.00	13.4	45.4
Feb	0.22	0.23	0.44	0.065	0.11	5.00	10.9	60.0
Mar	0.22	0.16	0.48	0.063	0.09	5.00	9.4	58.8
Apr	0.40	0.18	1.09	0.082	0.15	5.00	9.1	72.1
May	0.57	0.15	0.60	0.088	0.11	5.00	10.3	36.5
Jun	0.37	0.17	0.53	0.070	0.09	5.00	9.3	46.2
Jul	0.37	0.17	0.28	0.065	0.07	5.00	8.7	40.1
Aug	0.37	0.20	0.37	0.048	0.06	5.00	10.2	27.8
Sep	0.21	0.14	0.31	0.056	0.07	5.00	22.8	27.7
Oct	0.22	0.20	0.16	0.060	0.07	5.00	8.1	25.4
Nov	0.30	0.13	0.29	0.062	0.07	5.00	10.3	37.3
Dec	0.45	0.20	0.15	0.062	0.08	5.00	10.5	33.8

[58] The table of water quality concentrations in Thomann and Mueller (1987) did not include concentrations of NO3.

Table 78 Calibration and Validation Stations for the PB Model

Station ID	Station Name/Location	Measured Constituents
CRMS0164	Bayou Lafourche, LA	SAL
CRMS0171	Barataria Bay near Grand Terre, LA	SAL
CRMS0178	Between Bay Tambour and Bay Joyeux, LA	SAL
CRMS3054	West Lake Salvador, LA	SAL
CRMS3136	Lake Des Allemands, LA	SAL
CRMS3166	Lake Cataouatche, LA	SAL
CRMS3169	Davis Pond, LA	SAL
CRMS4218	Little Lake, LA	SAL
CRMS4245	Bayou Perot, LA	SAL
EPA LA01-0035	Grand Terre, LA	NO3, TMP
EPA LA02-0025	Bayou Perot, LA	NO3, TMP
EPA LA02-0034	Barataria Waterway SSE of Lafitte, LA	NO3, TMP
EPA LA02-0040	Grand Isle, LA	NO3
EPA LA03-0031	Barataria Waterway SSE of Lafitte, LA	NO3, TPH, TMP
EPA LA03-0035	Barataria Waterway SSE of Lafitte, LA	NO3, TPH, TMP
EPA LA03-0040	Grand Terre, LA	NO3, TPH, TMP
EPA LA91LR40	Lake Salvador, LA	TMP
EPA LA91SR13	Little Lake, LA	TMP
EPA LA92SR17	Lake Cataouatche, LA	TMP
EPA LA94LR40	Lake Salvador, LA	TMP
LDEQ 0008	Little Lake at Temple, LA	TMP
LDEQ 0035	Pass Rigolets (The Rigolets) SE of Slidell, LA	SAL, NO3, TPH
LDEQ 0036	Pass Manchac at Manchac, LA	SAL, NO3, TPH
LDEQ 0109	Chef Menteur Pass at Menteur, LA	SAL, NO3, TPH
LDEQ 0137	Lake Pontchartrain (Causeway Crossover #7) near Metairie, LA	SAL, NO3, TPH
LDEQ 0138	Lake Pontchartrain (Causeway Crossover #4) near Metairie, LA	TRG[59], SAL, NO3, TPH
LDEQ 0139	Lake Pontchartrain (Causeway Crossover #1) near Covington, LA	SAL, NO3, TPH
LDEQ 0216	Lake Pontchartrain (Causeway Crossover #6) N of Metairie, LA	SAL
LDEQ 0217	Lake Pontchartrain (Causeway Crossover #2) S of Mandeville, LA	SAL
LDEQ 0636	Lake Cataouatche S of Avondale, LA	TPH
LDEQ 0897	Little Lake S of Bayou Perot, LA	NO3, TPH, TMP
LDEQ 0900	Bayou Perot SW of Barataria, LA	NO3, TPH, TMP
LDEQ 0901	Lake Salvador NE of Point Chicot, LA	NO3, TPH, TMP
LDEQ 0904	Main Canal, 2.1 miles S of Highway 90 at water control structure, LA	NO3, TPH, TMP

[59] Observational data from Gabriel Retana's thesis (Retana, 2008).

Station ID	Station Name/Location	Measured Constituents
LDEQ 0905	Harvey Canal at Lapalco Blvd (E side of canal) S of Harvey, LA	NO3, TPH, TMP
LDEQ 0907	Barataria Waterway SSE of Lafitte, LA	NO3, TPH, TMP
LDEQ 0908	Wilkinson Bayou N of Barataria Bay, LA	TPH, TMP
LDEQ 0909	Bayou Dulac W of Bay Sanbois, LA	TPH, TMP
LDEQ 0910	Outer Cataouatche Canal W of Avondale, LA	TPH, TMP
LDEQ 0920	Lac Des Allemands N of Bayou Boeuf, LA	NO3, TPH, TMP
LDEQ 0925	Southwestern Louisiana Canal at North Lake, LA	TPH, TMP
LDEQ 0926	Bay Lizette E of Leeville, LA	TPH, TMP
LDEQ 1072	Lake St. Catherine, LA	SAL, NO3, TPH
LDEQ 1074	Lake Borgne near mouth of Blind Rigolets, LA	SAL, NO3, TPH
LDEQ 1075	Lake Pontchartrain S of Treasure Isle channel marker #6, LA	SAL, NO3, TPH
LDEQ 1105	Lake Maurepas, LA	SAL, NO3, TPH
LDEQ 3084	Bay Rambo NW of Grand Isle, LA	TMP
LDEQ 3085	Grand Bayou E of Galliano, LA	TMP
LDEQ 3090	Little Lake, LA	TMP
LUMCON 103	Lake Pontchartrain, LA	TMP
MRGO Study[60]	IHNC, LA	Q
MRGO Study[61]	Chef Menteur, LA	Q
MRGO Study [62]	Pass Manchac, LA	Q
MRGO Study [63]	Rigolets, LA	Q
NOAA 8747437	Bay Waveland Yacht Club, MS	TRG[64]
UNO[65]	Lake Pontchartrain, LA	SAL
USGS 073802375	Lake Salvador near Lafitte, LA	TRG, SAL
USGS 07380251	Barataria Bay N of Grand Isle, LA	TRG, SAL
USGS 073802516	Barataria Pass at Grand Isle, LA	SAL
USGS 07380335	Little Lake near Cutoff, LA	TRG, SAL
USGS 291929089562600	Barataria Bay near Grand Terre, LA	TRG, SAL
USGS 292800090060000	Little Lake near Bay Dosgris E of Galliano, LA	TRG, SAL
USGS	Barataria Waterway S of Lafitte, LA	TRG, SAL

[60] Georgiou et al, 2009
[61] Georgiou et al, 2009
[62] Georgiou et al, 2009
[63] Georgiou et al, 2009
[64] Observational data from Gabriel Retana's thesis (Retana, 2008)
[65] There are several stations located in Lake Pontchartrain that were monitored by the University of New Orleans (UNO) (Haralampides, 2000).

Station ID	Station Name/Location	Measured Constituents
292859090004000		
USGS 2951190901217	Lake Cataouatche at Whiskey Canal S of Waggaman, LA	TRG, SAL
USGS 295501090190400	Davis Pond, LA	TRG, SAL
USGS 3007220891501	Mississippi Sound at Grand Pass, LA	SAL
USGS 300910089374820	Rigolets at CSX RR near Rigolets, LA	TRG[66]
USGS 301001089442600	Rigolets at Highway 90 near Slidell, LA	SAL
USGS 301748090200900	Pass Manchac at Turtle Cove near Ponchatoula, LA	TRG[67], SAL
USGS Site 10A1 & 10A3	Rigolets, LA	SAL, TPH
USGS Site 10A2 & 10A4	Rigolets, LA	SAL
USGS Site 11A1-11A2, 11A4-11A5, 11A7	Causeway Bridge, LA	SAL
USGS Site 2A1 & 2A3	Pass Manchac, LA	SAL, TPH
USGS Site 2A2, 2B2-2B3, 2C2-2C3	Pass Manchac, LA	SAL
USGS Site 3A1-3A3, 3B2-3B3, 3C2-3C3	Tangipahoa River at Lake Pontchartrain, LA	SAL
USGS Site 4A1-4A3, 4B2-4B3, 4C2	IHNC, LA	SAL
USGS Site 5A1-5A3, 5B2-5B3, 5C2-5C3	17th Street Canal, LA	SAL
USGS Site 6A1-6A3, 6B2-6B3, 6C2-6C3	Tchefuncte River, LA	SAL
USGS Site 7A1-7A3, 7B2-7B3, 7C2-7C3	Bayou Castine, LA	SAL
USGS Site 8A1-8A3, 8B2-8B3, 8C2-8C3	Bayou Lacombe, LA	SAL
USGS Site 9A1 & 9A3	Chef Menteur, LA	SAL, TPH
USGS Site 9A2 & 9A4	Chef Menteur, LA	SAL

[66] Observational data from Gabriel Retana's thesis (Retana, 2008)
[67] Observational data from Gabriel Retana's thesis (Retana, 2008)

Table 79 Calibration and Validation Stations for the AA Model

Station ID	Station Name/Location	Measured Constituents
CRMS0175	West of Bay Diego, LA	STG, SAL, TMP
CRMS0178	Between Bay Tambour and Bay Joyeux, LA	SAL, TMP
CRMS0190	West of Little Lake near Cut Off, LA	STG, SAL, TMP
CRMS0303	West of Bay Junop, LA	STG, SAL, TMP
CRMS0309	South of Mosquito Bay, LA	STG, SAL, TMP
CRMS0312	Southwest of Pointe Aux Chenes Wildlife Management Area, LA	STG, SAL, TMP
CRMS0331	East of Lake Long near Lockport, LA	STG, SAL, TMP
CRMS0336	East of Lake Felicity, LA	STG, SAL, TMP
CRMS0371	North of Carencro Lake, LA	STG, SAL, TMP
CRMS0376	East of Caillou Bay, LA	STG, SAL, TMP
CRMS0383	South of Caillou Lake, LA	STG, SAL, TMP
CRMS0387	North of Catfish Lake near Galliano, LA	STG, SAL, TMP
CRMS0390	North of Lake Boudreaux, LA	STG, SAL, TMP
CRMS0396	South of Lake De Cade, LA	STG, SAL, TMP
CRMS0409	North of Lake Penchant, LA	STG, SAL
CRMS0421	North of Dog Lake and West of Lake Charlie, LA	STG, SAL, TMP
CRMS0434	East of Felix Lake, LA	STG, SAL, TMP
CRMS0461	West of Lake Salve, LA	STG, SAL, TMP
CRMS0479	Wax Lake Delta, LA	STG, SAL, TMP
CRMS0490	North of East Cote Blanche Bay and South of GIWW, LA	TMP
CRMS2568	Southeast of Towhead Lake, LA	STG, SAL, TMP
CRMS2862	South of Amelia, LA	STG, SAL, TMP
CRMS4014	West of Atchafalaya River, LA	STG, SAL, TMP
CRMS6008	North of Hog Bayou Lake, LA	STG, SAL, TMP
CRMS6038	Southwest of Spanish Lake, LA	STG, SAL, TMP
TE-26-05	Lake Chapeau, LA	STG, SAL, TMP
NOAA 8764044	Tesoro Marine Terminal, LA	STG
NOAA 8764227	Lawma, Amerada Pass, LA	STG
NOAA 8761724	Grand Isle, LA	STG
LUMCON 105	Tambour Bay, LA (TAML1)	SAL
USGS 07381235	GIWW W of Bayou Lafourche at Larose, LA	STG, Q, SAL
USGS 07381328	Houma Navigation Canal at Dulac, LA	STG
USGS 07381331	GIWW at Houma, LA	STG, Q, SAL, TMP
USGS 073813375	Bayou Terrebonne at Ctrl Str near Lapeyrouse, LA	STG
USGS 073813498	Caillou Bay SW of Cocodrie, LA	STG, SAL, TMP
USGS 07381355	Company Canal at Salt Barrier near Lockport, LA	STG, SAL, TMP

Station ID	Station Name/Location	Measured Constituents
USGS 073814675	Bayou Boeuf at Railroad Bridge at Amelia, LA	STG, Q, TMP
USGS 07381515	Atchafalaya River at Butte La Rose, LA	STG
USGS 073815450	Chicot Pass near Myette Point near Charenton, LA	STG
USGS 07381590	Wax Lake Outlet at Calumet, LA	STG, Q, TSS, ALG, TN, TPH
USGS 073815963	Murphy Lake near Bayou Sorrel, LA	STG, TMP
USGS 07381600	Lower Atchafalaya River at Morgan City, LA	STG, Q, TSS, ALG, TN, TPH
USGS 073816202	GIWW at Mile 103 S of Morgan City, LA	STG
USGS 073816503	Bayou Penchant S of Morgan City, LA	STG
USGS 07381654	Atchafalaya Bay at Eugene Island, LA	STG
USGS 07381670	GIWW at Bayou Sale Ridge near Franklin, LA	STG, Q
USGS 295447091191500	Middle Fork Bayou Long at Bayou Long, LA	STG, TMP
USGS 300312091320000	Arm of Grand Lake near Crook Chene Cove, LA	STG, TMP
USACE 03240	Whiskey Bay Pilot Channel below Head, LA	STG
USACE 03315	Blind Tensas Cut below Upper Grand River, LA	STG
USACE 03645	Six Mile Lake near Verdunville, LA	STG
USACE 03820	Lower Atchafalaya River below Sweet Bay Lake, LA	STG
USACE 49690	Intracoastal Waterway near Pierre Pass, LA	STG
USACE 76360	Bayou Boeuf (IWW) at Bayou Boeuf Lock East, LA	STG
USACE 76400	Bayou Boeuf (IWW) at Bayou Boeuf Lock West, LA	STG
LDEQ 0039	Atchafalaya River at Morgan City, LA	TSS, TPH
LDEQ 0110	Bayou Terrebonne at Houma, LA	TSS, TPH
LDEQ 0339	Bayou Black W of Houma, LA	TSS, TPH
LDEQ 0340	Intracoastal Waterway E of Houma, LA	TSS, TPH
LDEQ 0344	Houma Navigation Canal S of Houma, LA	TSS, TPH
LDEQ 0934	Intracoastal Waterway at Venvirotek Dock, LA	TSS, TPH
LDEQ 0942	Houma Navigation Canal at Gulf Island Dock, LA	TSS, TPH
LDEQ 0949	Bayou Petit Caillou at Cocodrie, LA	TSS, TPH
LDEQ 0950	Grand Bayou Du Large at Bayou Voison, LA	TSS, TPH
LDEQ 0952	Houma Navigation Canal N of Bayou Petit Caillou, LA	TSS, TPH
LDEQ 0953	Southwestern Louisiana Canal W of	TSS, TPH

Station ID	Station Name/Location	Measured Constituents
	Leeville, LA	
LDEQ 0954	Lake Boudreaux S of Bayou Chauvin, LA	TSS, TPH
LDEQ 0957	Caillou Bay S of Bayou Grand Caillou, LA	TSS, TPH
LDEQ 0958	Terrebonne Bay SE of Cocodrie, LA	TSS, TPH
LDEQ 0959	Timbalier Bay S of Devils Island, LA	TSS, TPH
LDEQ 0960	Lake Barre W of Cocodrie, LA	TSS, TPH
LDEQ 0961	Lake Pelto S of Cocodrie, LA	TSS, TPH
LDEQ 0962	Gulf of Mexico S of Wind Island Pass, LA	TSS, TPH
LDEQ 1199	ICWW S of Belle River, LA	TSS, TPH
LDEQ 1200	Bayou Teche at Patterson, LA	TSS, TPH
LDEQ 1201	Lower Atchafalaya River near Bateman Island, LA	TPH
LDEQ 1202	Wax Lake Outlet SW of Patterson, LA	TSS, TPH
LDEQ 1203	ICWW S of Patterson, LA	TSS, TPH
LDEQ 1209	Bayou Blue at North Bend Pumping Station, LA	TSS, TPH
LDEQ 3001	Bayou Terrebonne near Lapeyrouse, LA	TSS, TPH

Table 80 Calibration and Validation Stations for the CP Model

Station ID	Station Name/Location	Measured Constituents
CPRA ME-11	Mermentau River below Grand Lake, LA	STG, SAL
CPRA ME-16	South of White Lake, LA	STG, SAL
CPRA CS02-05	Near Wild Cow Lake, LA	STG, SAL
CPRA CS23-05	Southwest of Starks North Canal, LA	STG, SAL
CPRA CS27-25	West of Black Lake and South of GIWW, LA	STG, SAL
CRMS0494	North of West Cote Blanche Bay, LA	STG, SAL
CRMS0499	West of Lake Michael, LA	STG, SAL
CRMS0504	Northwest of Oyster Lake, LA	STG, SAL
CRMS0520	Bird Island Bayou, LA	SAL
CRMS0527	Northwest of West Cote Blanche Bay, LA	STG, SAL
CRMS0530	South of Vermilion Bay, LA	STG
CRMS0532	South of Tigre Lagoon, LA	STG, SAL
CRMS0543	Northeast of West Cote Blanche Bay, LA	STG, SAL
CRMS0549	North of Vermilion Bay, LA	STG, SAL
CRMS0553	North of Little Chenier Road, LA	STG, SAL
CRMS0554	Grand Lake Outlet, LA	STG, SAL
CRMS0562	Southeast of Little Pecan Lake, LA	STG, SAL
CRMS0581	West of North Island Canal, LA	SAL
CRMS0584	Northeast of Upper Mud Lake, LA	STG, SAL
CRMS0587	West of Upper Mud Lake, LA	STG, SAL
CRMS0588	Southeast of Dr. Miller Canal, LA	STG, SAL
CRMS0590	East of Latania Lake, LA	STG, SAL

Station ID	Station Name/Location	Measured Constituents
CRMS0595	West of Blackfish Lake, LA	STG, SAL
CRMS0599	West of Big Constance Lake, LA	STG, SAL
CRMS0603	Northeast of Little Pecan Lake, LA	STG, SAL
CRMS0605	South of Lake Misere, LA	STG, SAL
CRMS0608	North of Grassy Lake, LA	SAL
CRMS0610	Near Big Constance Lake, LA	SAL
CRMS0615	South of Price Lake, LA	STG, SAL
CRMS0618	Southwest of Schooner Bayou, LA	STG
CRMS0624	West of Grand Lake, LA	STG, SAL
CRMS 0626	Southwest of White Lake, LA	SAL
CRMS0630	South of Little Pecan Lake, LA	STG, SAL
CRMS0632	East of Freshwater City Road, LA	STG, SAL
CRMS0633	West of Freshwater Bayou and North of Gulf of Mexico, LA	SAL
CRMS0635	Southwest of Wild Cow Lake, LA	SAL
CRMS0639	Northwest of West Cove, LA	STG, SAL
CRMS0641	East of Five Lakes, LA	STG, SAL
CRMS0644	South of Calcasieu Lake, LA	STG
CRMS0655	East of Mud Lake, LA	STG, SAL
CRMS0660	South of Greens Lake, LA	STG, SAL
CRMS0683	North of Willow Bayou Canal, LA	STG, SAL
CRMS0685	North of West Cove, LA	STG, SAL
CRMS0694	Southeast of Five Lakes, LA	STG, SAL
CRMS1446	East of Latania Lake, LA	STG, SAL
CRMS2189	East of Sabine Lake, LA	STG, SAL
CRMS2334	East-Southeast of Five Lakes, LA	STG, SAL
LDEQ 0001	Vermilion River at Perry, LA	SAL
LDEQ 0003	Mermentau River at Mermentau, LA	SAL
LDEQ 0026	Calcasieu River near Burton Landing, LA	SAL, TMP, TSS, TN, TPH
LDEQ 0029	Mermentau River near Grand Cheniere, LA	SAL, TMP, TSS, TN, TPH
LDEQ 0091	Sabine River NE of Orange, TX	TMP, TSS, TN, TPH
LDEQ 0098	Bayou Lacassine near Lake Arthur, LA	SAL
LDEQ 0310	White Lake SW of Abbeville, LA	SAL, TMP, TSS, TN, TPH
LDEQ 0316	Vermilion Bay S of New Iberia, LA	TMP, TSS, TN, TPH
LDEQ 0654	Mermentau River at Lake Arthur, LA	SAL, TMP, TSS, TN, TPH
LDEQ 0655	Mermentau River (lower) at Lacassine National Wildlife Refuge, LA	SAL, TMP, TSS, TN, TPH
LDEQ 0657	Intracoastal Waterway SSW of Iowa, LA	SAL, TMP, TSS, TN, TPH
LDEQ 0659	Grand Lake near Talen's Landing, LA	SAL
LDEQ 0660	Intracoastal Waterway at Mile 170, LA	SAL, TMP, TSS, TN, TPH
LDEQ 0677	Vermilion River N of Intracoastal City, LA	SAL, TMP, TSS, TN, TPH
LDEQ 0678	Vermilion River Cutoff SW of Abbeville, LA	TMP, TSS, TN, TPH

Station ID	Station Name/Location	Measured Constituents
LDEQ 0679	Intracoastal Waterway SW of Abbeville, LA	SAL, TMP, TSS, TN, TPH
LDEQ 0691	West Cote Blanche Bay SE of Cypremort, LA	TMP, TSS, TPH
LDEQ 0695	Freshwater Bayou Canal S of Kaplan, LA	SAL, TMP, TSS, TN, TPH
LDEQ 0696	Bird Island Bayou at North end of Marsh Island, LA	TMP, TSS, TN, TPH
LDEQ 0852	Calcasieu River Coastal Waters SE of Cameron Jetties, LA	SAL, TMP, TSS, TN, TPH
LDEQ 1157	Black Bayou S of Orange, TX	SAL, TMP, TSS, TN, TPH
LDEQ 1158	Sabine Lake near Blue Buck Point, LA	SAL, TMP, TSS, TN, TPH
LDEQ 1159	Sabine Pass S of Port Arthur, TX	SAL, TMP, TSS, TN, TPH
LDEQ 1168	Vinton Waterway S of Vinton, LA	SAL
LDEQ 1169	Black Bayou S of Toomey, LA	TMP, TSS, TN, TPH
LDEQ 1170	Gulf of Mexico S of Louisiana Point, LA	SAL
LDEQ 1209	Bayou Blue at North Bend Pumping Station in North Bend, LA	SAL
LDEQ 2114	Gulf of Mexico SW of Grand Chenier, LA	SAL, TMP, TSS, TN, TPH
LDEQ 2115	Unnamed Canal near Big Constance Lake, LA	SAL, TMP, TSS, TN, TPH
LDEQ 2116	Intracoastal Waterway SW of Avery Island, LA	SAL, TMP, TSS, TN, TPH
LDEQ 2148	Boston Canal/ICWW N of ICWW at 2nd Oilfield Canal, LA	SAL, TMP, TSS, TN, TPH
NOAA 8765251	Vermilion Bay at Cypremort Point, LA	STG
NOAA 8766072	Freshwater Canal Locks, LA	STG
NOAA 8768094	Calcasieu Pass, LA	SAL
NOAA 8770570	Sabine Pass, LA	STG
TCEQ 10391	Sabine River Downstream of Cow Bayou, TX	SAL
TCEQ 10566	Neches River at City Park, TX	SAL
TCEQ 15653	ICWW 3.2 km East of Sabine River, TX	SAL
TCEQ 15654	Black Bayou in Cameron Parish, TX	SAL
USACE 70675	Catfish Point Control Structure – North, LA	STG
USACE 70750	Catfish Point Control Structure – South, LA	STG
USACE 73472	Calcasieu River Salt Water Barrier at Lake Charles, LA (Nav. E)	STG, SAL
USACE 73473	Calcasieu River Saltwater Barrier at Lake Charles, LA (Nav. W)	STG
USACE 76600	Schooner Bayou at Control Structure – East, LA	STG
USACE 76680	Schooner Bayou at Control Structure – West, LA	STG
USACE 76720	Leland Bowman Lock – East, LA	STG

Station ID	Station Name/Location	Measured Constituents
USACE 76800	Leland Bowman Lock – West, LA	STG
USACE 76880	Calcasieu Lock – East, LA	STG
USACE B1	Leland Bowman Lock/GIWW – Bowman East	SAL
USACE B1A	Leland Bowman Lock/GIWW – Bowman West	SAL
USACE CL10	Bell City Drainage Ditch, LA	SAL
USACE CL2	Calcasieu Lock East, LA	SAL
USACE CL7	Sweet Lake, LA	SAL
USACE S2	Schooner Bayou C.S., Westside, LA	SAL
USACE S3	Schooner Bayou C.S., Eastside, LA	SAL
USGS 07385790	Charenton Drainage Canal at Baldwin, LA	STG
USGS 07386980	Vermilion River at Perry, LA	STG
USGS 07387040	Vermilion Bay near Cypremort Point, LA	STG, SAL
USGS 08012150	Mermentau River at Mermentau, LA	STG
USGS 08015500	Calcasieu River near Kinder, LA	STG
USGS 08017044	Calcasieu River at I-10 at Lake Charles, LA	STG
USGS 08017095	North Calcasieu Lake near Hackberry, LA	STG, SAL
USGS 08017118	Calcasieu River at Cameron, LA	STG
USGS 08041780	Neches River Saltwater Barrier at Beaumont, TX	STG

Table 81 Group 1 Link Properties for the PB Model

Link ID	Compart-ment U/S	D/S	Depth (m)	Length (m)	Width (m)	Manning's *n*	K_m	K_{en}	K_{ex}	E_{xy} (m^2/s)
1	1	14	7.79	10000	11435	0.018	0.0075	0.25	1	10.9
2	3	1	11.5	12000	912	0.021	0.075	0.5	1.5	750
3	2	1	4.05	15000	12800	0.021	0.0075	0.1	1	50
4	3	2	10	10900	350	0.021	0.075	0.5	1	220
5	8	28	8	41677	320	9990	0	0.5	1	400
6	9	8	8	20539	300	9990	0	0.5	1	180
7	9	2	4.05	11000	203	0.019	0	0.5	1	155
8	4	9	8.75	14600	155	0.019	0.1	0.5	1	400
9	5	3	3.658	6000	7605	0.021	0	0.025	0.25	30
10	5	4	4.3	13400	23000	0.021	0	0.02	0.25	100
11	6	5	3.962	19000	22400	0.021	0	0.5	1	30.55
12	7	6	11.693	9850	240	0.026	0	0.5	1	140
13	8	2	4.05	2000	200	0.025	0	0.5	1	15
14	10	6	4.572	18657	24200	0.025	0	0.02	0.25	50.5
15	10	4	3.81	20900	16100	0.021	0	0.02	0.25	30.5
16	1	13	4.62	11508	600	0.018	0	0.02	1.25	50.5

Link ID	Compart-ment U/S	D/S	Depth (m)	Length (m)	Width (m)	Manning's *n*	K_m	K_{en}	K_{ex}	E_{xy} (m^2/s)
17	80	18	5	26000	12140	0.015	0	0.02	0.25	105.5
18	18	27	5	46000	10370	0.02	0	0.02	0.25	25.51
19	27	26	5	6740	2954	0.02	0	0.02	0.25	105.51
20	26	25	5	5000	4886	0.032	0	0.02	0.25	115.51
21	2	73	1	5000	650	0.075	0	0.02	0.25	270.51
22	14	13	1	5000	10000	0.08	0	0.02	0.25	200.51
23	14	17	10	3000	5300	0.02	0	0.08	0.25	200.1
24	78	17	2	3500	32000	0.058	0	0.12	0.25	200.1
25	17	22	10.5	10000	25000	0.0225	0	0.02	0.25	425.51
26	27	22	5	15000	10800	0.03	0	0.02	0.25	100.51
27	22	25	10.9	57400	64000	0.035	0	0.02	0.25	100.51
28	74	16	1	17000	28400	0.045	0	0.038	0.25	20.1
29	16	17	4.6	31800	32400	0.022	0	0.02	0.25	250.51
30	16	21	10.5	6000	18000	0.0225	0	0.02	0.25	255.51
31	21	22	8	48200	46400	0.02	0	0.02	0.25	1250.51
32	21	24	10	53774	50000	0.0265	0	0.02	0.25	25.1
33	24	25	11	64860	48000	0.02	0	0.02	0.25	500.51
34	28	20	5	20000	4900	0.02	0	0.02	0.25	215.51
35	28	16	5	20000	10000	0.02	0	0.02	0.25	700
36	15	28	5	9750	11200	0.018	0	0.02	0.25	700
37	28	74	2	8000	19940	0.08	0	0.02	0.25	300
38	20	21	8	41100	58000	0.018	0	0.02	0.25	605.51
39	20	23	18	39000	73000	0.02518	0	0.02	0.25	200.51
40	23	24	15	72020	42300	0.02	0	0.02	0.25	1500.51
41	11	79	0.91	10000	4400	0.06	0	0.02	0.25	12.551
42	12	15	2.75	20000	23200	0.03218	0	0.02	0.25	300.51
43	15	20	4	10000	14500	0.032	0	0.02	0.25	500.51
44	20	31	10	20000	10200	0.02	0	0.02	0.25	2500.51
45	23	32	12.6	45000	32000	0.032	0	0.02	0.25	10.51
46	19	29	12.6	29000	48000	0.03	0	0.02	0.25	450.51
47	73	74	1	5000	1000	0.1	0	0.12	0.25	200.1
48	18	17	2	12318	15000	0.023	0	0.02	0.25	300.51
49	30	15	2	10540	30000	0.0232	0	0.032	0.25	550.51
50	33	20	10	17000	32000	0.0232	0	0.02	0.25	400.51
51	12	30	5	11000	1500	0.02	0	0.02	0.25	450.51
52	32	29	12.5	60830	22000	0.032	0	0.02	0.25	1800.51
53	31	19	5	38700	50000	0.032	0	0.02	0.25	1800.51
54	85	32	14	39300	63000	0.033	0	0.02	0.25	1300.51
55	25	101	15.7	45100	73000	0.028	0	0.02	0.25	2000.51
56	24	102	16.8	42060	75000	0.0302	0	0.02	0.25	1500.51

Link ID	Compart-ment U/S	D/S	Depth (m)	Length (m)	Width (m)	Manning's *n*	K_m	K_{en}	K_{ex}	E_{xy} (m^2/s)
57	23	103	16.8	45600	100000	0.0302	0	0.02	0.25	1500.51
58	29	104	15.7	31800	45000	0.0302	0	0.02	0.25	2000.51
59	32	105	18	30000	75000	0.0302	0	0.02	0.25	2000.51
60	9	2	1.5	8156	100	0.041	0	0.12	1	175
61	34	19	2	5000	100	0.1	0	0.12	1	1000
62	35	19	3	2700	450	0.024	0	0.12	20.1	1201
63	36	19	10	911	522	0.024	0	0.12	1	1200
64	37	31	1	1560	2300	0.035	0	0.12	1	200
65	38	31	3.5	4646	862	0.0235	0	0.12	1	150
66	39	31	4.5	2000	870	0.0435	0	0.12	1	151
67	36	31	0.5	2000	500	0.1	0	0.12	1	51
68	37	31	0.5	3150	500	0.09	0	0.12	1	61
69	40	31	4	2000	6500	0.05	0	0.12	1	61
70	34	35	1.5	3000	10000	0.035	0	0.12	0.5	1000
71	35	36	2	9222	4400	0.025	0	0.12	0.5	1084.4
72	37	36	2	5173	8883.6	0.025	0	0.12	0.5	1087.3
73	38	37	2	9157	7800	0.025	0	0.12	0.5	1083.1
74	39	38	2	15047	8000	0.025	0	0.12	0.5	2000.9
75	39	40	2	6960	8300	0.0205	0	0.12	0.5	2027.4
76	70	72	2	33576	29000	0.025	0	0.12	0.5	1287.5
77	71	70	1.5	38280	643	0.035	0	0.12	0.5	524.2
78	40	41	1.5	6057	3218	0.025	0	0.12	0.5	1256.6
79	41	42	1	3300	9350.3	0.025	0	0.12	0.5	105.7
80	43	34	1	16238	11072.3	0.025	0	0.12	0.5	162.4
81	43	35	2	10815	4300	0.025	0	0.12	0.5	108.1
82	36	44	1.5	7804	6000	0.02	0	0.12	0.5	111.7
83	37	45	4	10026	5278.6	0.019	0	0.12	0.5	100.3
84	38	46	2.5	10499	8900	0.018	0	0.12	0.5	114.3
85	47	39	1.6	21300	80.5	0.025	0	0.12	0.5	260
86	43	44	1	12907	1896	0.025	0	0.12	0.5	129.1
87	45	44	1.6	5000	4169	0.0205	0	0.12	0.5	287.2
88	46	45	1.6	6727	4170	0.0205	0	0.12	0.5	72.4
89	47	46	1.5	2831	241.4	0.025	0	0.12	0.5	77.2
90	48	44	3	4522	1800	0.03	0	0.12	0.5	85
91	49	45	4.5	3312	950	0.025	0	0.12	0.5	88
92	50	45	1	805	80.5	0.03	0	0.12	0.5	21.4
93	51	46	1	1376	1448.4	0.025	0	0.12	0.5	134.4
94	51	47	1	1002	1062.2	0.025	0	0.12	0.5	90.6
95	48	49	1.5	4190	2043.9	0.025	0	0.12	0.5	75
96	54	48	1.5	11000	193.1	0.02	0	0.12	0.5	85

Link ID	Compart-ment U/S	D/S	Depth (m)	Length (m)	Width (m)	Manning's *n*	K_m	K_{en}	K_{ex}	E_{xy} (m^2/s)
97	55	48	5	2100	630	0.0205	0	0.12	0.5	140
98	52	49	2	5590	289.7	0.025	0	0.12	0.5	60
99	53	50	1	815	3600	0.025	0	0.12	0.5	70.8
100	56	52	2	12760	257.5	0.025	0	0.12	0.5	114.6
101	52	53	1	3390	160.9	0.025	0	0.12	0.5	48.3
102	53	51	1	1145	273.6	0.025	0	0.12	0.5	18.8
103	48	52	1.2	1613	450.6	0.025	0	0.12	0.5	532.7
104	55	56	2	4357	190	0.025	0	0.12	1	51.5
105	56	57	0.25	7916	3379.6	0.07	0	0.12	0.5	17.9
106	57	51	1.5	2846	450	0.035	0	0.12	0.5	114.3
107	57	53	1.5	4989	530	0.05	0	0.12	0.5	124.9
108	59	55	6.5	2295	550	0.023	0	0.12	0.5	110.6
109	58	54	5.48	6952	160.9	0.025	0	0.12	0.5	114.4
110	60	55	4	2969	2912	0.024	0	0.12	0.5	260.8
111	61	60	2	4708	80.5	0.04	0	0.12	0.5	91.4
112	61	56	1	3546	338	0.04	0	0.12	0.5	67.6
113	61	57	1	3484	482.8	0.06	0	0.12	0.5	45.9
114	65	59	5.49	9597	160.9	0.025	0	0.12	2	162.6
115	65	61	2	3074	32.2	0.035	0	0.12	0.5	61.5
116	66	61	1	2639	16.1	0.1	0	0.12	0.5	26.4
117	69	61	3.5	10425	136.8	0.0203	0	0.12	1	47.5
118	64	59	2.74	2284	517	0.0205	0	0.12	1	141.6
119	64	58	2.74	2523	600	0.0205	0	0.12	1	112.7
120	63	58	2.25	14000	241.4	0.02	0	0.12	1	50
121	62	63	2.1	5343	48.3	0.024	0	0.12	0.5	53.4
122	67	63	2.8	10114	1142.6	0.024	0	0.12	1	50
123	68	64	1.8	3713	350	0.0235	0	0.12	0.5	90
124	58	59	2.29	10372	8181	0.0205	0	0.12	0.5	33
125	66	61	4.89	14827	160	0.03	0	0.12	0.5	1026.8
126	51	50	1	6759	804	0.08	0	0.12	0.5	67.6
127	59	49	1	4869	1448	0.08	0	0.12	0.5	67.6
128	72	29	10	48766	10000	0.0232	0	0.025	0.25	850.51
129	72	19	8	10704	15000	0.0232	0	0.02	0.25	850.51
130	72	106	9	40311	12000	0.02532	0	0.02	0.25	850.51
131	74	17	1	8724	100	0.1	0	0.12	0.25	13.1
132	1	73	1.2	5378	1000	0.05	0	0.12	0.25	235.1
133	73	13	1.1	5331	8500	0.078	0	0.12	0.25	500.1
134	74	78	1.1	8864	15000	0.078	0	0.12	0.25	485.1
135	8	73	1.25	3228	520	0.1	0	0.12	0.25	115.1
136	8	2	6	129	140.55	0.0239	0	0.12	1.25	135.1

Link ID	Compart-ment U/S	D/S	Depth (m)	Length (m)	Width (m)	Manning's *n*	K_m	K_{en}	K_{ex}	E_{xy} (m^2/s)
137	76	80	2.65	5774	19000	0.023	0	0.12	0.25	55.1
138	77	18	2.31	10515	23241	0.023	0	0.12	0.25	35.1
139	13	78	1.8	8244	19000	0.0352	0	0.02	0.25	140.51
140	79	12	1.2	10000	3400	0.052	0	0.02	0.25	205.305
141	75	9	4.03	556	50	0.03	0	0.512	10.25	135.1
142	75	8	4.05	500	50	0.03	0	0.5	10	155
143	30	33	1.035	12000	3500	0.05218	0	0.02	0.25	100.51
144	12	28	3.035	3000	78	0.05218	0	0.02	0.25	100.51
145	75	8	4.05	10000	170	0.03	0	0.5	1	155
146	80	14	2.7	12230	26000	0.023	0	0.02	0.25	250.51
147	71	107	4	8000	500	0.025	0	0.12	1	200
148	71	58	4.25	15000	180	0.025	0	0.12	1	200
149	50	49	1	791	160.9	0.025	0	0.12	0.5	48.3
150	62	58	2	19650	241.4	0.05	0	0.12	0.5	393
151	71	48	2.5	38500	20.4	0.027	0	0.12	0.5	1393
152	55	54	3	10811	50	0.03	0	0.12	0.5	33
153	48	43	2	6000	50	0.03	0	0.12	0.5	67.6
154	57	51	0.2	6000	10000	0.1	0	0.12	0.5	14.3
155	61	57	0.2	6000	4820.8	0.1	0	0.12	0.5	45.9
156	59	61	1	11370	50	0.1	0	0.12	1	45.9
157	61	60	0.5	4571	3000	0.1	0	0.12	0.5	91.4
158	61	56	0.5	6759	4000	0.1	0	0.12	0.5	67.6
159	61	57	0.5	4587	5000	0.1	0	0.12	0.5	45.9
160	41	89	2	10000	10000	0.03	0	0	1	1000
161	34	81	2.7	300	10	0.023	0	0.02	0.25	250.51
162	58	81	2	20000	20.13	0.023	0	0.02	0.25	250.51
163	58	43	2	15000	20.13	0.023	0	0.02	0.25	250.51
164	83	107	4.7	1500	3300	0.023	0	0.02	0.25	250.51
165	83	106	7	45210	13000	0.023	0	0.02	0.25	1250.51
166	83	72	7	74000	23000	0.023	0	0.02	0.25	450.51
167	3	82	2.5	1000	100	0.02354	0.075	0.5	1.5	500
168	84	2	2.5	1500	100	0.0231	0.0075	0.1	1	60
169	82	84	2	1500	50	0.028	0.0075	0.1	1	60
170	48	49	4	10182	500	0.026	0	0.12	0.5	35
171	54	55	5	10700	185	0.021	0	0	1	100
172	31	85	8	10000	10500	0.0352	0	0.02	0.25	1.51
173	19	85	10	20000	10500	0.0352	0	0.02	0.25	1.51
174	62	67	2	10000	500	0.0352	0	0.02	0.25	1.51
175	86	89	3.5	10000	2000	0.025305	0	0.025	0.25	10.51
176	89	31	3.9	10000	5000	0.03052	0	0.025	0.25	10.51

Link ID	Compart-ment U/S	D/S	Depth (m)	Length (m)	Width (m)	Manning's *n*	K_m	K_{en}	K_{ex}	E_{xy} (m^2/s)
177	87	33	2.5	10000	5000	0.03052	0	0.025	0.25	10.51
178	86	87	1.5	10000	500	0.0352	0	0.025	0.25	10.51
179	42	86	2	2000	650	0.08	0	0.12	1	10.1
180	89	33	3	10000	5000	0.082	0	0.025	0.25	10.51
181	88	87	1.5	12000	1500	0.045218	0	0.02	0.25	100.51
182	12	88	2	11000	1200	0.02	0	0.02	0.25	1000.51
183	88	30	1	10540	30000	0.0232	0	0.032	0.25	50.51

Attachment B

Pontchartrain and Barataria Basin Model Calibration & Validation Plots

Tidal Range (TRG)

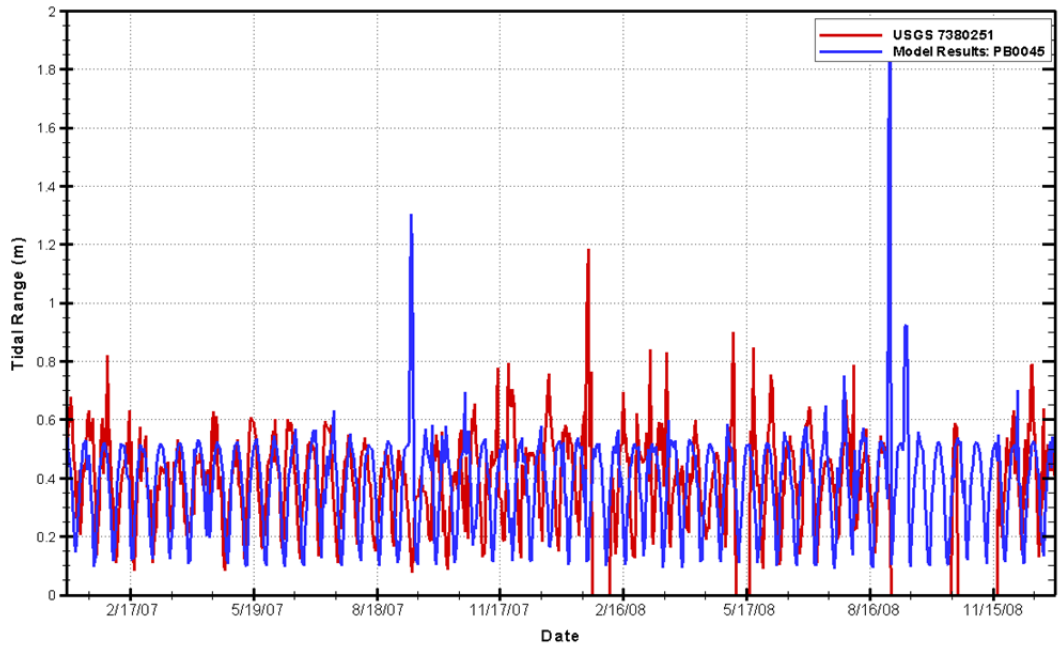

Figure 107 TRG Calibration (2008) & Validation (2007) Results for Barataria Bay North of Grand Isle in the PB Model

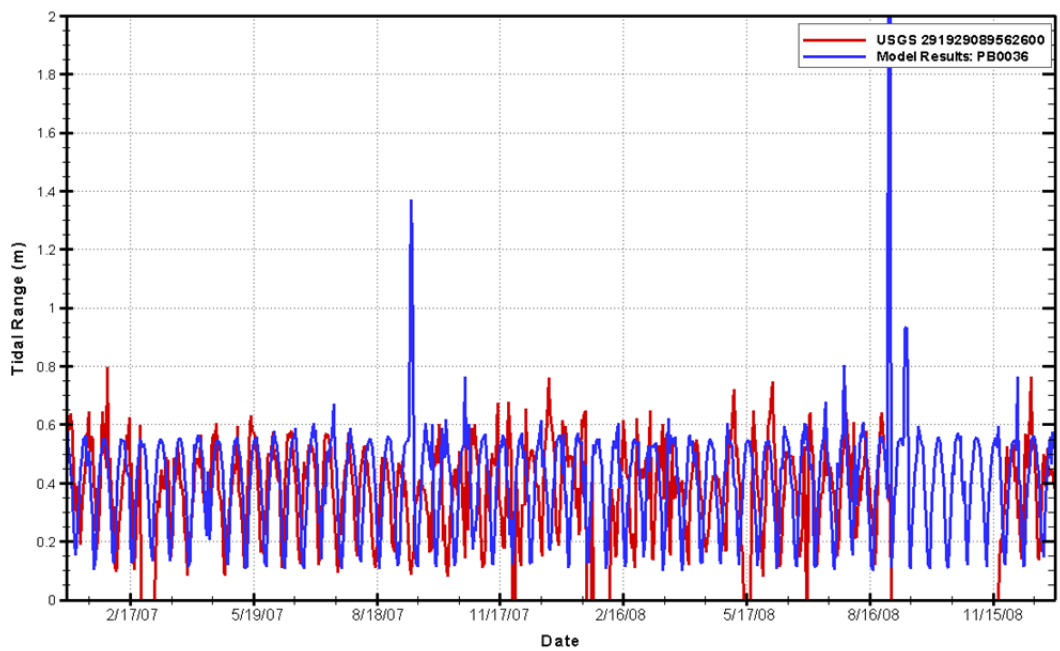

Figure 108 TRG Calibration (2008) & Validation (2007) Results for Barataria Bay near Grand Terre in the PB Model

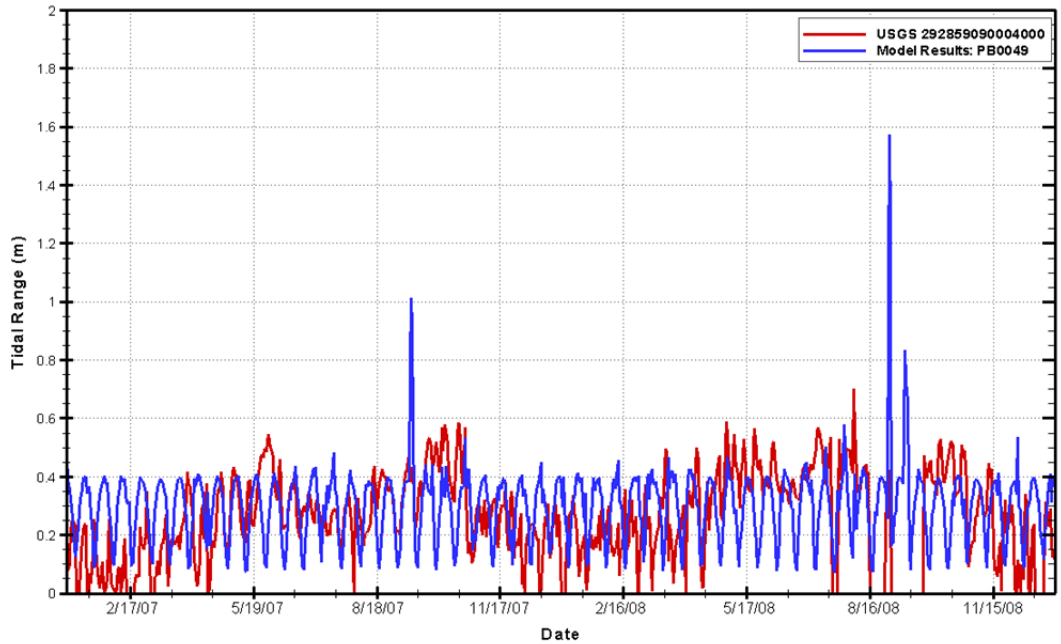

Figure 109 TRG Calibration (2008) & Validation (2007) Results for Barataria Waterway South of Lafitte in the PB Model

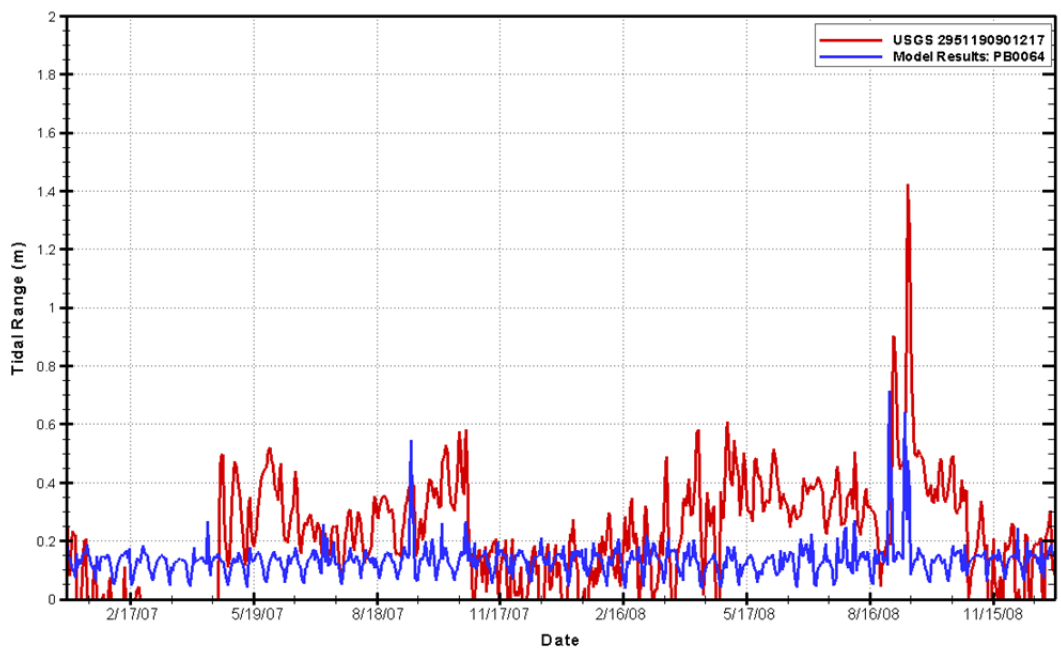

Figure 110 TRG Calibration (2008) & Validation (2007) Results for Lake Cataouatche in the PB Model

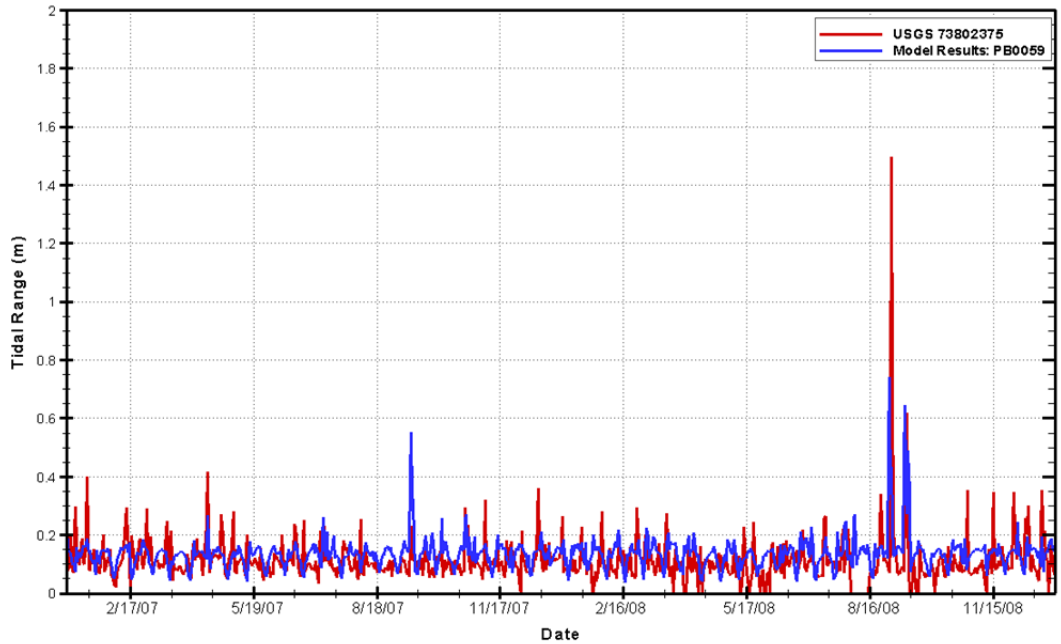

Figure 111 TRG Calibration (2008) & Validation (2007) Results for Lake Salvador in the PB Model

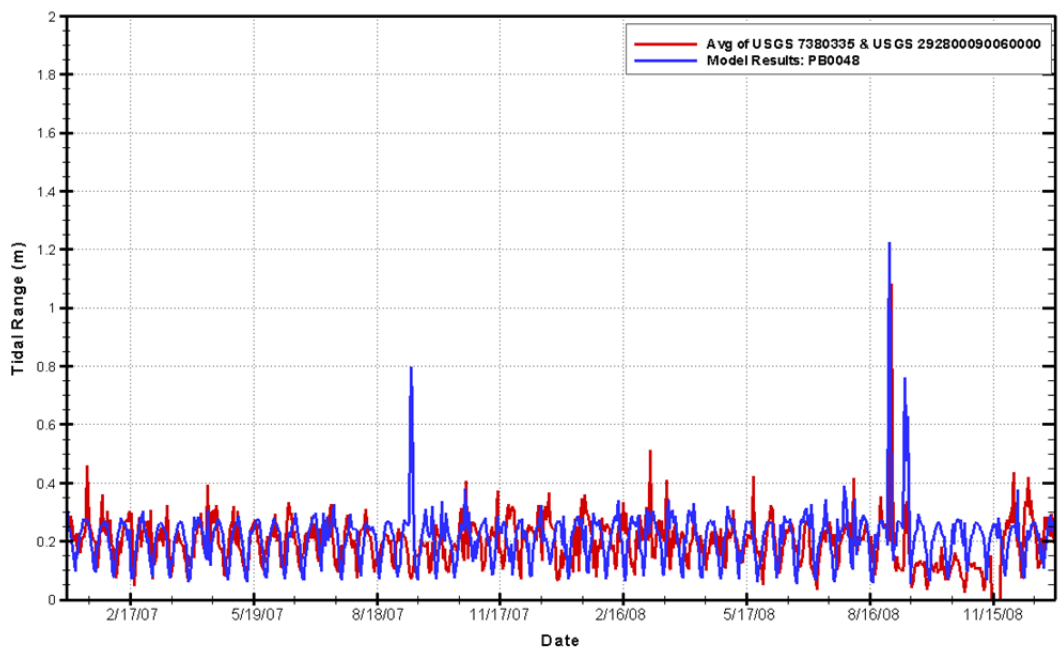

Figure 112 TRG Calibration (2008) & Validation (2007) Results for Little Lake in the PB Model

Salinity (SAL)

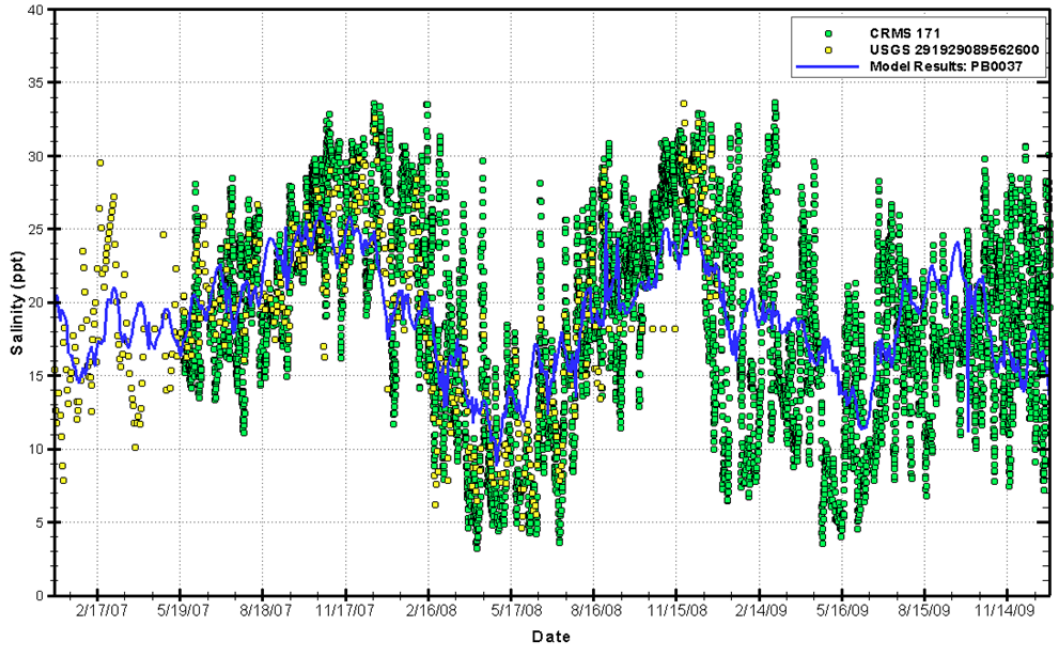

Figure 113 SAL Calibration (2008 – 2009) and Validation (2007) Results for Barataria Bay near Grand Terre in the PB Model

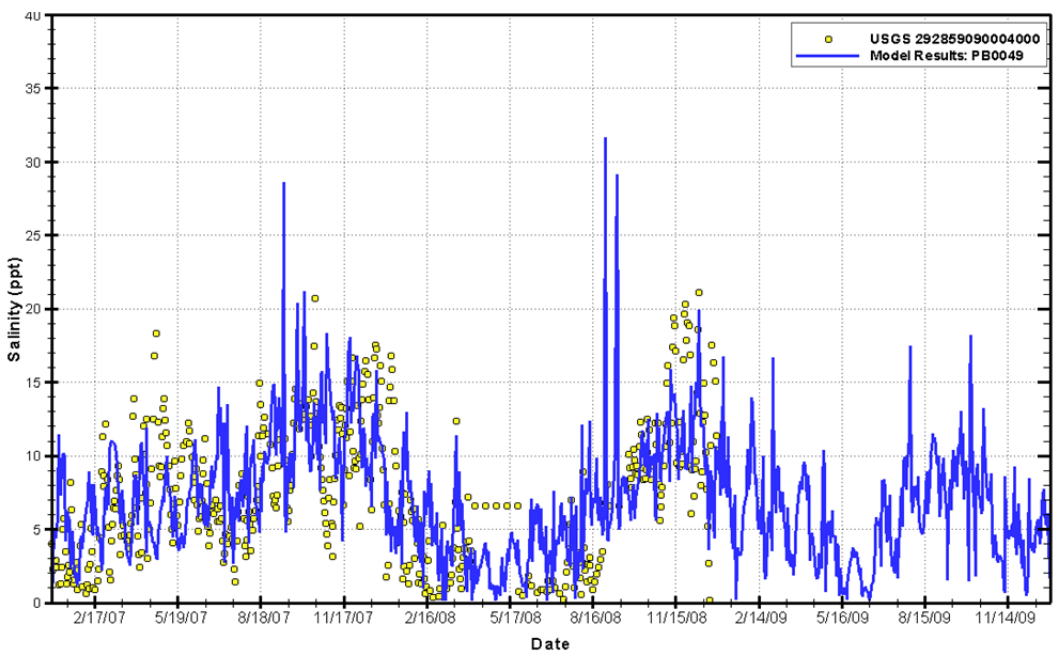

Figure 114 SAL Calibration (2008 – 2009) and Validation (2007) Results for Barataria Waterway South of Lafitte in the PB Model

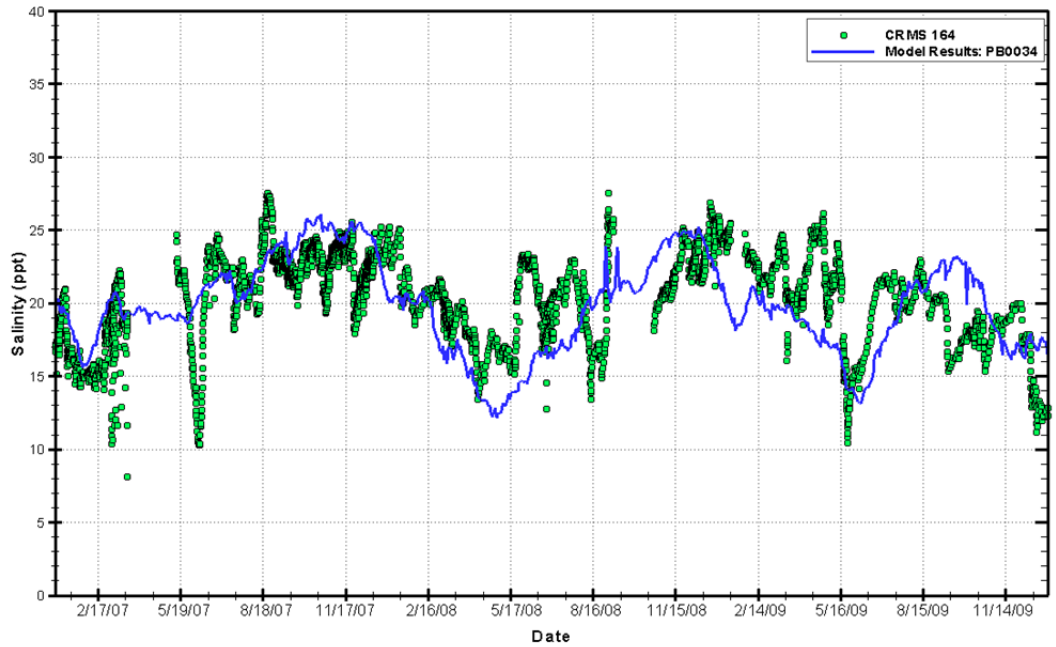

Figure 115 SAL Calibration (2008 – 2009) and Validation (2007) Results for Bayou Lafourche in the PB Model

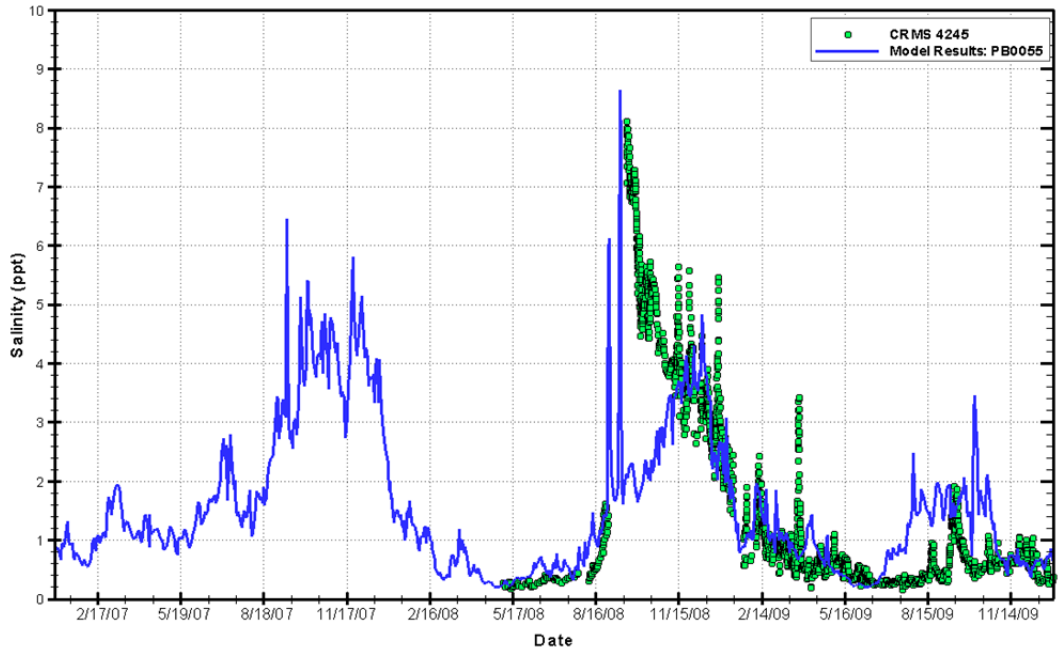

Figure 116 SAL Calibration (2008 – 2009) Results for Bayou Perot in the PB Model[68]

[68] There was no validation due to limited measured data.

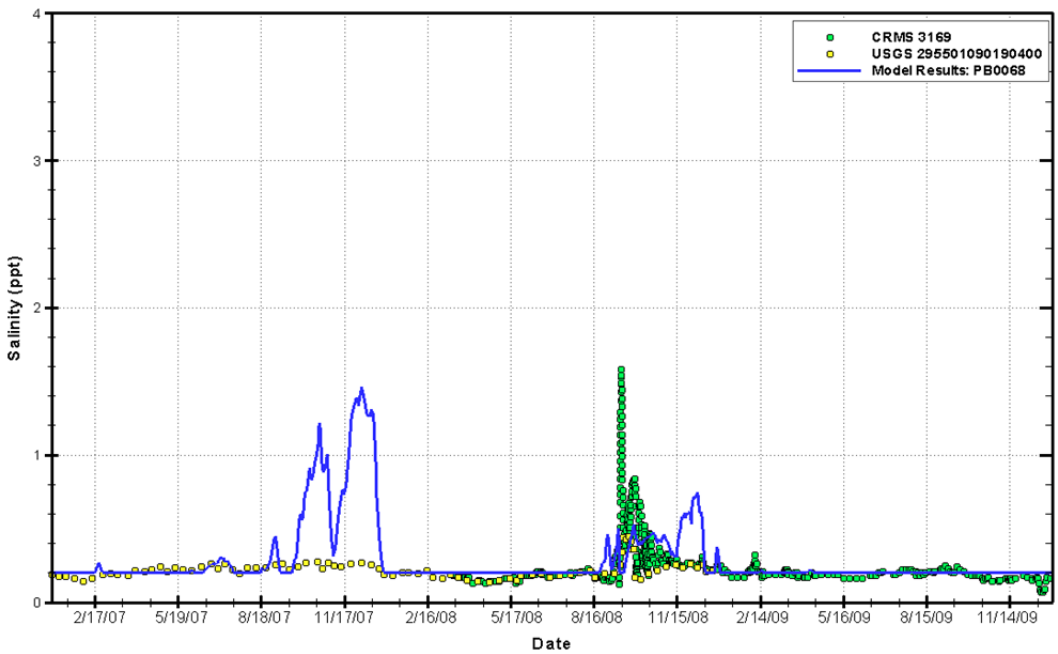

Figure 117 SAL Calibration (2008 – 2009) and Validation (2007) Results for Davis Pond in the PB Model

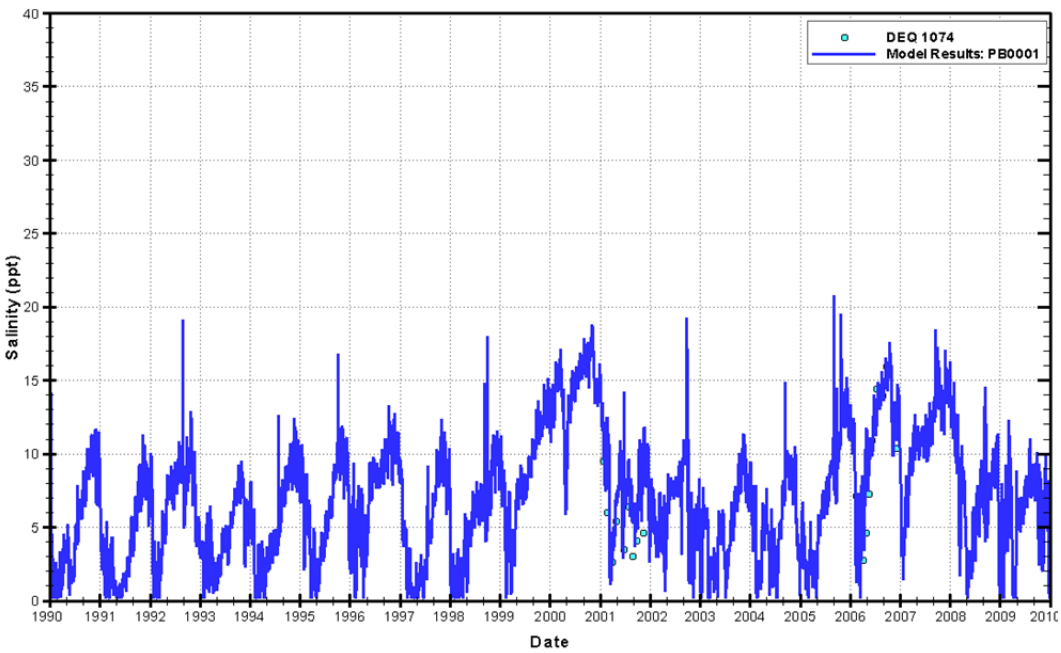

Figure 118 SAL Calibration (2001 – 2007) Results for East Lake Borgne in the PB Model[69]

[69] There was no validation due to limited measured data.

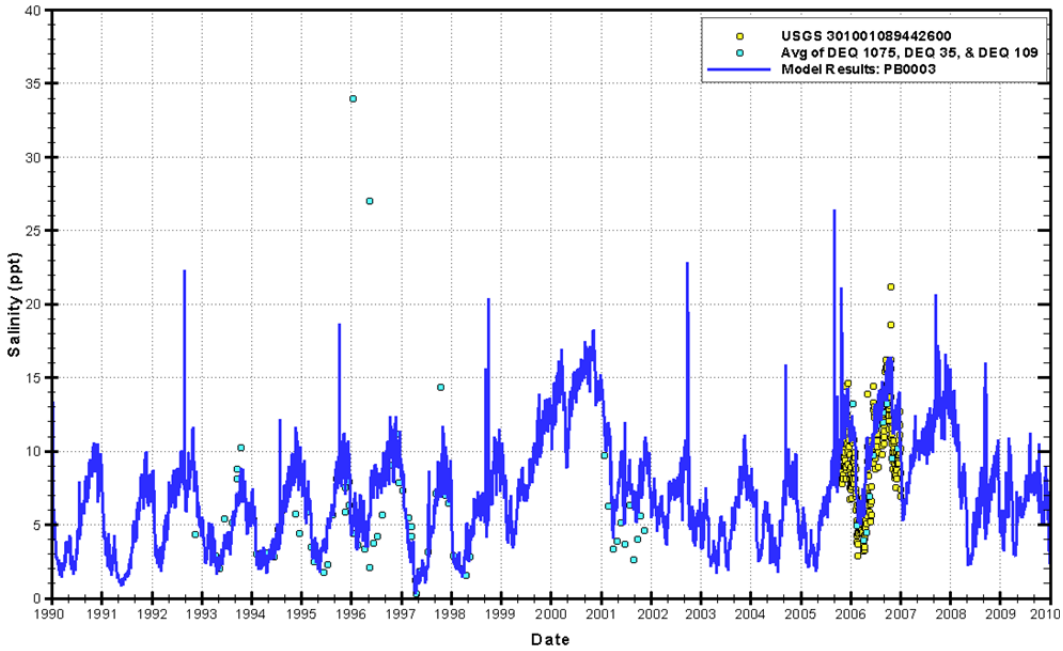

Figure 119 SAL Calibration (1990 – 1999) and Validation (2000 – 2007) Results for East Lake Pontchartrain in the PB Model

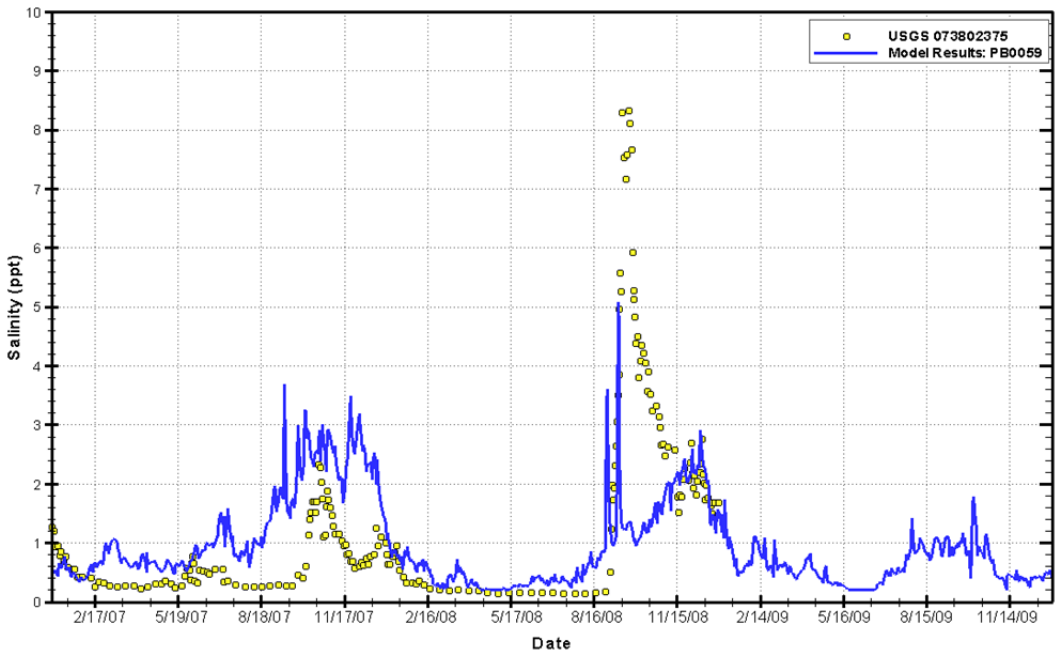

Figure 120 SAL Calibration (2008 – 2009) and Validation (2007) Results for East Lake Salvador in the PB Model

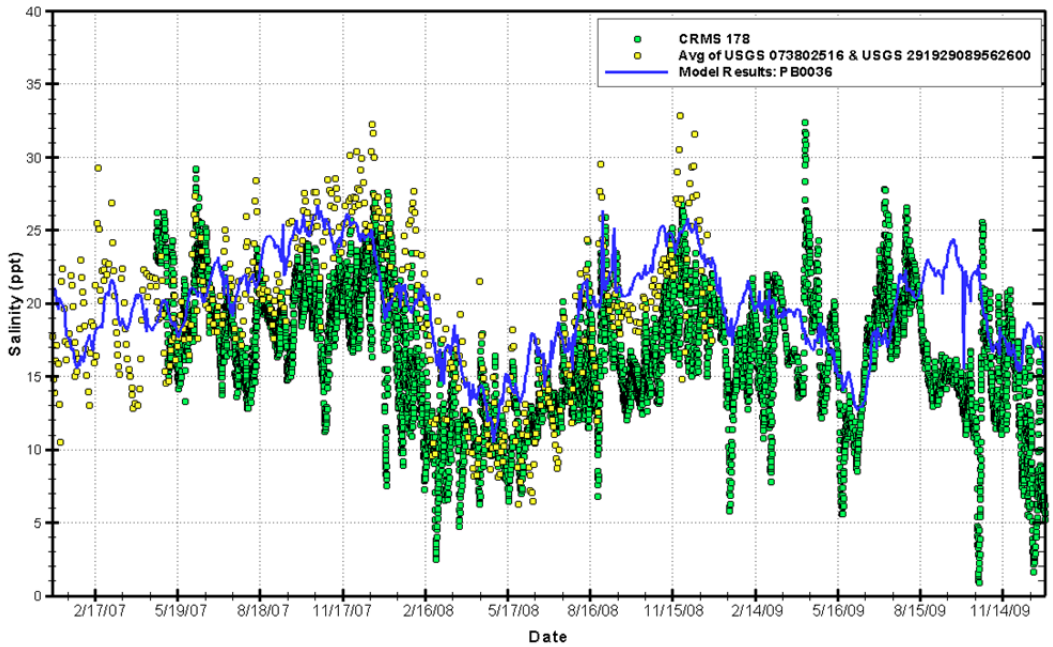

Figure 121 SAL Calibration (2008 – 2009) and Validation (2007) Results for Grand Isle/Grand Terre in the PB Model

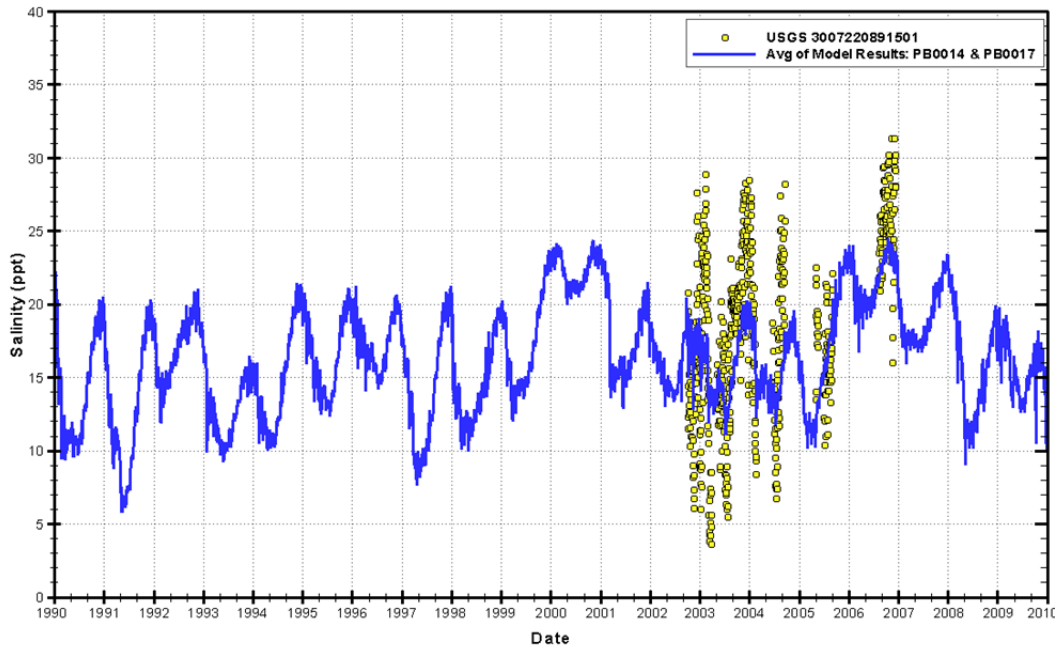

Figure 122 SAL Calibration (2002 – 2007) Results for Mississippi Sound at Grand Pass in the PB Model[70]

[70] There was no validation due to limited measured data.

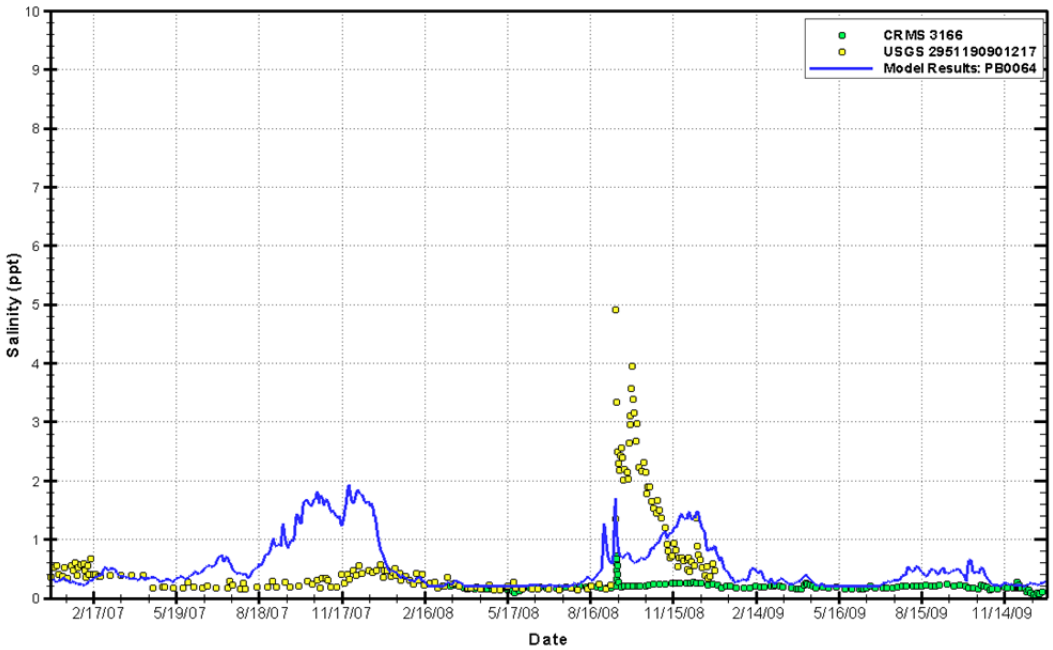

Figure 123 SAL Calibration (2008 – 2009) and Validation (2007) Results for Lake Cataouatche in the PB Model

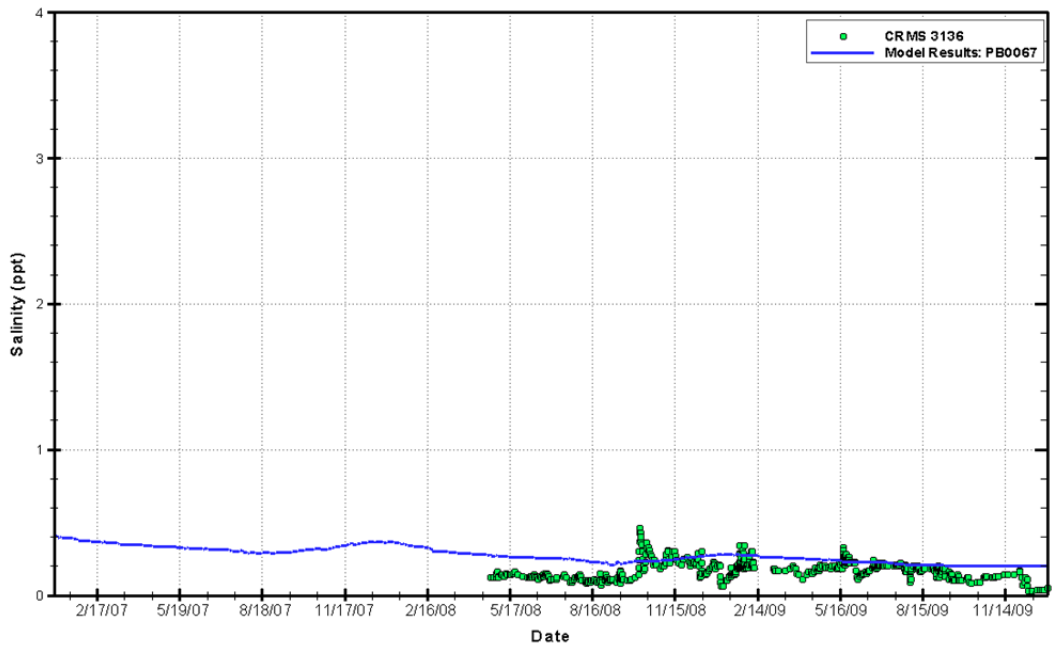

Figure 124 SAL Calibration (2008 – 2009) Results for Lake Des Allemands in the PB Model[71]

[71] There was no validation due to limited measured data.

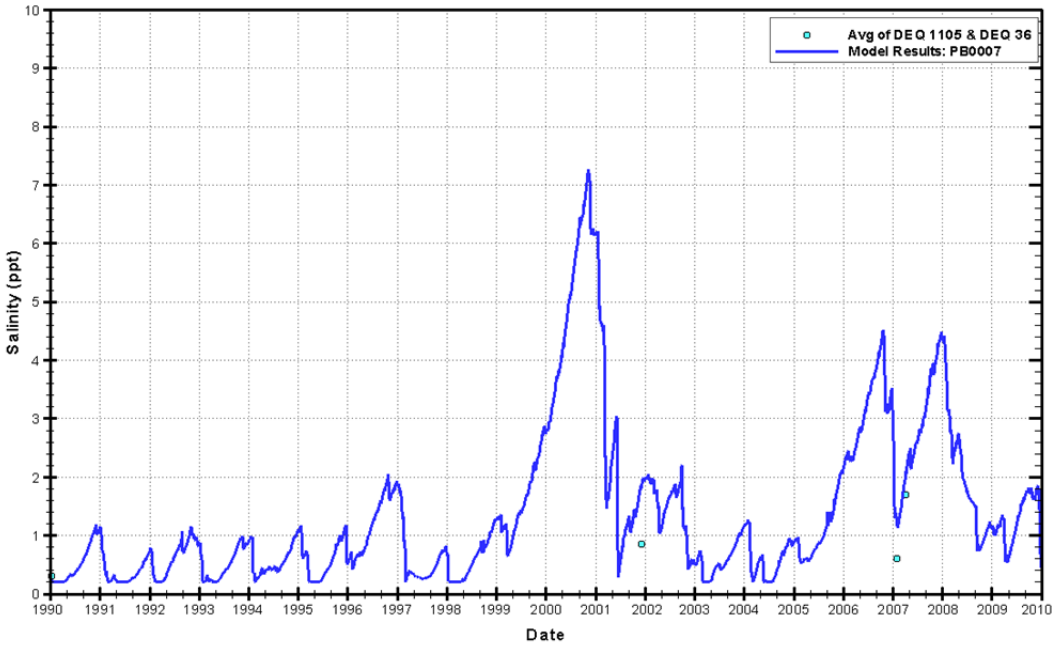

Figure 125 SAL Calibration (2001 – 2008) Results for Lake Maurepas in the PB Model[72]

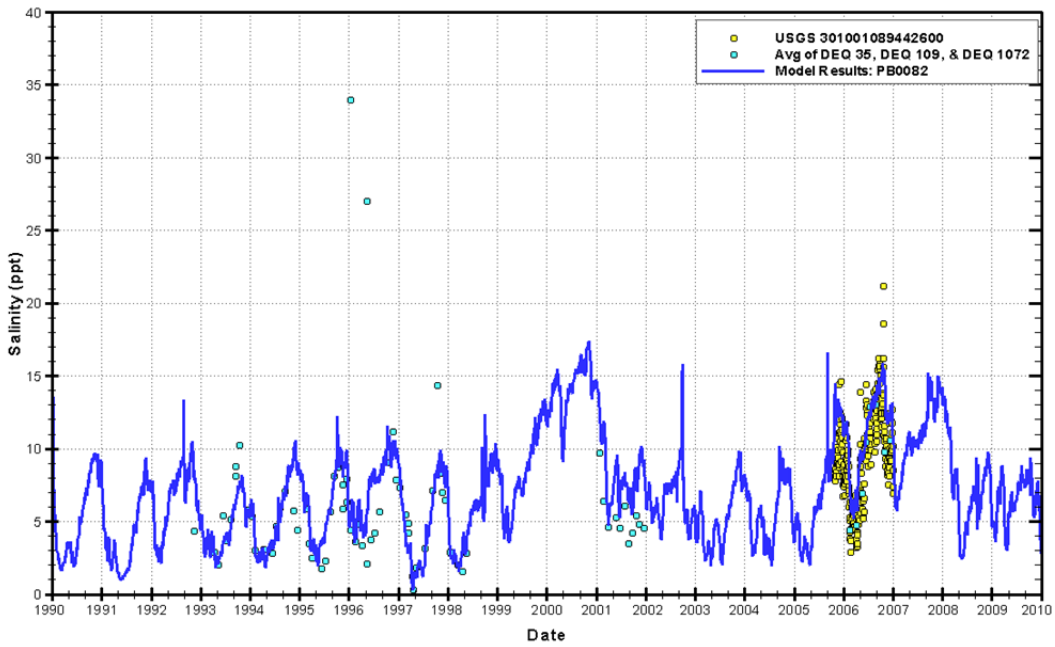

Figure 126 SAL Calibration (1990 – 1999) and Validation (2000 – 2007) Results for Lake St. Catherine in the PB Model

[72] There was no validation due to limited measured data.

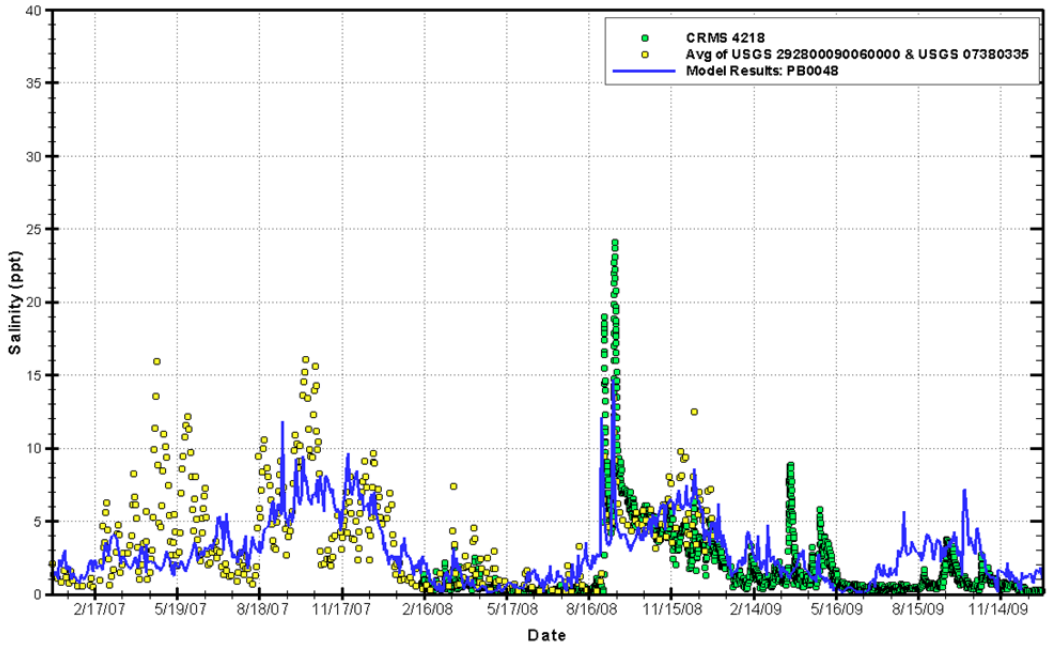

Figure 127 SAL Calibration (2008 – 2009) and Validation (2007) Results for Little Lake in the PB Model

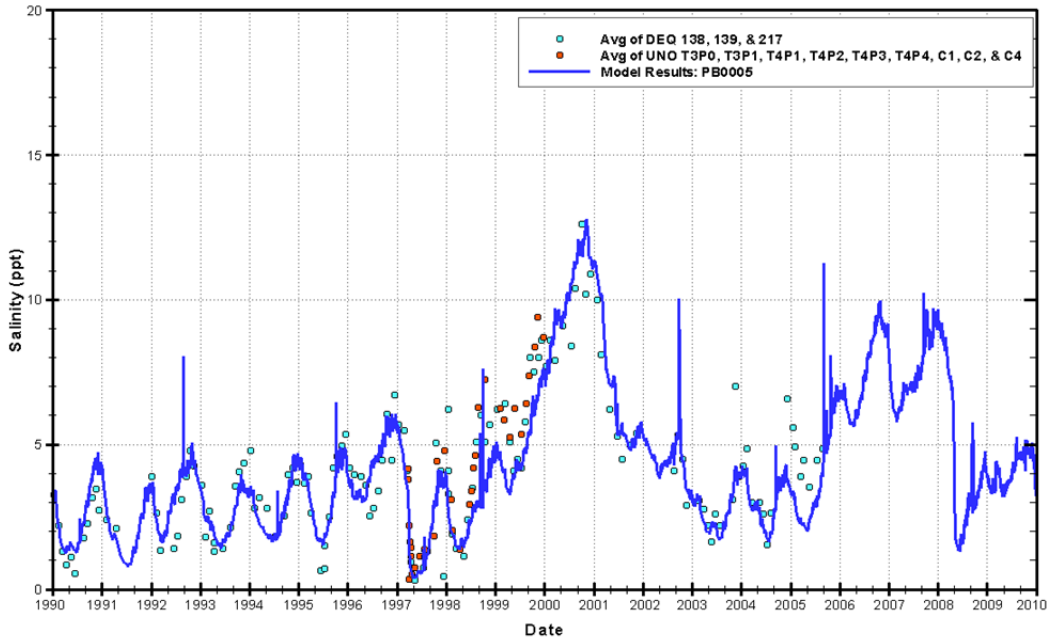

Figure 128 SAL Calibration (1990 – 1994) and Validation (1995 – 2007) Results for Northeast Lake Pontchartrain in the PB Model

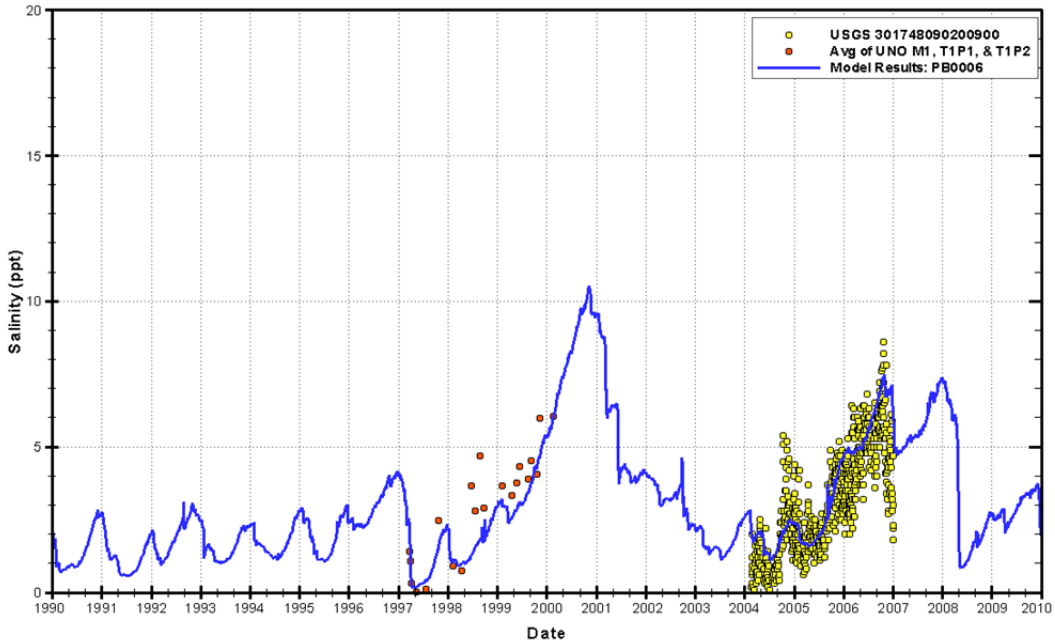

Figure 129 SAL Calibration (1997 – 2001) and Validation (2004 – 2007) Results for Northwest Lake Pontchartrain in the PB Model

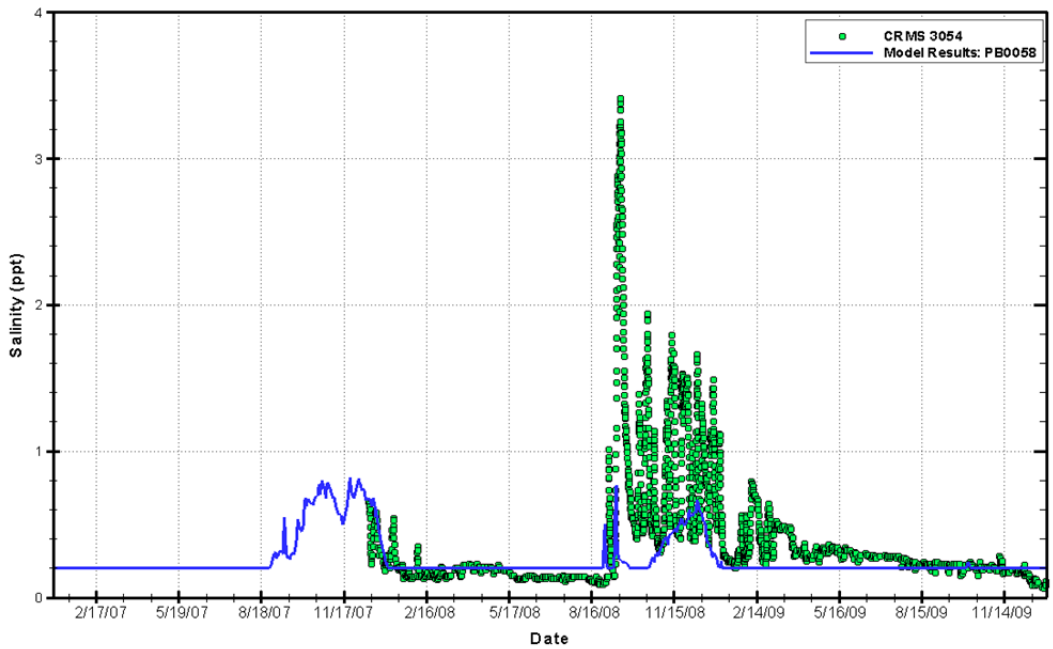

Figure 130 SAL Calibration (2008 – 2009) and Validation (2007) Results for West Lake Salvador in the PB Model

Temperature (TMP)

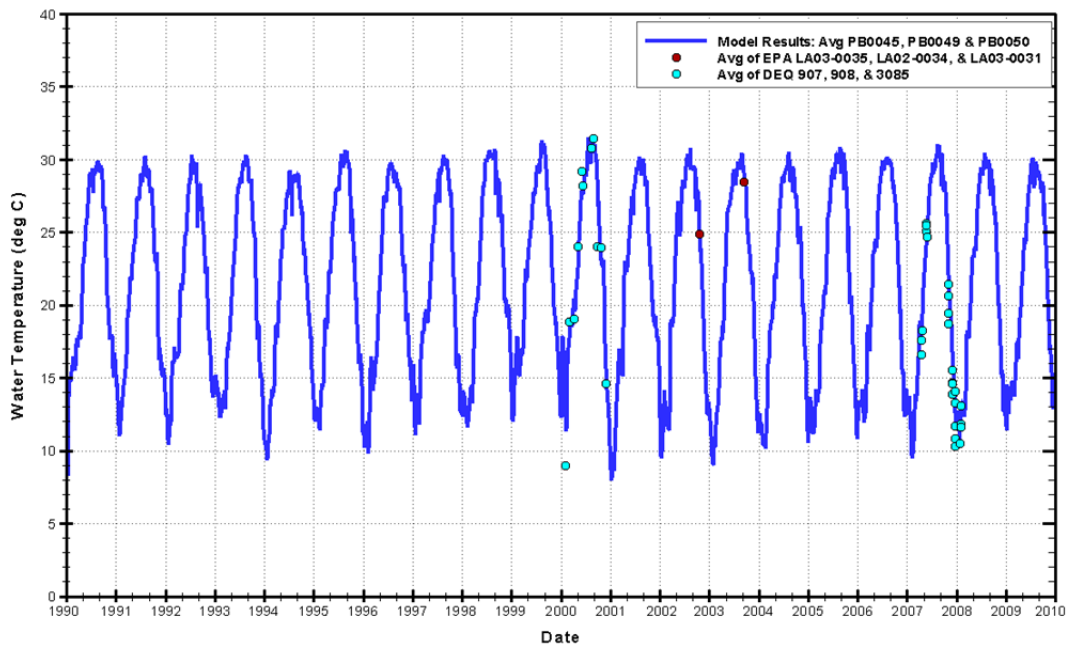

Figure 131 TMP Calibration (2007 – 2008) and Validation (1990 – 2006) Results for Barataria Waterway South of Lafitte in the PB Model

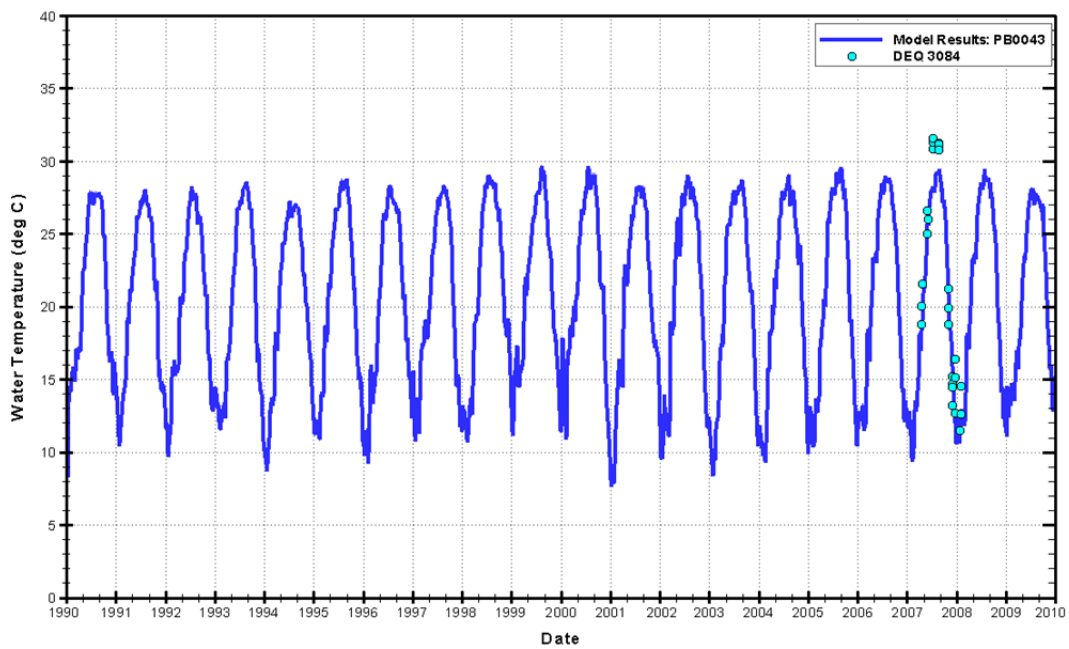

Figure 132 TMP Calibration (2007 – 2008) and Validation (1990 – 2006) Results for Bay Rambo in the PB Model

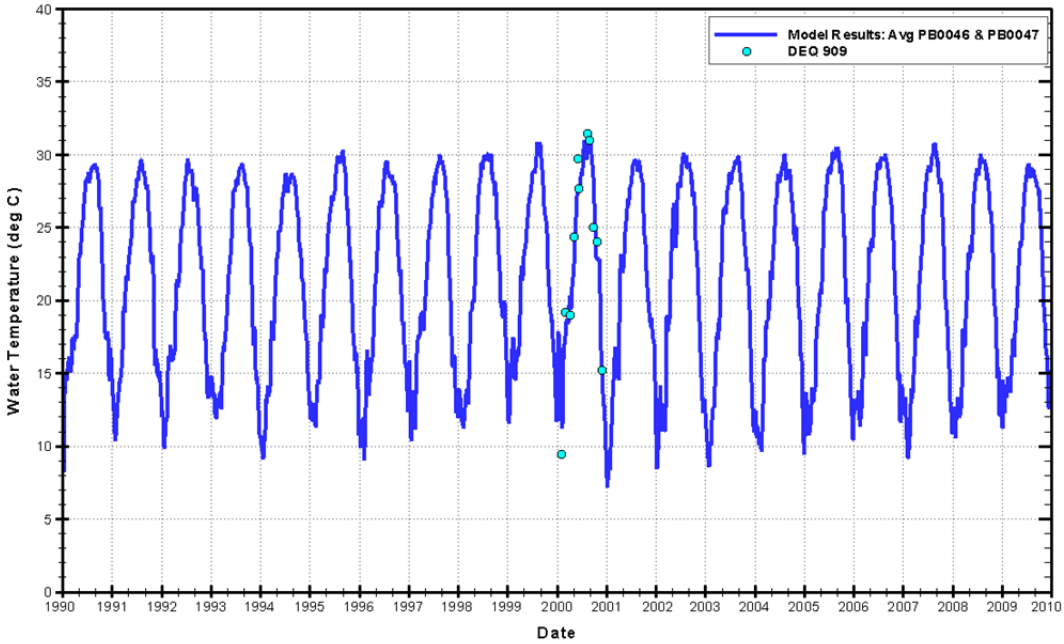

Figure 133 TMP Validation (1990 – 2006) Results for Bayou Dulac in the PB Model

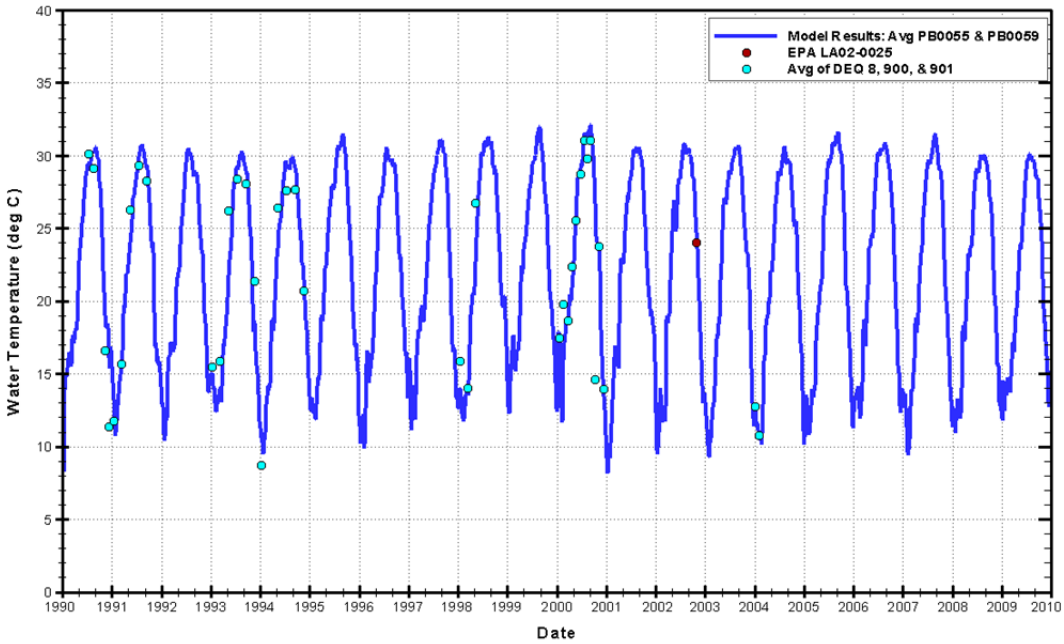

Figure 134 TMP Validation (1990 – 2006) Results for Bayou Perot in the PB Model

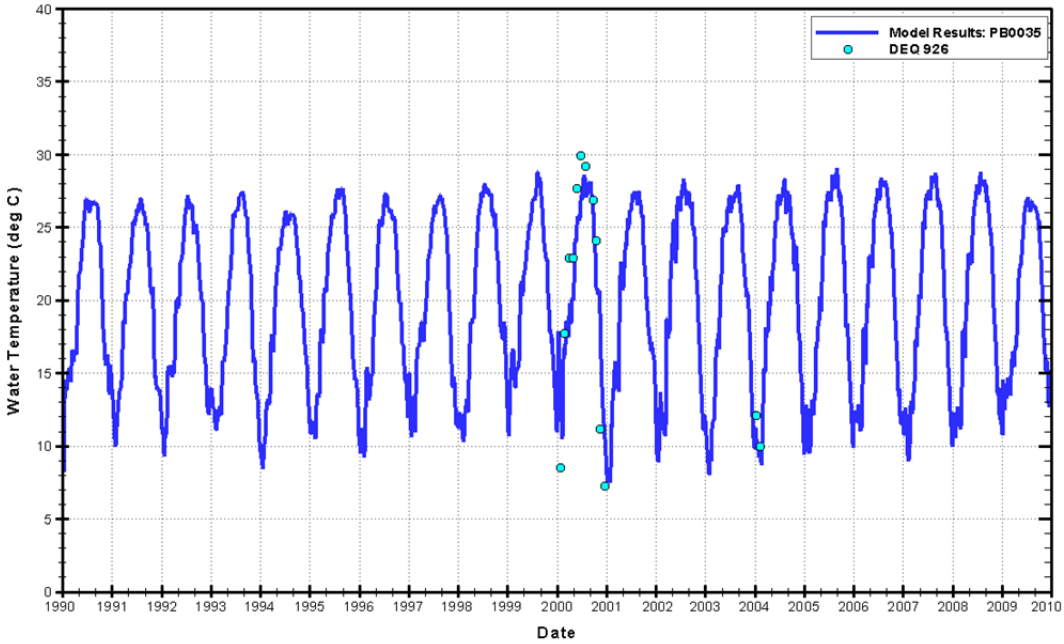

Figure 135 TMP Validation (1990 – 2006) Results for Grand Isle in the PB Model

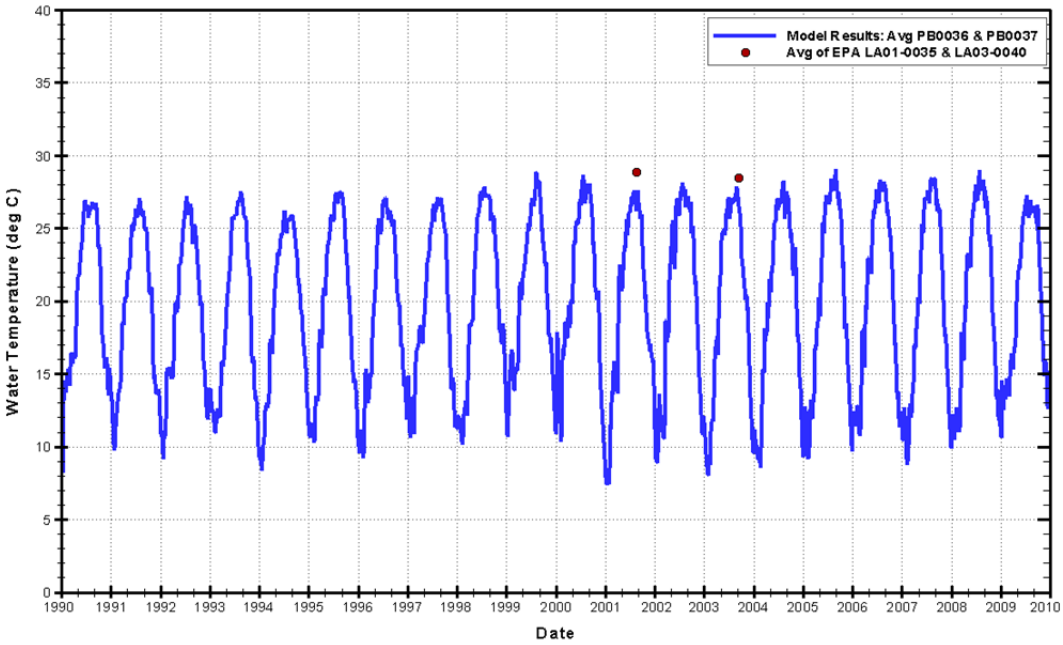

Figure 136 TMP Validation (1990 – 2006) Results for Grand Terre in the PB Model

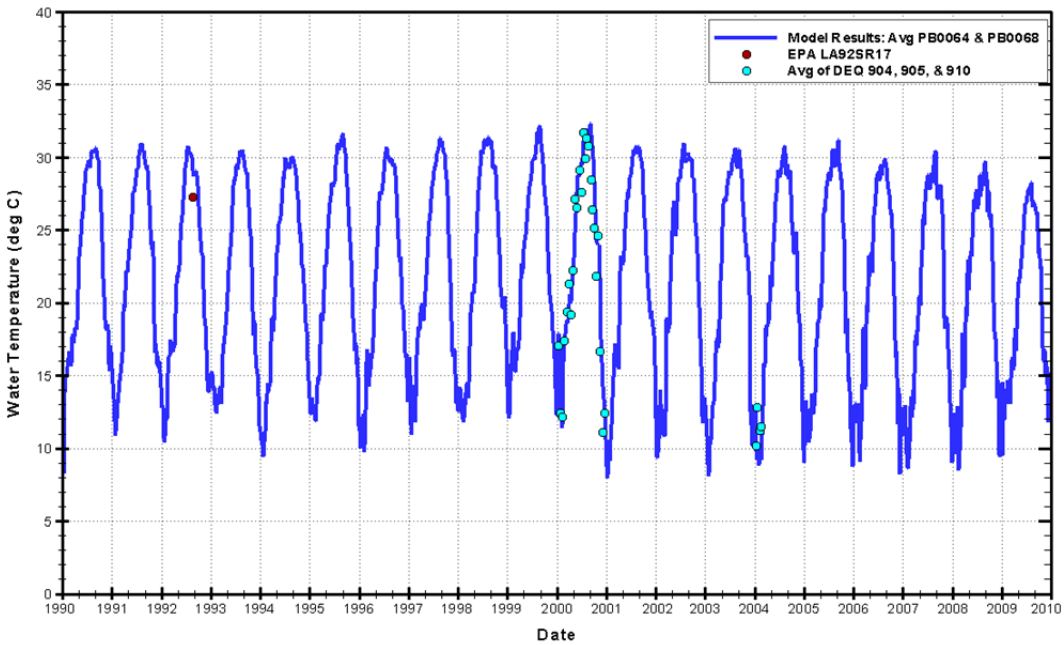

Figure 137 TMP Validation (1990 – 2006) Results for Lake Cataouatche in the PB Model

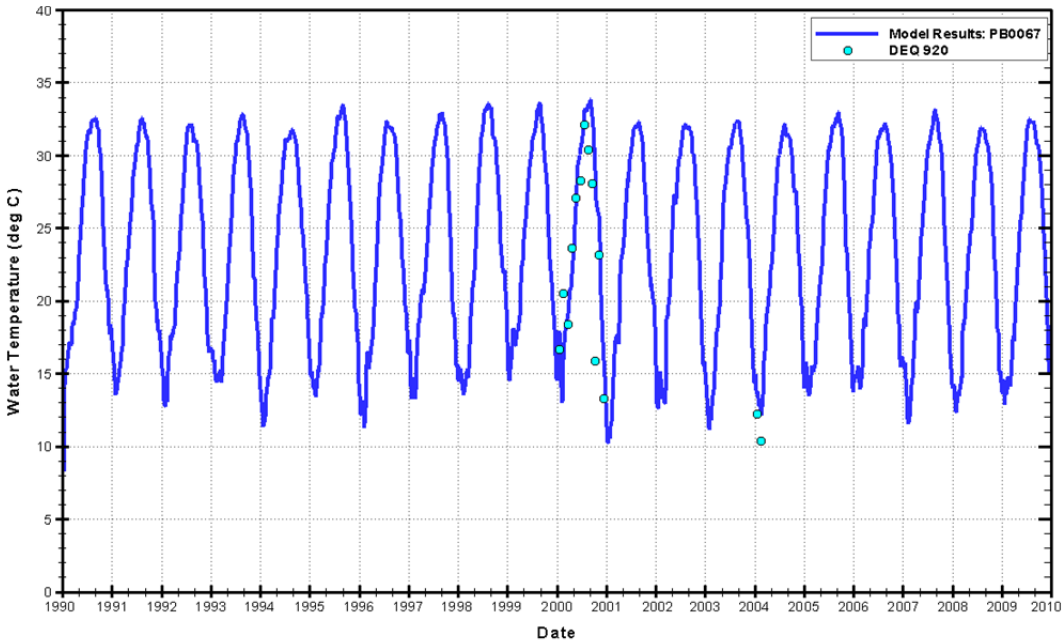

Figure 138 TMP Validation (1990 – 2006) Results for Lake Des Allemands in the PB Model

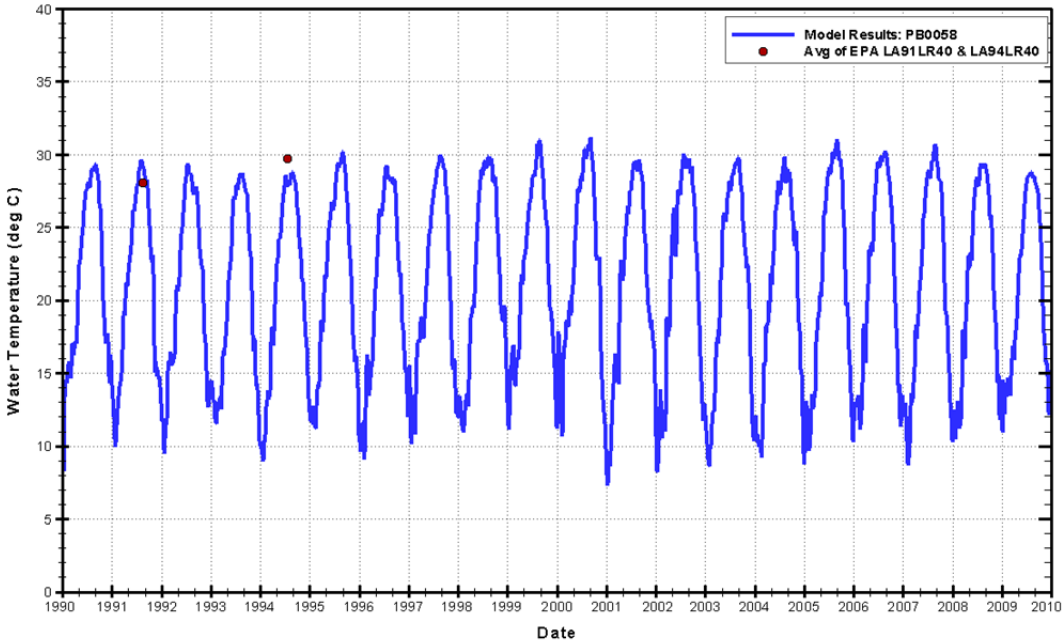

Figure 139 TMP Validation (1990 – 2006) Results for Lake Salvador in the PB Model

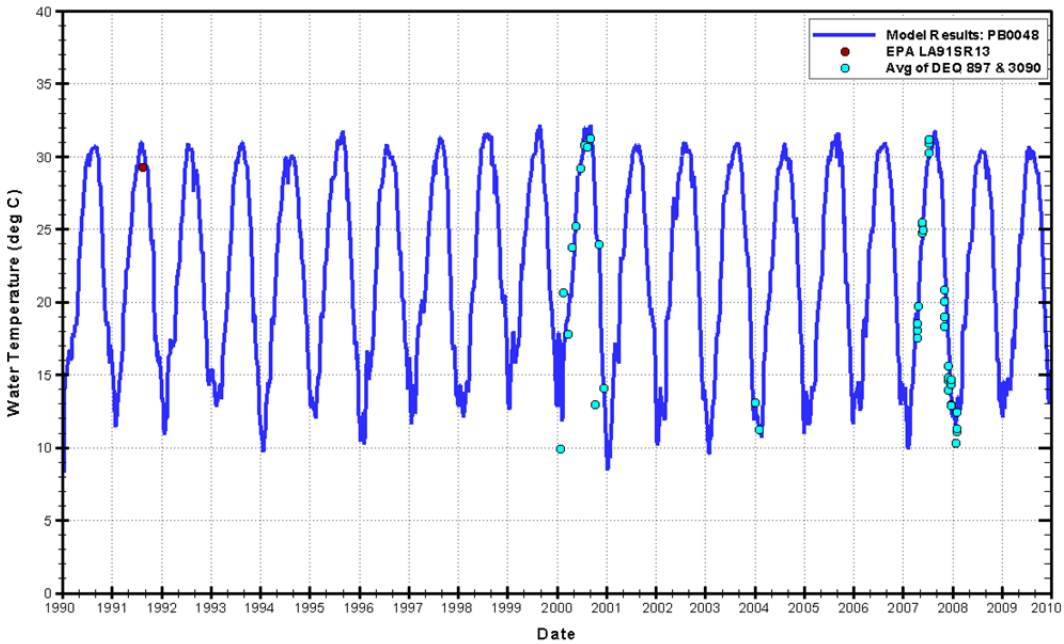

Figure 140 TMP Calibration (2007 – 2008) and Validation (1990 – 2006) Results for Little Lake in the PB Model

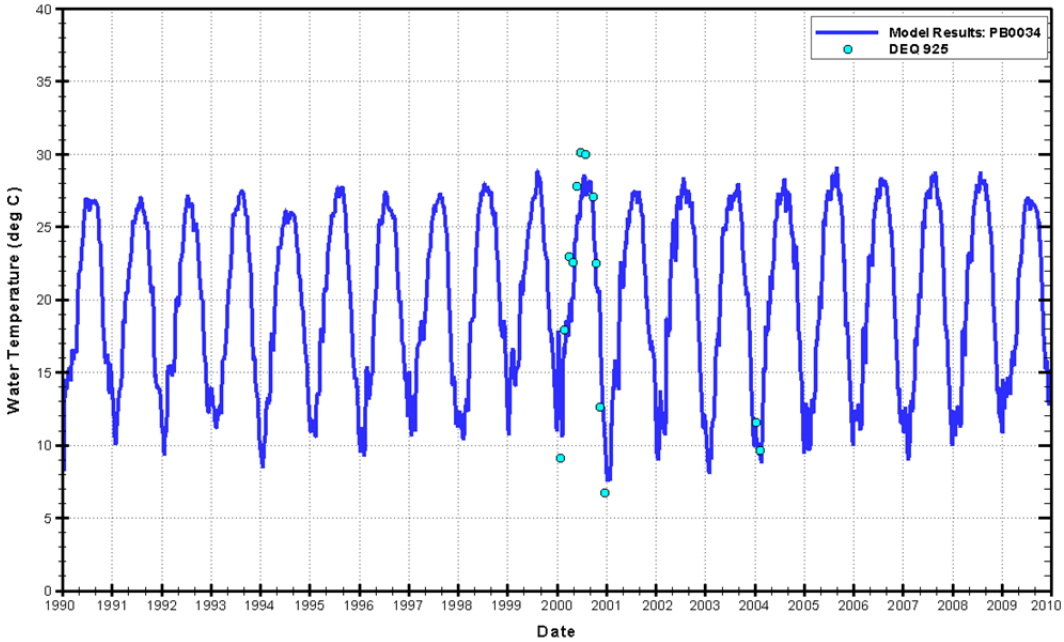

Figure 141 TMP Validation (1990 – 2006) Results for Northwest Grand Isle in the PB Model

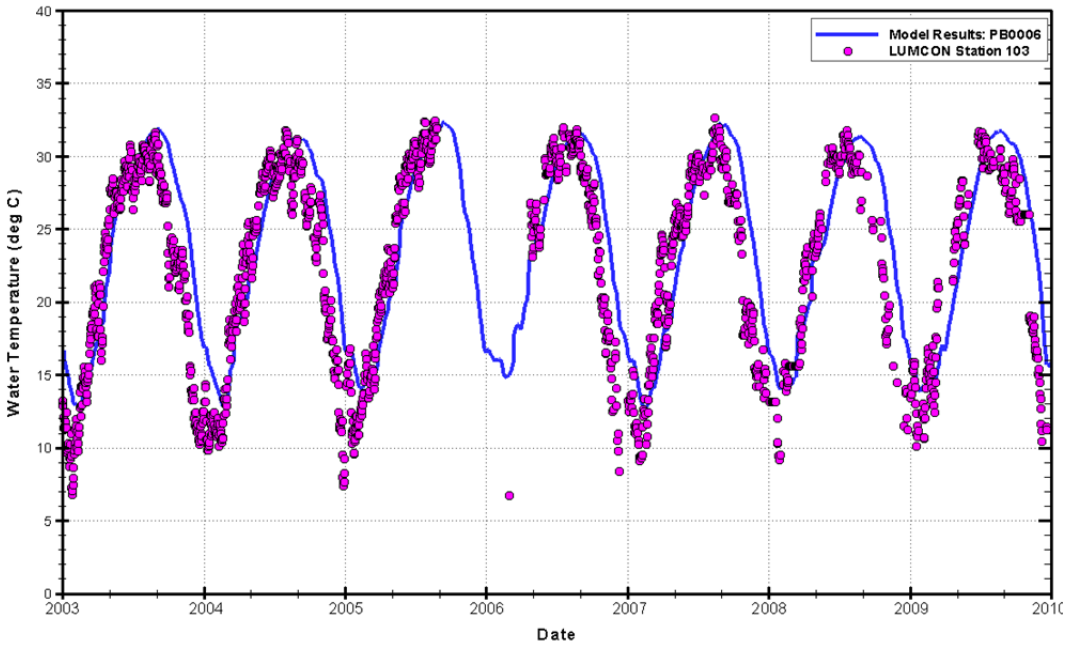

Figure 142 TMP Calibration (2007 – 2008) and Validation (1990 – 2006) Results for Northwest Lake Pontchartrain in the PB Model

Nitrate + Nitrite (NO3)

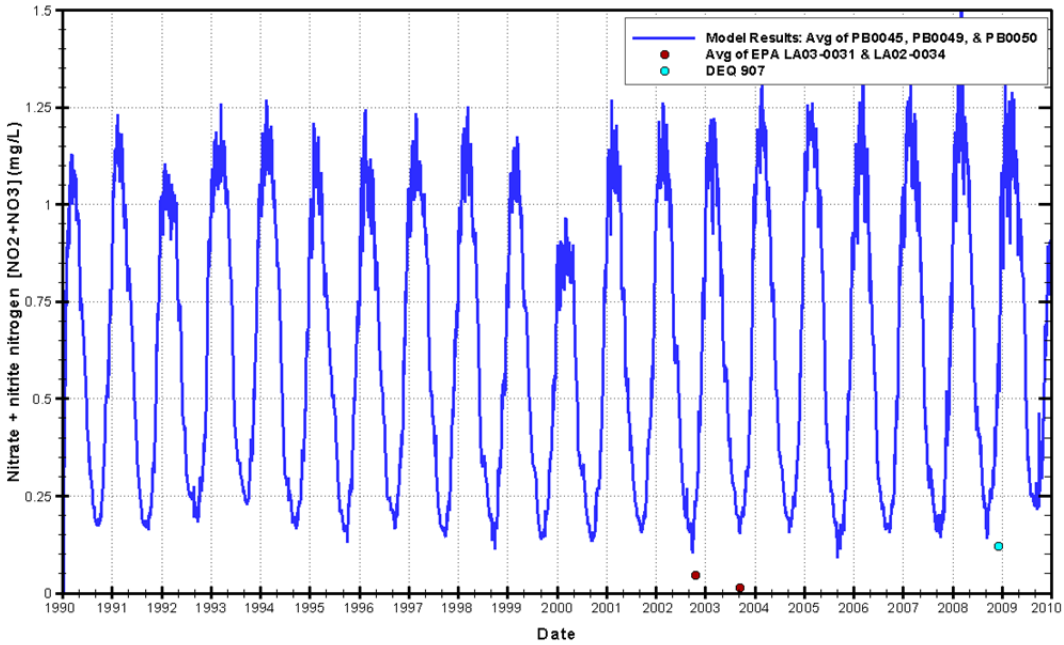

Figure 143 NO3 Calibration (2007 – 2008) and Validation (1990 – 2006) Results for Barataria Waterway South of Lafitte in the PB Model

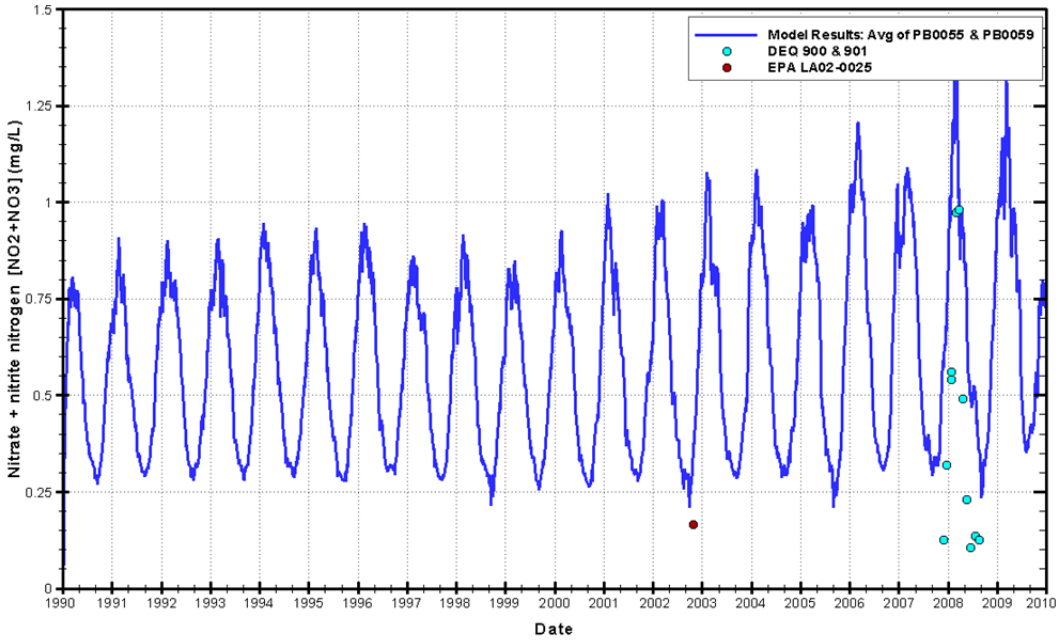

Figure 144 NO3 Calibration (2007 – 2008) and Validation (1990 – 2006) Results for Bayou Perot in the PB Model

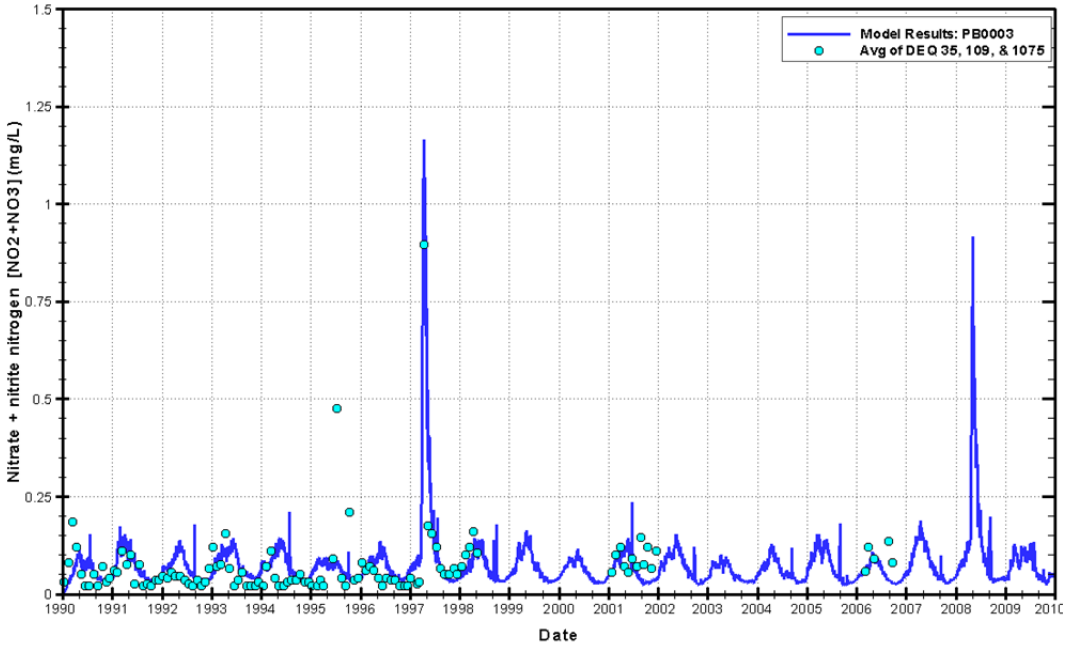

Figure 145 NO3 Calibration (1990 – 1994) and Validation (1995 – 2009) Results for East Lake Pontchartrain in the PB Model

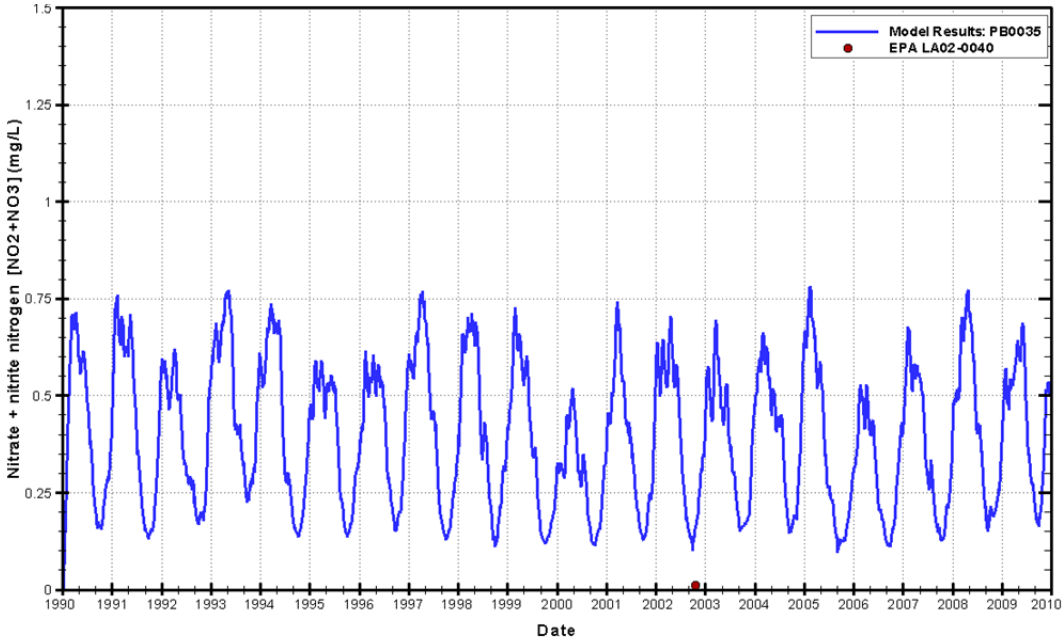

Figure 146 NO3 Validation (1990 – 2006) Results for Grand Isle in the PB Model

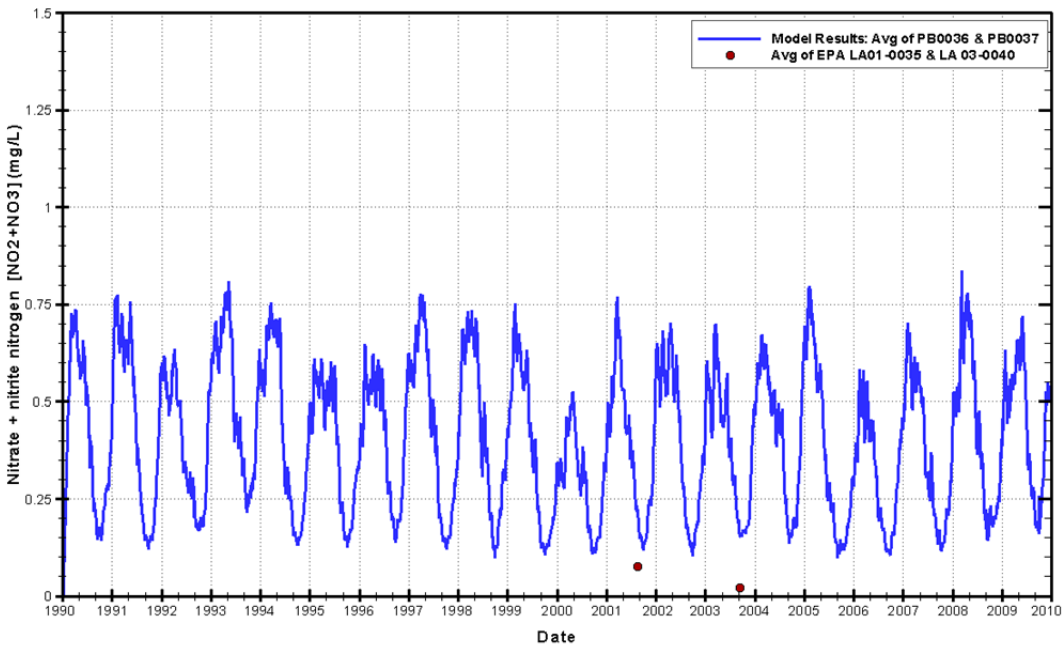

Figure 147 NO3 Validation (1990 – 2006) Results for Grand Terre in the PB Model

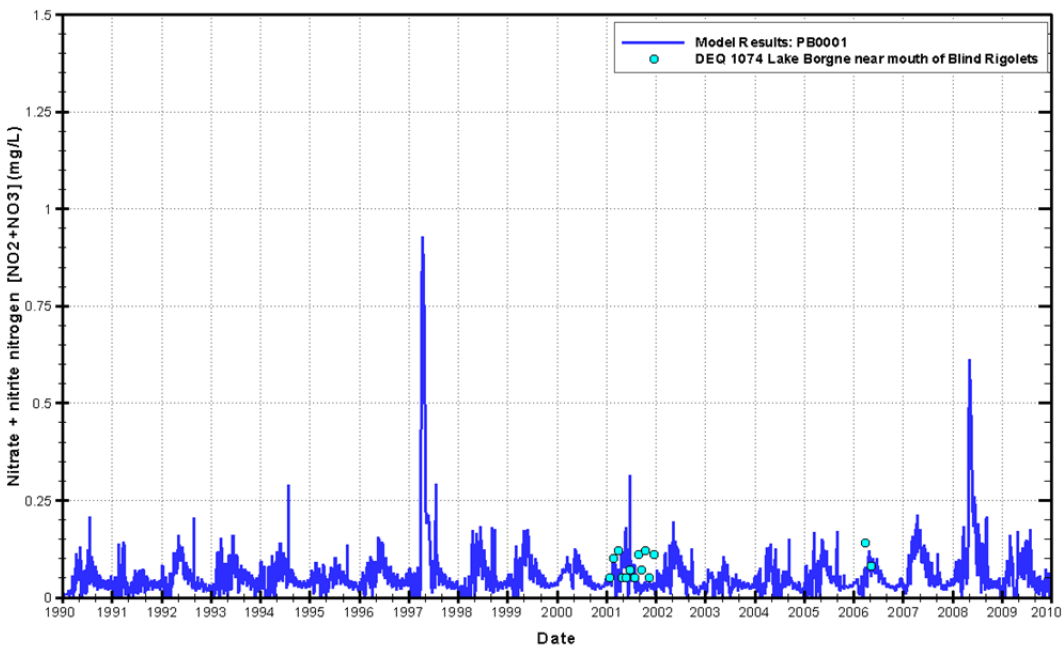

Figure 148 NO3 Validation (1990 – 2006) Results for Lake Borgne in the PB Model

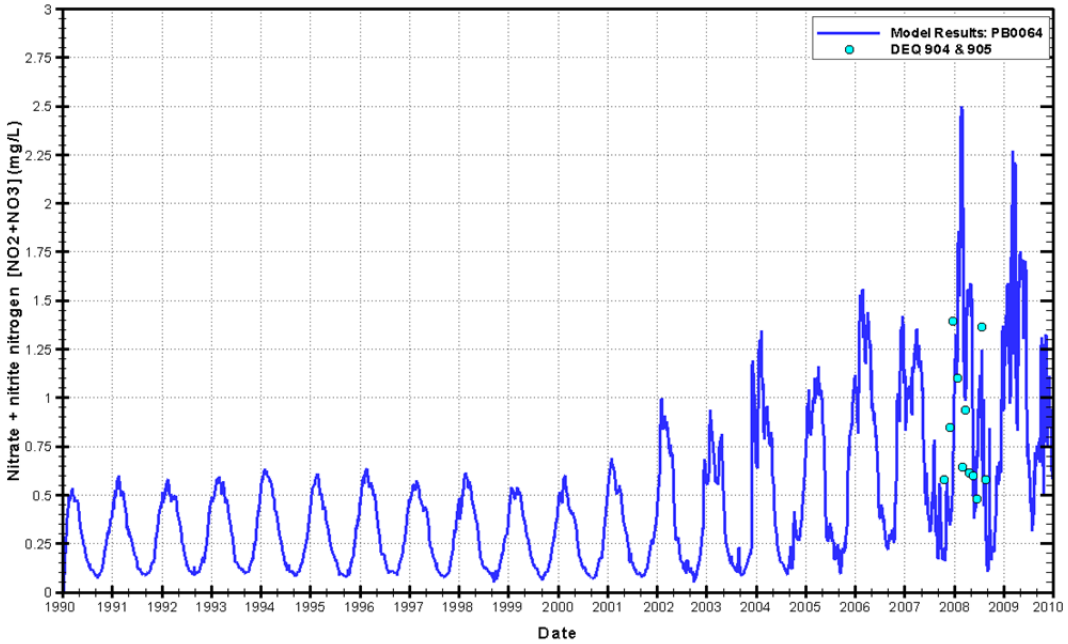

Figure 149 NO3 Calibration (2008) and Validation (2007) Results for Lake Cataouatche in the PB Model

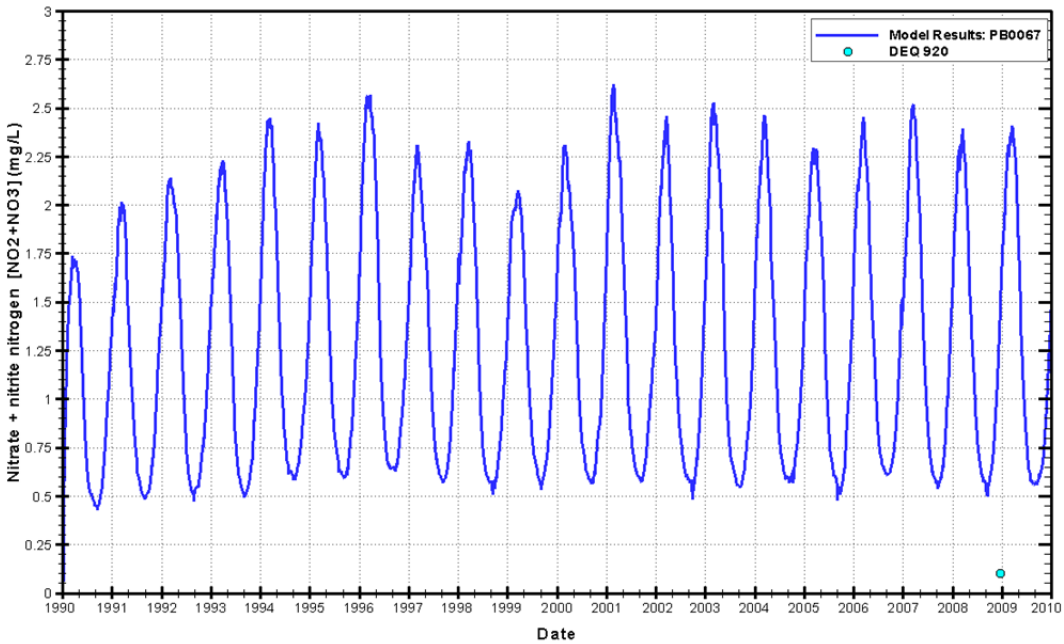

Figure 150 NO3 Validation (1990 – 2006) Results for Lake Des Allemands in the PB Model

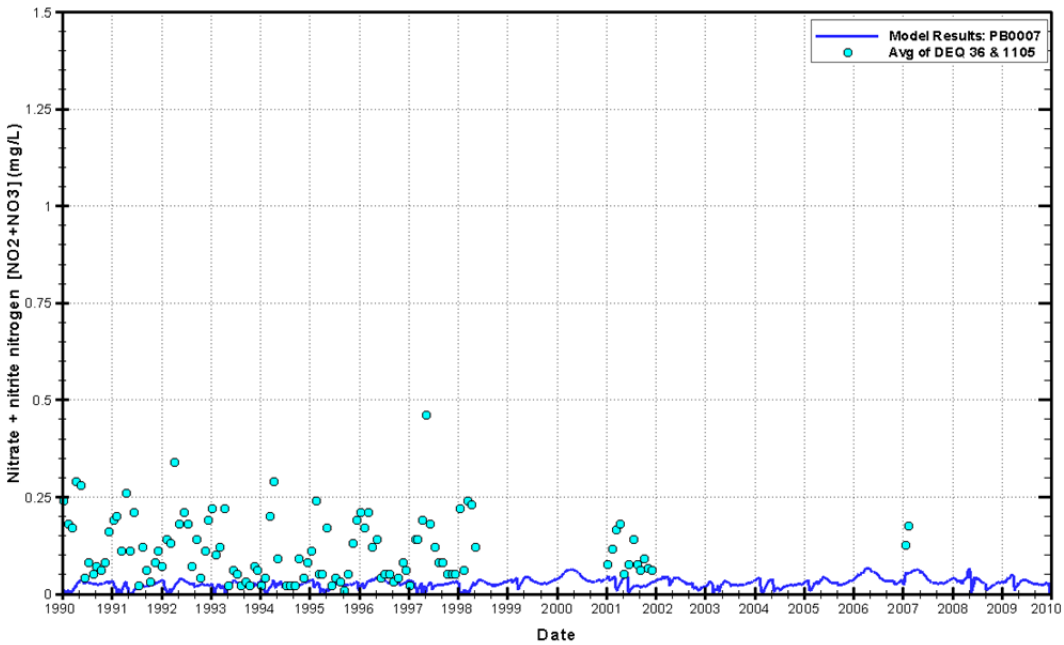

Figure 151 NO3 Calibration (1990 – 1994) and Validation (1995 – 2009) Results for Lake Maurepas in the PB Model

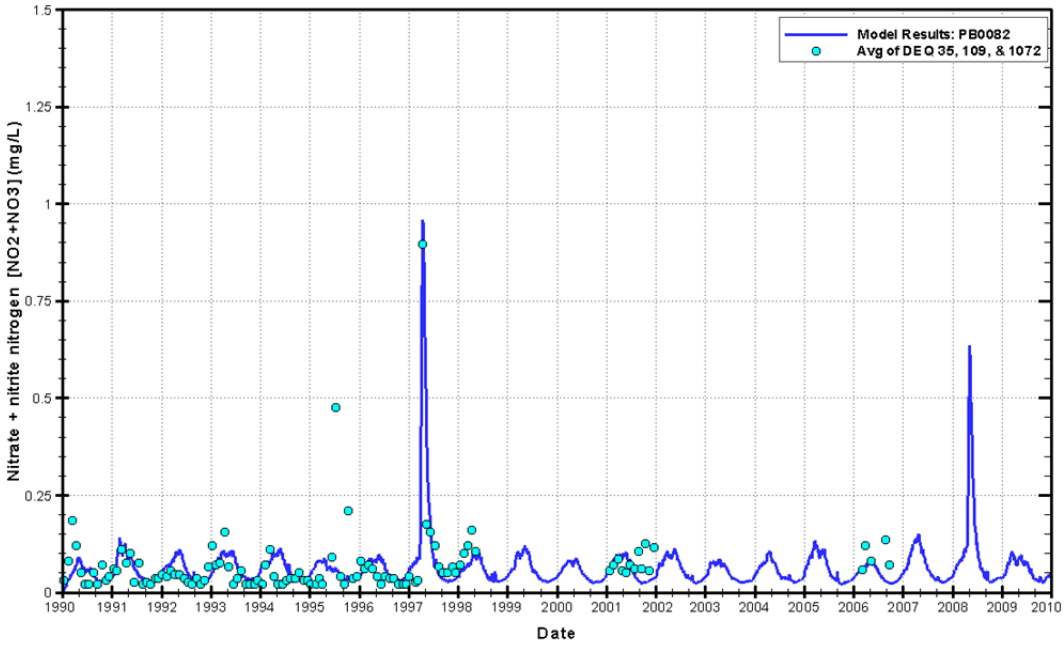

Figure 152 NO3 Calibration (1990 – 1994) and Validation (1995 – 2009) Results for Lake St. Catherine in the PB Model

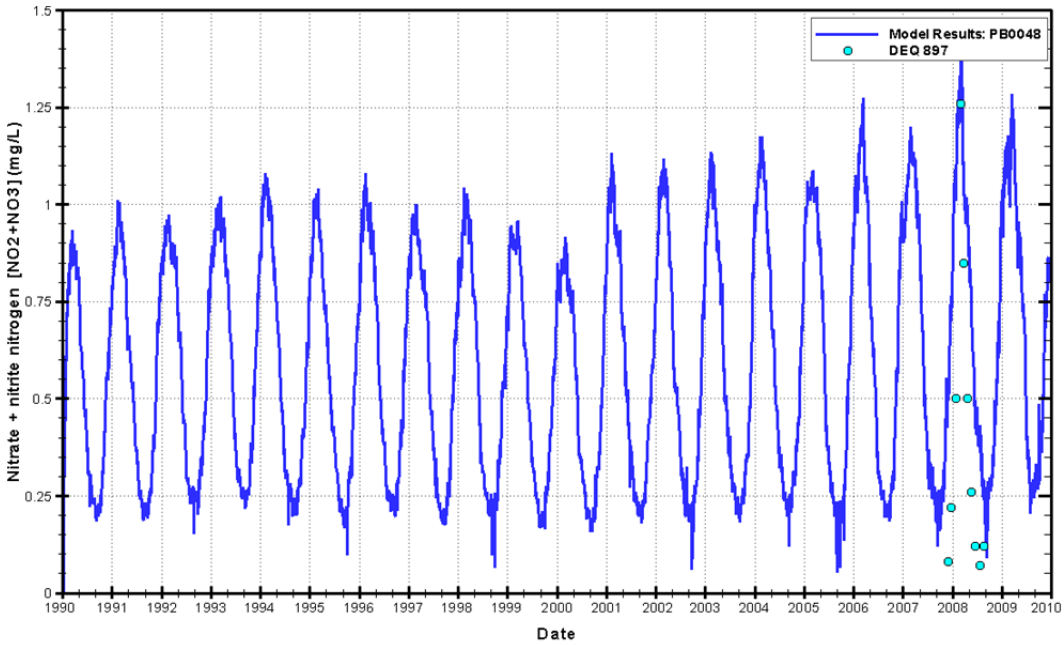

Figure 153 NO3 Calibration (2008) and Validation (2007) Results for Little Lake in the PB Model

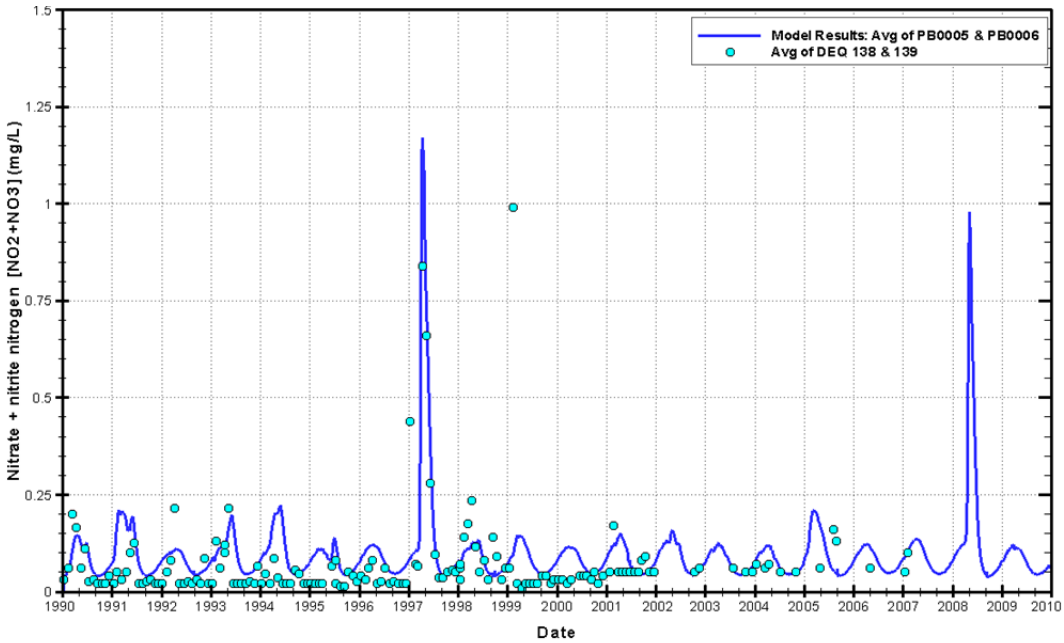

Figure 154 NO3 Calibration (1990 – 1994) and Validation (1995 – 2009) Results for North Lake Pontchartrain in the PB Model

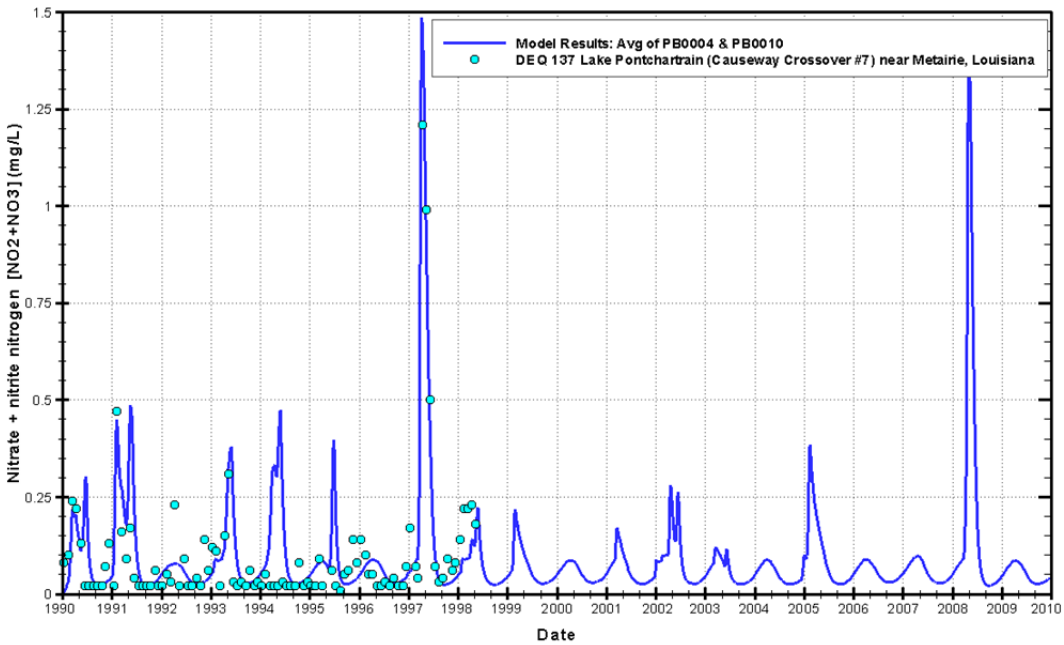

Figure 155 NO3 Calibration (1990 – 1994) and Validation (1995 – 2009) Results for South Lake Pontchartrain in the PB Model

Total Phosphorus (TPH)

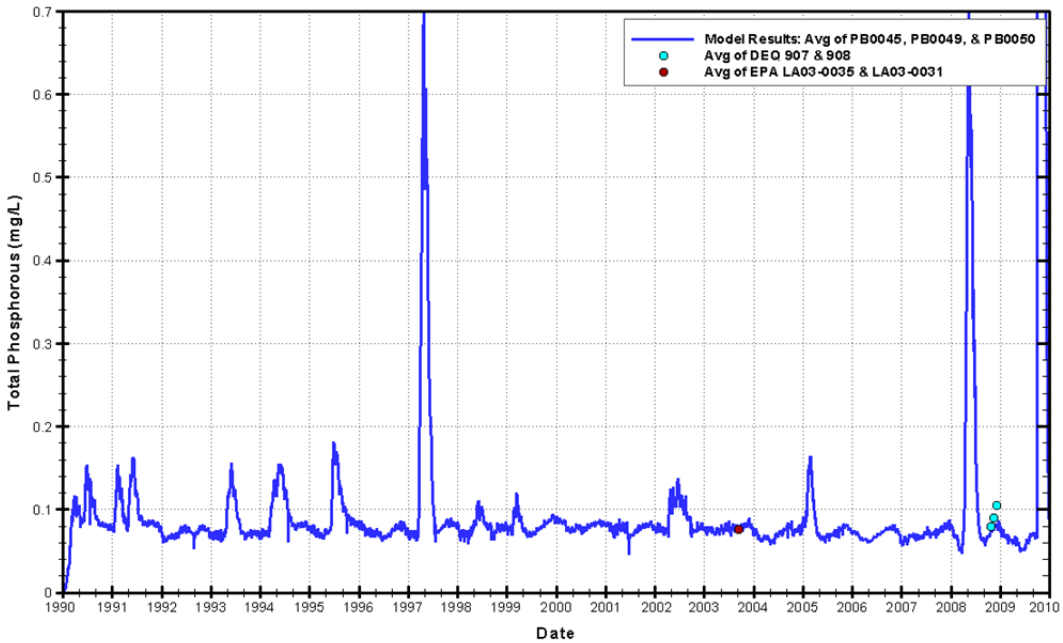

Figure 156 TPH Calibration (2007 – 2008) and Validation (1990 – 2006) Results for Barataria Waterway South of Lafitte in the PB Model

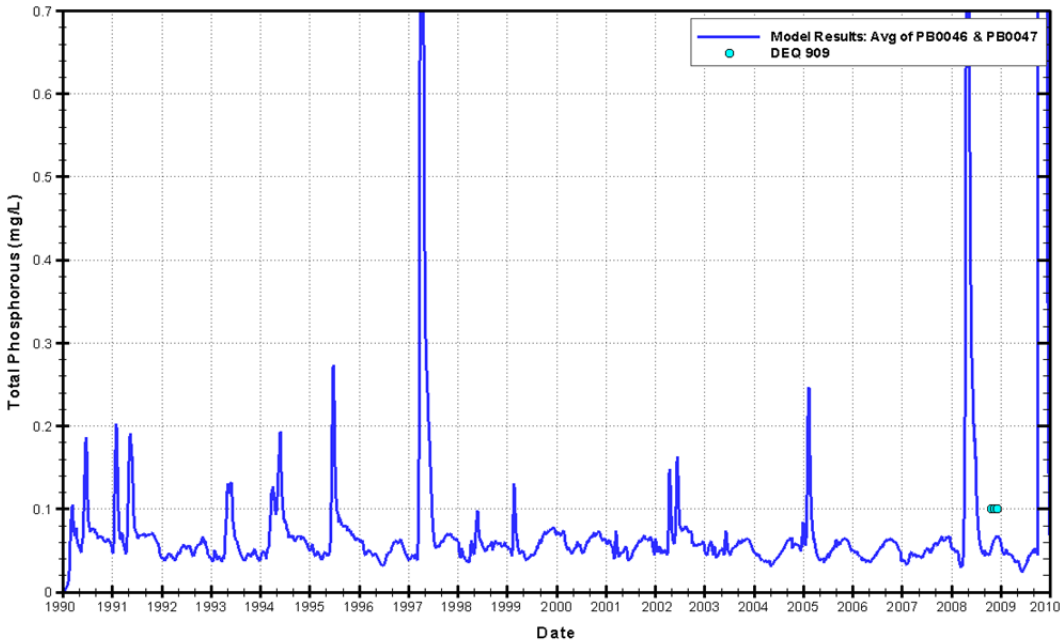

Figure 157 TPH Validation (2007 – 2008) Results for Bayou Dulac in the PB Model

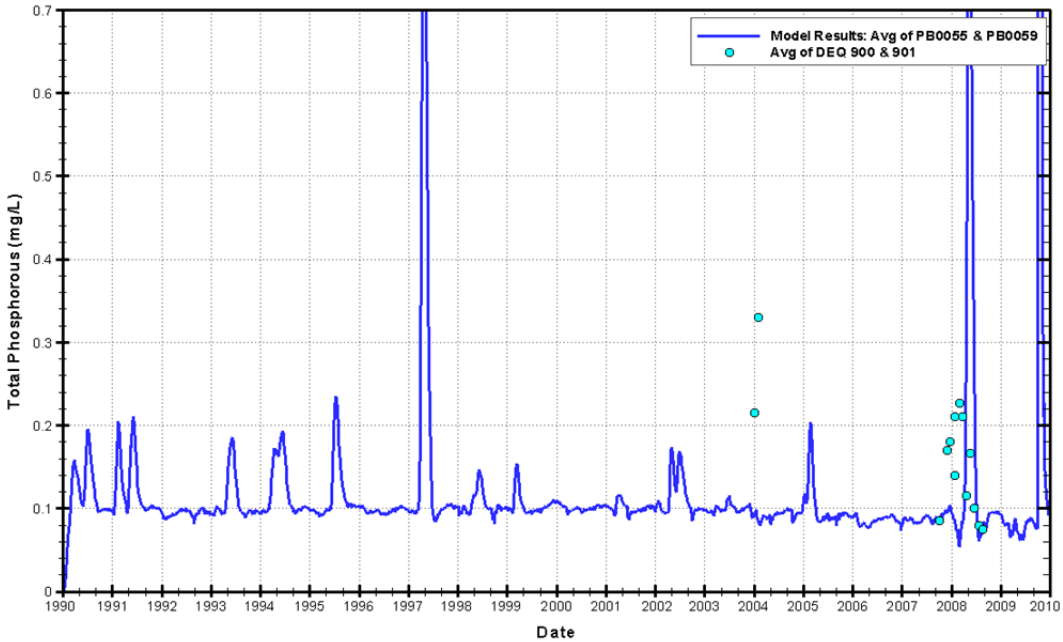

Figure 158 TPH Calibration (2007 – 2008) and Validation (1990 – 2006) Results for Bayou Perot in the PB Model

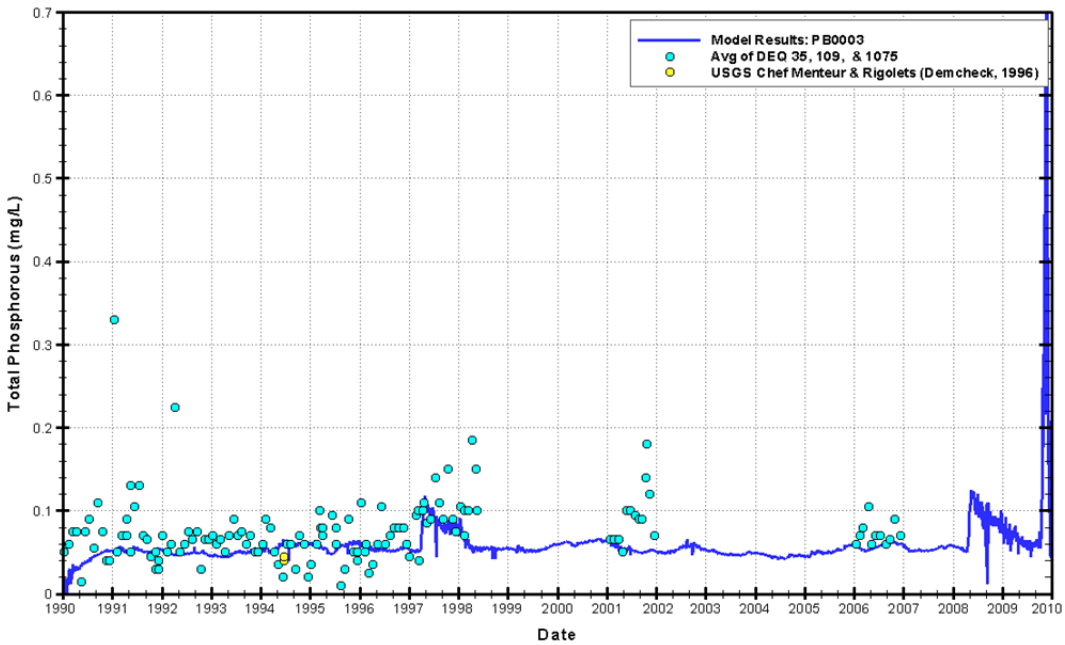

Figure 159 TPH Calibration (1990 – 1994) and Validation (1995 – 2009) Results for East Lake Pontchartrain in the PB Model

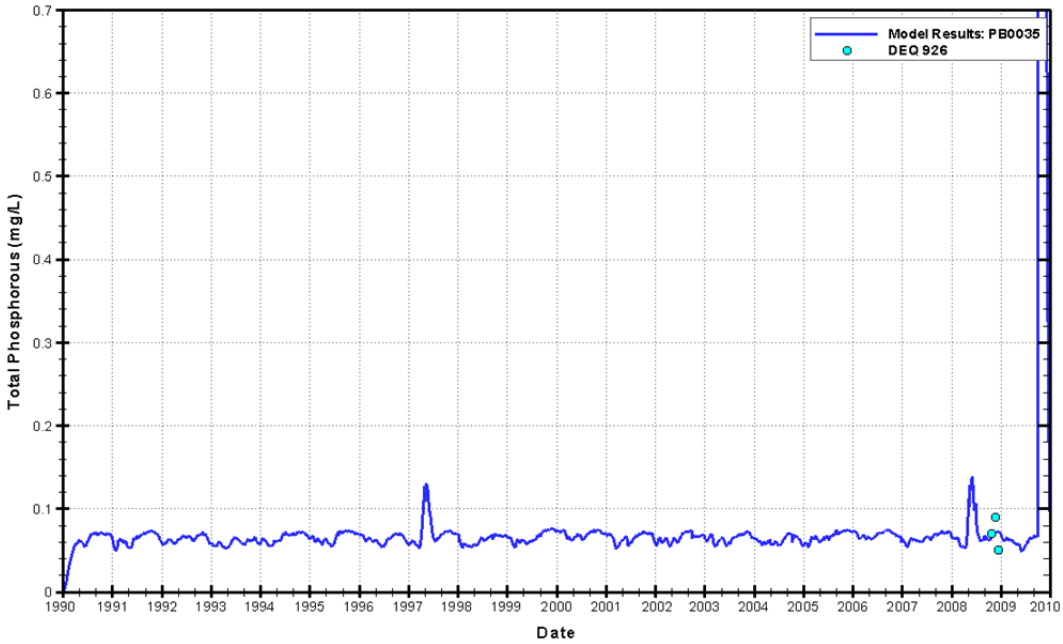

Figure 160 TPH Validation (2008 – 2009) Results for Grand Isle in the PB Model

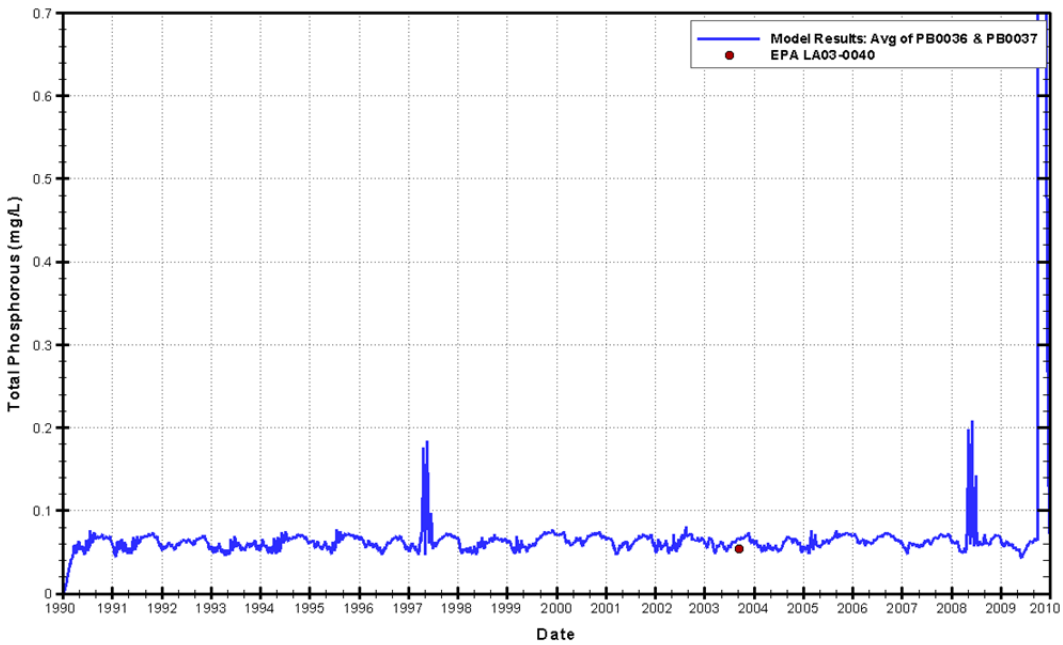

Figure 161 TPH Validation (1990 – 2006) Results for Grand Terre in the PB Model

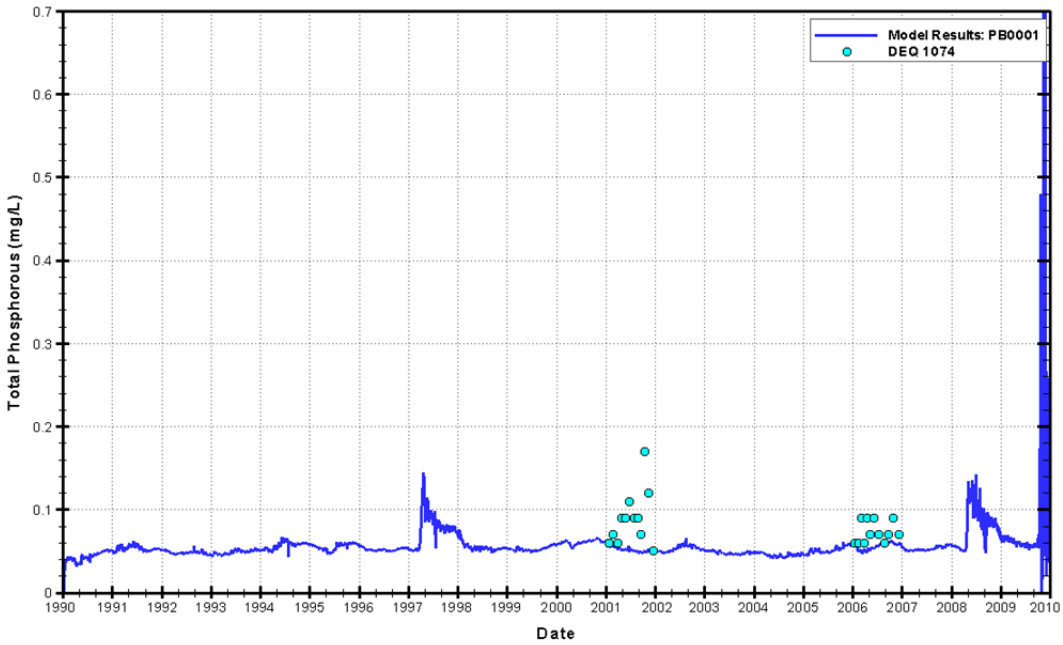

Figure 162 TPH Validation (1990 – 2006) Results for Lake Borgne in the PB Model

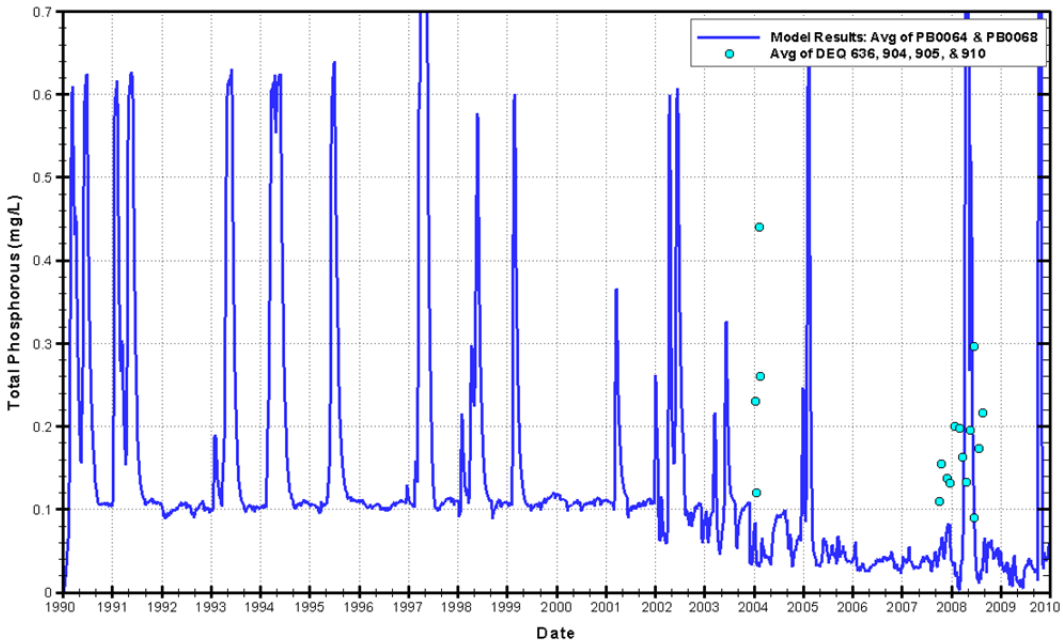

Figure 163 TPH Calibration (2007 – 2008) and Validation (1990 – 2006) Results for Lake Cataouatche in the PB Model

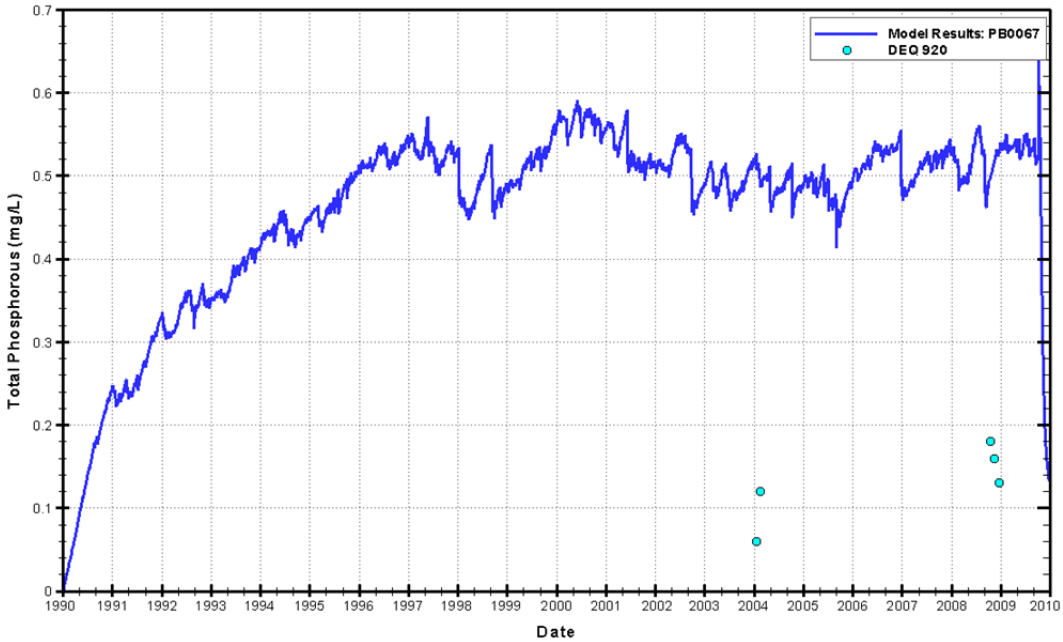

Figure 164 TPH Validation (1990 – 2009) Results for Lake Des Allemands in the PB Model

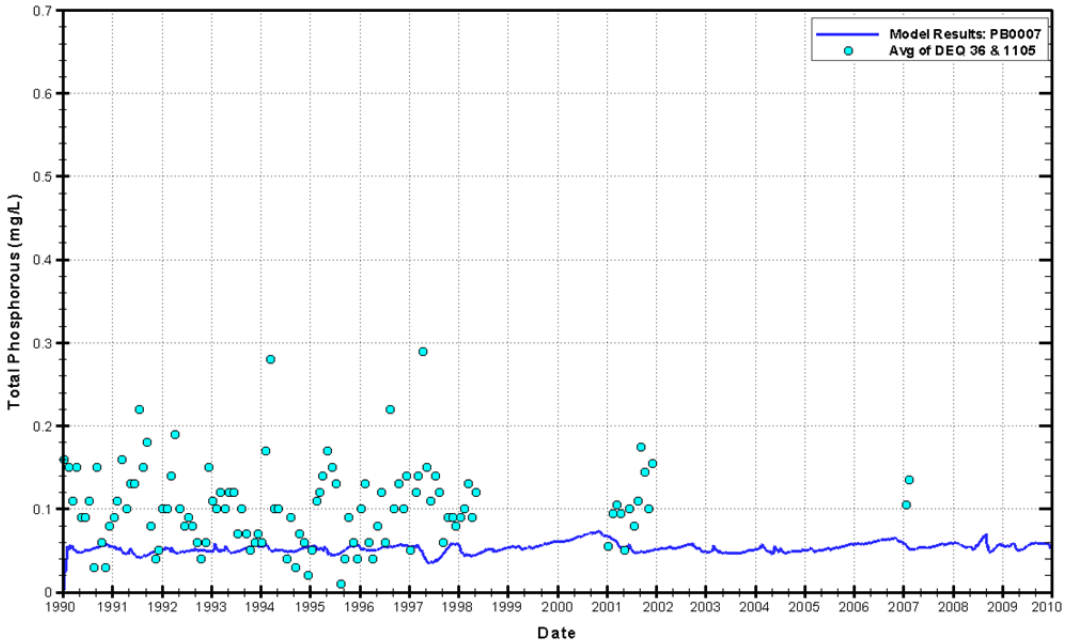

Figure 165 TPH Validation (1990 – 2009) Results for Lake Maurepas in the PB Model

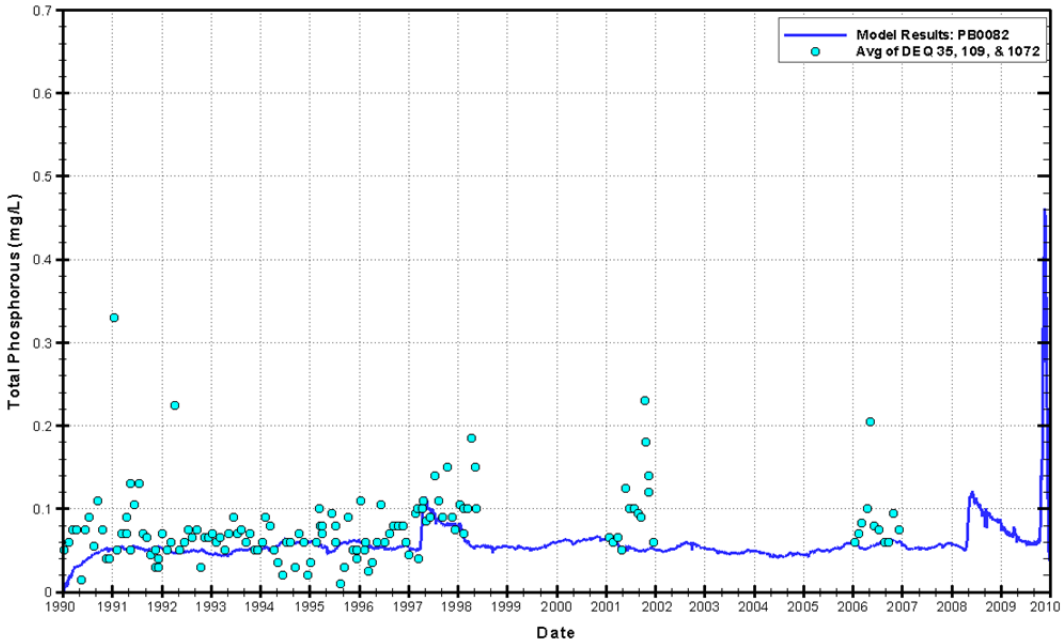

Figure 166 TPH Calibration (1990 – 1994) and Validation (1995 – 2009) Results for Lake St. Catherine in the PB Model

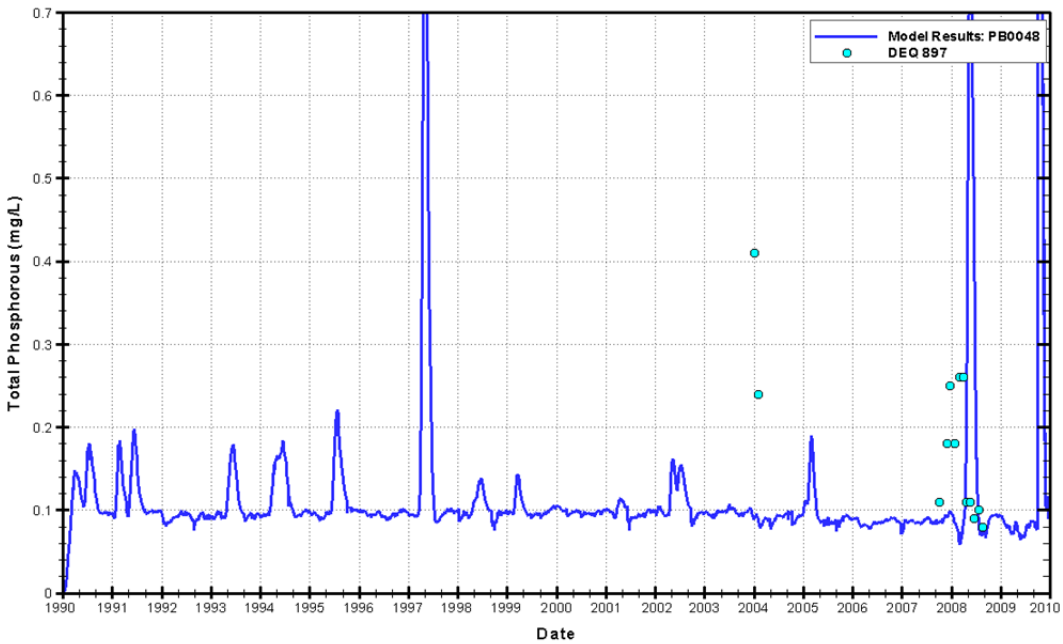

Figure 167 TPH Calibration (2007 – 2008) and Validation (1990 – 2006) Results for Little Lake in the PB Model

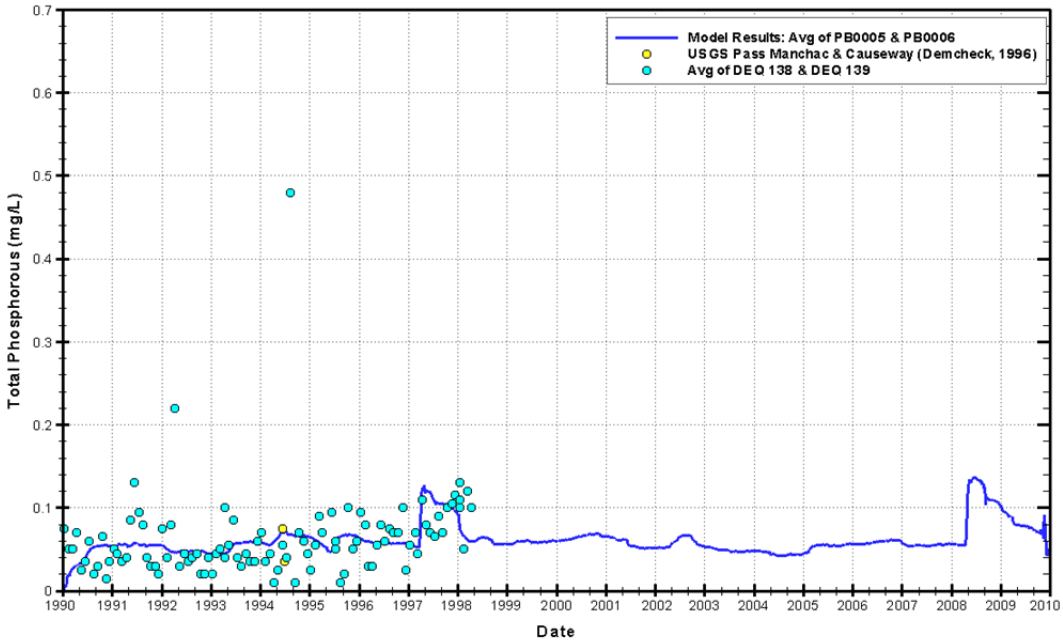

Figure 168 TPH Calibration (1990 – 1994) and Validation (1995 – 2009) Results for North Lake Pontchartrain in the PB Model

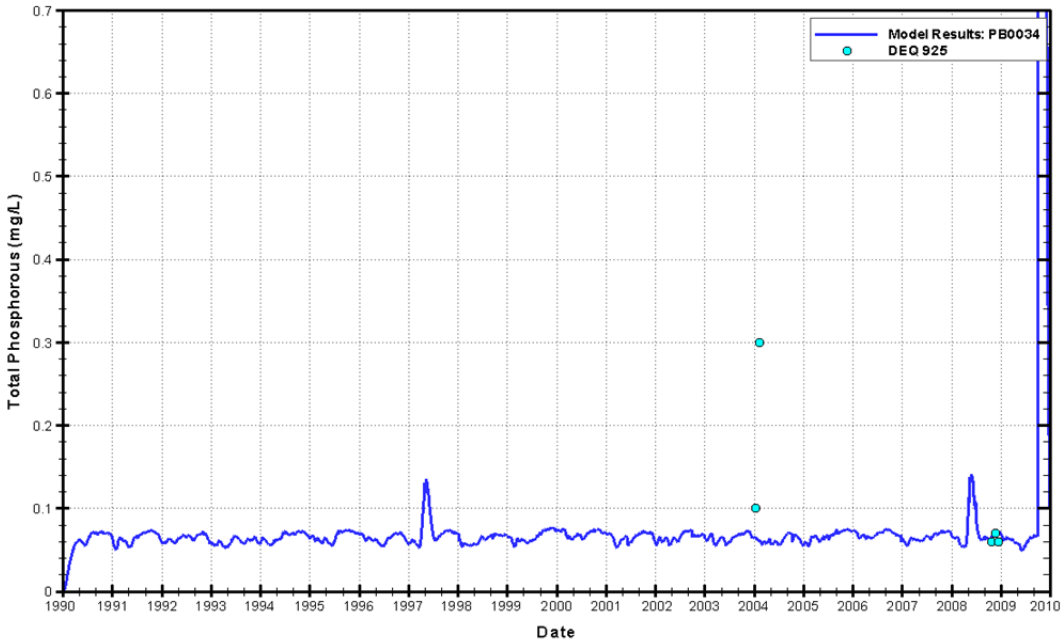

Figure 169 TPH Calibration (2007 – 2008) and Validation (1990 – 2006) Results for Northwest Grand Isle in the PB Model

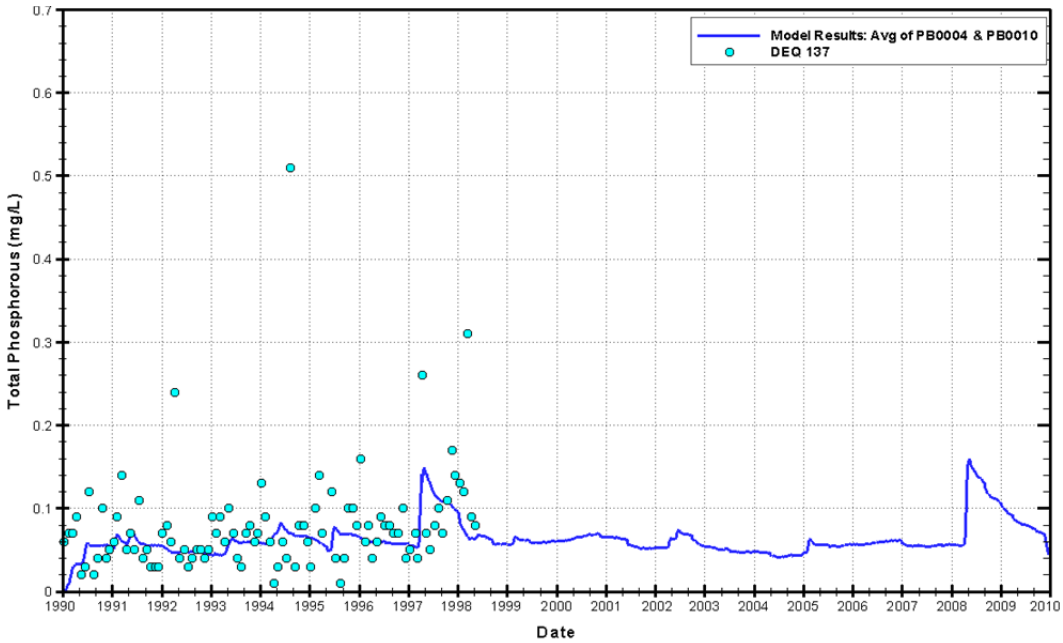

Figure 170 TPH Calibration (1990 – 1994) and Validation (1995 – 2009) Results for South Lake Pontchartrain in the PB Model

Atchafalaya Basin Model Calibration Plots

Stage (STG)

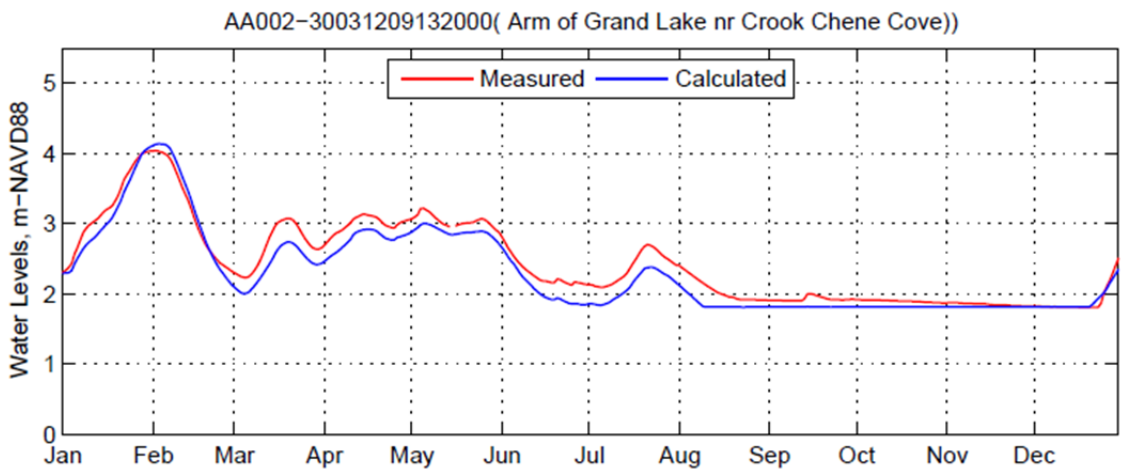

Figure 171 STG Calibration Results for Grand Lake in the AA Model

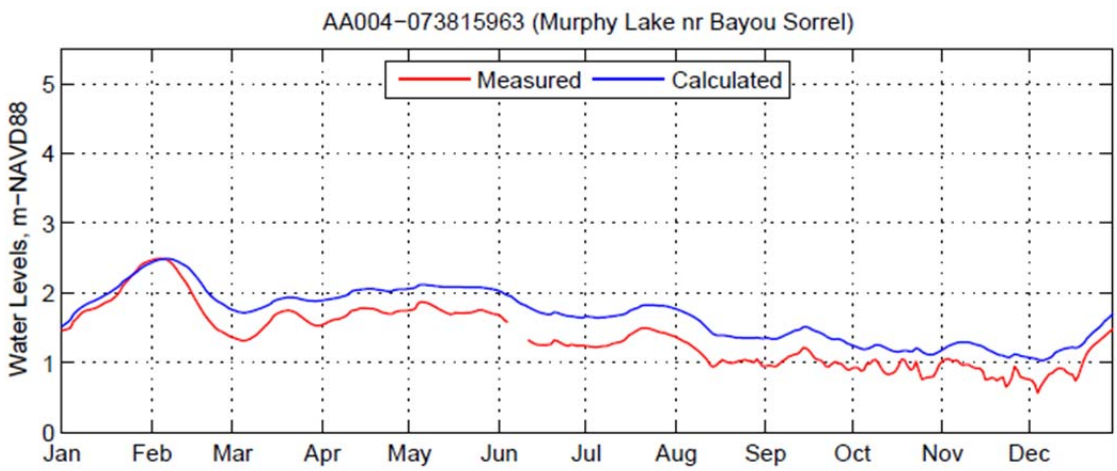

Figure 172 STG Calibration Results for Murphy Lake in the AA Model

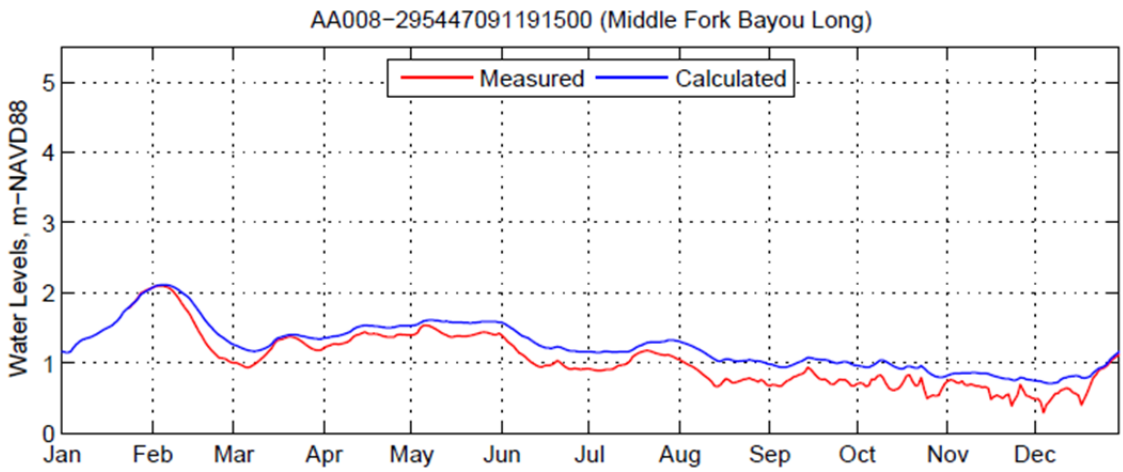

Figure 173 STG Calibration Results for Bayou Long in the AA Model

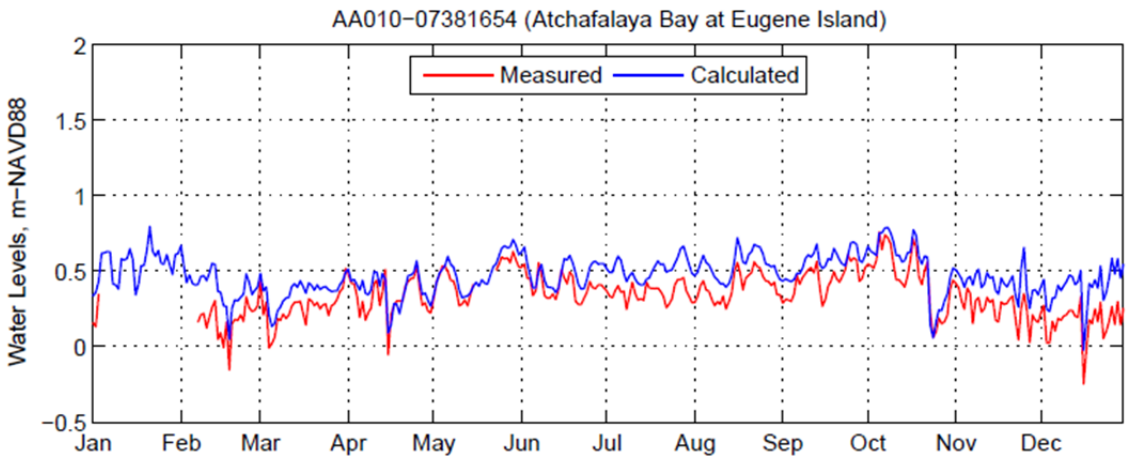

Figure 174 STG Calibration Results for Atchafalaya Bay in the AA Model

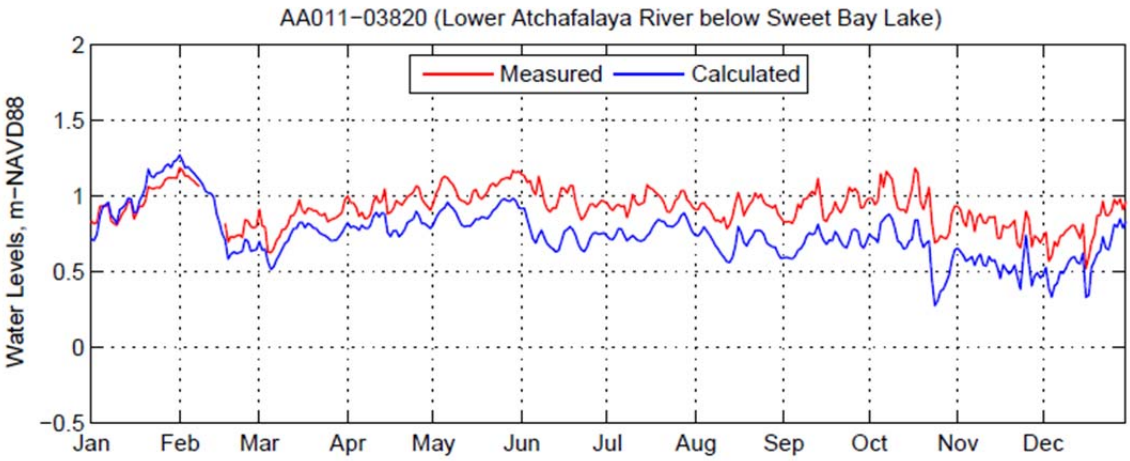

Figure 175 STG Calibration Results for Lower Atchafalaya River below Sweet Bay Lake in the AA Model

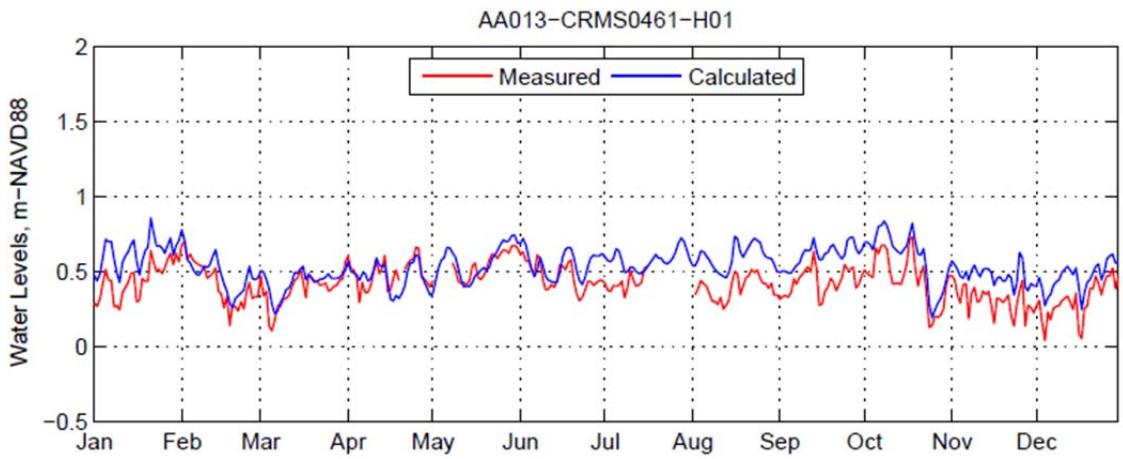

Figure 176 STG Calibration Results for AA013 in the AA Model

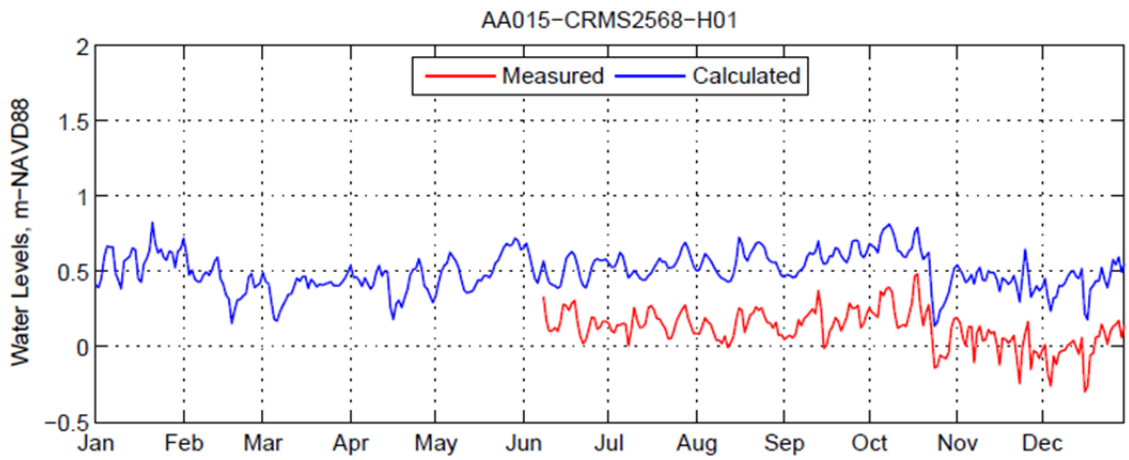

Figure 177 STG Calibration Results for AA015 in the AA Model

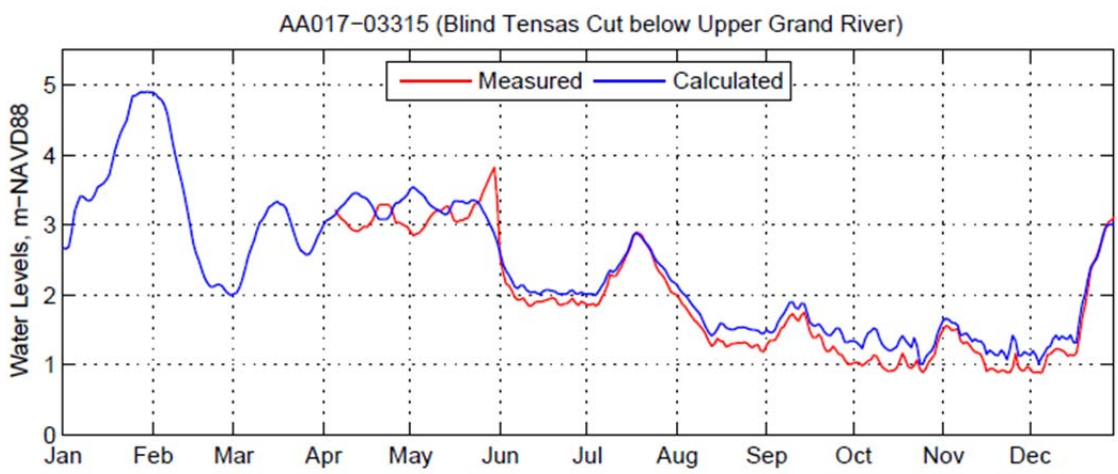

Figure 178 STG Calibration Results for Blind Tensas Cut in the AA Model

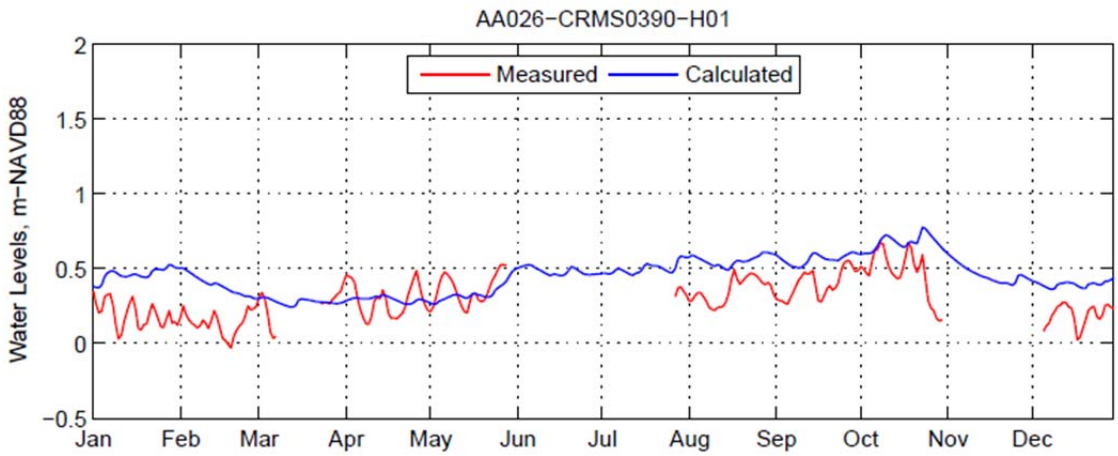

Figure 179 STG Calibration Results for AA026 in the AA Model

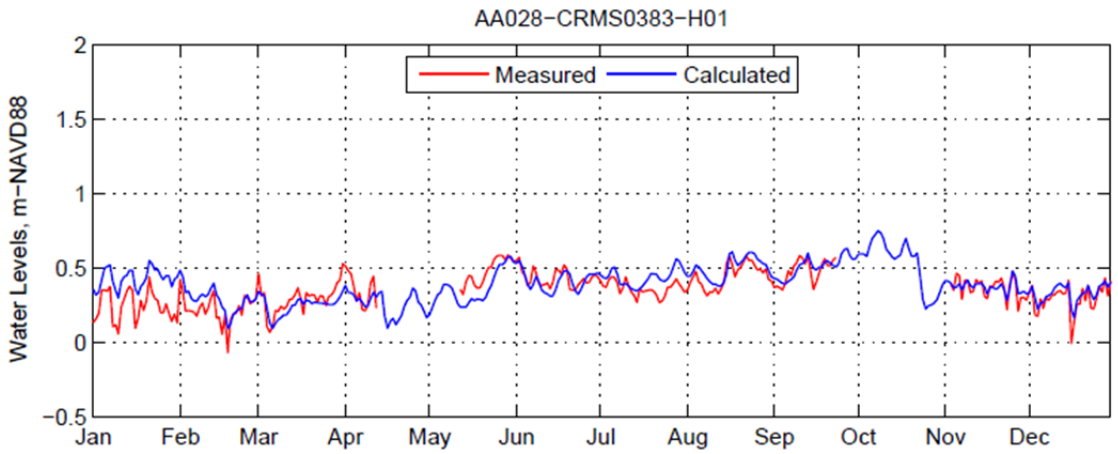

Figure 180 STG Calibration Results for AA028 in the AA Model

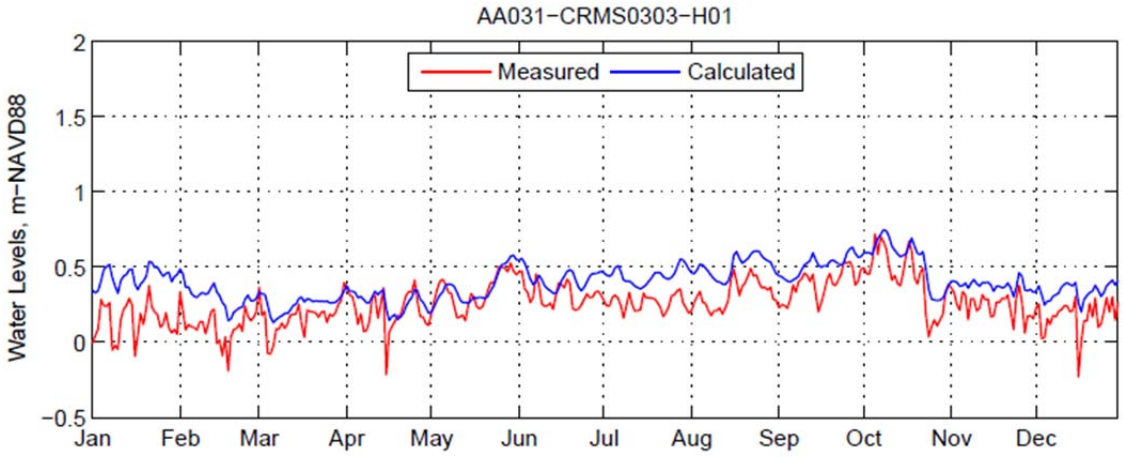

Figure 181 STG Calibration Results for AA031 in the AA Model

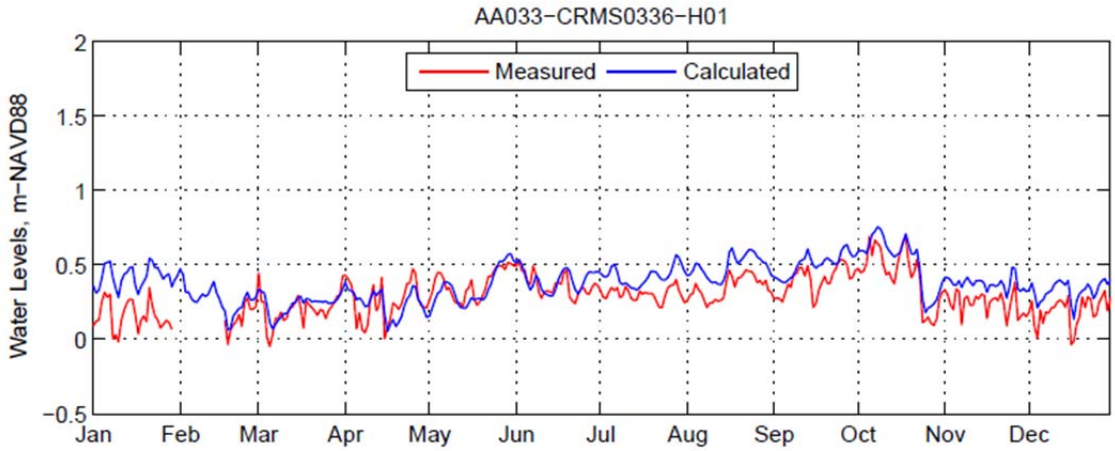

Figure 182 STG Calibration Results for AA033 in the AA Model

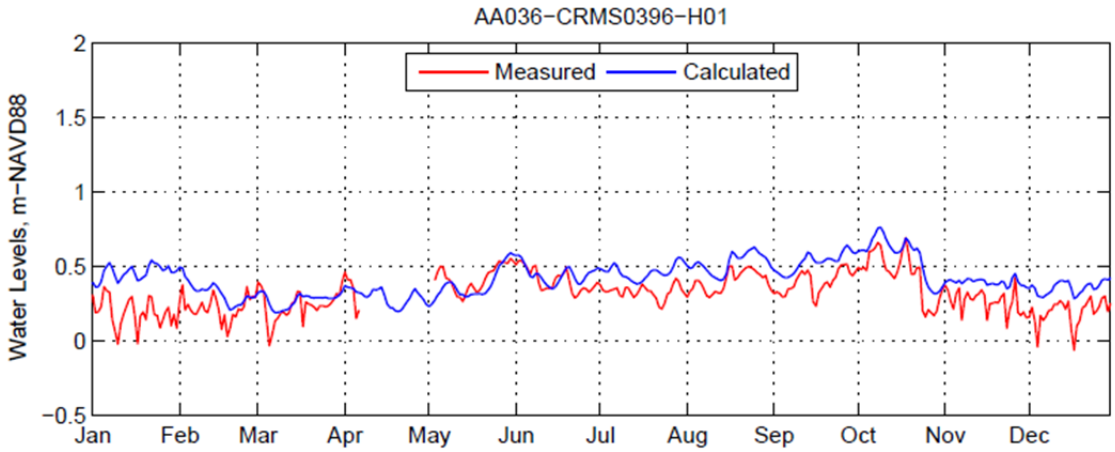

Figure 183 STG Calibration Results for AA036 in the AA Model

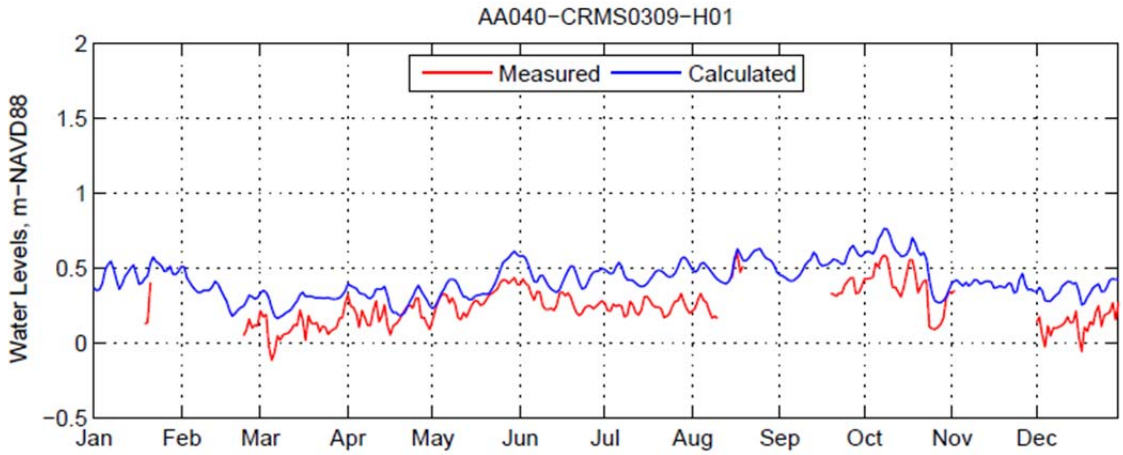

Figure 184 STG Calibration Results for AA040 in the AA Model

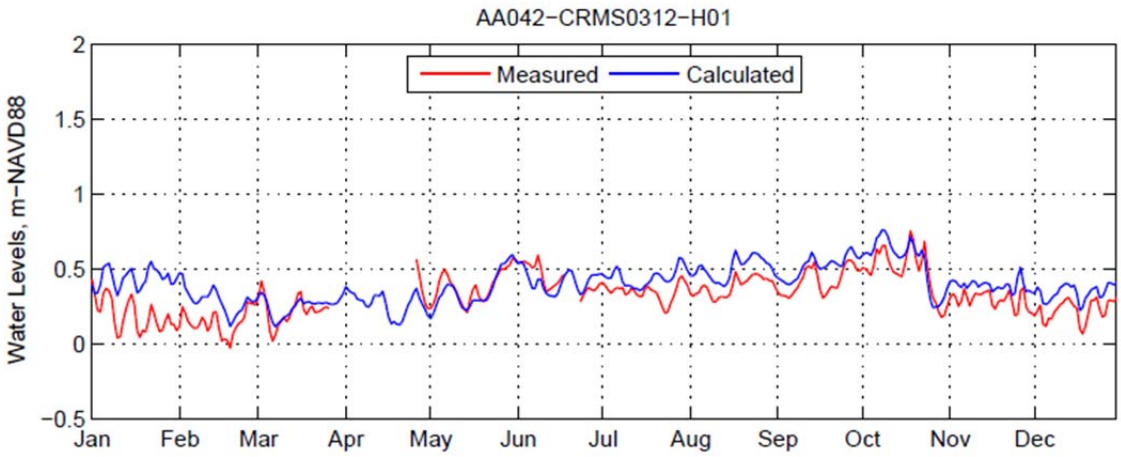

Figure 185 STG Calibration Results for AA042 in the AA Model

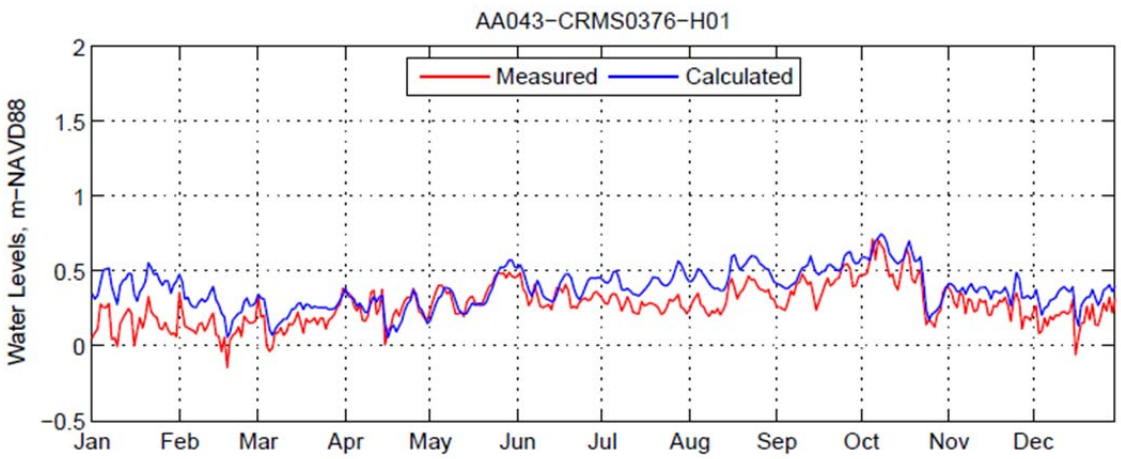

Figure 186 STG Calibration Results for AA043 in the AA Model

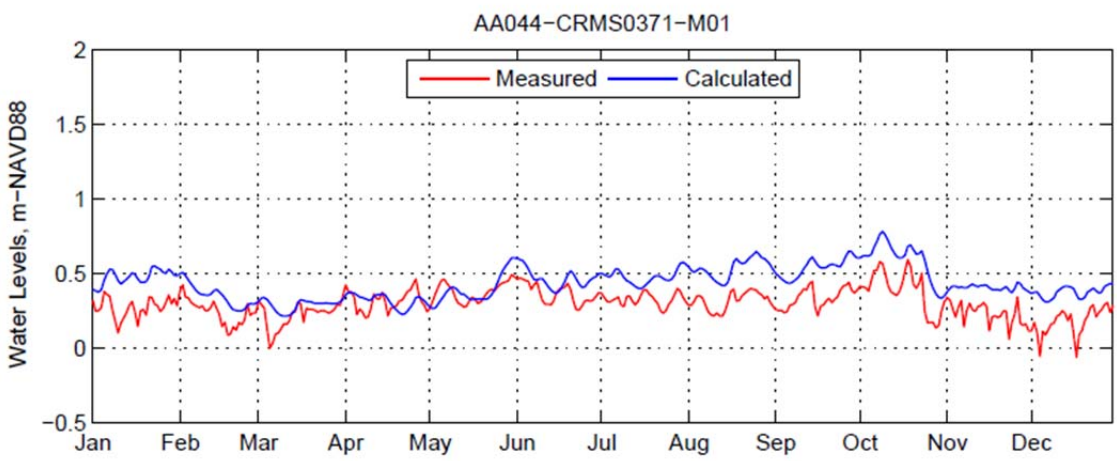

Figure 187 STG Calibration Results for AA044 in the AA Model

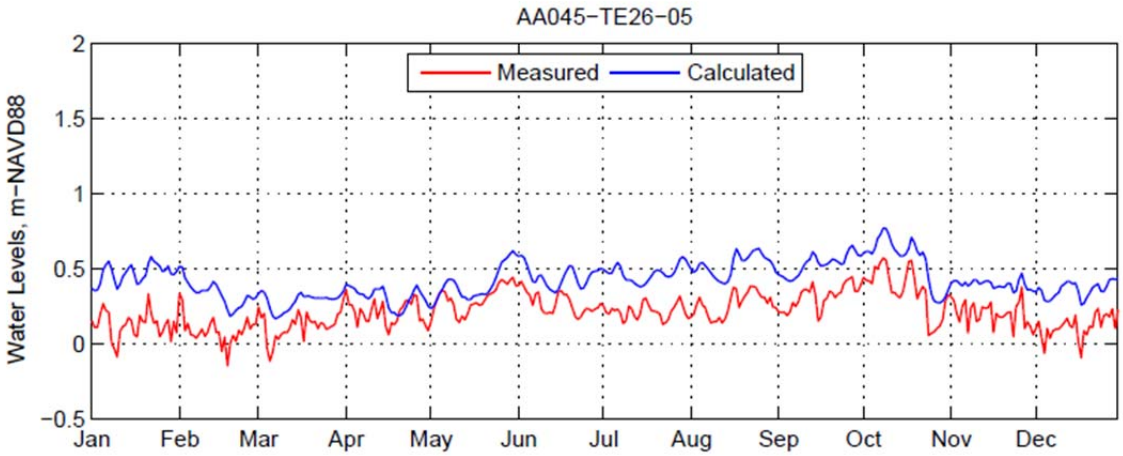

Figure 188 STG Calibration Results for Lake Chapeau in the AA Model

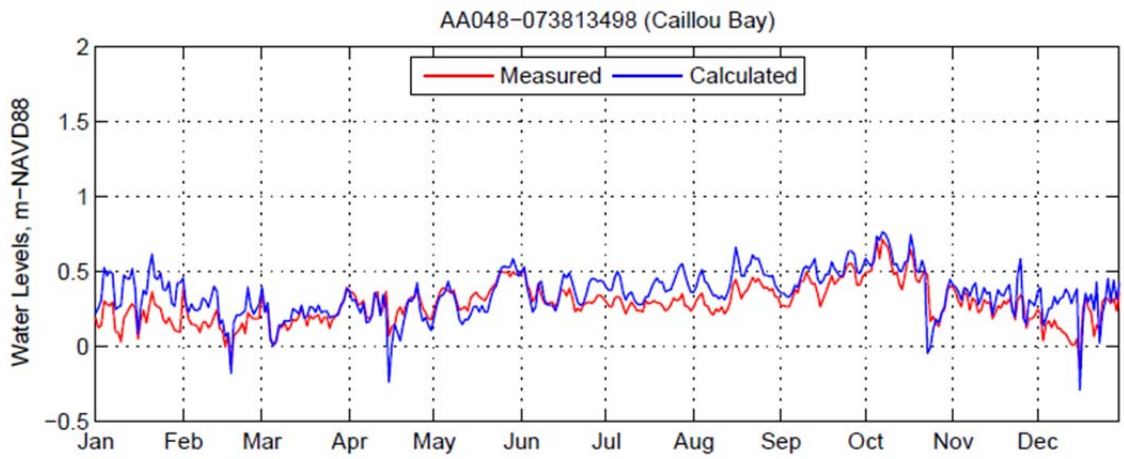

Figure 189 STG Calibration Results for Caillou Bay in the AA Model

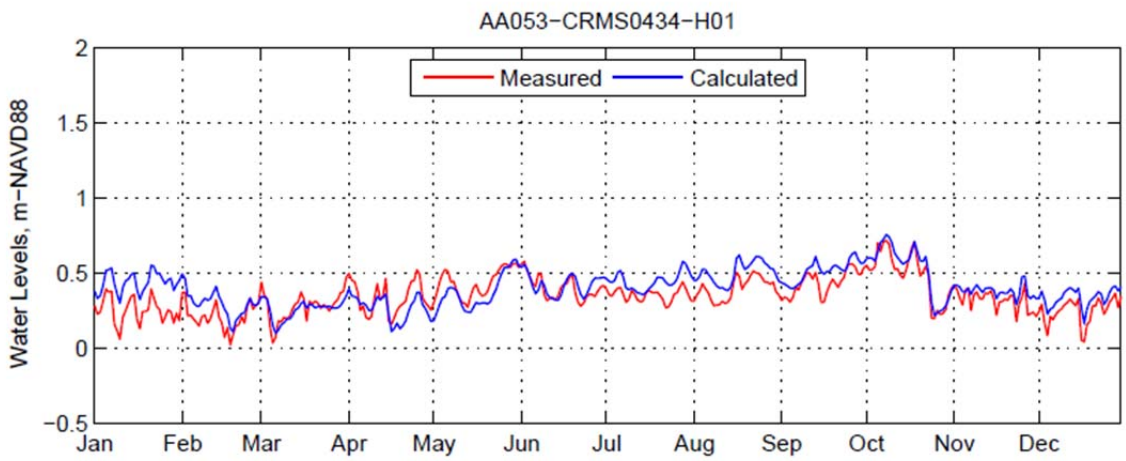

Figure 190 STG Calibration Results for AA053 in the AA Model

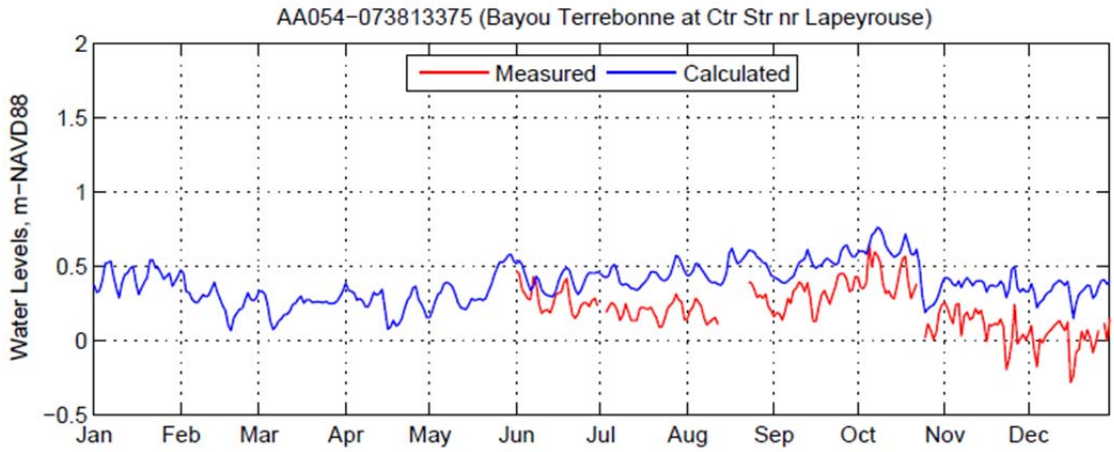

Figure 191 STG Calibration Results for Bayou Terrebonne in the AA Model

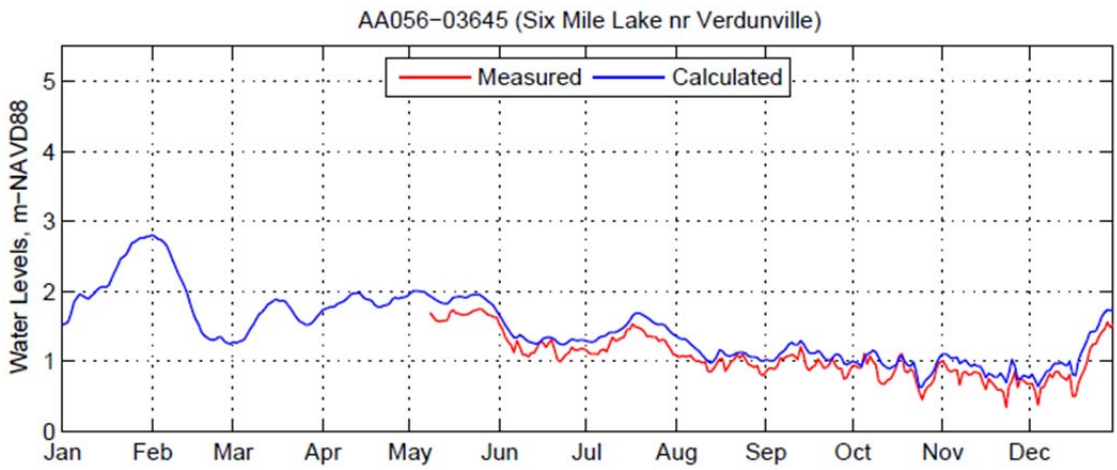

Figure 192 STG Calibration Results for Six Mile Lake in the AA Model

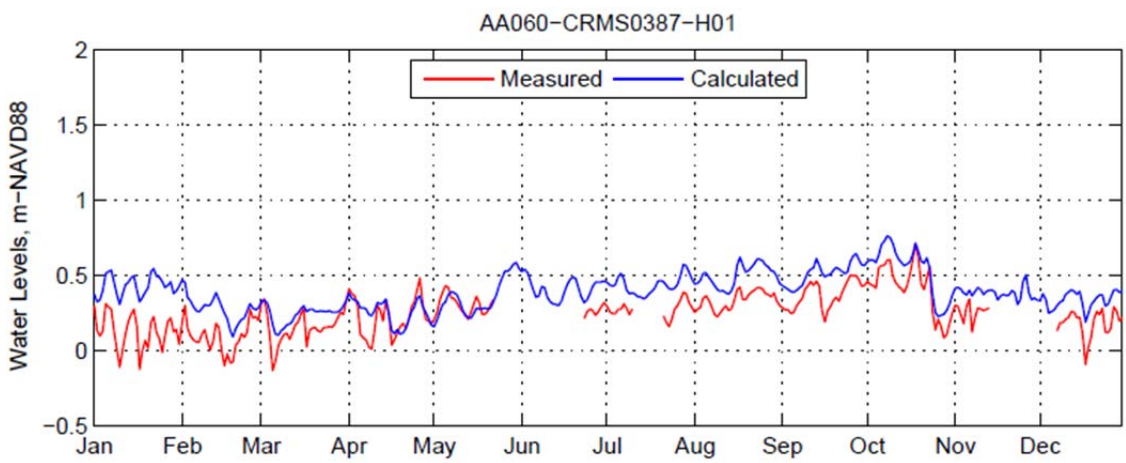

Figure 193 STG Calibration Results for AA060 in the AA Model

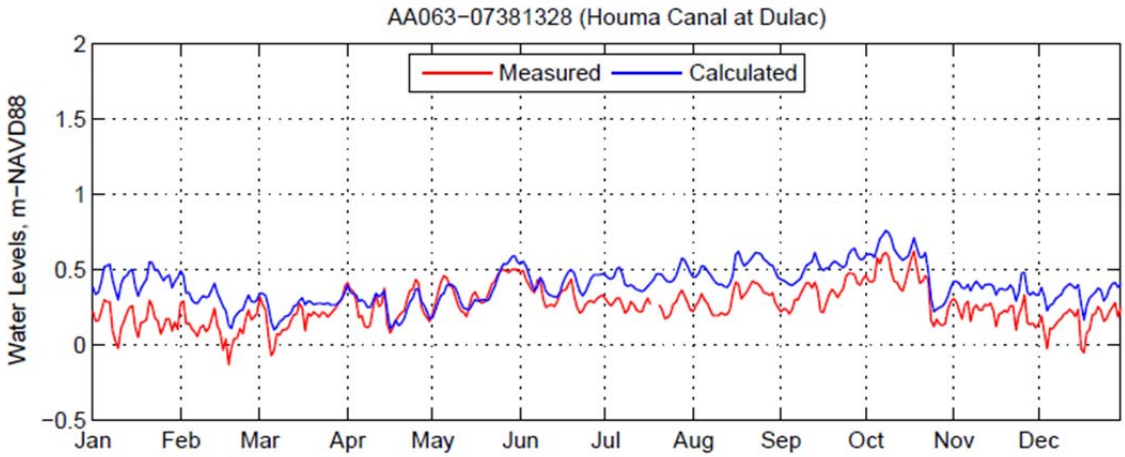

Figure 194 STG Calibration Results for Houma Navigation Canal at Dulac in the AA Model

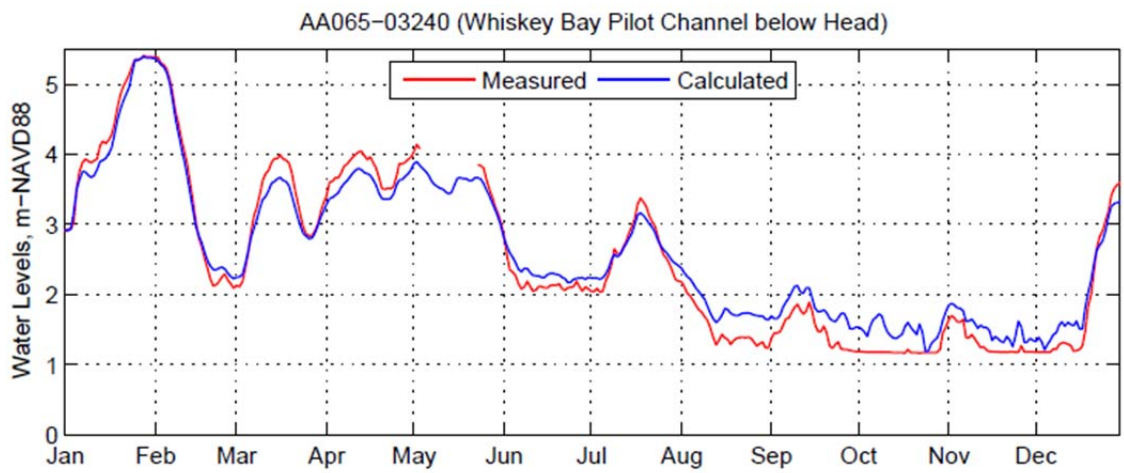

Figure 195 STG Calibration Results for Whiskey Bay Pilot Channel in the AA Model

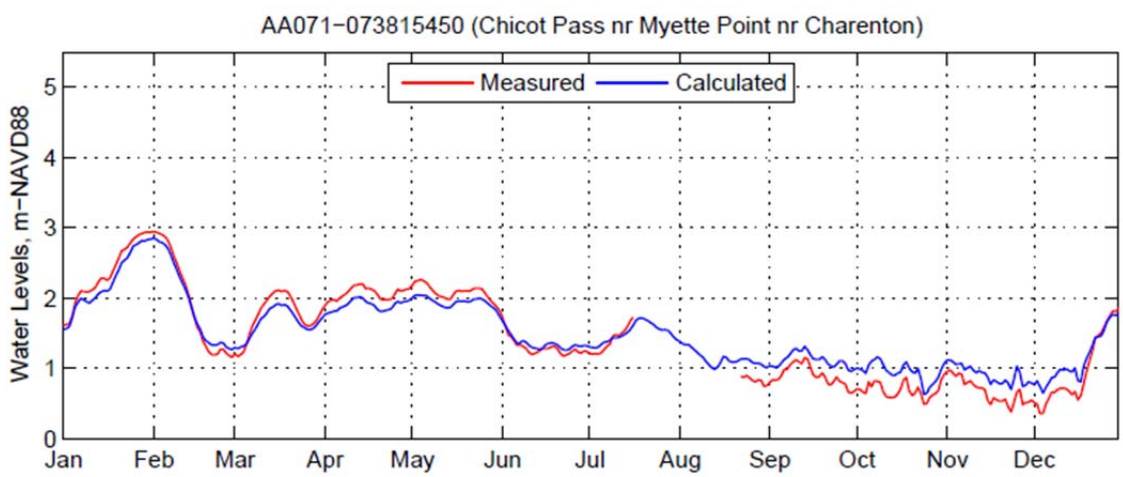

Figure 196 STG Calibration Results for Chicot Pass in the AA Model

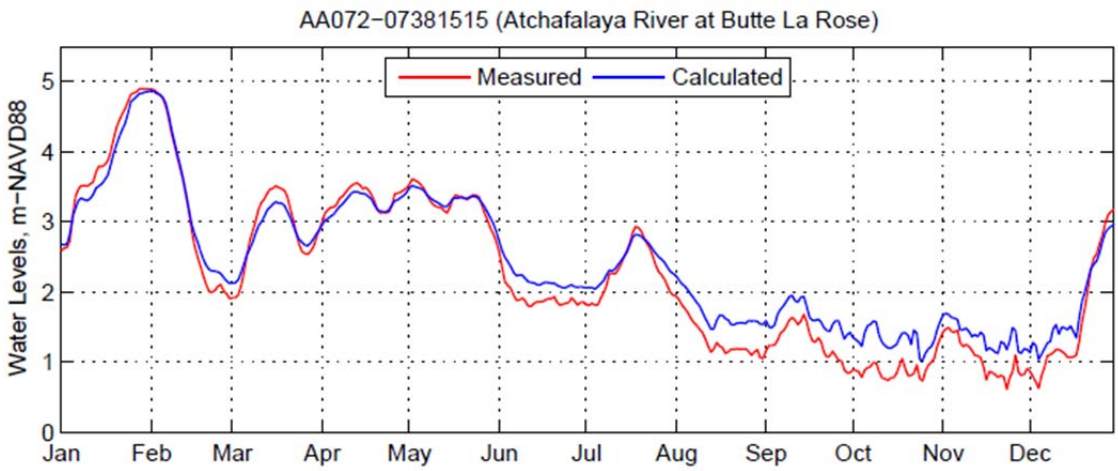

Figure 197 STG Calibration Results for Atchafalaya River at Butte La Rose in the AA Model

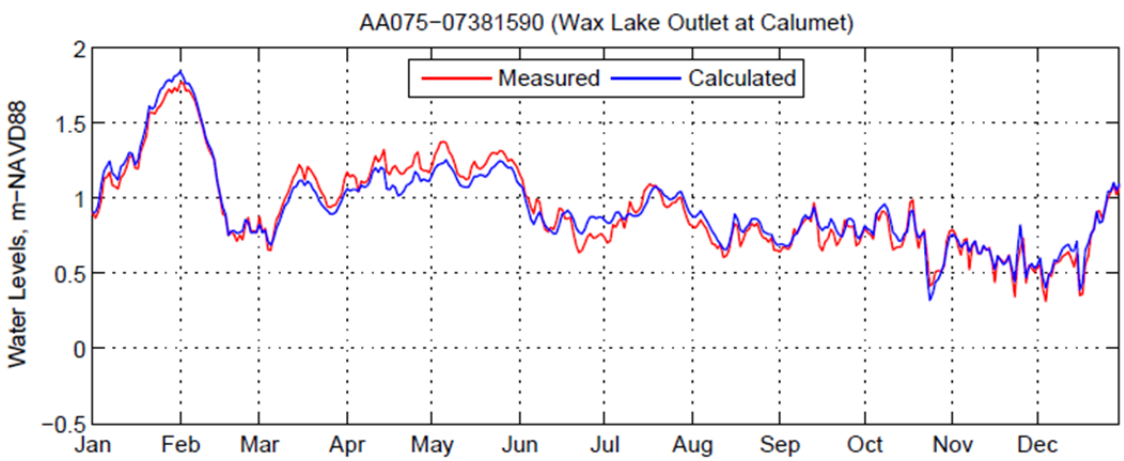

Figure 198 STG Calibration Results for Wax Lake Outlet at Calumet in the AA Model

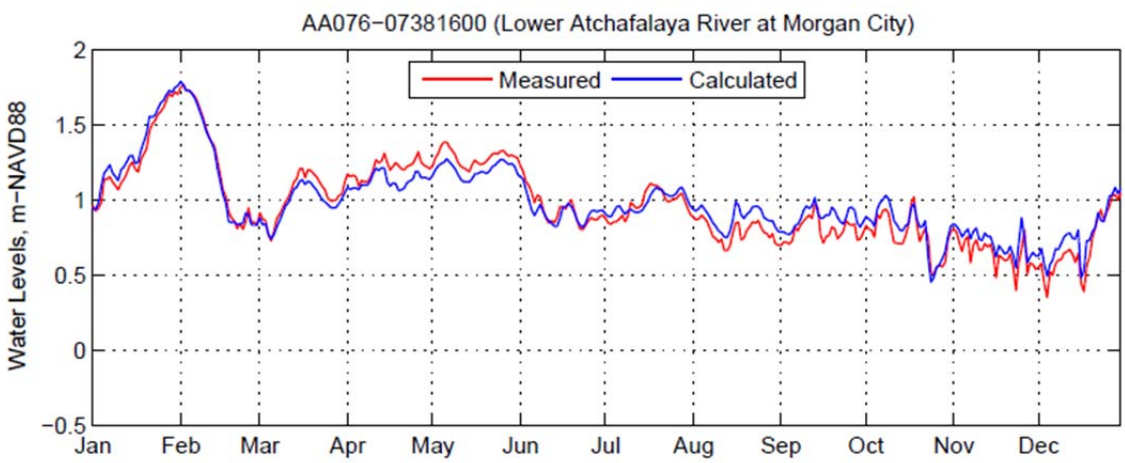

Figure 199 STG Calibration Results for Lower Atchafalaya River at Morgan City in the AA Model

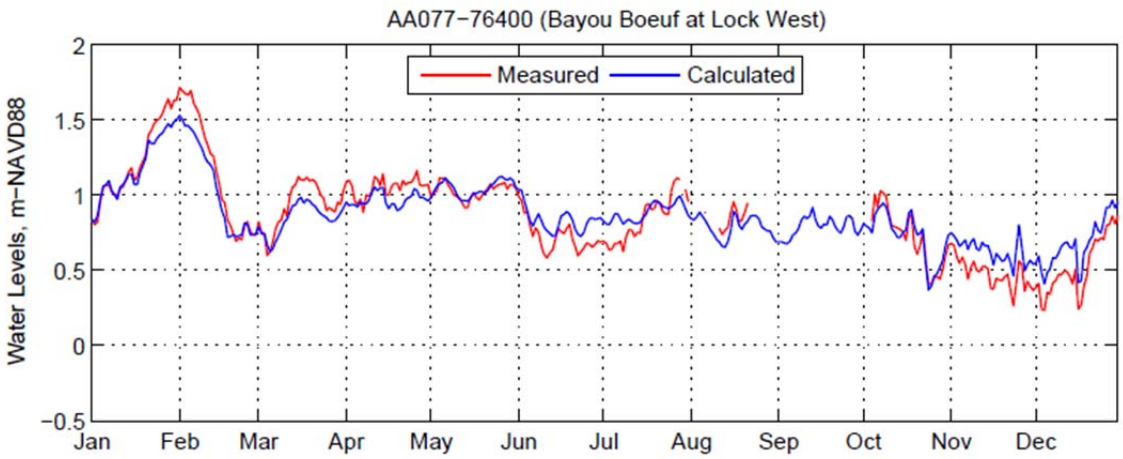

Figure 200 STG Calibration Results for Bayou Boeuf Lock West in the AA Model

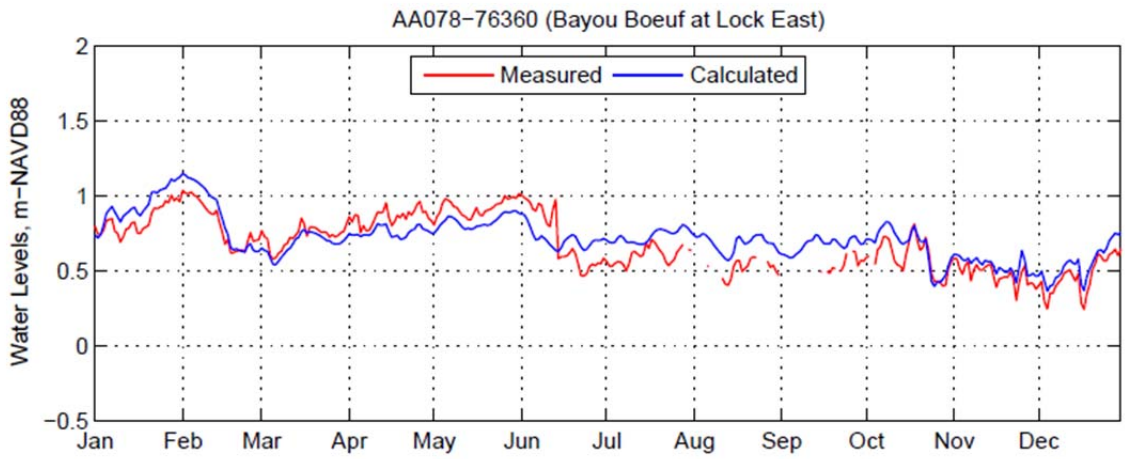

Figure 201 STG Calibration Results for Bayou Boeuf Lock East in the AA Model

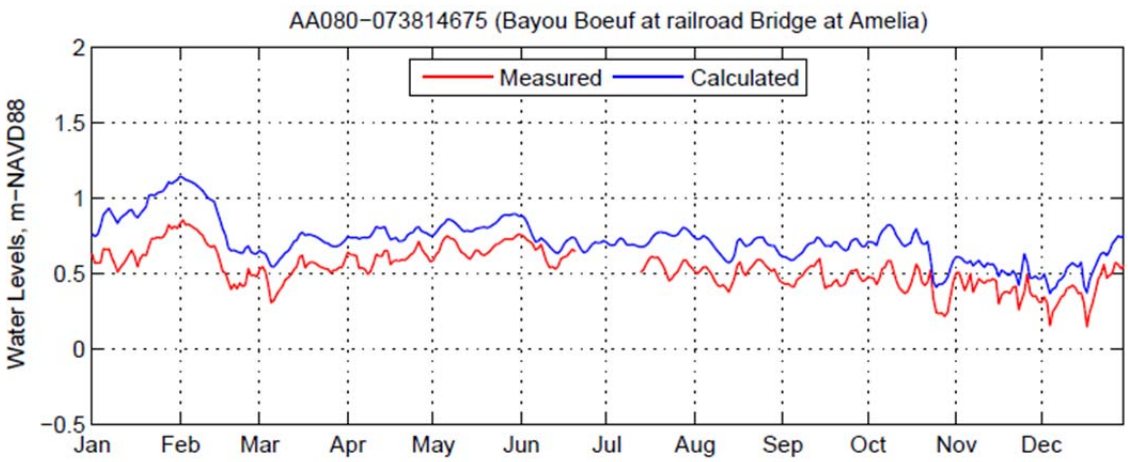

Figure 202 STG Calibration Results for Bayou Boeuf at Amelia in the AA Model

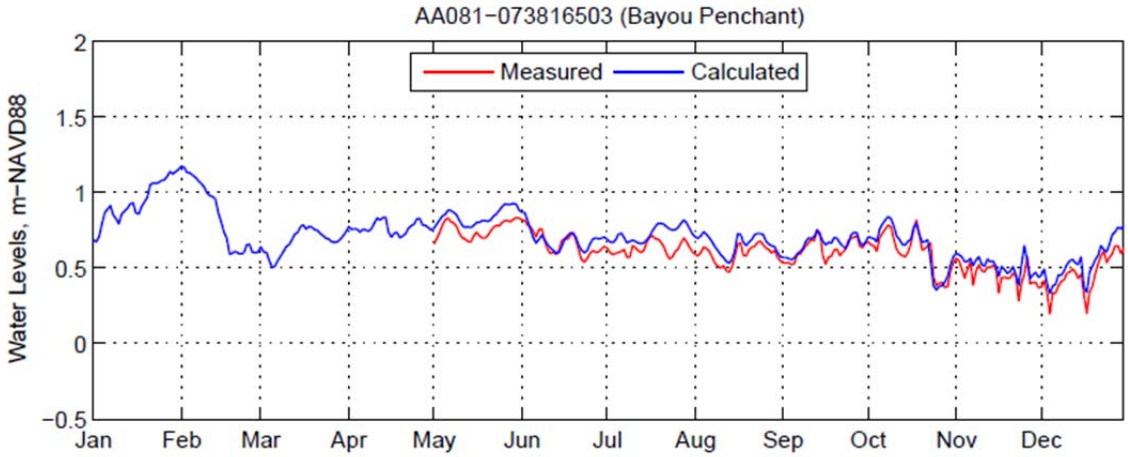

Figure 203 STG Calibration Results for Bayou Penchant in the AA Model

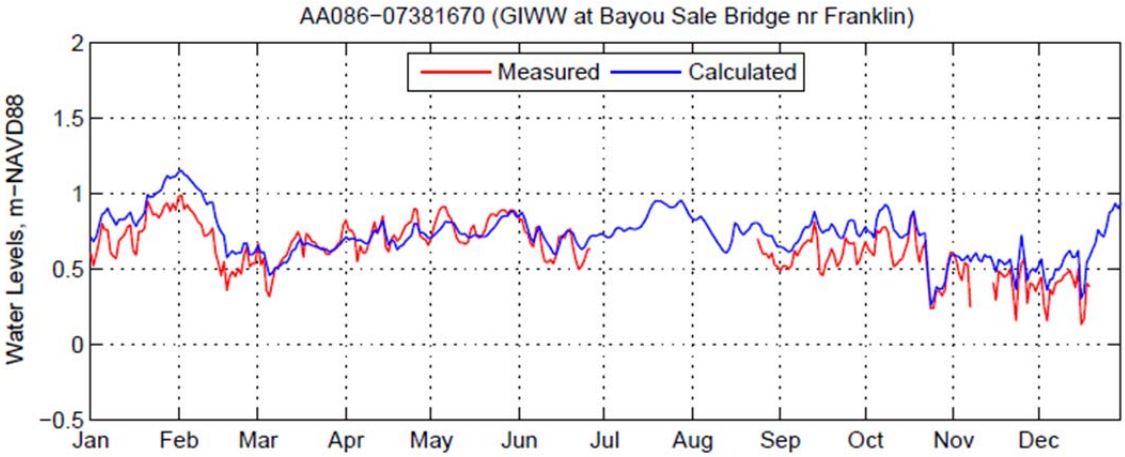

Figure 204 STG Calibration Results for GIWW at Bayou Sale Ridge in the AA Model

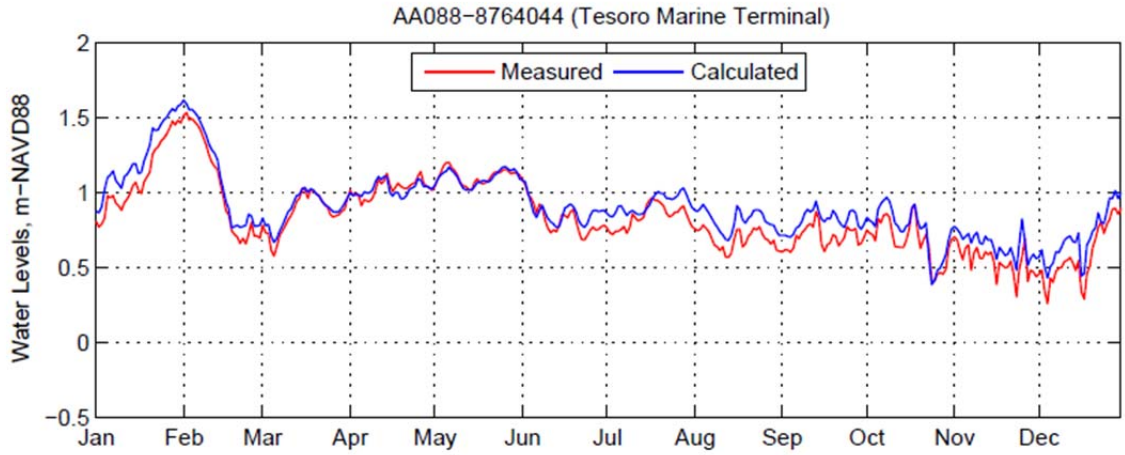

Figure 205 STG Calibration Results for Tesoro Marine Terminal in the AA Model

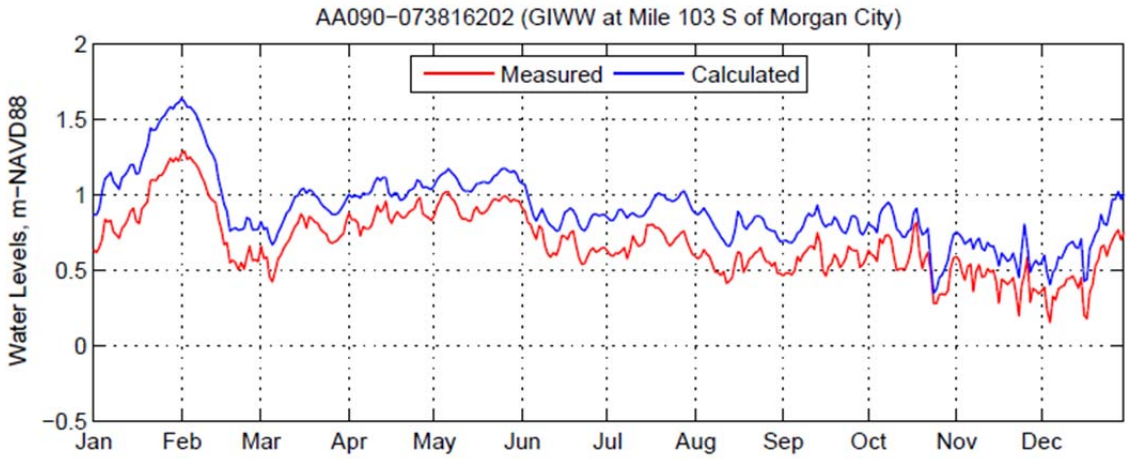

Figure 206 STG Calibration Results for GIWW at Mile 103 in the AA Model

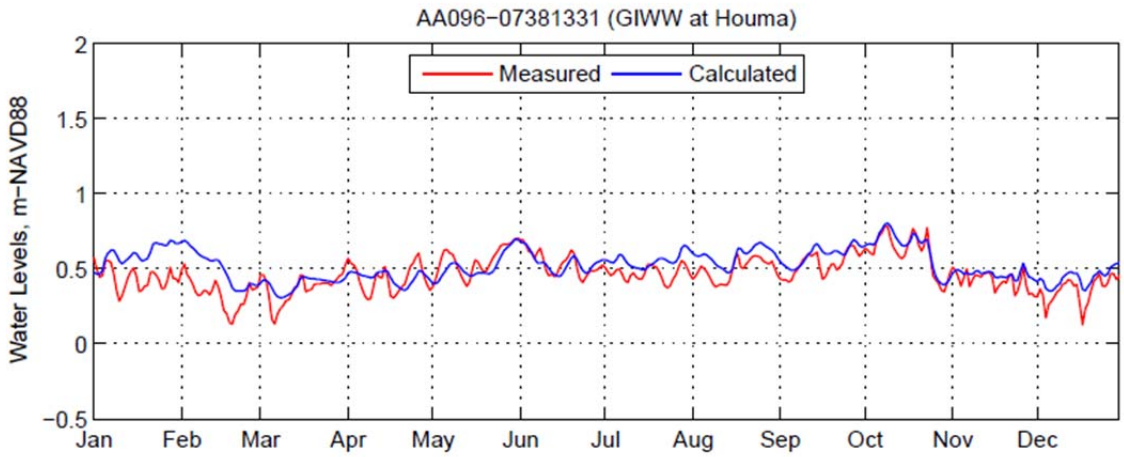

Figure 207 STG Calibration Results for GIWW at Houma in the AA Model

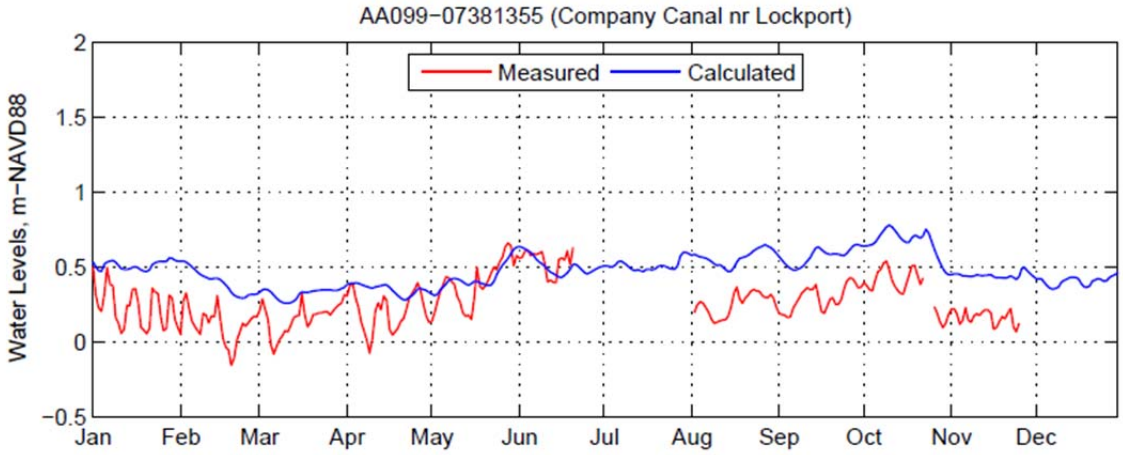

Figure 208 STG Calibration Results for Company Canal near Lockport in the AA Model

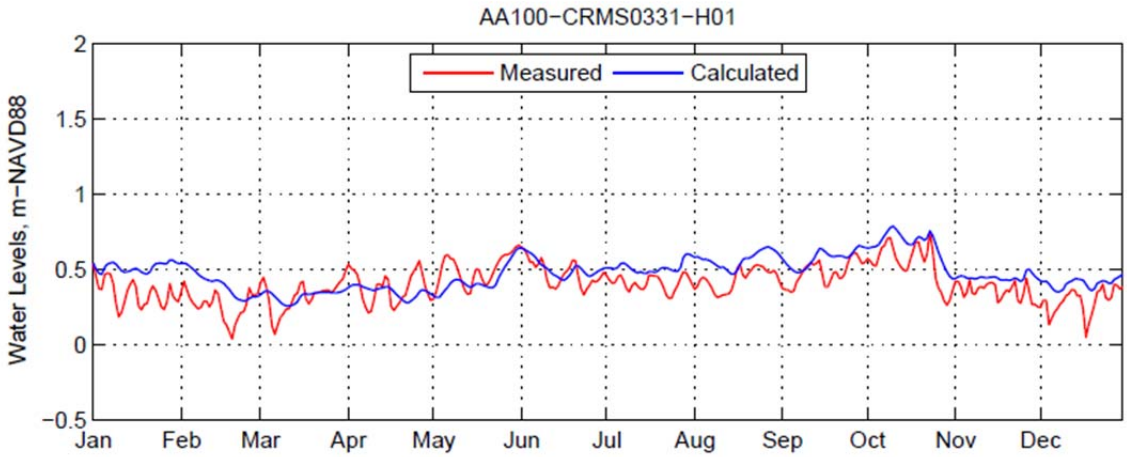

Figure 209 STG Calibration Results for AA100 in the AA Model

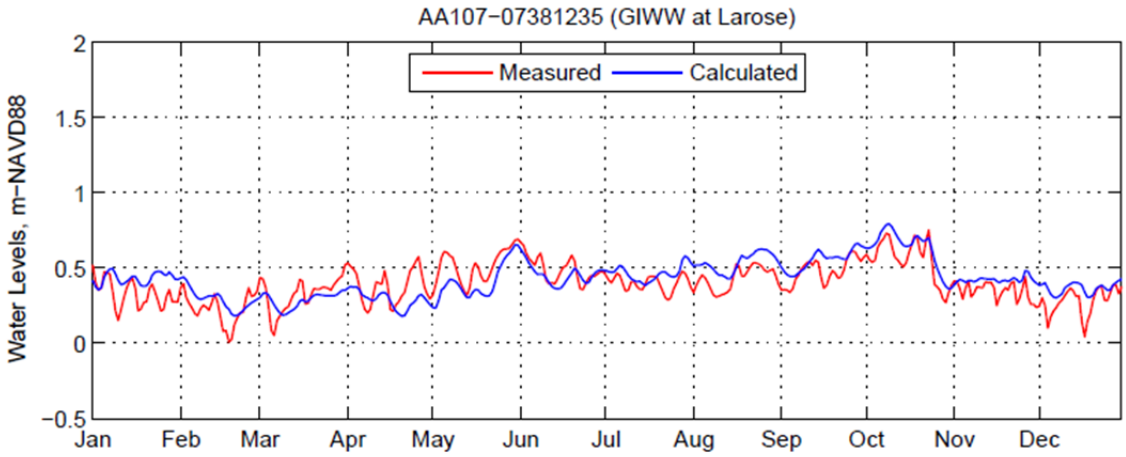

Figure 210 STG Calibration Results for GIWW at Larose in the AA Model

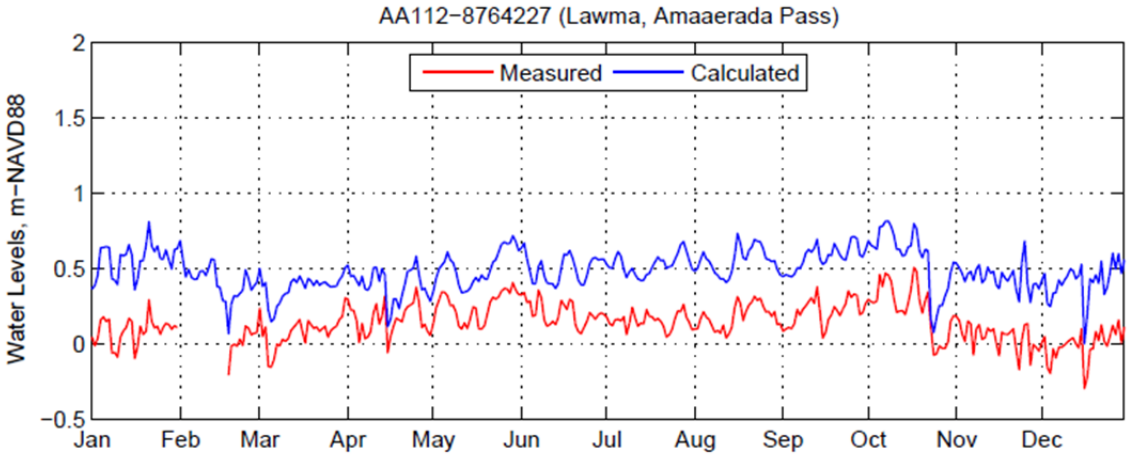

Figure 211 STG Calibration Results for Lawma, Amerada Pass in the AA Model

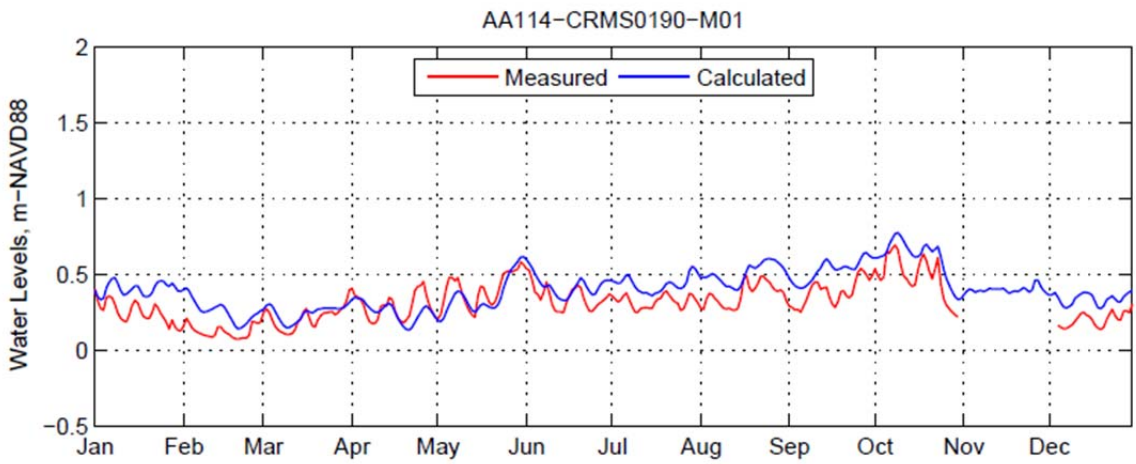

Figure 212 STG Calibration Results for AA114 in the AA Model

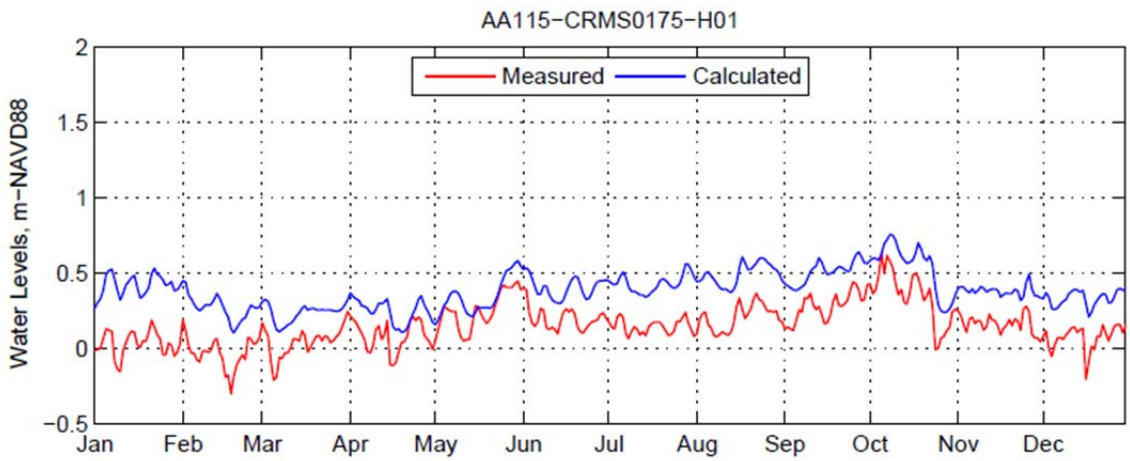

Figure 213 STG Calibration Results for AA115 in the AA Model

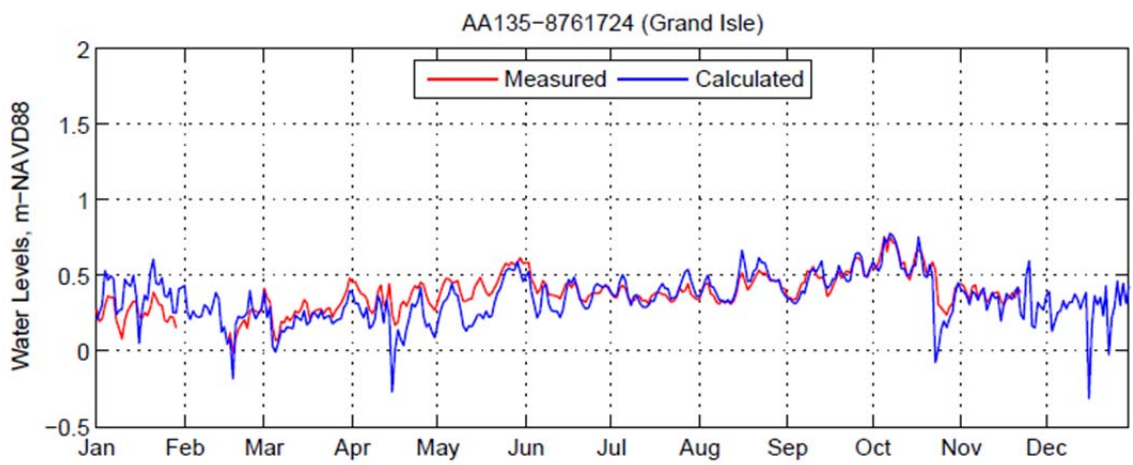

Figure 214 STG Calibration Results for Grand Isle in the AA Model

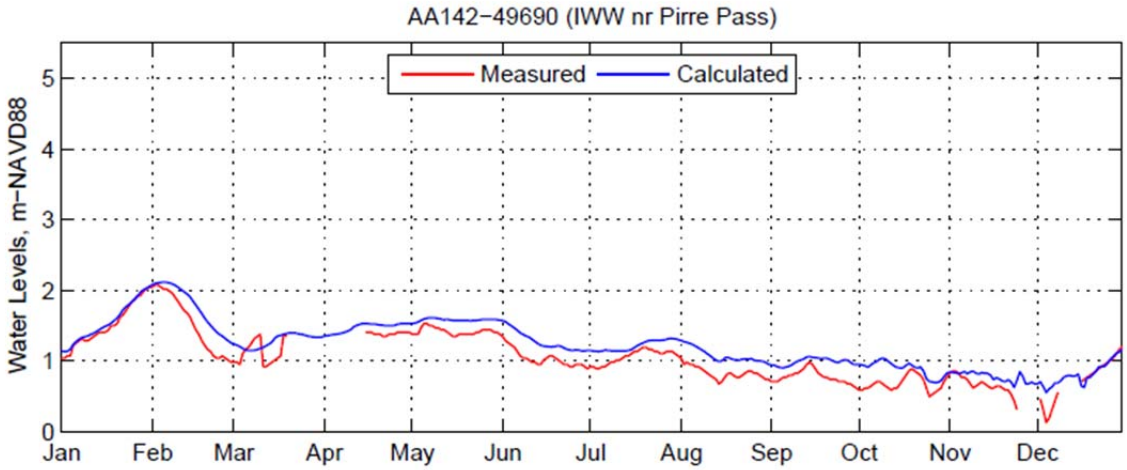

Figure 215 STG Calibration Results for ICWW near Pierre Pass in the AA Model

Discharge

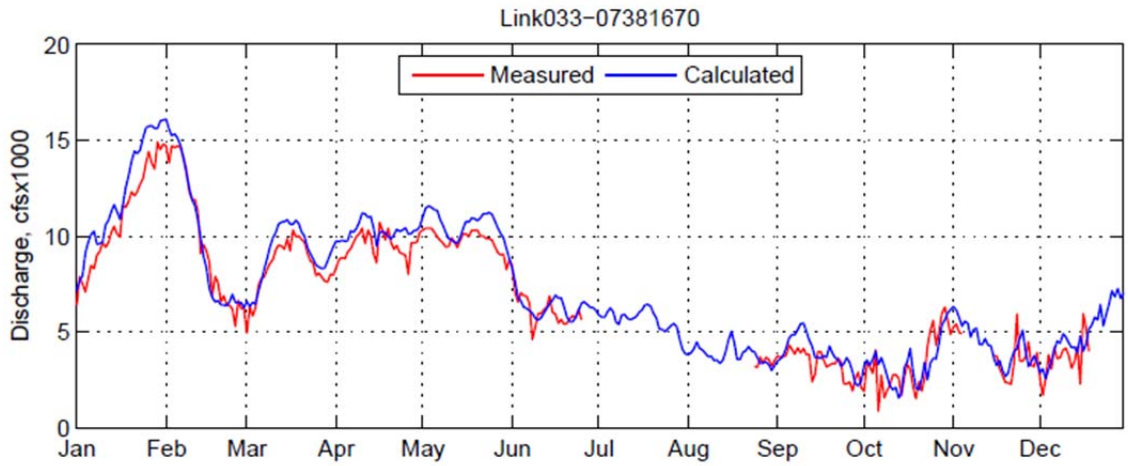

Figure 216 Discharge Calibration Results for Link 033 in the AA Model

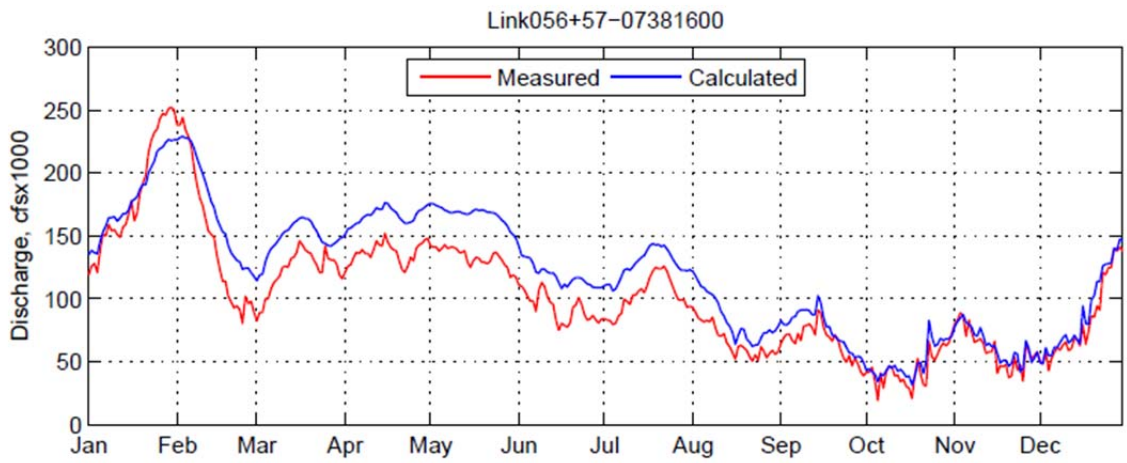

Figure 217 Discharge Calibration Results for Links 056 and 057 in the AA Model

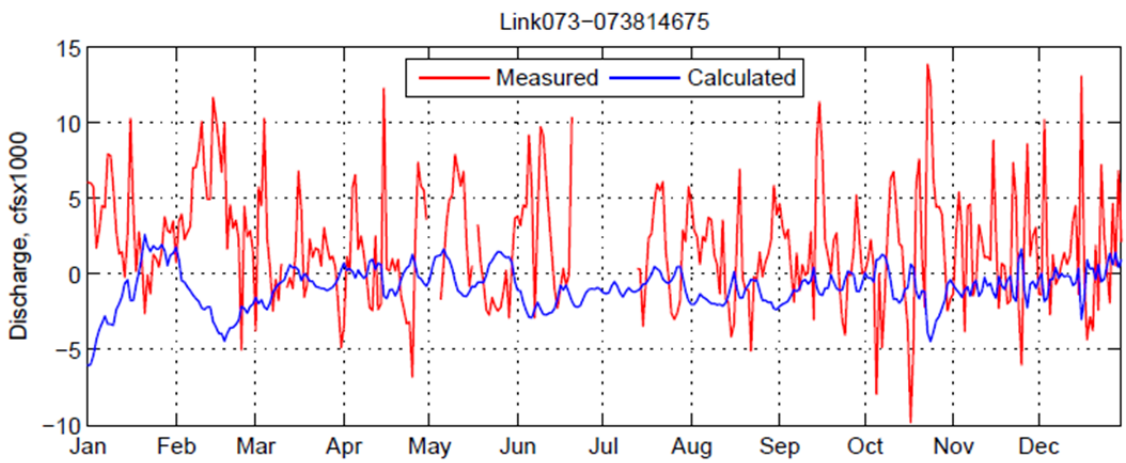

Figure 218 Discharge Calibration Results for Link 073 in the AA Model

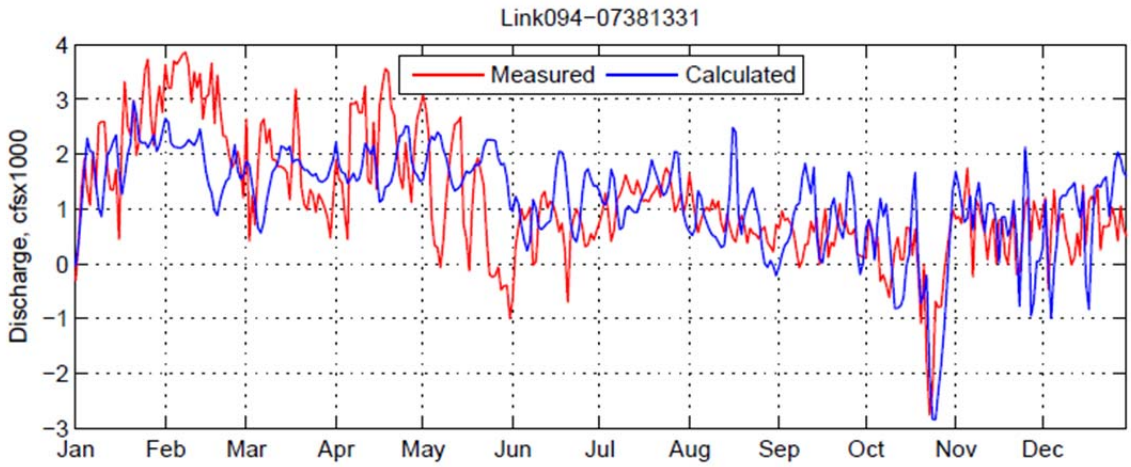

Figure 219 Discharge Calibration Results for Link 094 in the AA Model

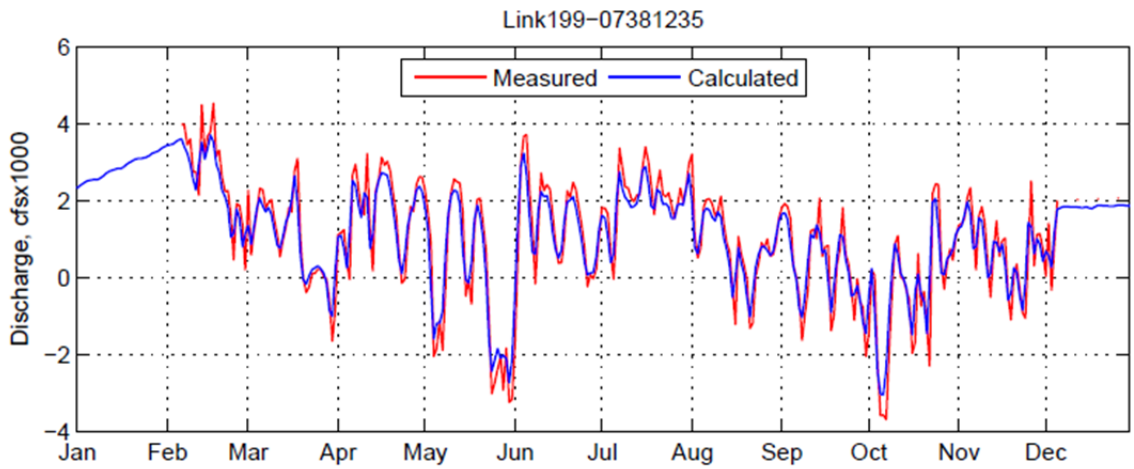

Figure 220 Discharge Calibration Results for Link 199 in the AA Model

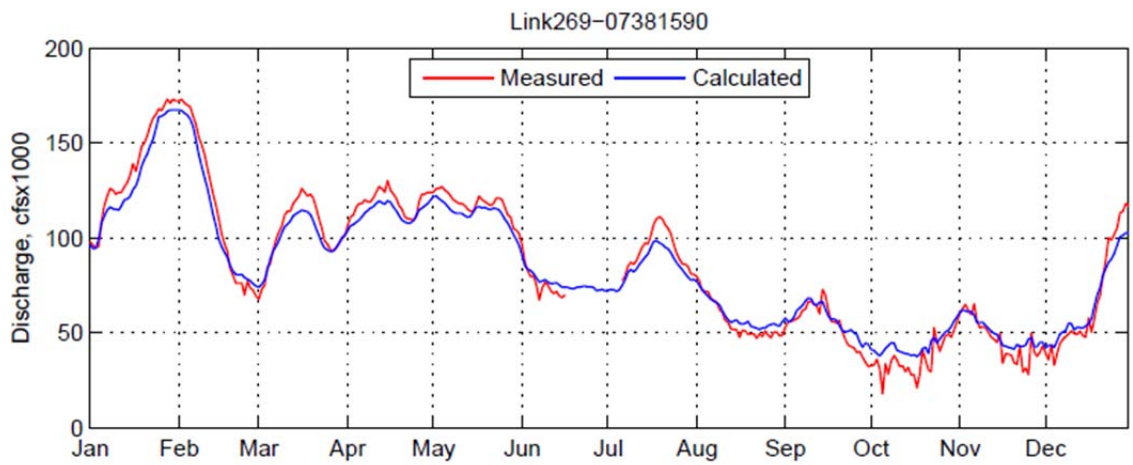

Figure 221 Discharge Calibration Results for Link 269 in the AA Model

Salinity (SAL)

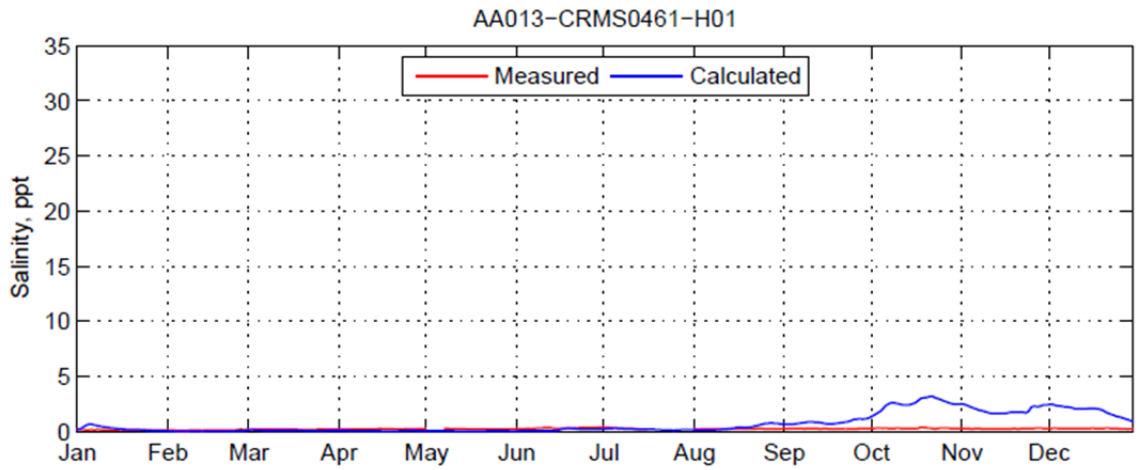

Figure 222 SAL Calibration Results for AA013 in the AA Model

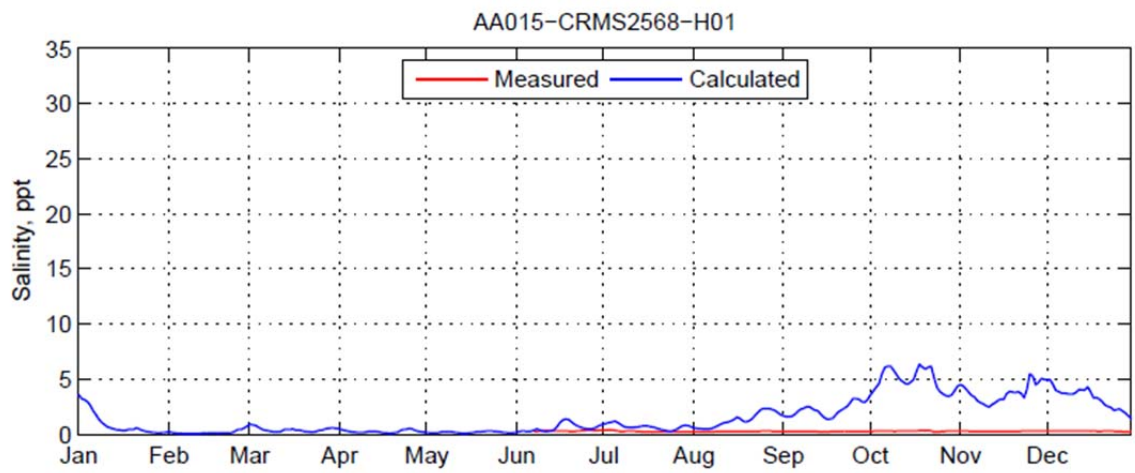

Figure 223 SAL Calibration Results for AA015 in the AA Model

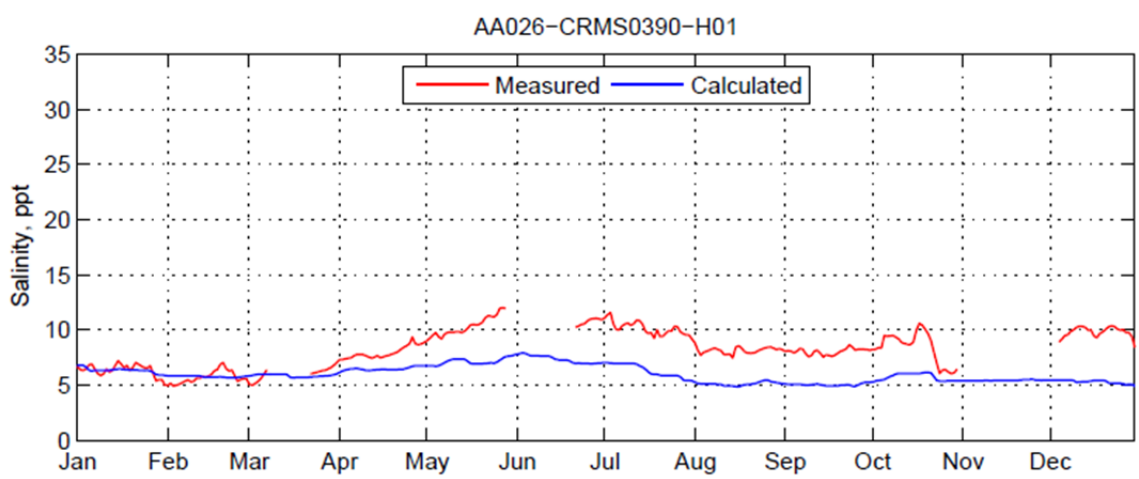

Figure 224 SAL Calibration Results for AA026 in the AA Model

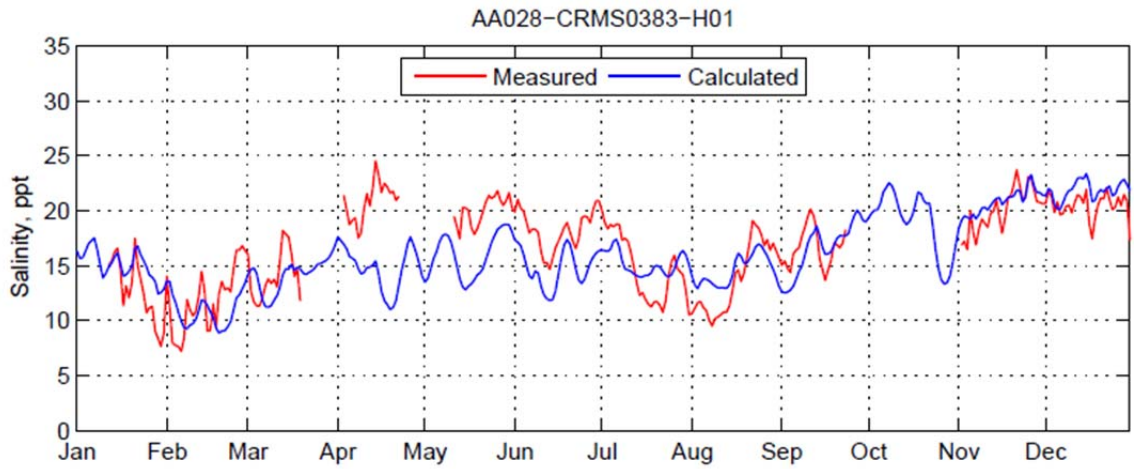

Figure 225 SAL Calibration Results for AA028 in the AA Model

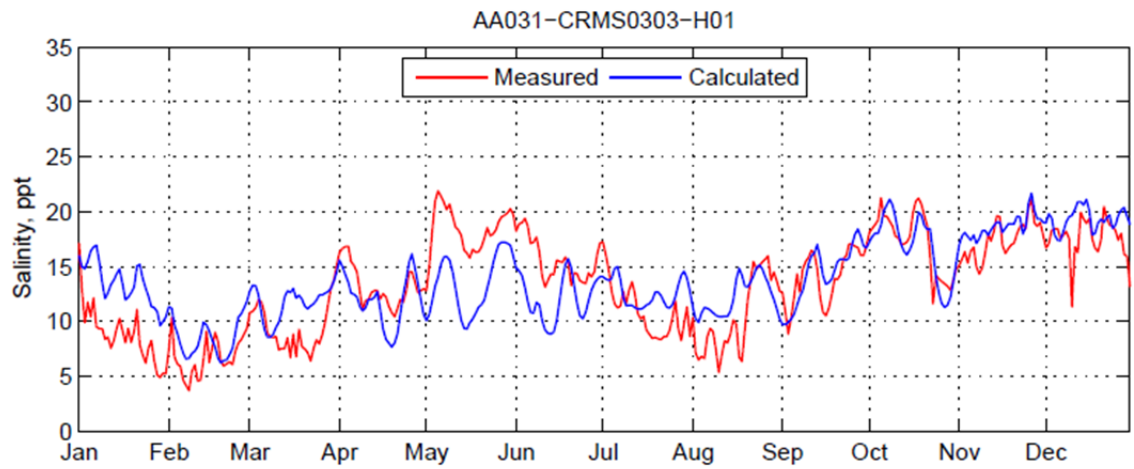

Figure 226 SAL Calibration Results for AA031 in the AA Model

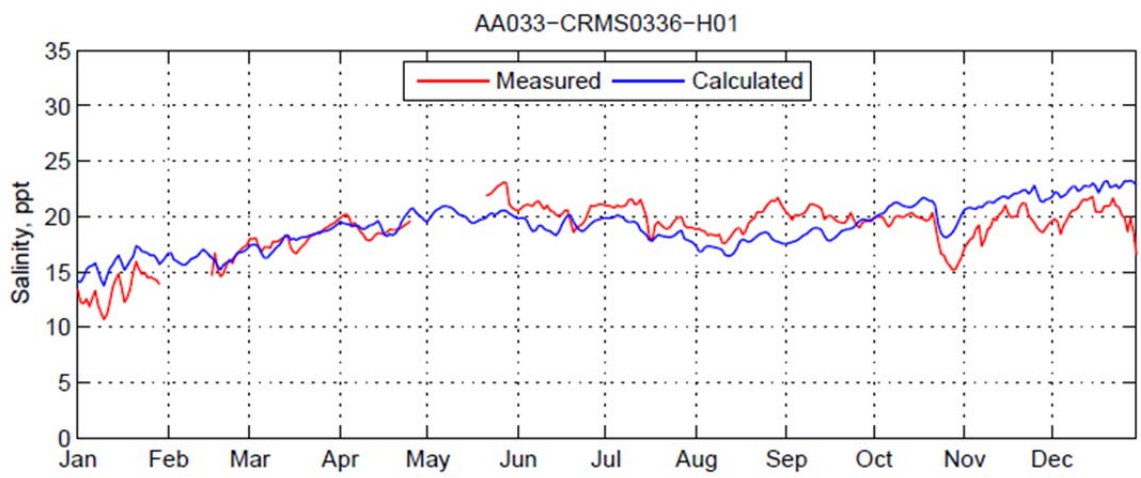

Figure 227 SAL Calibration Results for AA033 in the AA Model

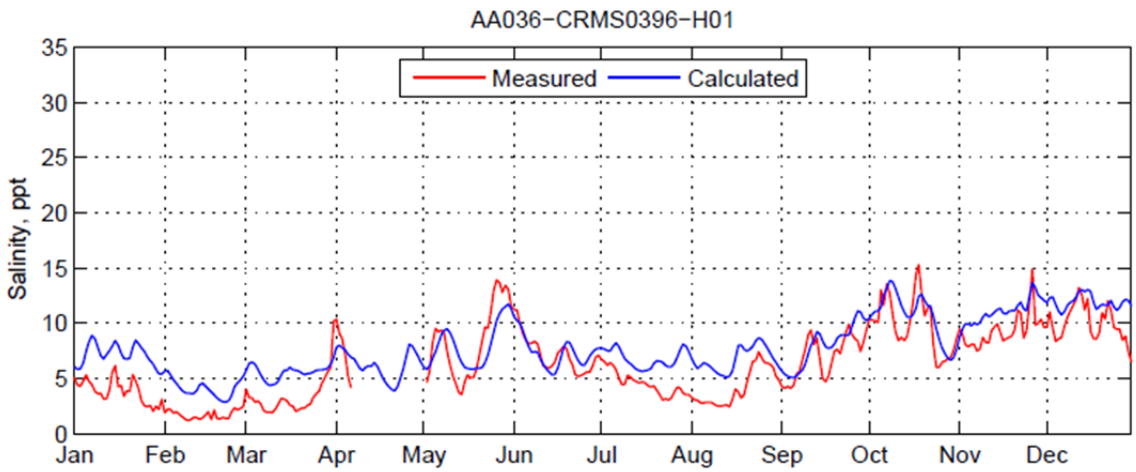

Figure 228 SAL Calibration Results for AA036 in the AA Model

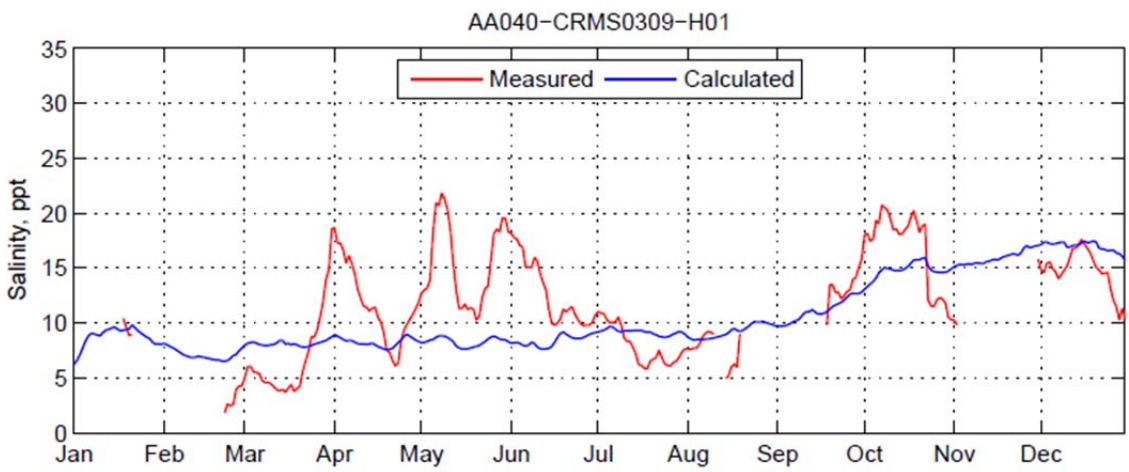

Figure 229 SAL Calibration Results for AA040 in the AA Model

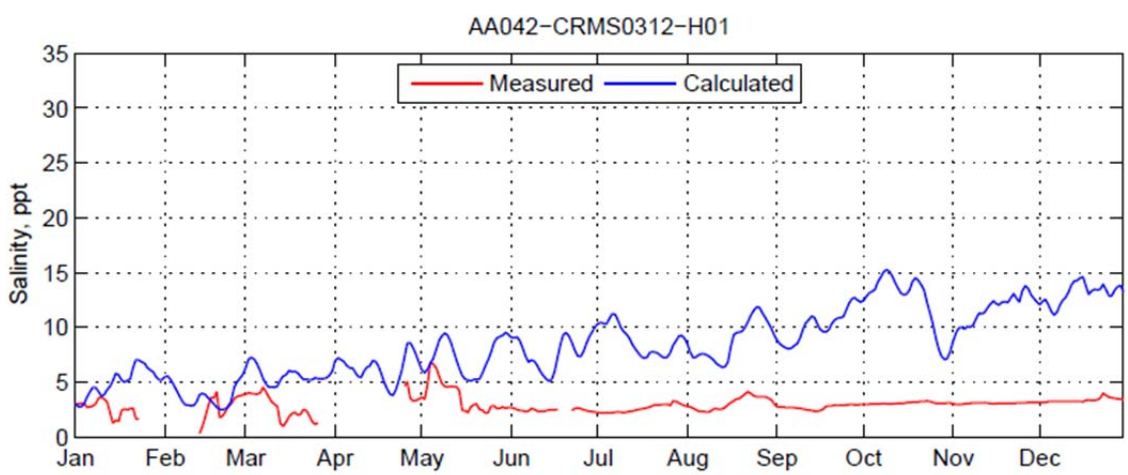

Figure 230 SAL Calibration Results for AA042 in the AA Model

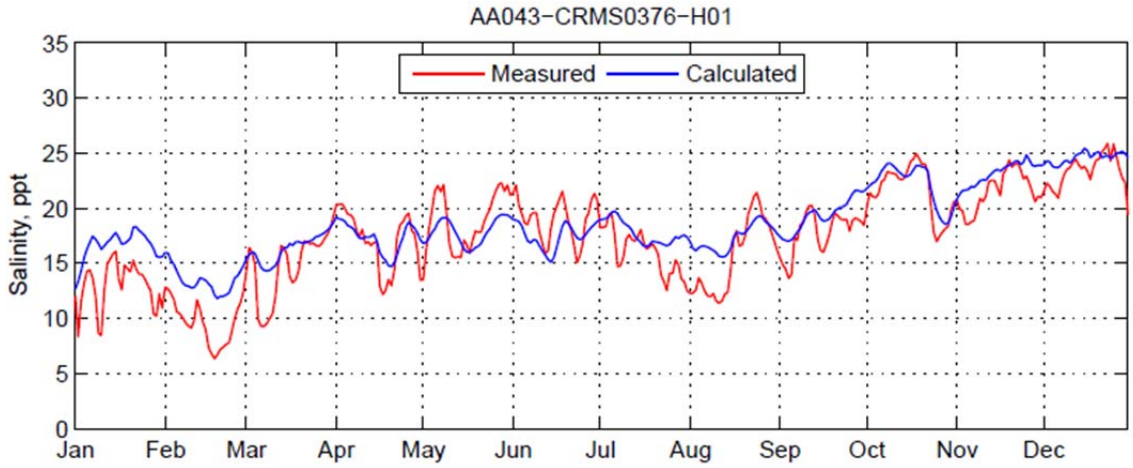

Figure 231 SAL Calibration Results for AA043 in the AA Model

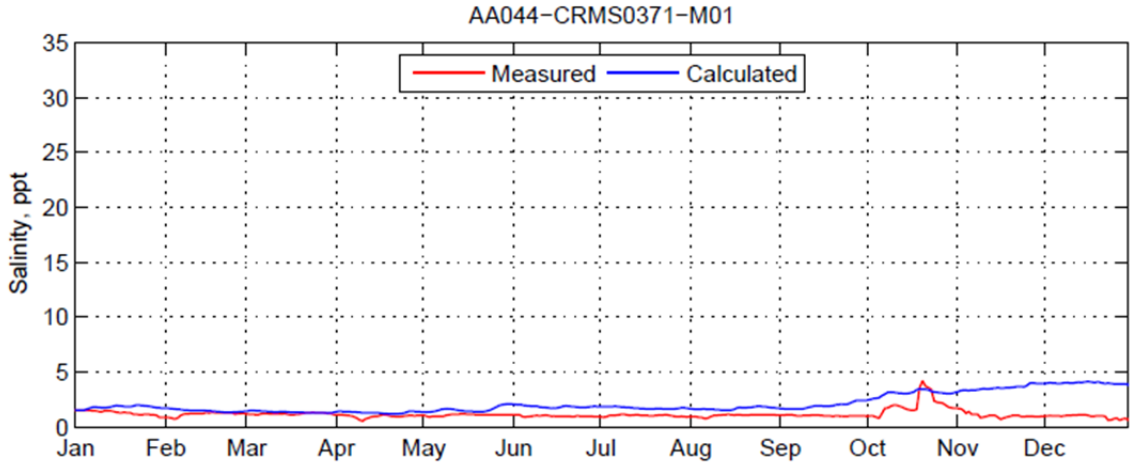

Figure 232 SAL Calibration Results for AA044 in the AA Model

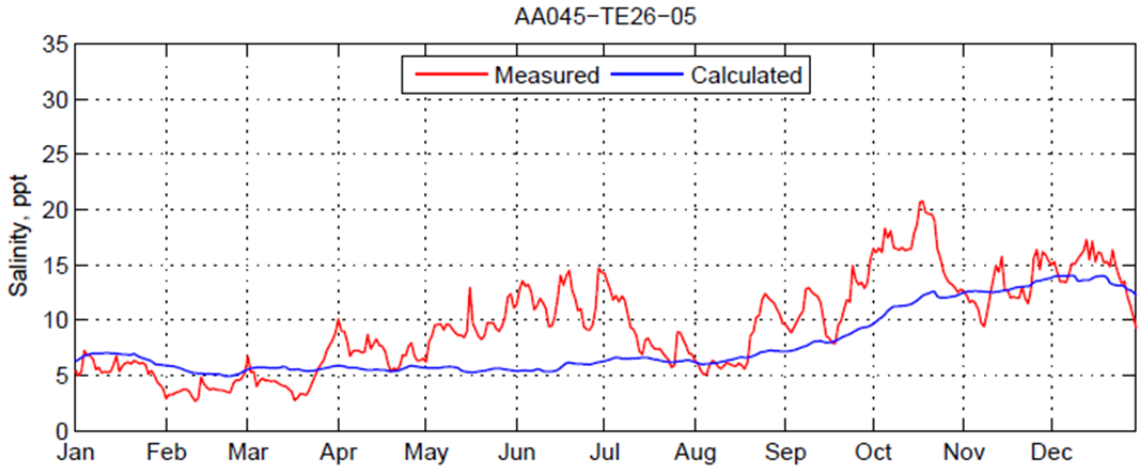

Figure 233 SAL Calibration Results for Lake Chapeau in the AA Model

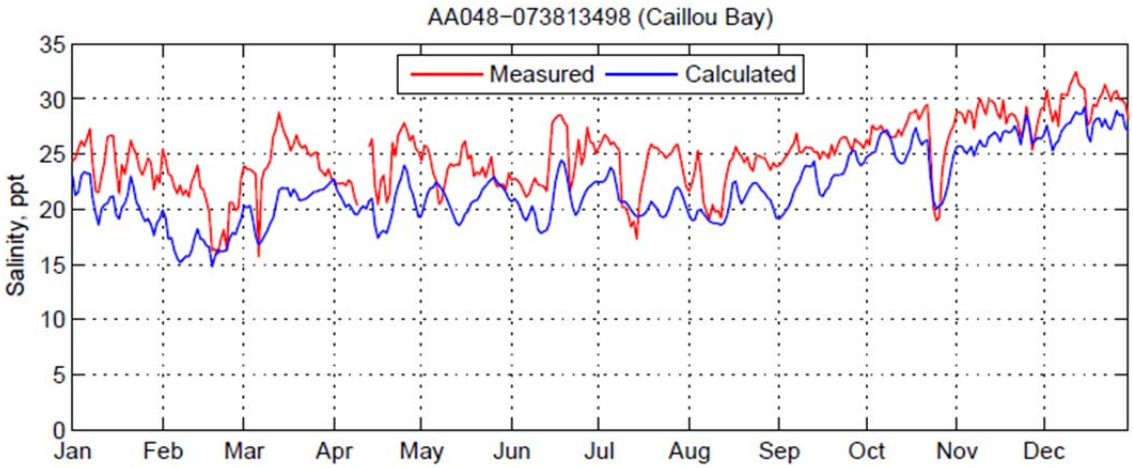

Figure 234 SAL Calibration Results for Caillou Bay in the AA Model

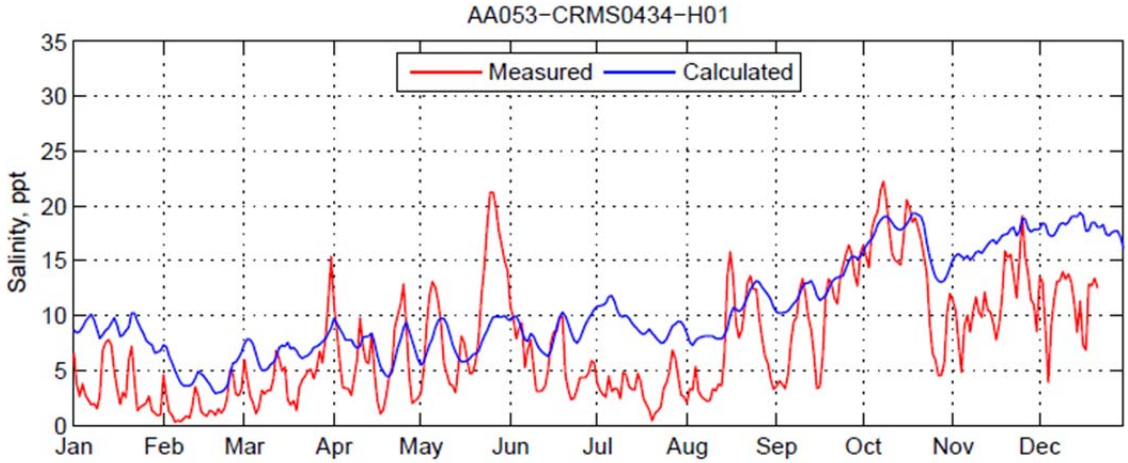

Figure 235 SAL Calibration Results for AA053 in the AA Model

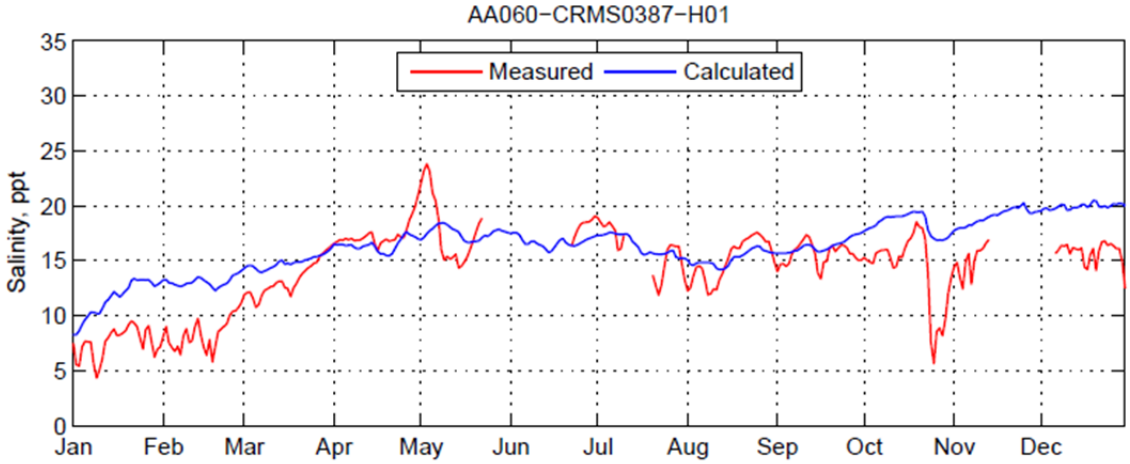

Figure 236 SAL Calibration Results for AA060 in the AA Model

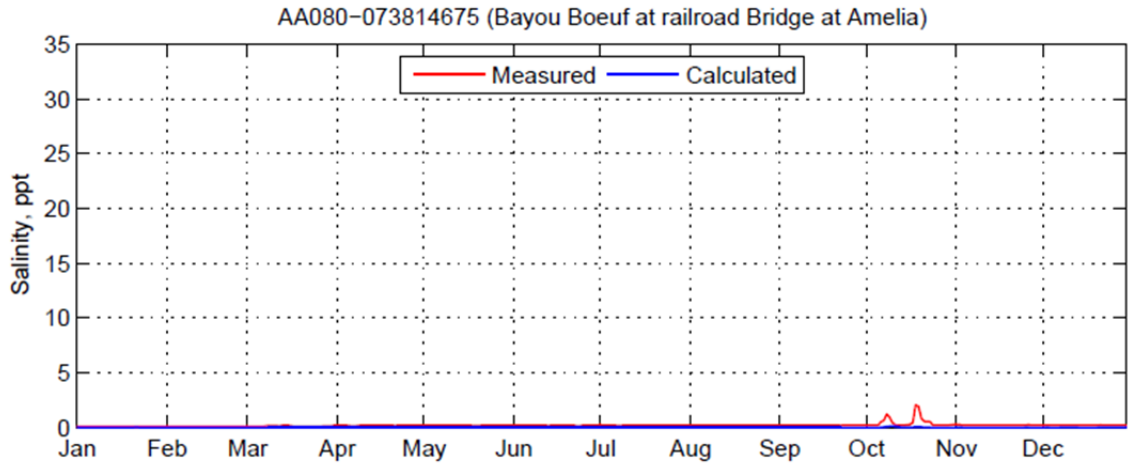

Figure 237 SAL Calibration Results for Bayou Boeuf at Amelia in the AA Model

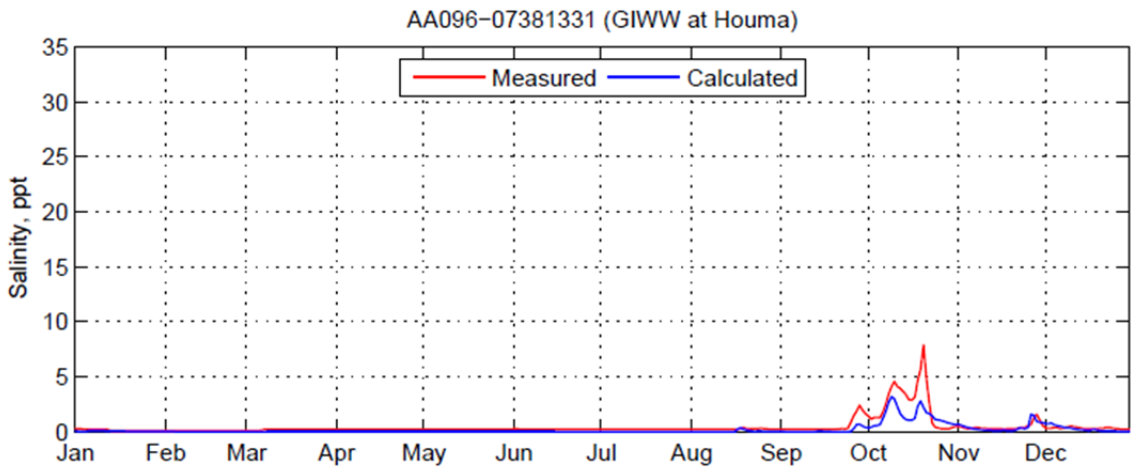

Figure 238 SAL Calibration Results for GIWW at Houma in the AA Model

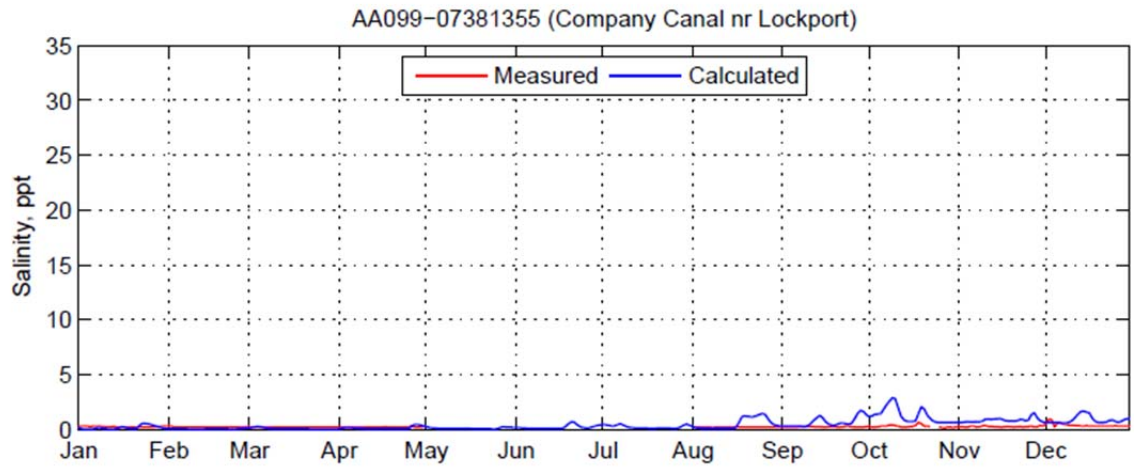

Figure 239 SAL Calibration Results for Company Canal near Lockport in the AA Model

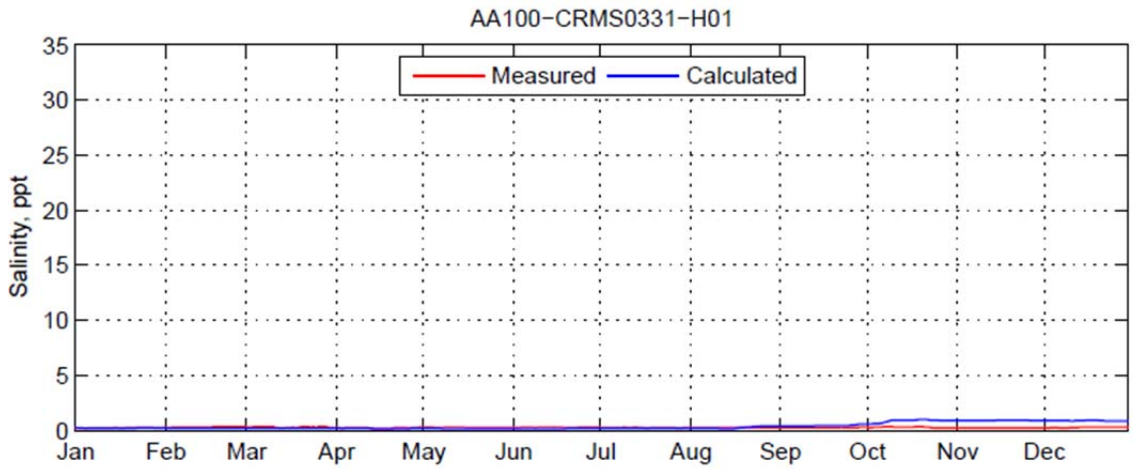

Figure 240 SAL Calibration Results for AA100 in the AA Model

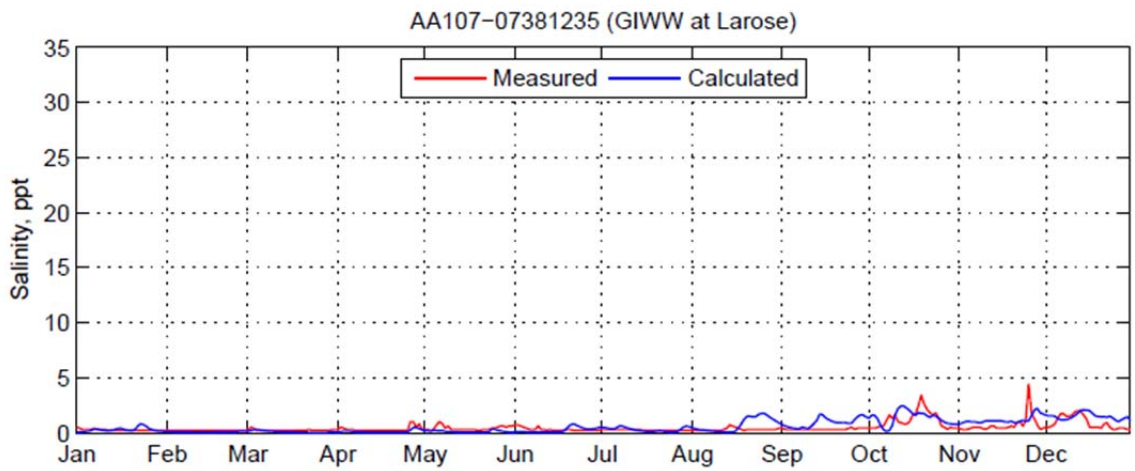

Figure 241 SAL Calibration Results for GIWW at Larose in the AA Model

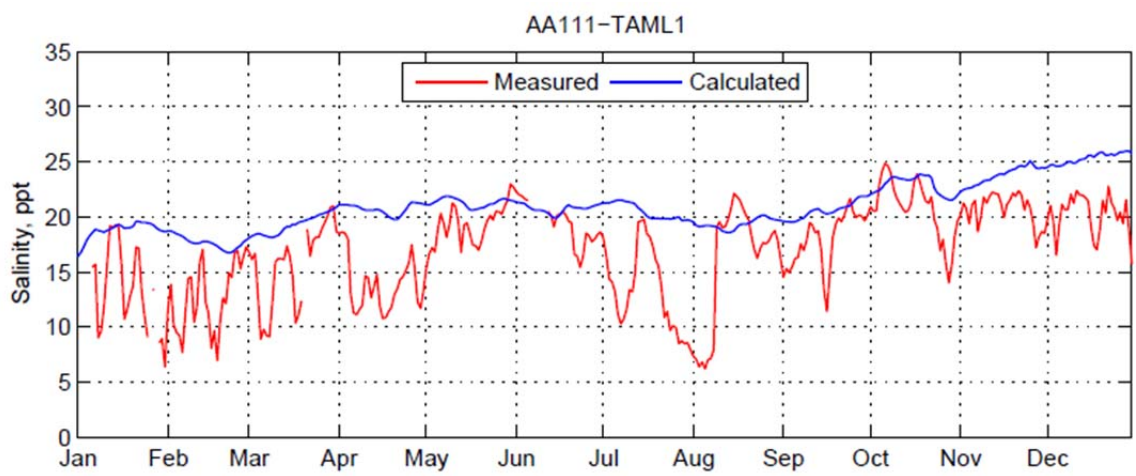

Figure 242 SAL Calibration Results for Tambour Bay in the AA Model

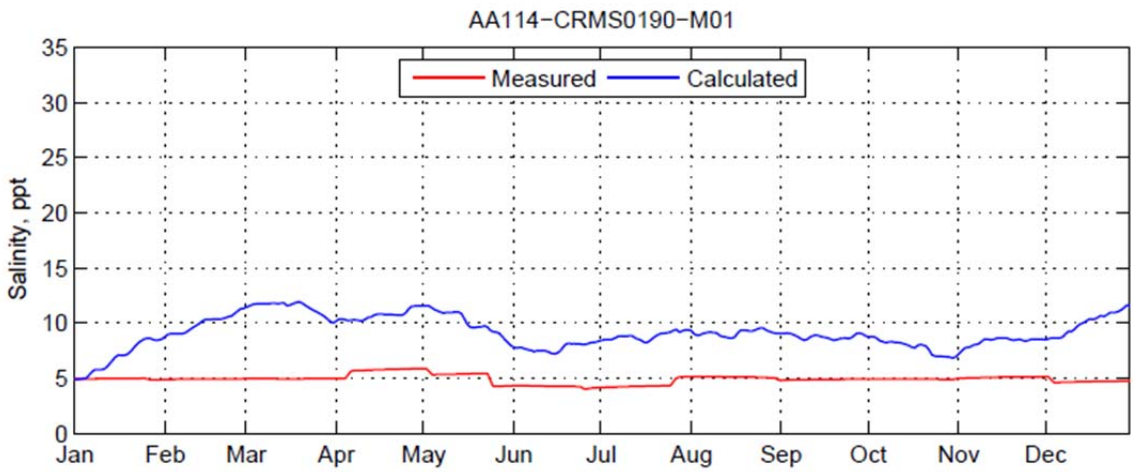

Figure 243 SAL Calibration Results for AA114 in the AA Model

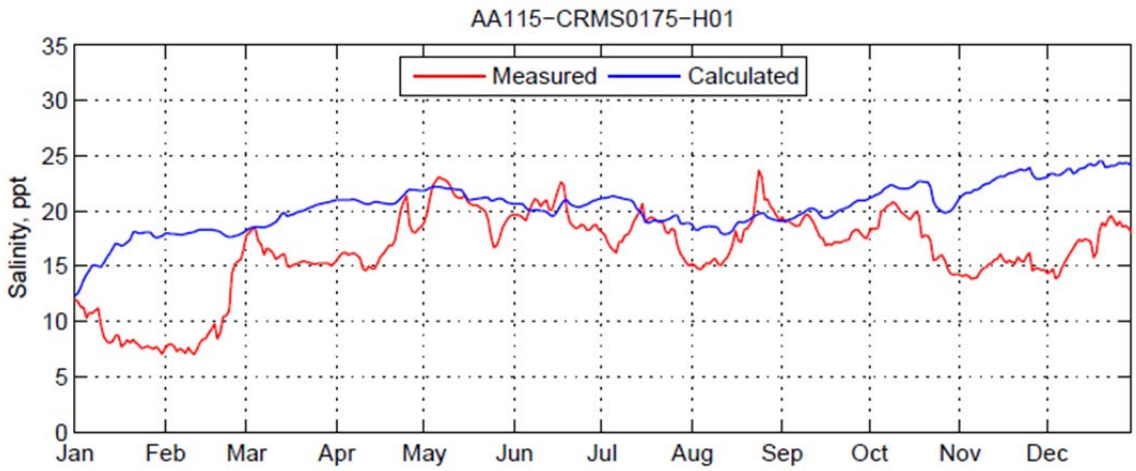

Figure 244 SAL Calibration Results for AA115 in the AA Model

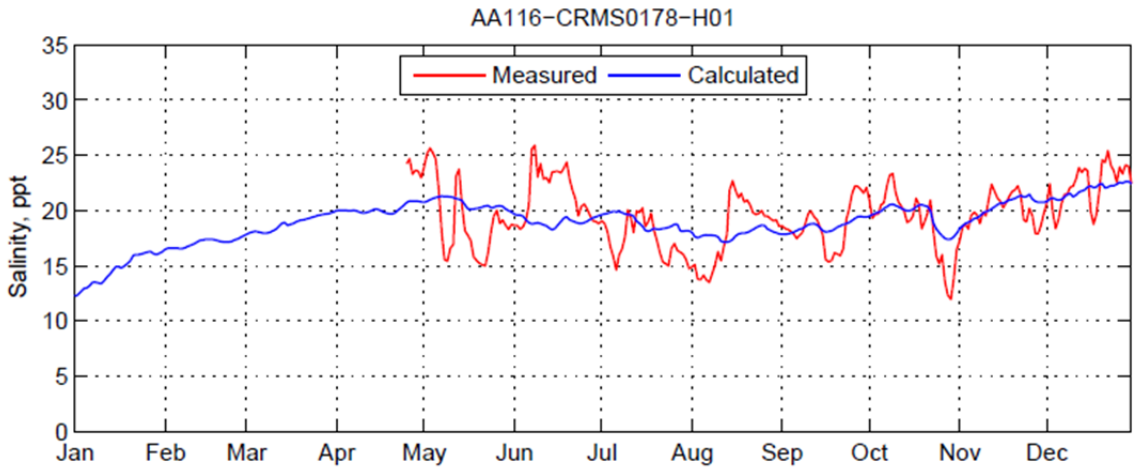

Figure 245 SAL Calibration Results for AA116 in the AA Model

Temperature (TMP)

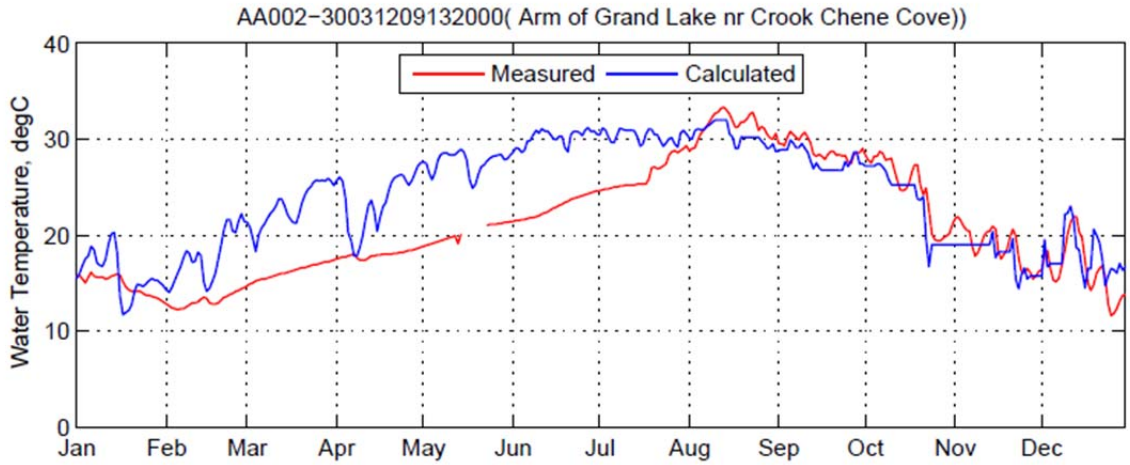

Figure 246 TMP Calibration Results for Grand Lake in the AA Model

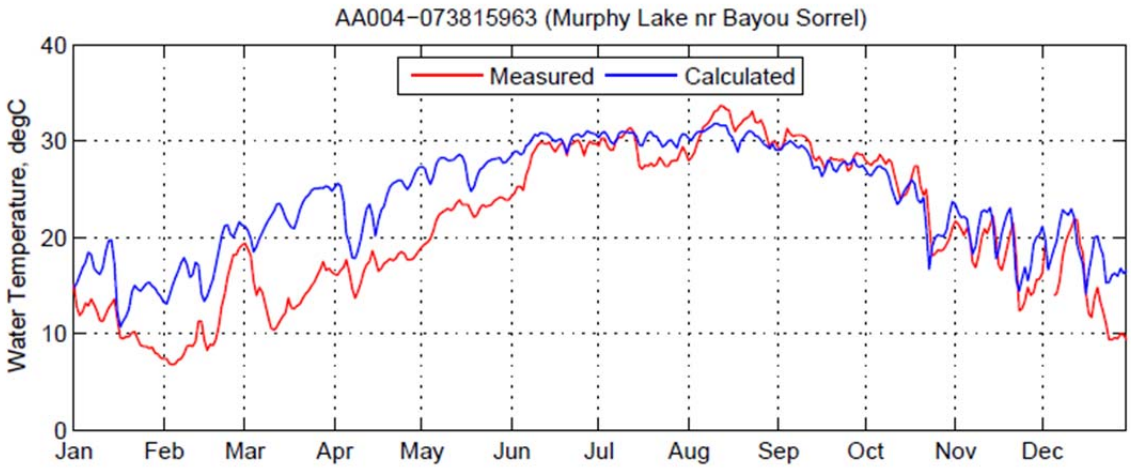

Figure 247 TMP Calibration Results for Murphy Lake in the AA Model

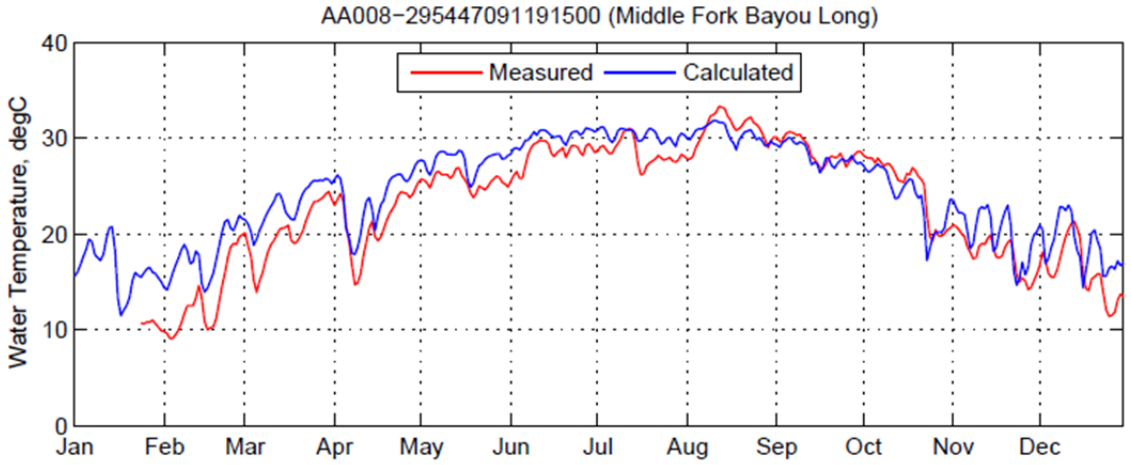

Figure 248 TMP Calibration Results for Bayou Long in the AA Model

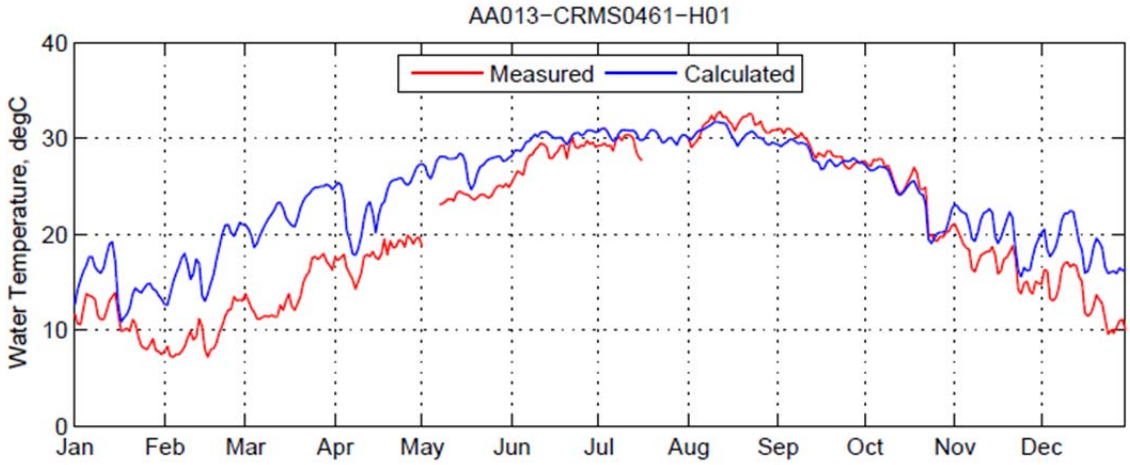

Figure 249 TMP Calibration Results for AA013 in the AA Model

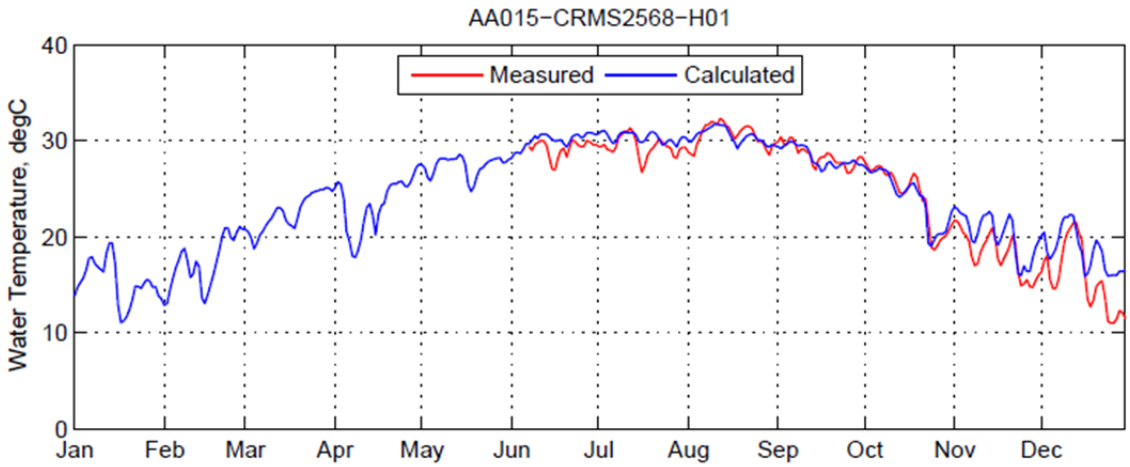

Figure 250 TMP Calibration Results for AA015 in the AA Model

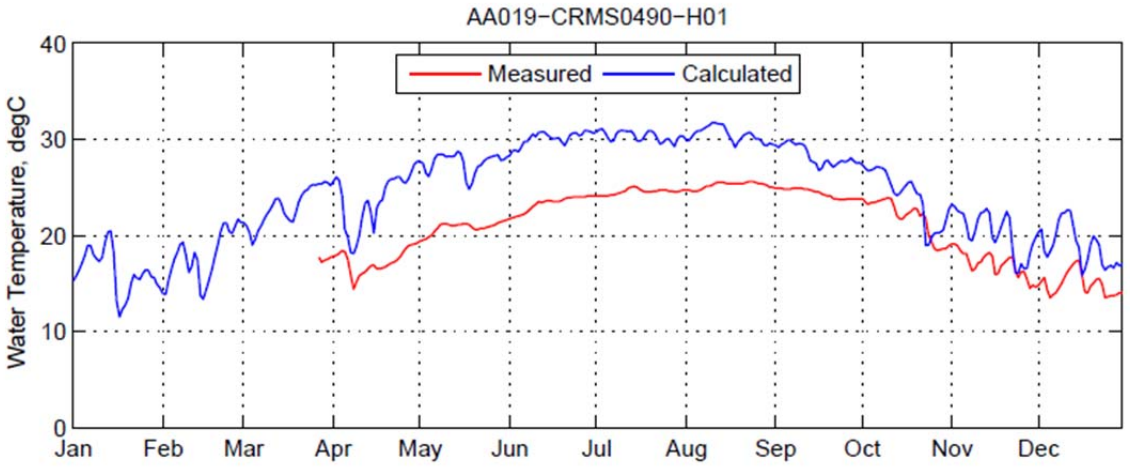

Figure 251 TMP Calibration Results for AA019 in the AA Model

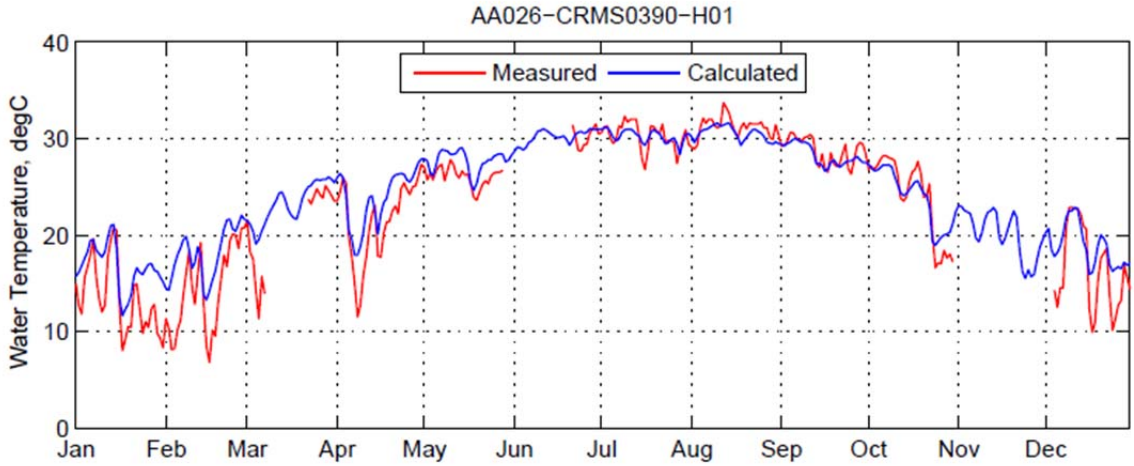

Figure 252 TMP Calibration Results for AA026 in the AA Model

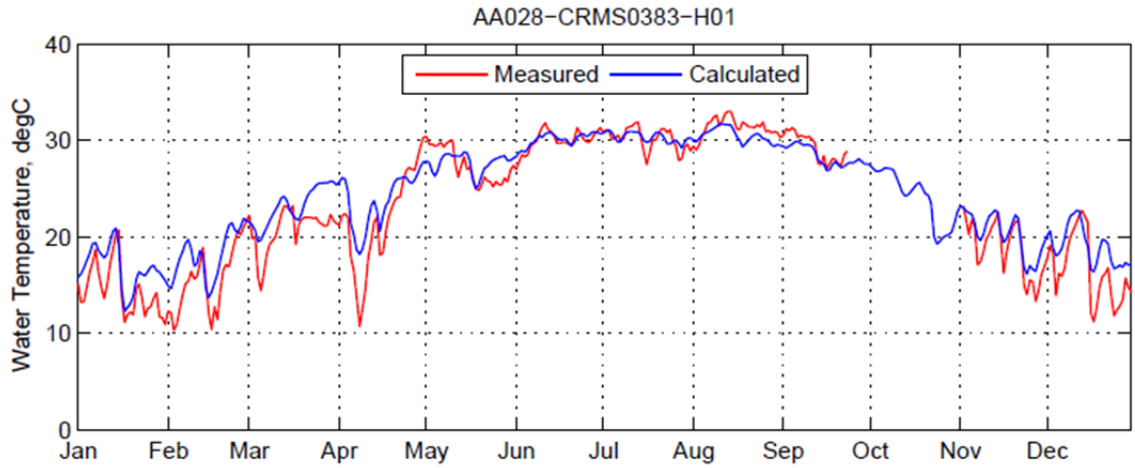

Figure 253 TMP Calibration Results for AA028 in the AA Model

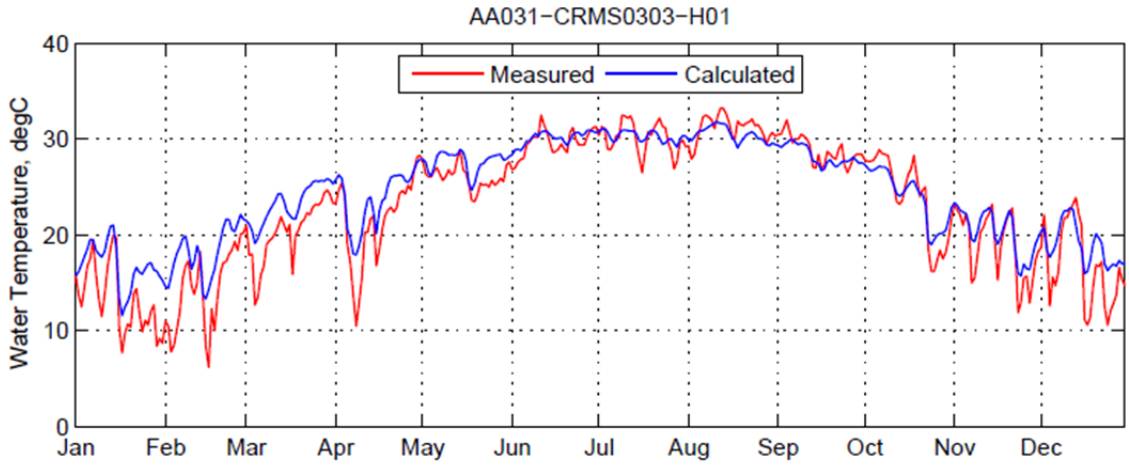

Figure 254 TMP Calibration Results for AA031 in the AA Model

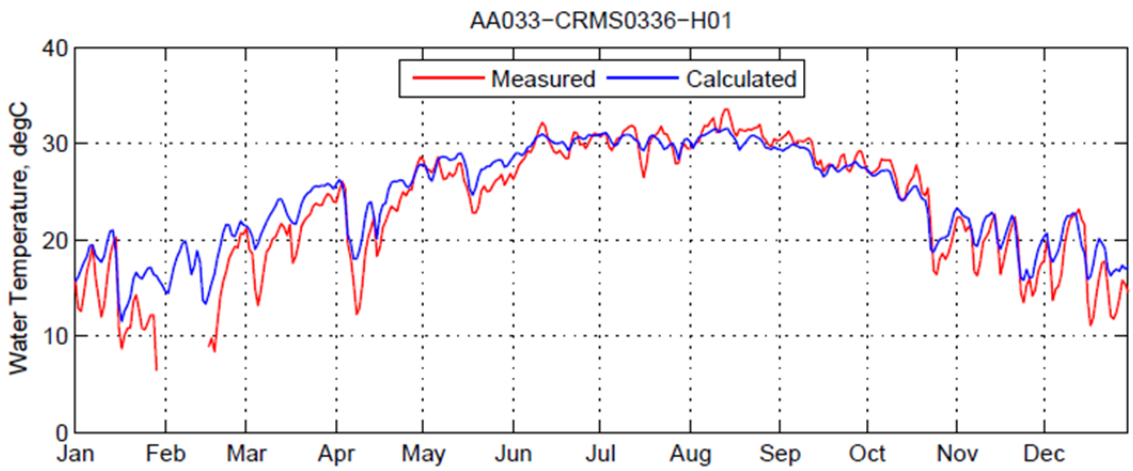

Figure 255 TMP Calibration Results for AA033 in the AA Model

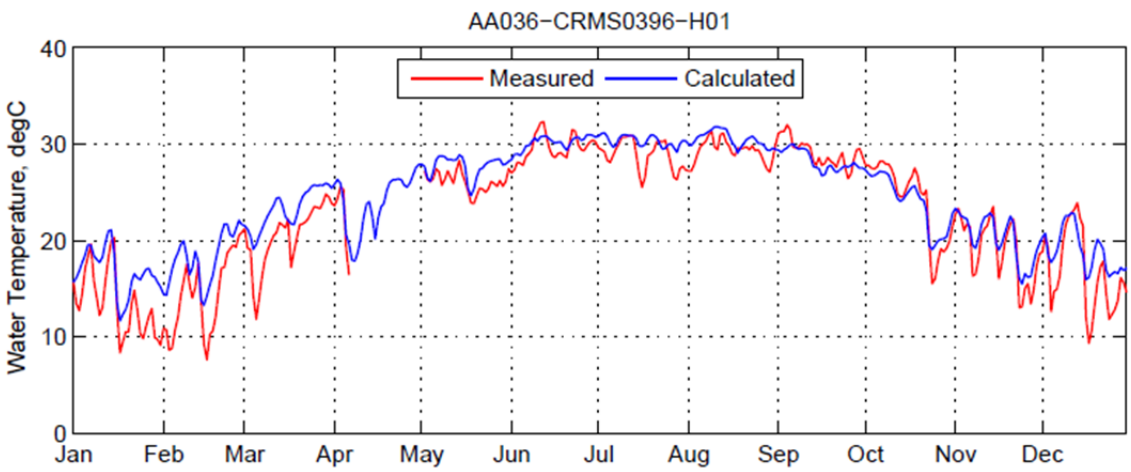

Figure 256 TMP Calibration Results for AA036 in the AA Model

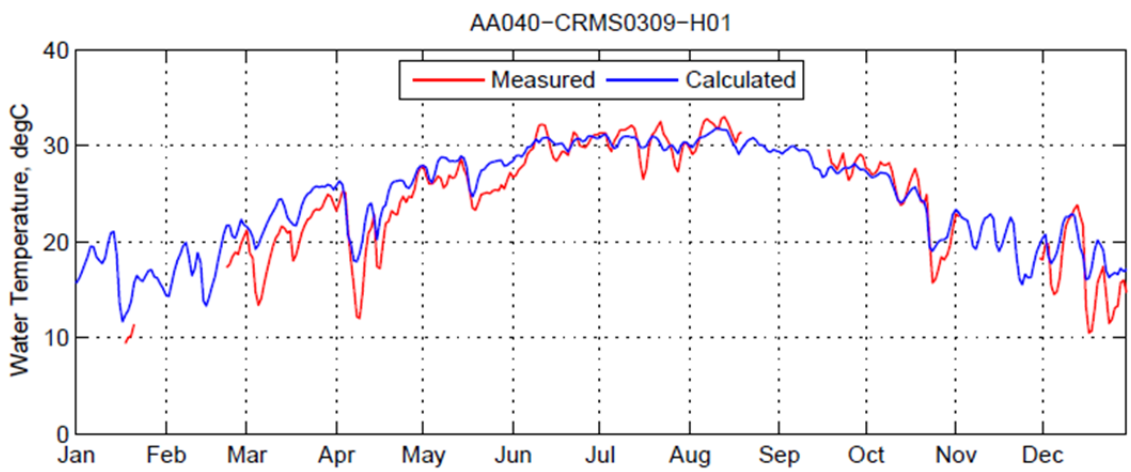

Figure 257 TMP Calibration Results for AA040 in the AA Model

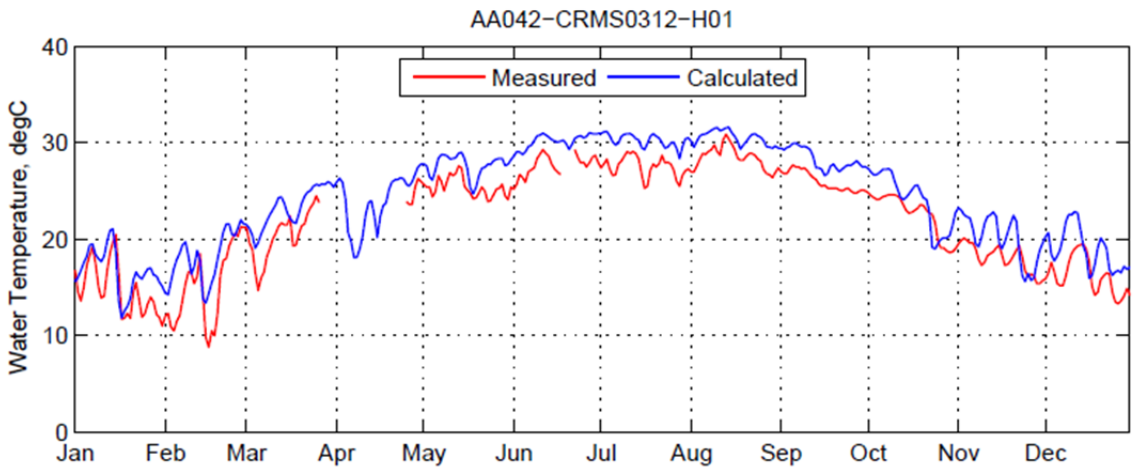

Figure 258 TMP Calibration Results for AA042 in the AA Model

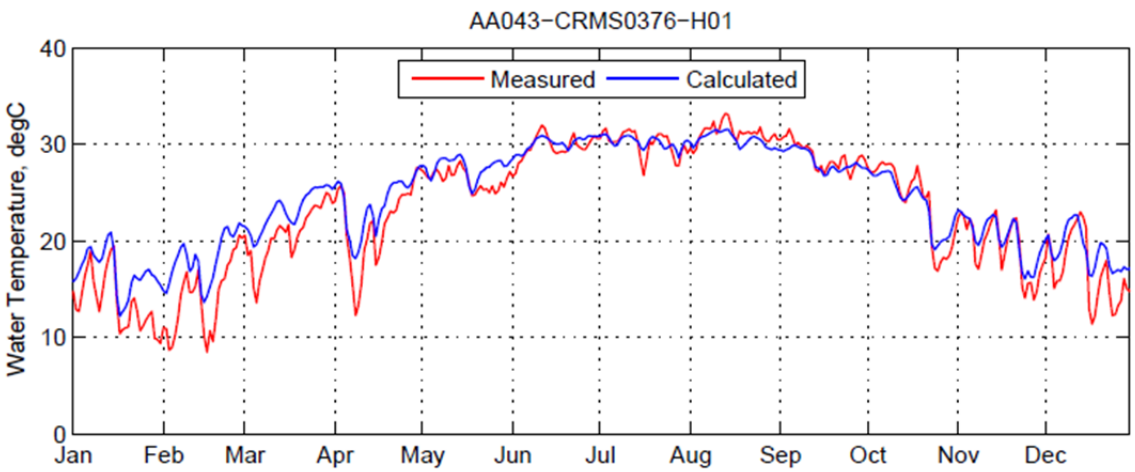

Figure 259 TMP Calibration Results for AA043 in the AA Model

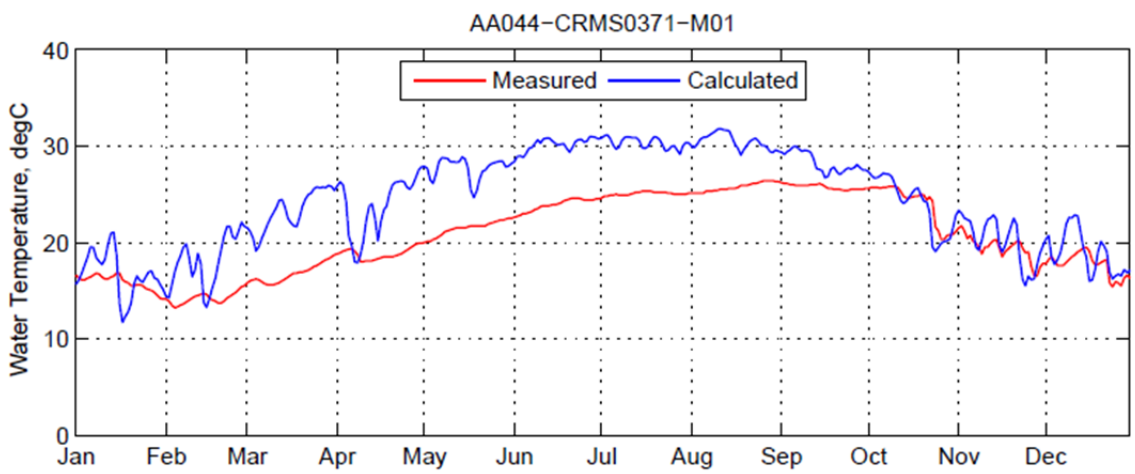

Figure 260 TMP Calibration Results for AA044 in the AA Model

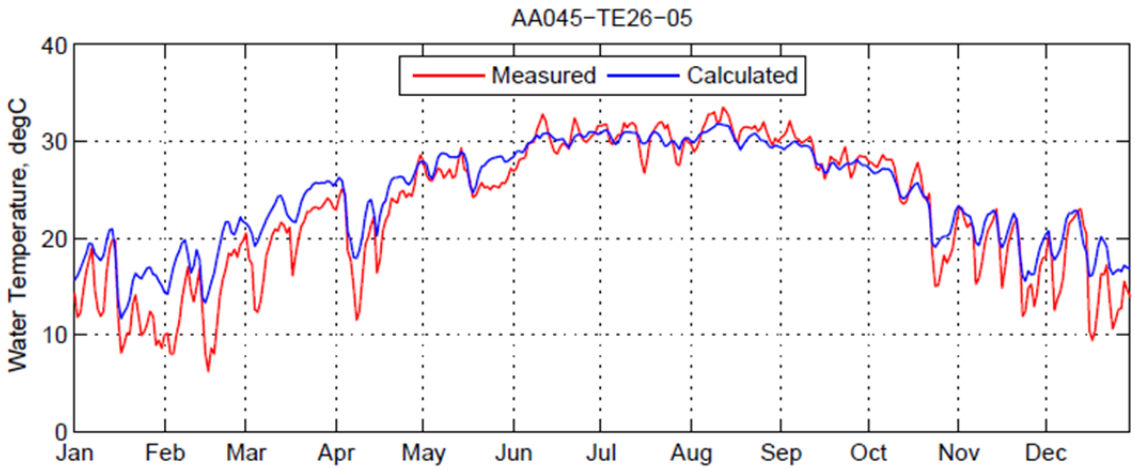

Figure 261 TMP Calibration Results for Lake Chapeau in the AA Model

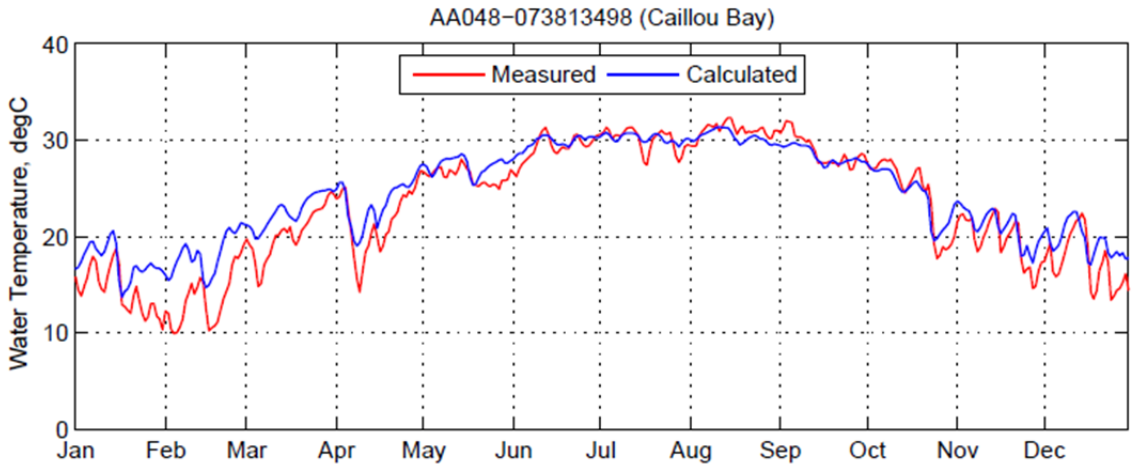

Figure 262 TMP Calibration Results for Caillou Bay in the AA Model

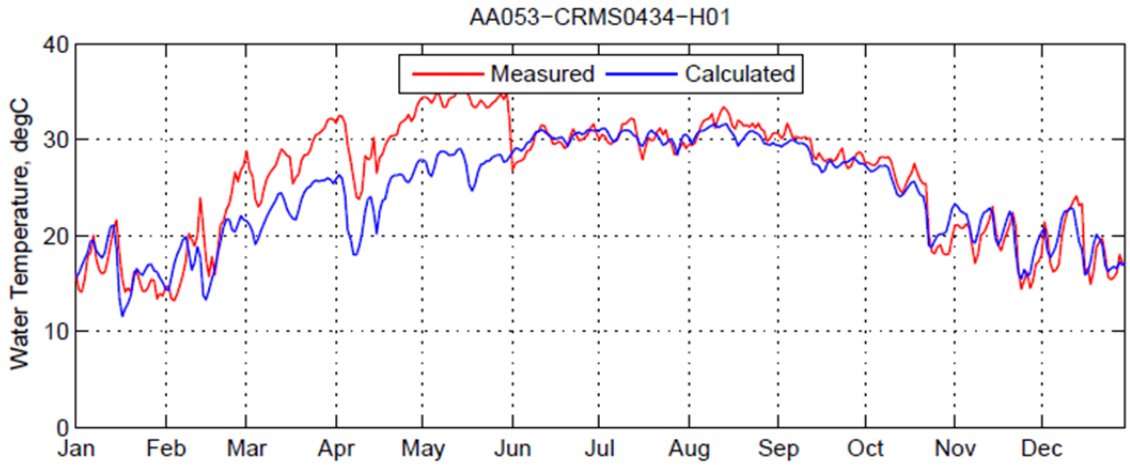

Figure 263 TMP Calibration Results for AA053 in the AA Model

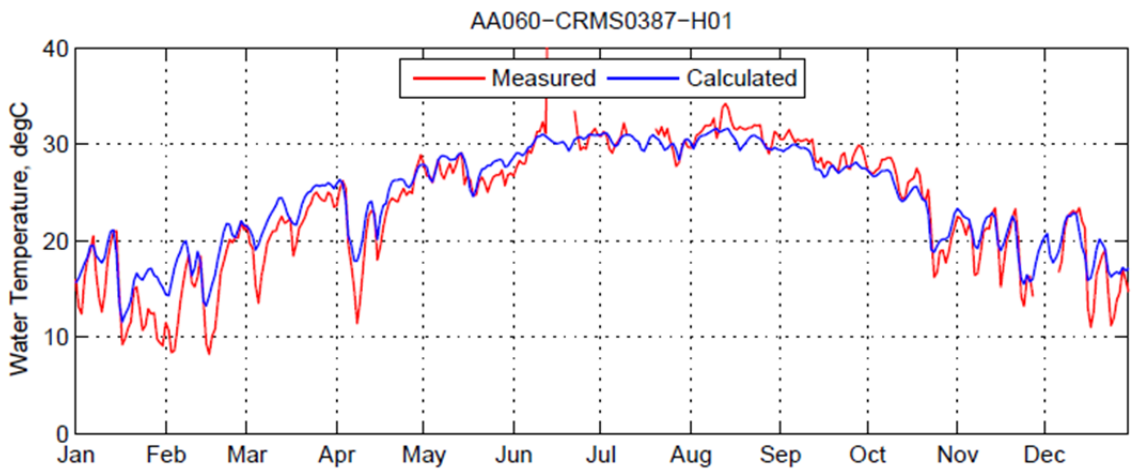

Figure 264 TMP Calibration Results for AA060 in the AA Model

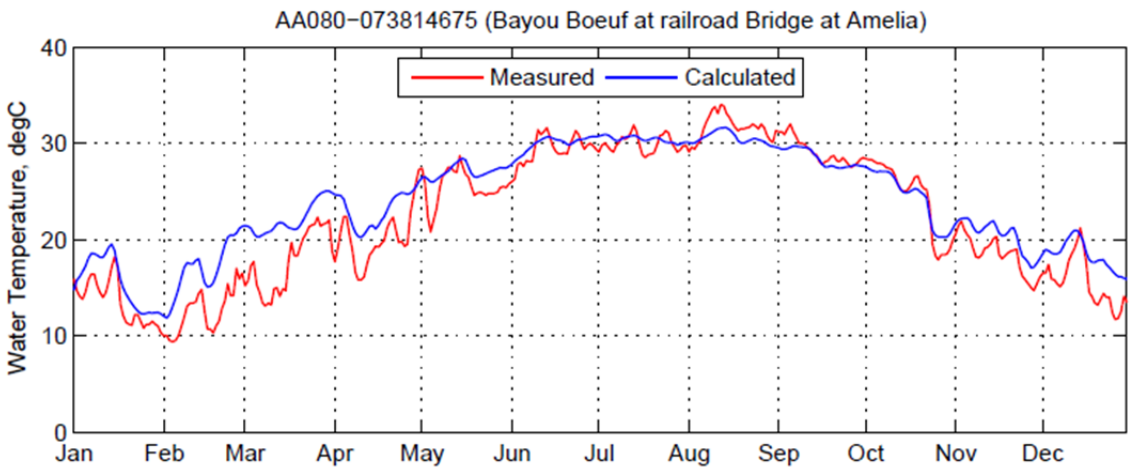

Figure 265 TMP Calibration Results for Bayou Boeuf at Amelia in the AA Model

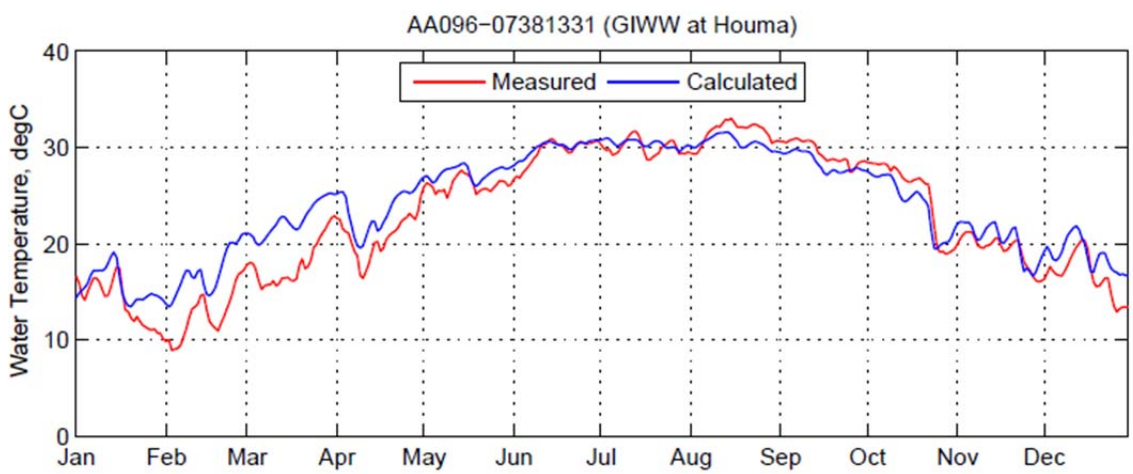

Figure 266 TMP Calibration Results for GIWW at Houma in the AA Model

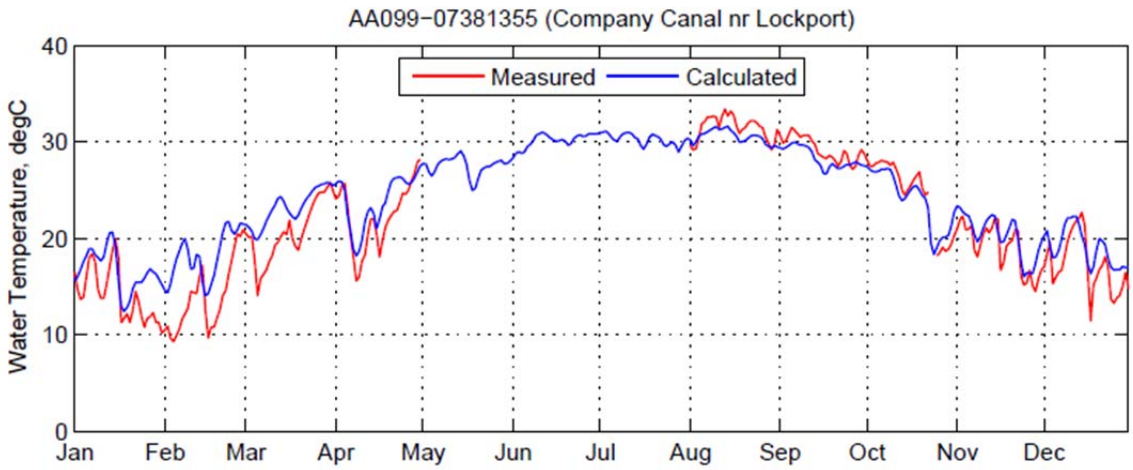

Figure 267 TMP Calibration Results for Company Canal near Lockport in the AA Model

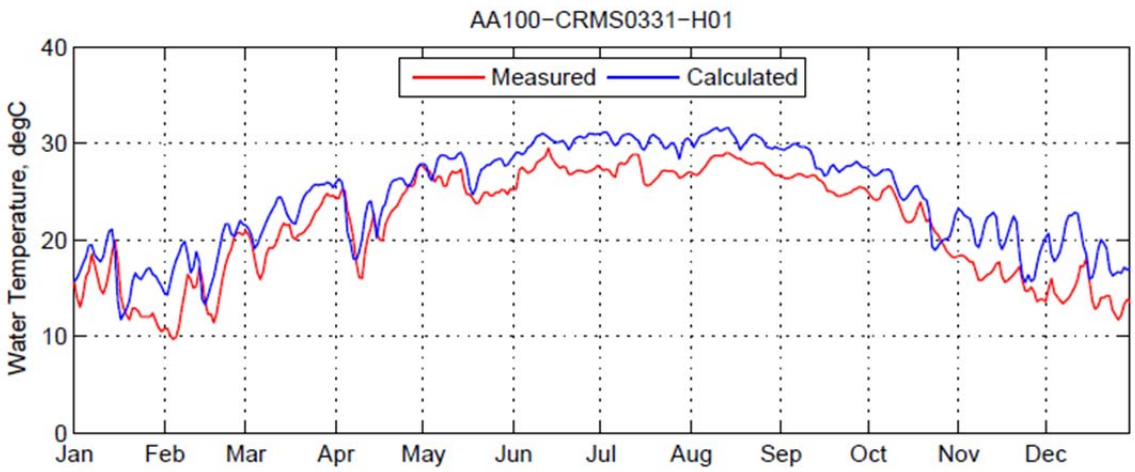

Figure 268 TMP Calibration Results for AA100 in the AA Model

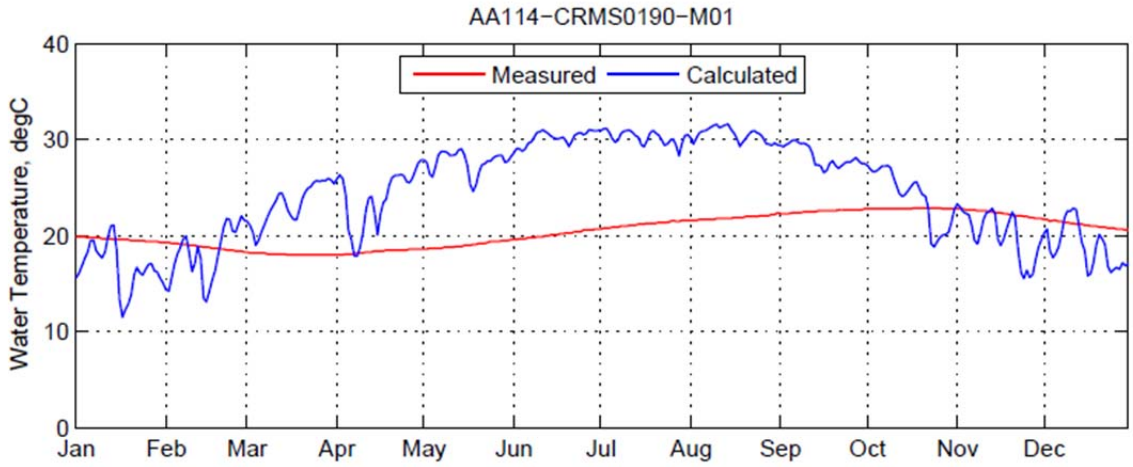

Figure 269 TMP Calibration Results for AA114 in the AA Model

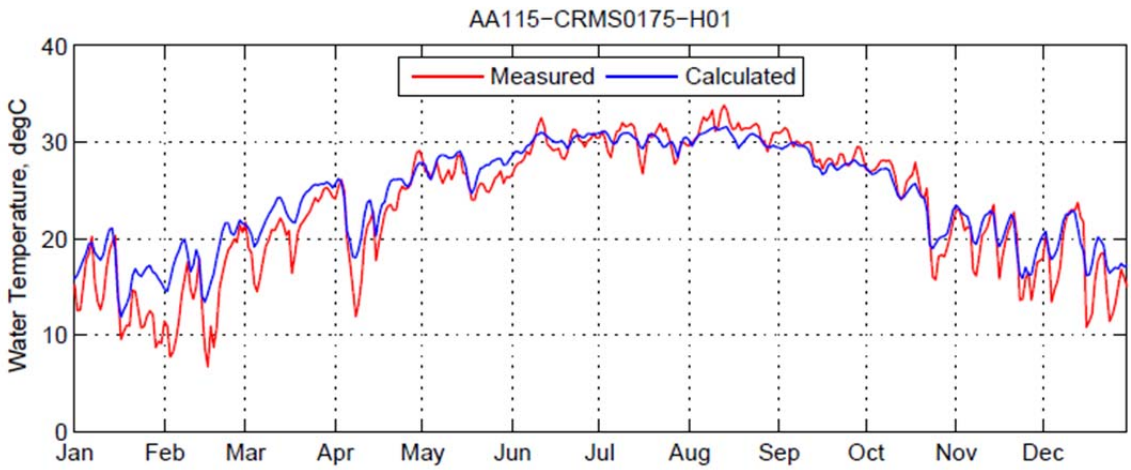

Figure 270 TMP Calibration Results for AA115 in the AA Model

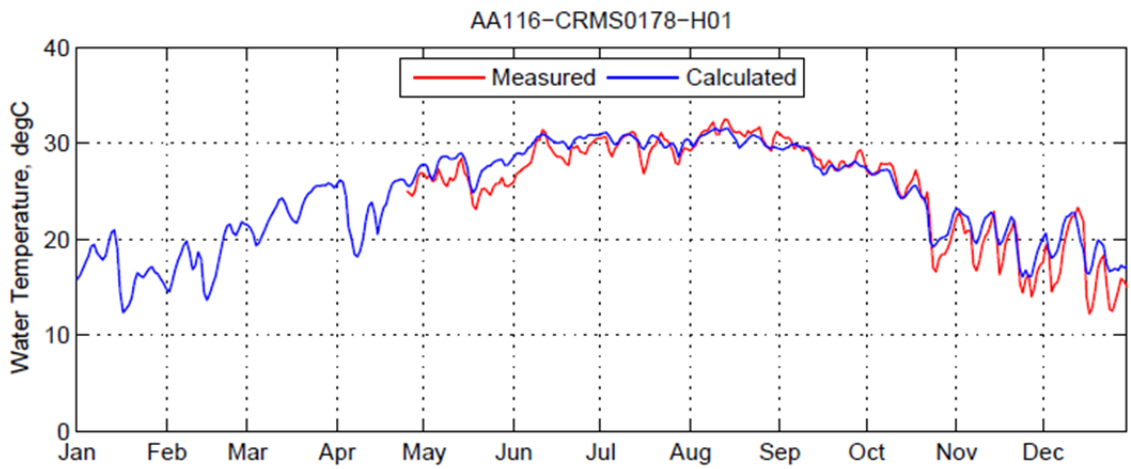

Figure 271 TMP Calibration Results for AA116 in the AA Model

Total Suspended Solids (TSS)

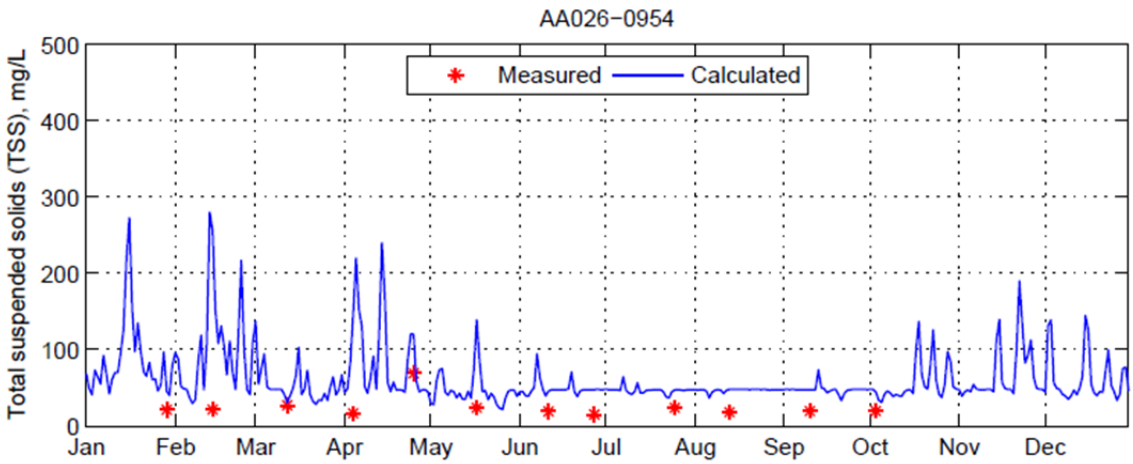

Figure 272 TSS Calibration Results for Lake Boudreaux South of Bayou Chauvin in the AA Model

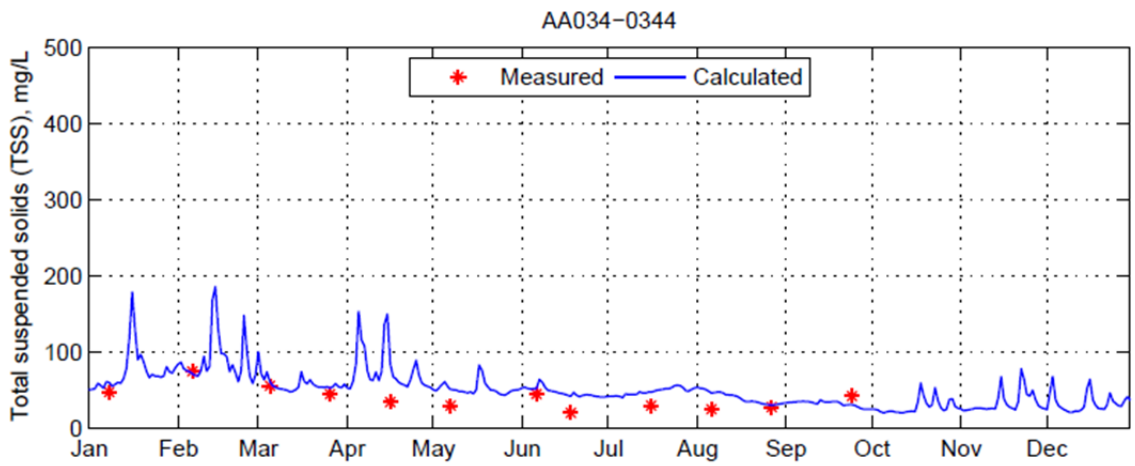

Figure 273 TSS Calibration Results for Houma Navigation Canal South of Houma in the AA Model

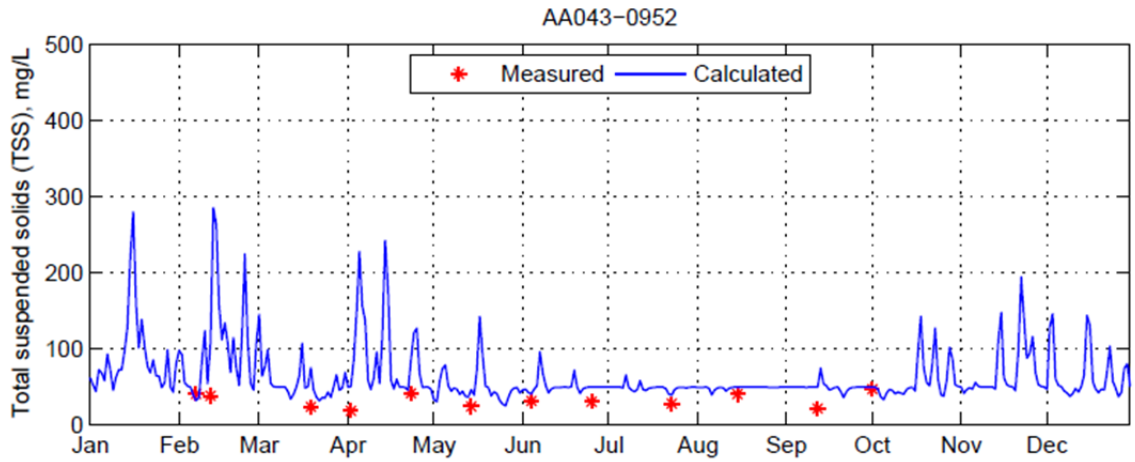

Figure 274 TSS Calibration Results for Houma Navigation Canal Northof Bayou Petit Caillou in the AA Model

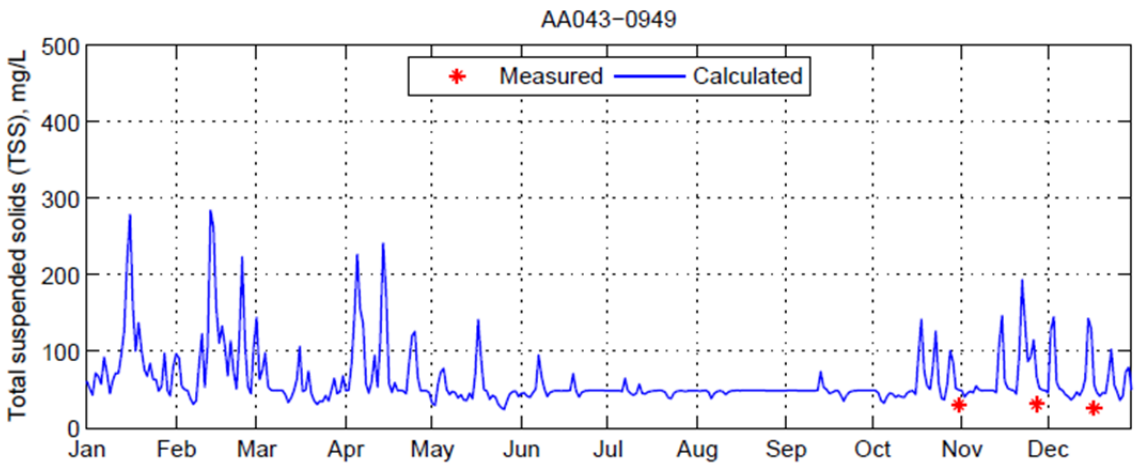

Figure 275 TSS Calibration Results for Bayou Petit Caillou at Cocodrie in the AA Model

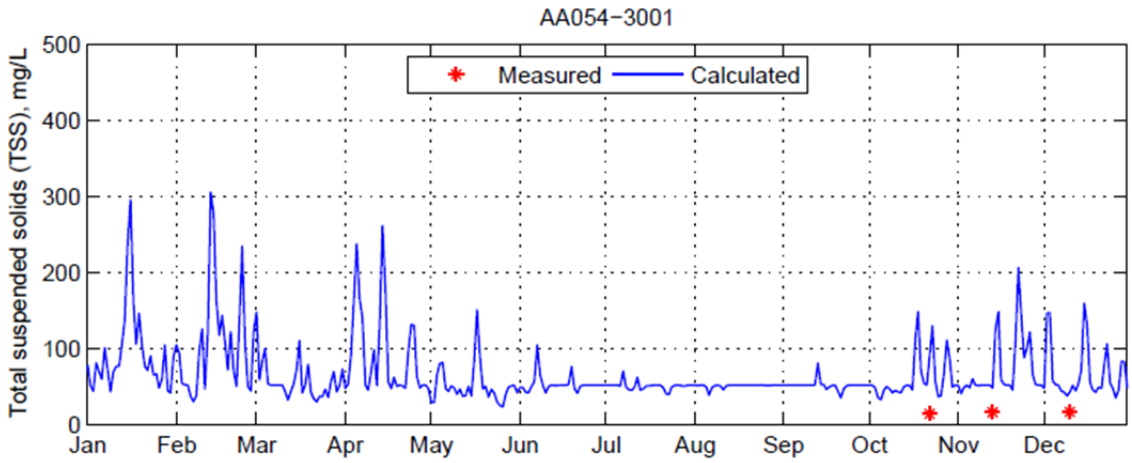

Figure 276 TSS Calibration Results for Bayou Terrebonne near Lapeyrouse in the AA Model

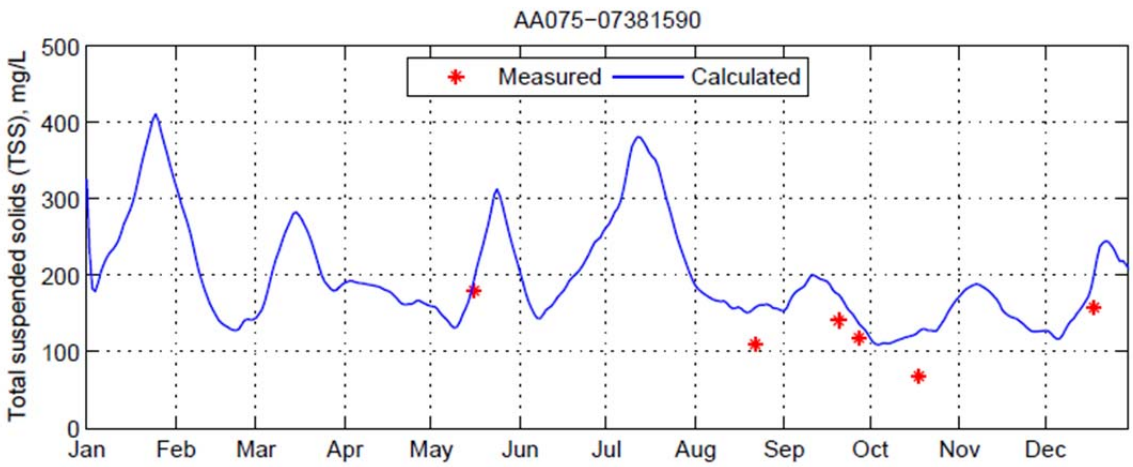

Figure 277 TSS Calibration Results for Wax Lake Outlet at Calumet in the AA Model

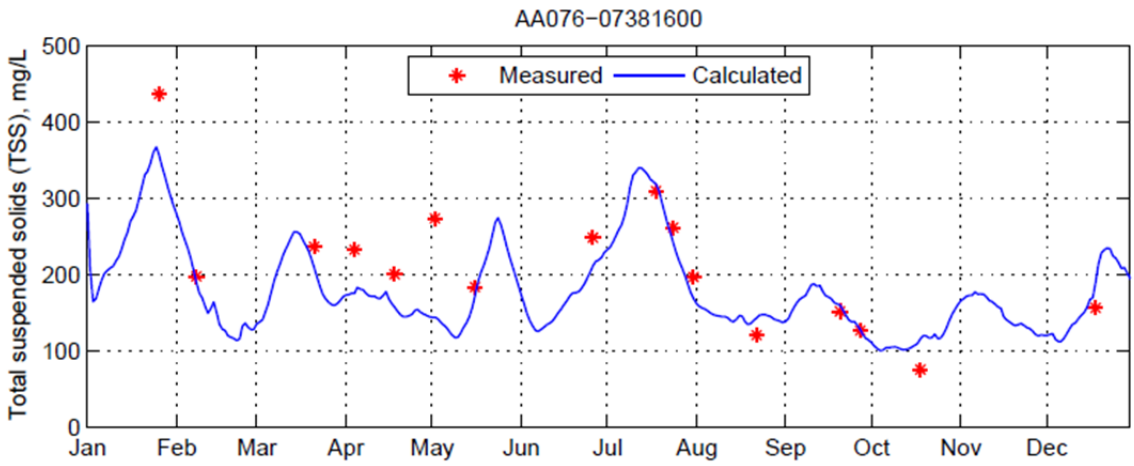

Figure 278 TSS Calibration Results for Lower Atchafalaya River at Morgan City in the AA Model

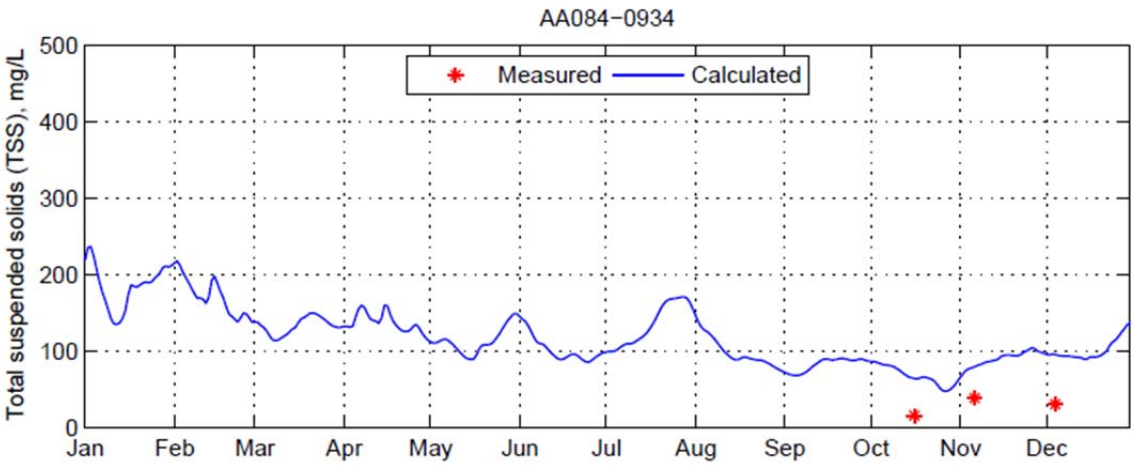

Figure 279 TSS Calibration Results for ICWW at Venvirotek Dock in the AA Model

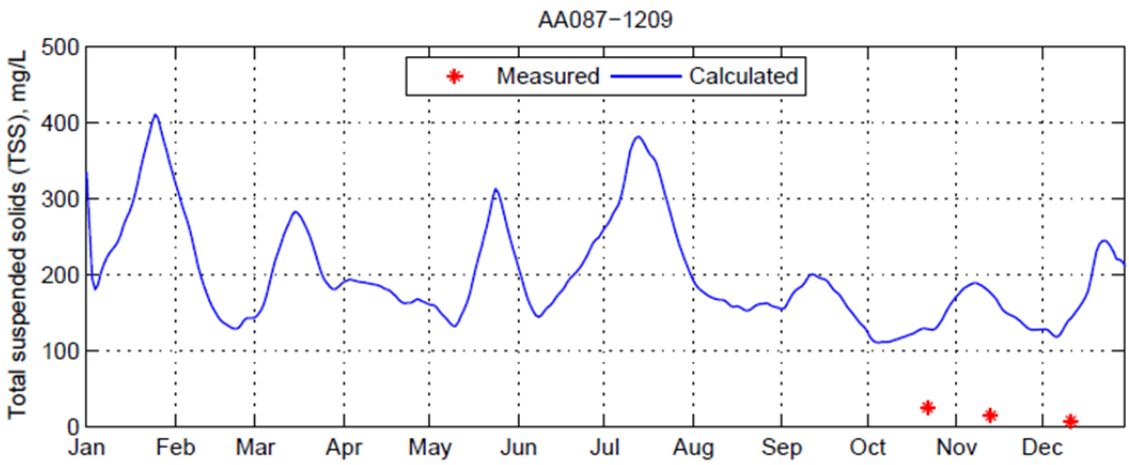

Figure 280 TSS Calibration Results for Bayou Blue at North End Pumping Station in the AA Model

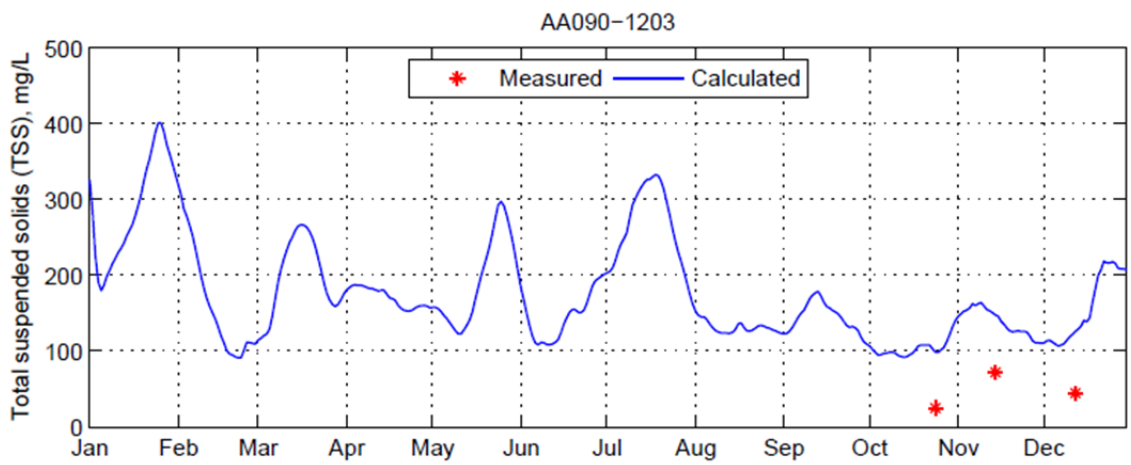

Figure 281 TSS Calibration Results for ICWW South of Patterson in the AA Model

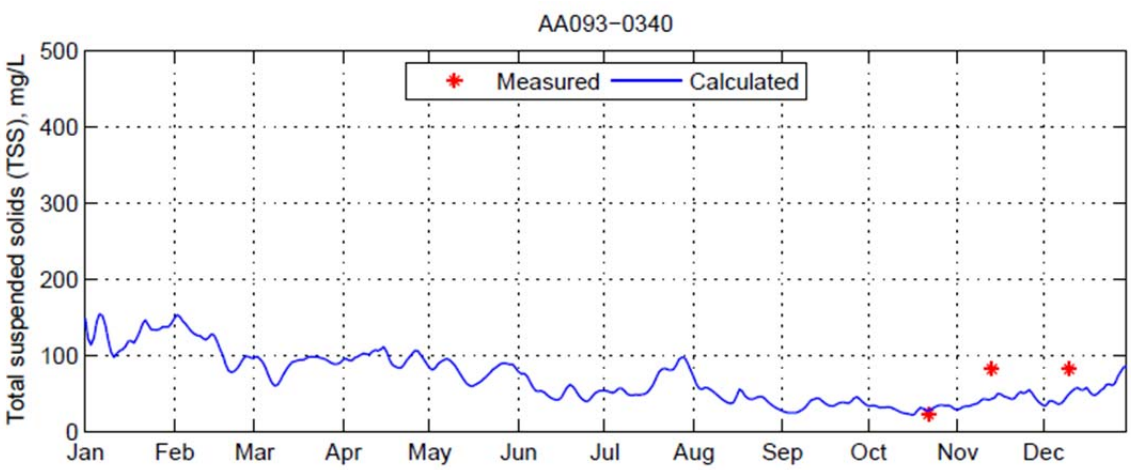

Figure 282 TSS Calibration Results for ICWW East of Houma in the AA Model

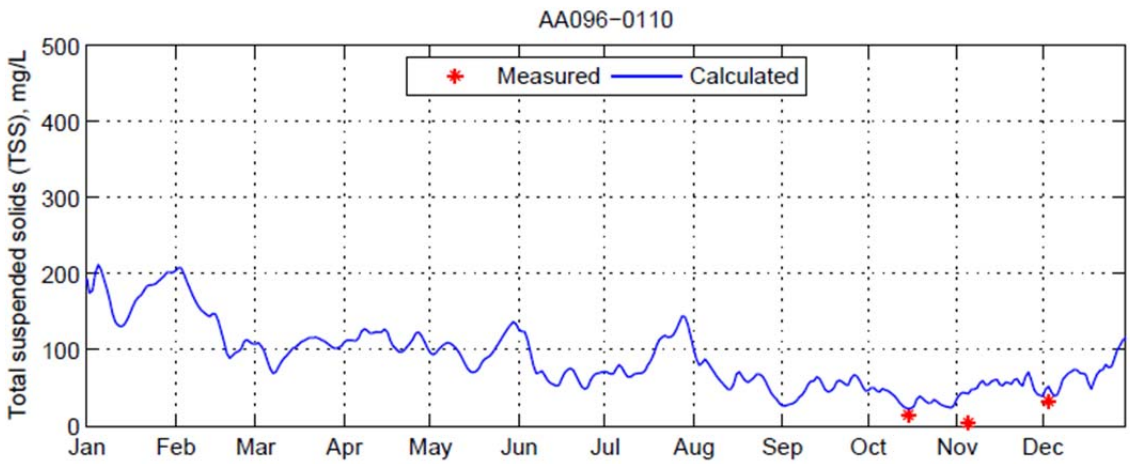

Figure 283 TSS Calibration Results for Bayou Terrebonne at Houma in the AA Model

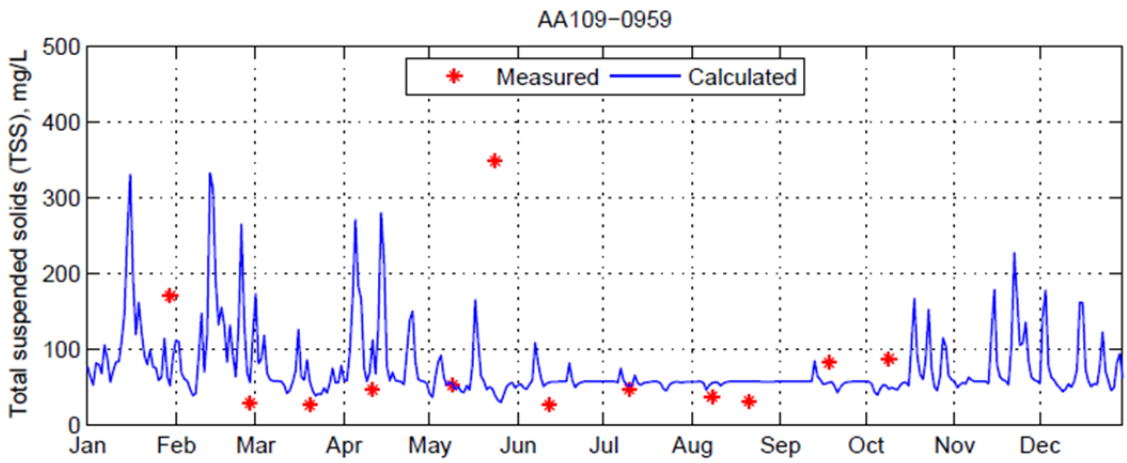

Figure 284 TSS Calibration Results for Timbalier Bay South of Devils Island in the AA Model

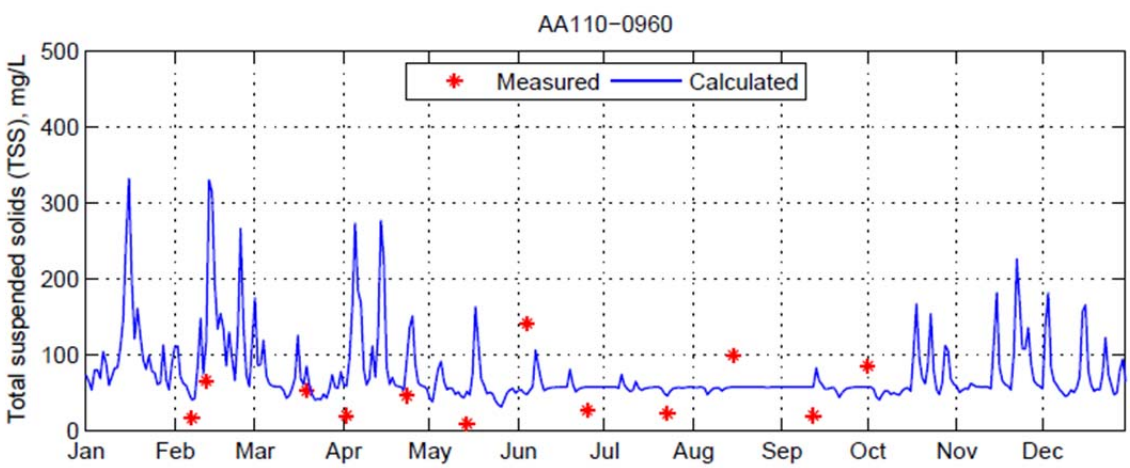

Figure 285 TSS Calibration Results for Lake Barre West of Cocodrie in the AA Model

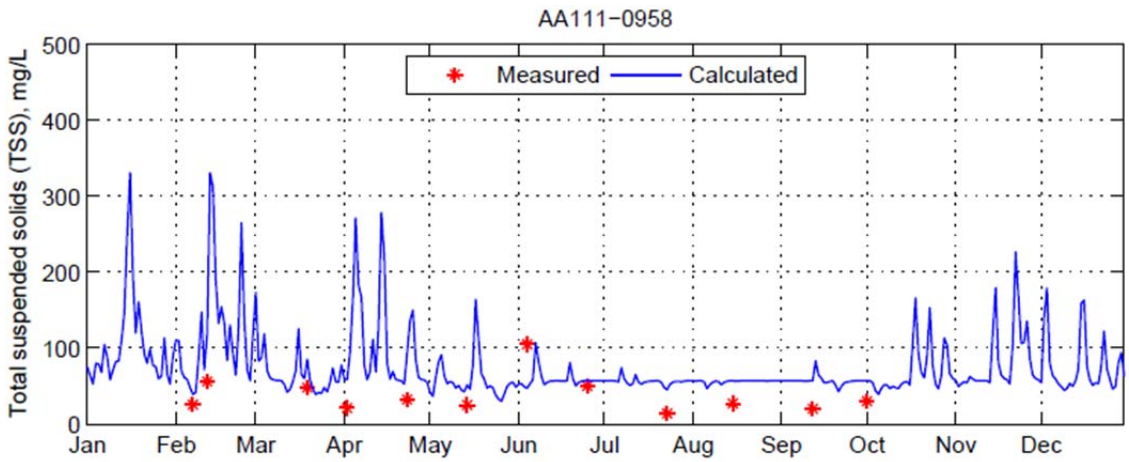

Figure 286 TSS Calibration Results for Terrebonne Bay Southeast of Cocodrie in the AA Model

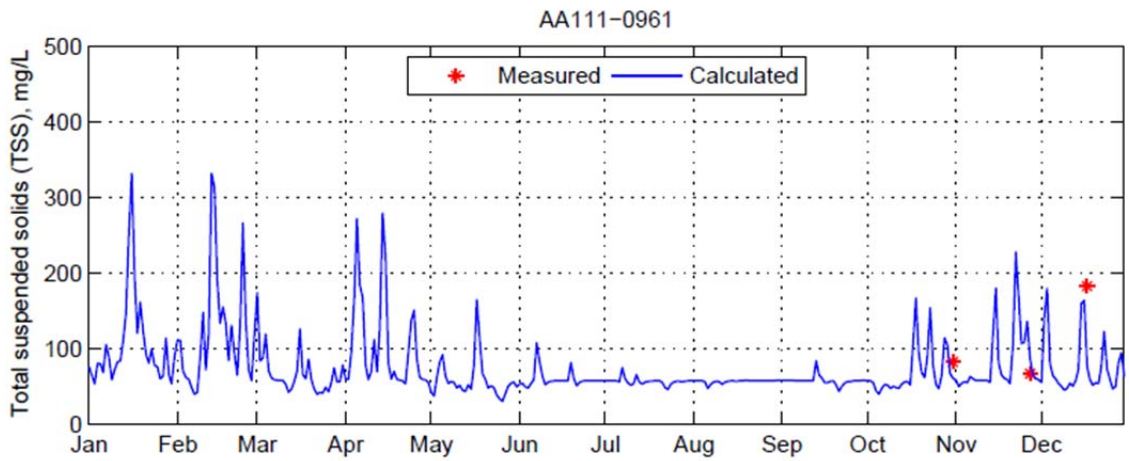

Figure 287 TSS Calibration Results for Lake Pelto South of Cocodrie in the AA Model

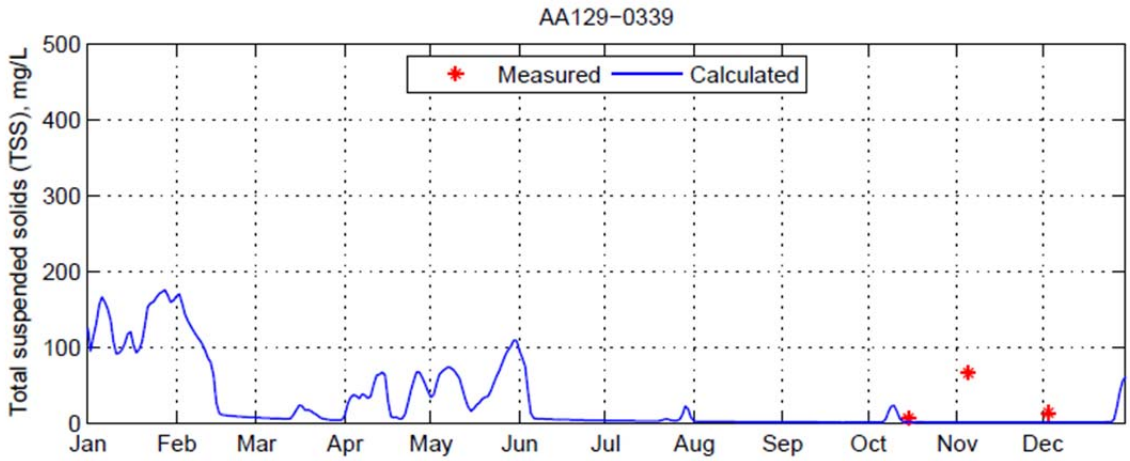

Figure 288 TSS Calibration Results for Bayou Black West of Houma in the AA Model

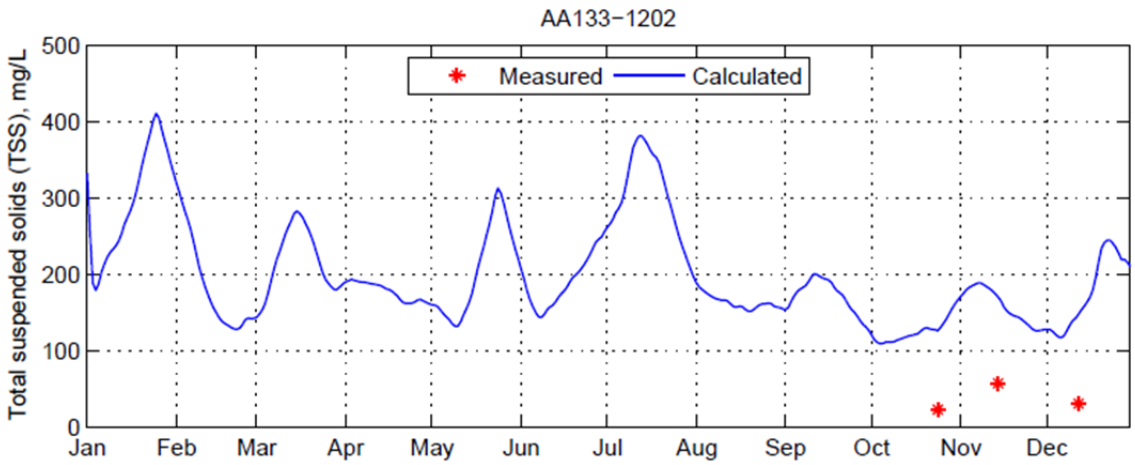

Figure 289 TSS Calibration Results for Wax Lake Outlet Southwest of Patterson in the AA Model

Algae (ALG)

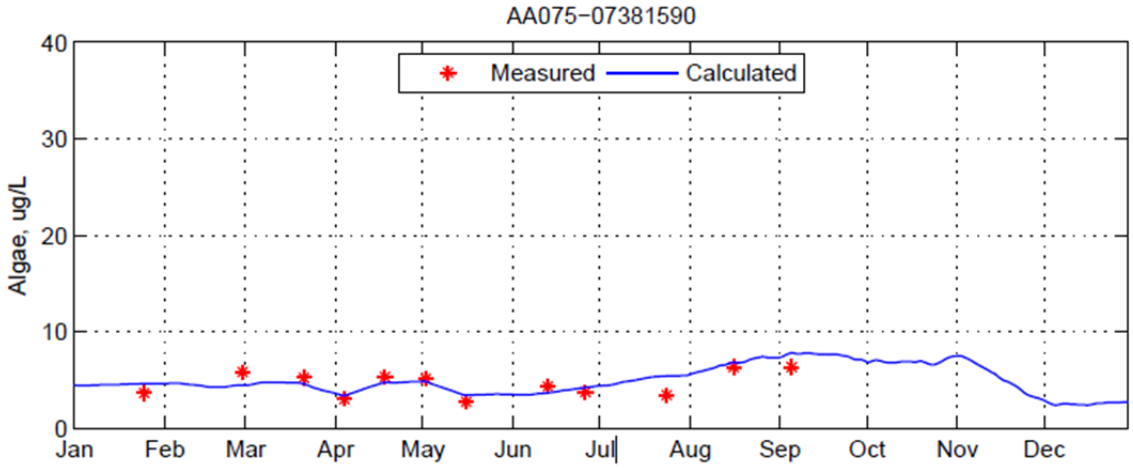

Figure 290 ALG Calibration Results for Wax Lake Outlet at Calumet in the AA Model

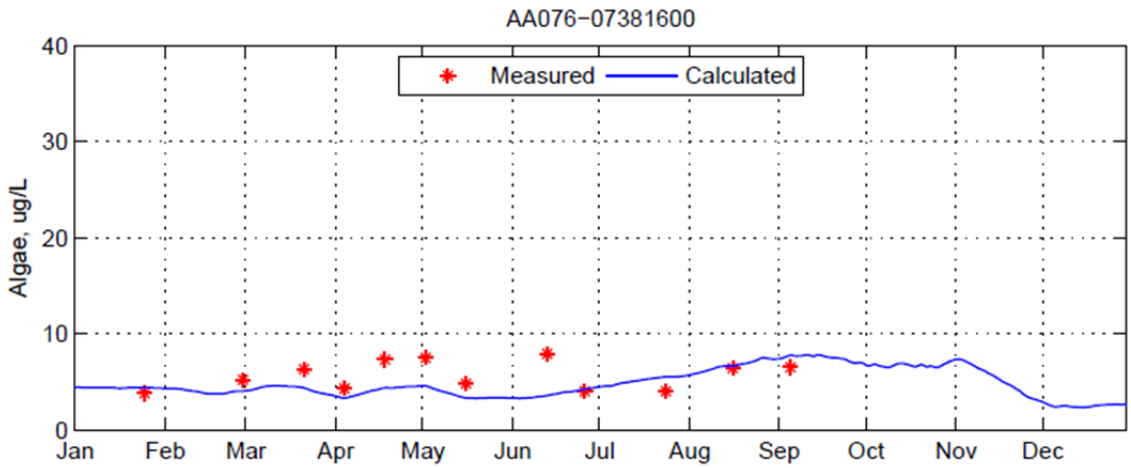

Figure 291 ALG Calibration Results for Lower Atchafalaya River at Morgan City in the AA Model

Total Nitrogen (TN)

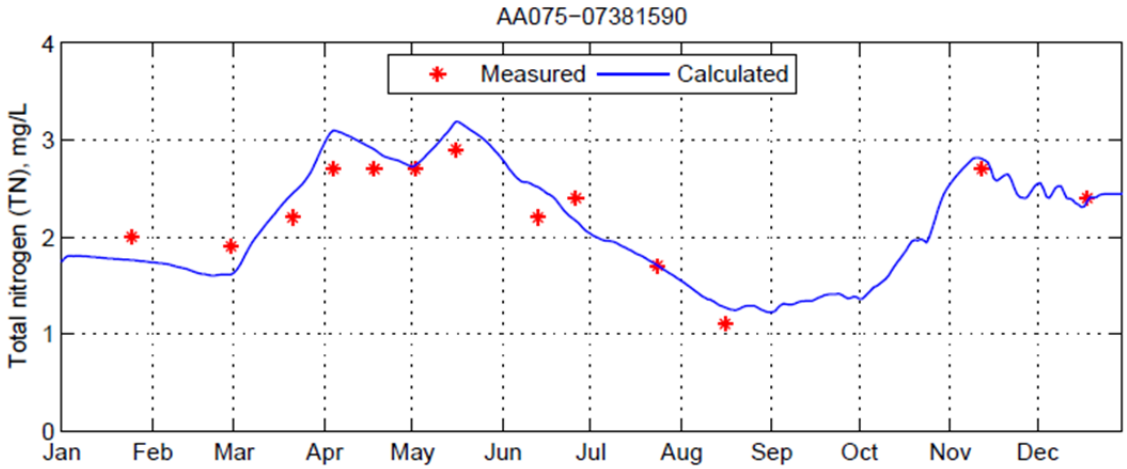

Figure 292 TN Calibration Results for Wax Lake Outlet at Calumet in the AA Model

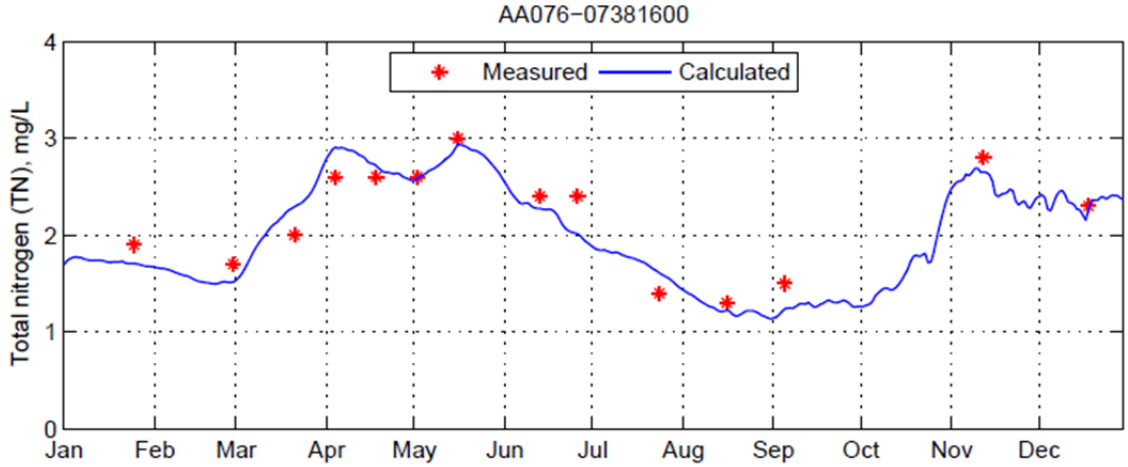

Figure 293 TN Calibration Results for Lower Atchafalaya River at Morgan City in the AA Model

Total Phosphorus (TPH)

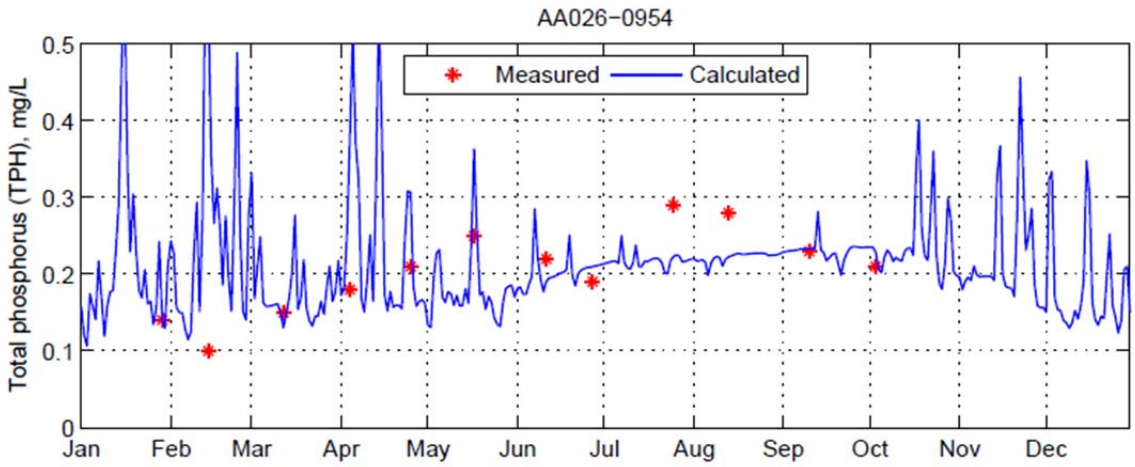

Figure 294 TPH Calibration Results for Lake Boudreaux South of Bayou Chauvin in the AA Model

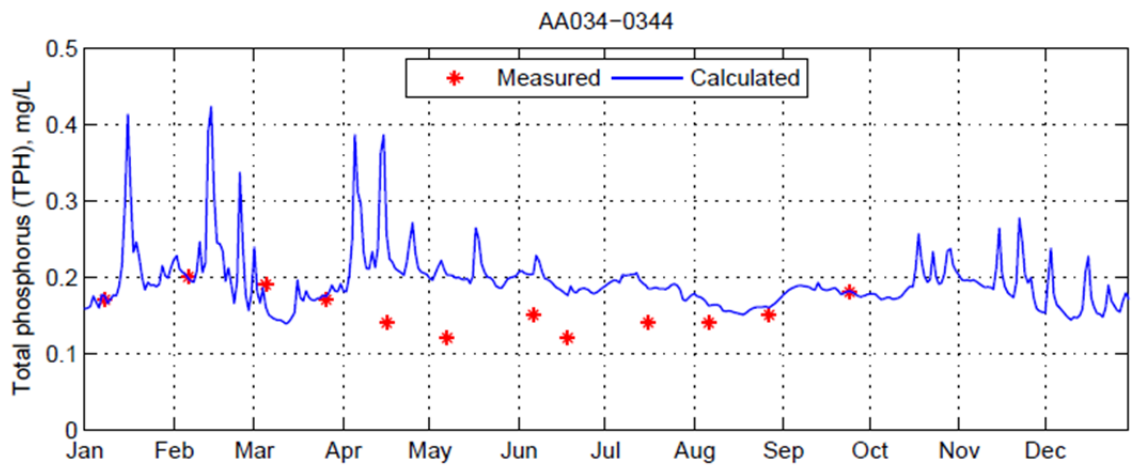

Figure 295 TPH Calibration Results for Houma Navigation Canal South of Houma in the AA Model

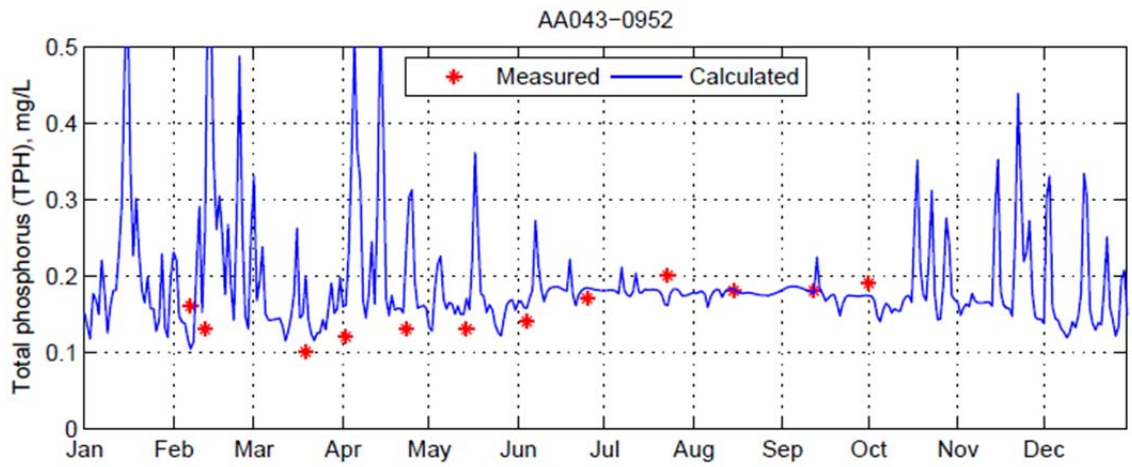

Figure 296 TPH Calibration Results for Houma Navigation Canal North of Bayou Petit Caillou in the AA Model

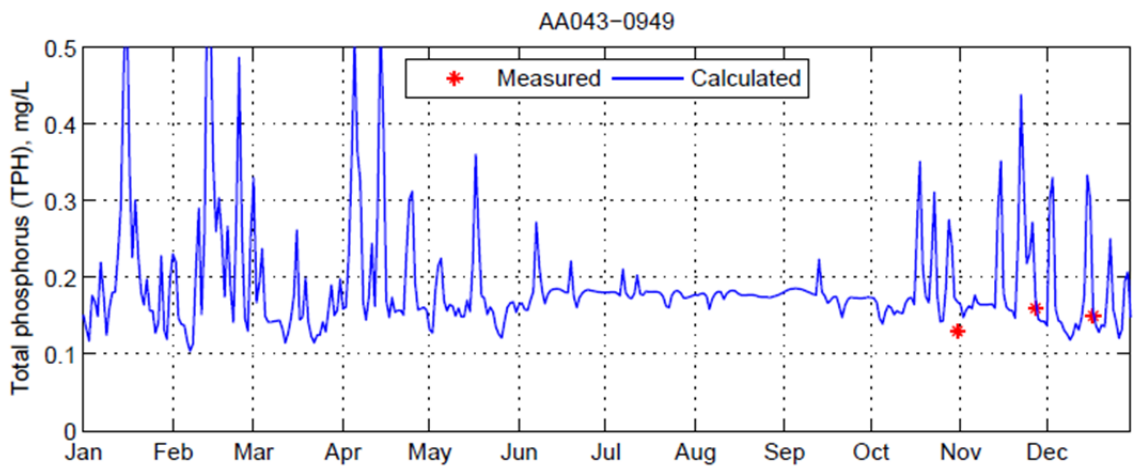

Figure 297 TPH Calibration Results for Bayou Petit Caillou at Cocodrie in the AA Model

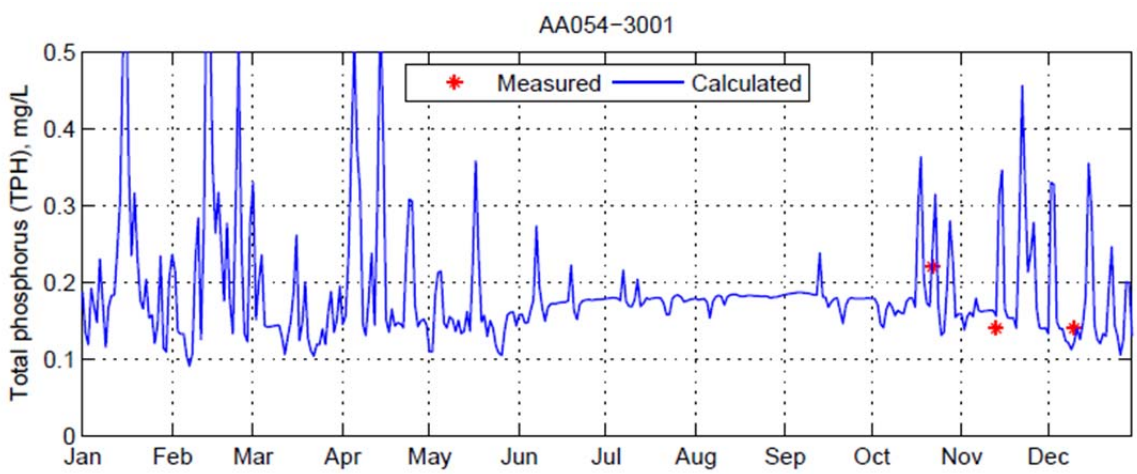

Figure 298 TPH Calibration Results for Bayou Terrebonne near Lapeyrouse in the AA Model

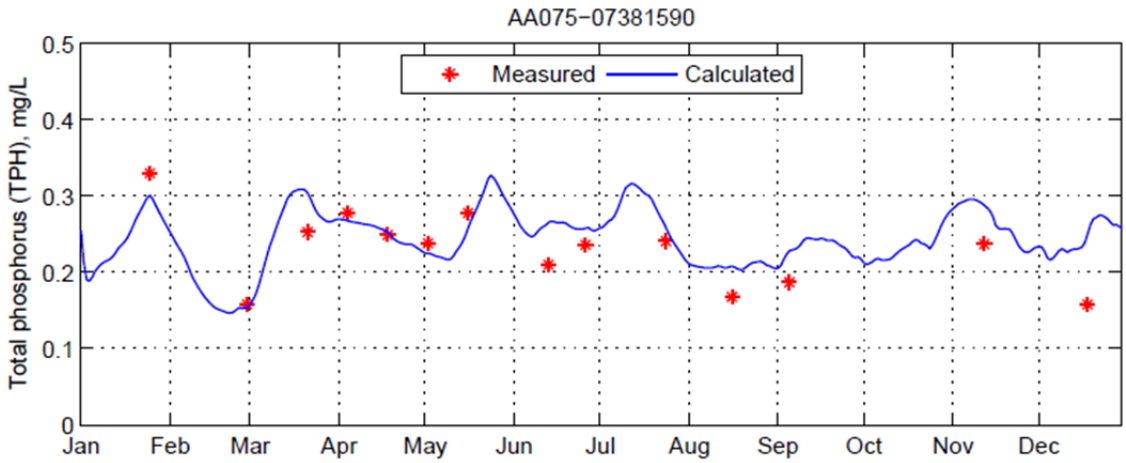

Figure 299 TPH Calibration Results for Wax Lake Outlet at Calumet in the AA Model

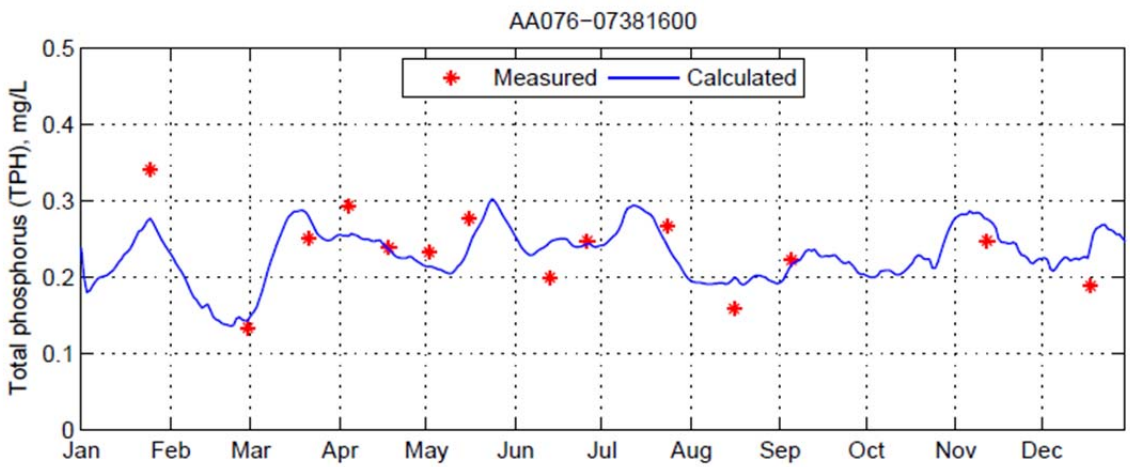

Figure 300 TPH Calibration Results for Lower Atchafalaya River at Morgan City in the AA Model

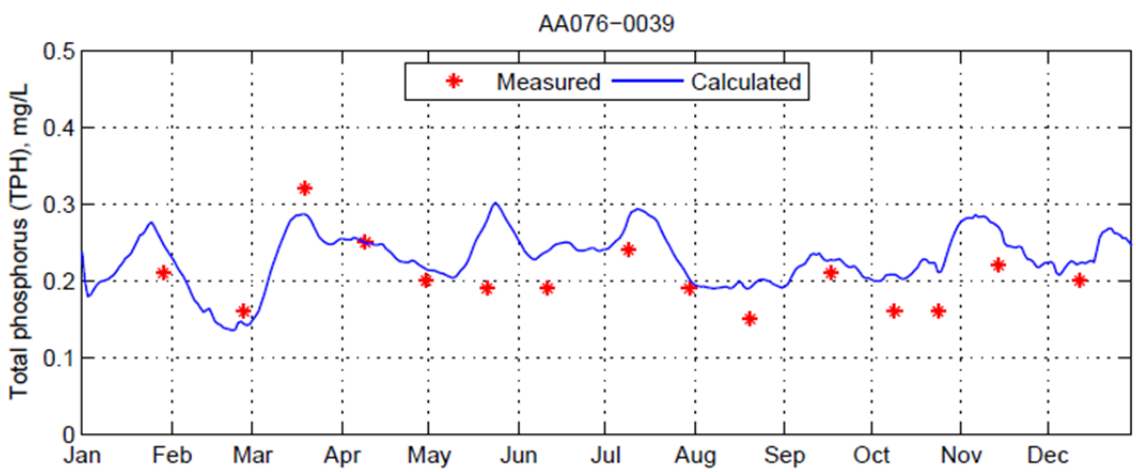

Figure 301 TPH Calibration Results for Atchafalaya River at Morgan City in the AA Model

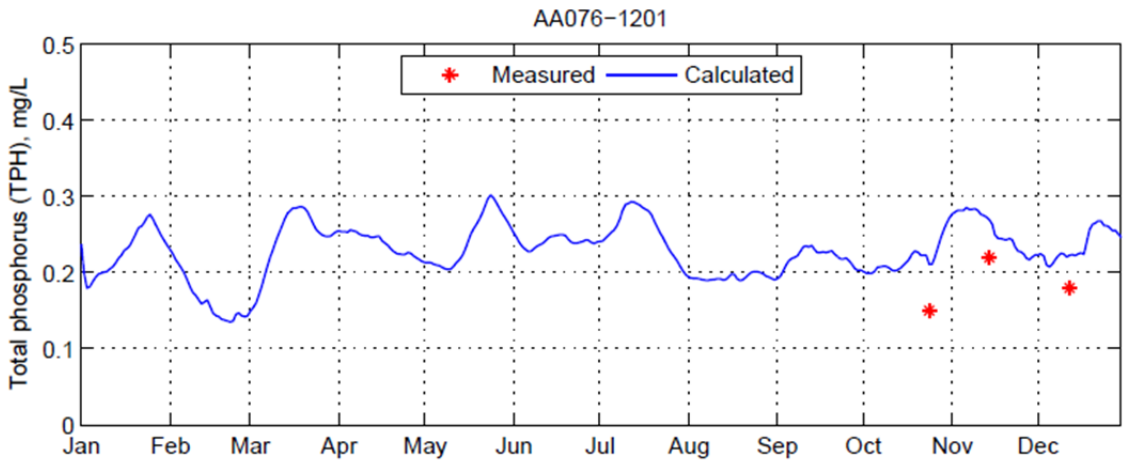

Figure 302 TPH Calibration Results for Lower Atchafalaya River near Bateman Island in the AA Model

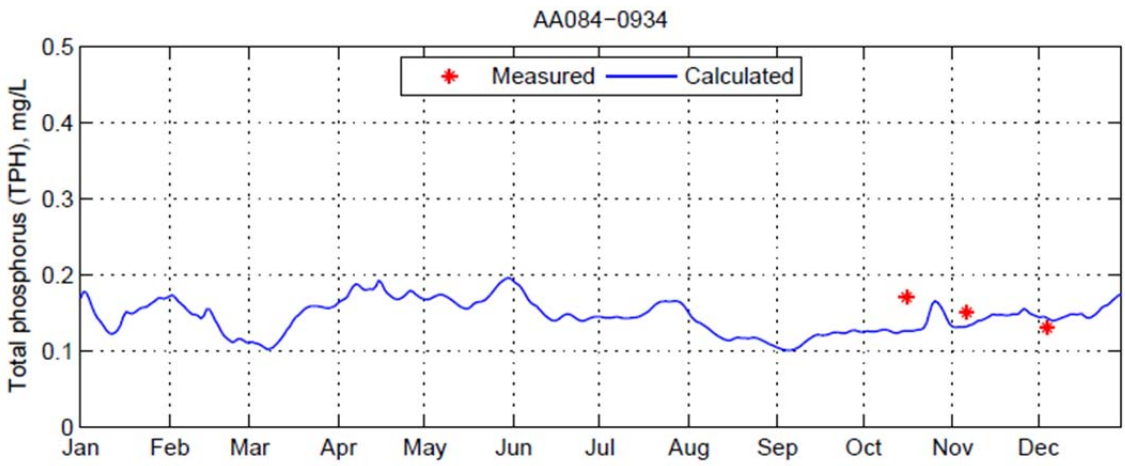

Figure 303 TPH Calibration Results for ICWW at Venvirotek Dock in the AA Model

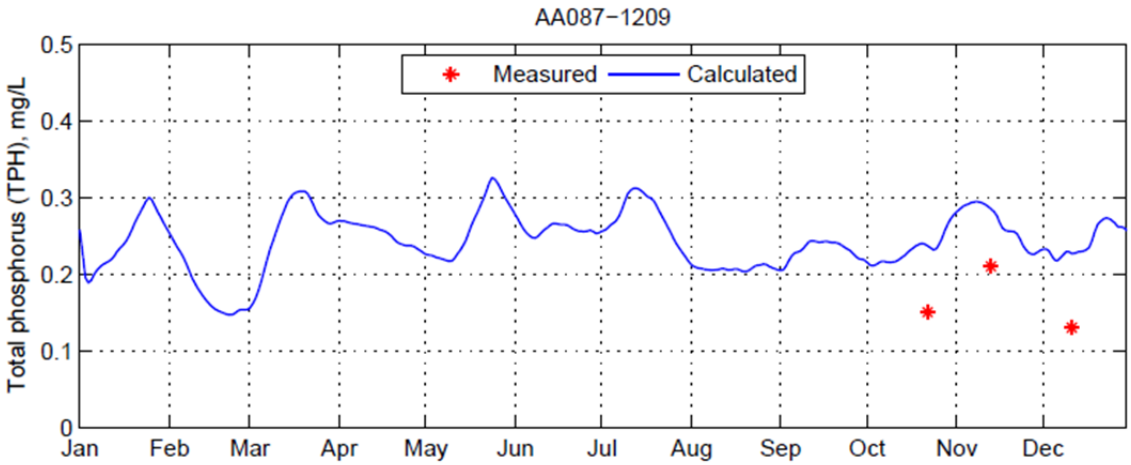

Figure 304 TPH Calibration Results for Bayou Blue at North Bend Pumping Station in the AA Model

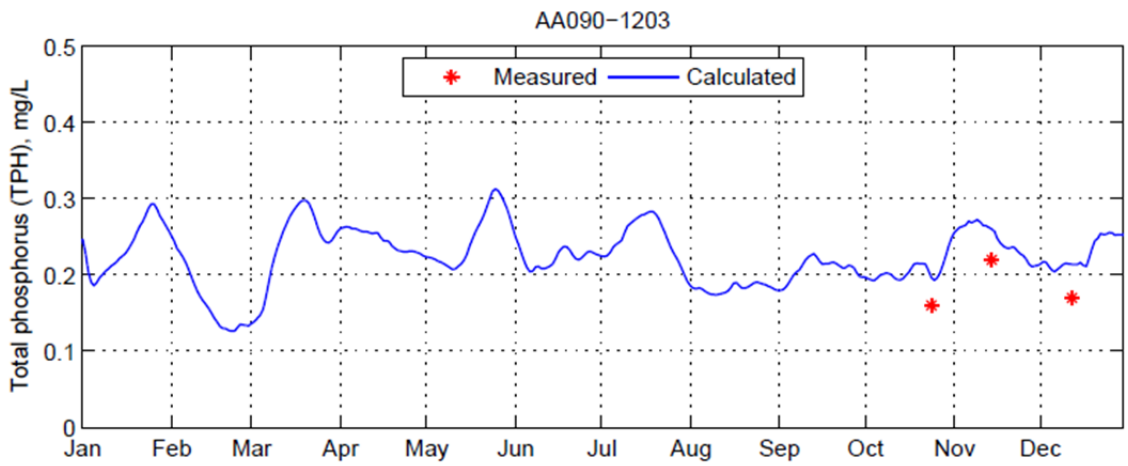

Figure 305 TPH Calibration Results for ICWW South of Patterson in the AA Model

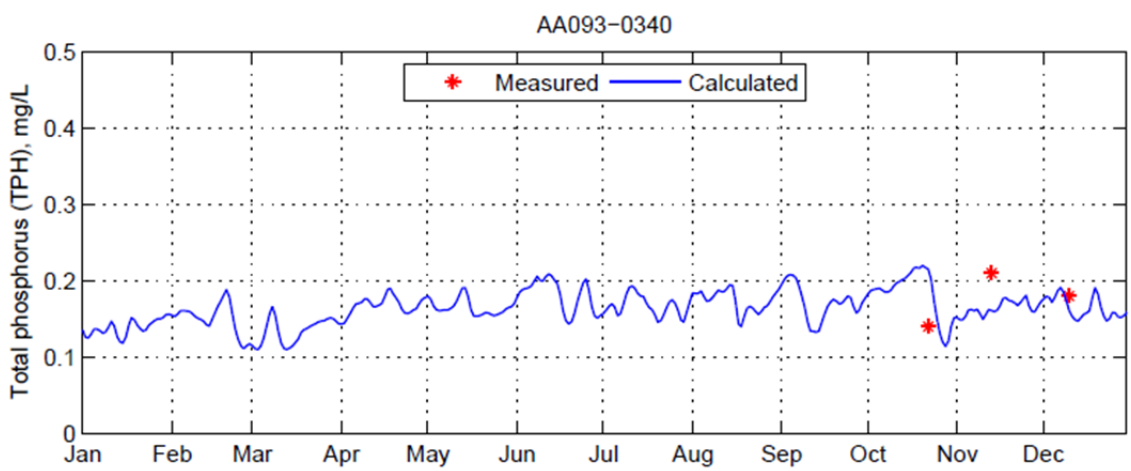

Figure 306 TPH Calibration Results for ICWW East of Houma in the AA Model

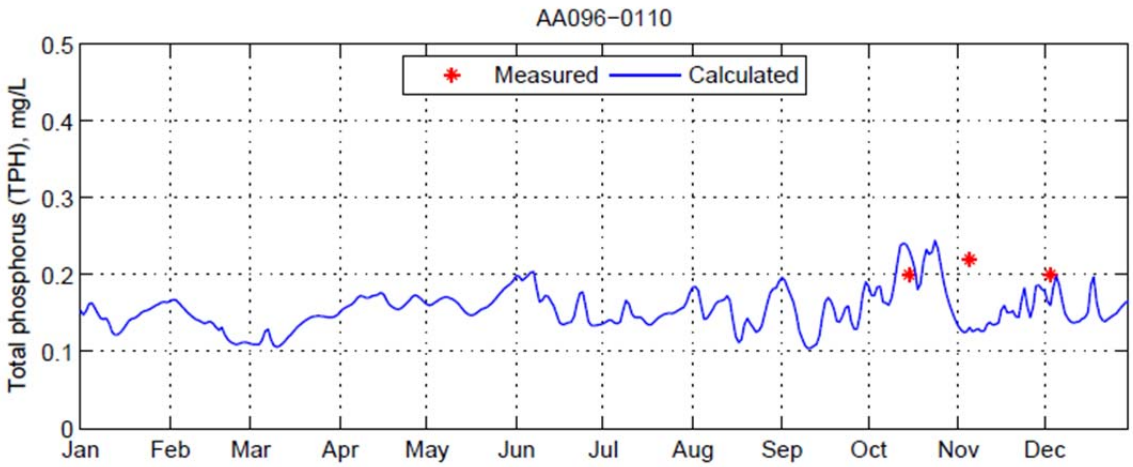

Figure 307 TPH Calibration Results for Bayou Terrebonne at Houma in the AA Model

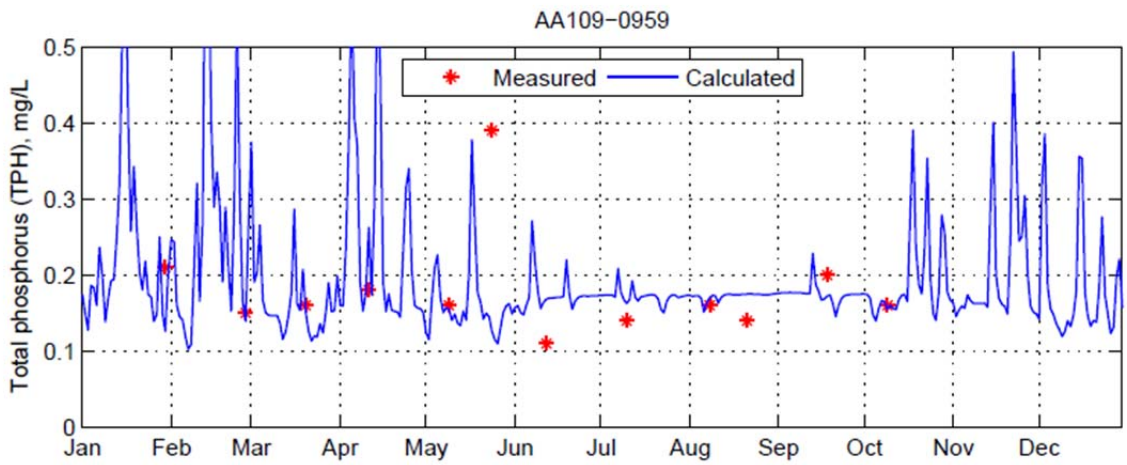

Figure 308 TPH Calibration Results for Timbalier Bay South of Devils Island in the AA Model

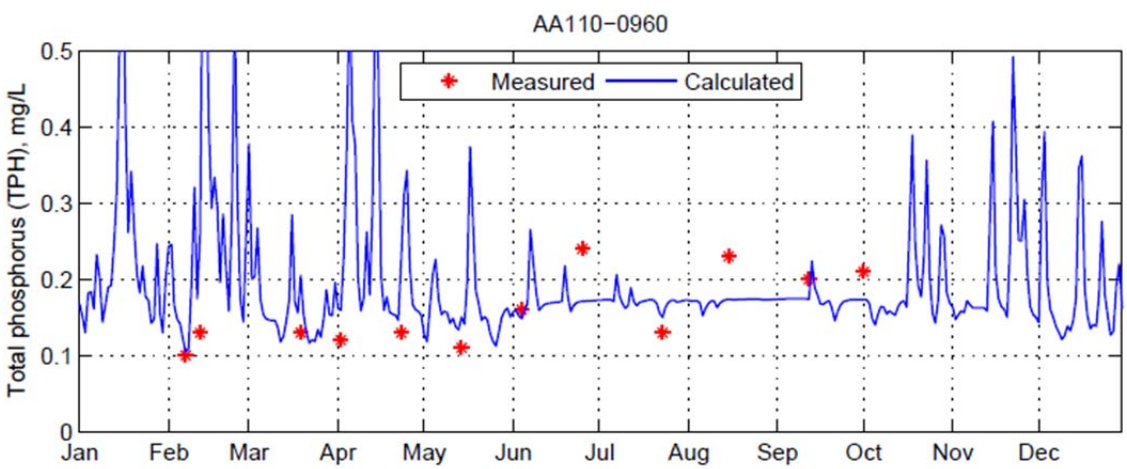

Figure 309 TPH Calibration Results for Lake Barre West of Cocodrie in the AA Model

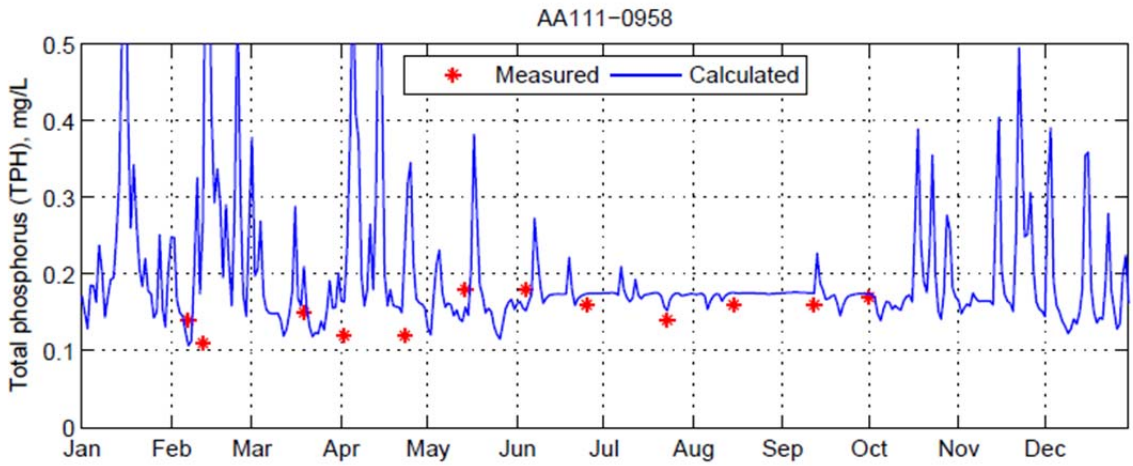

Figure 310 TPH Calibration Results for Terrebonne Bay Southeast of Cocodrie in the AA Model

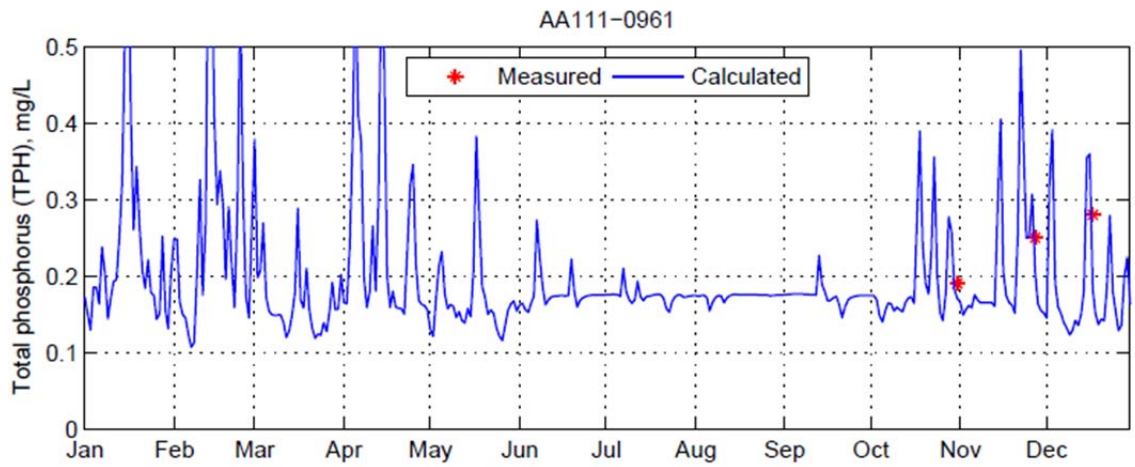

Figure 311 TPH Calibration Results for Lake Pelto South of Cocodrie in the AA Model

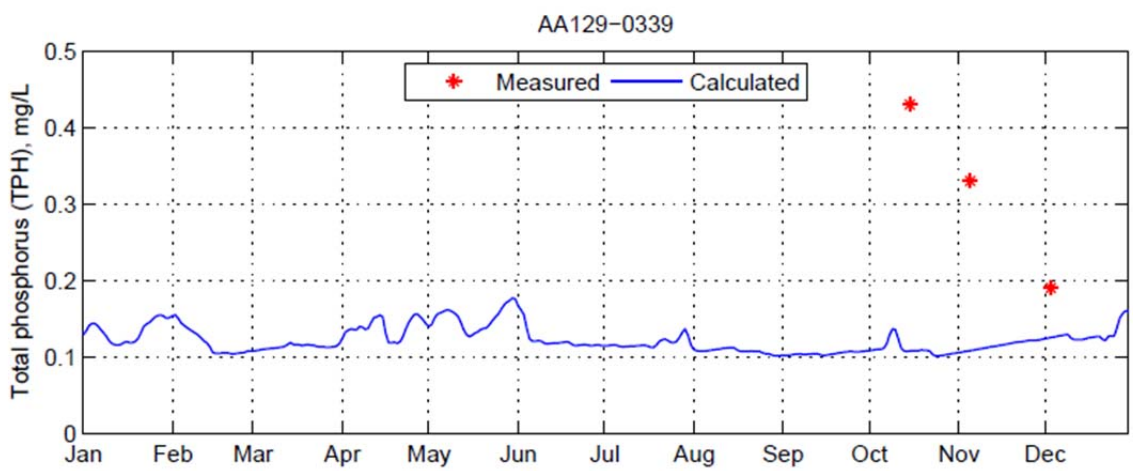

Figure 312 TPH Calibration Results for Bayou Black West of Houma in the AA Model

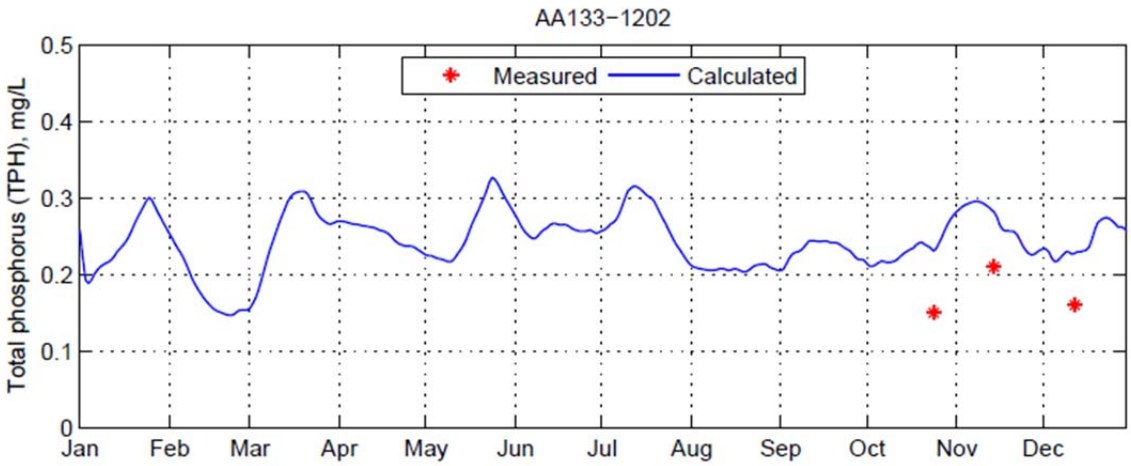

Figure 313 TPH Calibration Results for Wax Lake Outlet Southwest of Patterson in the AA Model

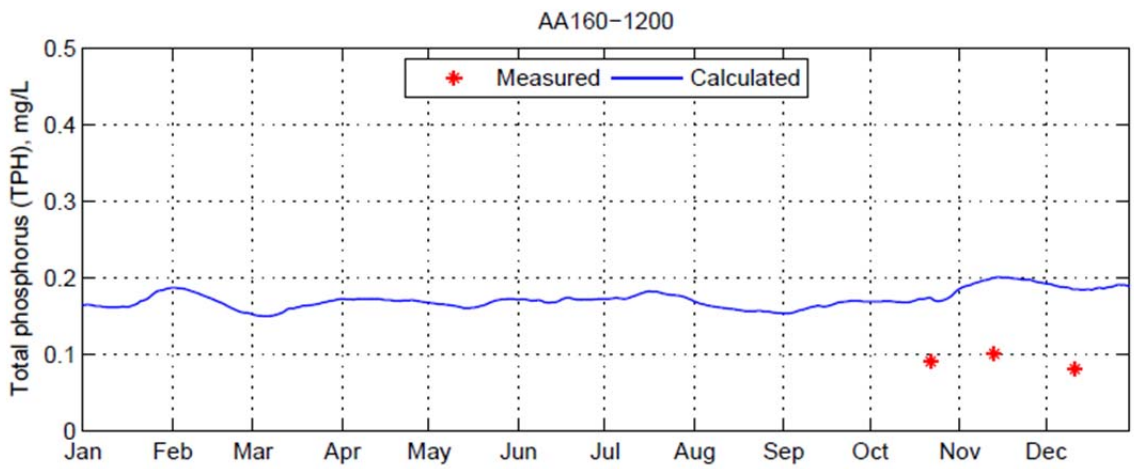

Figure 314 TPH Calibration Results for Bayou Teche at Patterson in the AA Model

Atchafalaya Basin Validation Plots

Stage (STG)

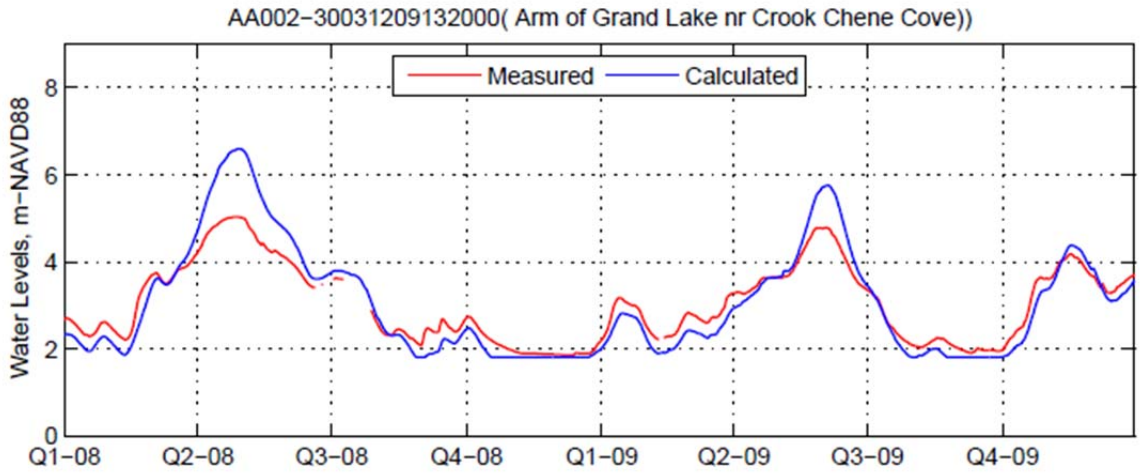

Figure 315 STG Validation Results for Grand Lake in the AA Model

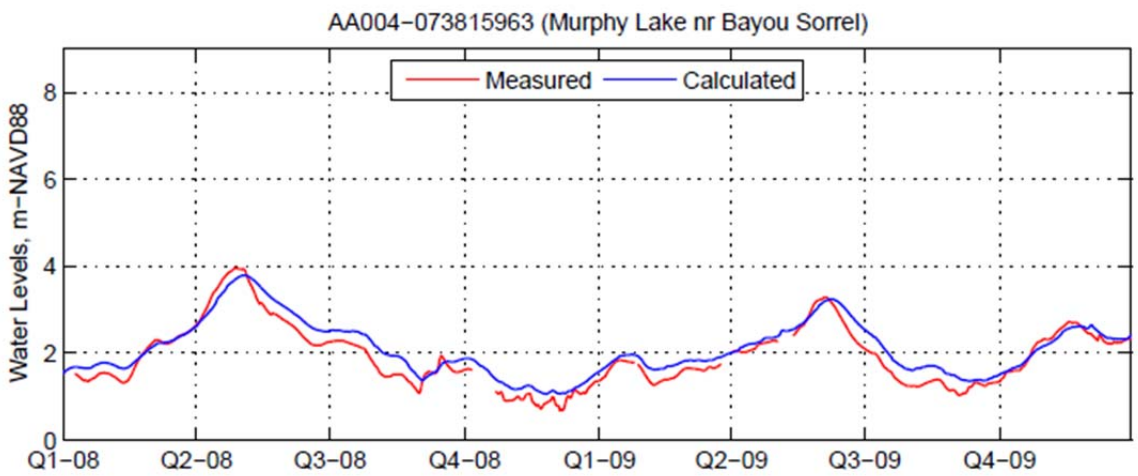

Figure 316 STG Validation Results for Murphy Lake in the AA Model

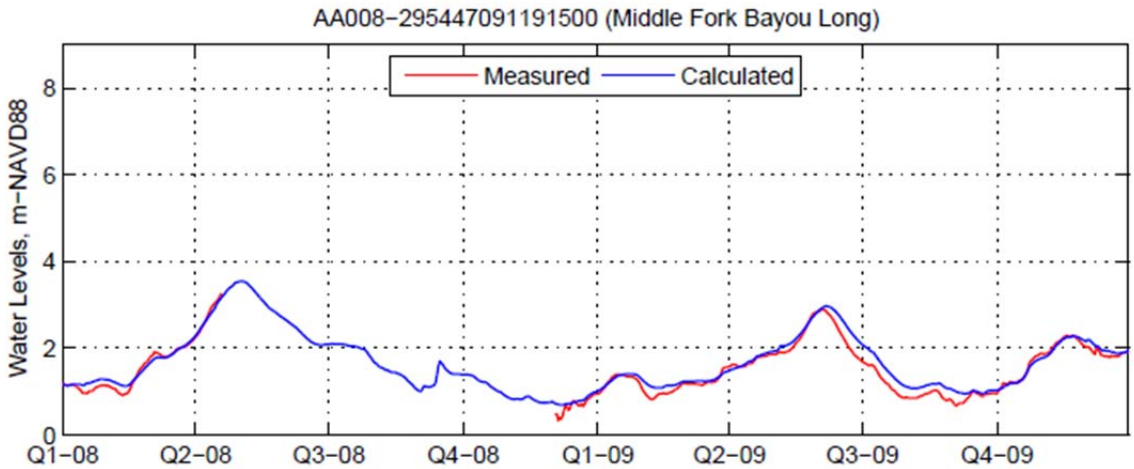

Figure 317 STG Validation Results for Bayou Long in the AA Model

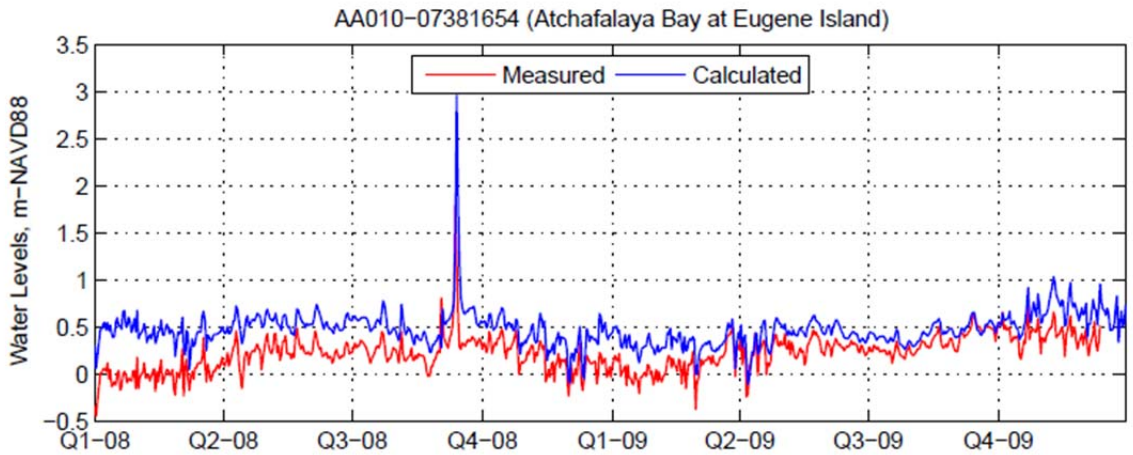

Figure 318 STG Validation Results for Atchafalaya Bay in the AA Model

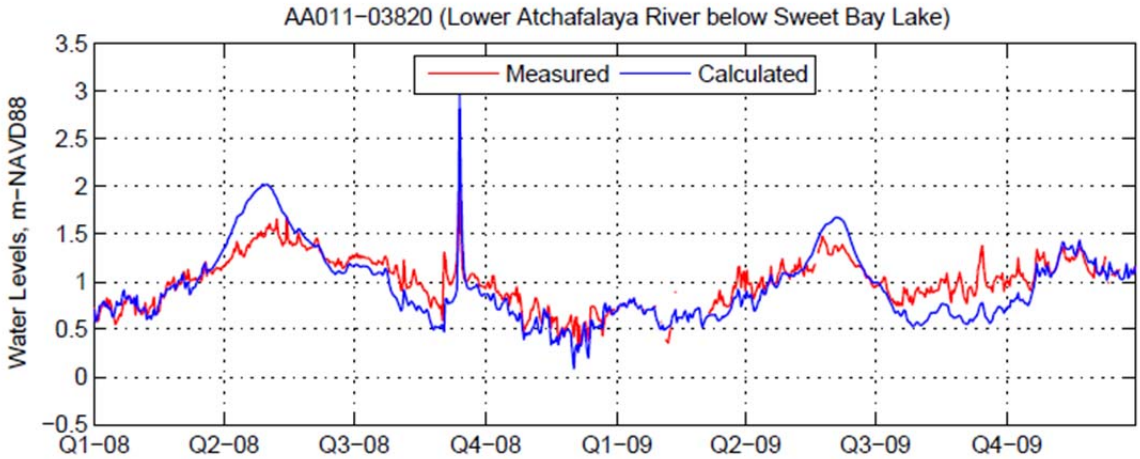

Figure 319 STG Validation Results for Lower Atchafalaya River below Sweet Bay Lake in the AA Model

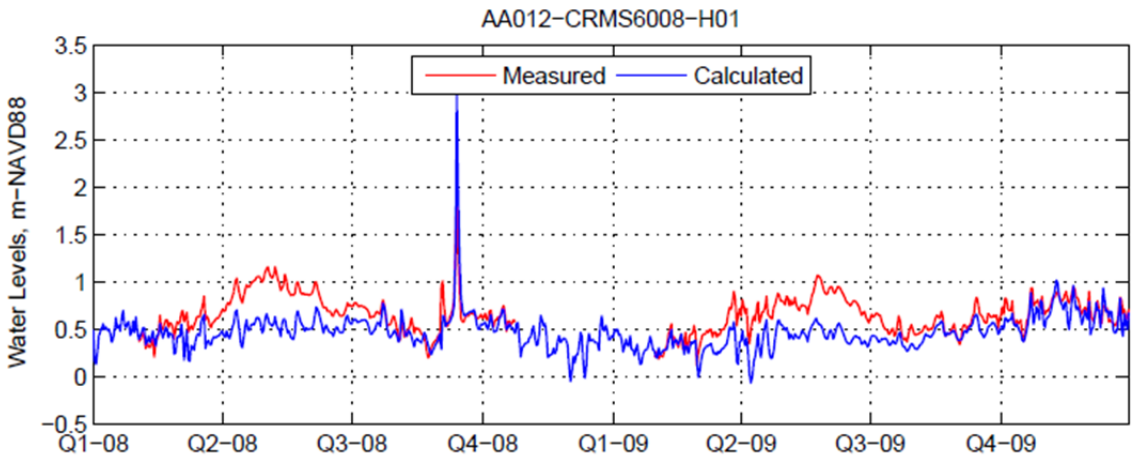

Figure 320 STG Validation Results for AA012 in the AA Model

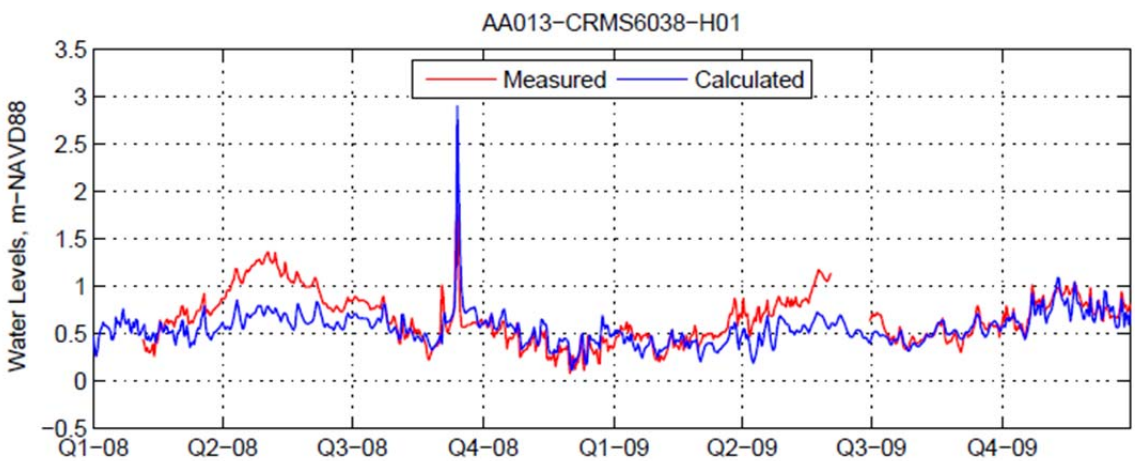

Figure 321 STG Validation Results for AA013 in the AA Model

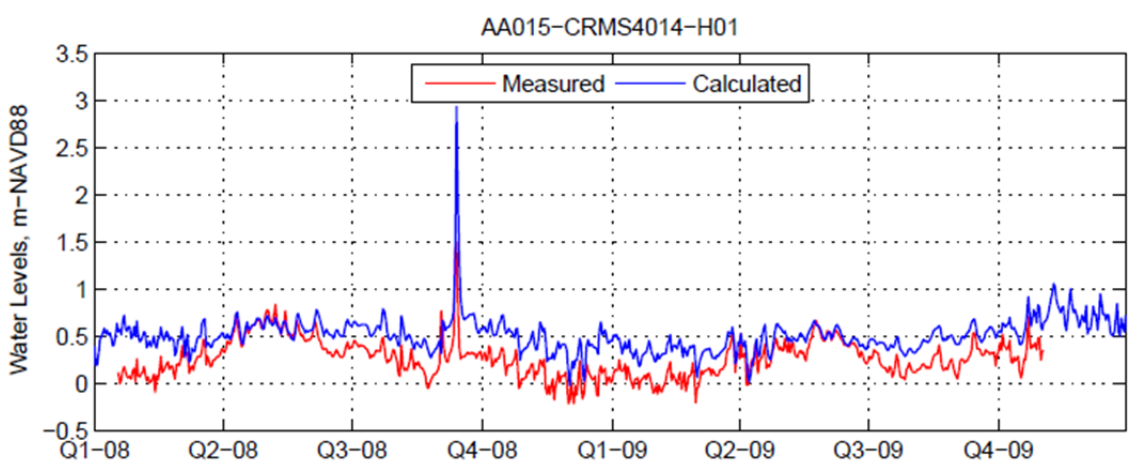

Figure 322 STG Validation Results for AA015 in the AA Model

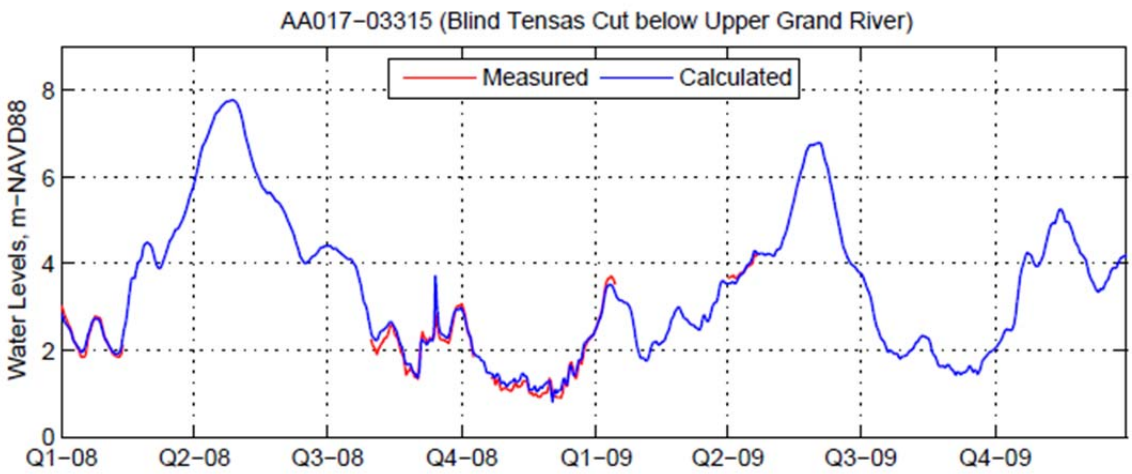

Figure 323 STG Validation Results for Blind Tensas Cut in the AA Model

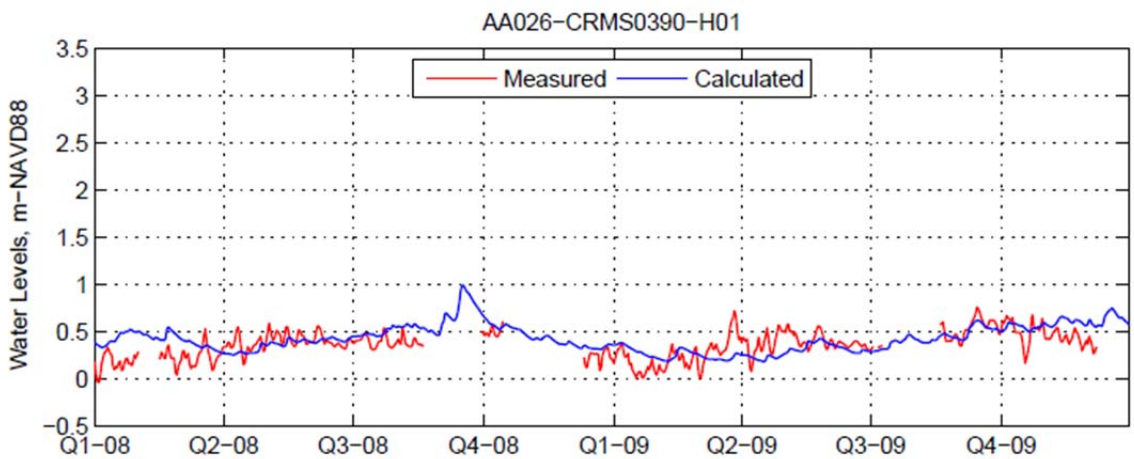

Figure 324 STG Validation Results for AA026 in the AA Model

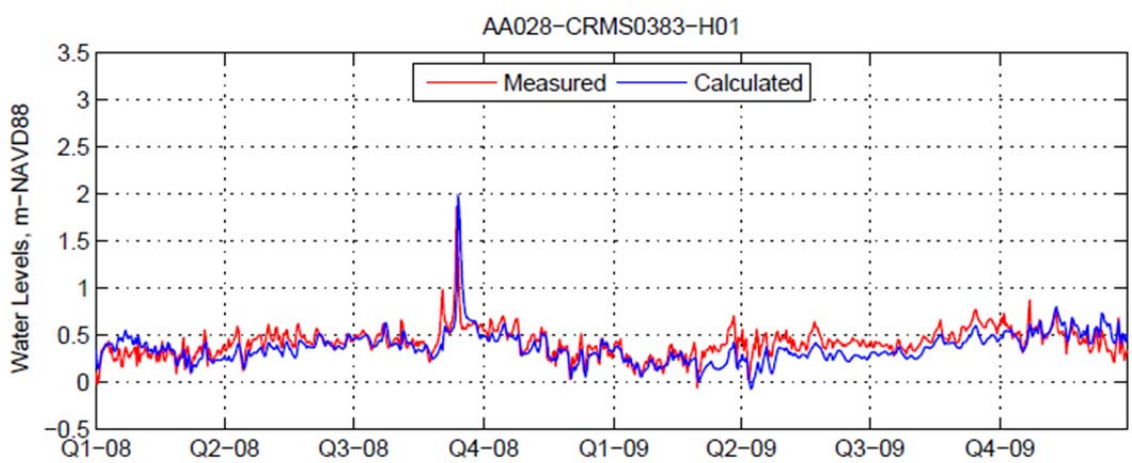

Figure 325 STG Validation Results for AA028 in the AA Model

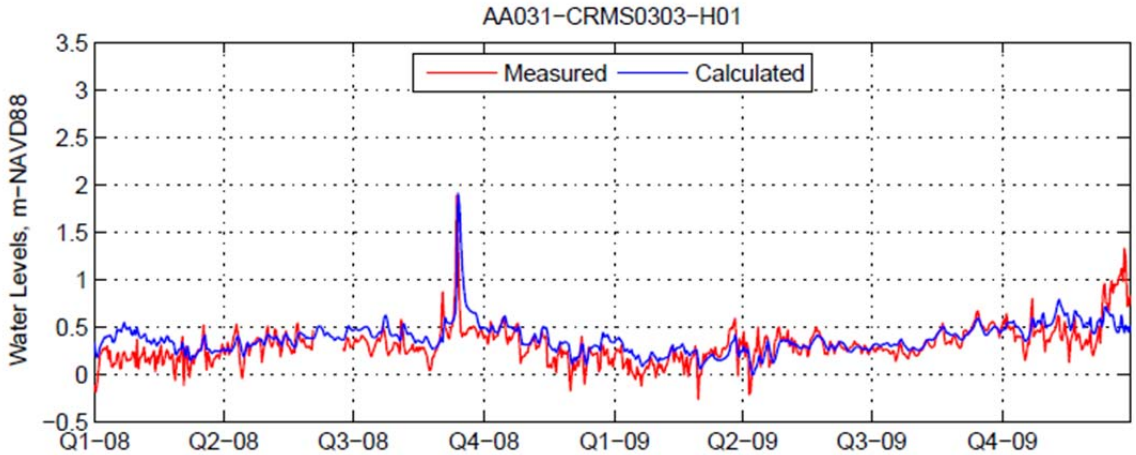

Figure 326 STG Validation Results for AA031 in the AA Model

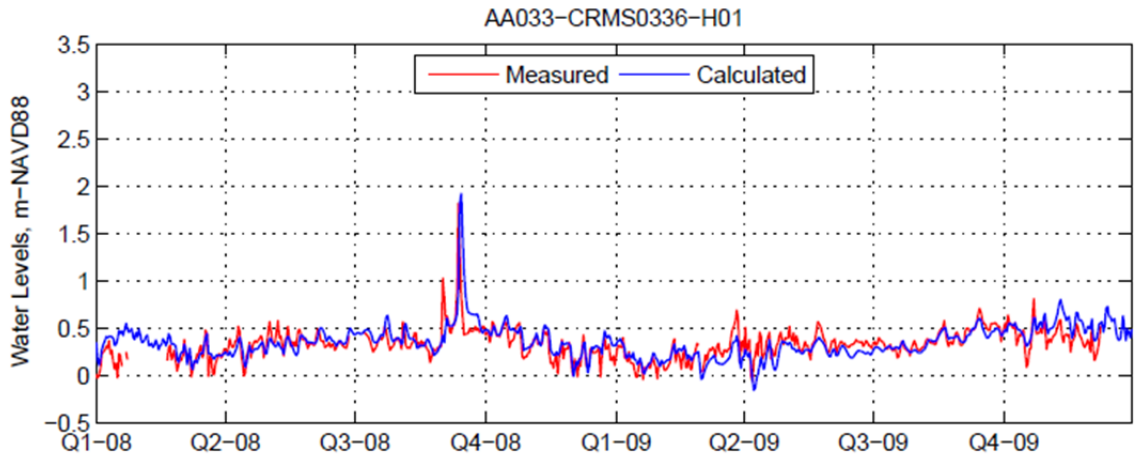

Figure 327 STG Validation Results for AA033 in the AA Model

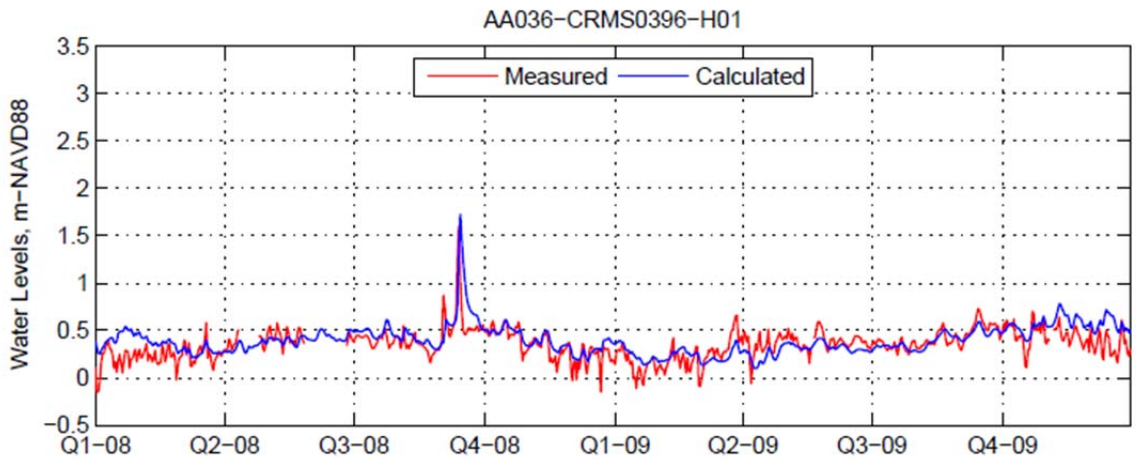

Figure 328 STG Validation Results for AA036 in the AA Model

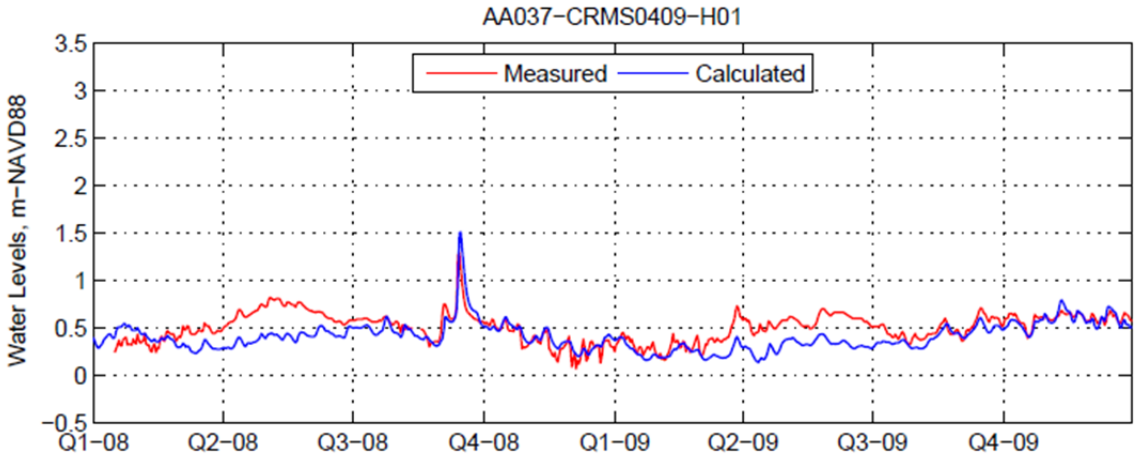

Figure 329 STG Validation Results for AA037 in the AA Model

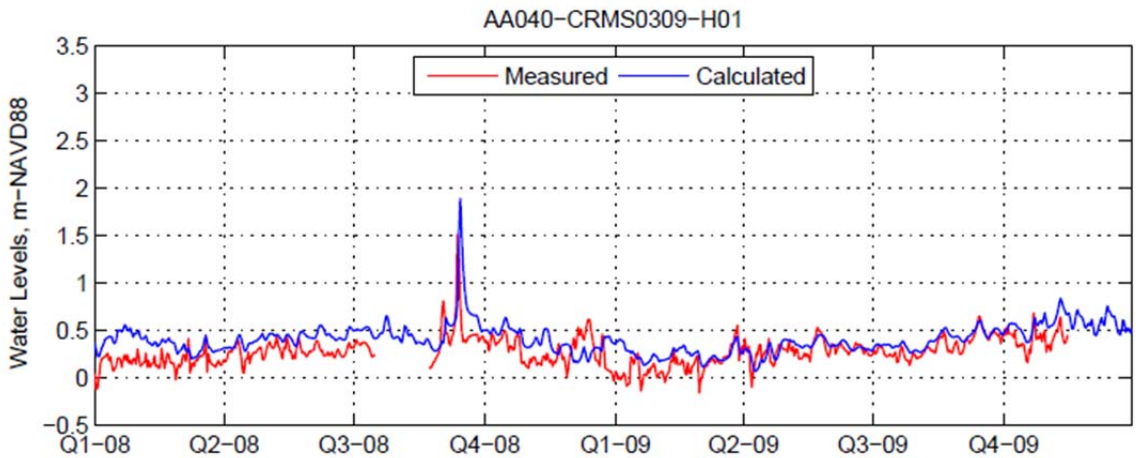

Figure 330 STG Validation Results for AA040 in the AA Model

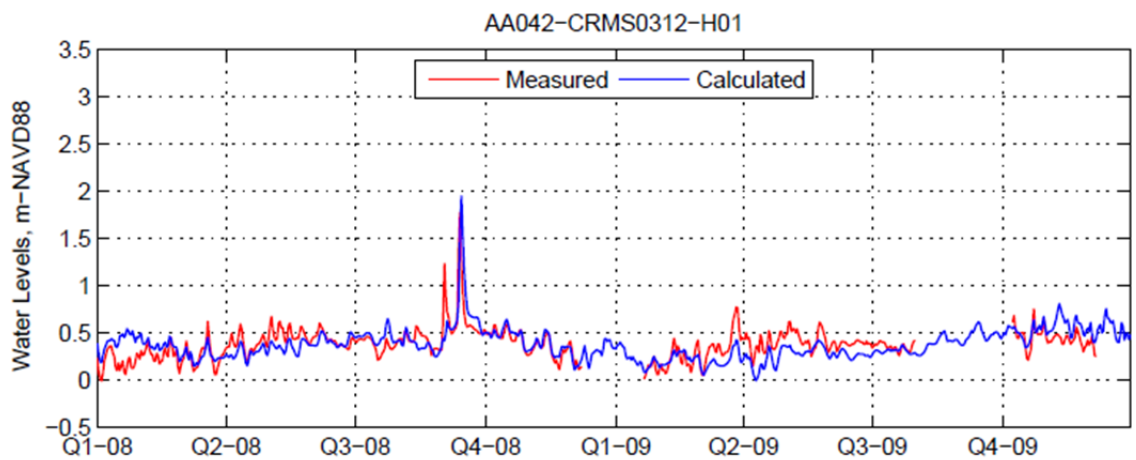

Figure 331 STG Validation Results for AA042 in the AA Model

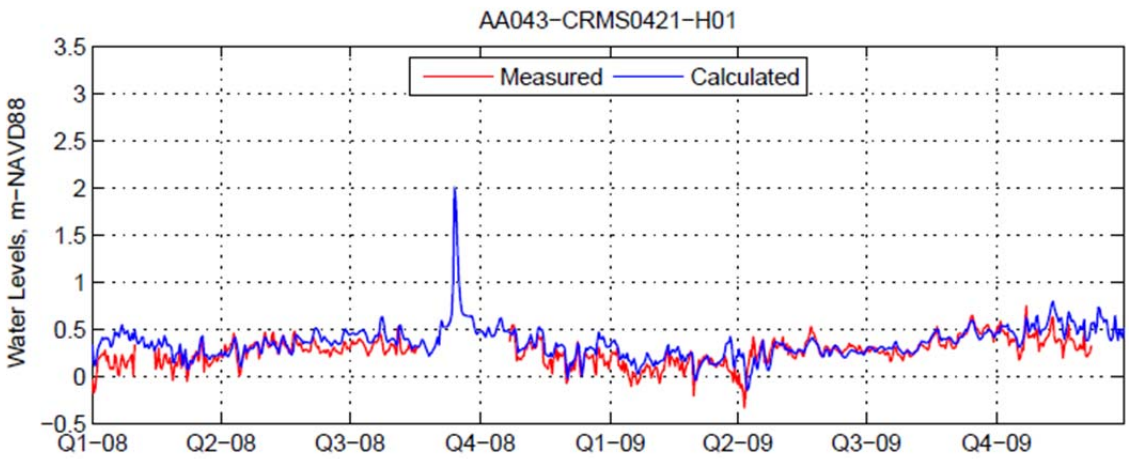

Figure 332 STG Validation Results for AA043 in the AA Model

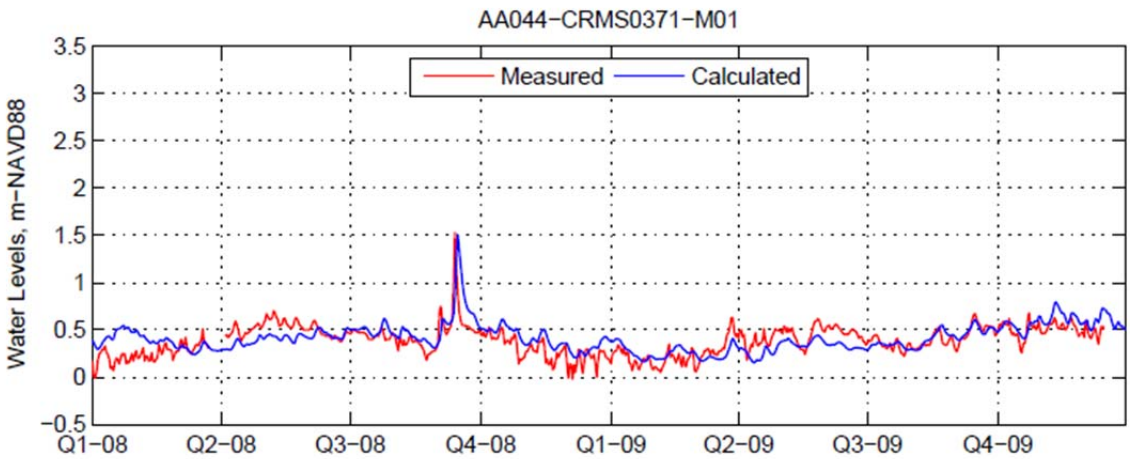

Figure 333 STG Validation Results for AA044 in the AA Model

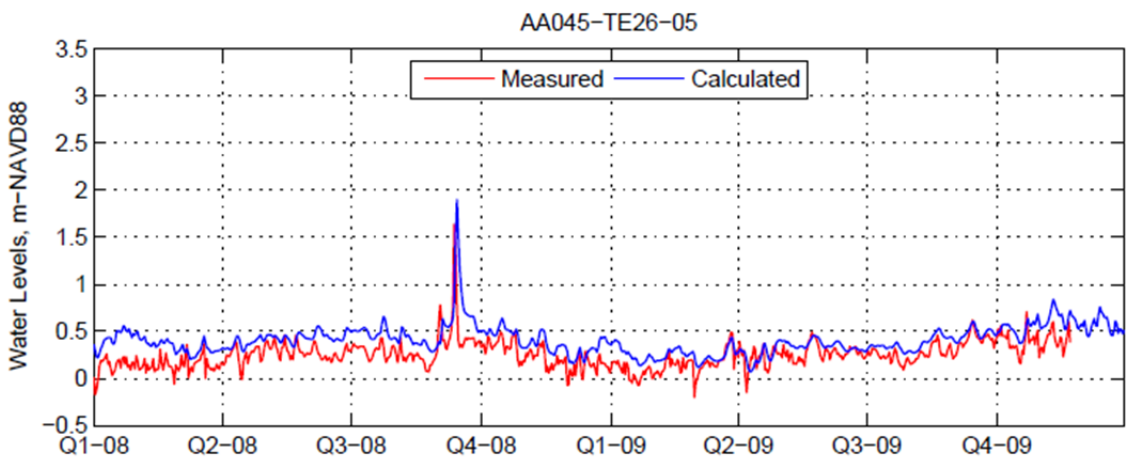

Figure 334 STG Validation Results for Lake Chapeau in the AA Model

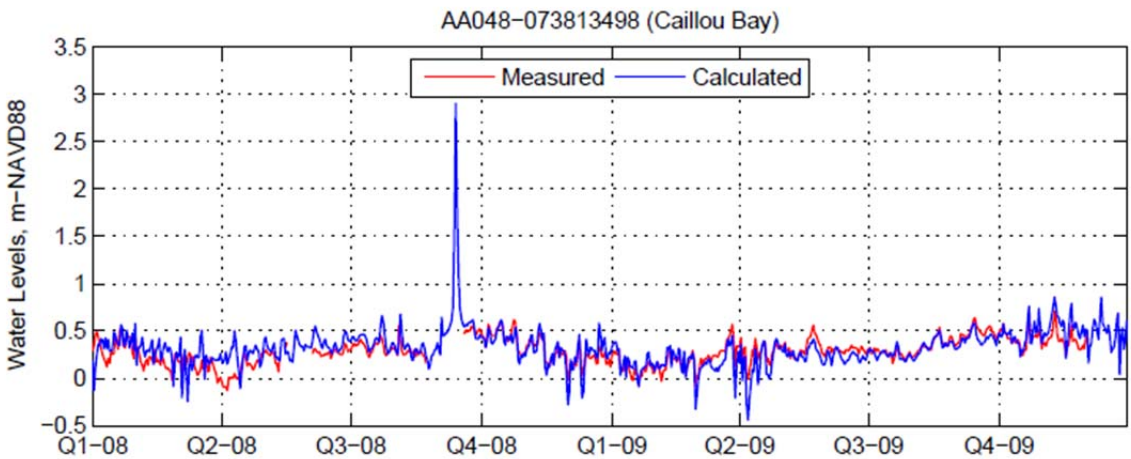

Figure 335 STG Validation Results for Caillou Bay in the AA Model

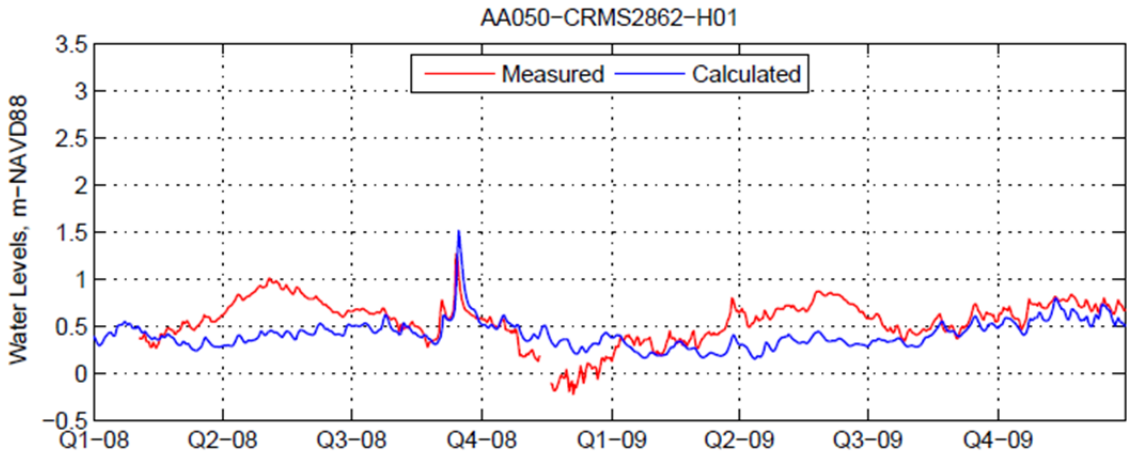

Figure 336 STG Validation Results for AA050 in the AA Model

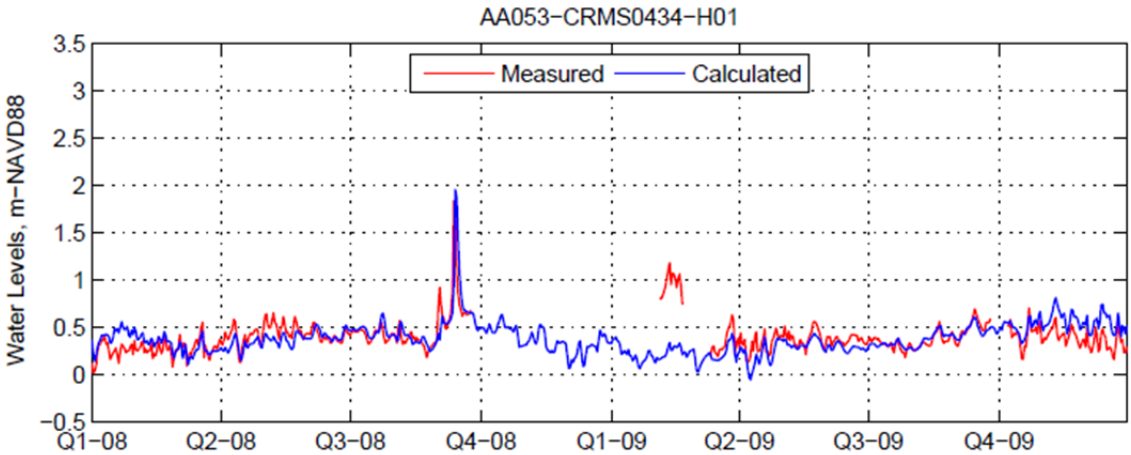

Figure 337 STG Validation Results for AA053 in the AA Model

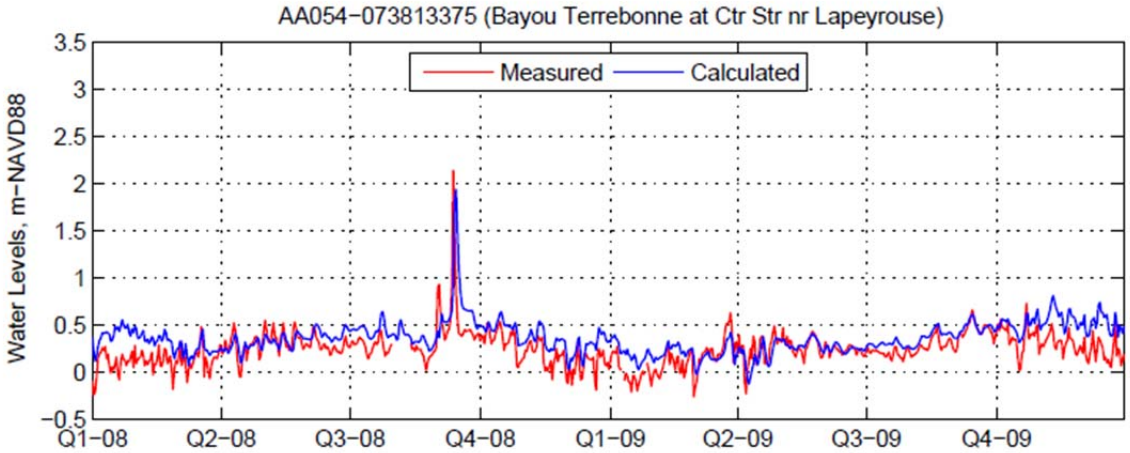

Figure 338 STG Validation Results for Bayou Terrebonne in the AA Model

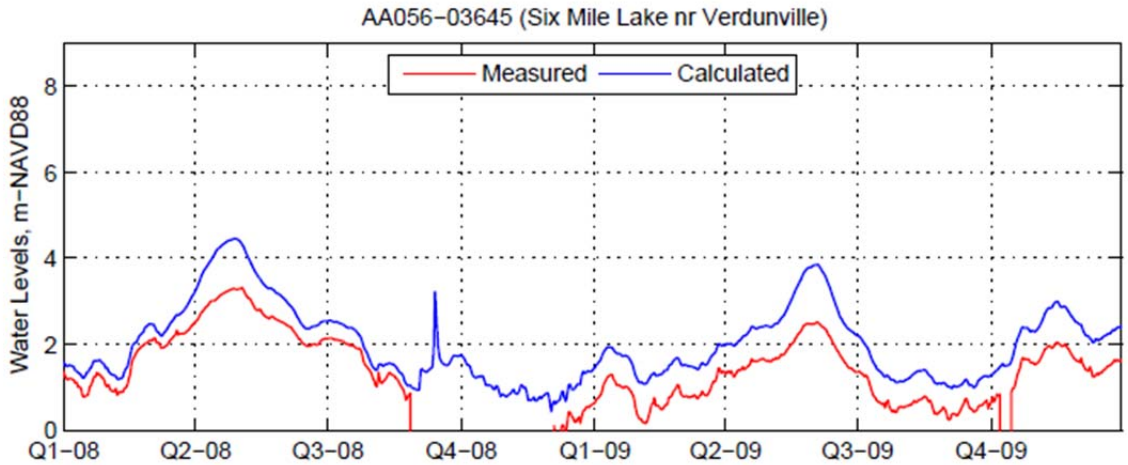

Figure 339 STG Validation Results for Six Mile Lake in the AA Model

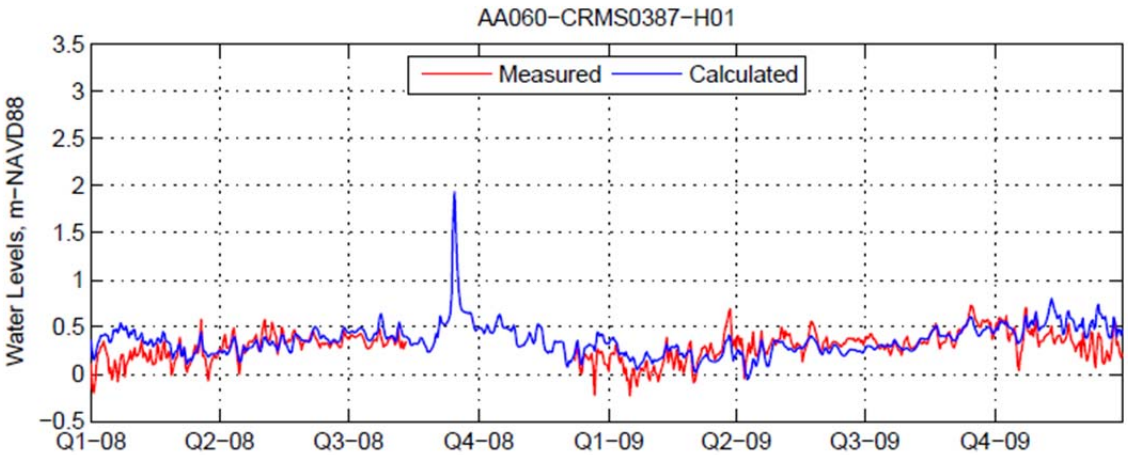

Figure 340 STG Validation Results for AA060 in the AA Model

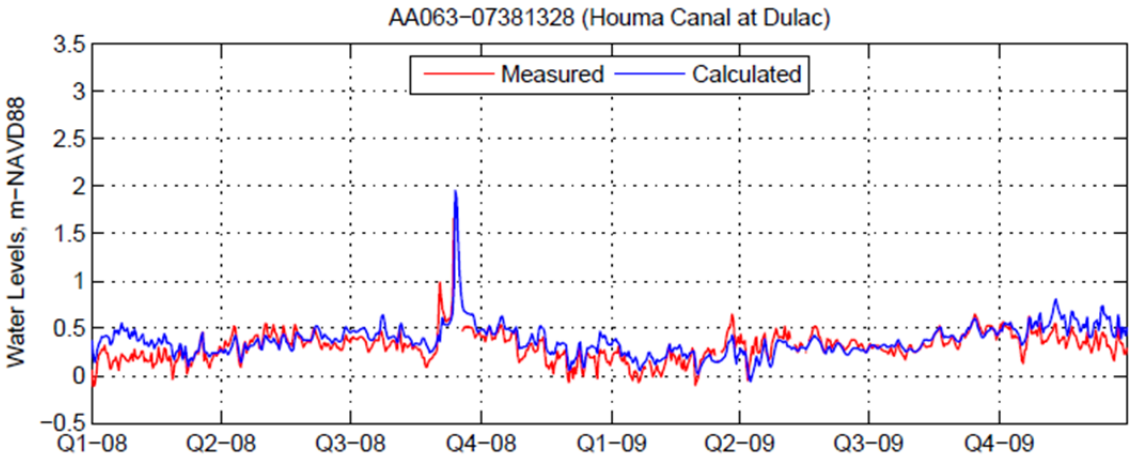

Figure 341 STG Validation Results for Houma Navigation Canal at Dulac in the AA Model

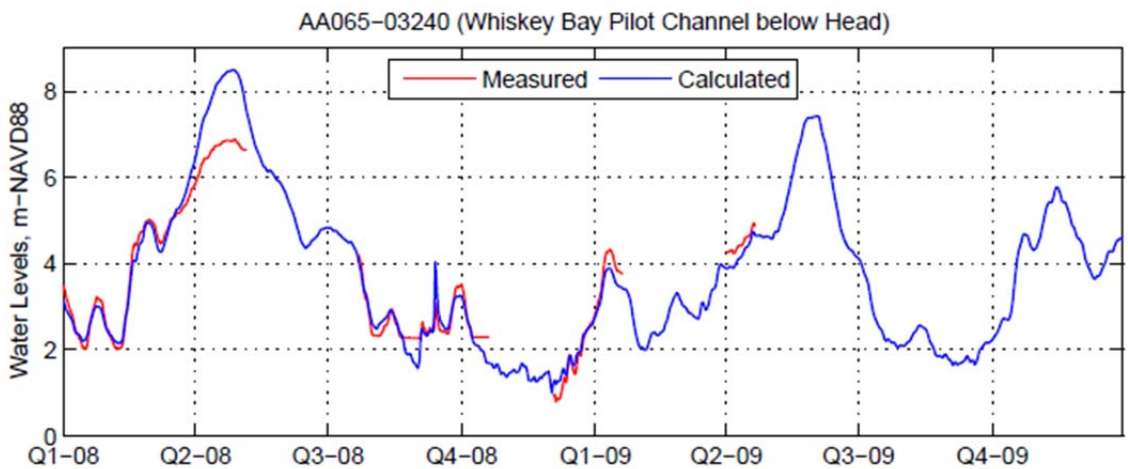

Figure 342 STG Validation Results for Whiskey Bay Pilot Channel in the AA Model

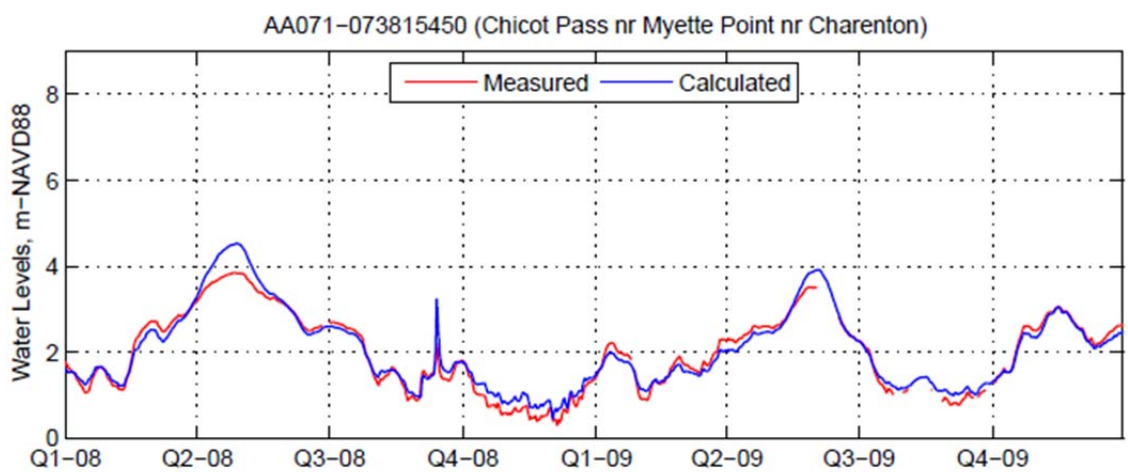

Figure 343 STG Validation Results for Chicot Pass in the AA Model

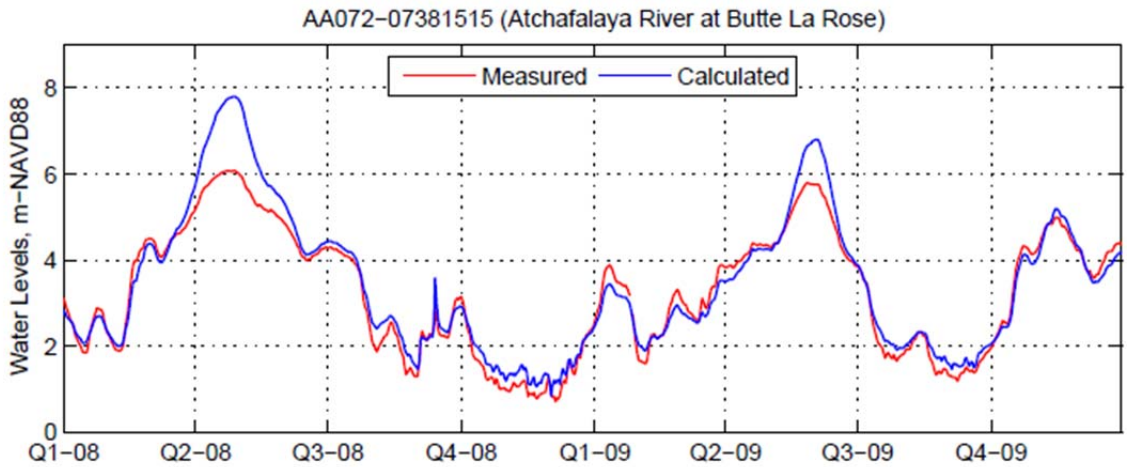

Figure 344 STG Validation Results for Atchafalaya River at Butte La Rose in the AA Model

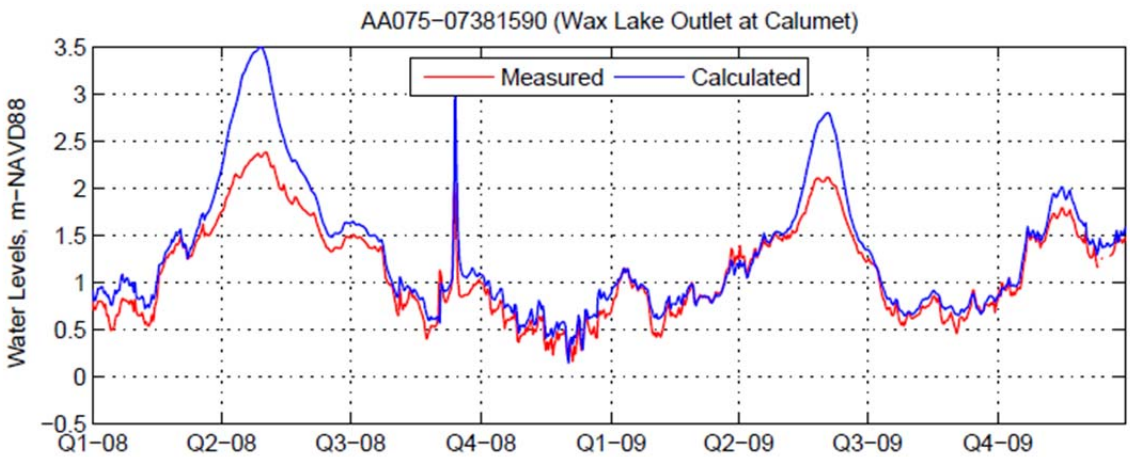

Figure 345 STG Validation Results for Wax Lake Outlet at Calumet in the AA Model

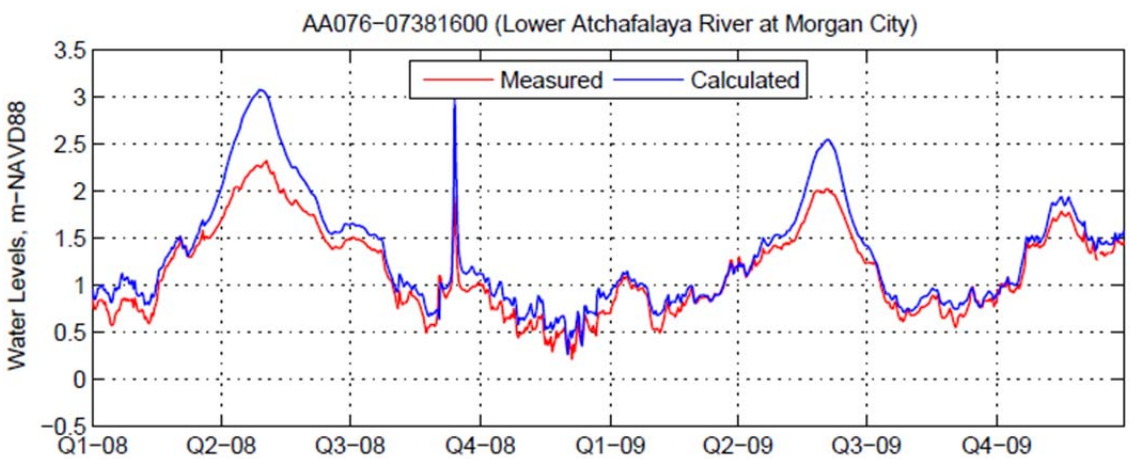

Figure 346 STG Validation Results for Lower Atchafalaya River at Morgan City in the AA Model

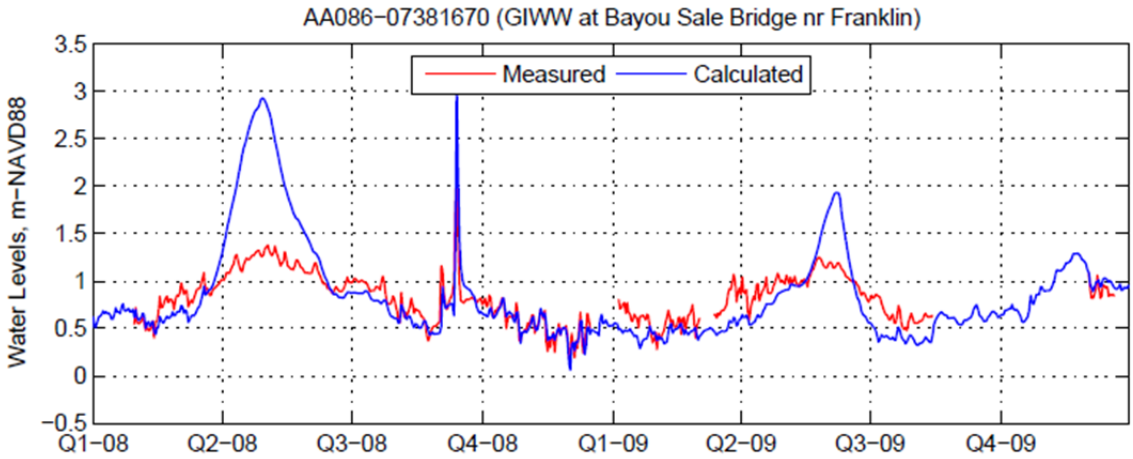

Figure 347 STG Validation Results for GIWW at Bayou Sale Ridge in the AA Model

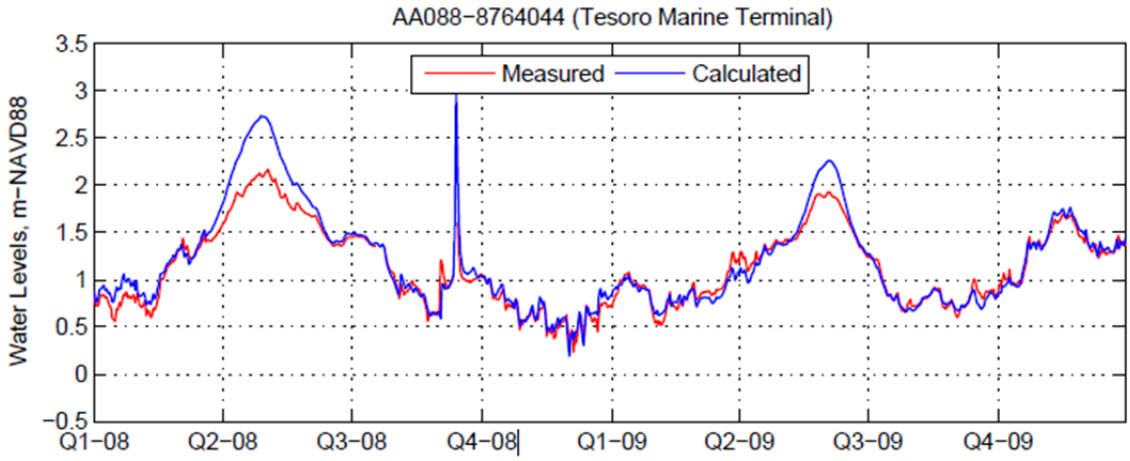

Figure 348 STG Validation Results for Tesoro Marine Terminal in the AA Model

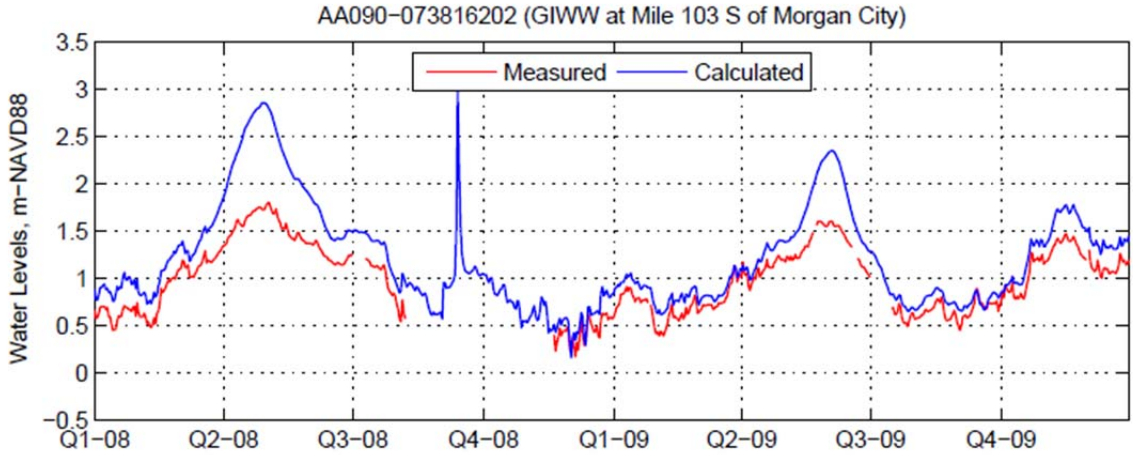

Figure 349 STG Validation Results for GIWW at Mile 103 in the AA Model

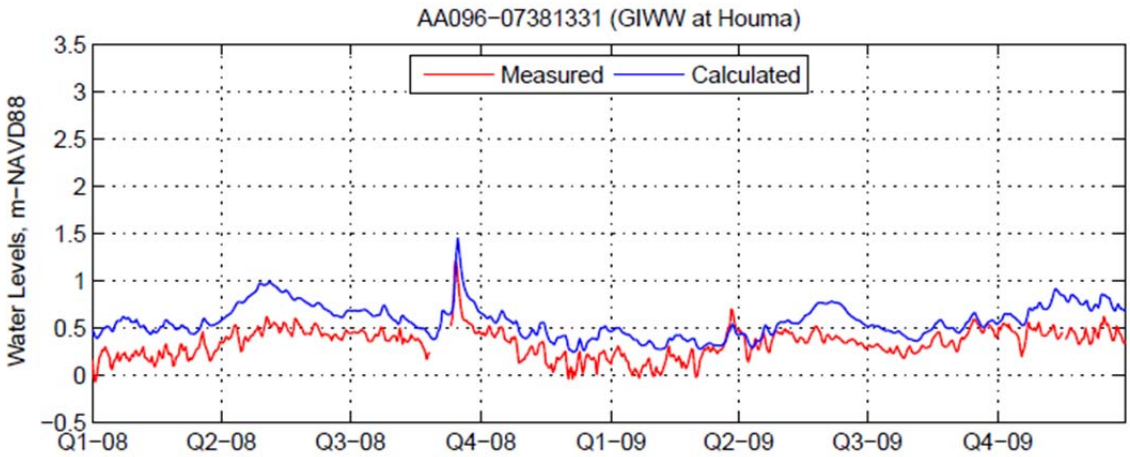

Figure 350 STG Validation Results for GIWW at Houma in the AA Model

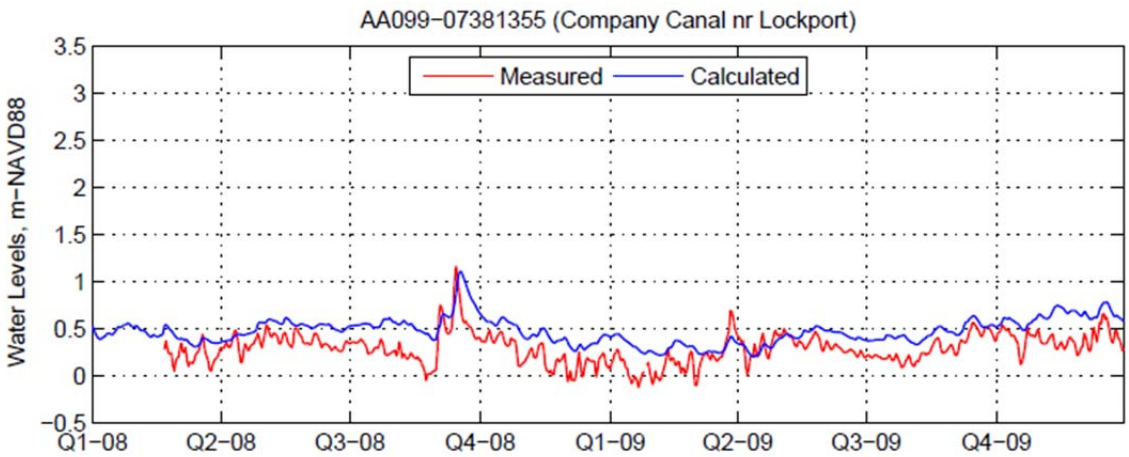

Figure 351 STG Validation Results for Company Canal near Lockport in the AA Model

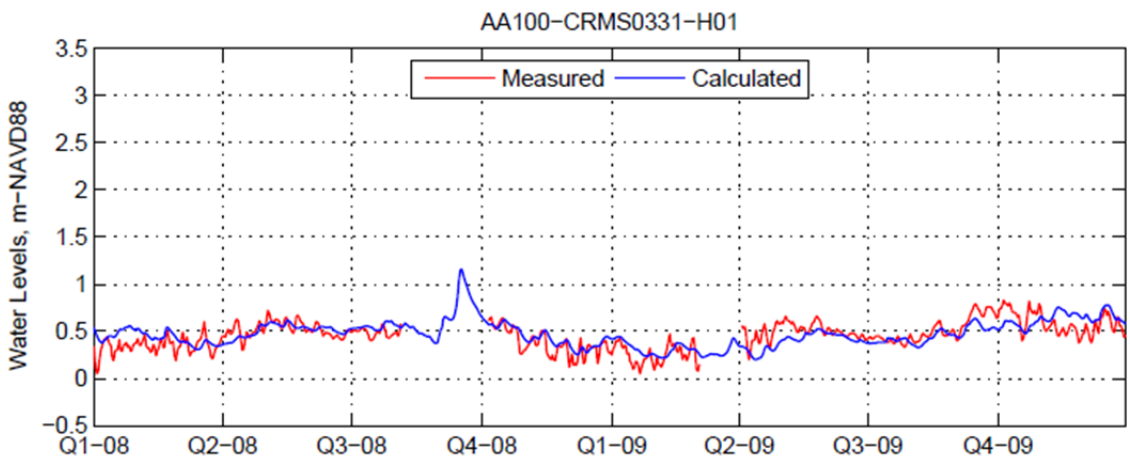

Figure 352 STG Validation Results for AA100 in the AA Model

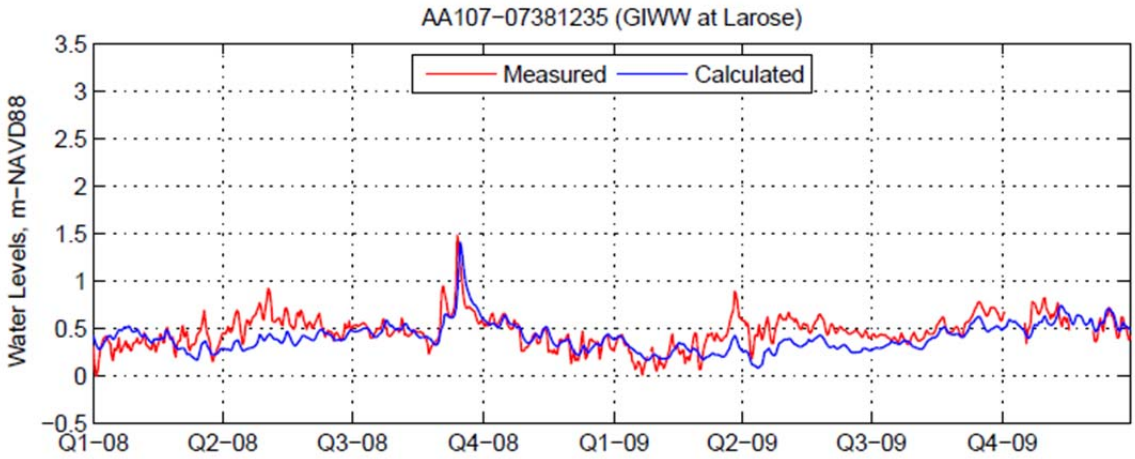

Figure 353 STG Validation Results for GIWW at Larose in the AA Model

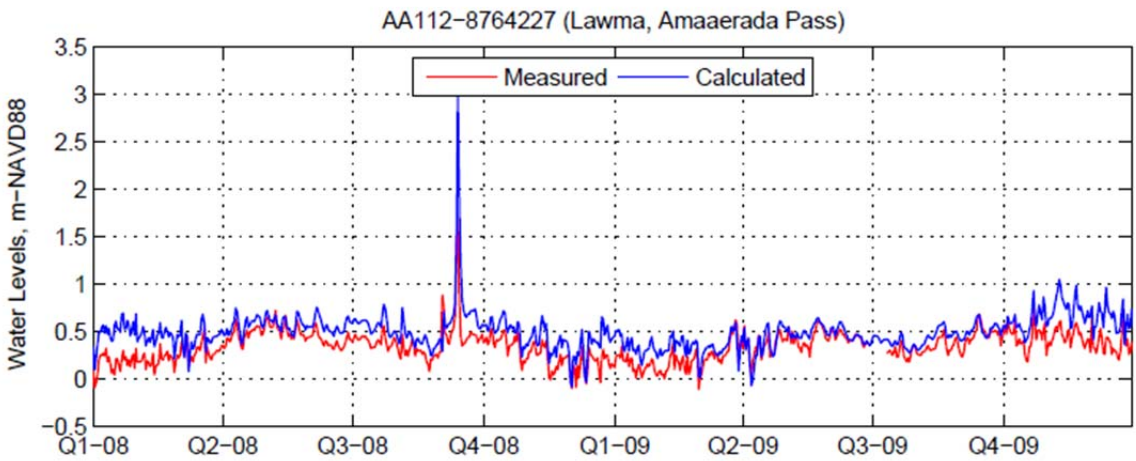

Figure 354 STG Validation Results for Lawma, Amerada Pass in the AA Model

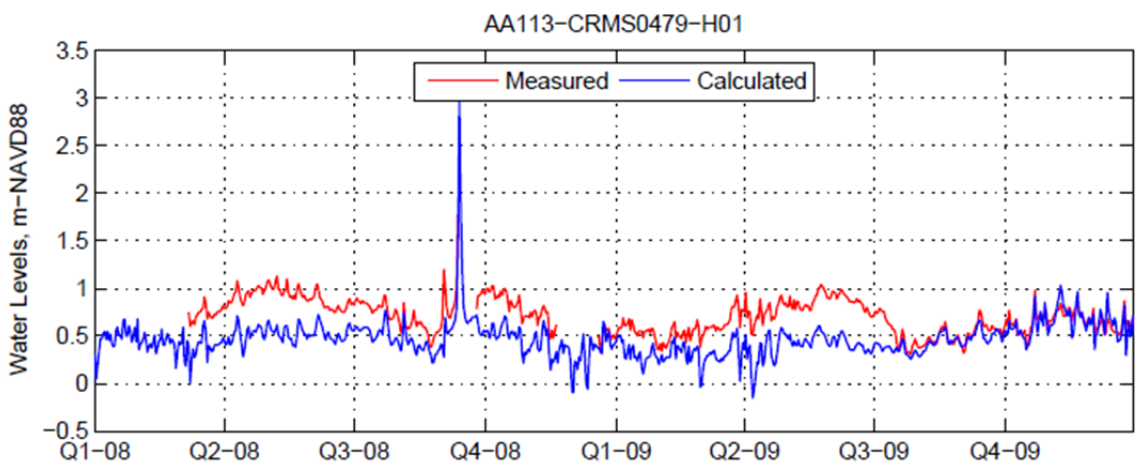

Figure 355 STG Validation Results for AA113 in the AA Model

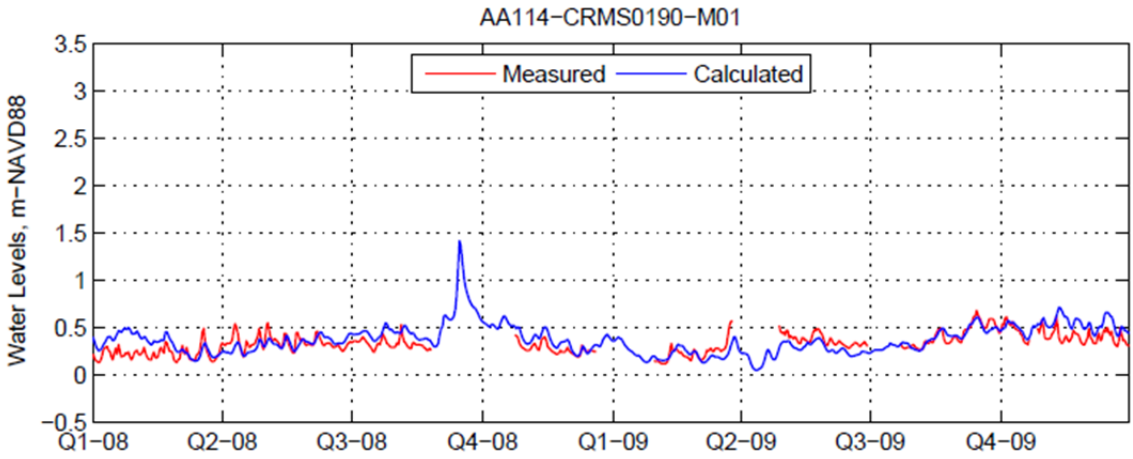

Figure 356 STG Validation Results for AA114 in the AA Model

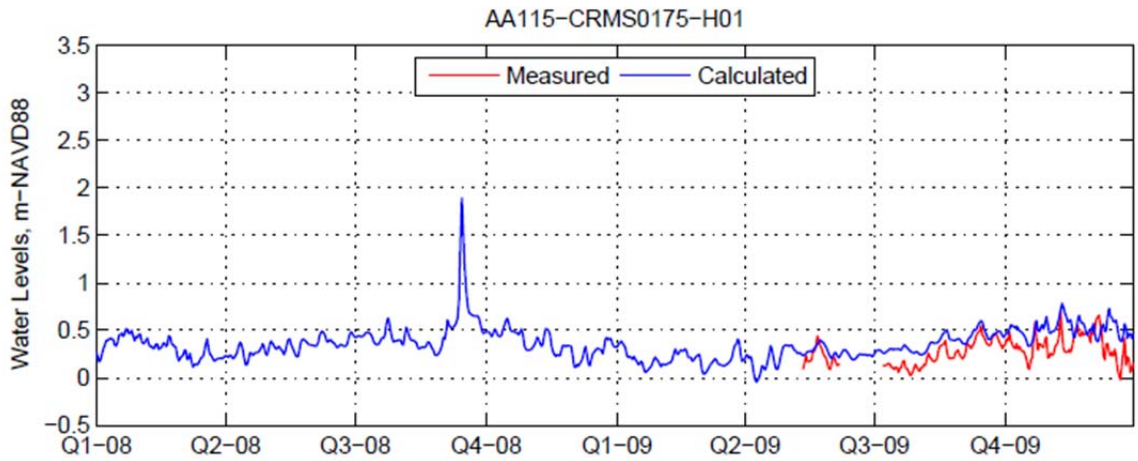

Figure 357 STG Validation Results for AA115 in the AA Model

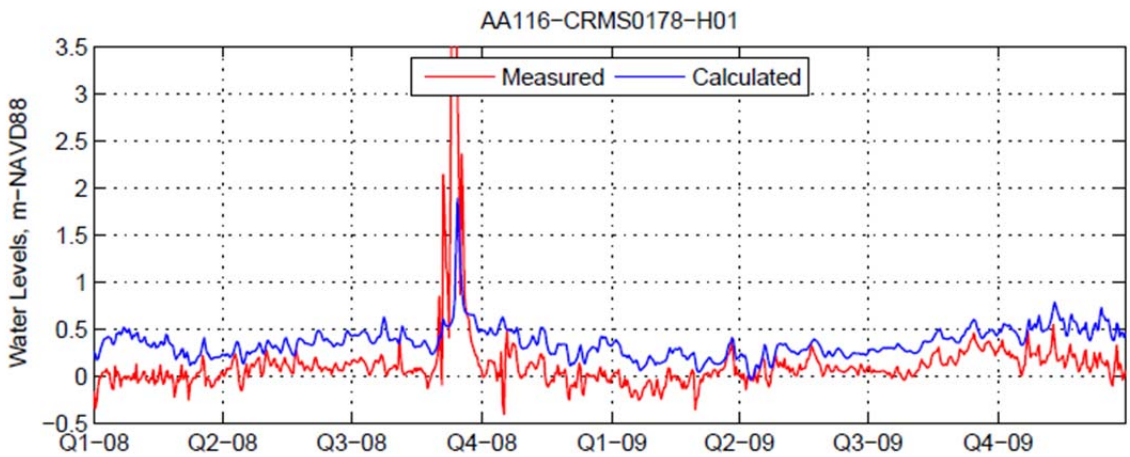

Figure 358 STG Validation Results for AA116 in the AA Model

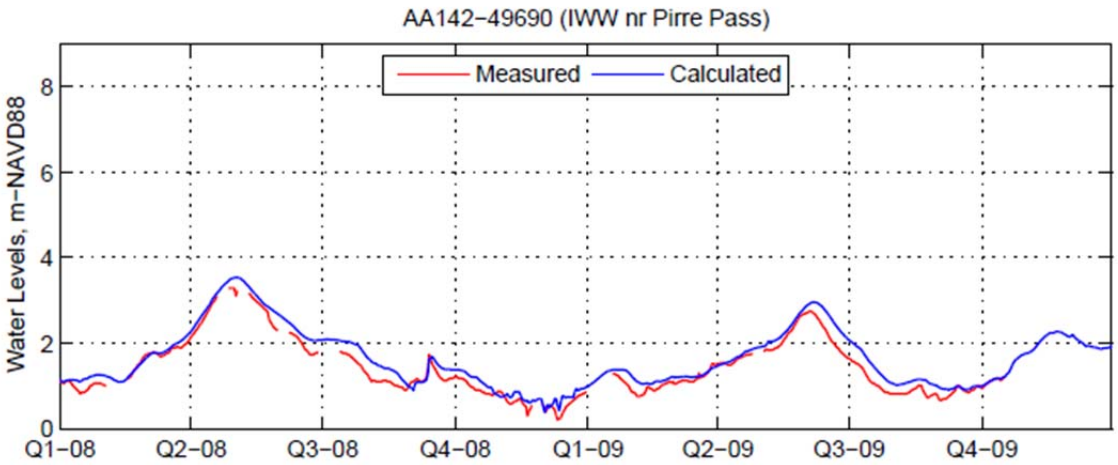

Figure 359 STG Validation Results for ICWW near Pierre Pass in the AA Model

Discharge

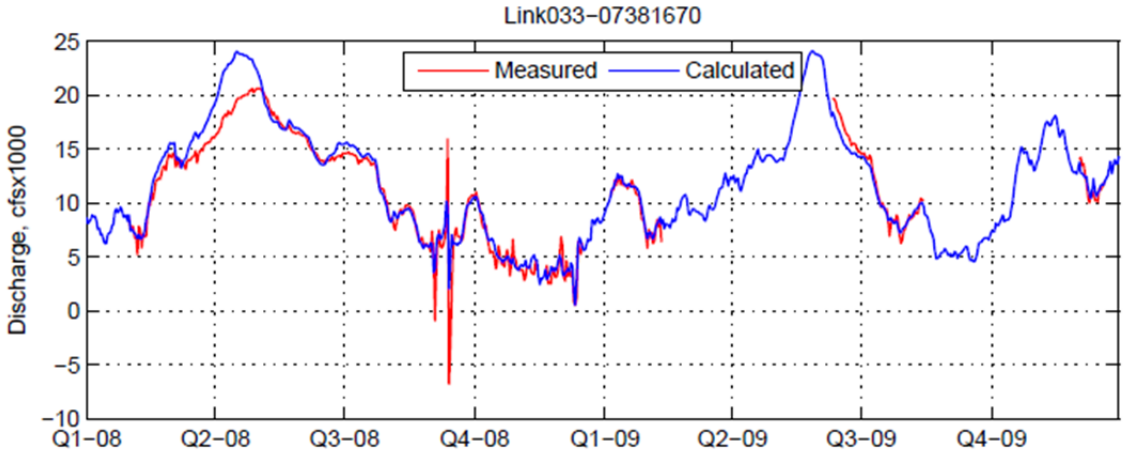

Figure 360 Discharge Validation Results for Link 033 in the AA Model

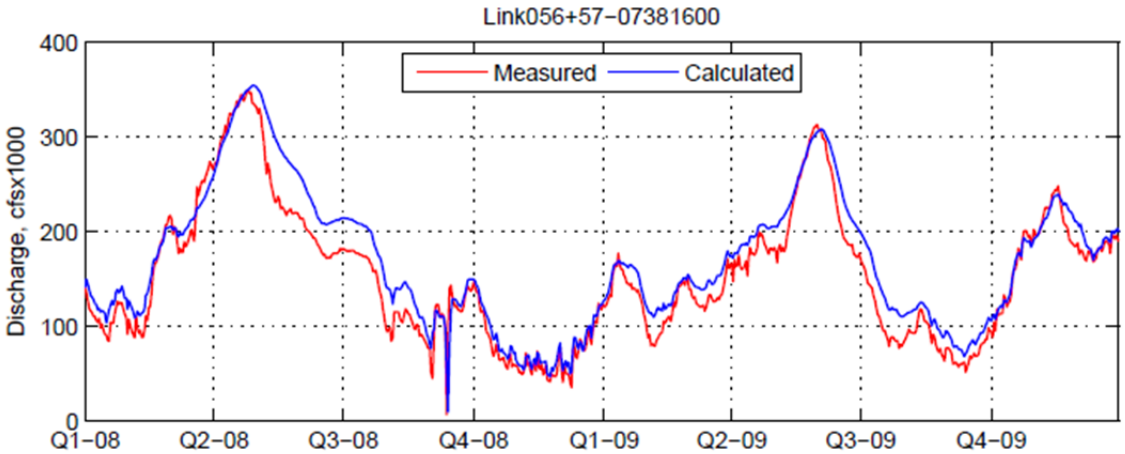

Figure 361 Discharge Validation Results for Links 056 and 057 in the AA Model

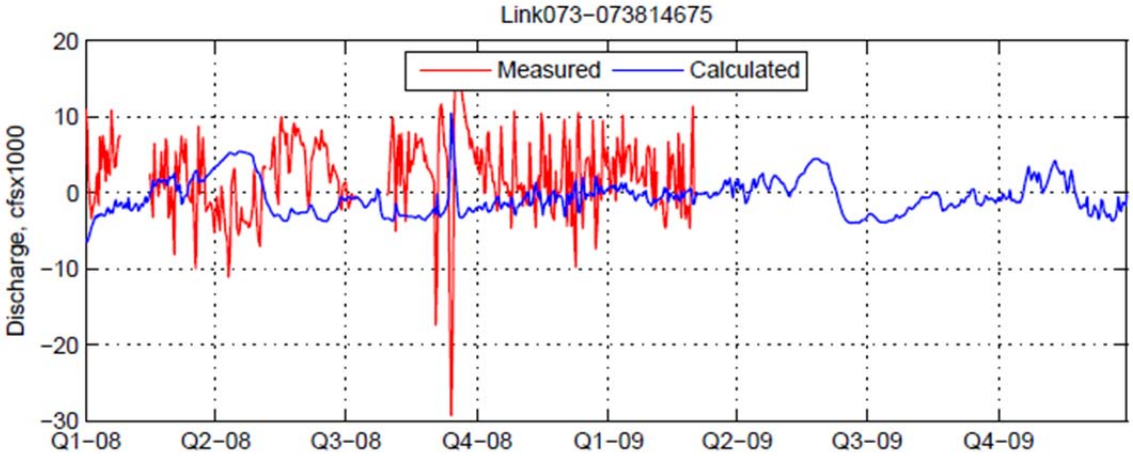

Figure 362 Discharge Validation Results for Link 073 in the AA Model

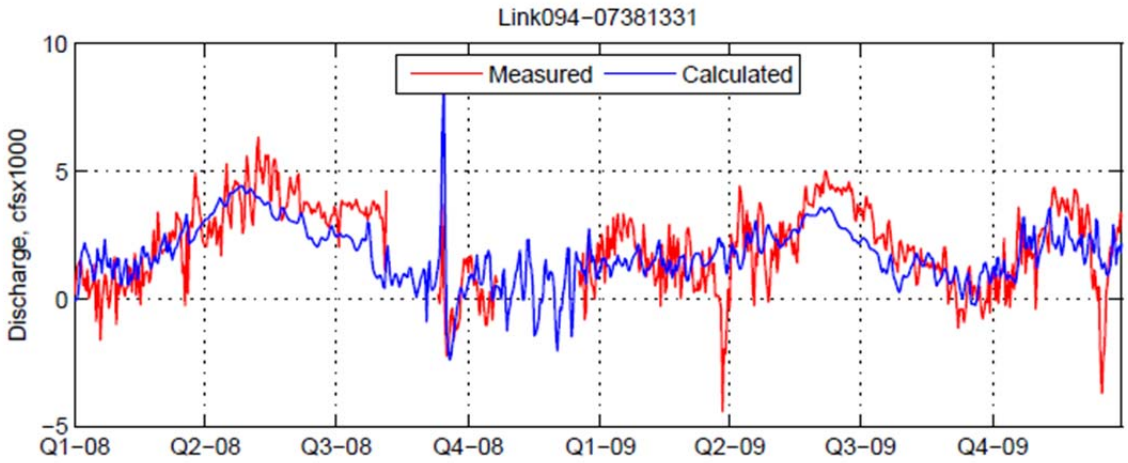

Figure 363 Discharge Validation Results for Link 094 in the AA Model

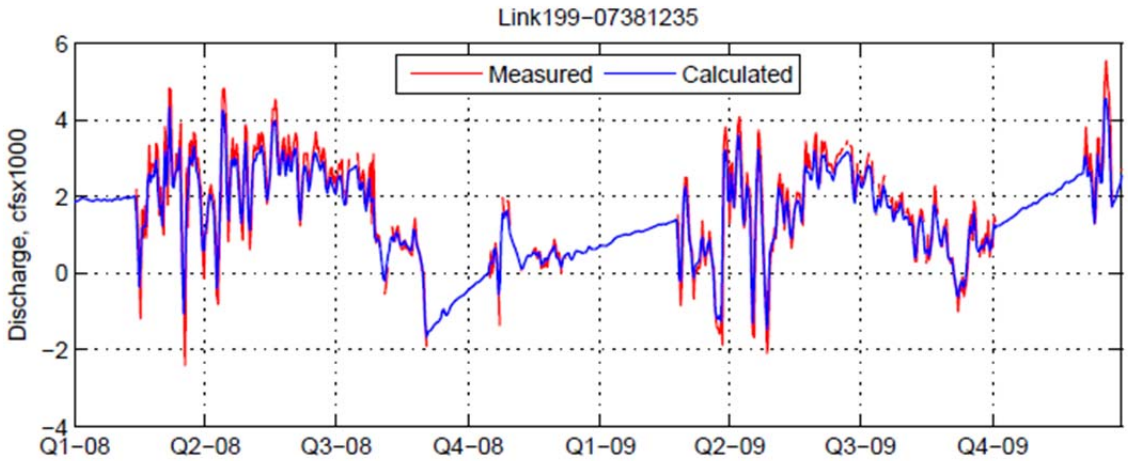

Figure 364 Discharge Validation Results for Link 199 in the AA Model

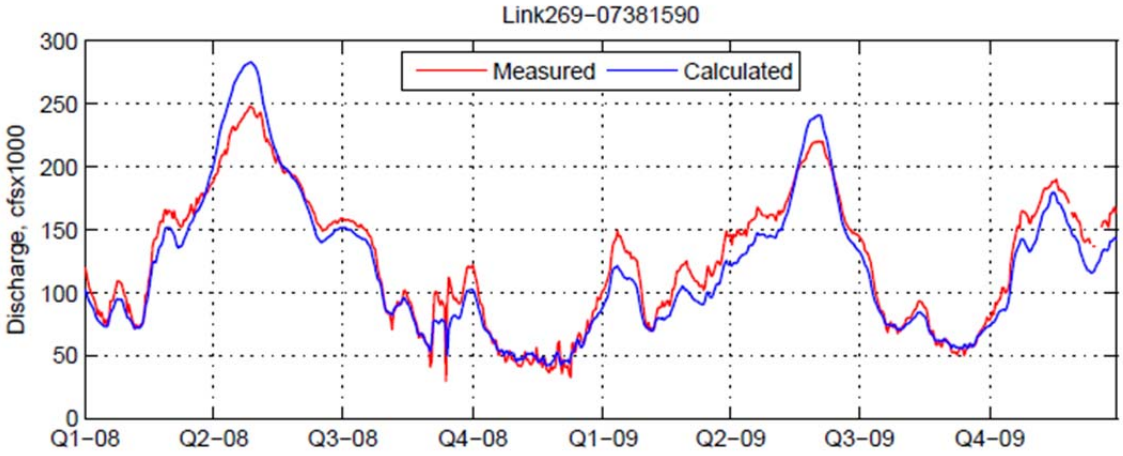

Figure 365 Discharge Validation Results for Link 269 in the AA Model

Salinity (SAL)

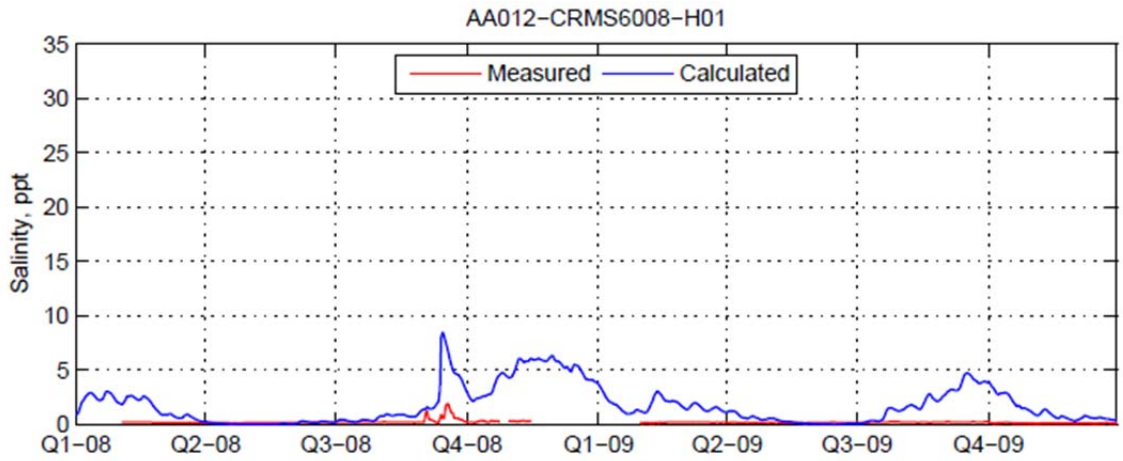

Figure 366 SAL Validation Results for AA012 in the AA Model

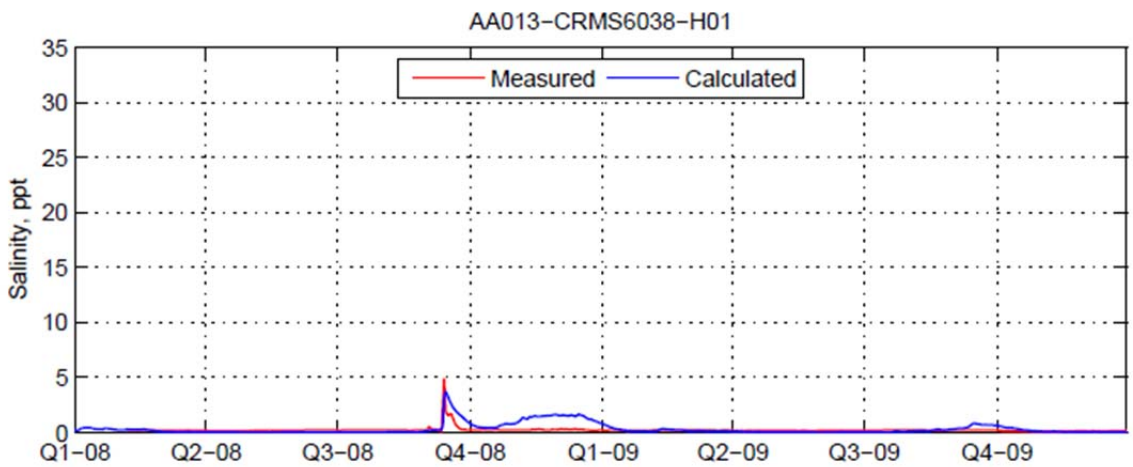

Figure 367 SAL Validation Results for AA013 in the AA Model

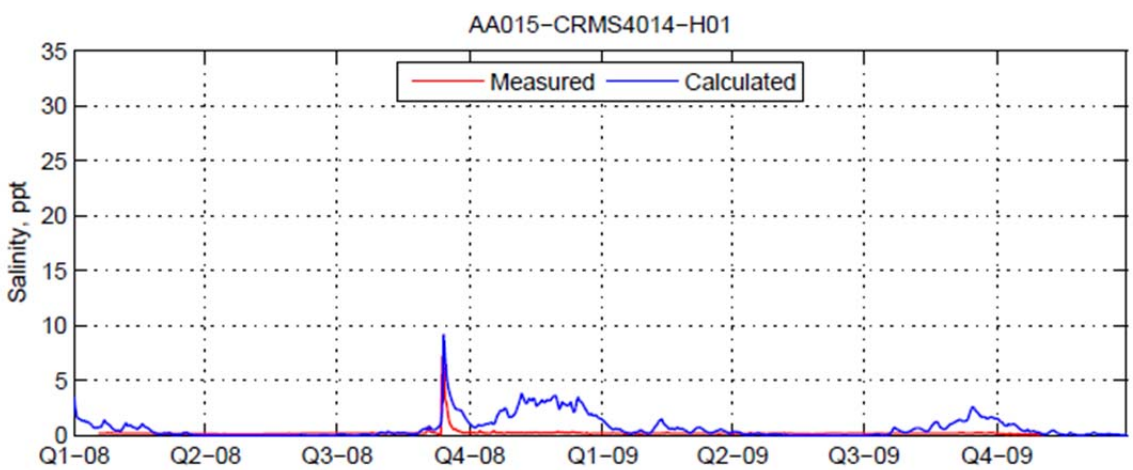

Figure 368 SAL Validation Results for AA015 in the AA Model

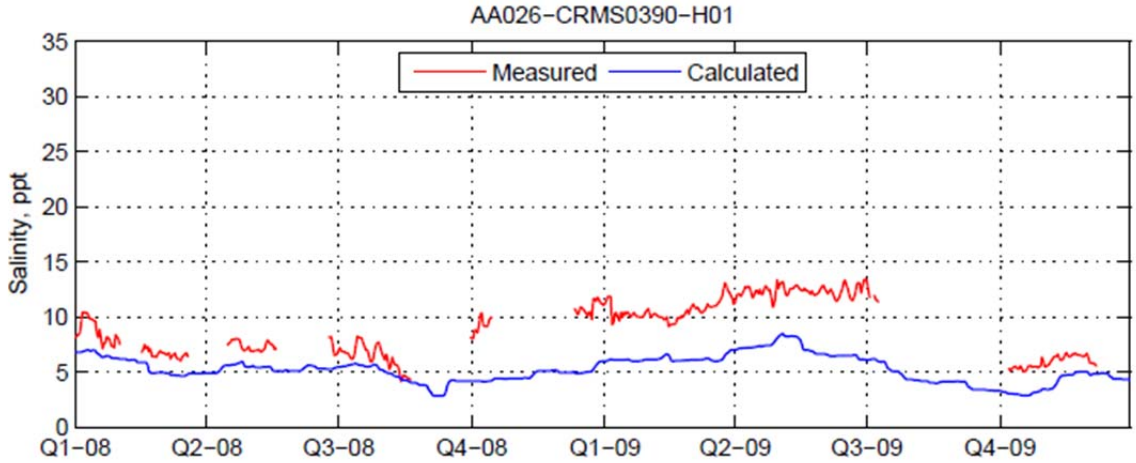

Figure 369 SAL Validation Results for AA026 in the AA Model

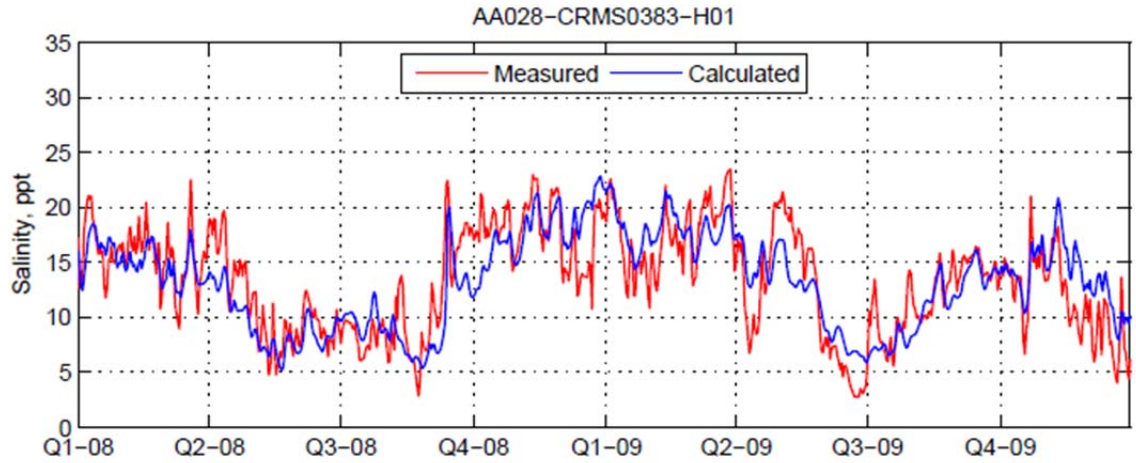

Figure 370 SAL Validation Results for AA028 in the AA Model

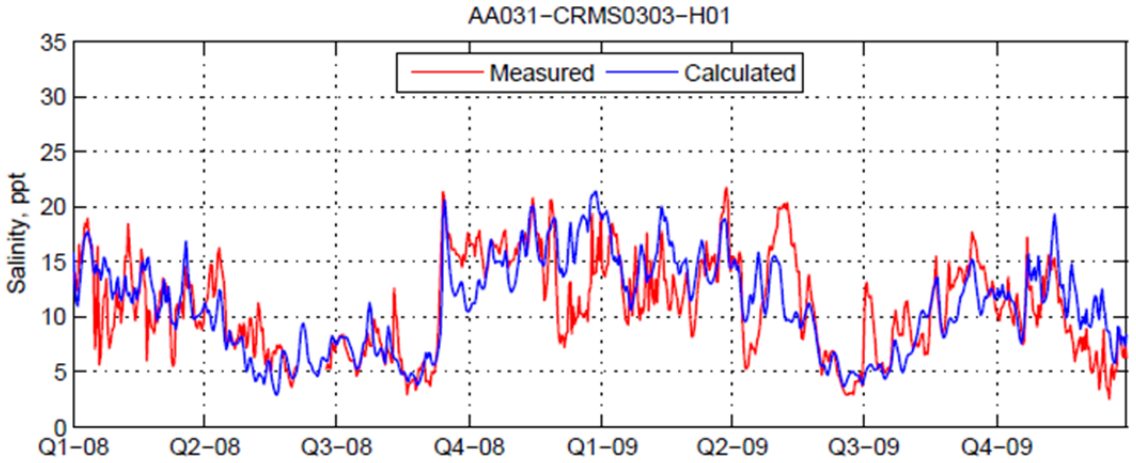

Figure 371 SAL Validation Results for AA031 in the AA Model

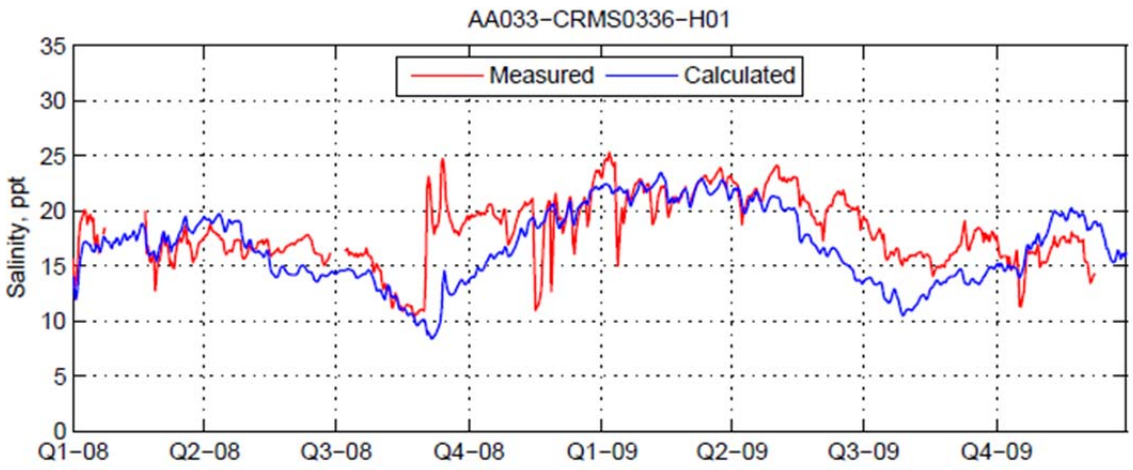

Figure 372 SAL Validation Results for AA033 in the AA Model

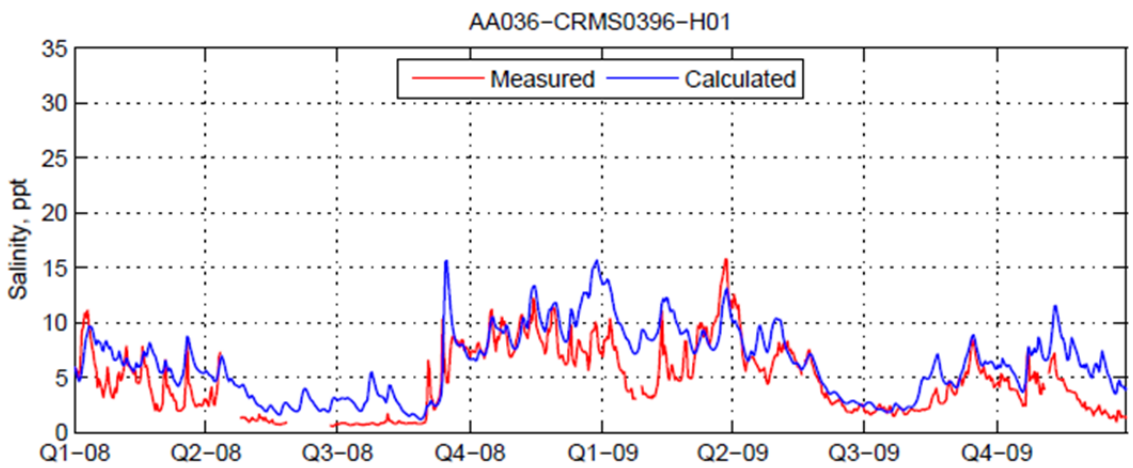

Figure 373 SAL Validation Results for AA036 in the AA Model

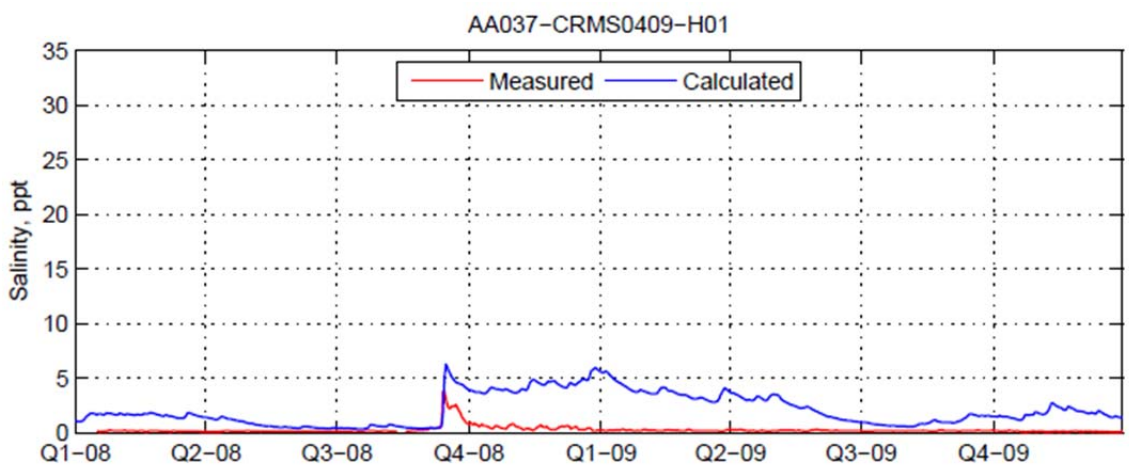

Figure 374 SAL Validation Results for AA037 in the AA Model

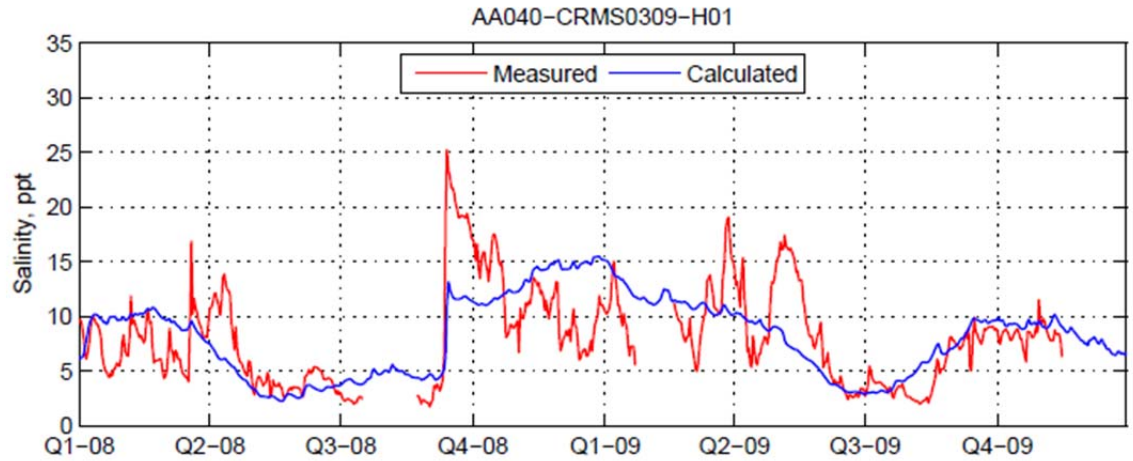

Figure 375 SAL Validation Results for AA040 in the AA Model

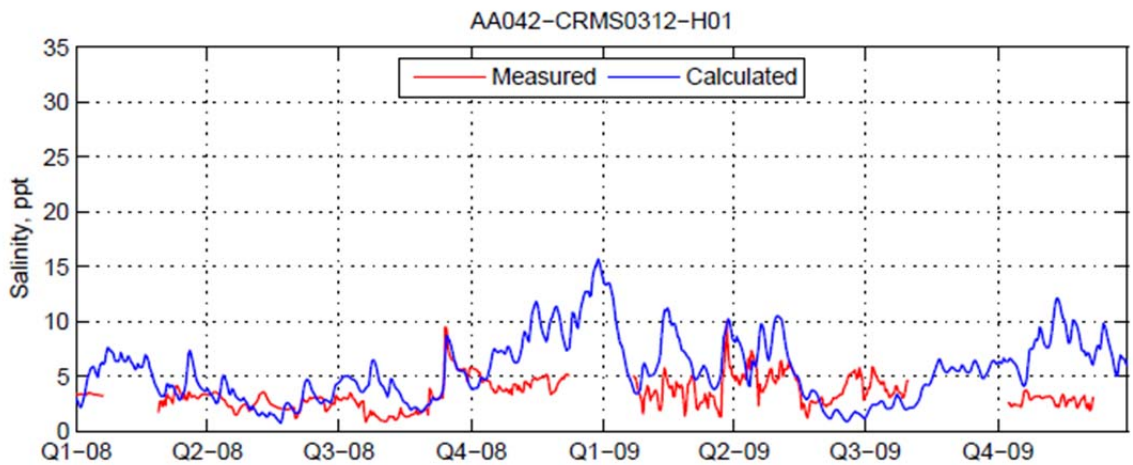

Figure 376 SAL Validation Results for AA042 in the AA Model

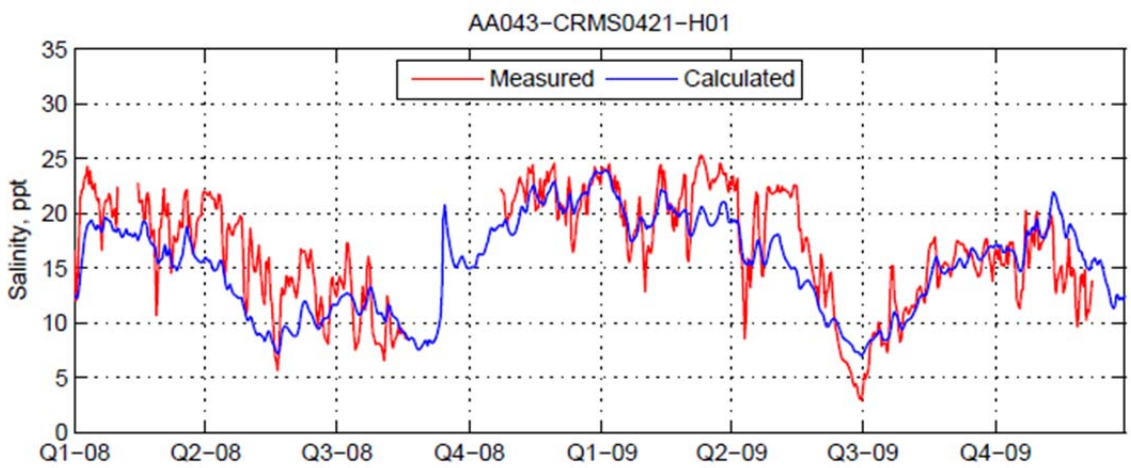

Figure 377 SAL Validation Results for AA043 in the AA Model

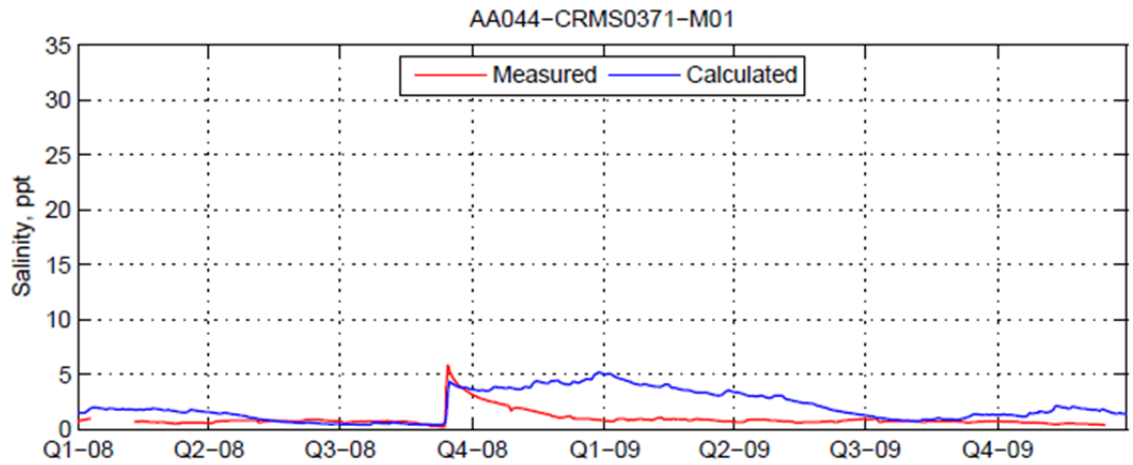

Figure 378 SAL Validation Results for AA044 in the AA Model

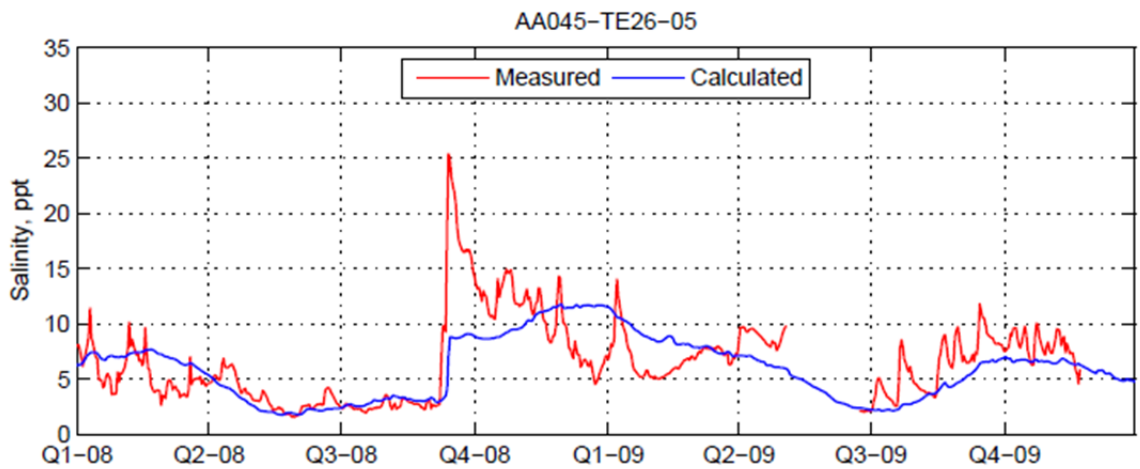

Figure 379 SAL Validation Results for Lake Chapeau in the AA Model

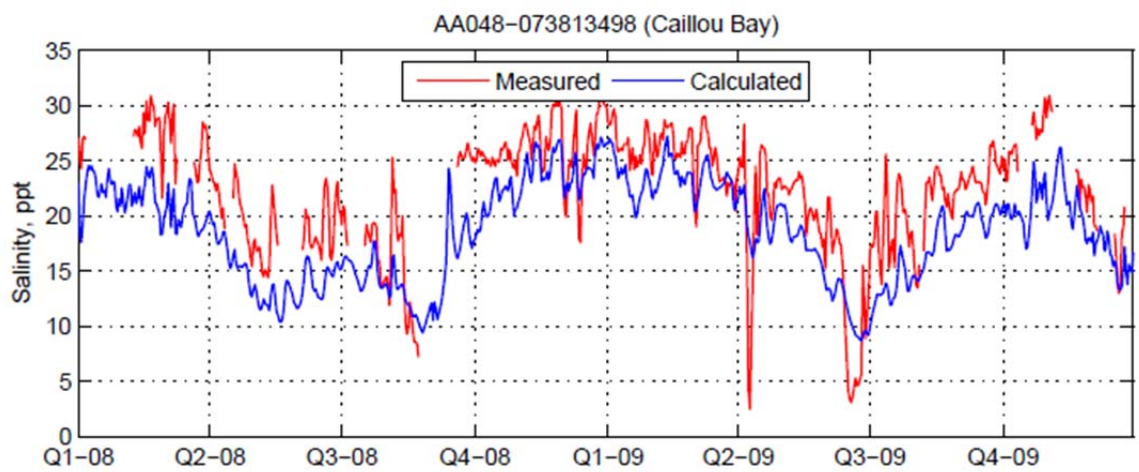

Figure 380 SAL Validation Results for Caillou Bay in the AA Model

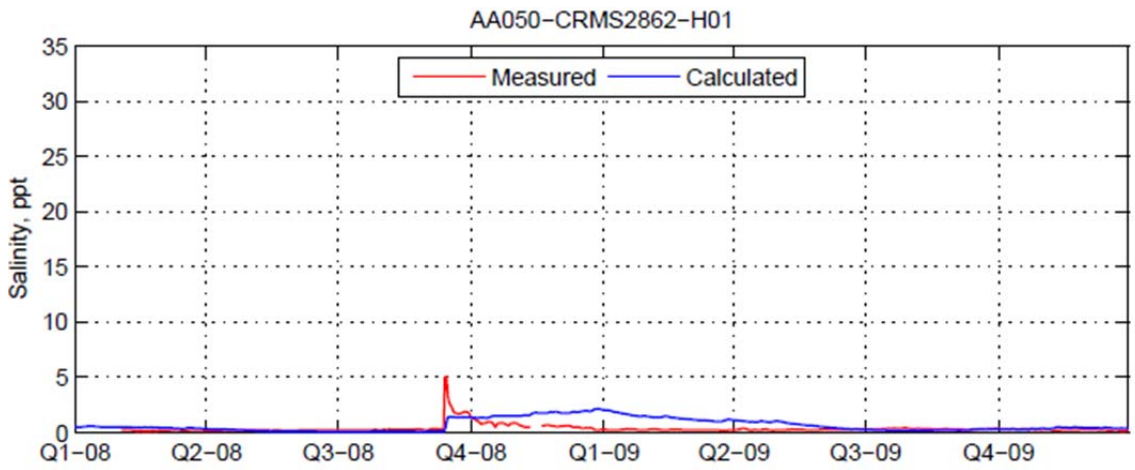

Figure 381 SAL Validation Results for AA050 in the AA Model

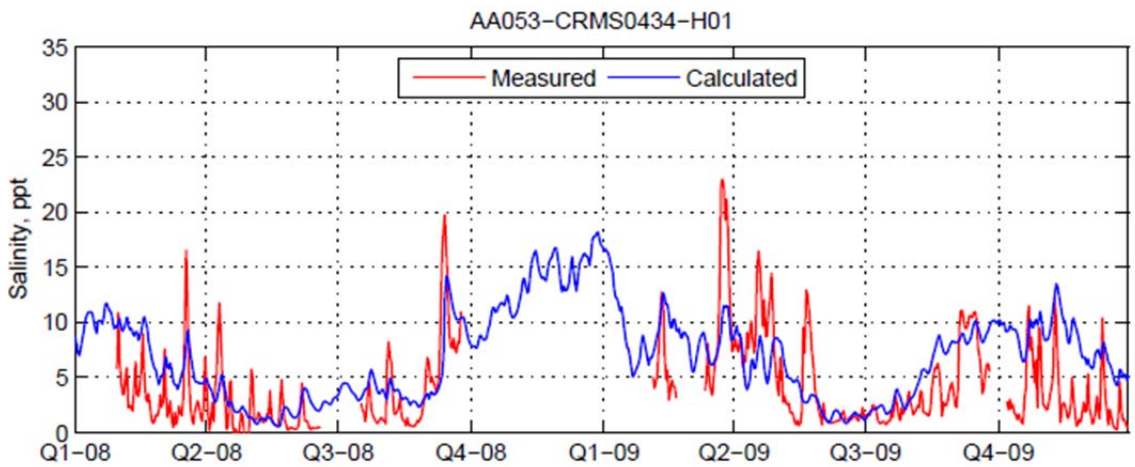

Figure 382 SAL Validation Results for AA053 in the AA Model

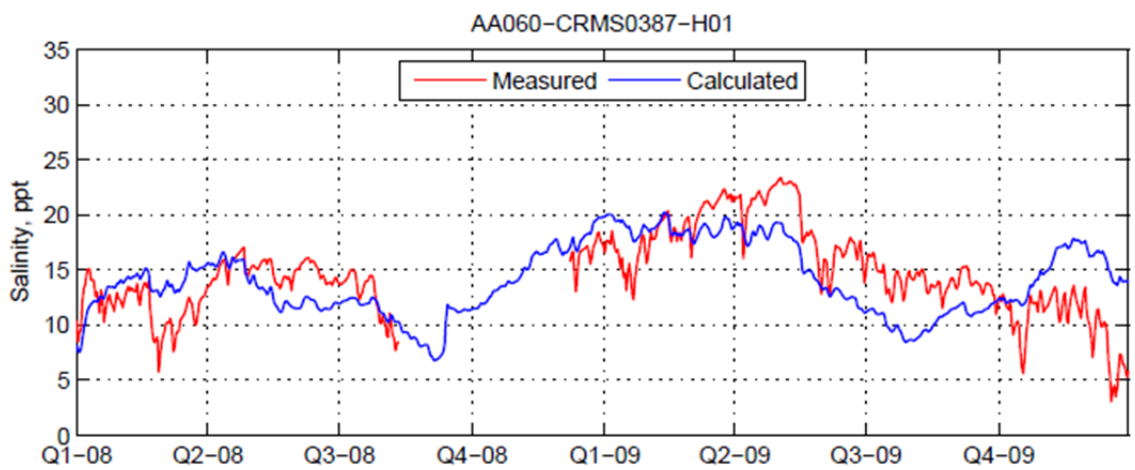

Figure 383 SAL Validation Results for AA060 in the AA Model

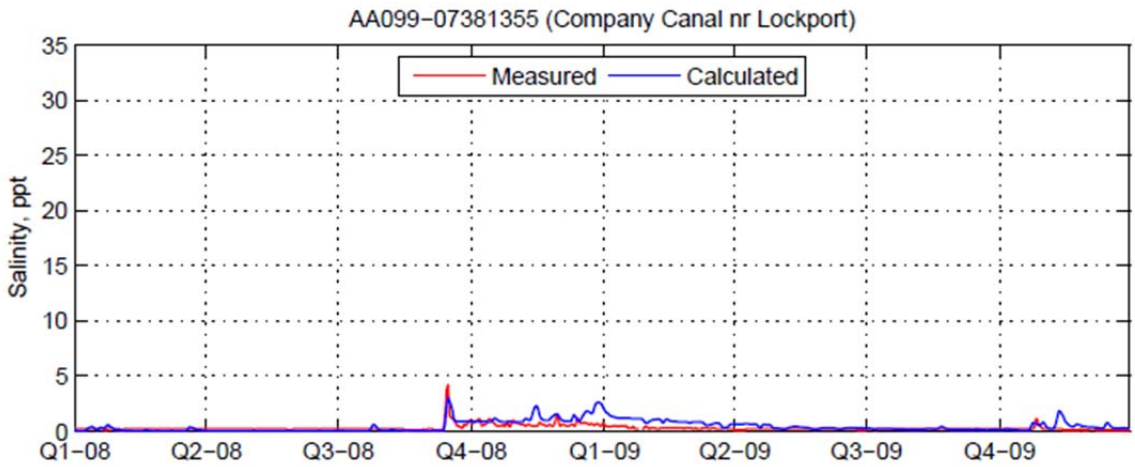

Figure 384 SAL Validation Results for Company Canal near Lockport in the AA Model

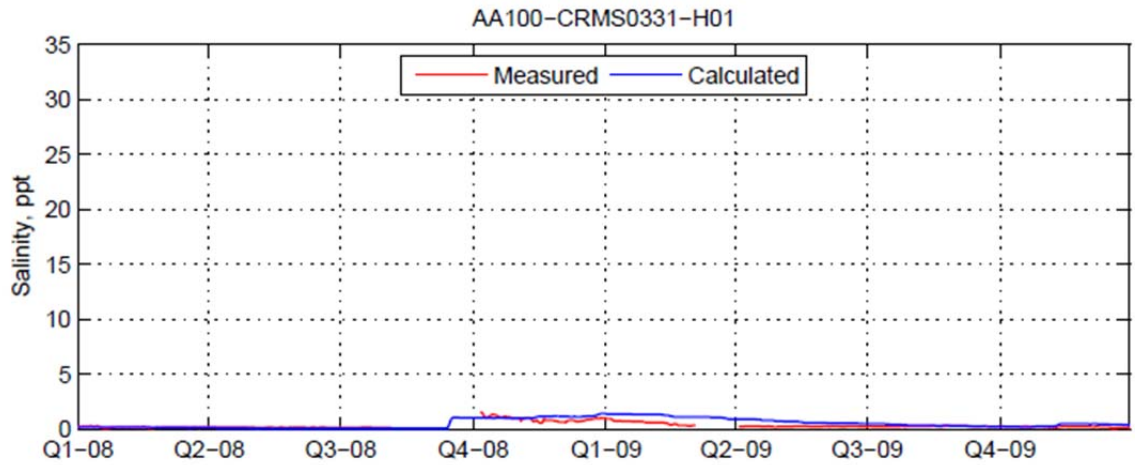

Figure 385 SAL Validation Results for AA100 in the AA Model

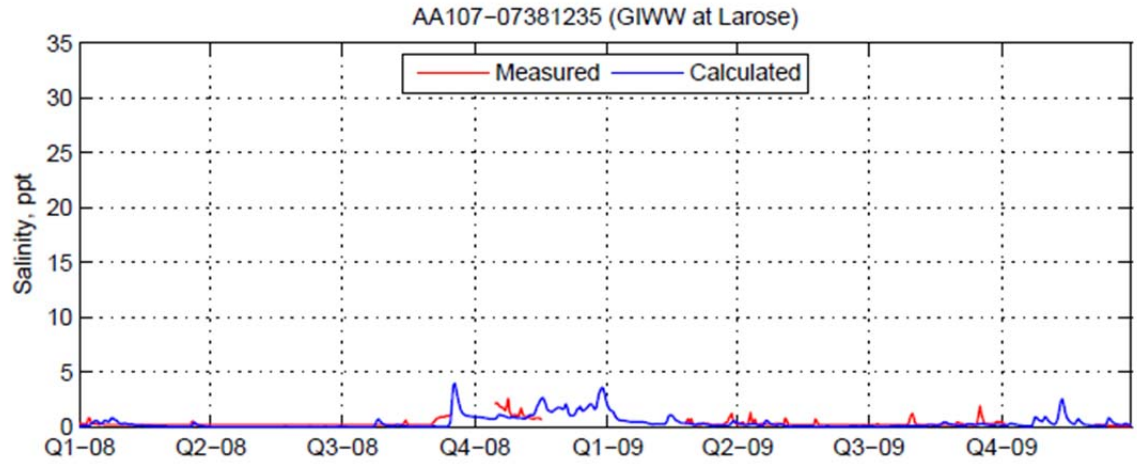

Figure 386 SAL Validation Results for GIWW at Larose in the AA Model

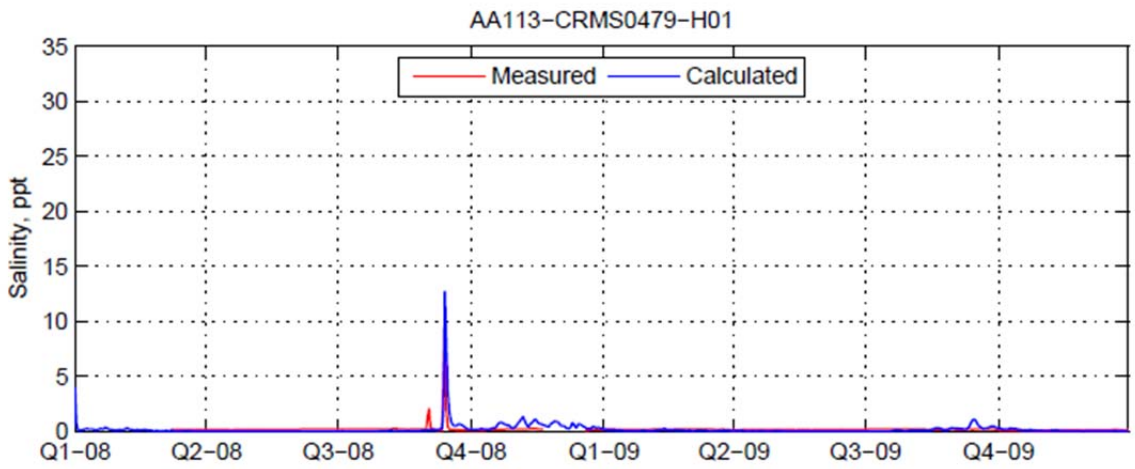

Figure 387 SAL Validation Results for AA113 in the AA Model

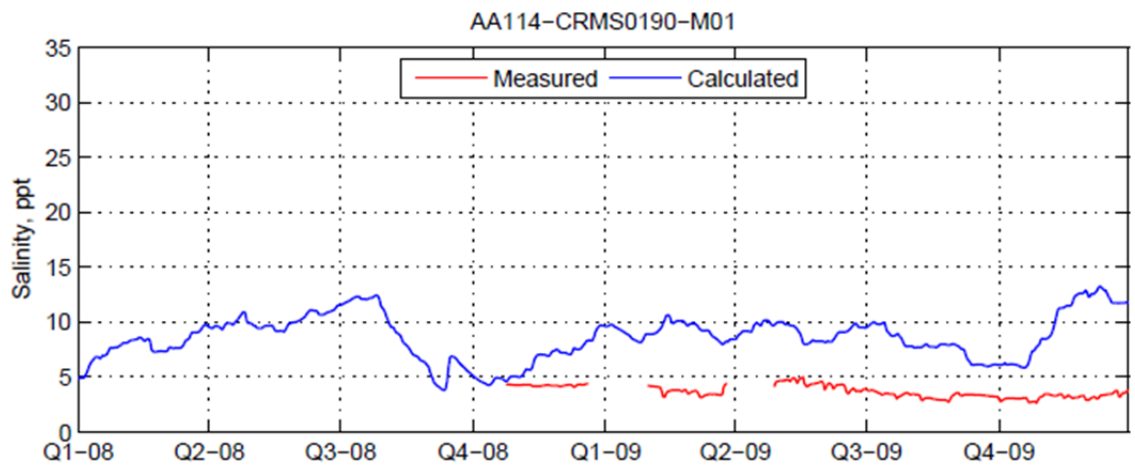

Figure 388 SAL Validation Results for AA114 in the AA Model

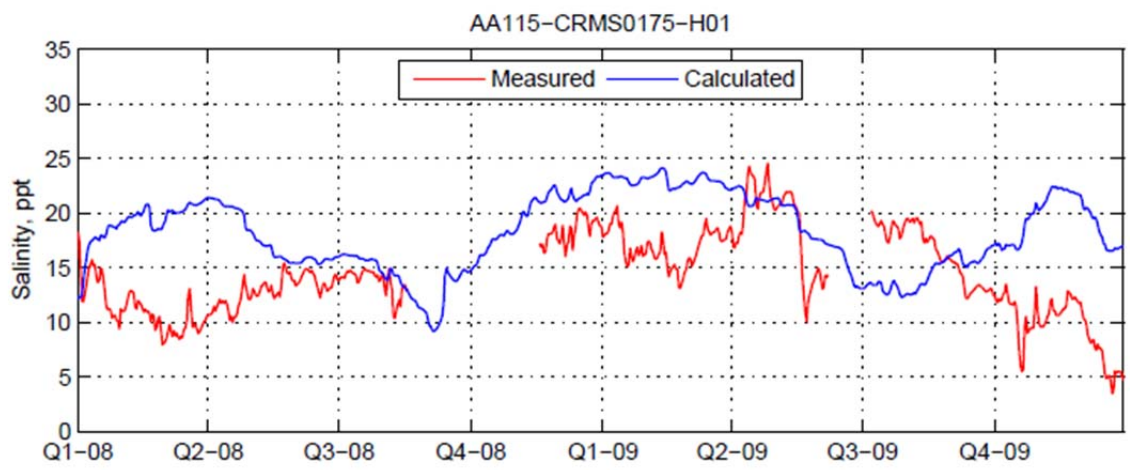

Figure 389 SAL Validation Results for AA115 in the AA Model

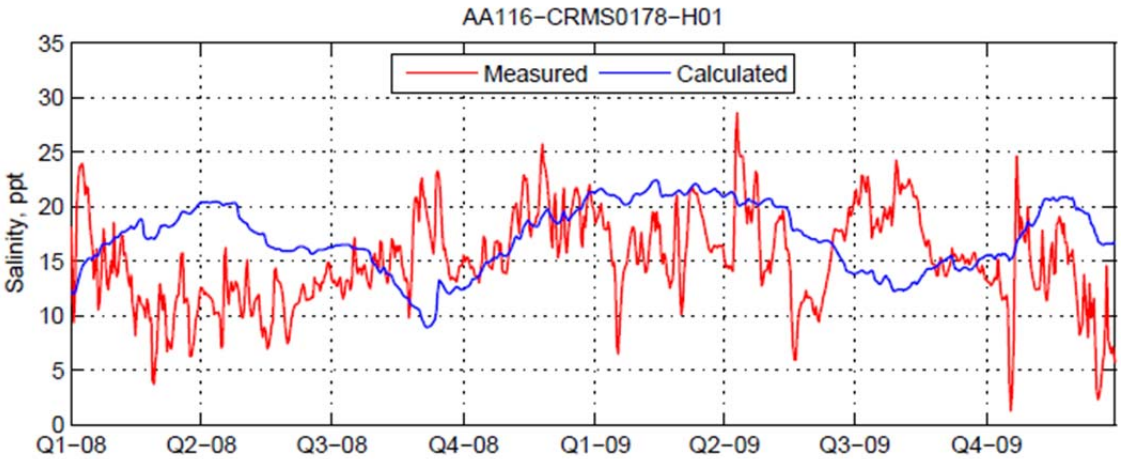

Figure 390 SAL Validation Results for AA116 in the AA Model

Temperature (TMP)

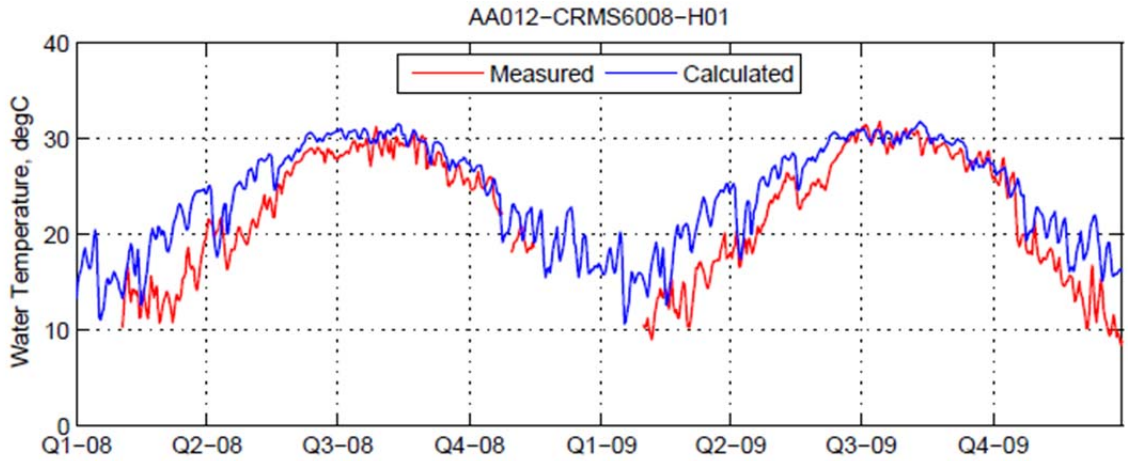

Figure 391 TMP Validation Results for AA012 in the AA Model

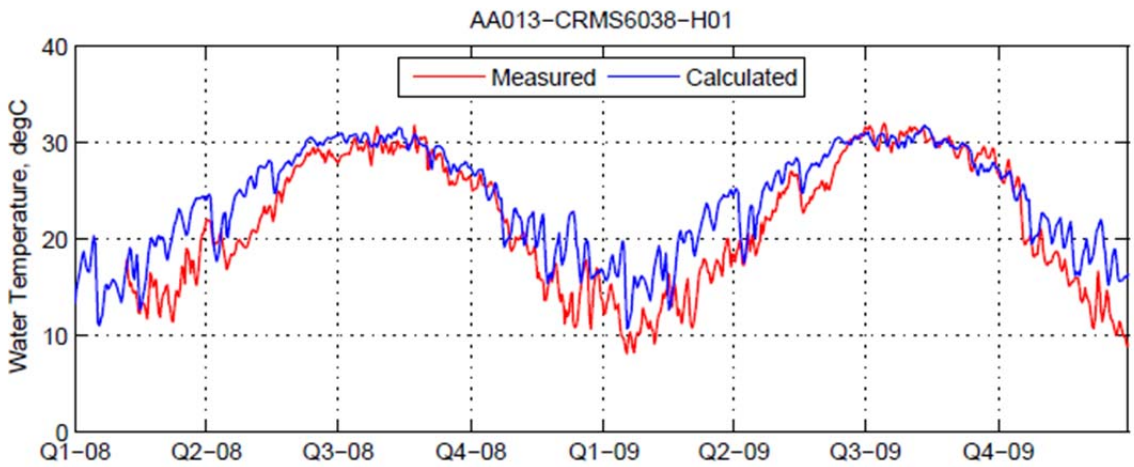

Figure 392 TMP Validation Results for AA013 in the AA Model

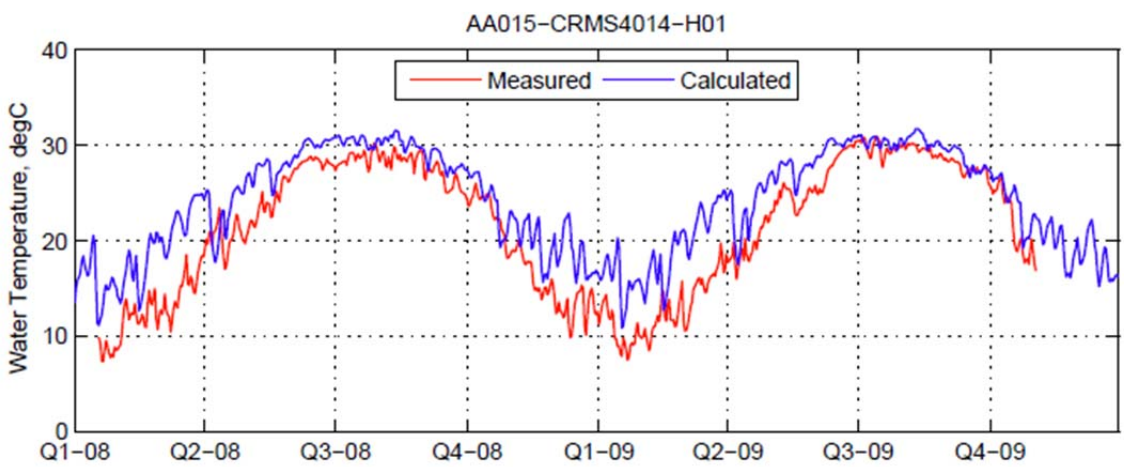

Figure 393 TMP Validation Results for AA015 in the AA Model

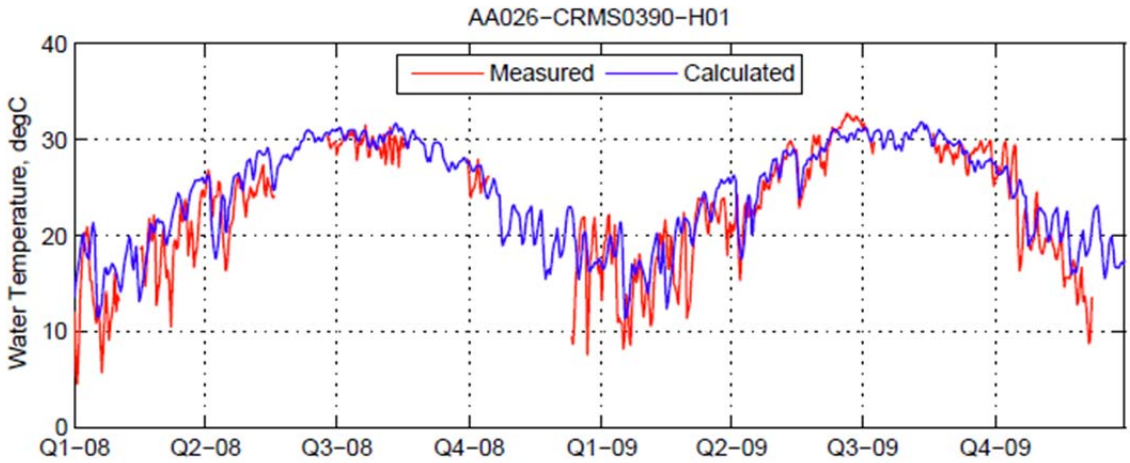

Figure 394 TMP Validation Results for AA026 in the AA Model

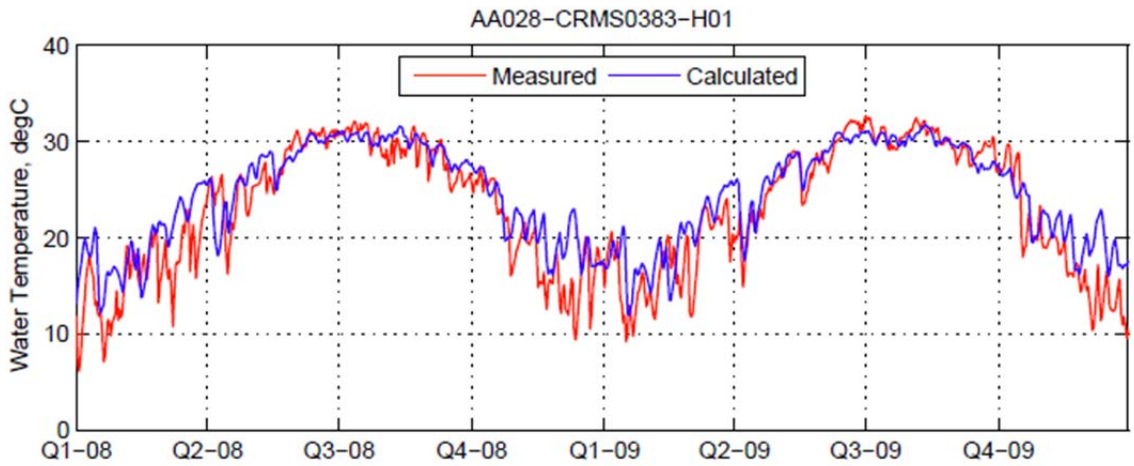

Figure 395 TMP Validation Results for AA028 in the AA Model

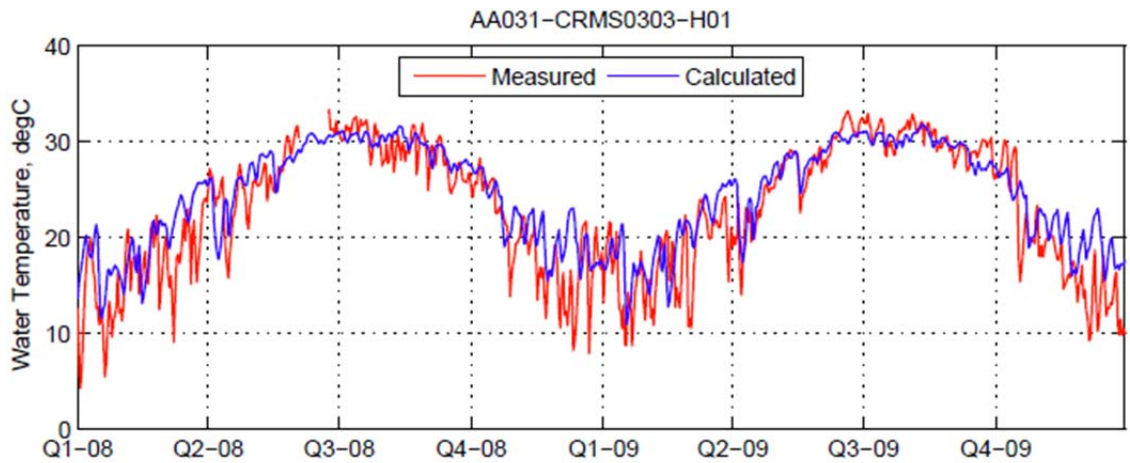

Figure 396 TMP Validation Results for AA031 in the AA Model

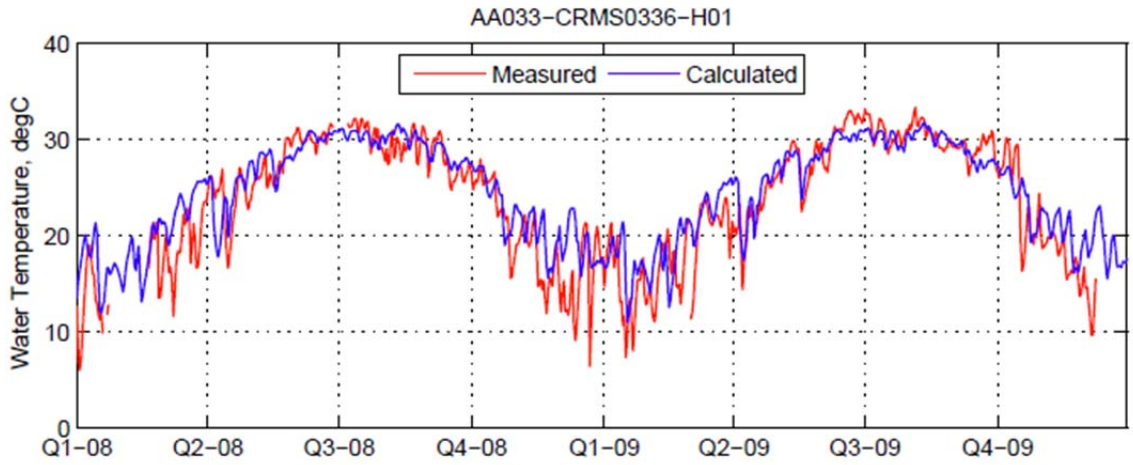

Figure 397 TMP Validation Results for AA033 in the AA Model

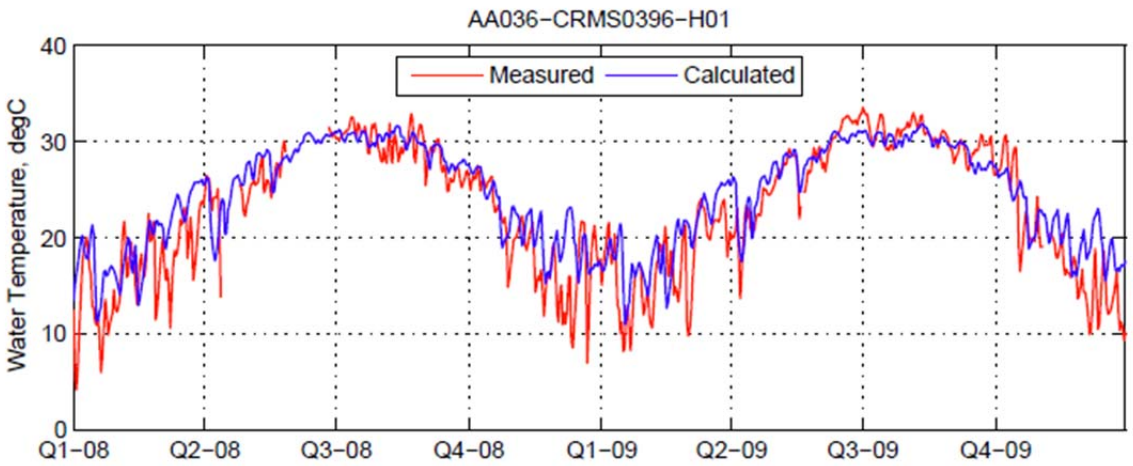

Figure 398 TMP Validation Results for AA036 in the AA Model

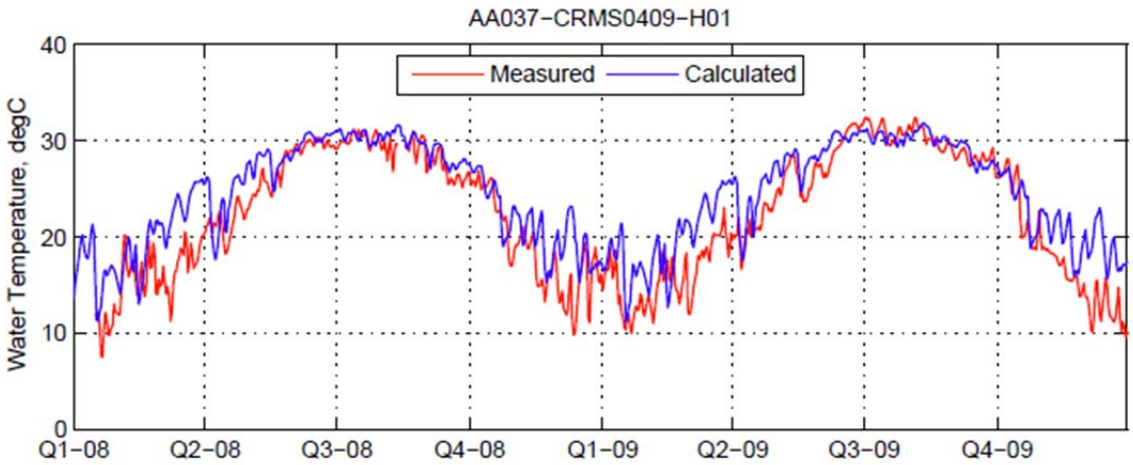

Figure 399 TMP Validation Results for AA037 in the AA Model

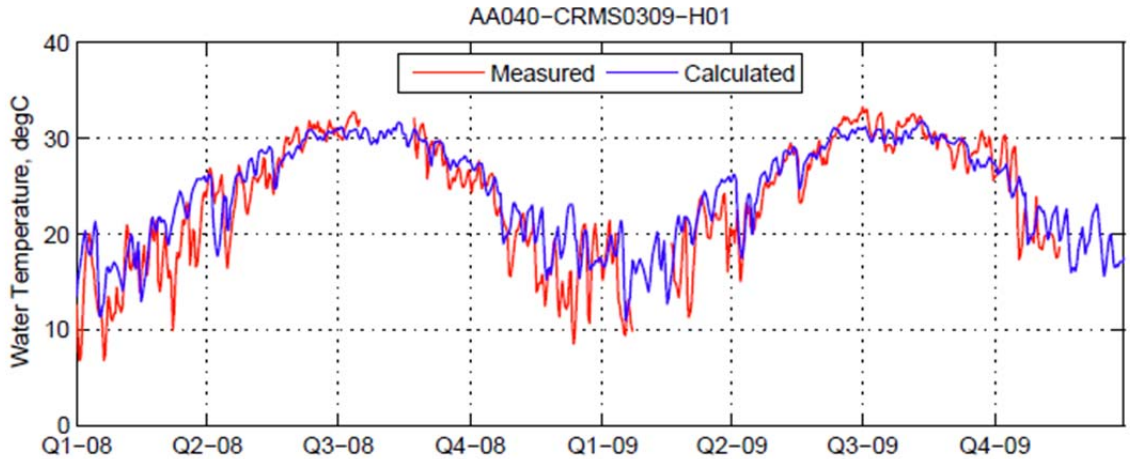

Figure 400 TMP Validation Results for AA040 in the AA Model

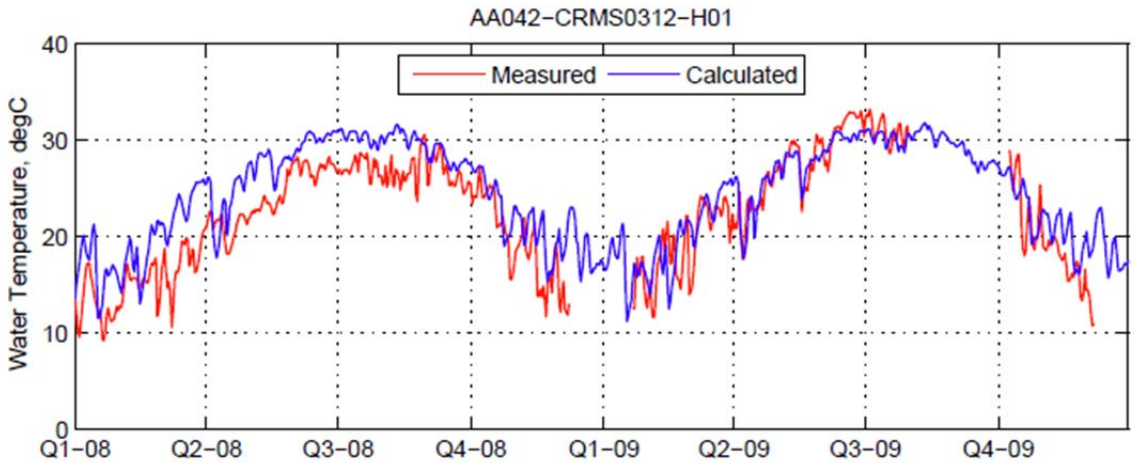

Figure 401 TMP Validation Results for AA042 in the AA Model

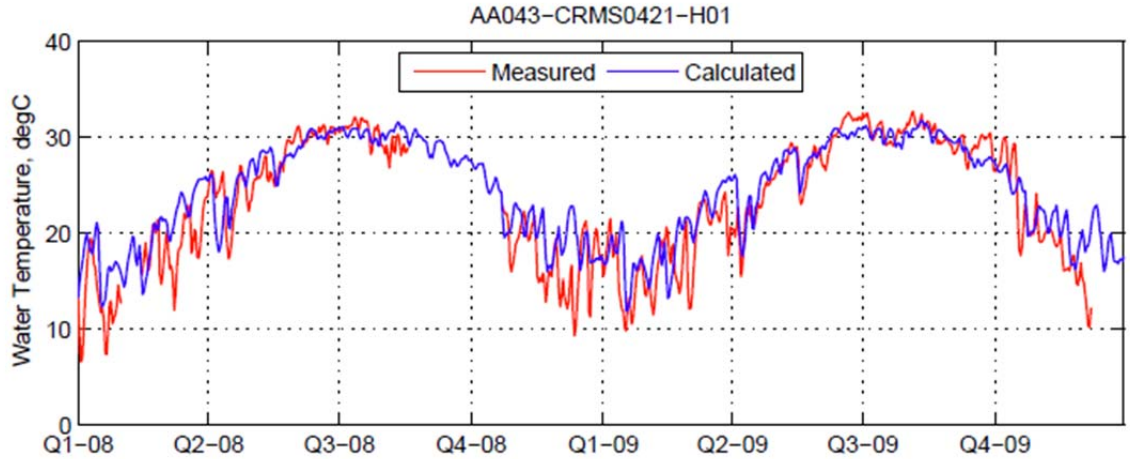

Figure 402 TMP Validation Results for AA043 in the AA Model

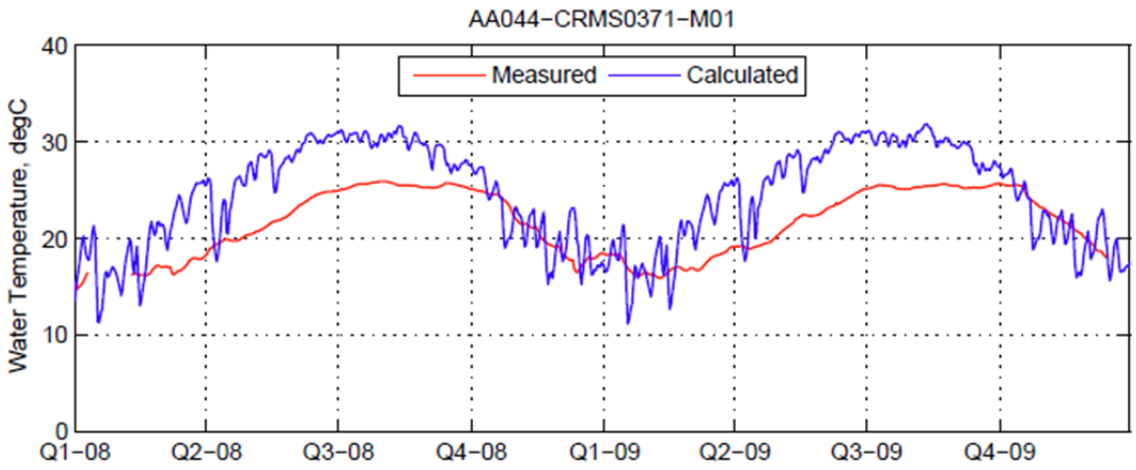

Figure 403 TMP Validation Results for AA044 in the AA Model

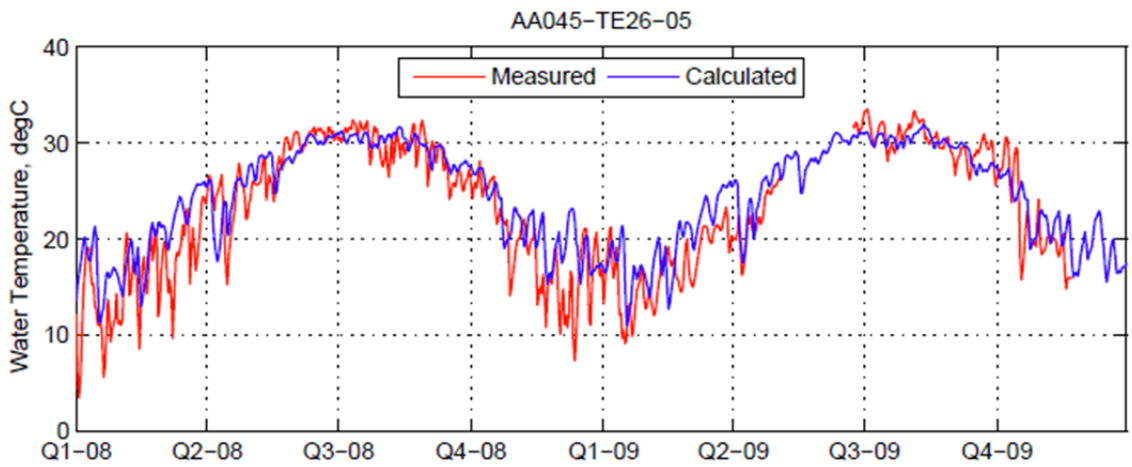

Figure 404 TMP Validation Results for Lake Chapeau in the AA Model

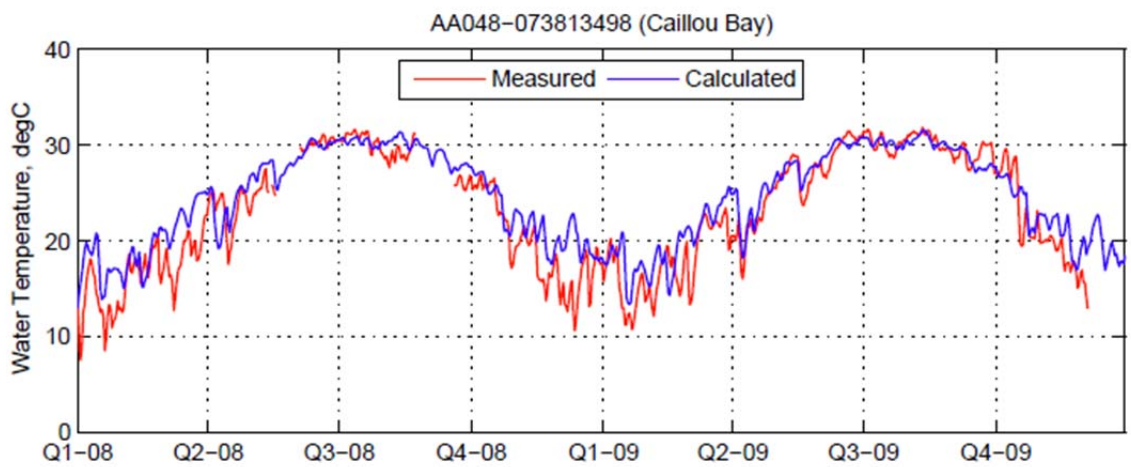

Figure 405 TMP Validation Results for Caillou Bay in the AA Model

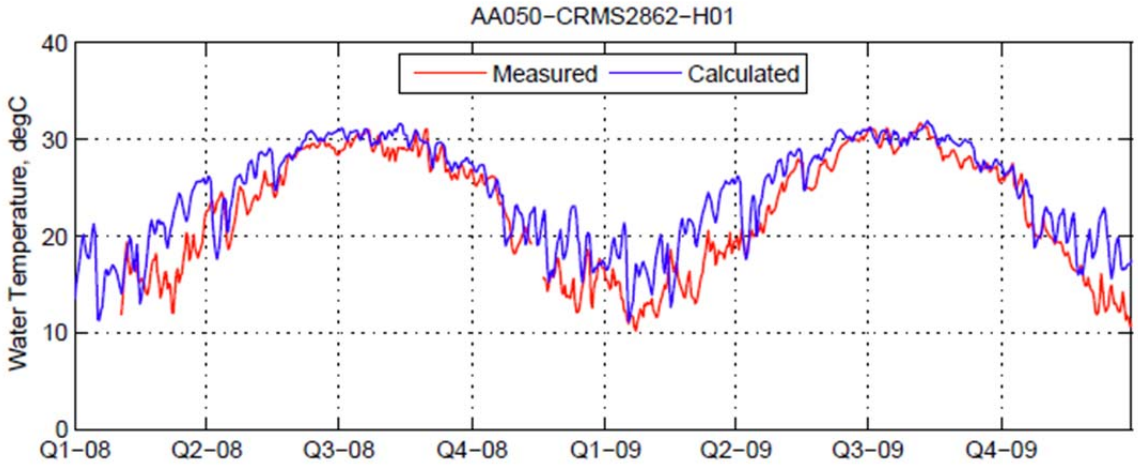

Figure 406 TMP Validation Results for AA050 in the AA Model

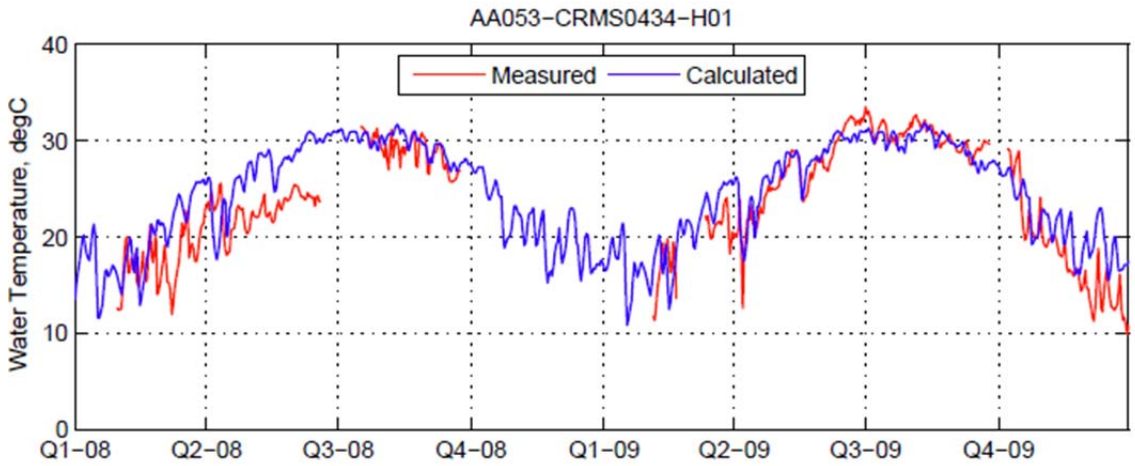

Figure 407 TMP Validation Results for AA053 in the AA Model

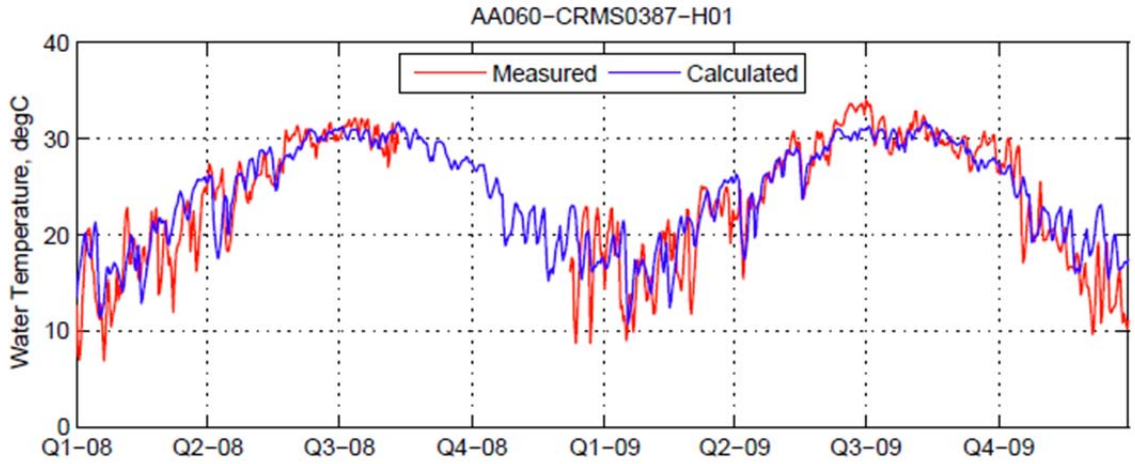

Figure 408 TMP Validation Results for AA060 in the AA Model

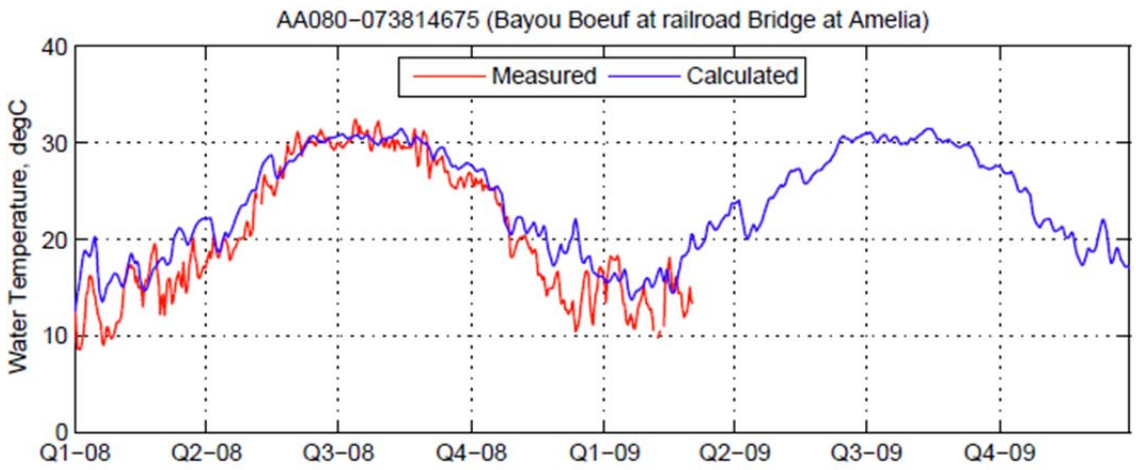

Figure 409 TMP Validation Results for Bayou Boeuf at Amelia in the AA Model

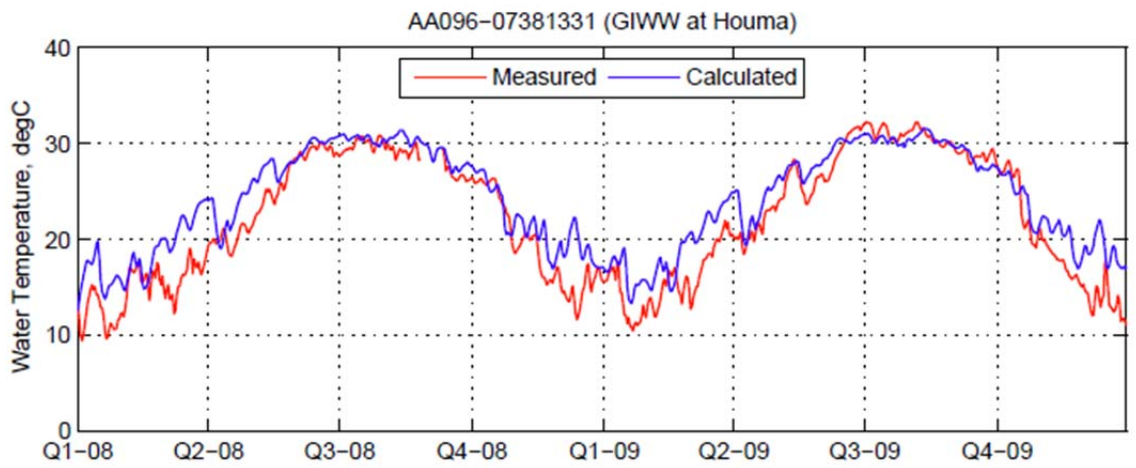

Figure 410 TMP Validation Results for GIWW at Houma in the AA Model

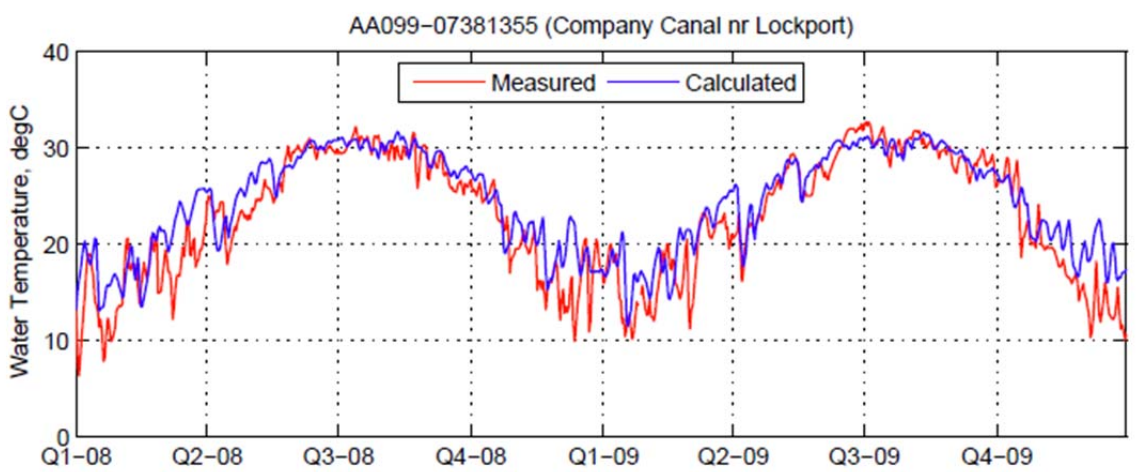

Figure 411 TMP Validation Results for Company Canal near Lockport in the AA Model

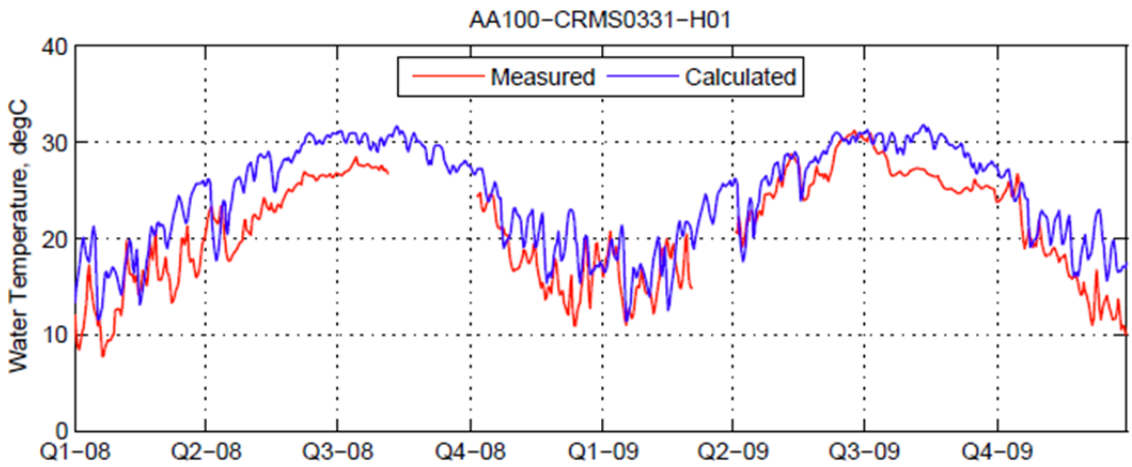

Figure 412 TMP Validation Results for AA100 in the AA Model

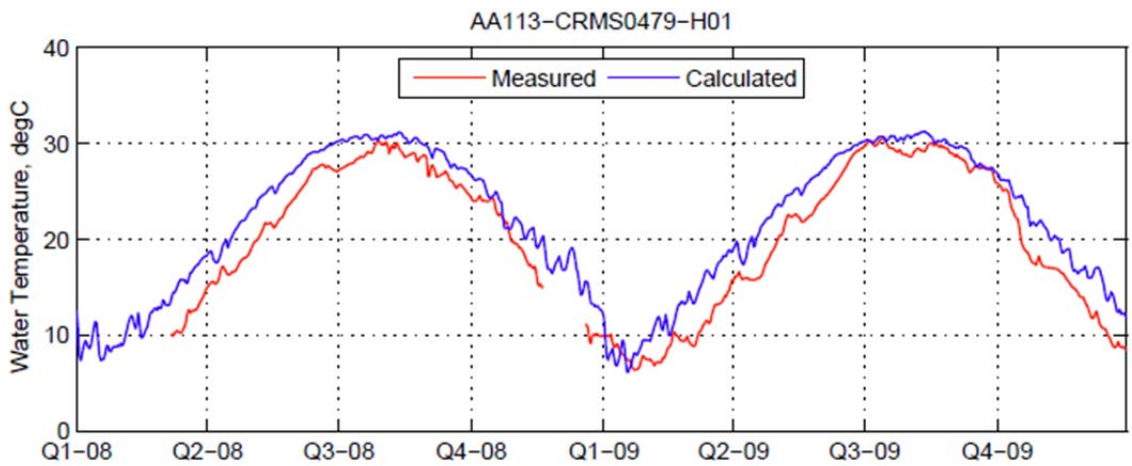

Figure 413 TMP Validation Results for AA113 in the AA Model

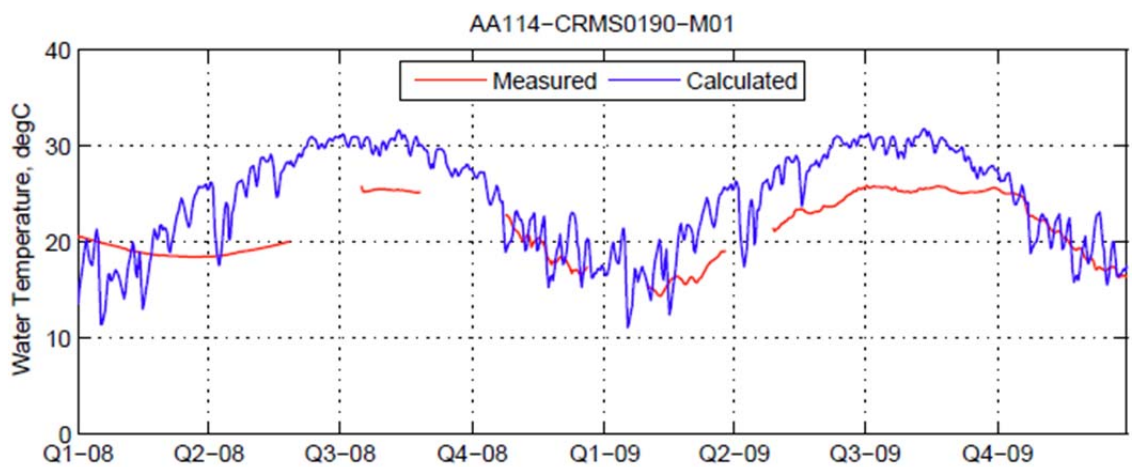

Figure 414 TMP Validation Results for AA114 in the AA Model

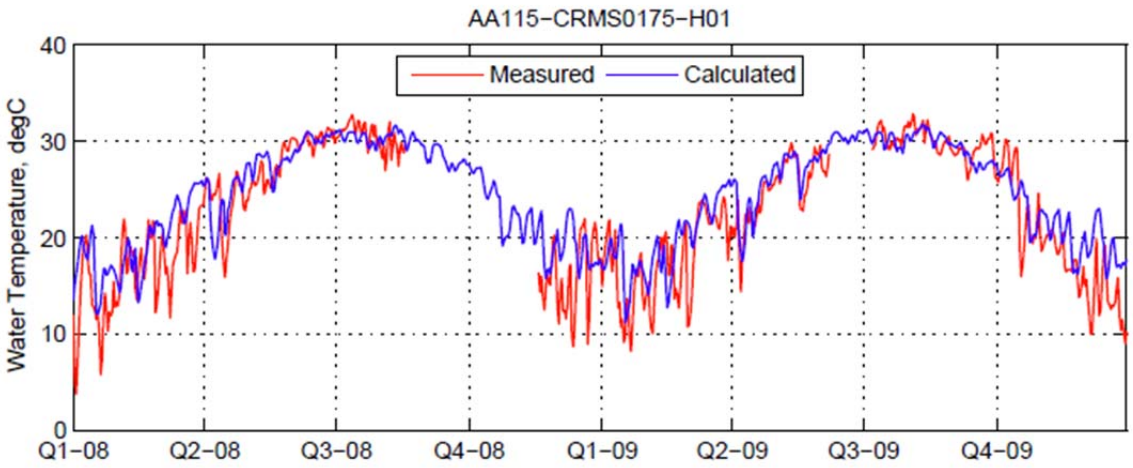

Figure 415 TMP Validation Results for AA115 in the AA Model

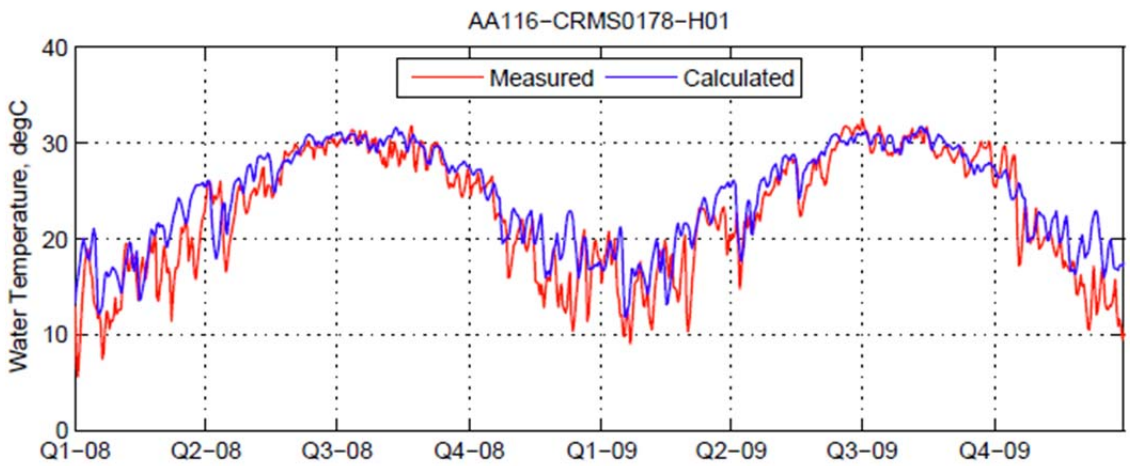

Figure 416 TMP Validation Results for AA116 in the AA Model

Total Suspended Solids (TSS)

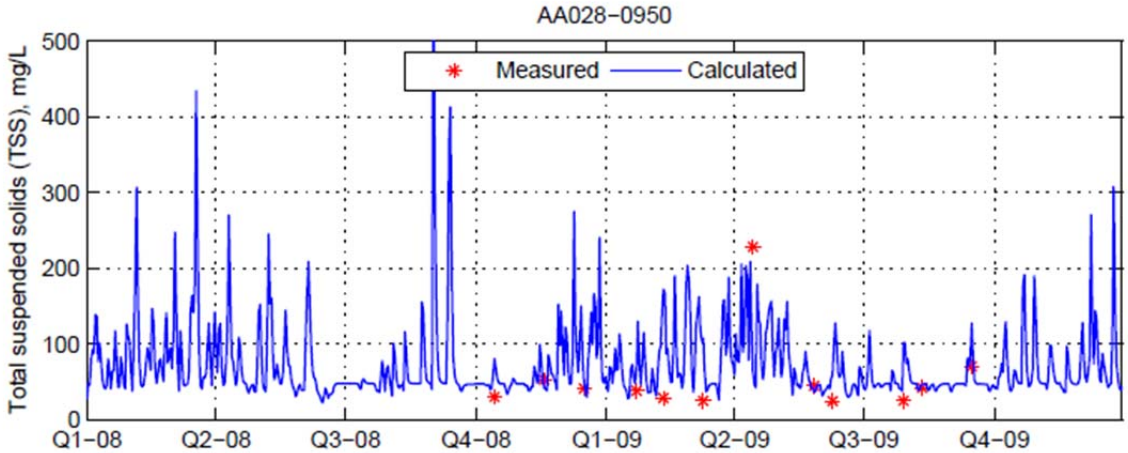

Figure 417 TSS Validation Results for Grand Bayou Du Large at Bayou Voison in the AA Model

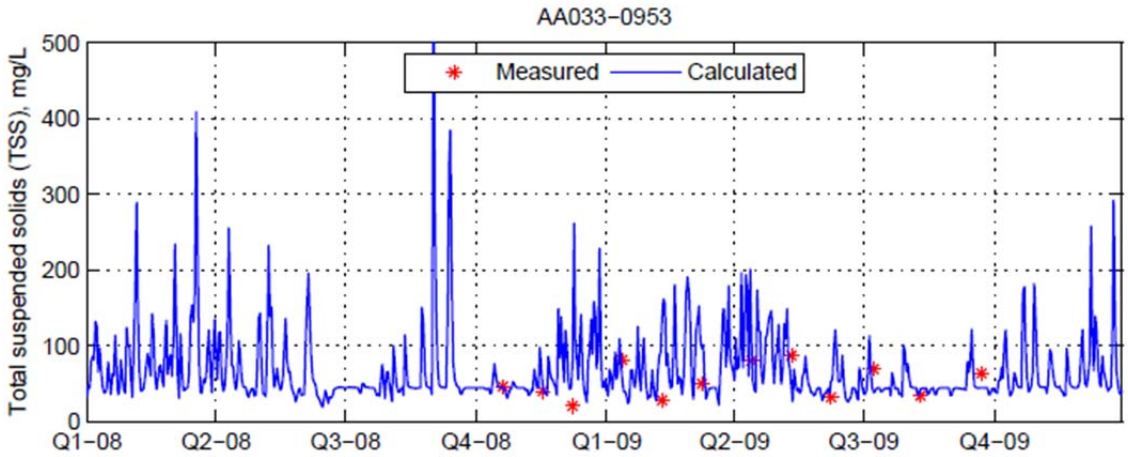

Figure 418 TSS Validation Results for Southwestern Louisiana Canal West of Leeville in the AA Model

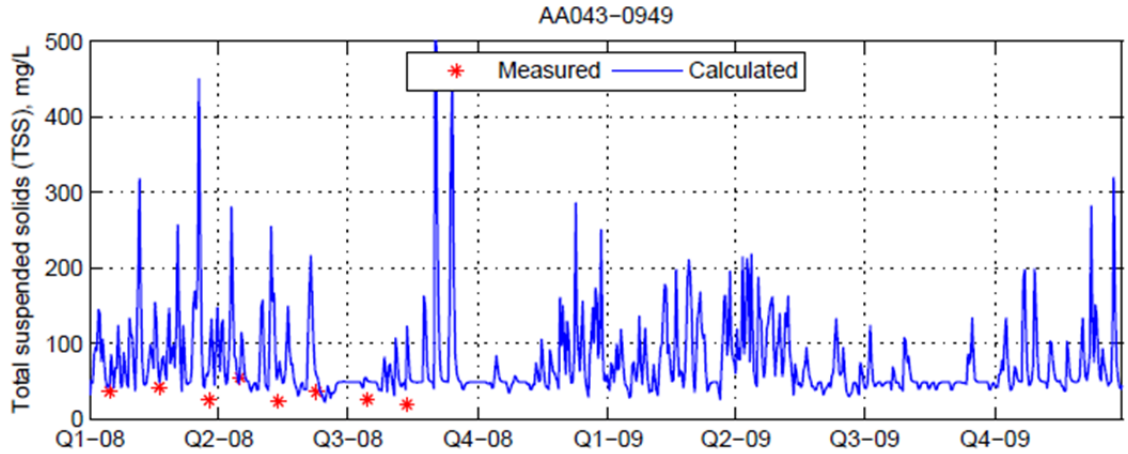

Figure 419 TSS Validation Results for Bayou Petit Canal at Cocodrie in the AA Model

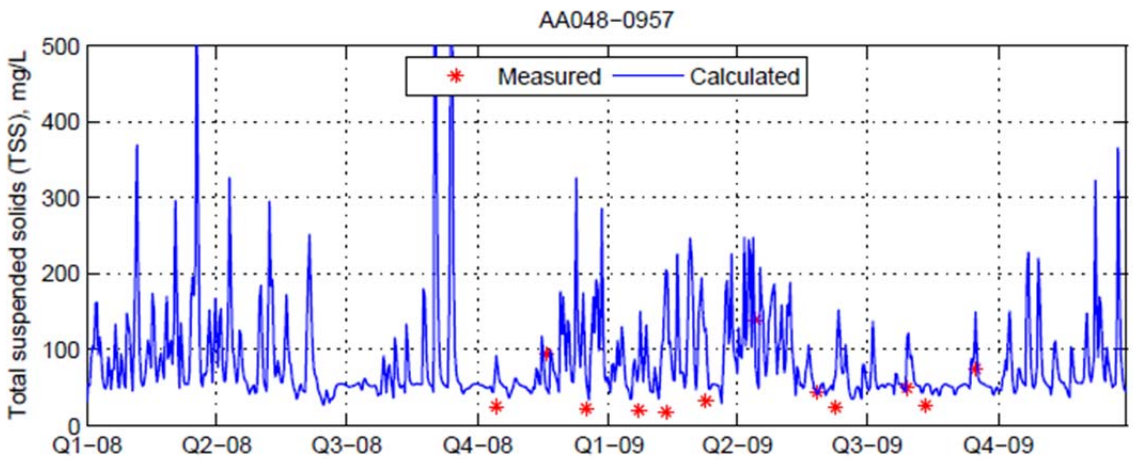

Figure 420 TSS Validation Results for Caillou Bay South of Bayou Grand Caillou in the AA Model

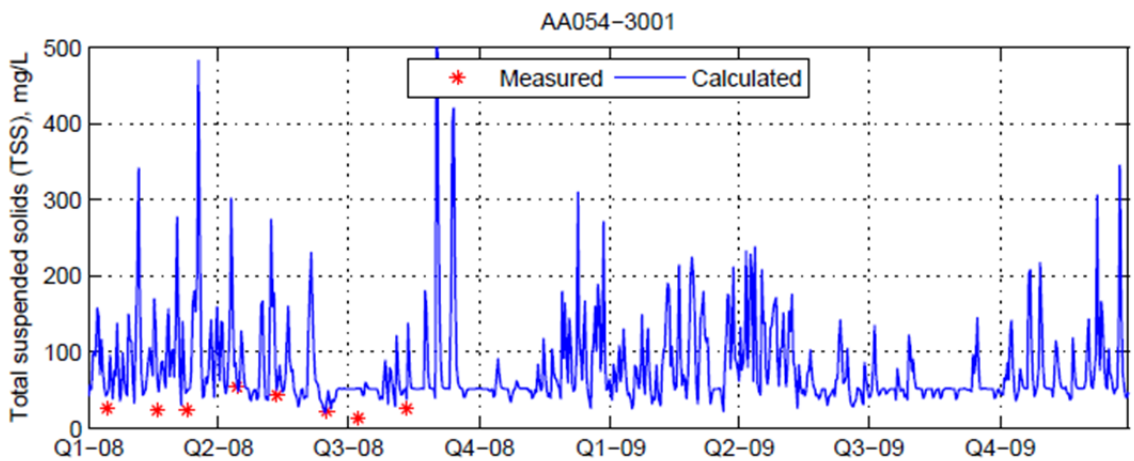

Figure 421 TSS Validation Results for Bayou Terrebonne near Lapeyrouse in the AA Model

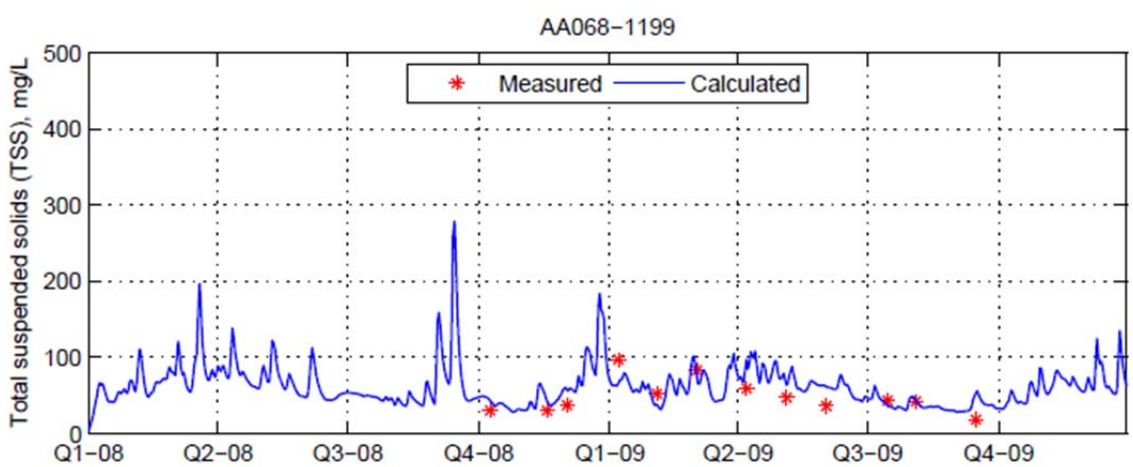

Figure 422 TSS Validation Results for ICWW South of Belle River in the AA Model

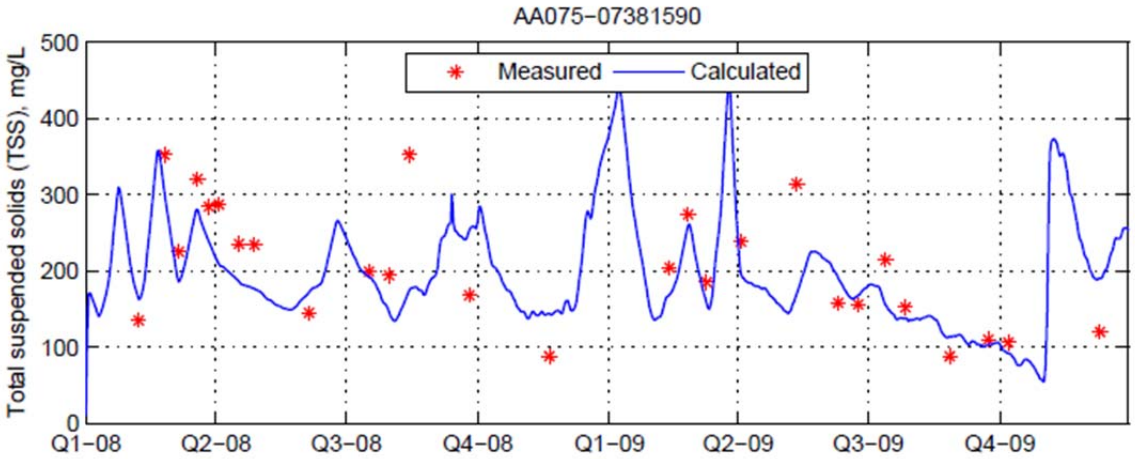

Figure 423 TSS Validation Results for Wax Lake Outlet at Calumet in the AA Model

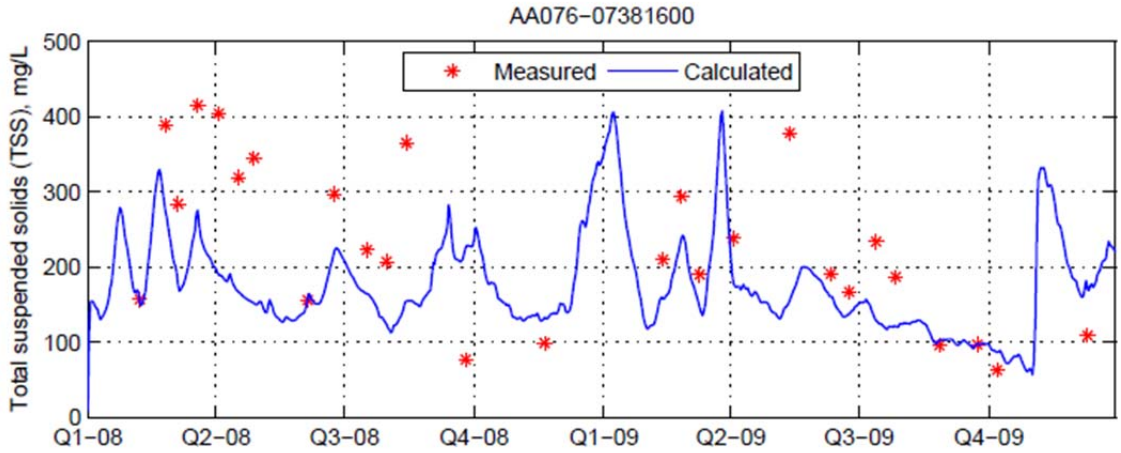

Figure 424 TSS Validation Results for Lower Atchafalaya River at Morgan City in the AA Model

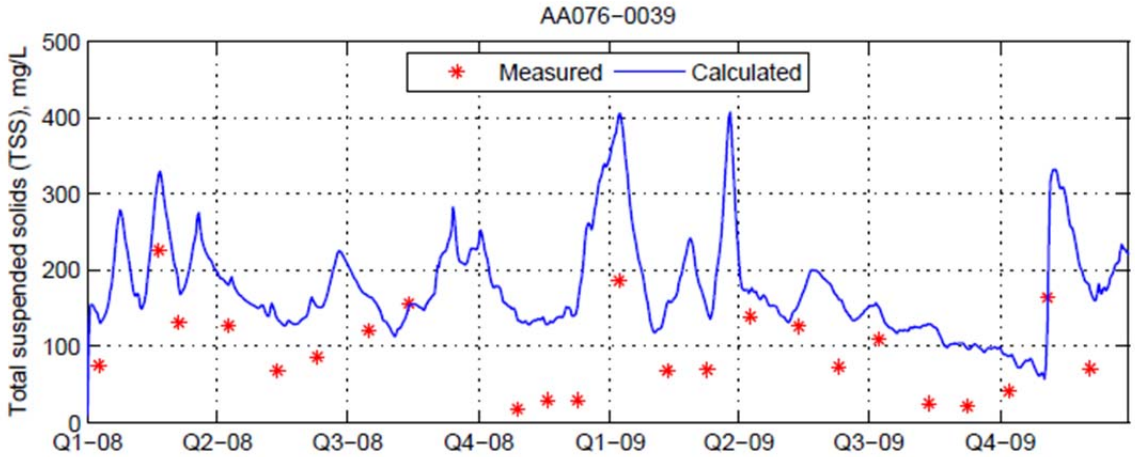

Figure 425 TSS Validation Results for Lower Atchafalaya River at Morgan City in the AA Model

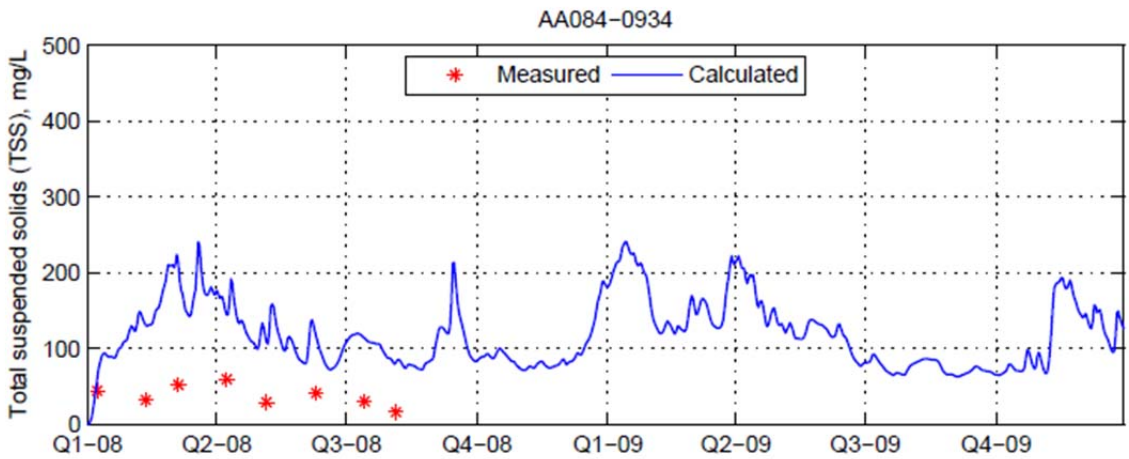

Figure 426 TSS Validation Results for ICWW at Venvirotek Dock in the AA Model

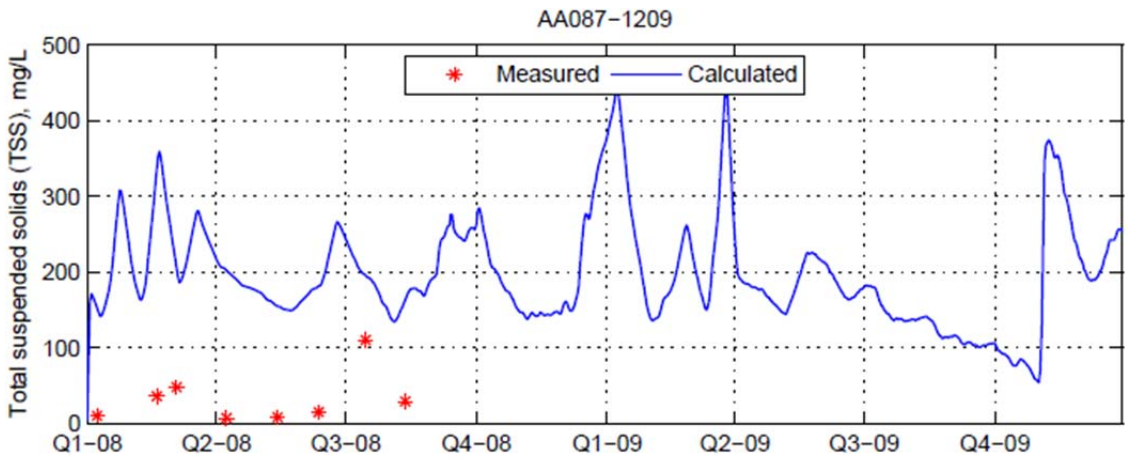

Figure 427 TSS Validation Results for Bayou Blue at North Bend Pumping Station in the AA Model

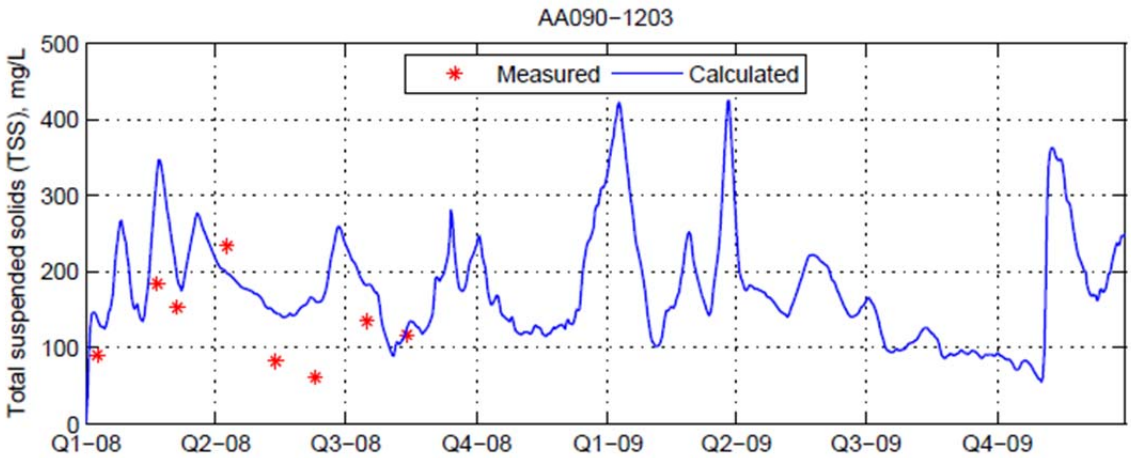

Figure 428 TSS Validation Results for ICWW South of Patterson in the AA Model

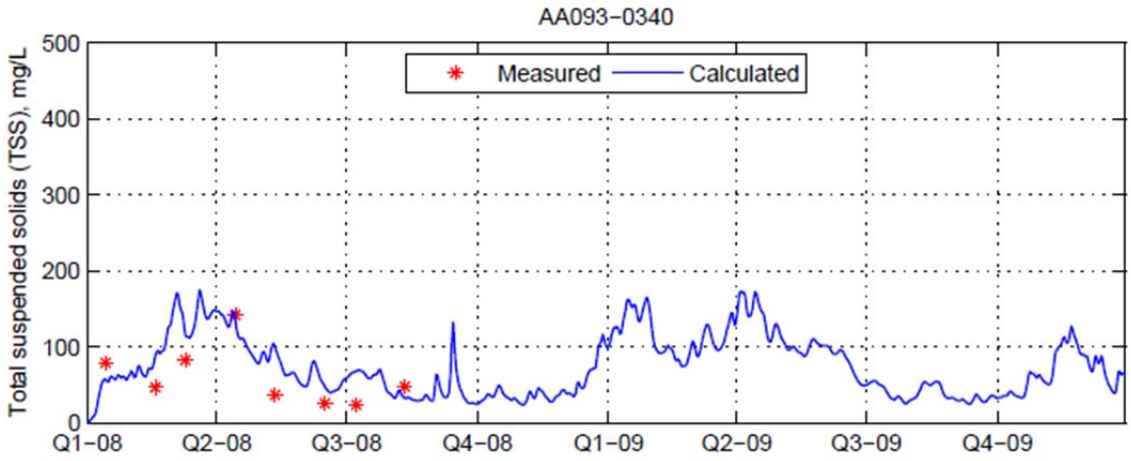

Figure 429 TSS Validation Results for ICWW East of Houma in the AA Model

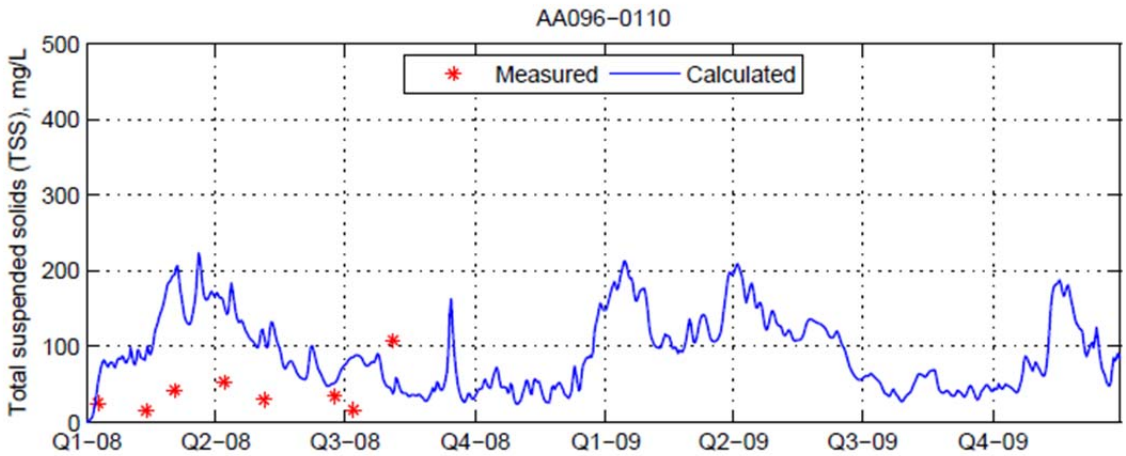

Figure 430 TSS Validation Results for Bayou Terrebonne at Houma in the AA Model

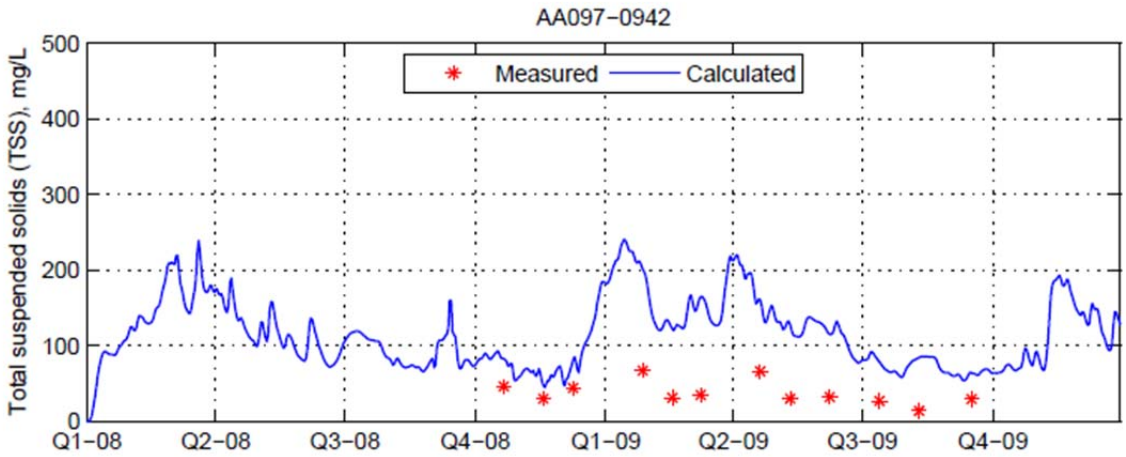

Figure 431 TSS Validation Results for Bayou Terrebonne at Houma in the AA Model

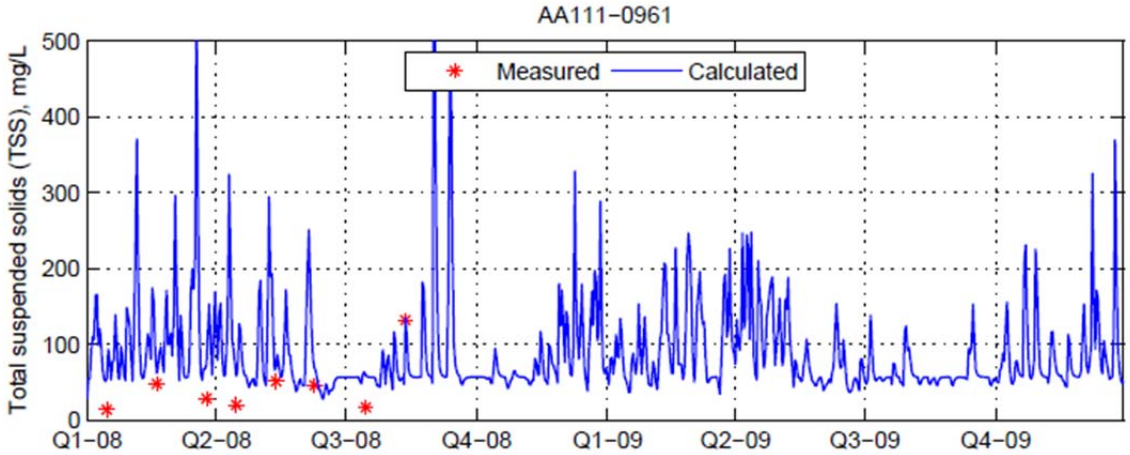

Figure 432 TSS Validation Results for Lake Pelto South of Cocodrie in the AA Model

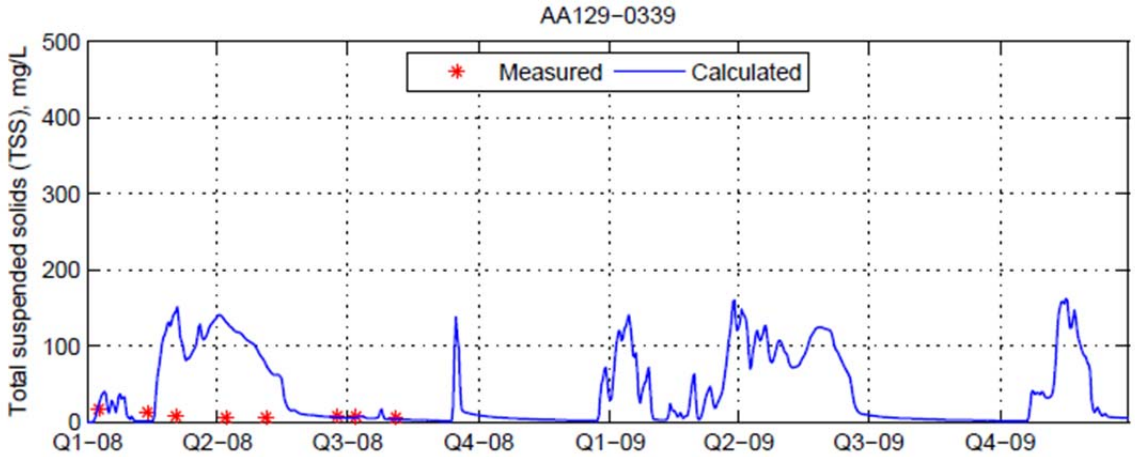

Figure 433 TSS Validation Results for Bayou Black West of Houma in the AA Model

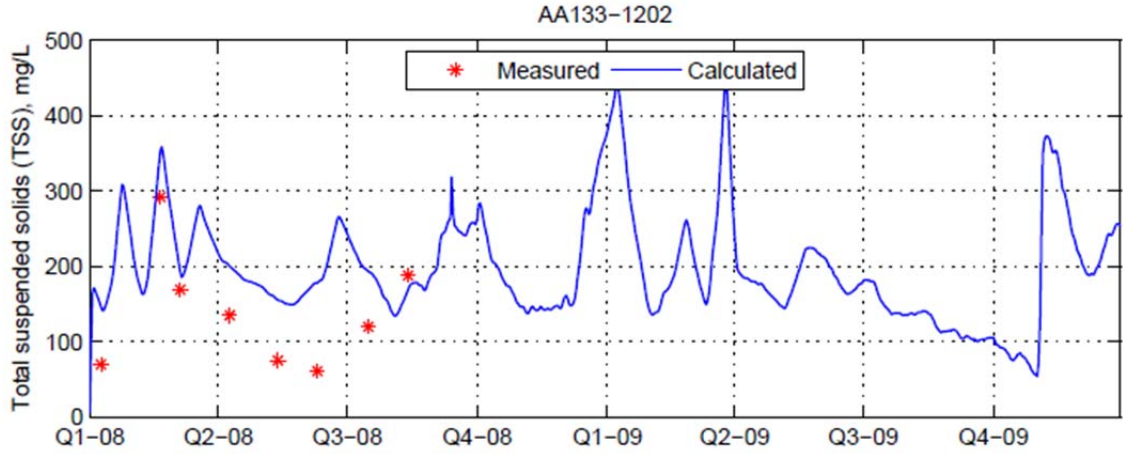

Figure 434 TSS Validation Results for Wax Lake Outlet Southwest of Patterson in the AA Model

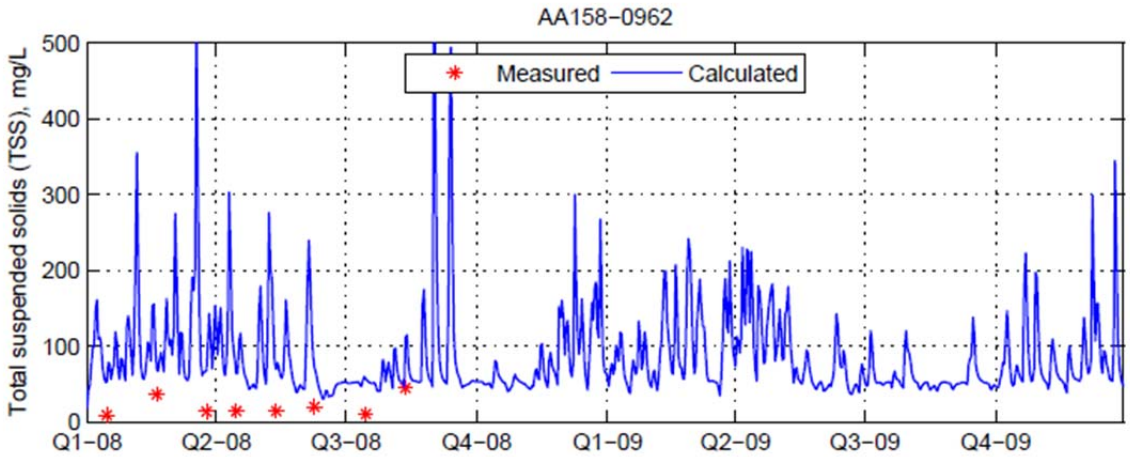

Figure 435 TSS Validation Results for Gulf of Mexico South of Wind Island Pass in the AA Model

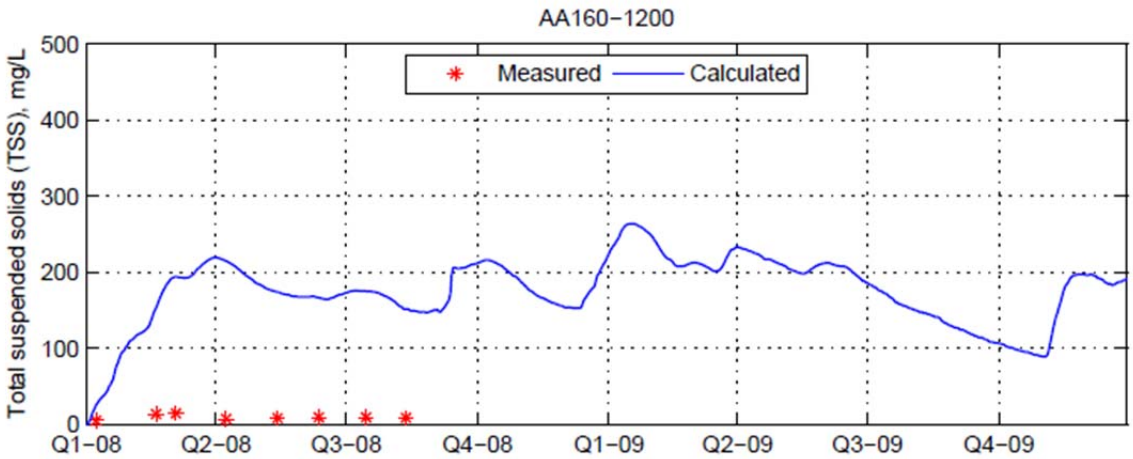

Figure 436 TSS Validation Results for Bayou Teche at Patterson in the AA Model

Total Nitrogen (TN)

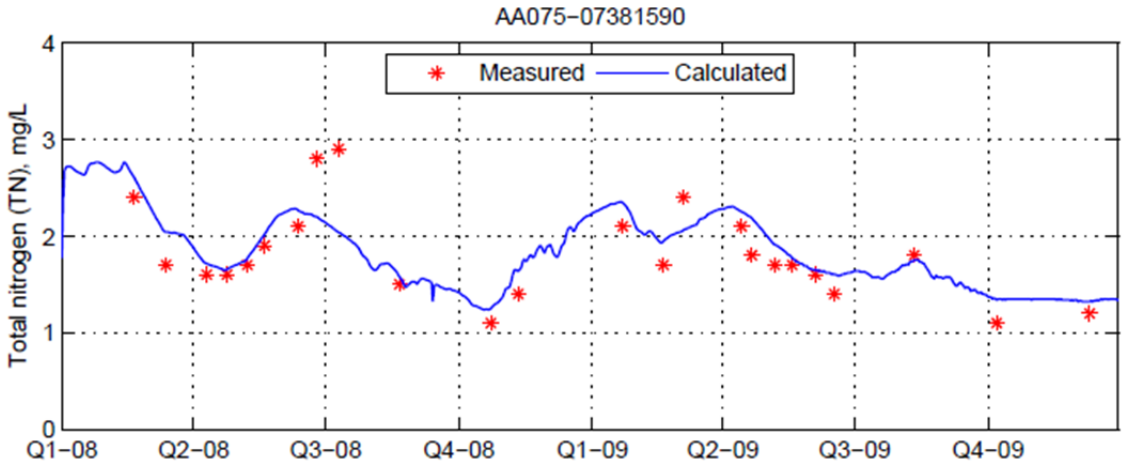

Figure 437 TN Validation Results for Wax Lake Outlet at Calumet in the AA Model

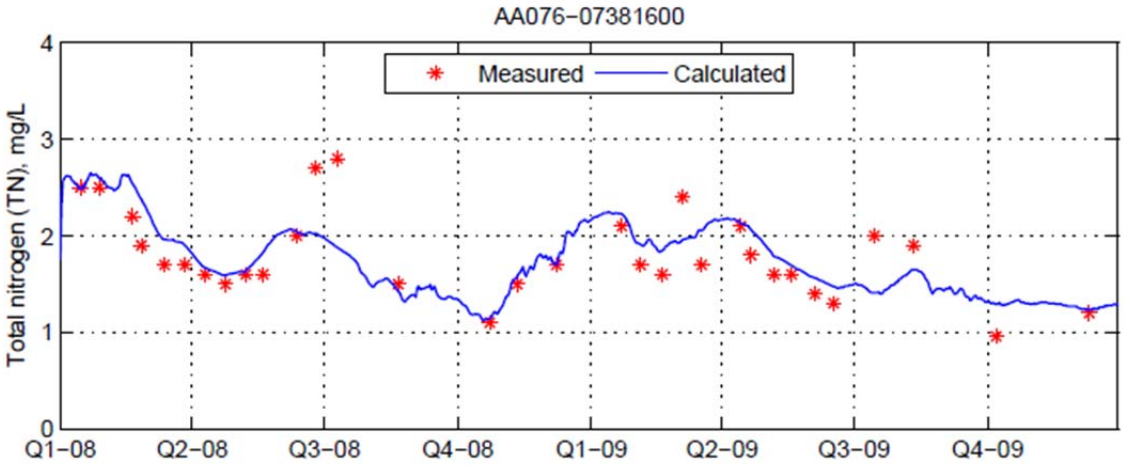

Figure 438 TN Validation Results for Lower Atchafalaya River at Morgan City in the AA Model

Total Phosphorus (TPH)

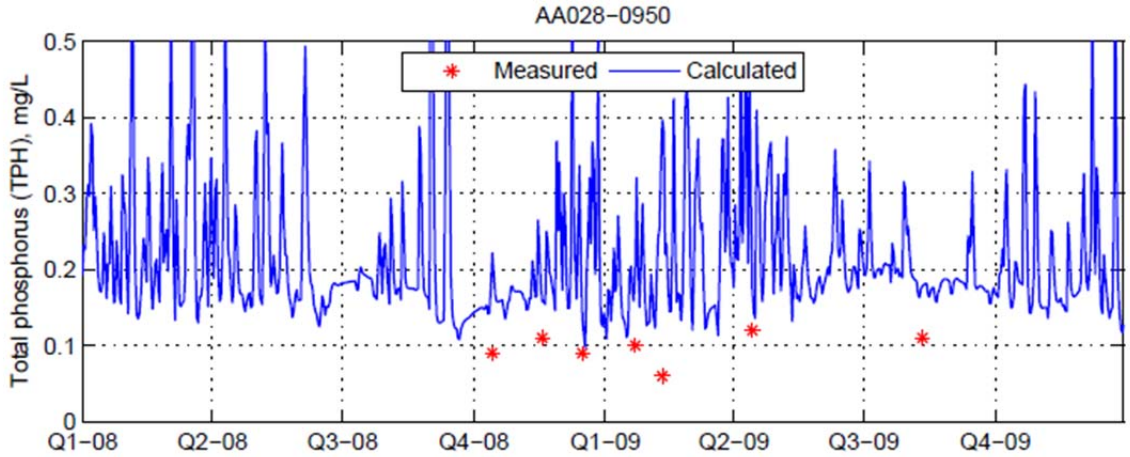

Figure 439 TPH Validation Results for Grand Bayou Du Large at Bayou Voison in the AA Model

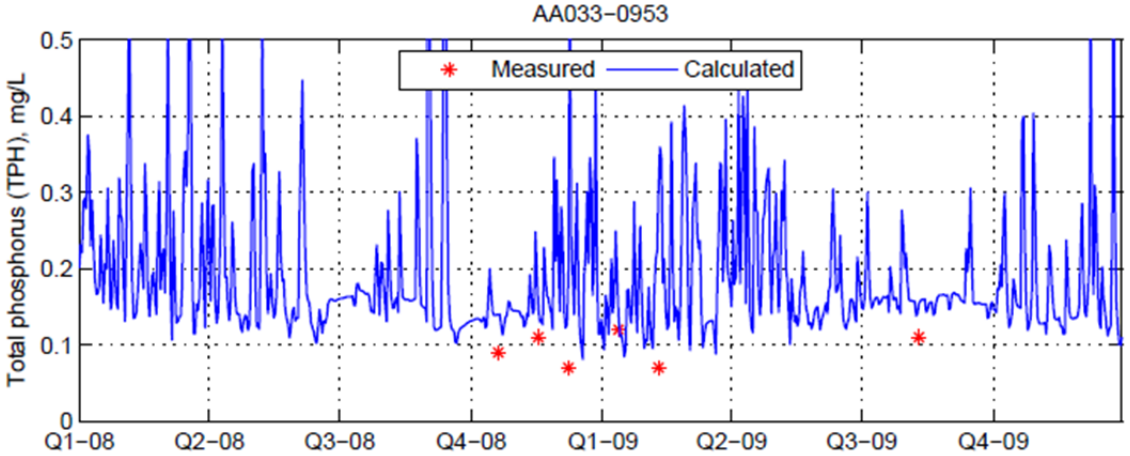

Figure 440 TPH Validation Results for Southwestern Louisiana Canal West of Leeville in the AA Model

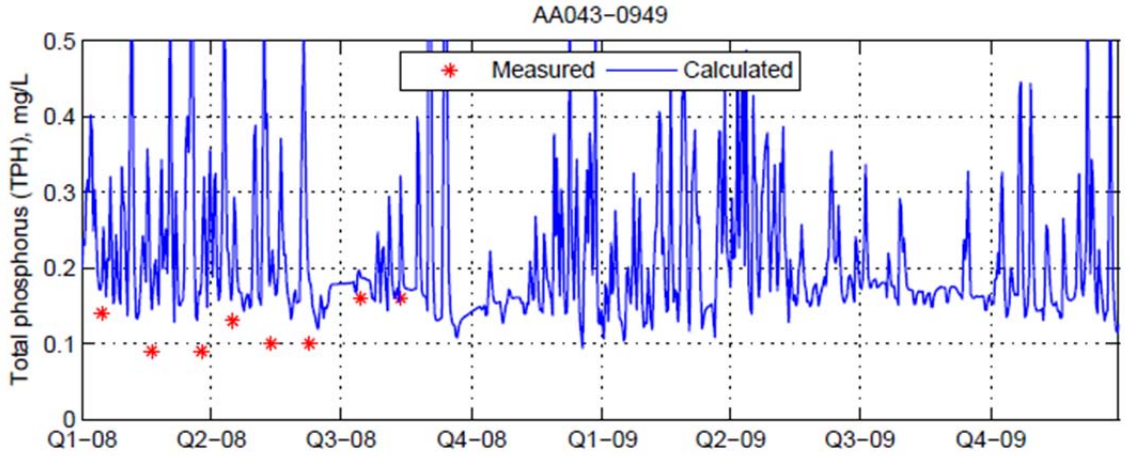

Figure 441 TPH Validation Results for Bayou Petit Caillou at Cocodrie in the AA Model

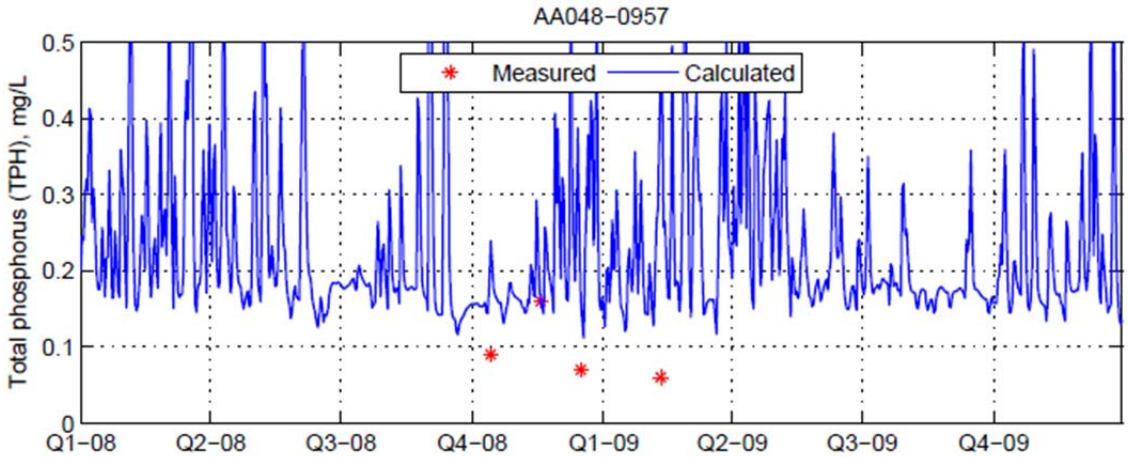

Figure 442 TPH Validation Results for Caillou Bay South of Bayou Grand Caillou in the AA Model

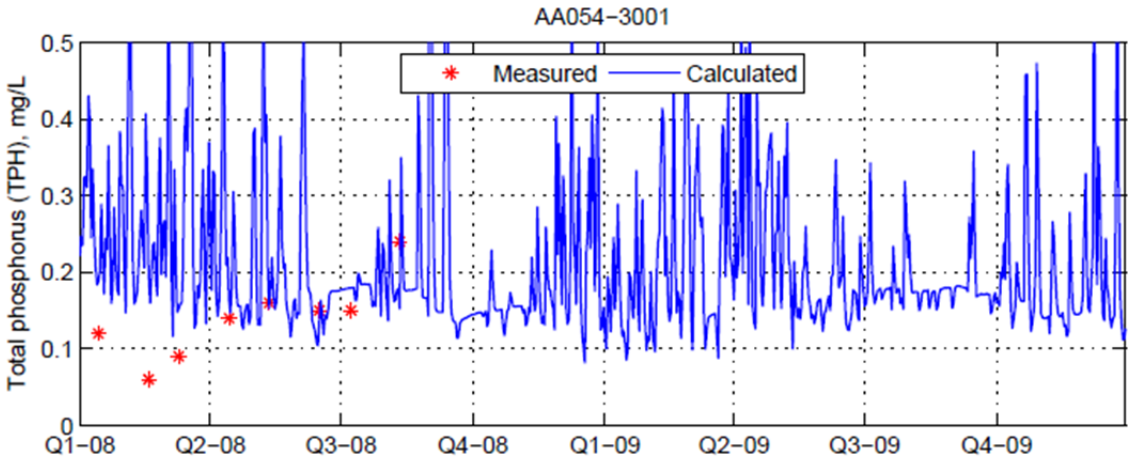

Figure 443 TPH Validation Results for Bayou Terrebonne near Lapeyrouse in the AA Model

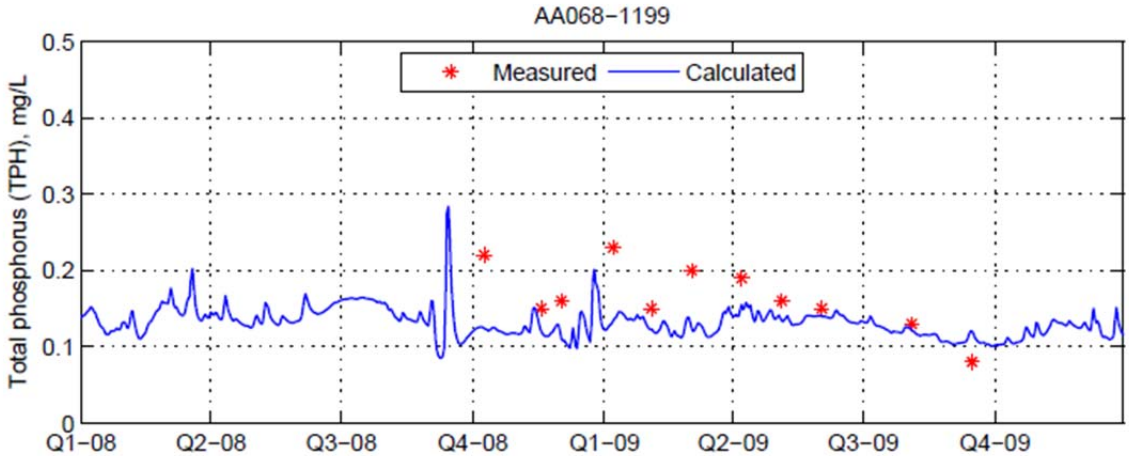

Figure 444 TPH Validation Results for ICWW South of Belle River in the AA Model

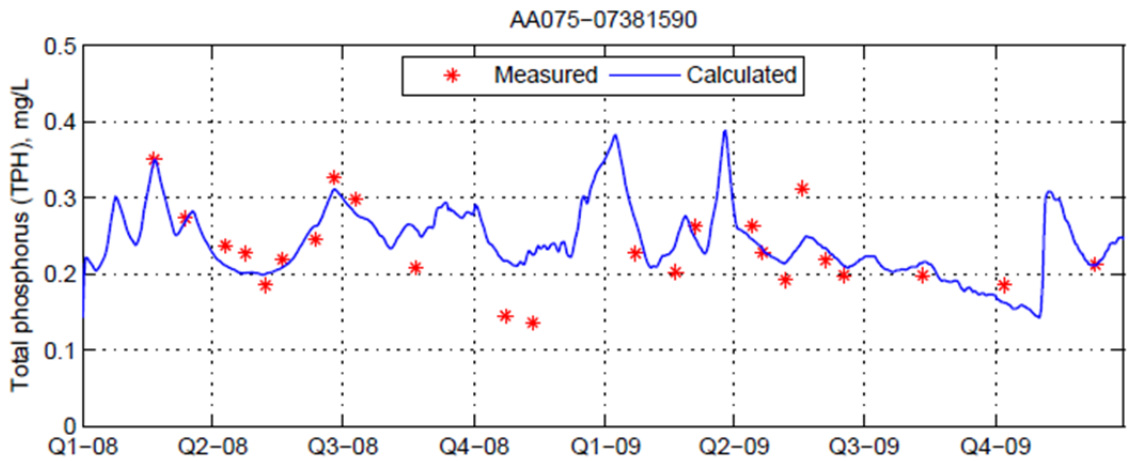

Figure 445 TPH Validation Results for Wax Lake Outlet at Calumet in the AA Model

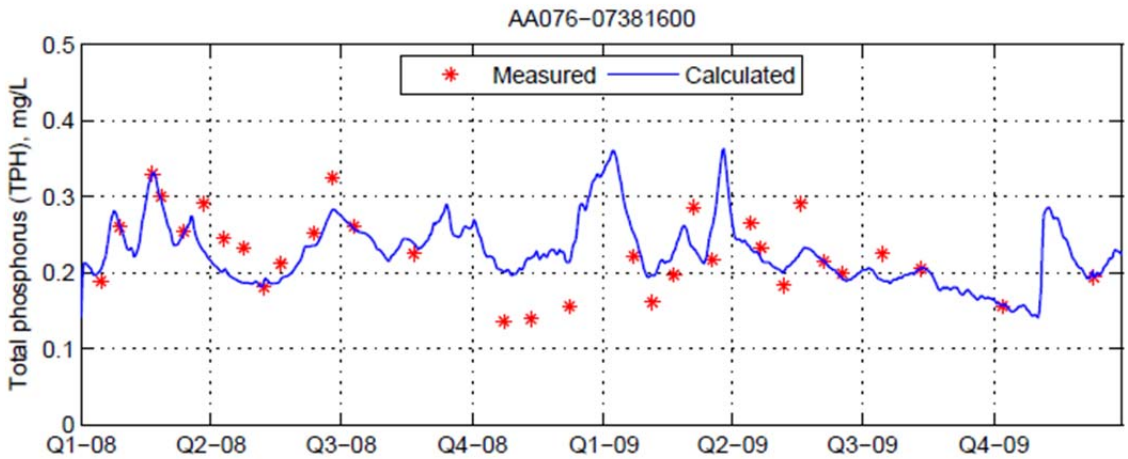

Figure 446 TPH Validation Results for Lower Atchafalaya River at Morgan City in the AA Model

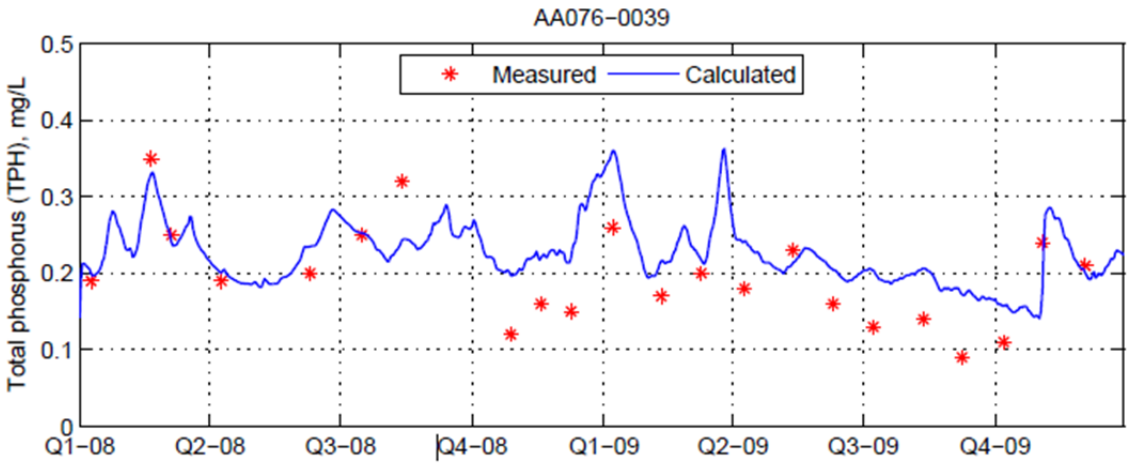

Figure 447 TPH Validation Results for Atchafalaya River at Morgan City in the AA Model

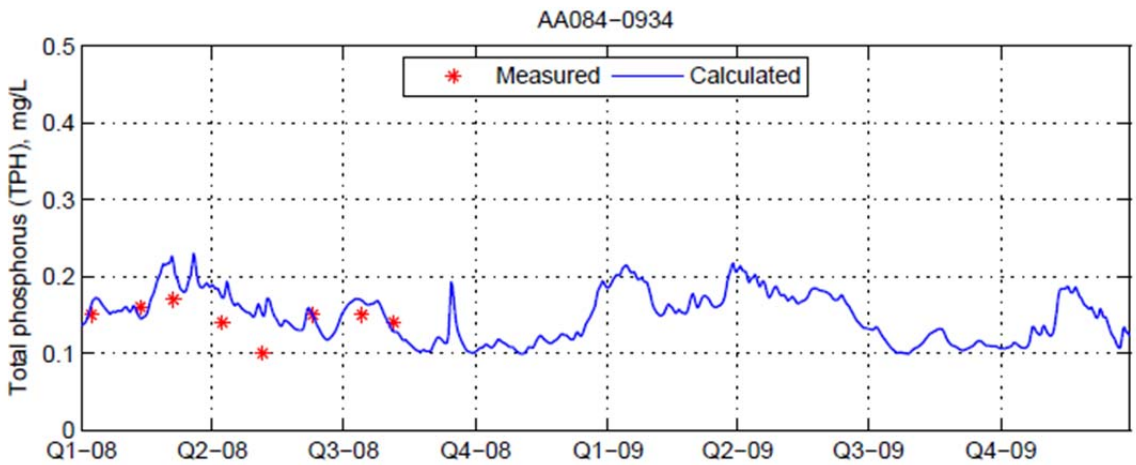

Figure 448 TPH Validation Results for ICWW at Venvirotek Dock in the AA Model

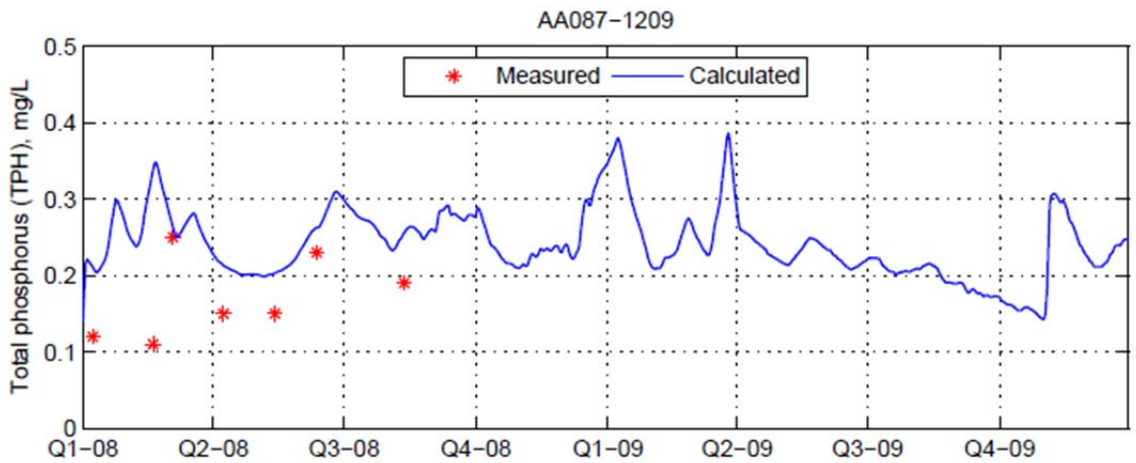

Figure 449 TPH Validation Results for Bayou Blue at North Bend Pumping Station in the AA Model

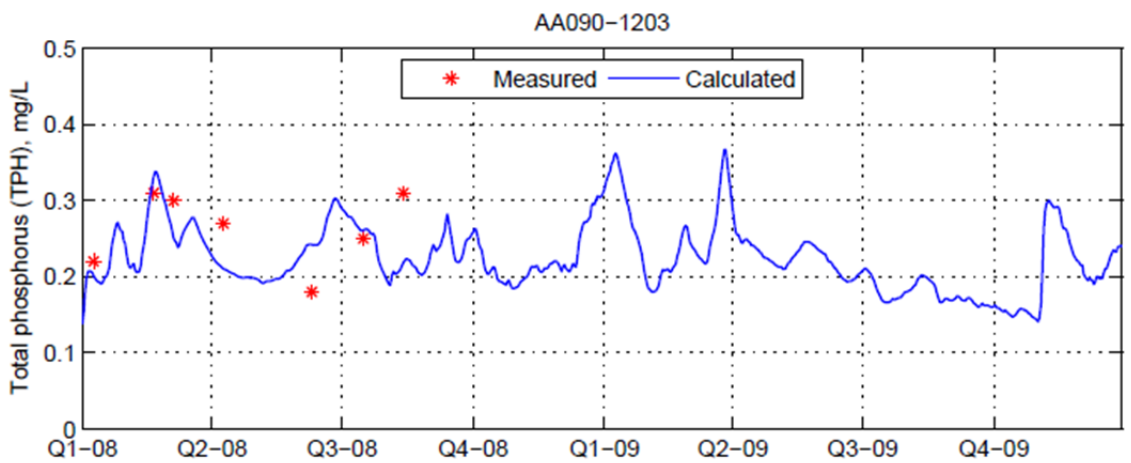

Figure 450 TPH Validation Results for ICWW South of Patterson in the AA Model

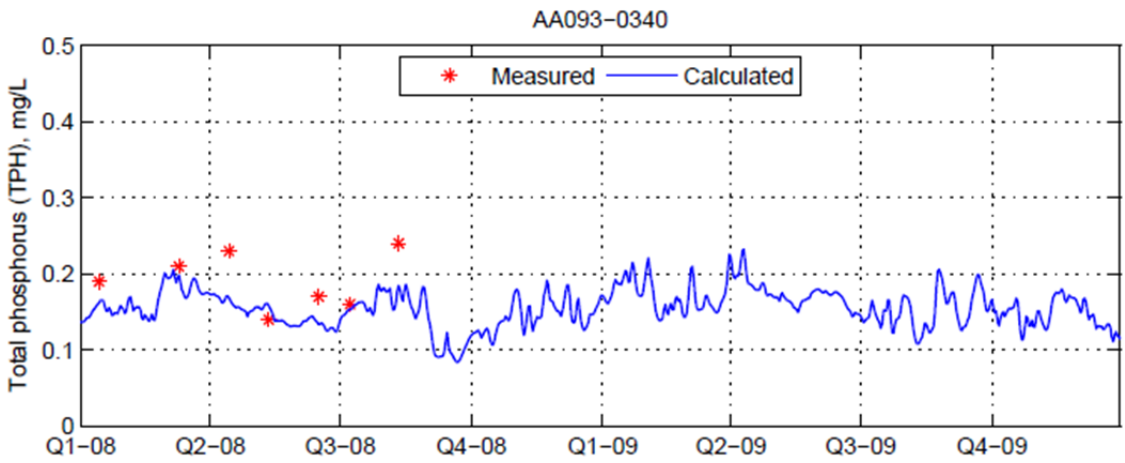

Figure 451 TPH Validation Results for ICWW East of Houma in the AA Model

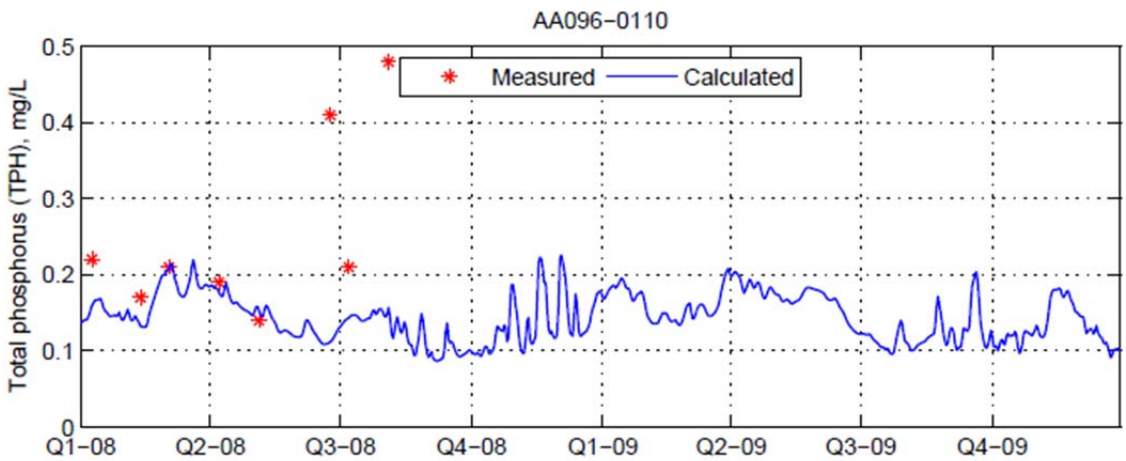

Figure 452 TPH Validation Results for Bayou Terrebonne at Houma in the AA Model

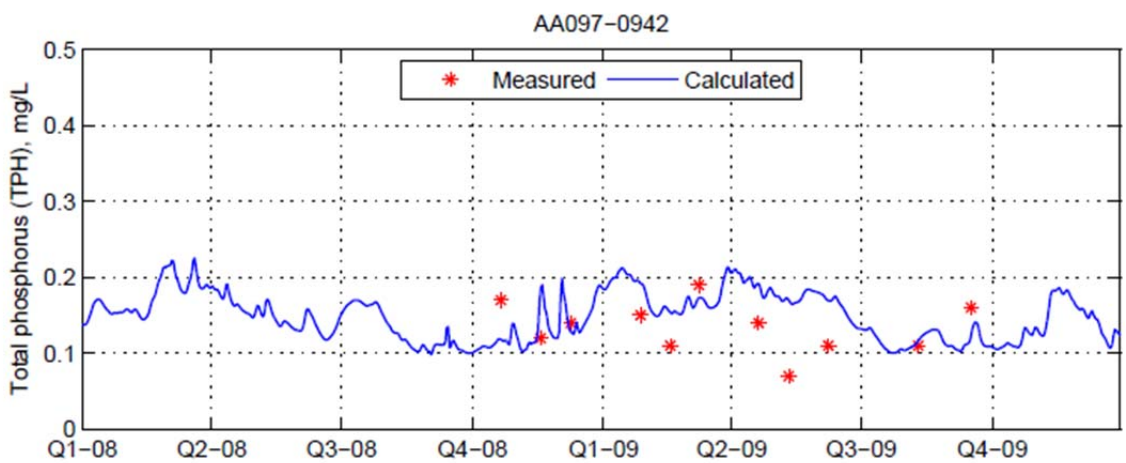

Figure 453 TPH Validation Results for Houma Navigation Canal at Gulf Island Dock in the AA Model

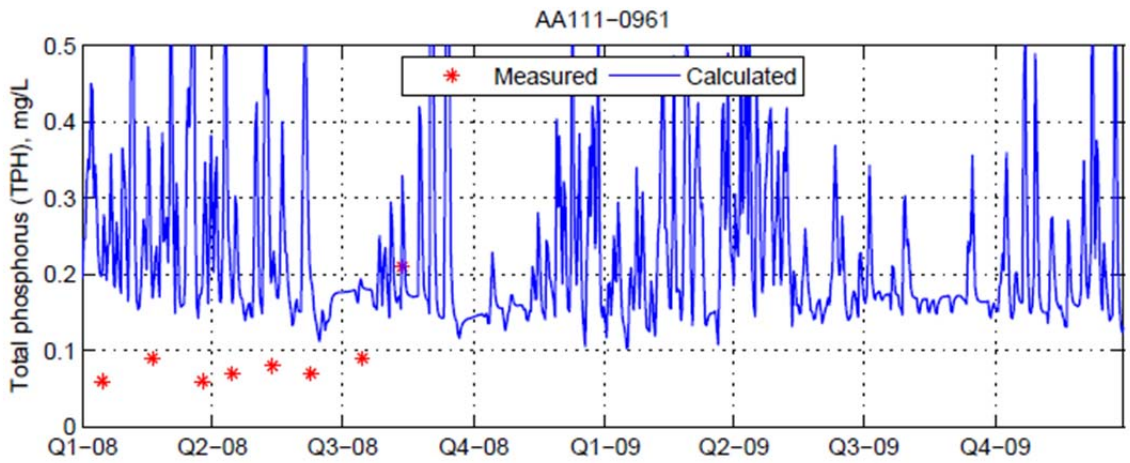

Figure 454 TPH Validation Results for Lake Pelto South of Cocodrie in the AA Model

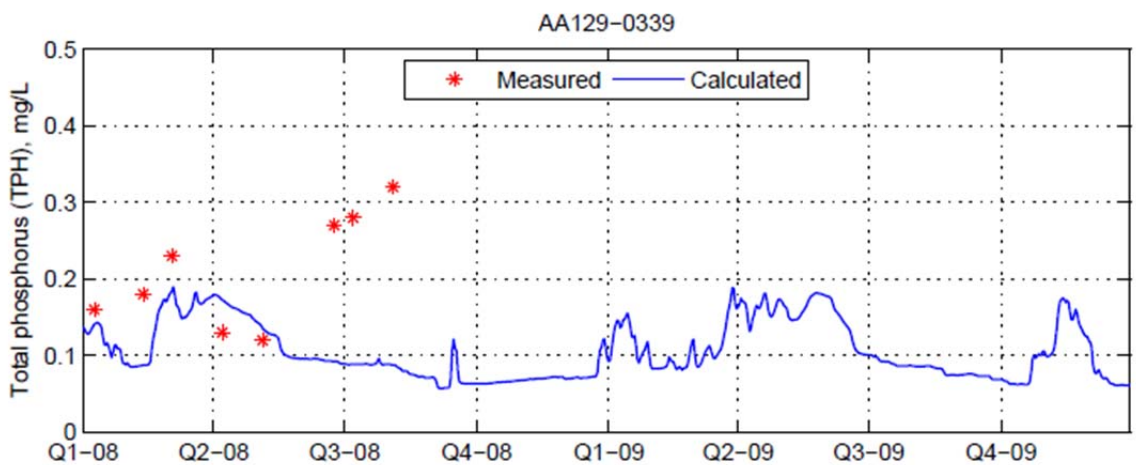

Figure 455 TPH Validation Results for Bayou Black West of Houma in the AA Model

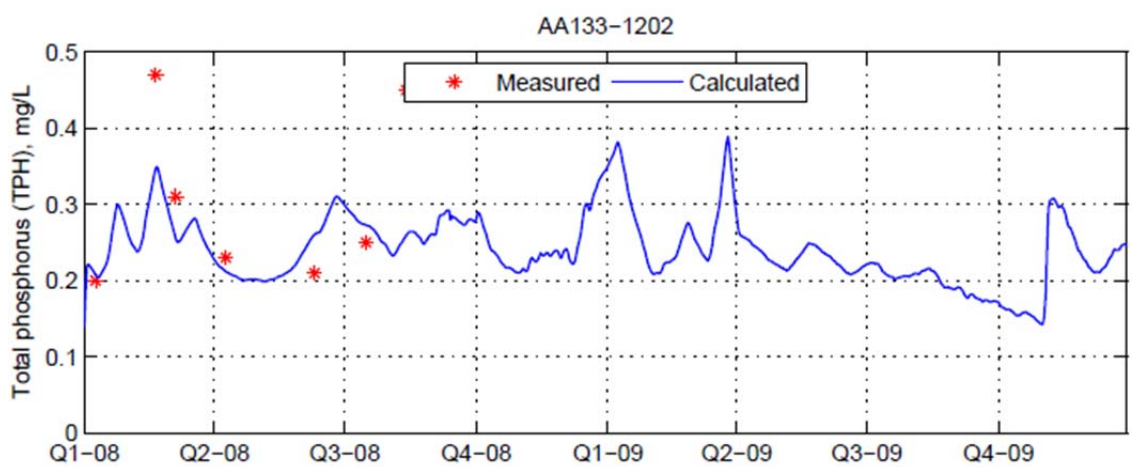

Figure 456 TPH Validation Results for Wax Lake Outlet Southwest of Patterson in the AA Model

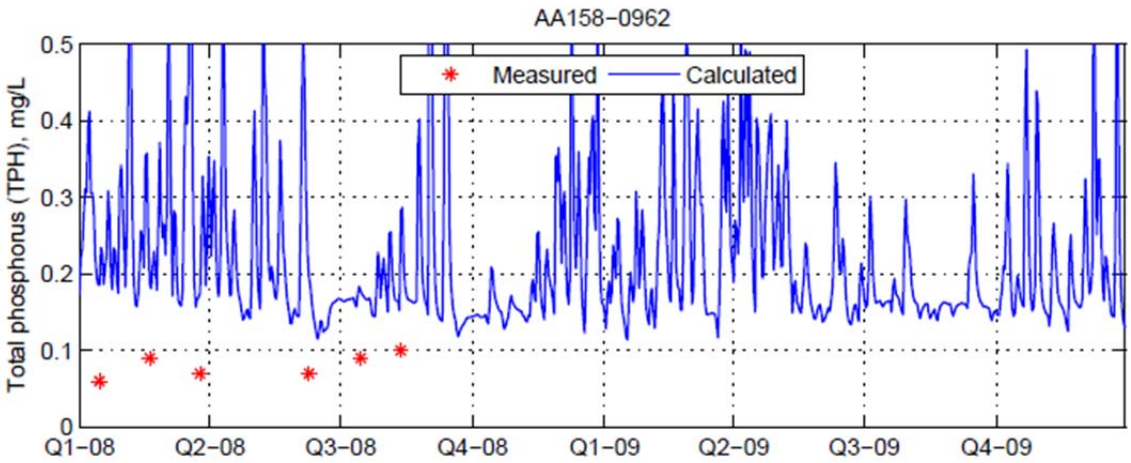

Figure 457 TPH Validation Results for Gulf of Mexico South of Wind Island Pass in the AA Model

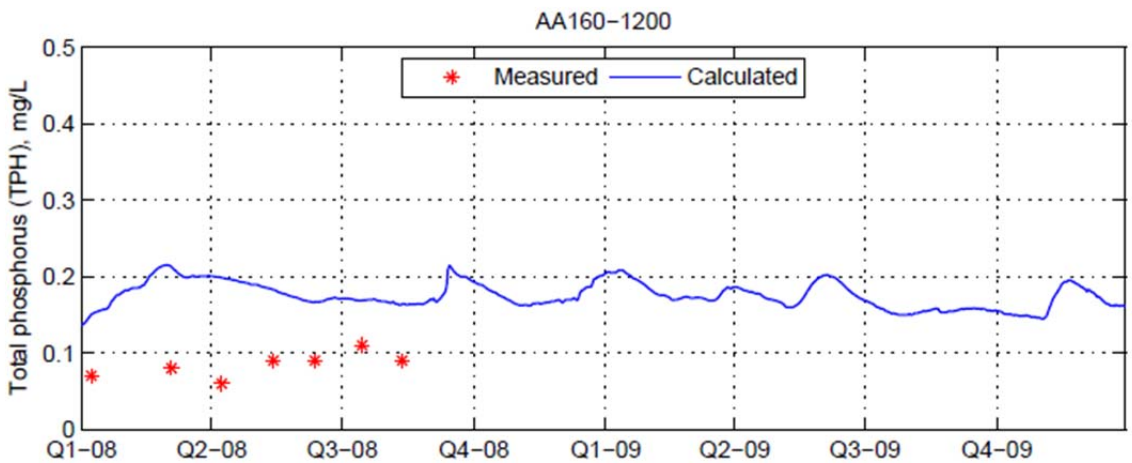

Figure 458 TPH Validation Results for Bayou Teche at Patterson in the AA Model

Chenier Plain Model Calibration Plots

Stage (STG)

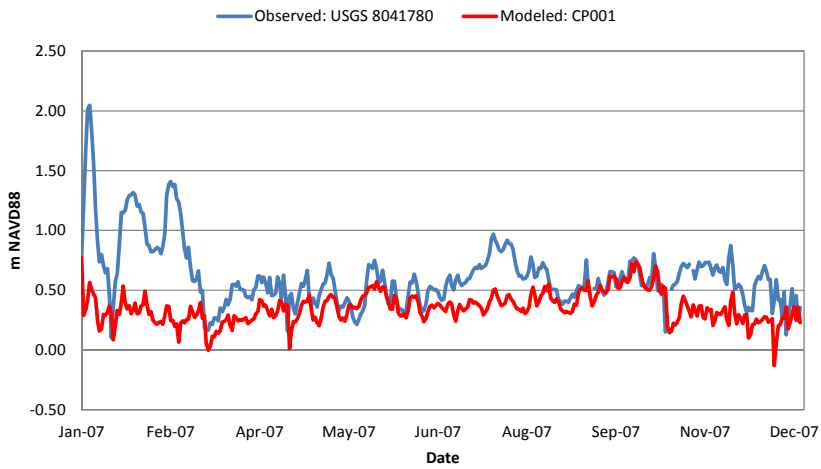

Figure 459 STG Calibration Results for the Neches River in the CP Model

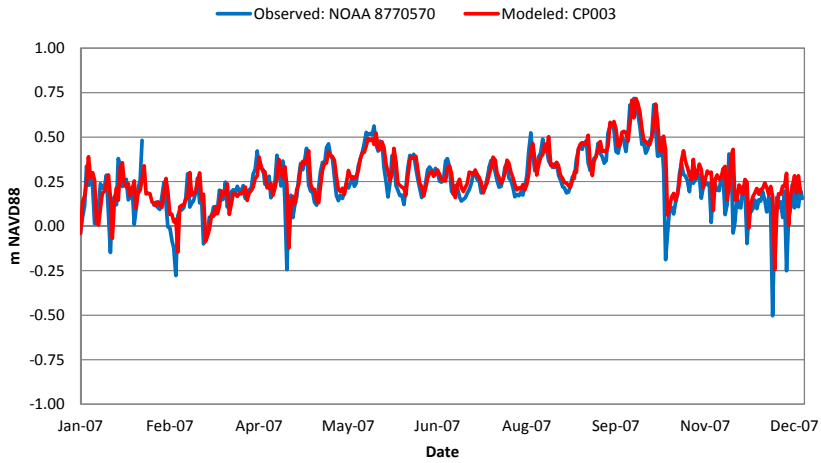

Figure 460 STG Calibration Results for Sabine Pass in the CP Model

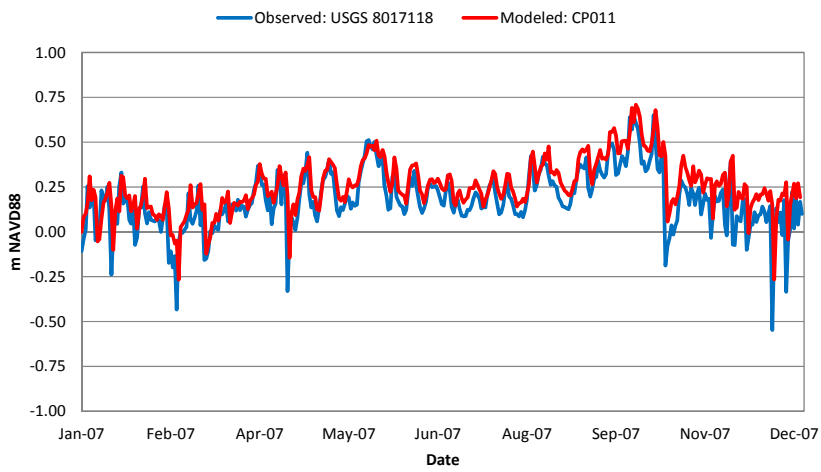

Figure 461 STG Calibration Results for Calcasieu Pass in the CP Model

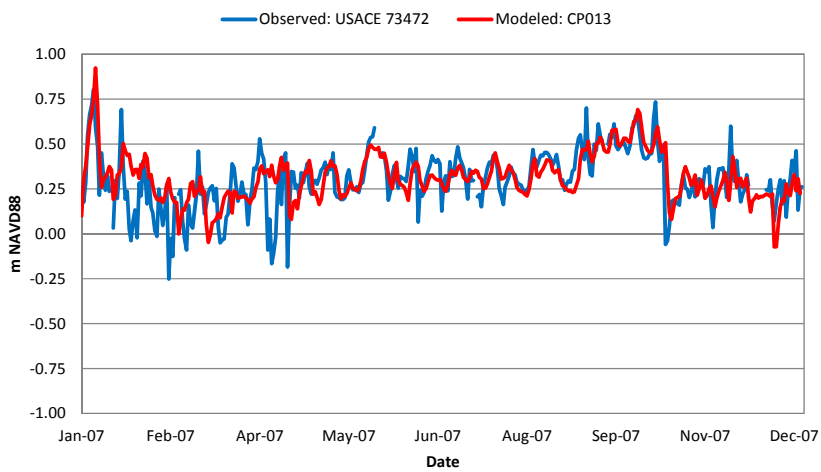

Figure 462 STG Calibration Results for Calcasieu River North of the Saltwater Barrier in the CP Model

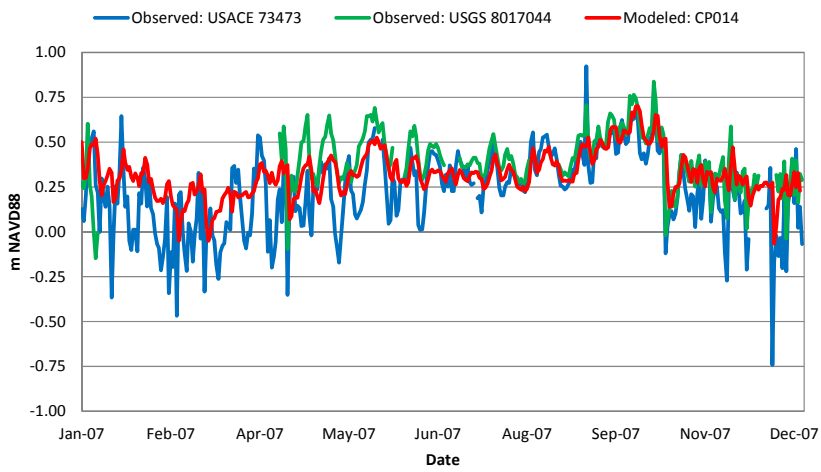

Figure 463 STG Calibration Results for Calcasieu River North of the GIWW and South of the Saltwater Barrier in the CP Model

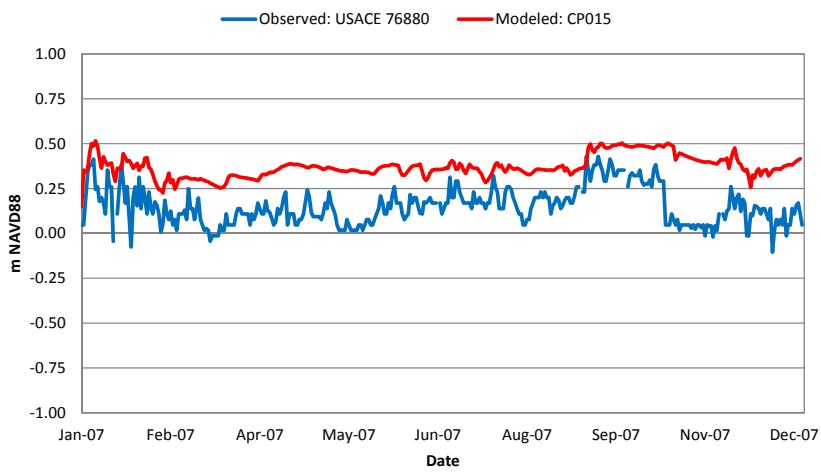

Figure 464 STG Calibration Results for GIWW East of Calcasieu Lock and West of Grand Lake in the CP Model

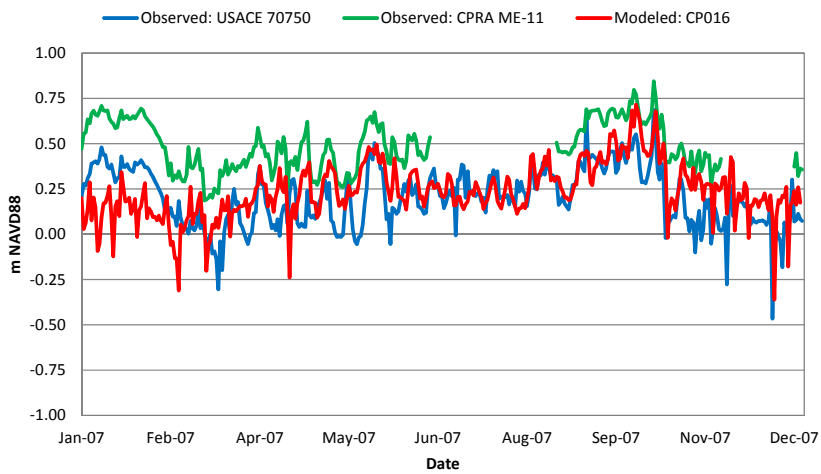

Figure 465 STG Calibration Results for the Mermentau River South of Grand Lake in the CP Model

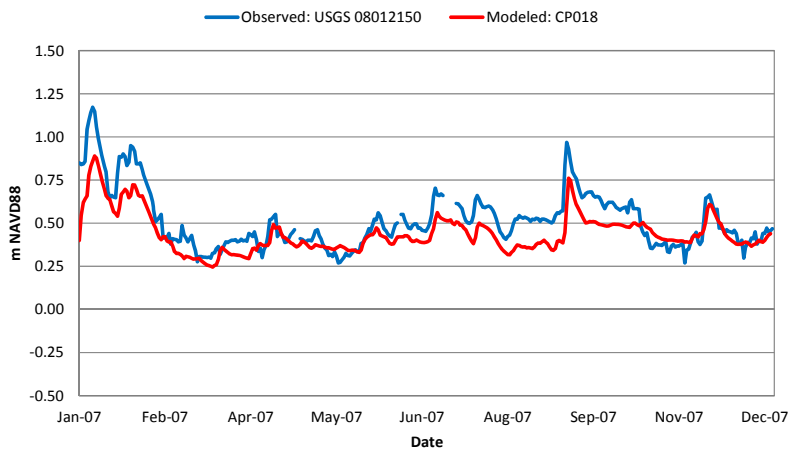

Figure 466 STG Calibration Results for Mermentau River North of Grand Lake in the CP Model

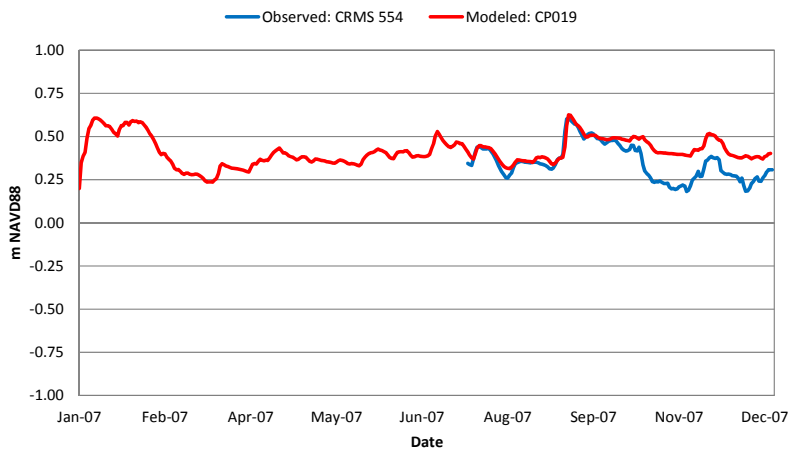

Figure 467 STG Calibration Results for the Channel Connecting Grand Lake and White Lake in the CP Model

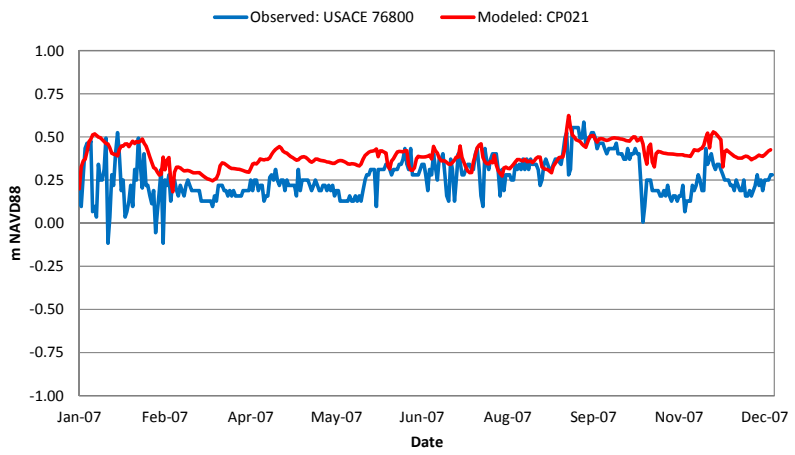

Figure 468 STG Calibration Results for the GIWW East of Grand Lake and West of the Leland Bowman Lock in the CP Model

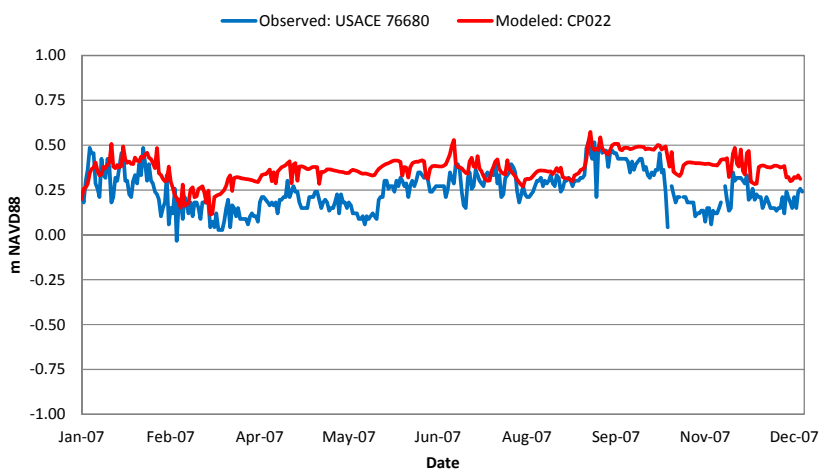

Figure 469 STG Calibration Results Schooner Bayou West of the Lock in the CP Model

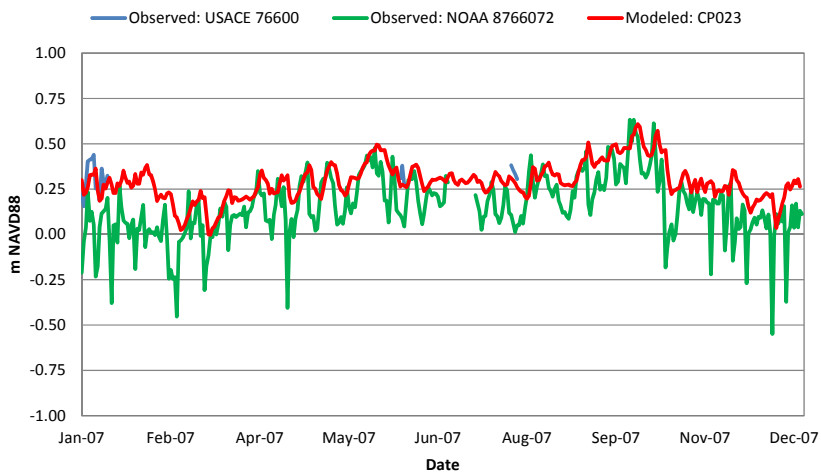

Figure 470 STG Calibration Results for Freshwater Bayou in the CP Model

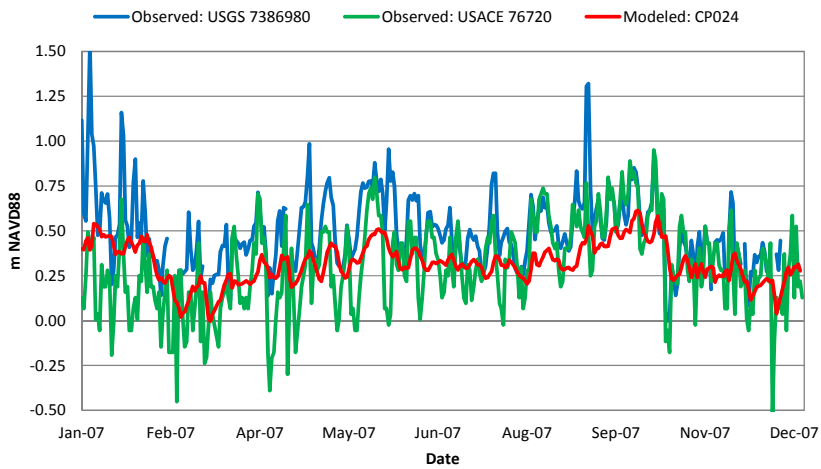

Figure 471 STG Calibration Results for Vermilion River in the CP Model

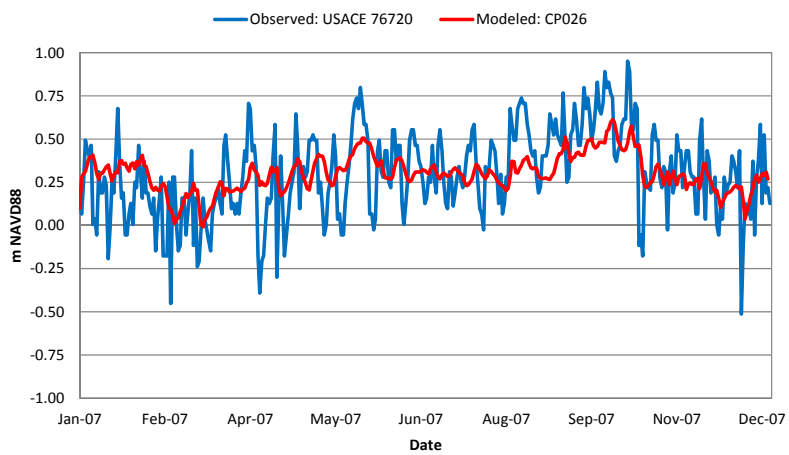

Figure 472 STG Calibration Results for the GIWW East of the Leland Bowman Lock and West of Franklin, LA in the CP Model

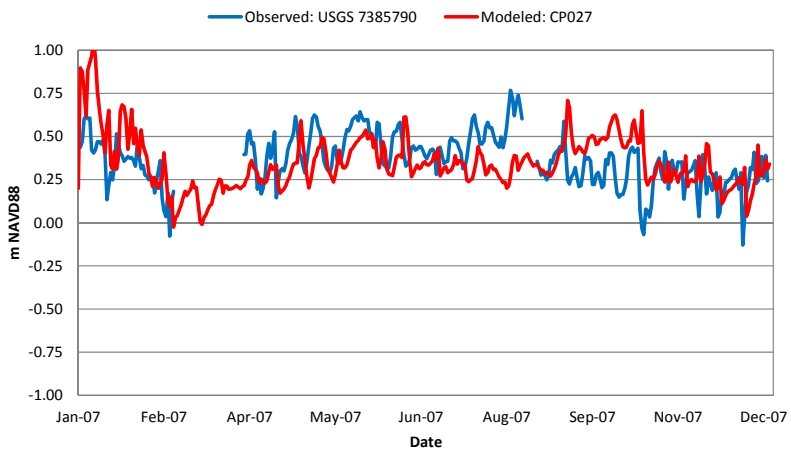

Figure 473 STG Calibration Results for Charenton Drainage Canal in the CP Model

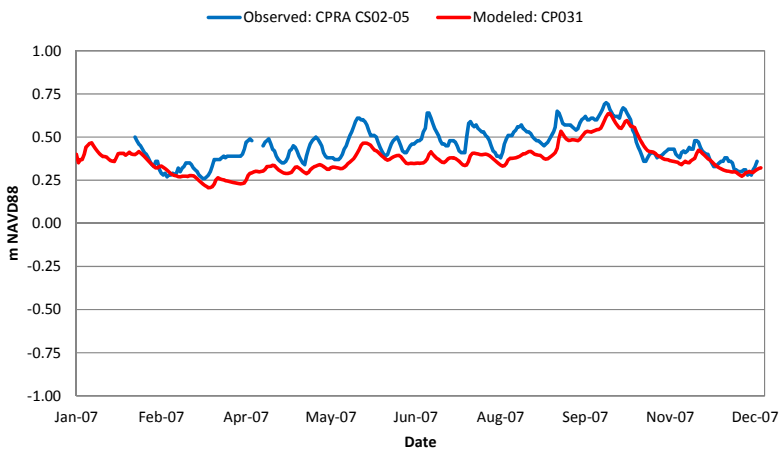

Figure 474 STG Calibration Results for Starks North Canal, Wild Cow Lake, and Browns Lake in the CP Model

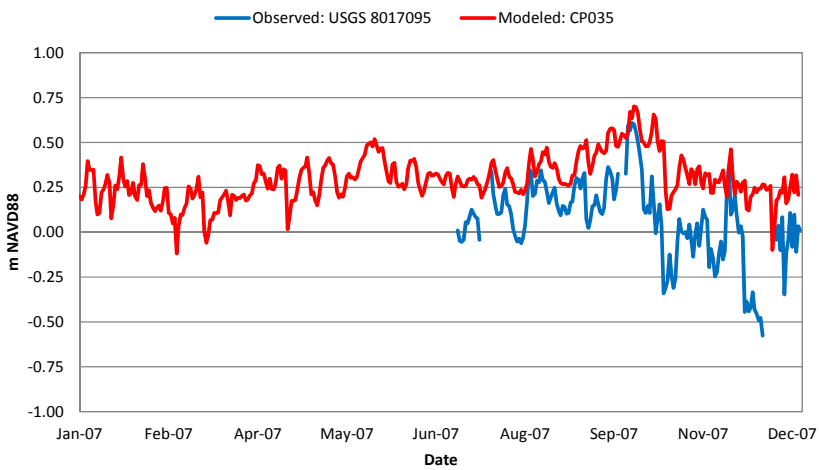

Figure 475 STG Calibration Results for Calcasieu Lake in the CP Model

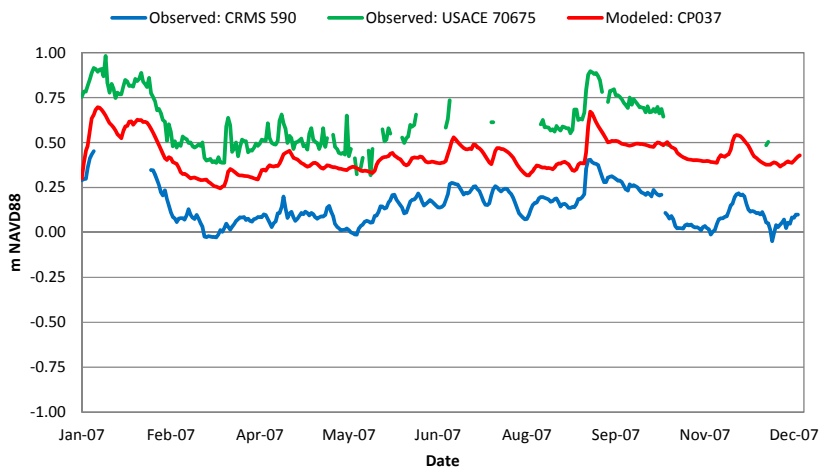

Figure 476 STG Calibration Results for Grand Lake in the CP Model

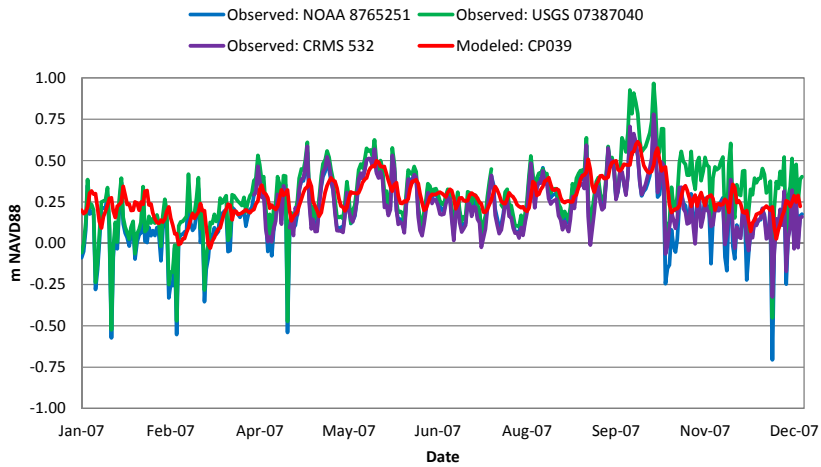

Figure 477 STG Calibration Results for Vermilion Bay in the CP Model

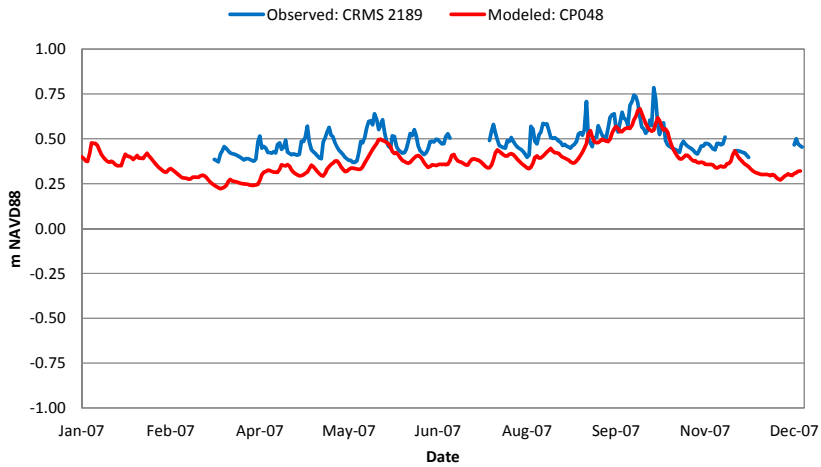

Figure 478 STG Calibration Results for the Marsh East of Central Sabine Lake and West of Greens Lake in the CP Model

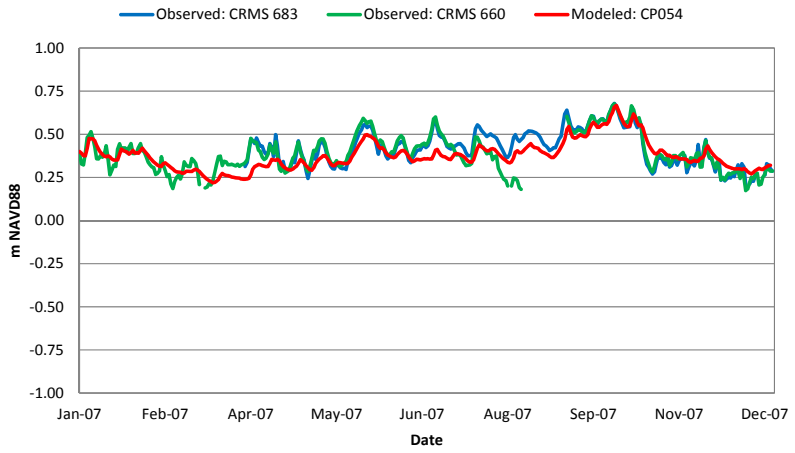

Figure 479 STG Calibration Results for Greens Lake and Surrounding Marshes in the CP Model

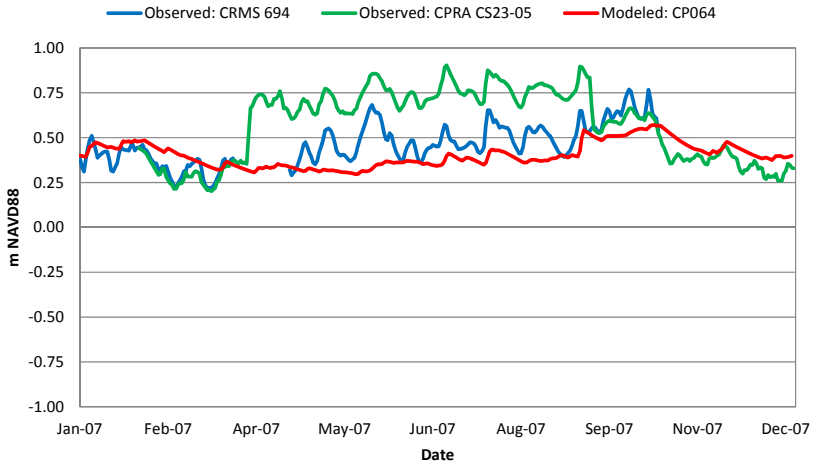

Figure 480 STG Calibration Results for Sabine National Wildlife Refuge in the CP Model

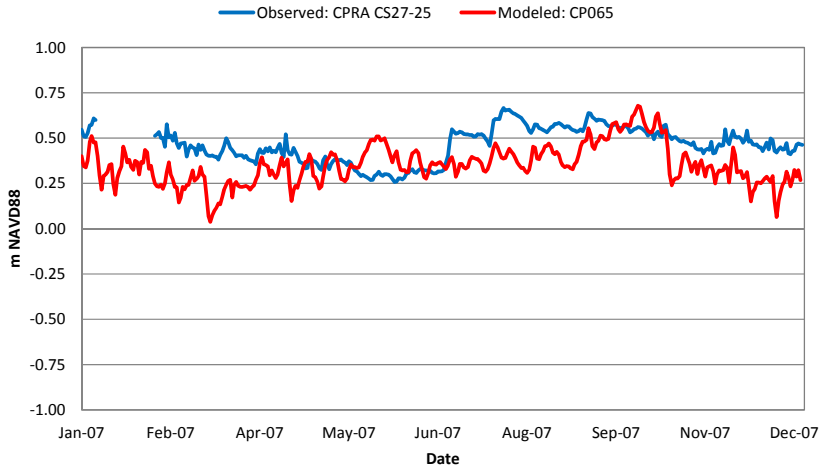

Figure 481 STG Calibration Results for CP065 in the CP Model

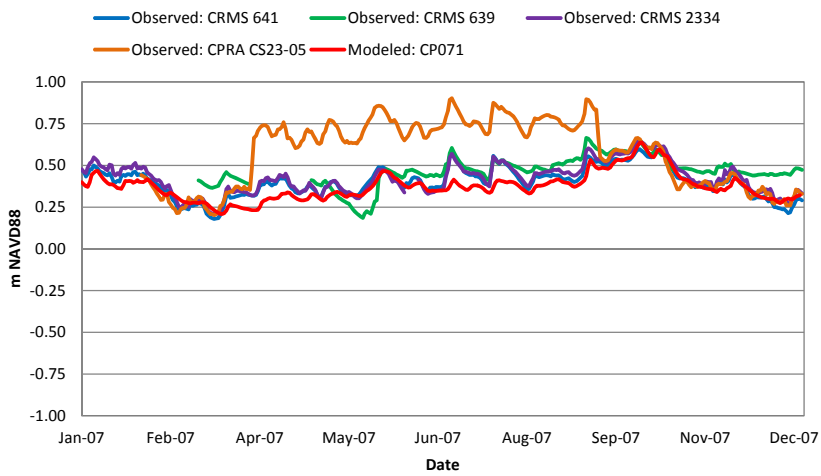

Figure 482 STG Calibration Results for CP071 in the CP Model

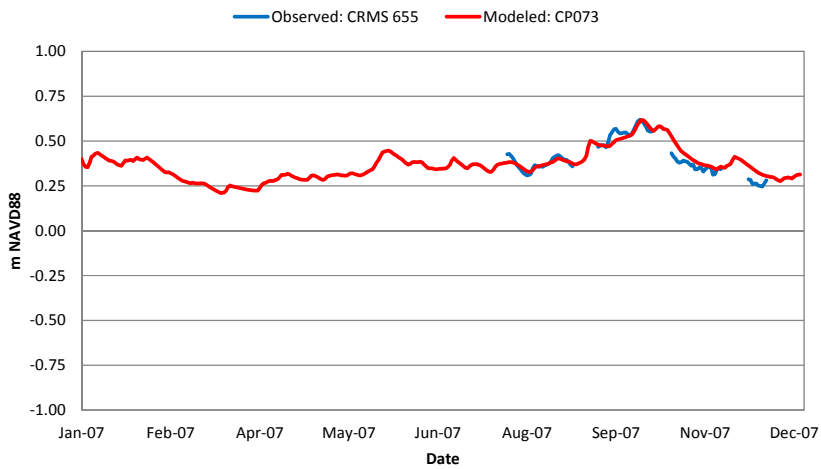

Figure 483 STG Calibration Results for CP073 in the CP Model

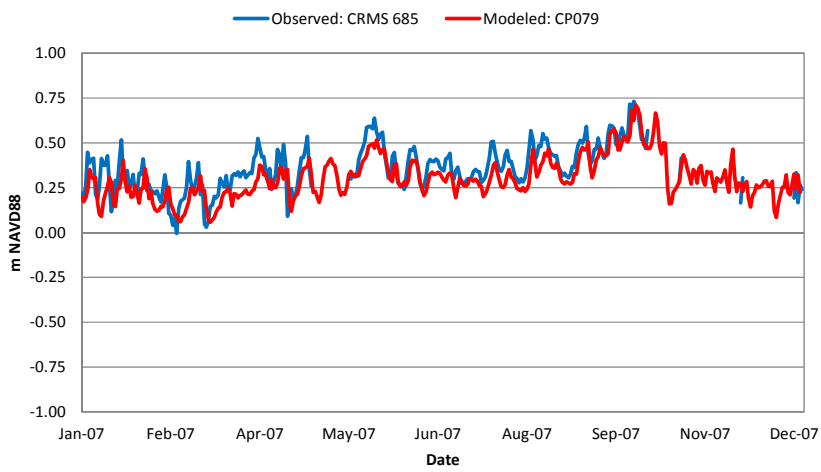

Figure 484 STG Calibration Results for CP079 in the CP Model

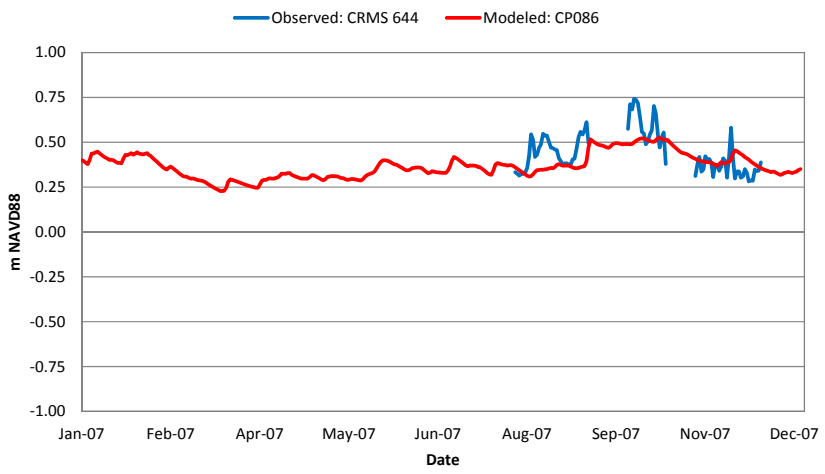

Figure 485 STG Calibration Results for CP086 in the CP Model

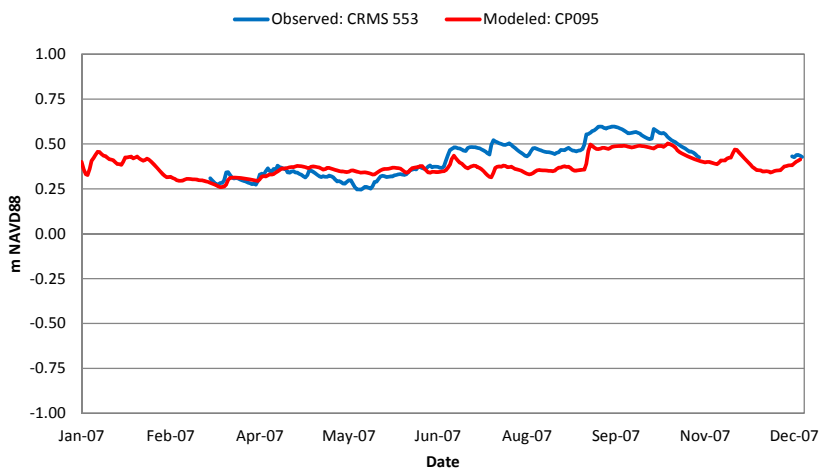

Figure 486 STG Calibration Results for CP095 in the CP Model

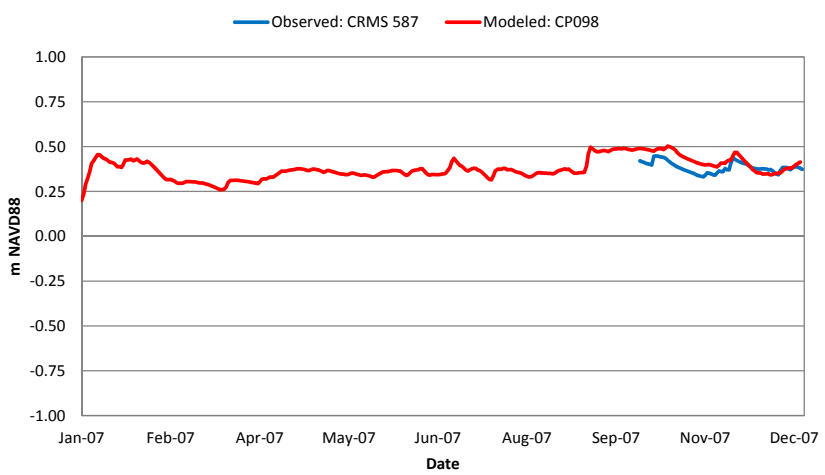

Figure 487 STG Calibration Results for CP098 in the CP Model

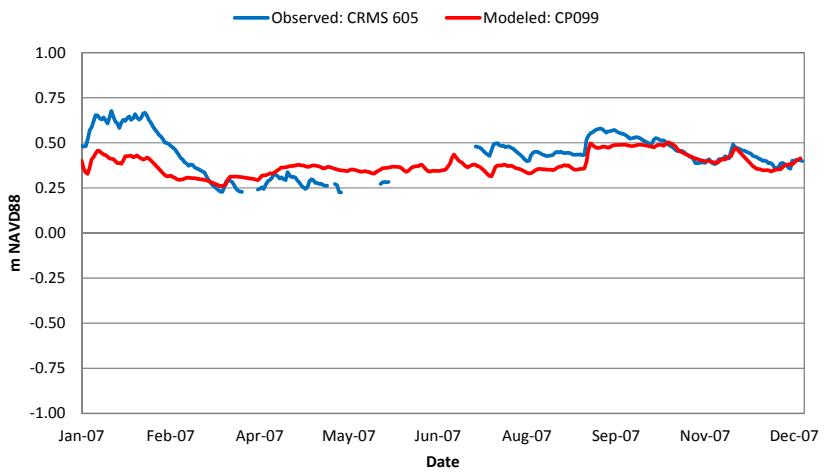

Figure 488 STG Calibration Results for CP099 in the CP Model

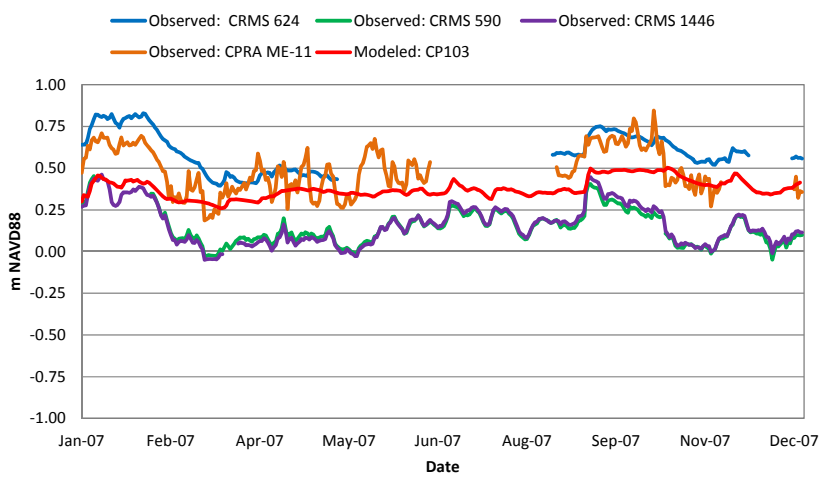

Figure 489 STG Calibration Results for CP103 in the CP Model

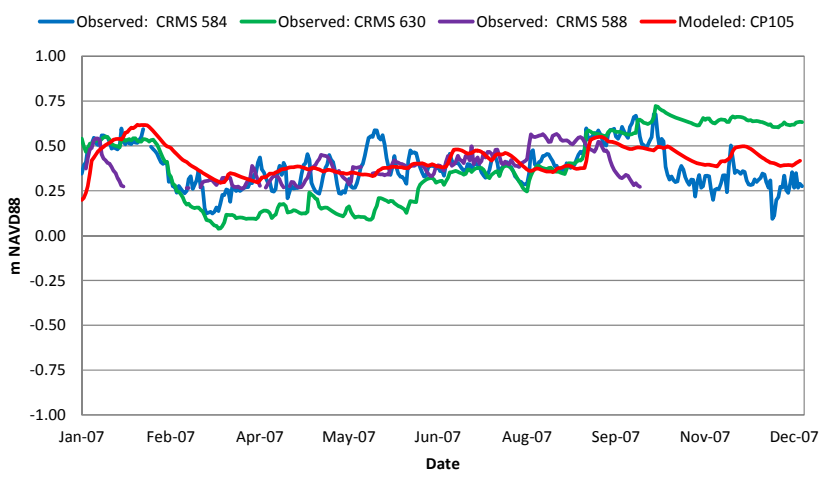

Figure 490 STG Calibration Results for CP105 in the CP Model

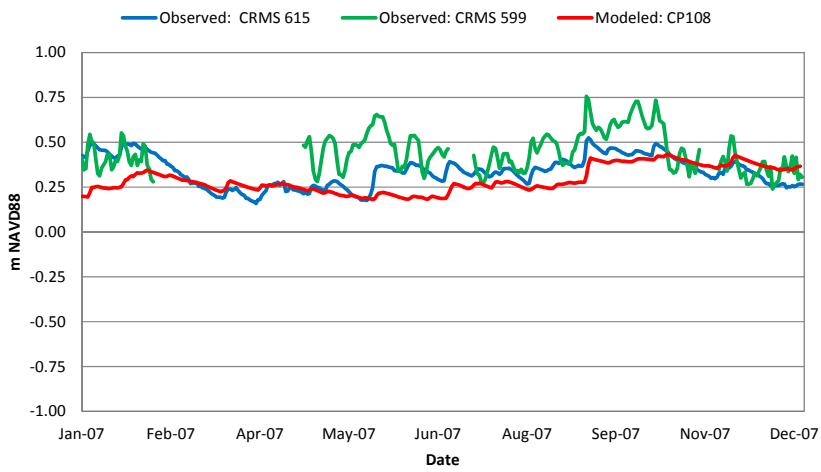

Figure 491 STG Calibration Results for CP108 in the CP Model

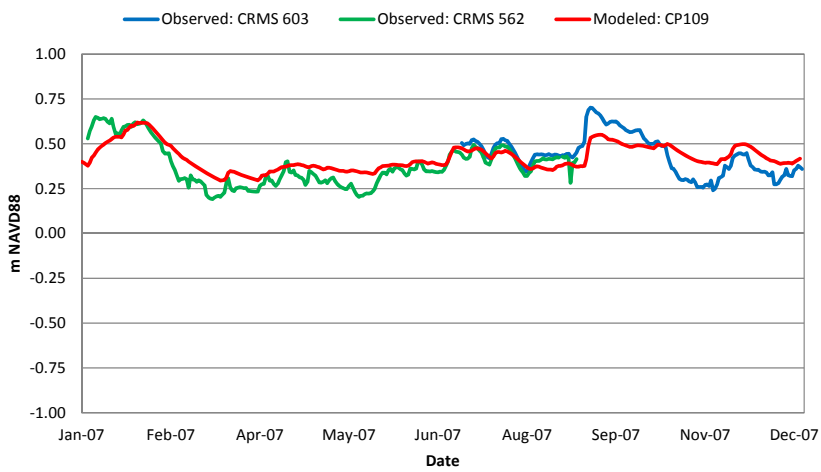

Figure 492 STG Calibration Results for CP109 in the CP Model

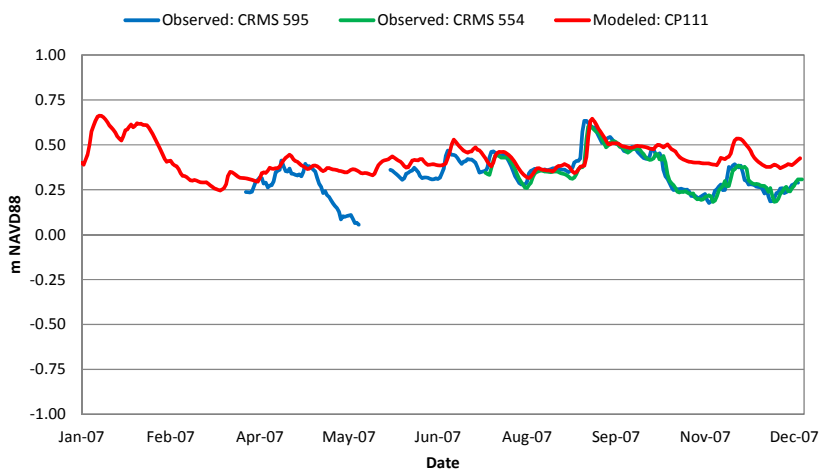

Figure 493 STG Calibration Results for CP111 in the CP Model

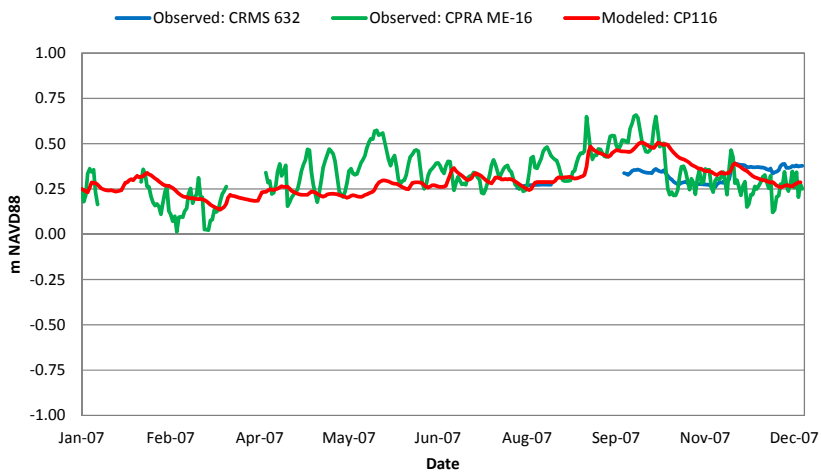

Figure 494 STG Calibration Results for CP116 in the CP Model

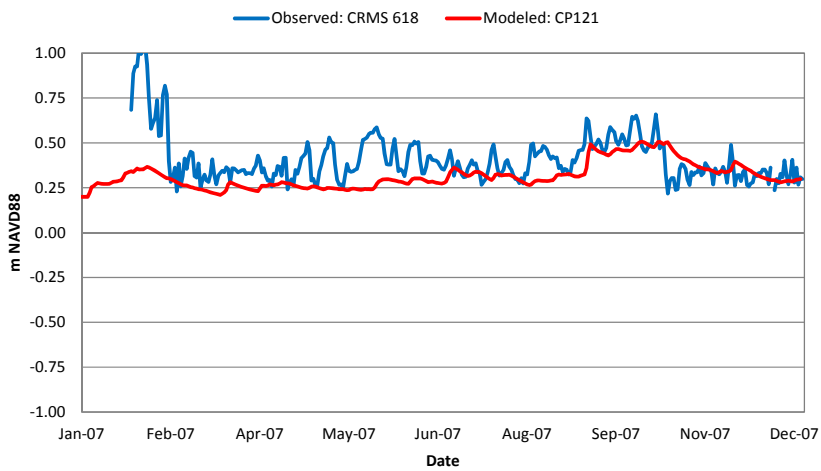

Figure 495 STG Calibration Results for CP121 in the CP Model

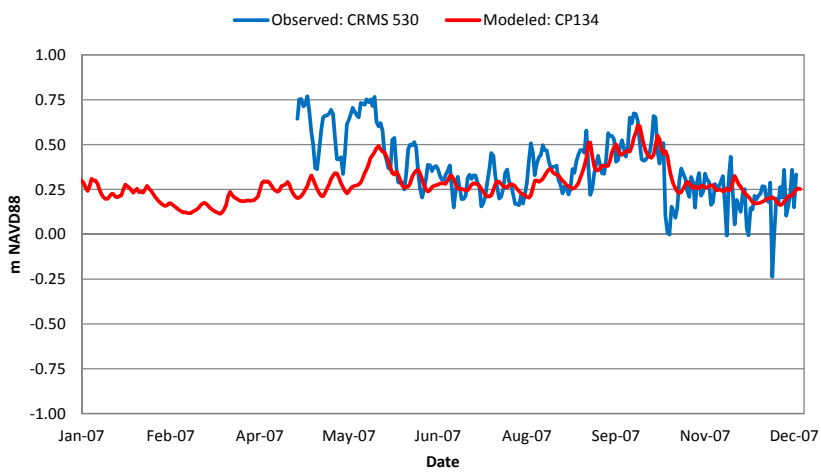

Figure 496 STG Calibration Results for Northwest Marsh Island in the CP Model

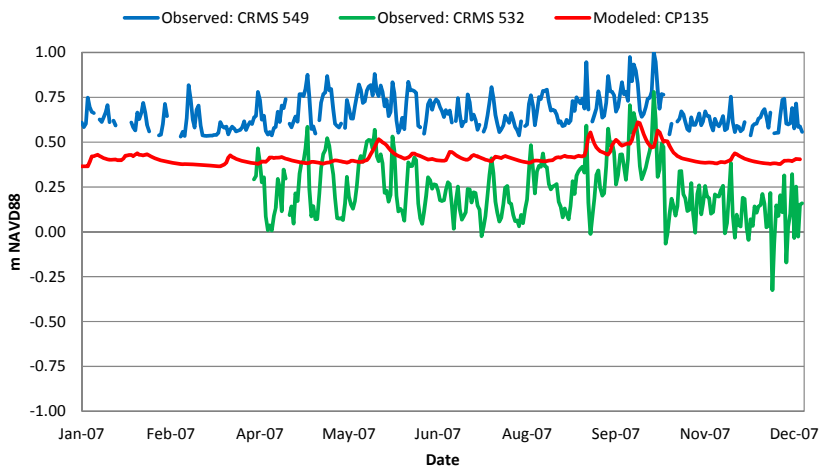

Figure 497 STG Calibration Results for CP135 in the CP Model

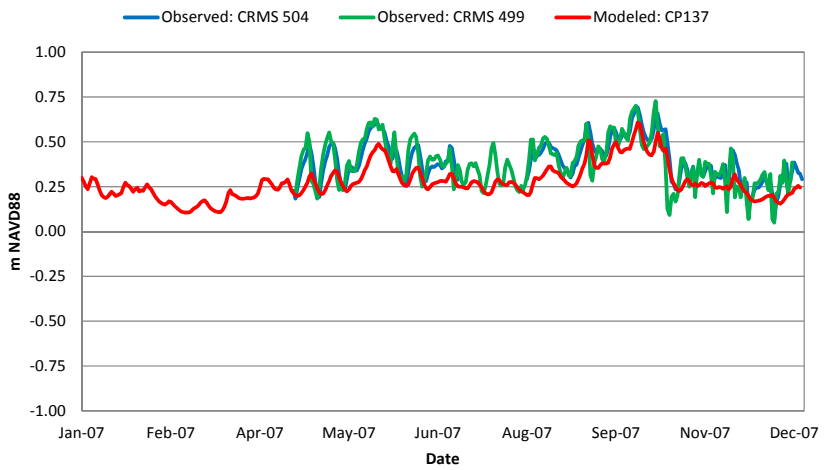

Figure 498 STG Calibration Results for East Marsh Island in the CP Model

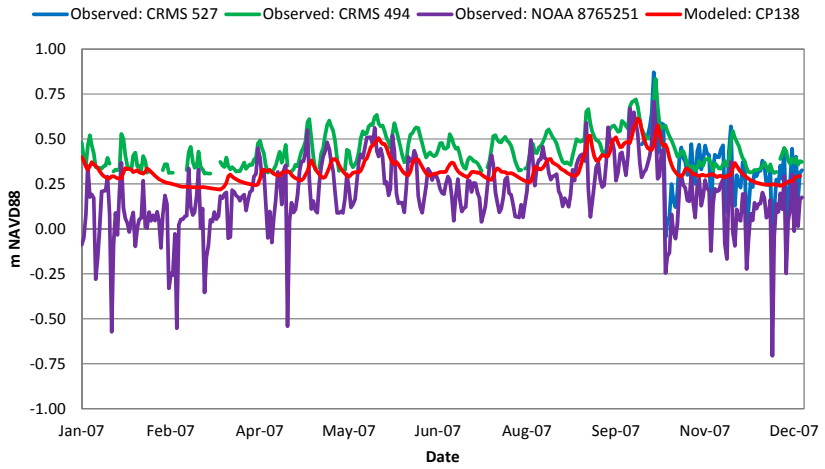

Figure 499 STG Calibration Results for CP138 in the CP Model

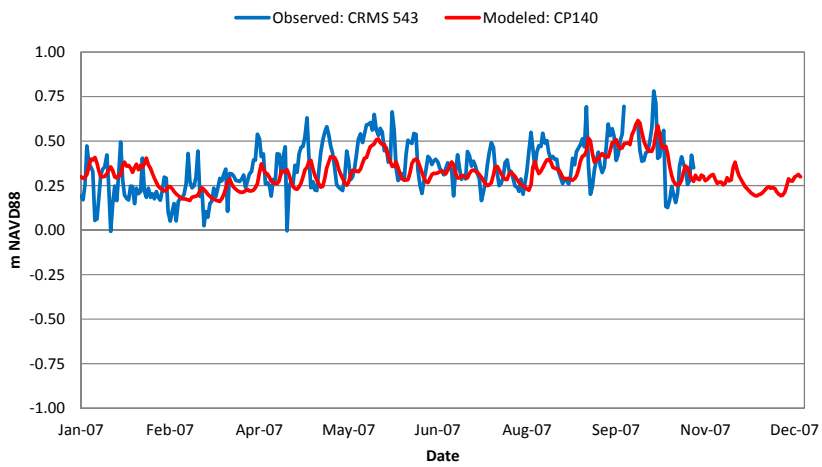

Figure 500 STG Calibration Results for CP140 in the CP Model

Salinity (SAL)

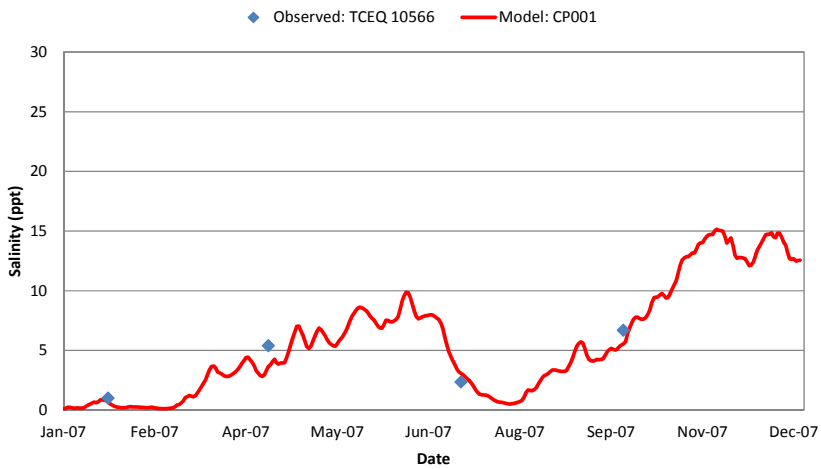

Figure 501 SAL Calibration Results for Neches River in the CP Model

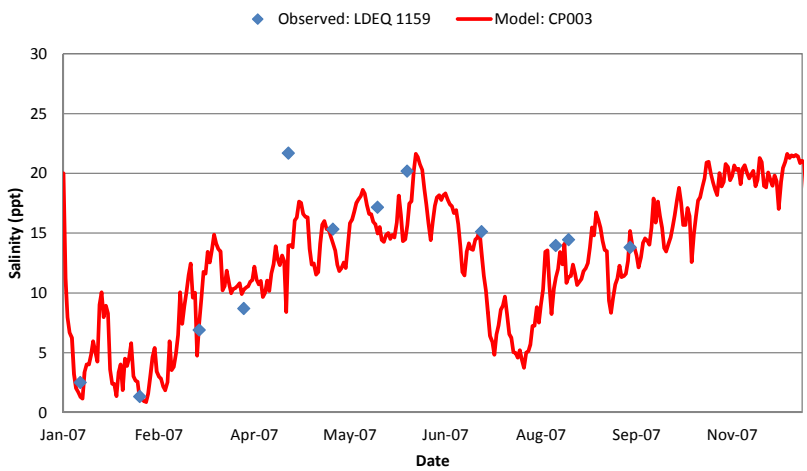

Figure 502 SAL Calibration Results for Sabine Pass in the CP Model

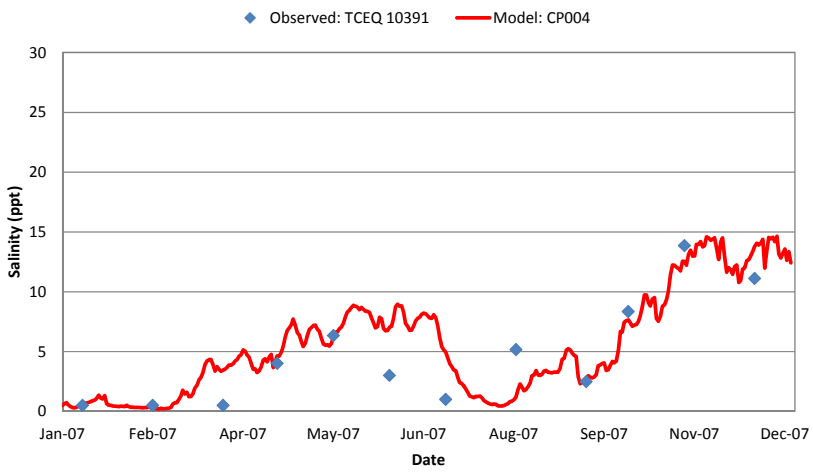

Figure 503 SAL Calibration Results for CP004 in the CP Model

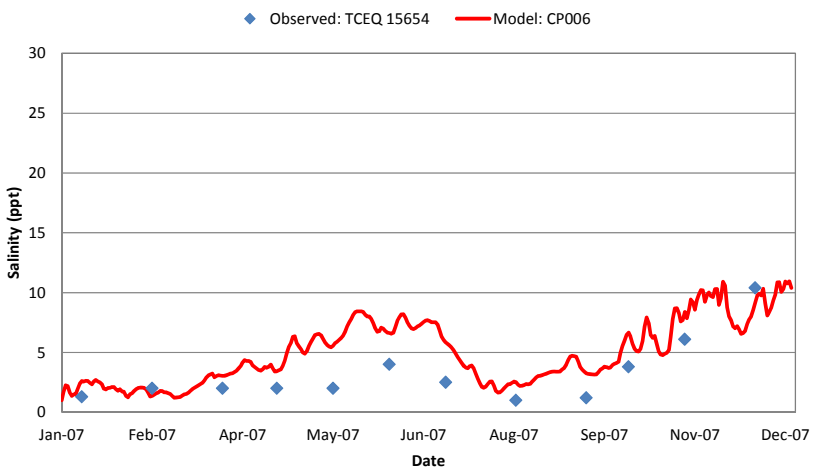

Figure 504 SAL Calibration Results for Black Bayou in the CP Model

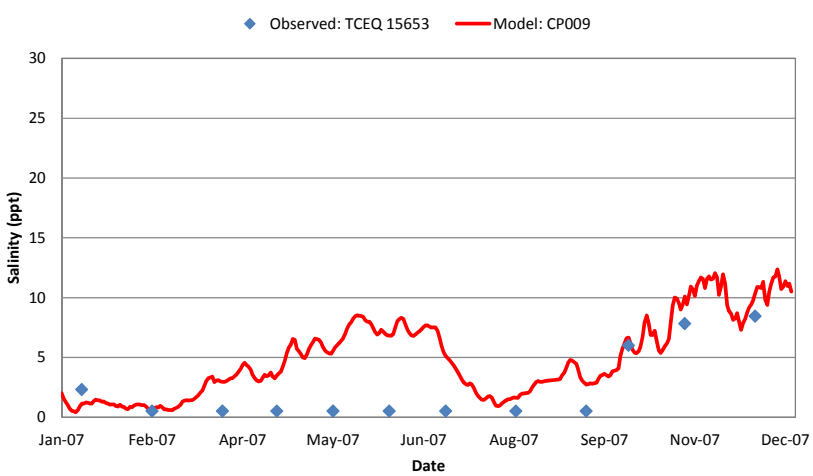

Figure 505 SAL Calibration Results for the GIWW between Sabine and Calcasieu Rivers in the CP Model

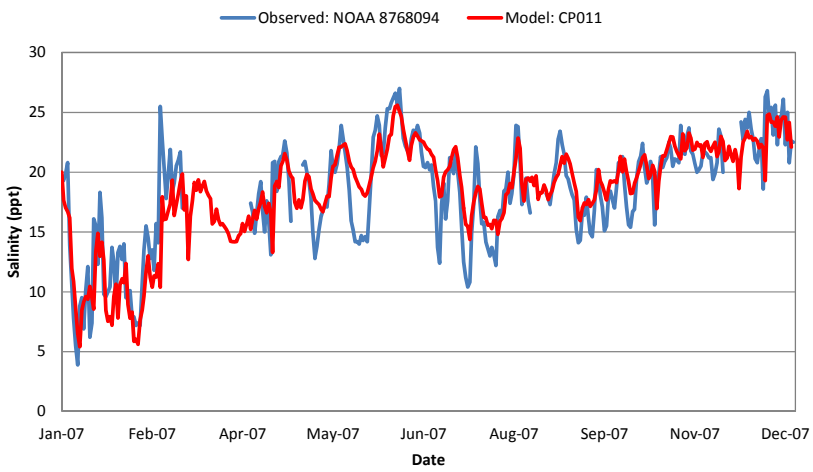

Figure 506 SAL Calibration Results for Calcasieu Pass in the CP Model

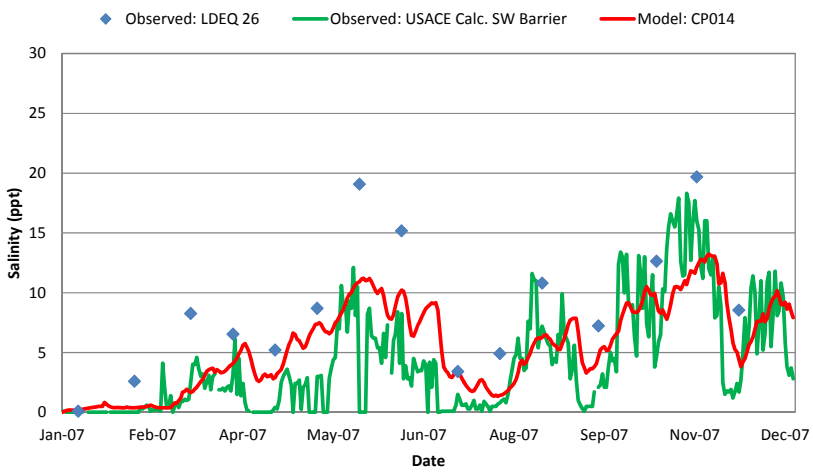

Figure 507 SAL Calibration Results for Calcasieu River North of the GIWW in the CP Model

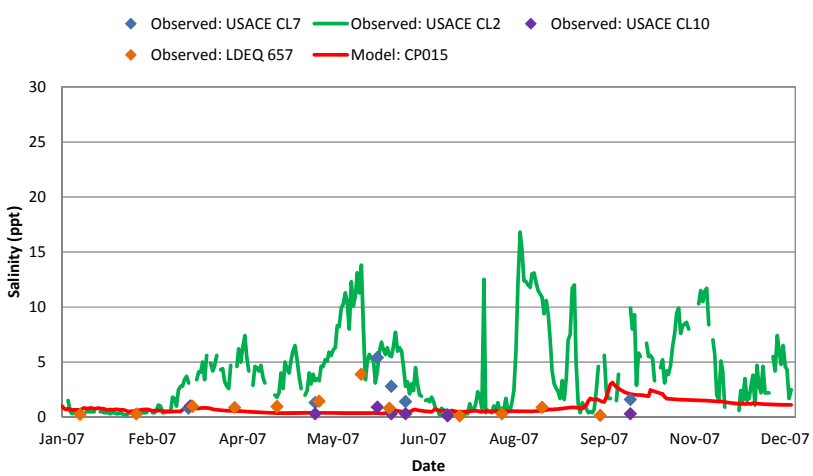

Figure 508 SAL Calibration Results for the GIWW between Calcasieu River and Grand Lake in the CP Model

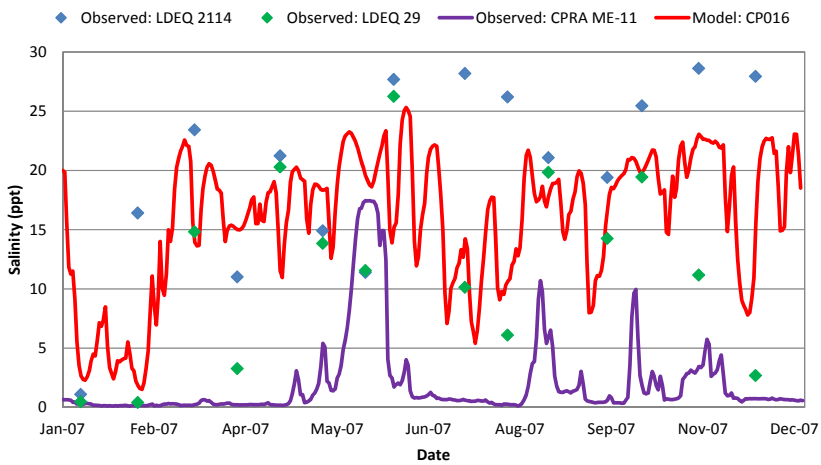

Figure 509 SAL Calibration Results for the Mermentau River South of Grand Lake in the CP Model

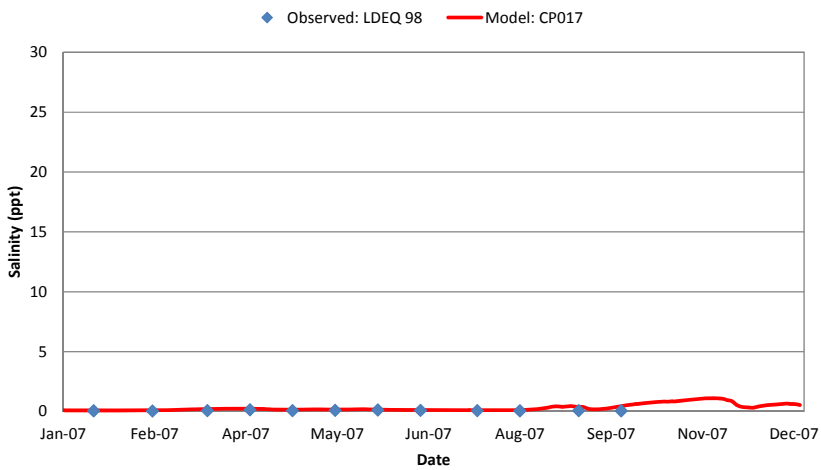

Figure 510 SAL Calibration Results for Lacassine River in the CP Model

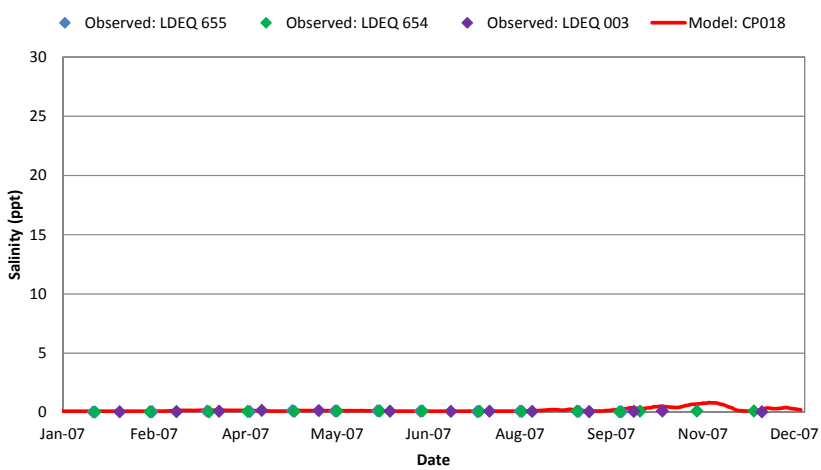

Figure 511 SAL Calibration Results for Mermentau River North of Grand Lake in the CP Model

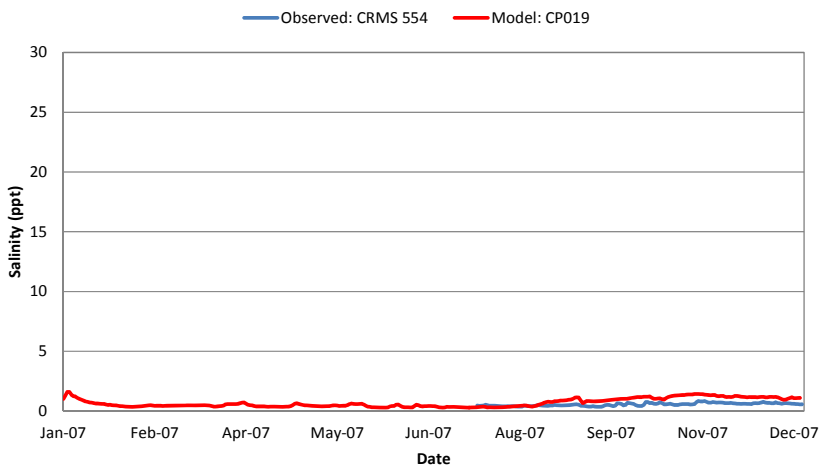

Figure 512 SAL Calibration Results for the Channel Connecting Grand and White Lakes in the CP Model

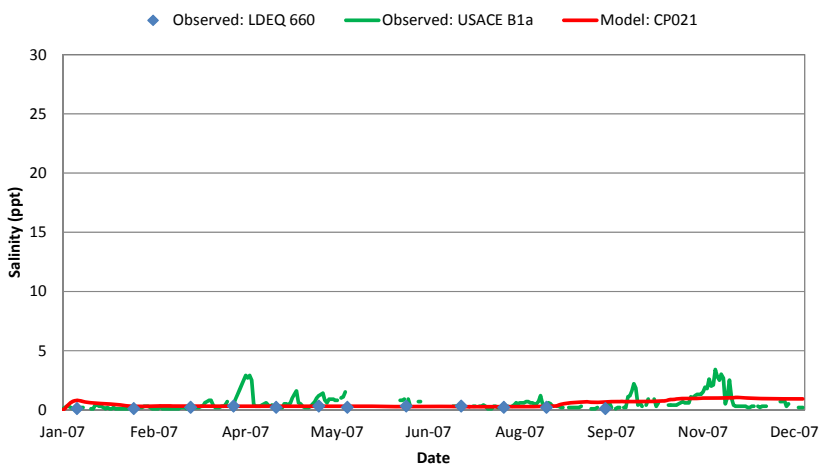

Figure 513 SAL Calibration Results for the GIWW East of Grand Lake and West of Leland Bowman Lock in the CP Model

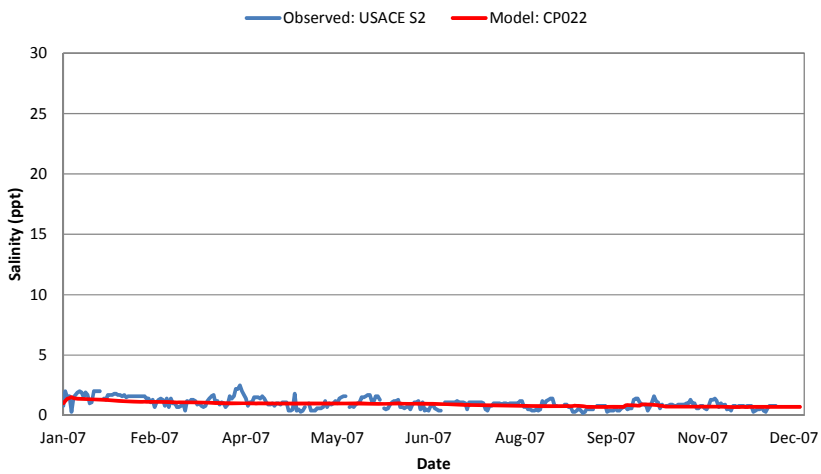

Figure 514 SAL Calibration Results for Schooner Bayou West of the Lock in the CP Model

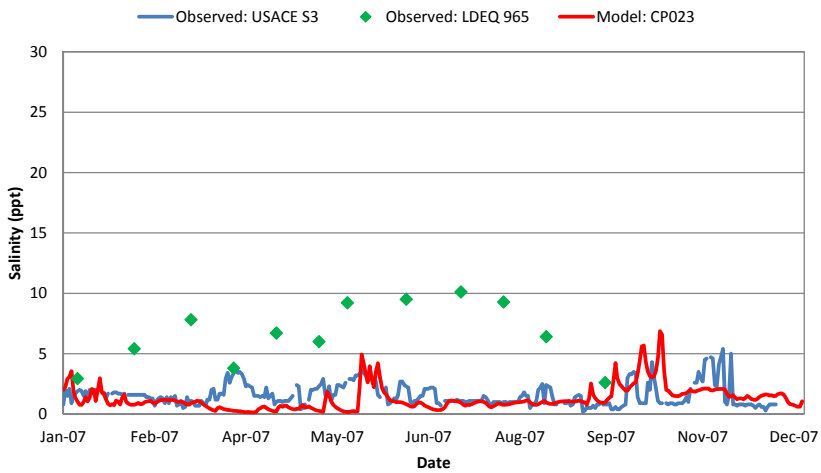

Figure 515 SAL Calibration Results for Freshwater Bayou in the CP Model

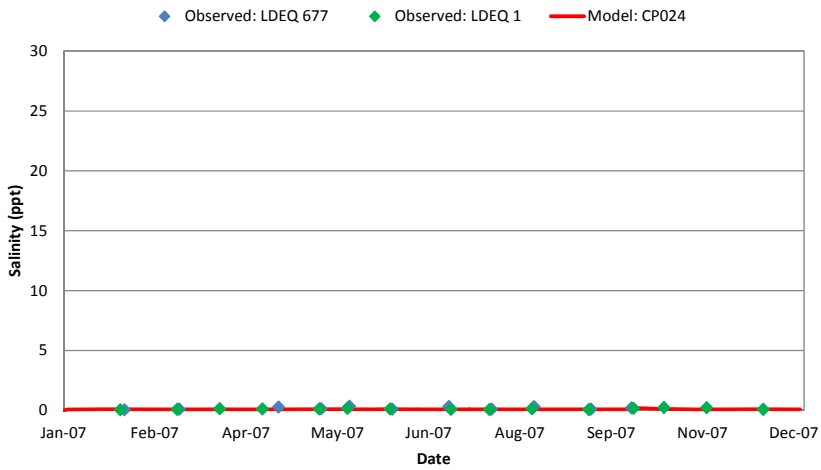

Figure 516 SAL Calibration Results for Vermilion River in the CP Model

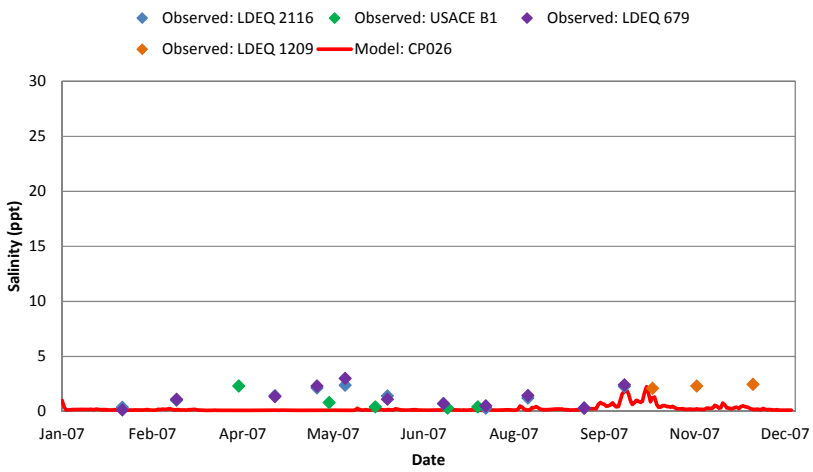

Figure 517 SAL Calibration Results for the GIWW North of Vermilion Bay in the CP Model

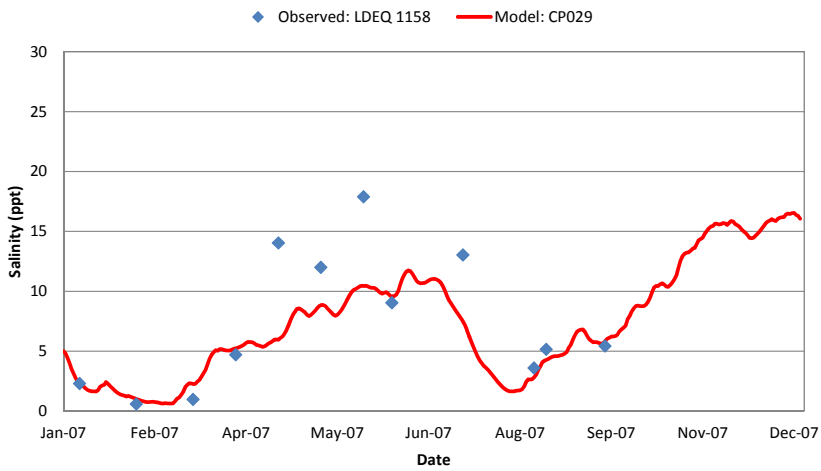

Figure 518 SAL Calibration Results for Sabine Lake in the CP Model

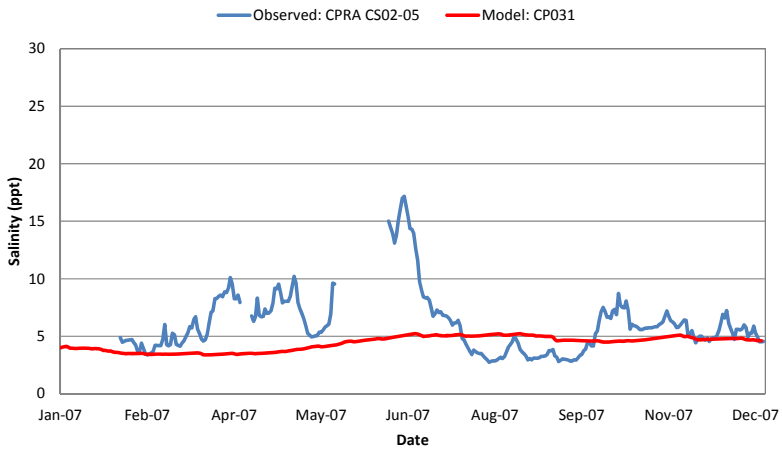

Figure 519 SAL Calibration Results for Starks North Canal, Wild Cow Lake, and Browns Lake in the CP Model

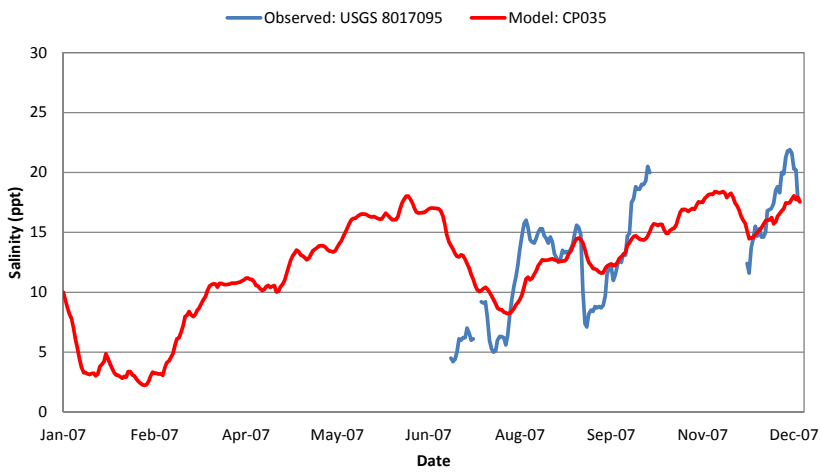

Figure 520 SAL Calibration Results for Calcasieu Lake in the CP Model

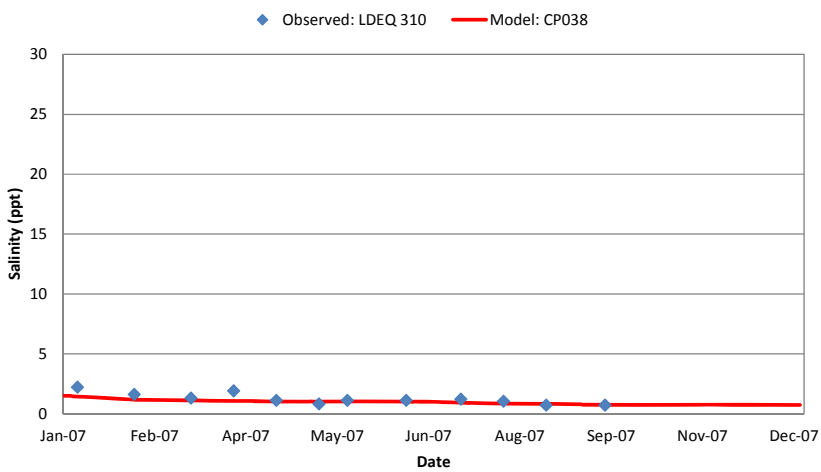

Figure 521 SAL Calibration Results for White Lake in the CP Model

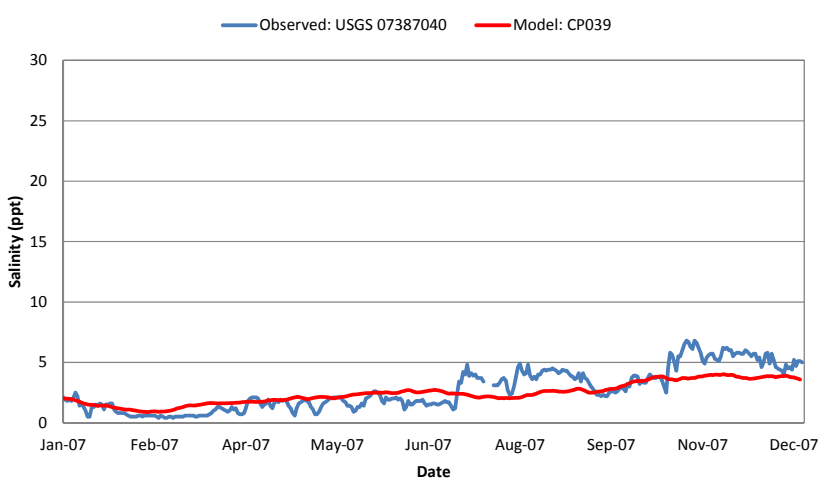

Figure 522 SAL Calibration Results for Vermilion Bay in the CP Model

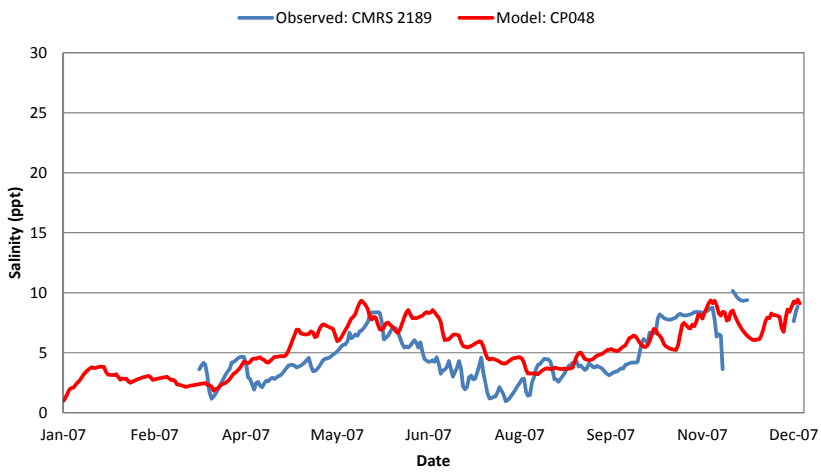

Figure 523 SAL Calibration Results for the Marsh East of Central Sabine Lake in the CP Model

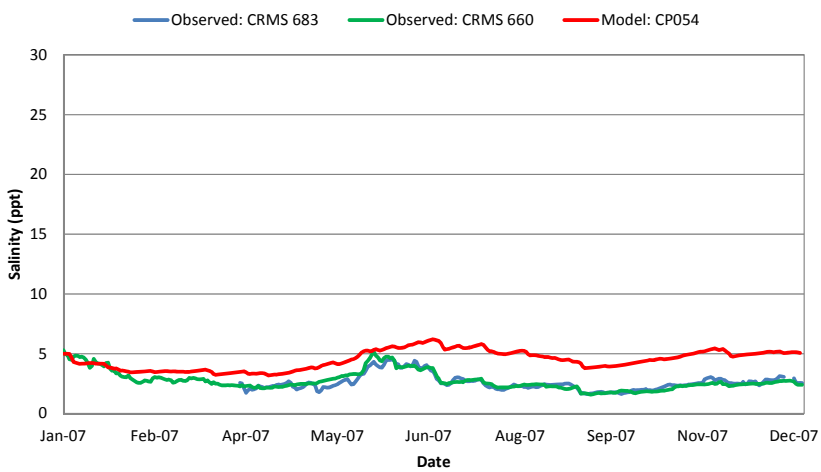

Figure 524 SAL Calibration Results for Greens Lake and Surrounding Marshes in the CP Model

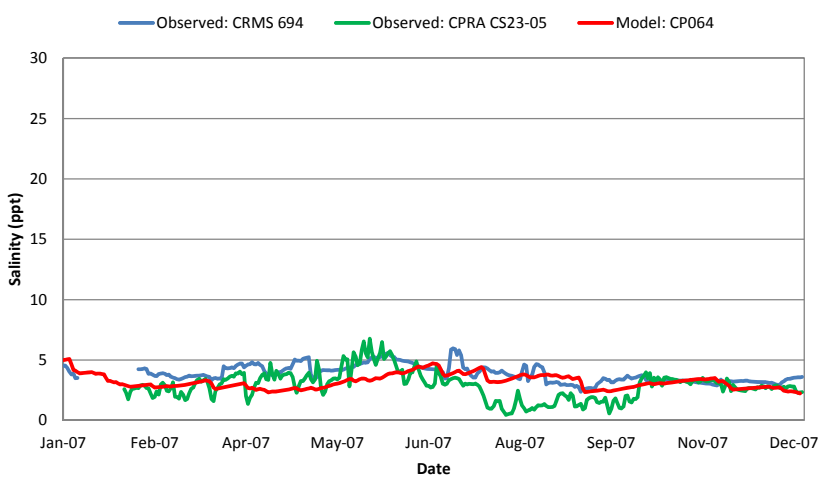

Figure 525 SAL Calibration Results for CP064 in the CP Model

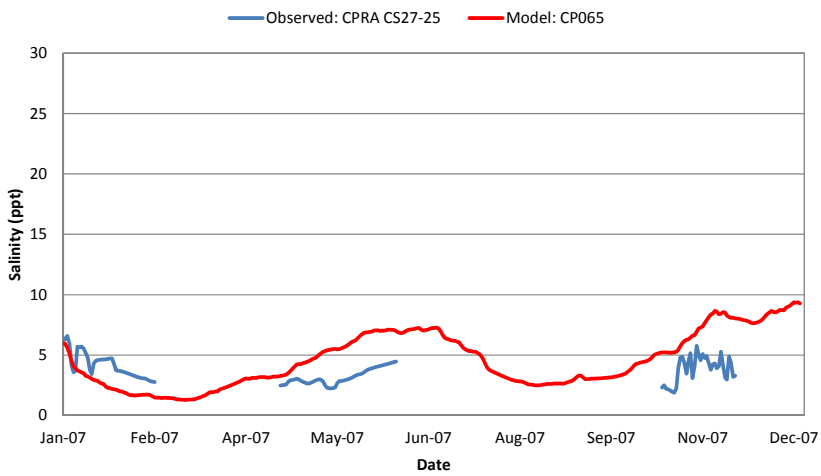

Figure 526 SAL Calibration Results for CP065 in the CP Model

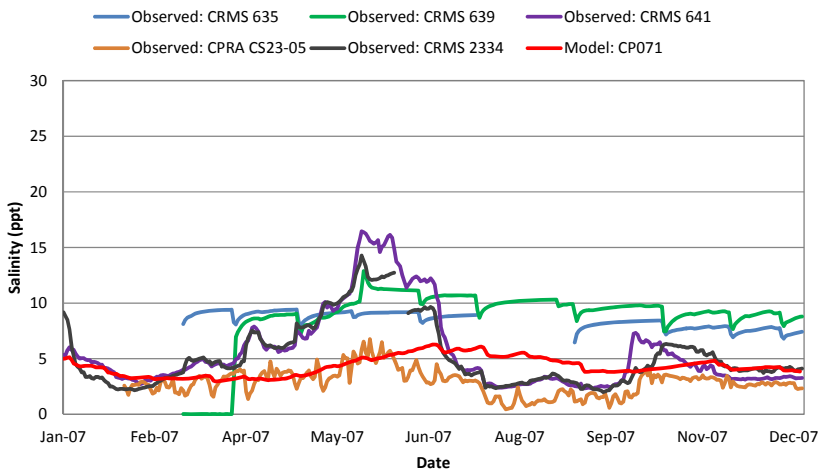

Figure 527 SAL Calibration Results for CP071 in the CP Model

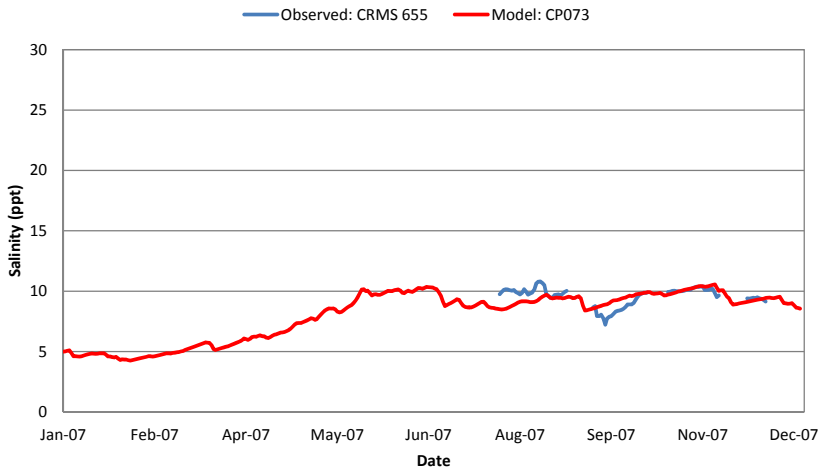

Figure 528 SAL Calibration Results for CP073 in the CP Model

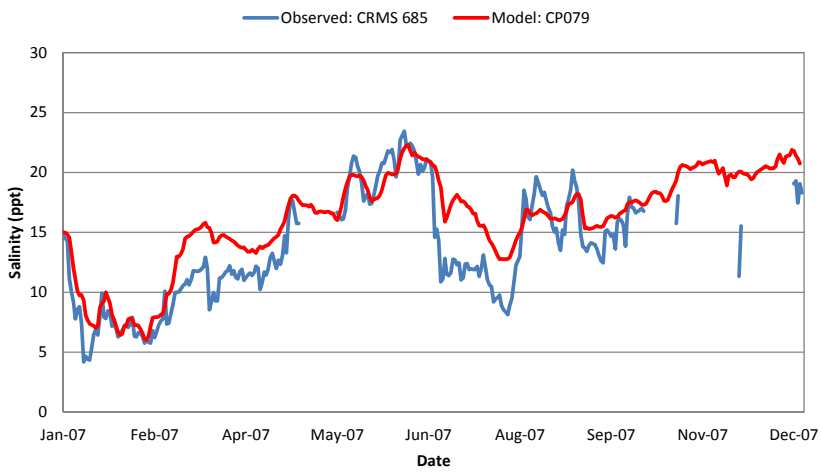

Figure 529 SAL Calibration Results for CP079 in the CP Model

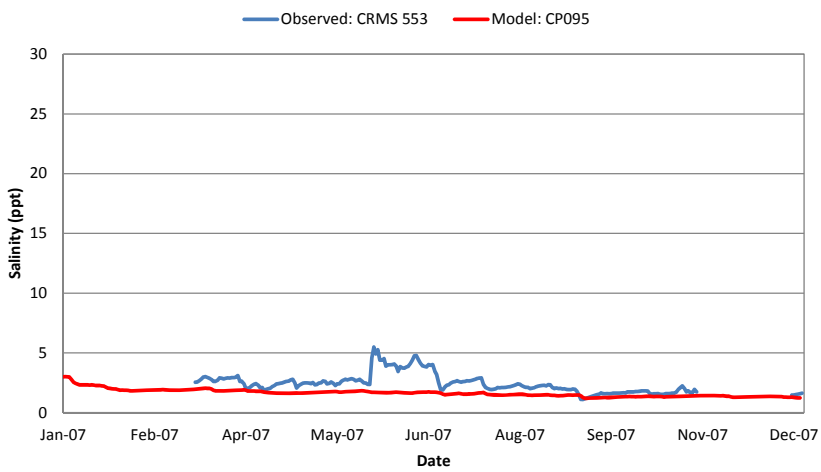

Figure 530 SAL Calibration Results for CP095 in the CP Model

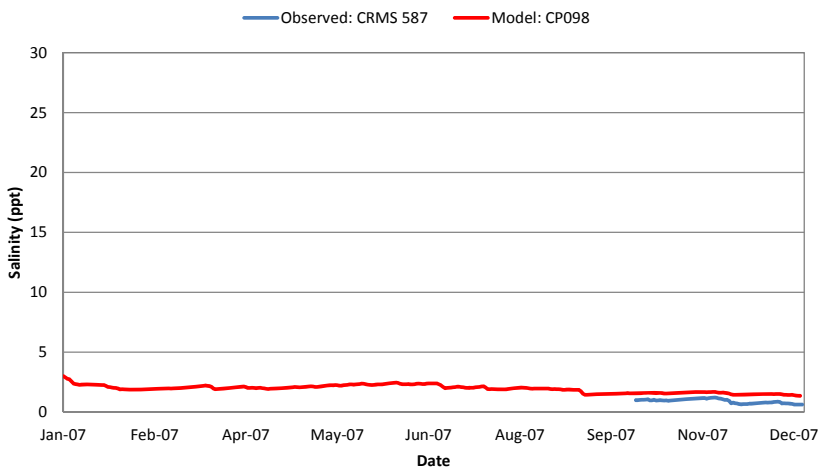

Figure 531 SAL Calibration Results for CP098 in the CP Model

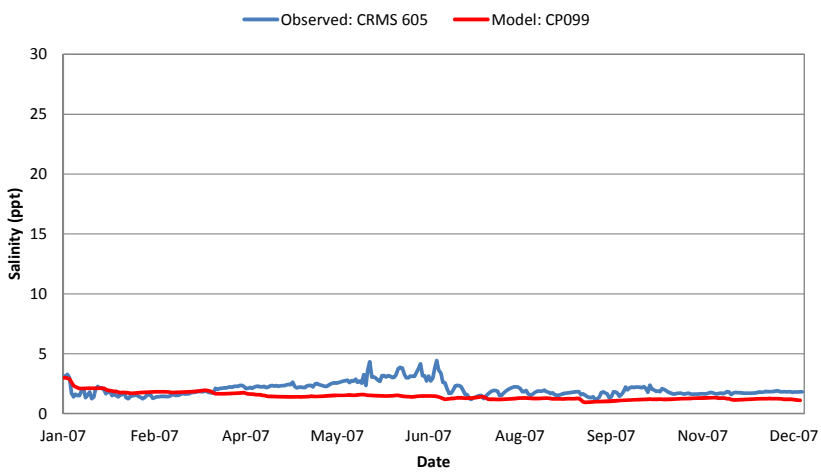

Figure 532 SAL Calibration Results for CP099 in the CP Model

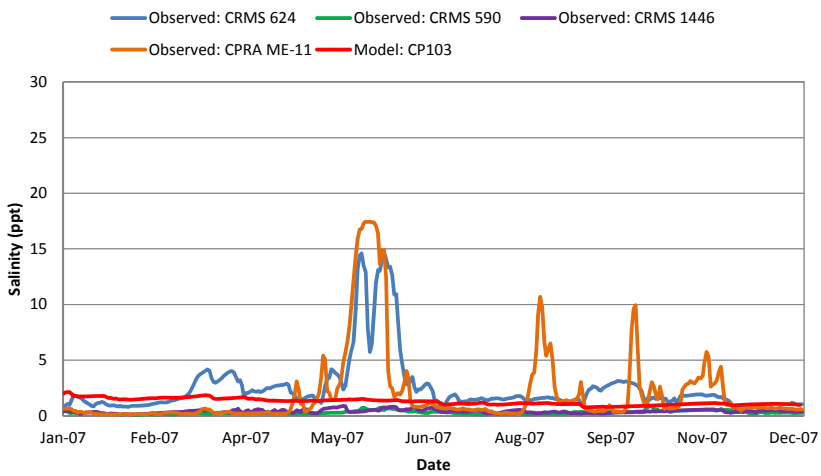

Figure 533 SAL Calibration Results for CP103 in the CP Model

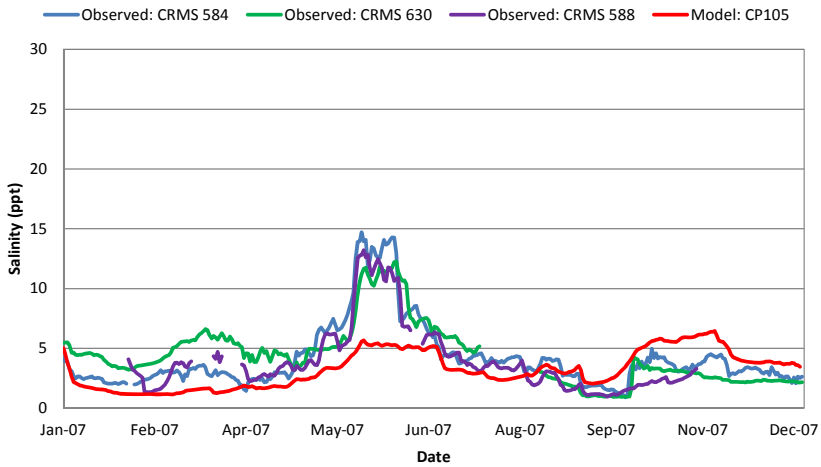

Figure 534 SAL Calibration Results for CP105 in the CP Model

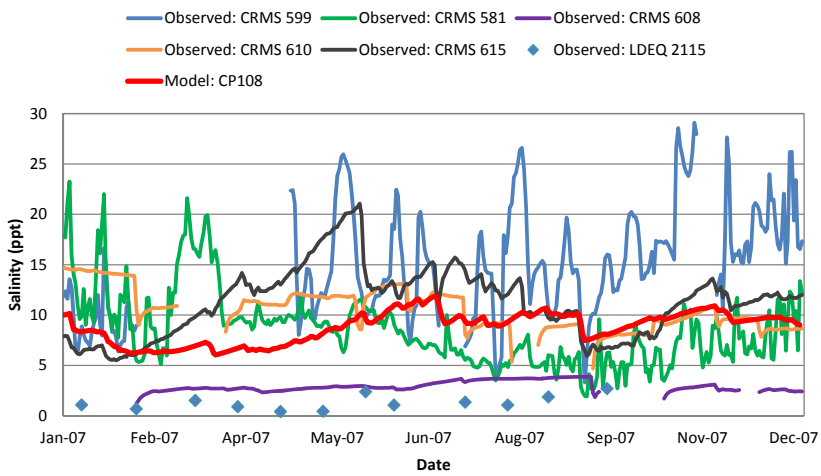

Figure 535 SAL Calibration Results for CP108 in the CP Model

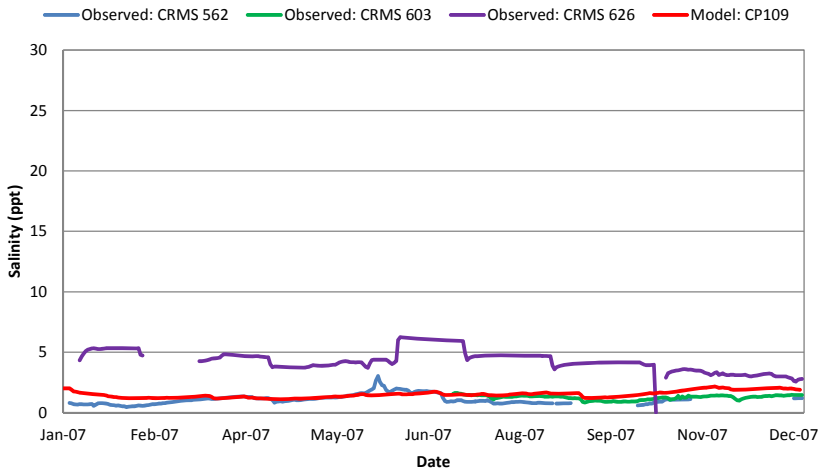

Figure 536 SAL Calibration Results for CP109 in the CP Model

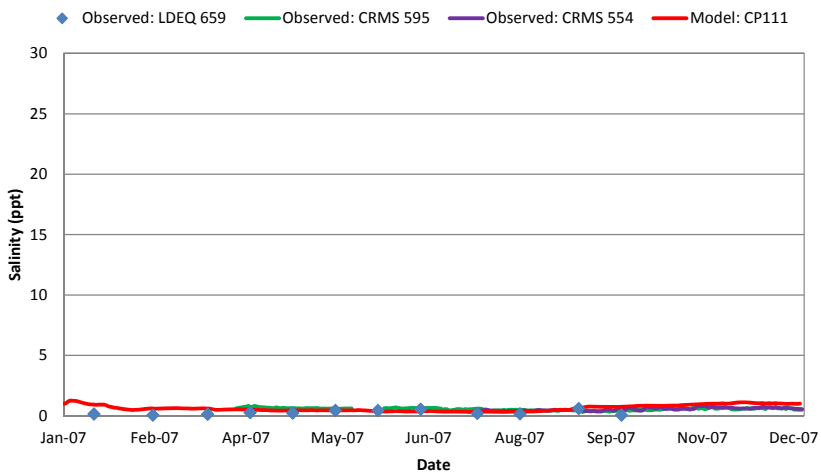

Figure 537 SAL Calibration Results for CP111 in the CP Model

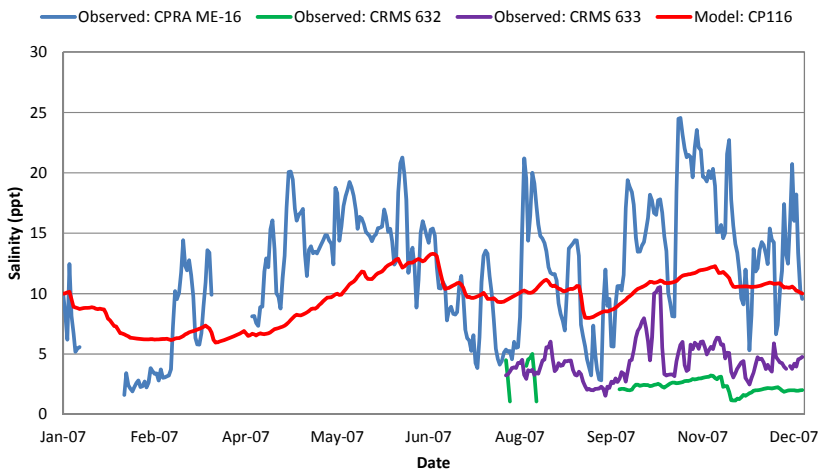

Figure 538 SAL Calibration Results for CP116 in the CP Model

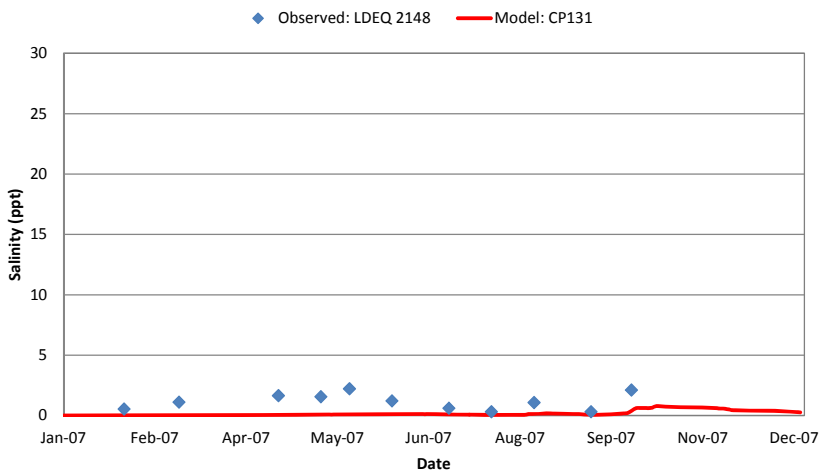

Figure 539 SAL Calibration Results for CP131 in the CP Model

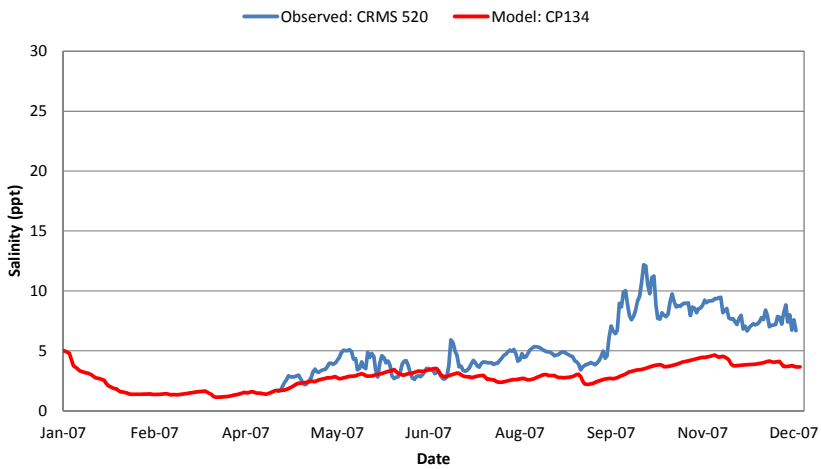

Figure 540 SAL Calibration Results for CP134 in the CP Model

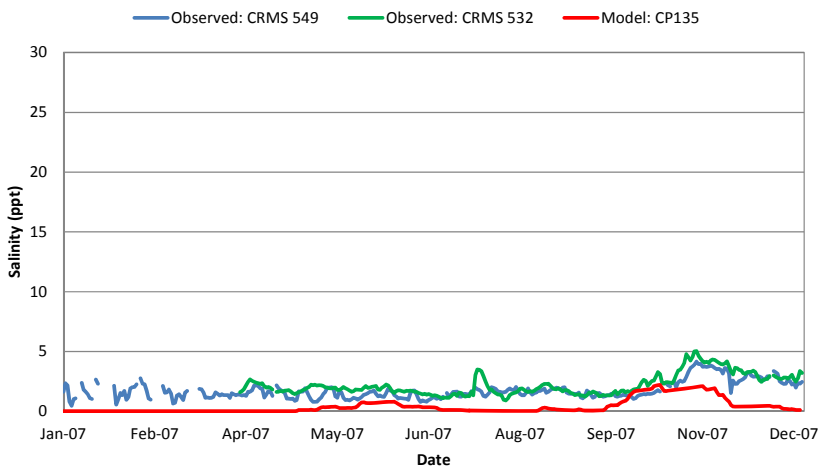

Figure 541 SAL Calibration Results for CP135 in the CP Model

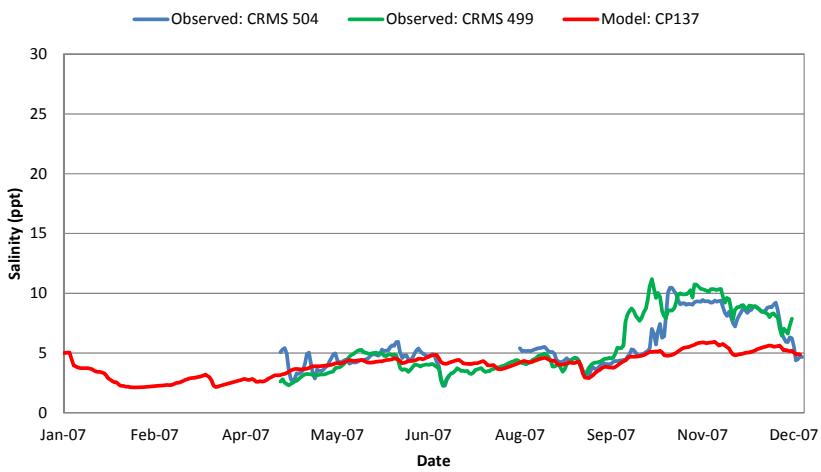

Figure 542 SAL Calibration Results for East Marsh Island in the CP Model

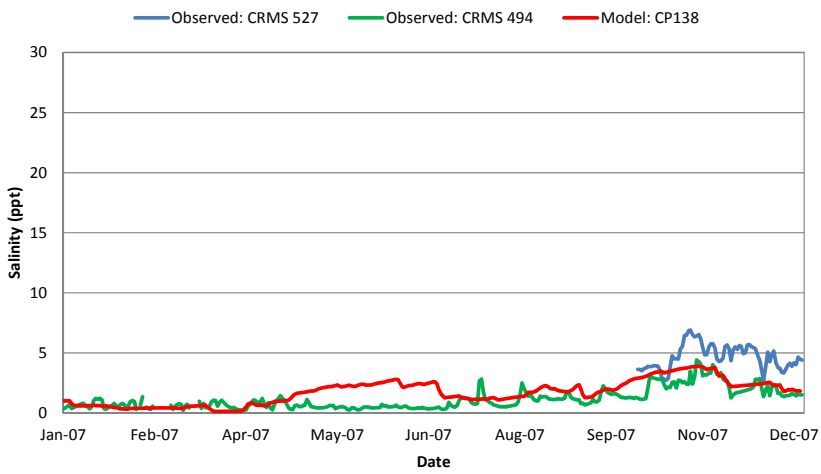

Figure 543 SAL Calibration Results for CP138 in the CP Model

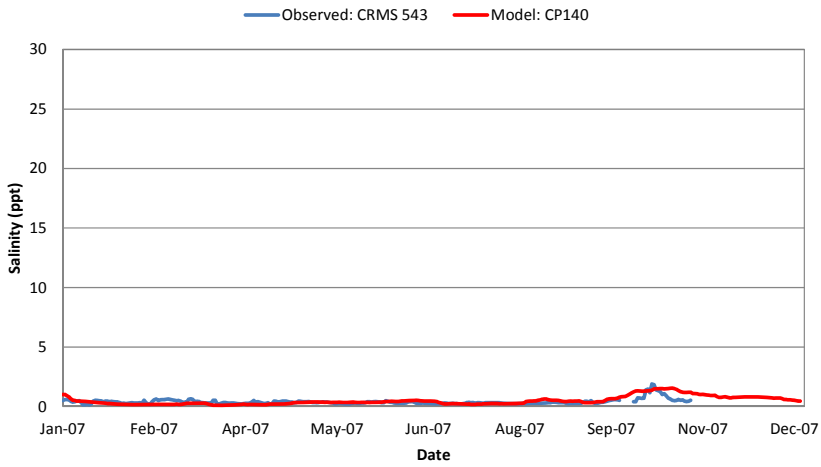

Figure 544 SAL Calibration Results for CP140 in the CP Model

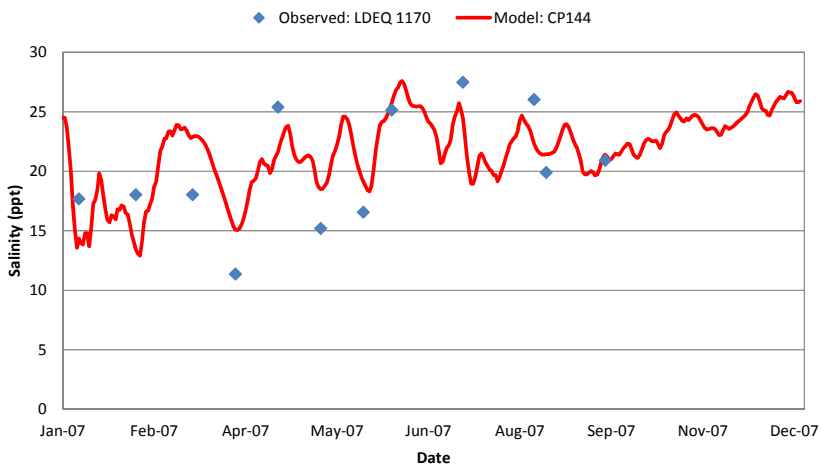

Figure 545 SAL Calibration Results for Offshore of Sabine Pass in the CP Model

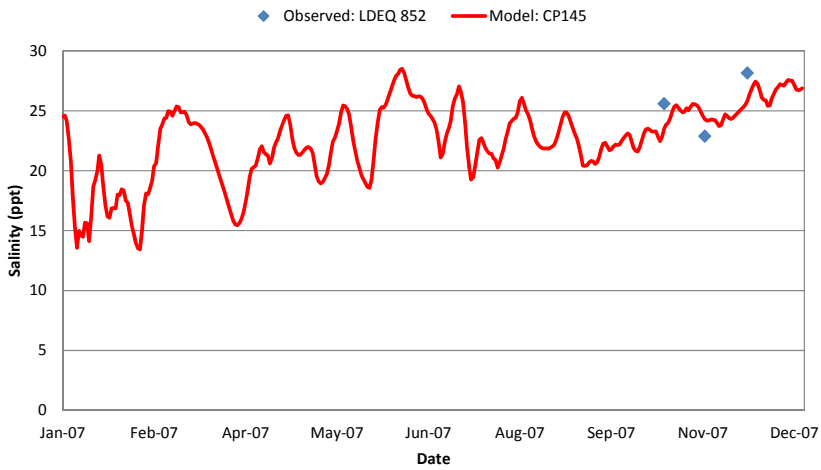

Figure 546 SAL Calibration Results for Offshore of Calcasieu Pass in the CP Model

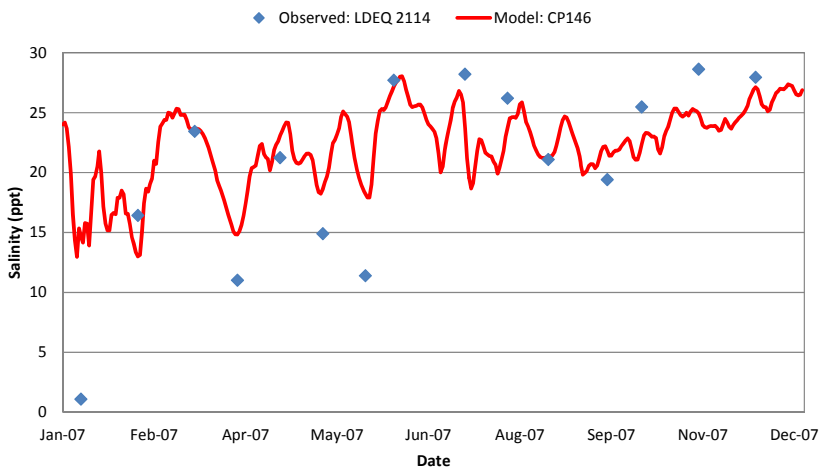

Figure 547 SAL Calibration Results for Offshore of Mermentau River in the CP Model

Temperature (TMP)

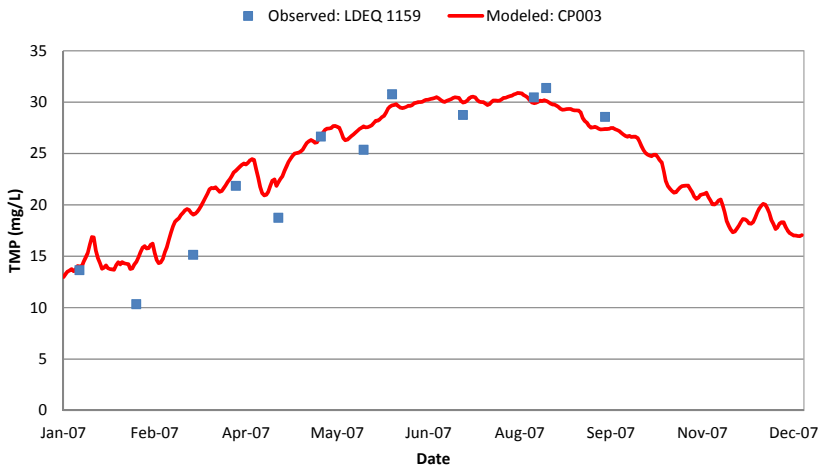

Figure 548 TMP Calibration Results for Sabine Pass in the CP Model

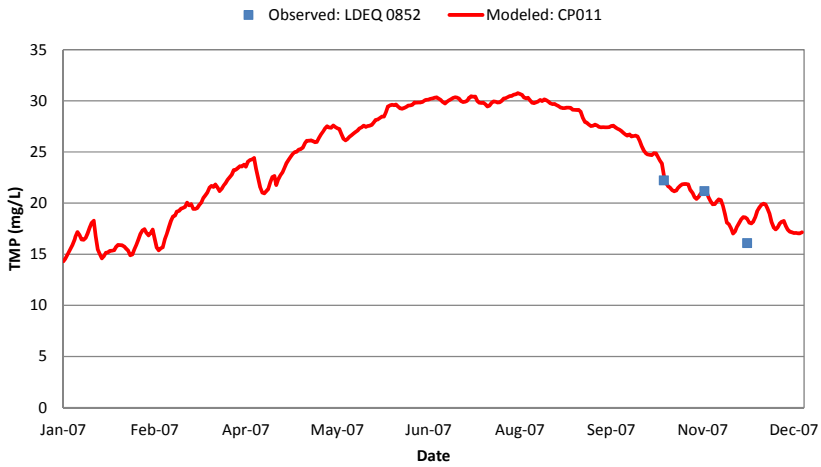

Figure 549 TMP Calibration Results for Calcasieu Pass in the CP Model

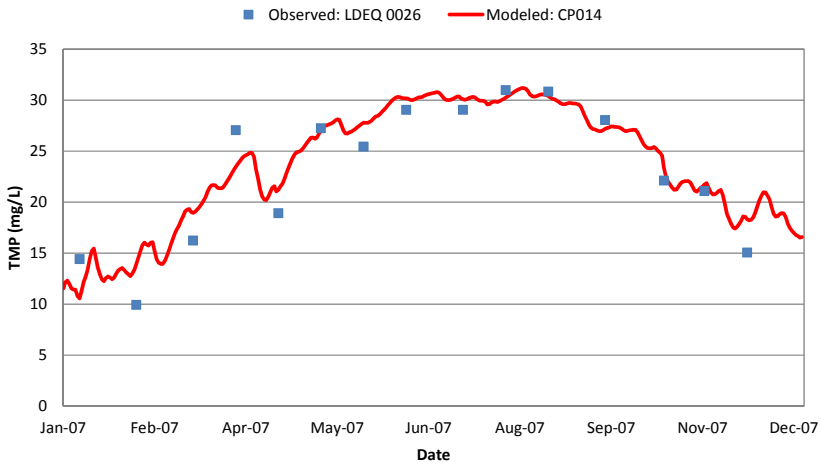

Figure 550 TMP Calibration Results for Calcasieu River North of the GIWW in the CP Model

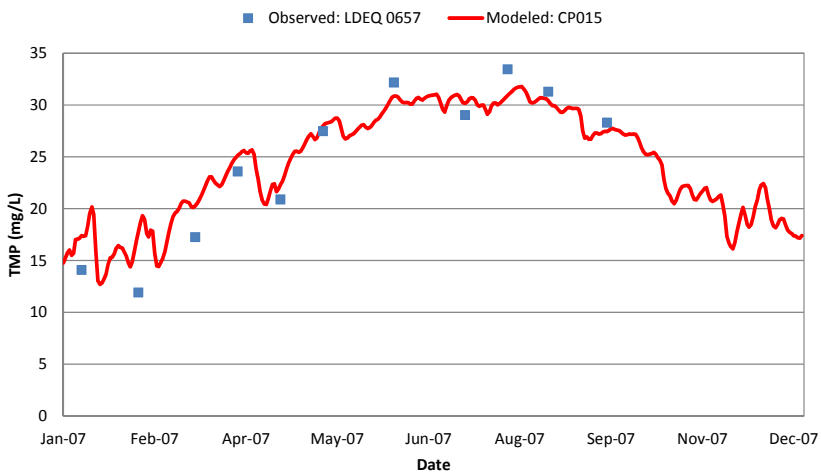

Figure 551 TMP Calibration Results for GIWW East of Calcasieu Lock and West of Grand Lake in the CP Model

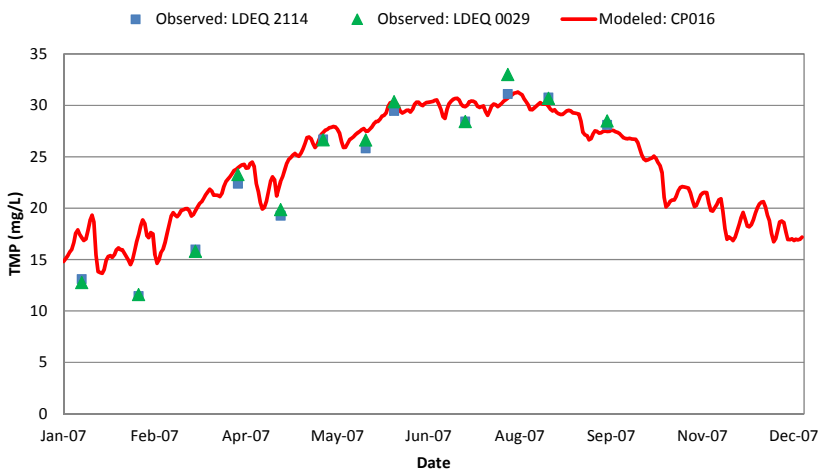

Figure 552 TMP Calibration Results for Mermentau River South of Grand Lake in the CP Model

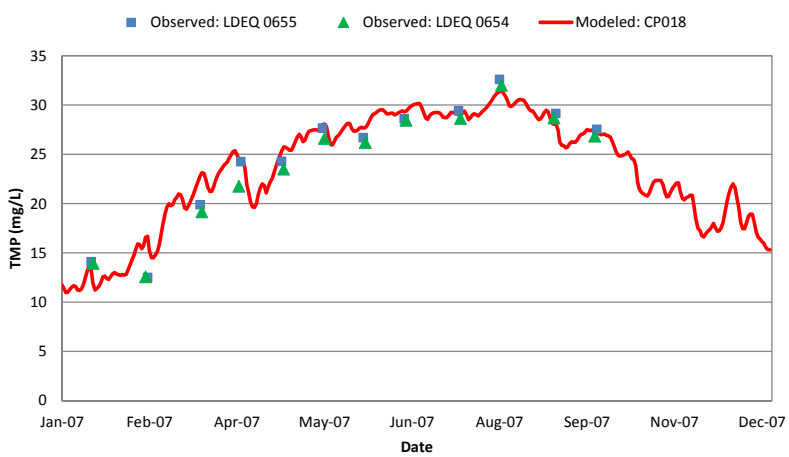

Figure 553 TMP Calibration Results for Mermentau River North of Grand Lake in the CP Model

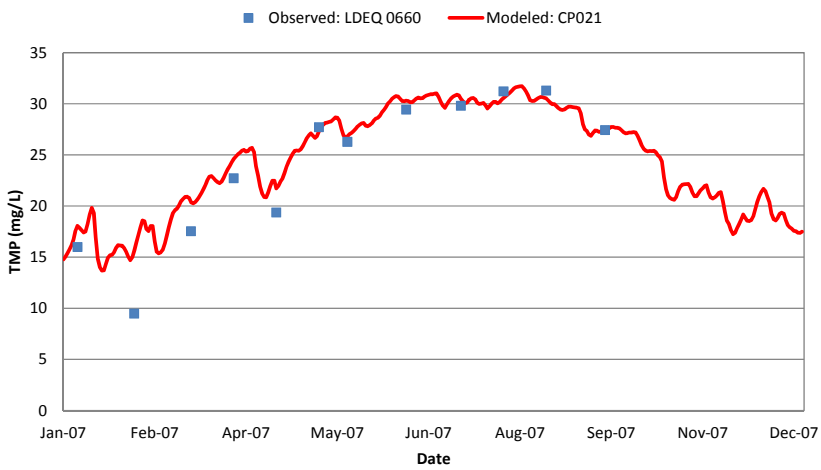

Figure 554 TMP Calibration Results for the GIWW East of Grand Lake and West of Leland Bowman Lock in the CP Model

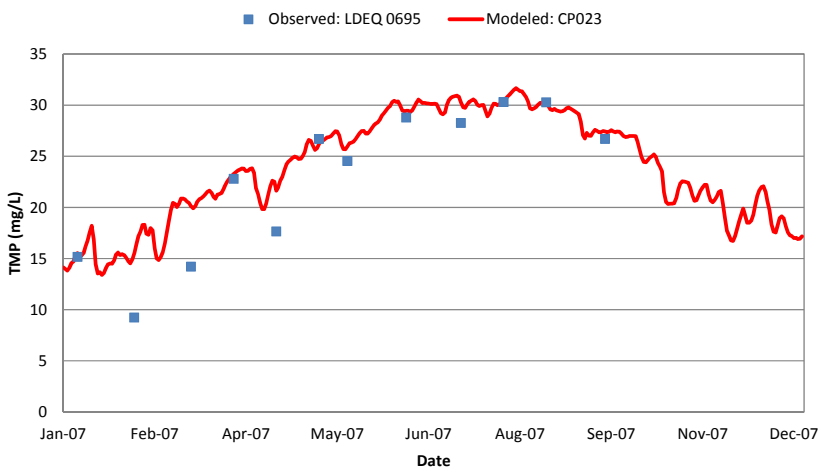

Figure 555 TMP Calibration Results for Freshwater Bayou in the CP Model

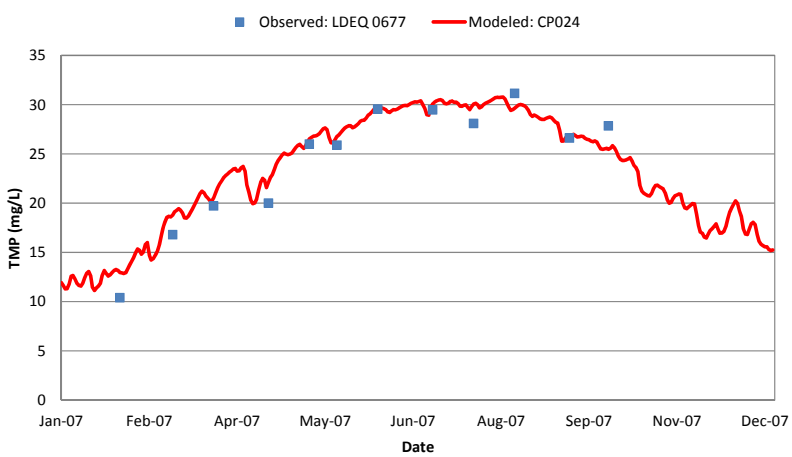

Figure 556 TMP Calibration Results for Vermilion River in the CP Model

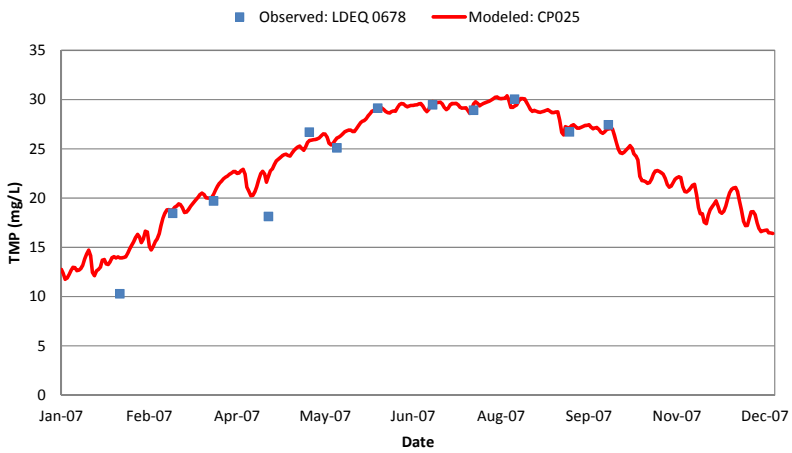

Figure 557 TMP Calibration Results for Vermilion River Channel South of the GIWW in the CP Model

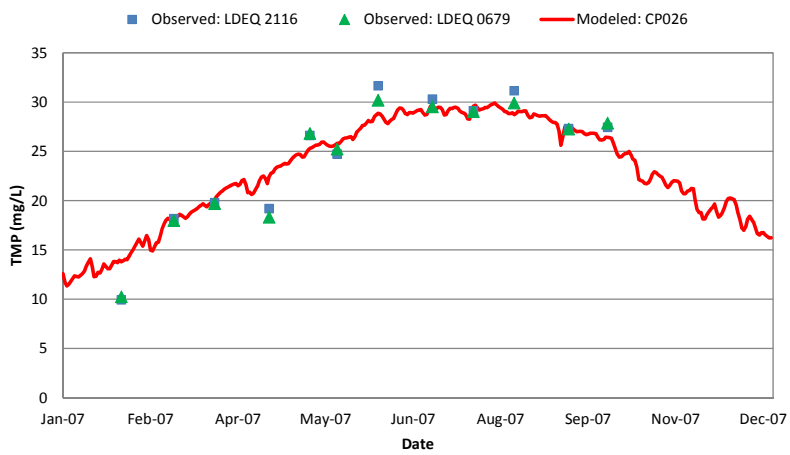

Figure 558 TMP Calibration Results for GIWW North of Vermilion Bay in the CP Model

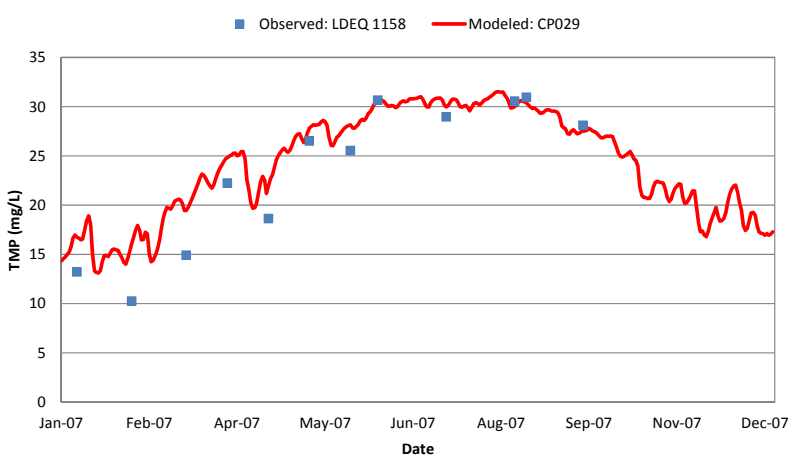

Figure 559 TMP Calibration Results for Sabine Lake in the CP Model

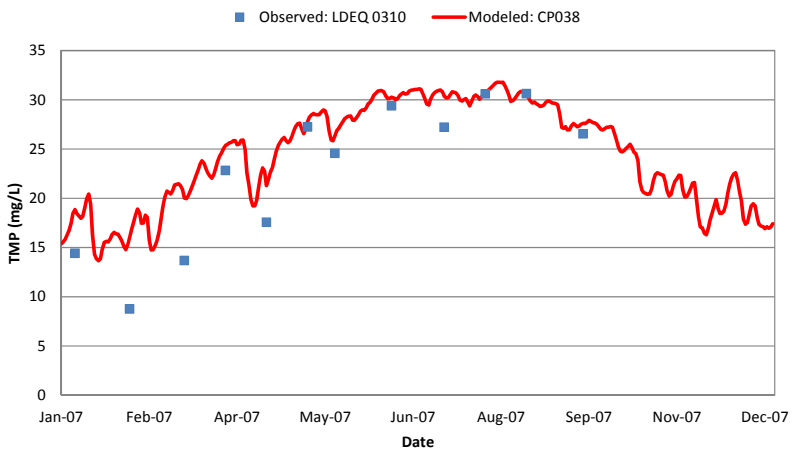

Figure 560 TMP Calibration Results for White Lake in the CP Model

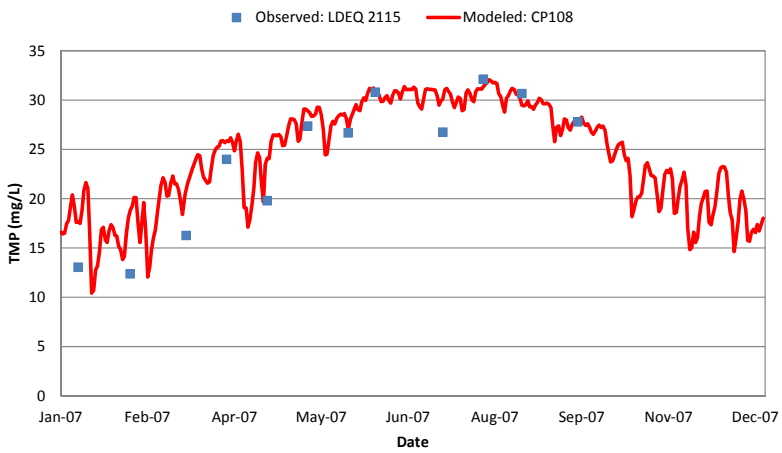

Figure 561 TMP Calibration Results for CP108 in the CP Model

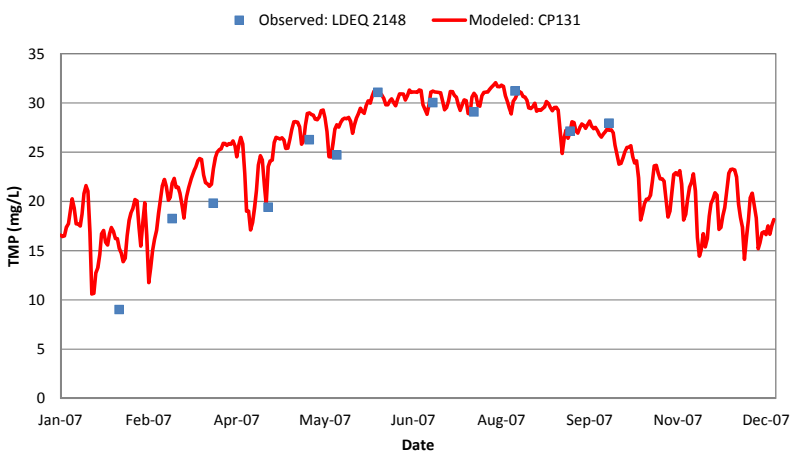

Figure 562 TMP Calibration Results for CP131 in the CP Model

Total Suspended Solids (TSS)

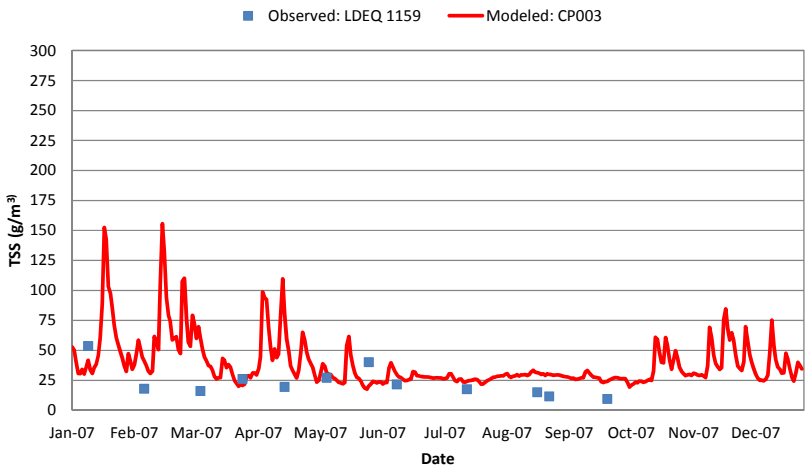

Figure 563 TSS Calibration Results for Sabine Pass in the CP Model

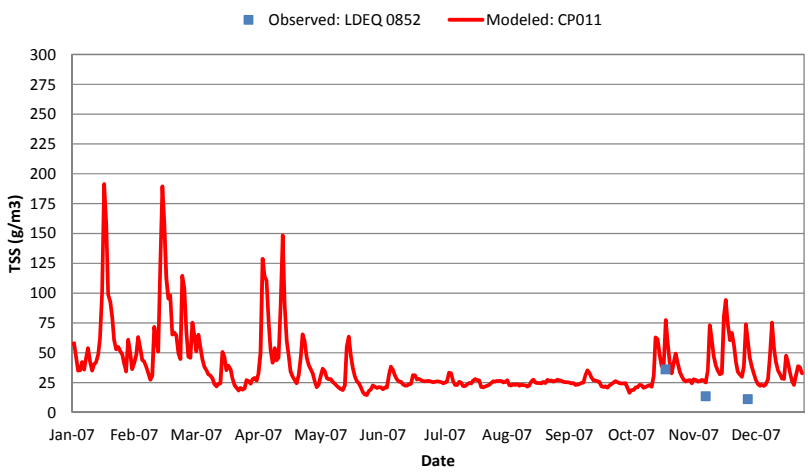

Figure 564 TSS Calibration Results for Calcasieu Pass in the CP Model

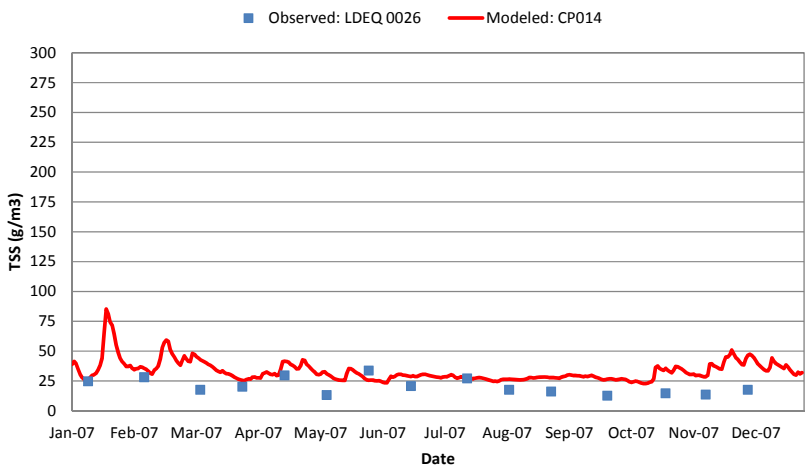

Figure 565 TSS Calibration Results for Calcasieu River North of the GIWW in the CP Model

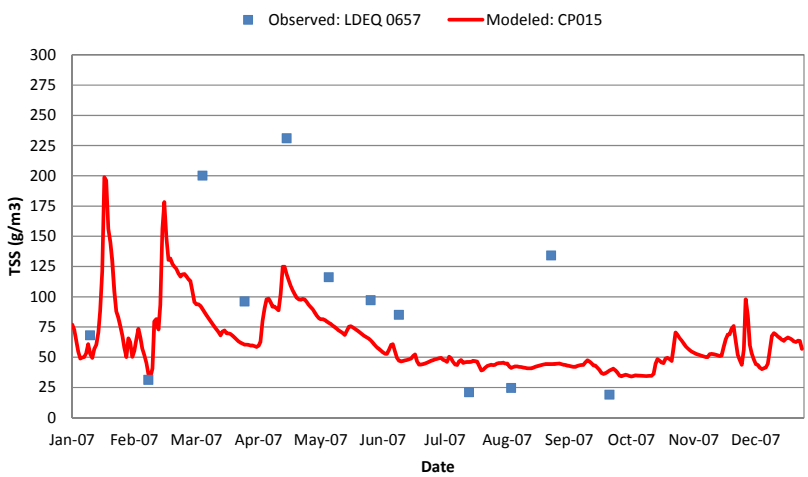

Figure 566 TSS Calibration Results for GIWW East of Calcasieu Lock and West of Grand Lake in the CP Model

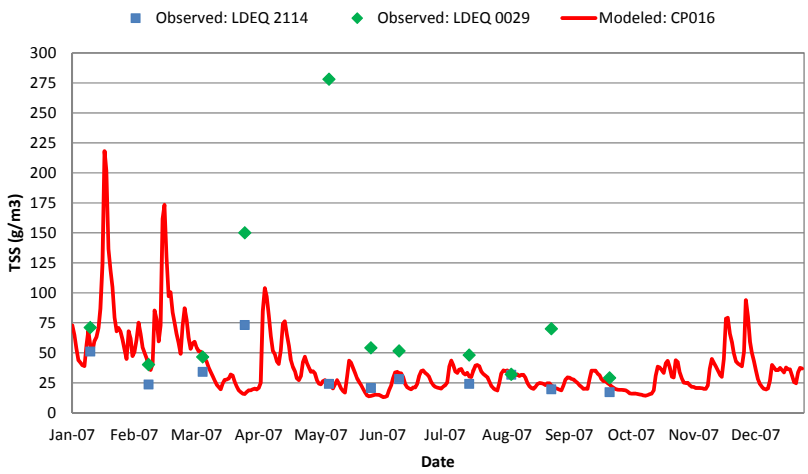

Figure 567 TSS Calibration Results for Mermentau River South of Grand Lake in the CP Model

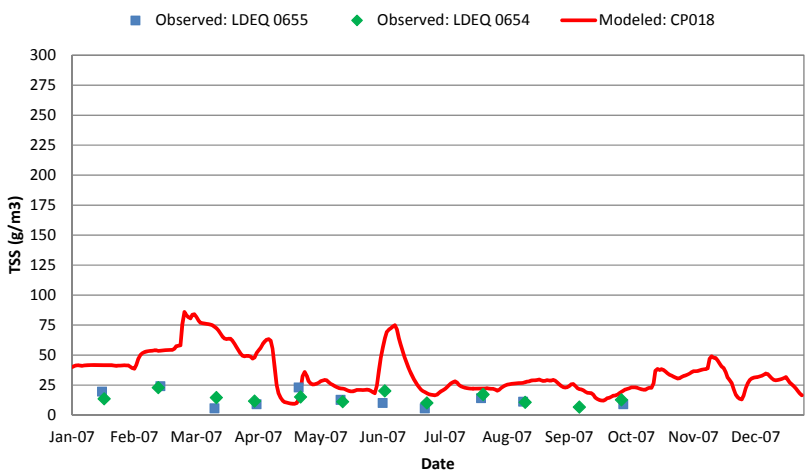

Figure 568 TSS Calibration Results for Mermentau River North of Grand Lake in the CP Model

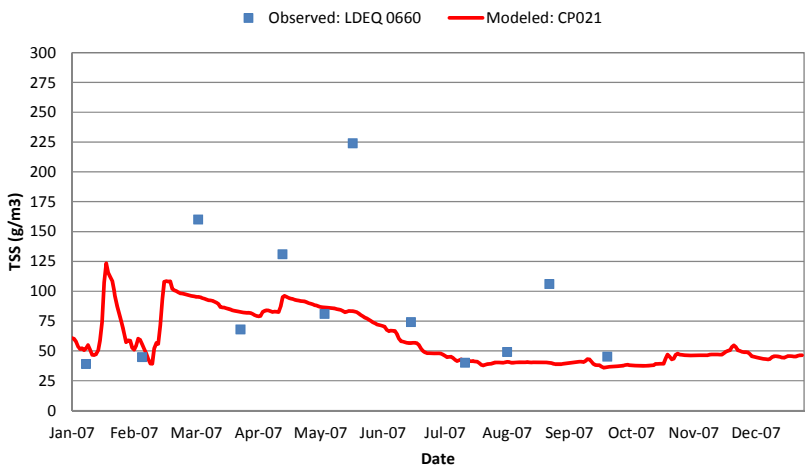

Figure 569 TSS Calibration Results for the GIWW East of Grand Lake and West of Leland Bowman Lock in the CP Model

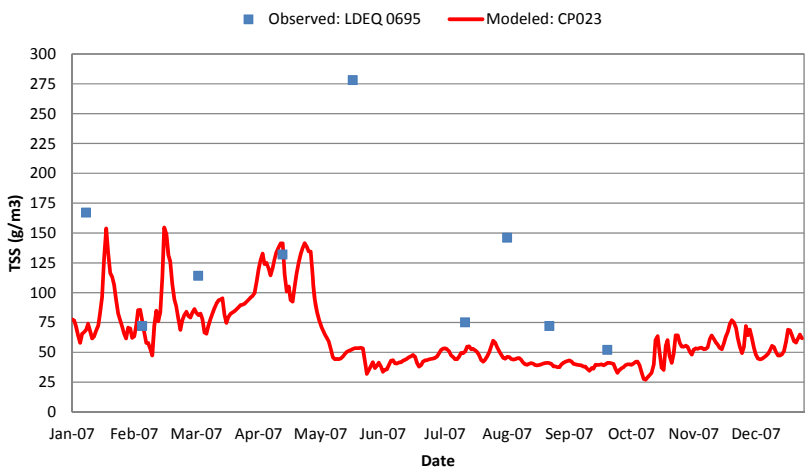

Figure 570 TSS Calibration Results for Freshwater Bayou in the CP Model

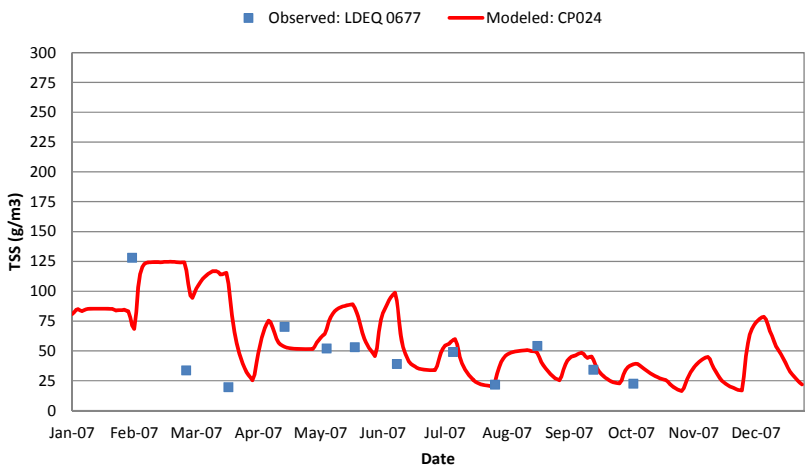

Figure 571 TSS Calibration Results for Vermilion River in the CP Model

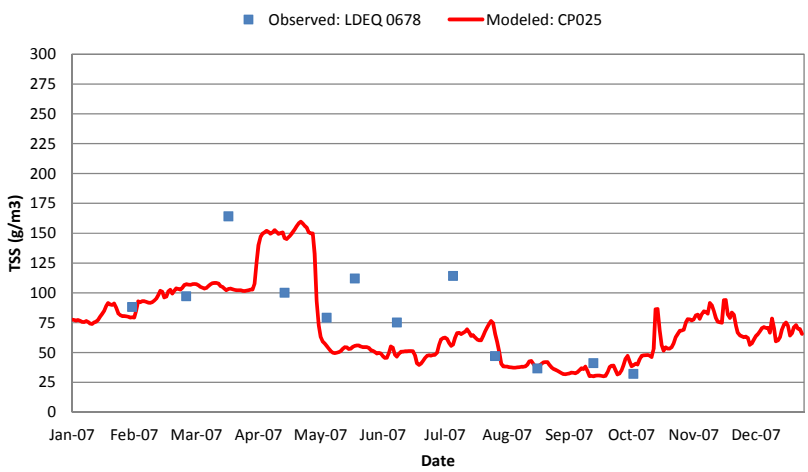

Figure 572 TSS Calibration Results for Vermilion River Channel South of the GIWW in the CP Model

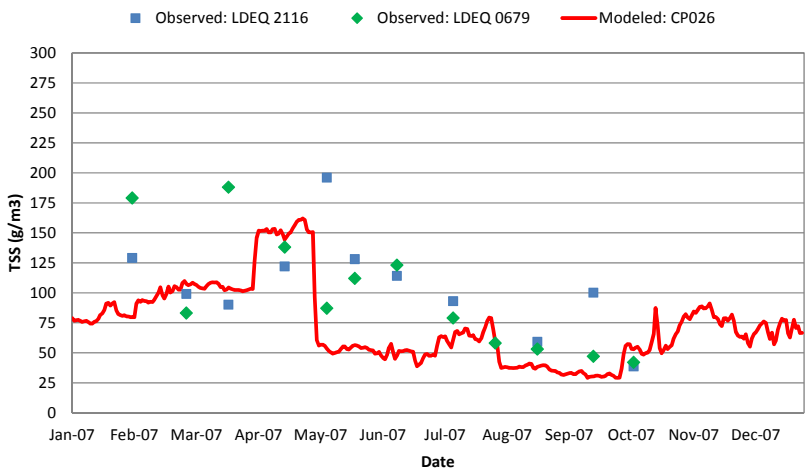

Figure 573 TSS Calibration Results for GIWW North of Vermilion Bay in the CP Model

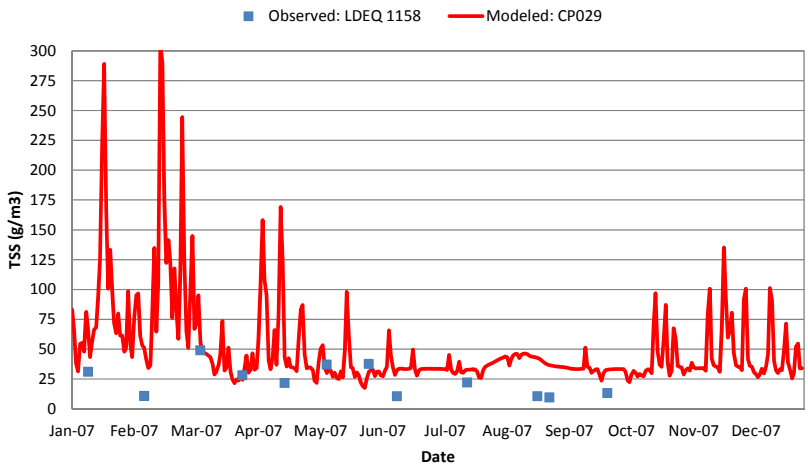

Figure 574 TSS Calibration Results for Sabine Lake in the CP Model

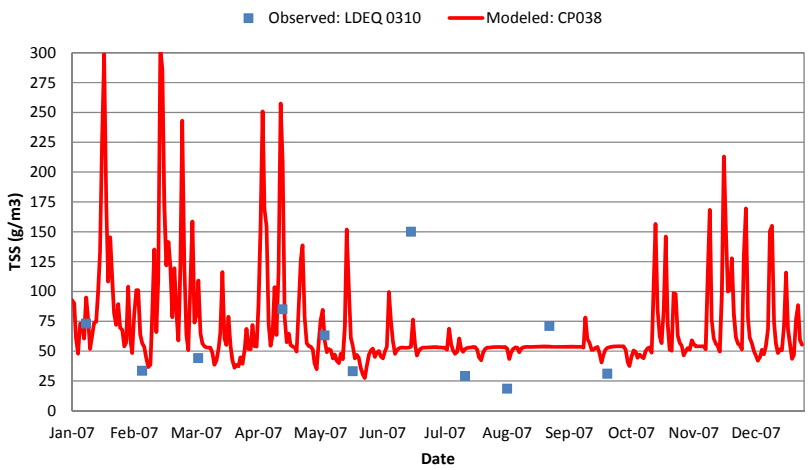

Figure 575 TSS Calibration Results for White Lake in the CP Model

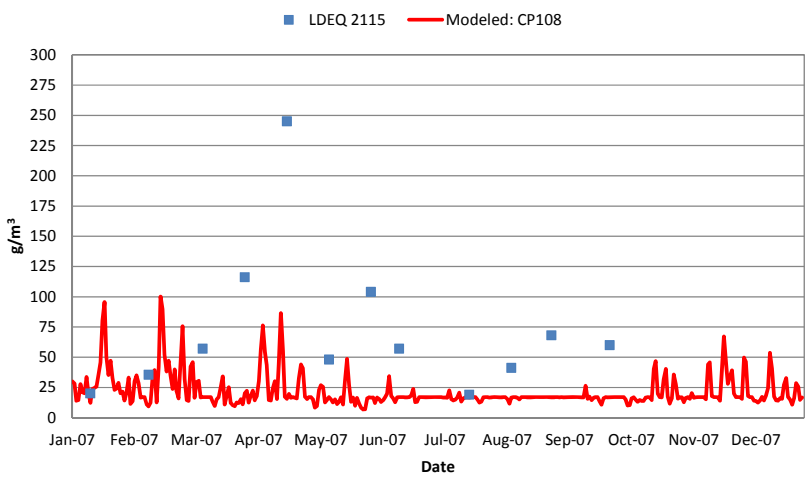

Figure 576 TSS Calibration Results for CP108 in the CP Model

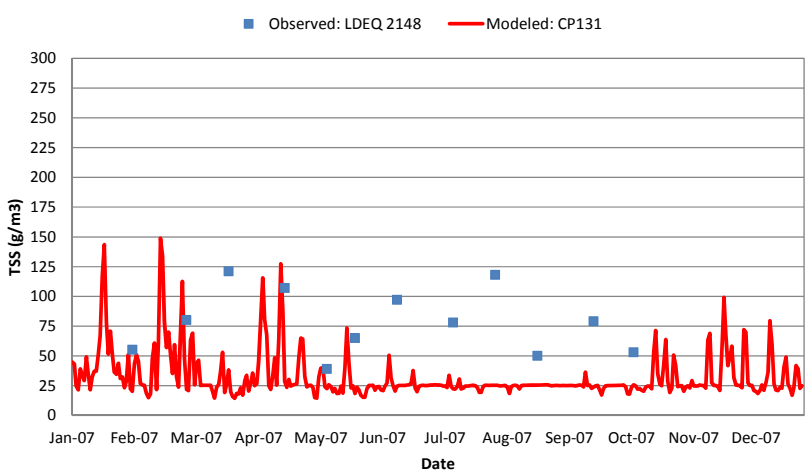

Figure 577 TSS Calibration Results for CP131 in the CP Model

Total Nitrogen (TN)

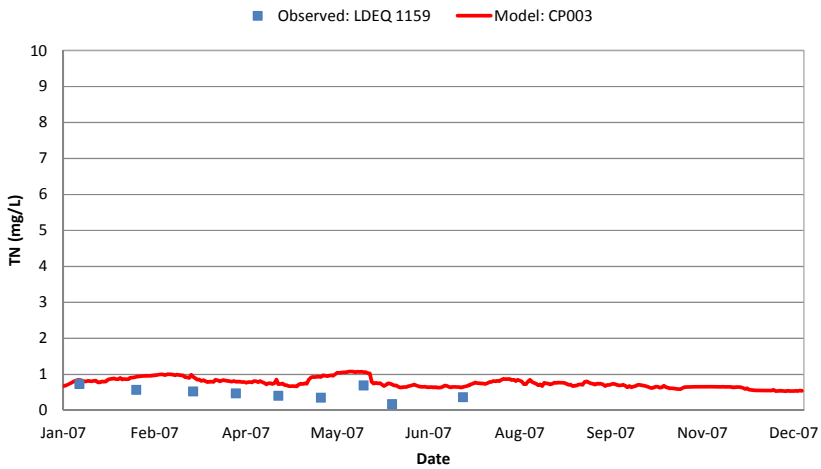

Figure 578 TN Calibration Results for Sabine Pass in the CP Model

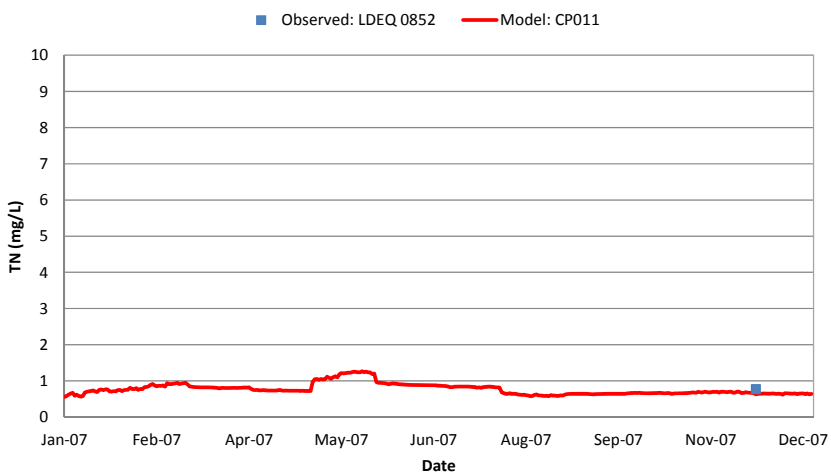

Figure 579 TN Calibration Results for Calcasieu Pass in the CP Model

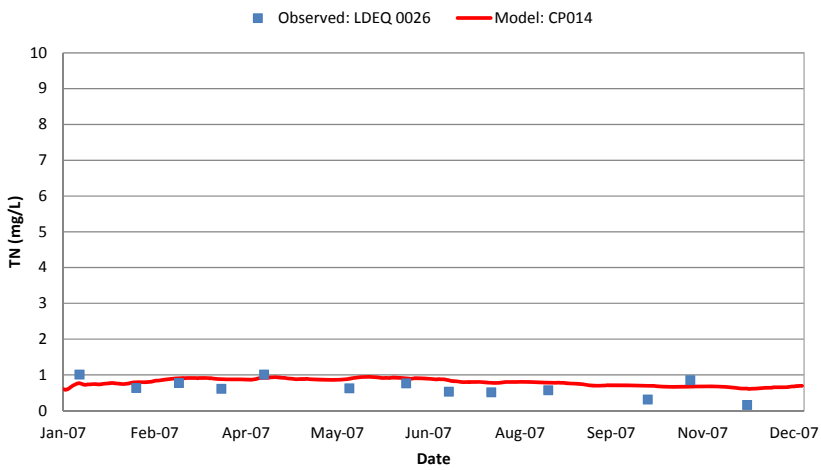

Figure 580 TN Calibration Results for Calcasieu River North of the GIWW in the CP Model

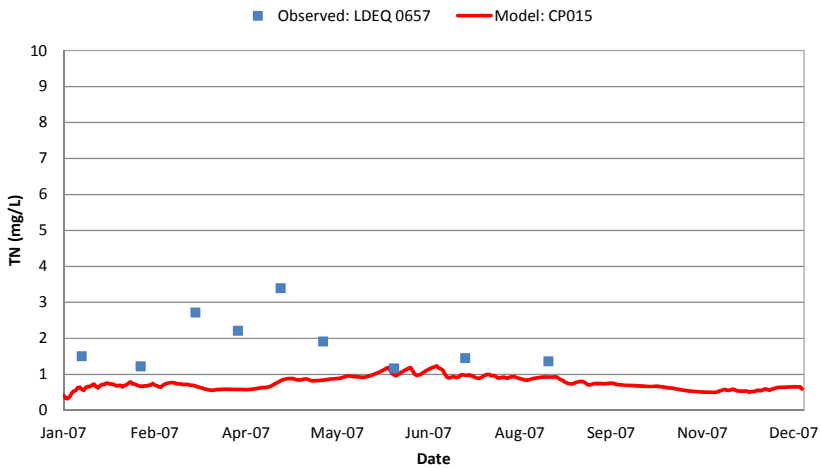

Figure 581 TN Calibration Results for GIWW East of Calcasieu Lock and West of Grand Lake in the CP Model

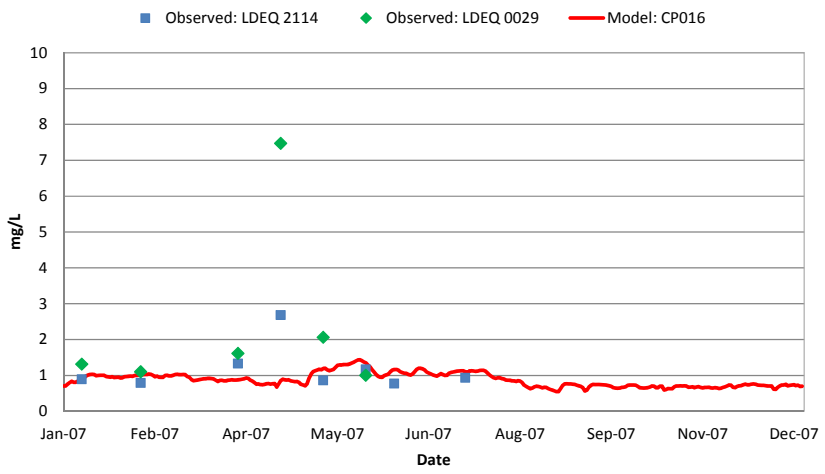

Figure 582 TN Calibration Results for Mermentau River South of Grand Lake in the CP Model

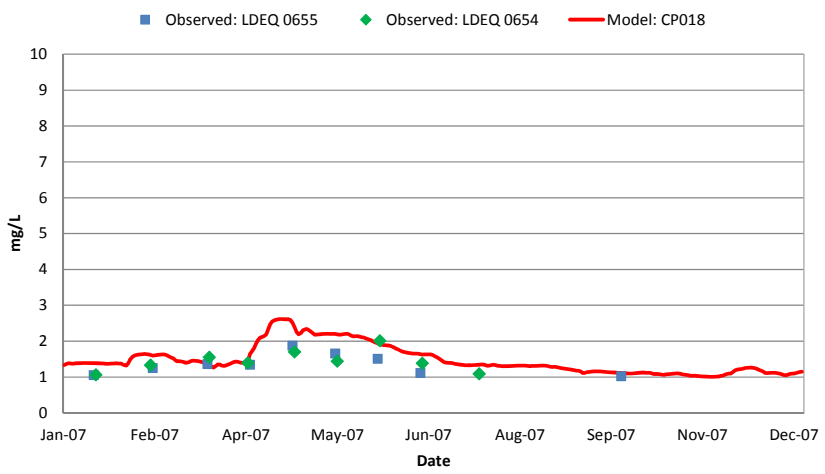

Figure 583 TN Calibration Results for Mermentau River North of Grand Lake in the CP Model

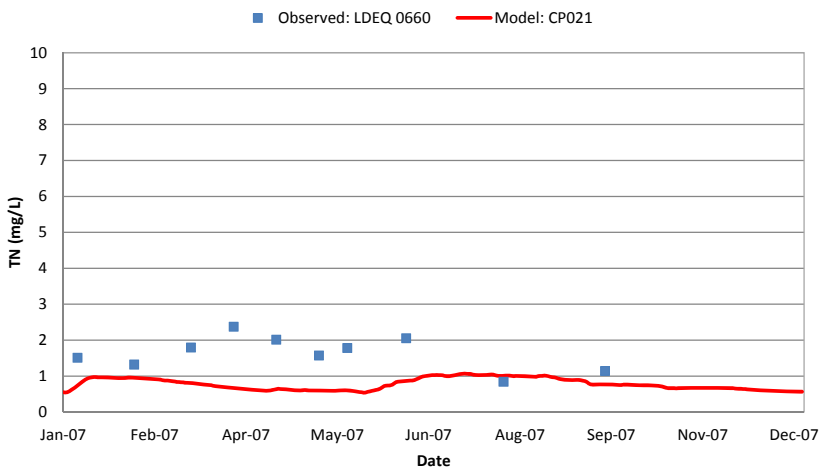

Figure 584 TN Calibration Results for the GIWW East of Grand Lake and West of Leland Bowman Lock in the CP Model

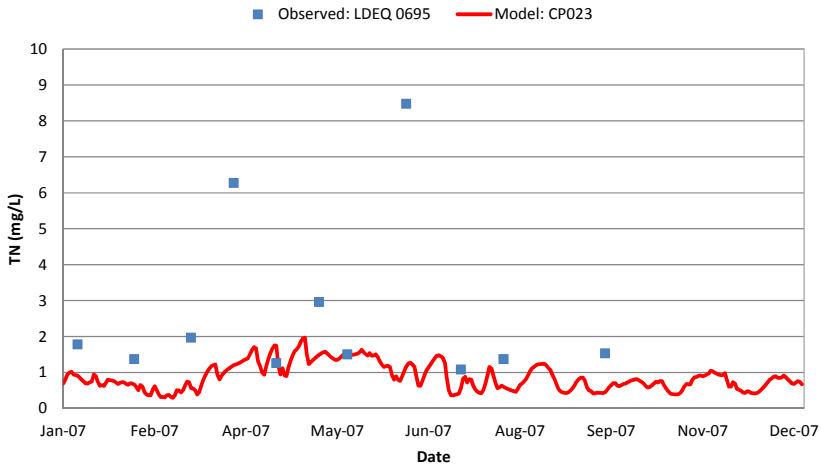

Figure 585 TN Calibration Results for Freshwater Bayou in the CP Model

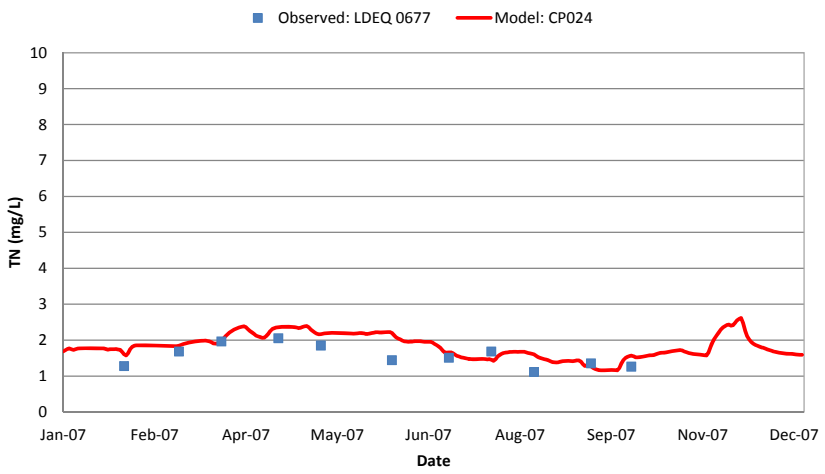

Figure 586 TN Calibration Results for Vermilion River in the CP Model

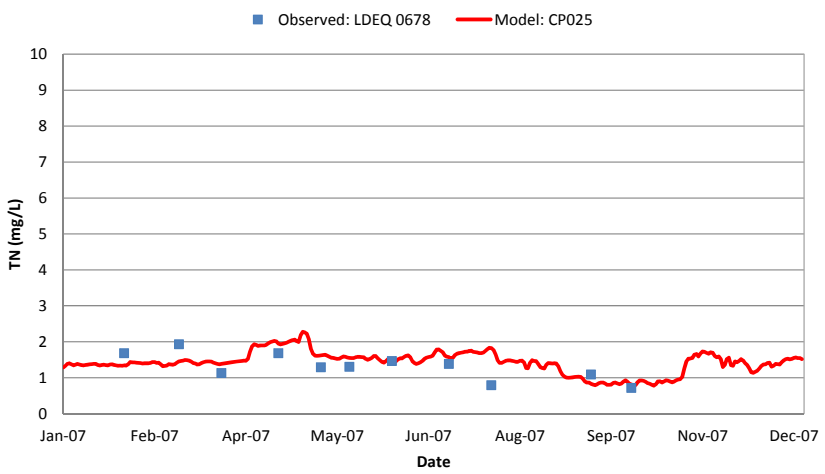

Figure 587 TN Calibration Results for Vermilion River Channel South of the GIWW in the CP Model

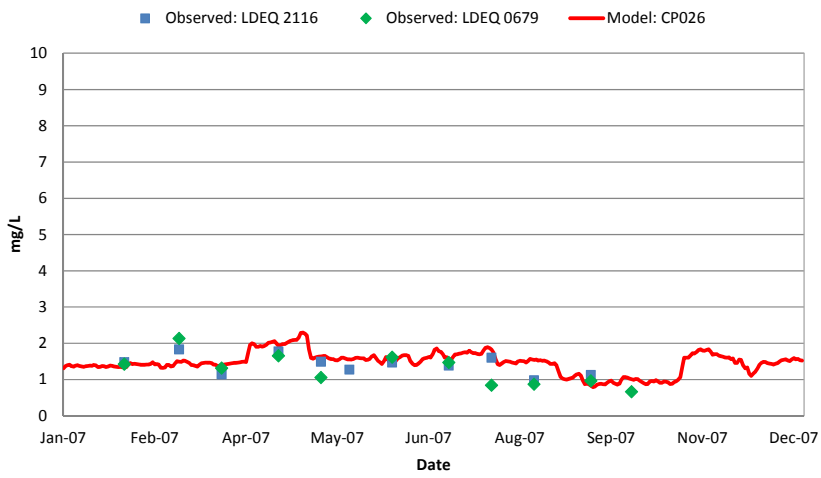

Figure 588 TN Calibration Results for GIWW North of Vermilion Bay in the CP Model

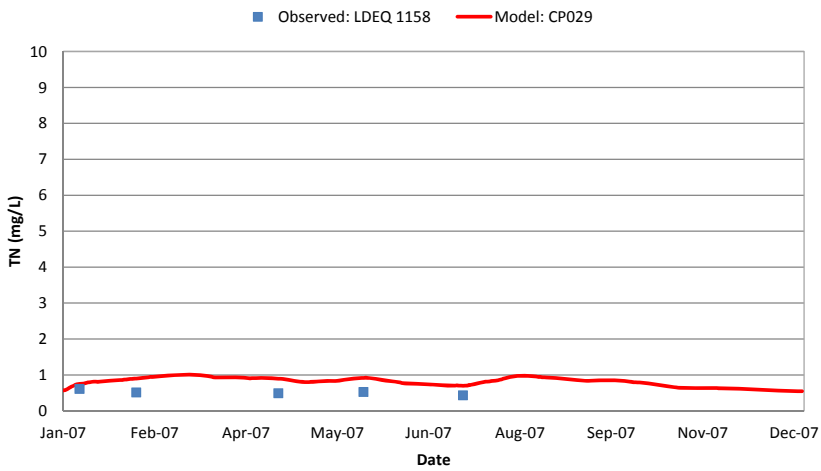

Figure 589 TN Calibration Results for Sabine Lake in the CP Model

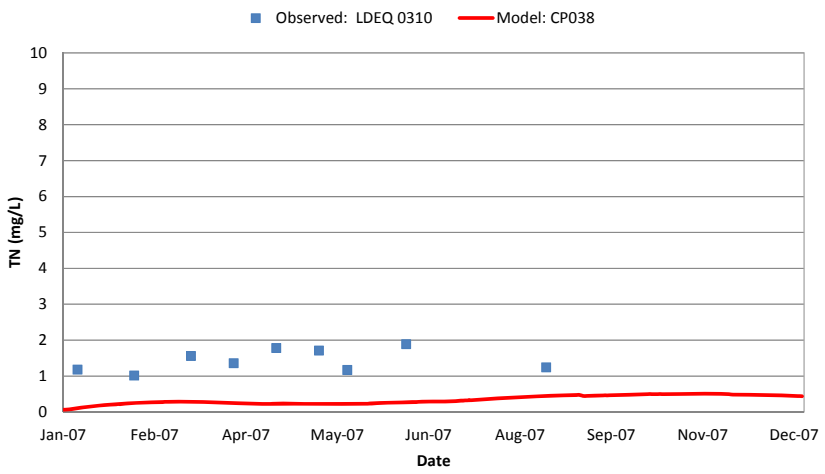

Figure 590 TN Calibration Results for White Lake in the CP Model

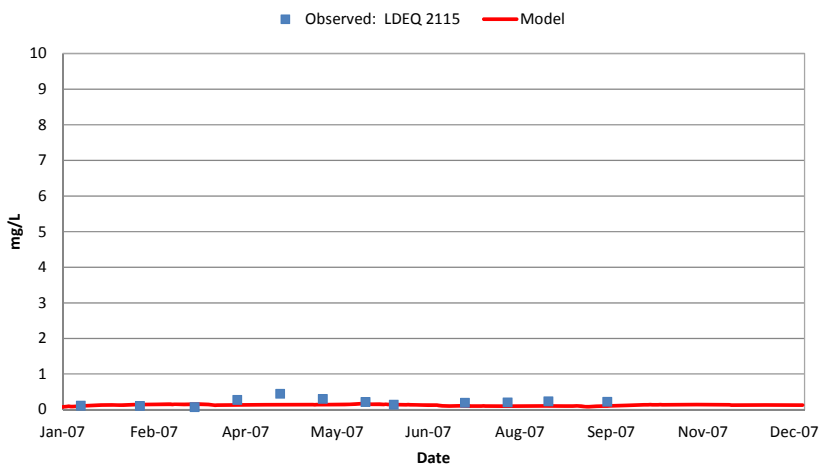

Figure 591 TN Calibration Results for CP108 in the CP Model

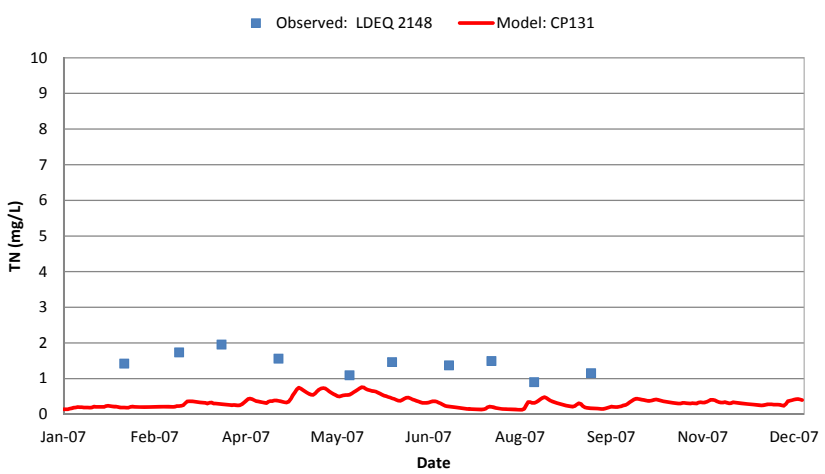

Figure 592 TN Calibration Results for CP131 in the CP Model

Total Phosphorus (TPH)

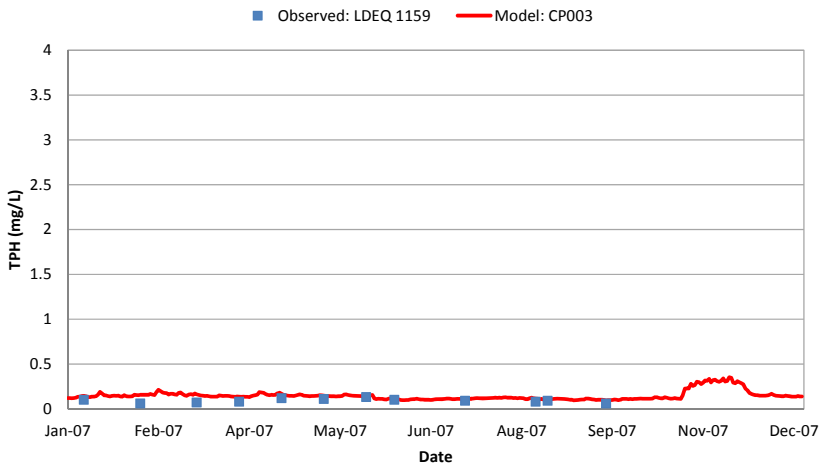

Figure 593 TPH Calibration Results for Sabine Pass in the CP Model

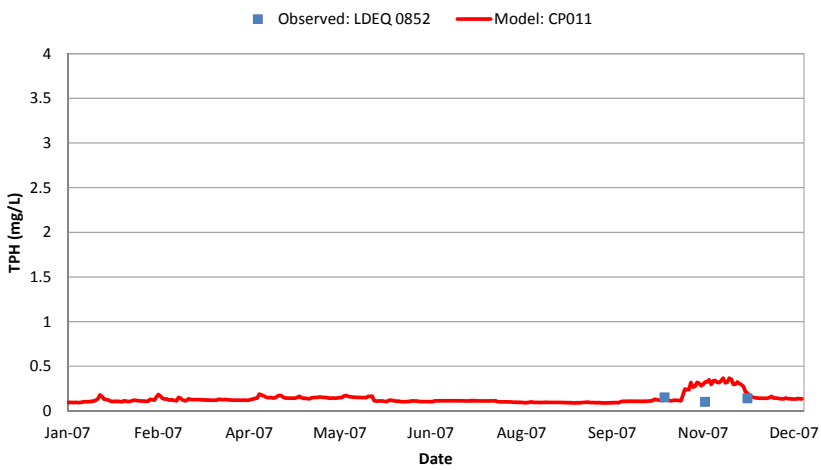

Figure 594 TPH Calibration Results for Calcasieu Pass in the CP Model

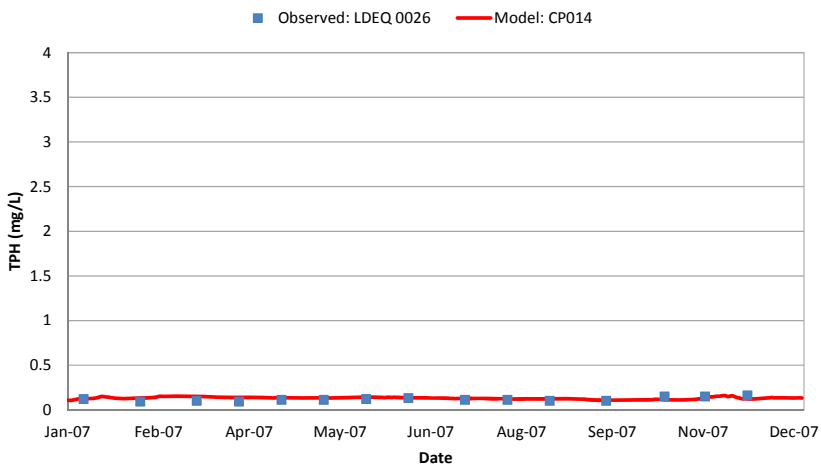

Figure 595 TPH Calibration Results for Calcasieu River North of the GIWW in the CP Model

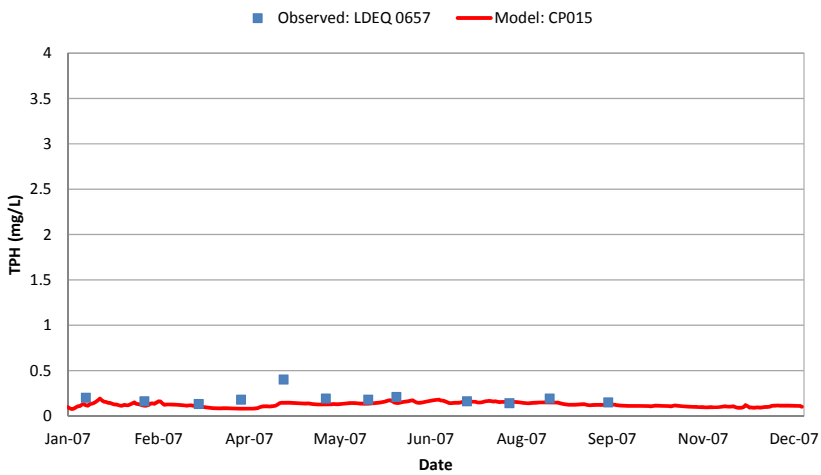

Figure 596 TPH Calibration Results for GIWW East of Calcasieu Lock and West of Grand Lake in the CP Model

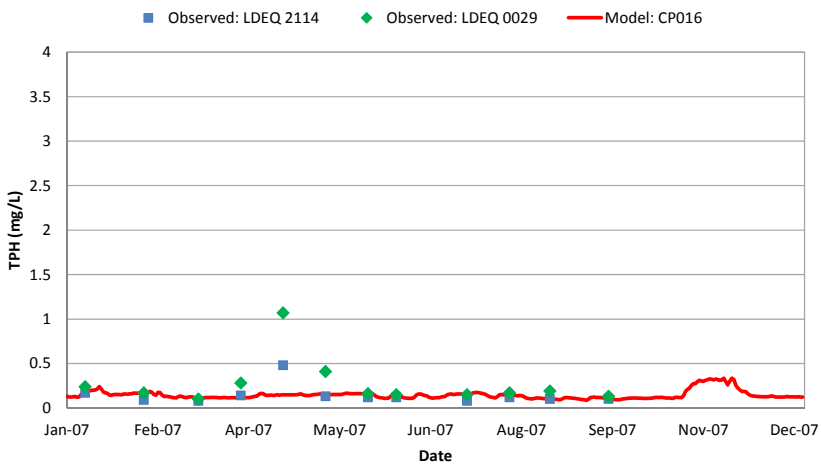

Figure 597 TPH Calibration Results for Mermentau River South of Grand Lake in the CP Model

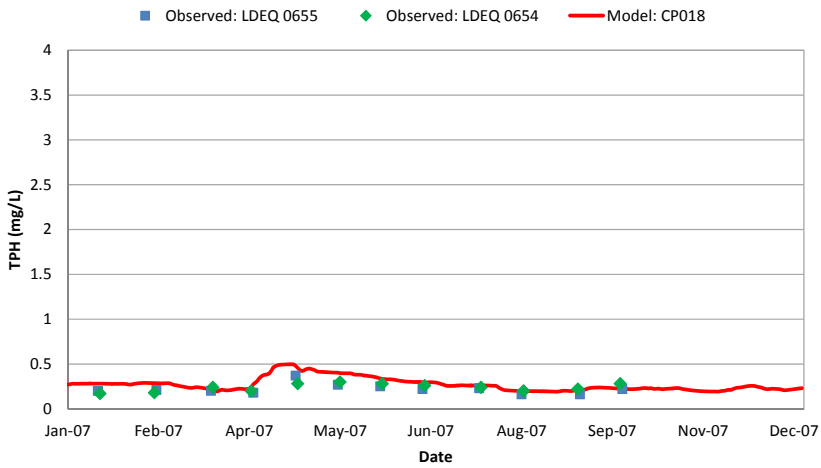

Figure 598 TPH Calibration Results for Mermentau River North of Grand Lake in the CP Model

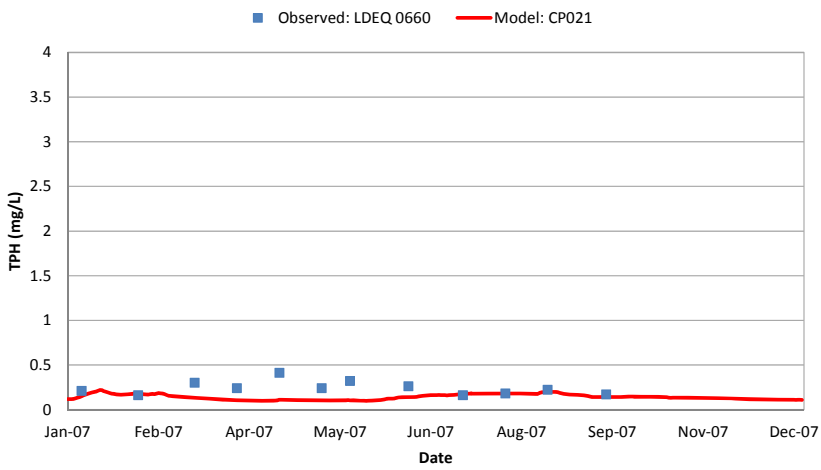

Figure 599 TPH Calibration Results for the GIWW East of Grand Lake and West of Leland Bowman Lock in the CP Model

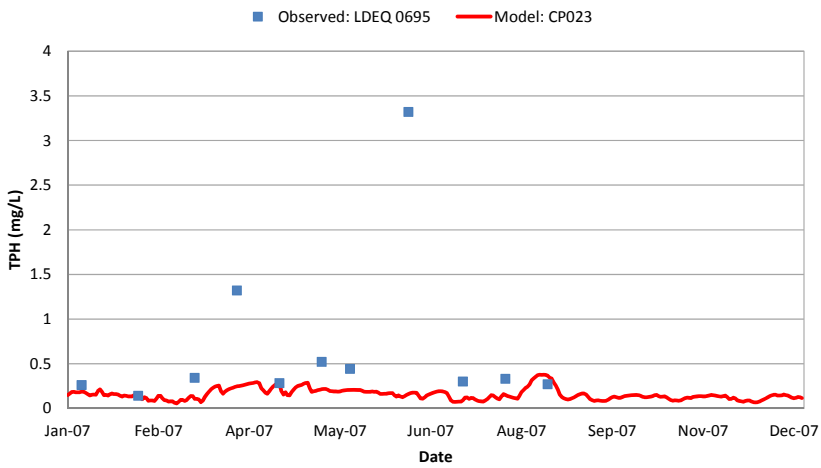

Figure 600 TPH Calibration Results for Freshwater Bayou in the CP Model

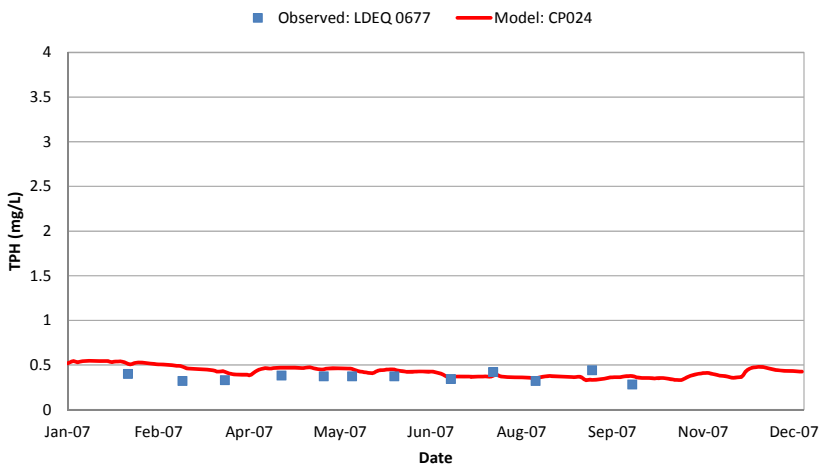

Figure 601 TPH Calibration Results for Vermilion River in the CP Model

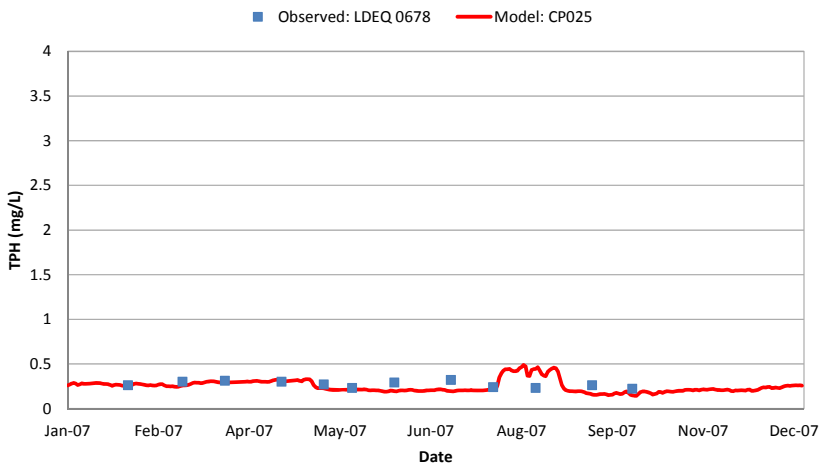

Figure 602 TPH Calibration Results for Vermilion River Channel South of the GIWW in the CP Model

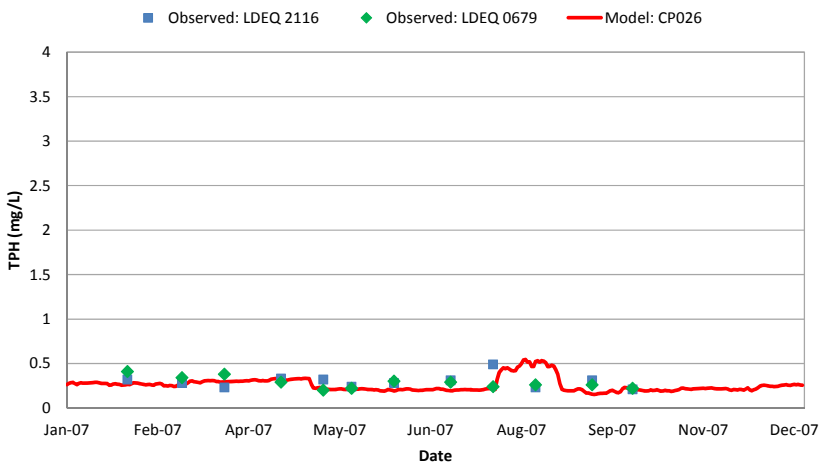

Figure 603 TPH Calibration Results for the GIWW North of Vermilion Bay in the CP Model

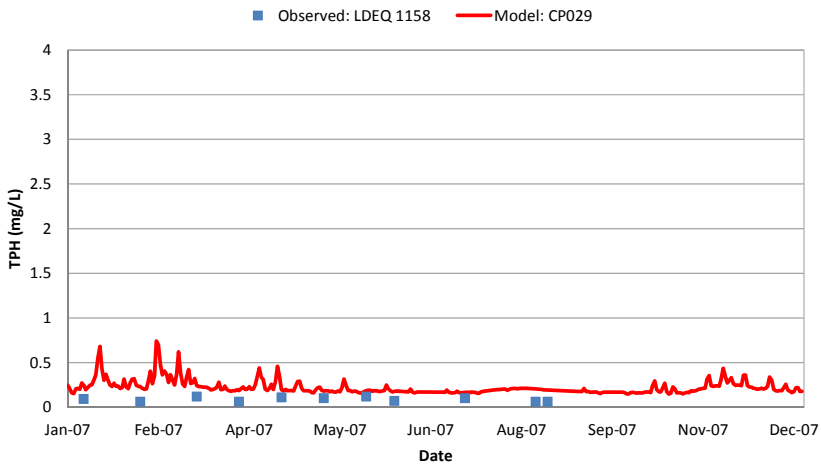

Figure 604 TPH Calibration Results for Sabine Lake in the CP Model

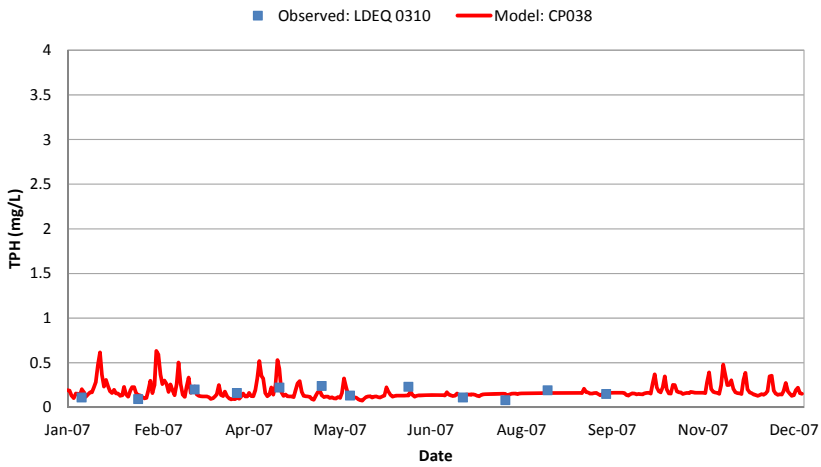

Figure 605 TPH Calibration Results for White Lake in the CP Model

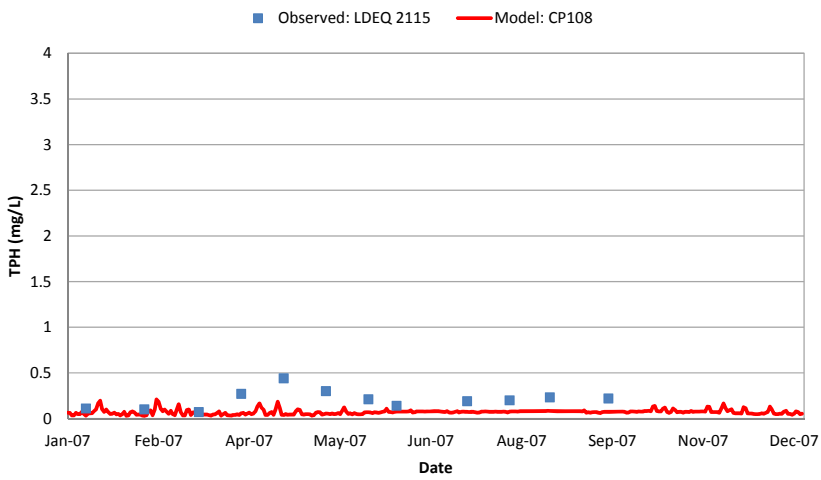

Figure 606 TPH Calibration Results for CP108 in the CP Model

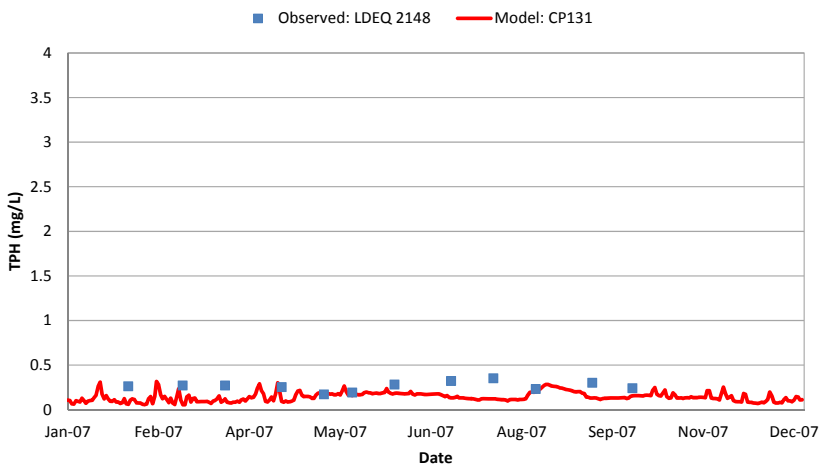

Figure 607 TPH Calibration Results for CP131 in the CP Model

Chenier Plain Model Validation Plots

Stage (STG)

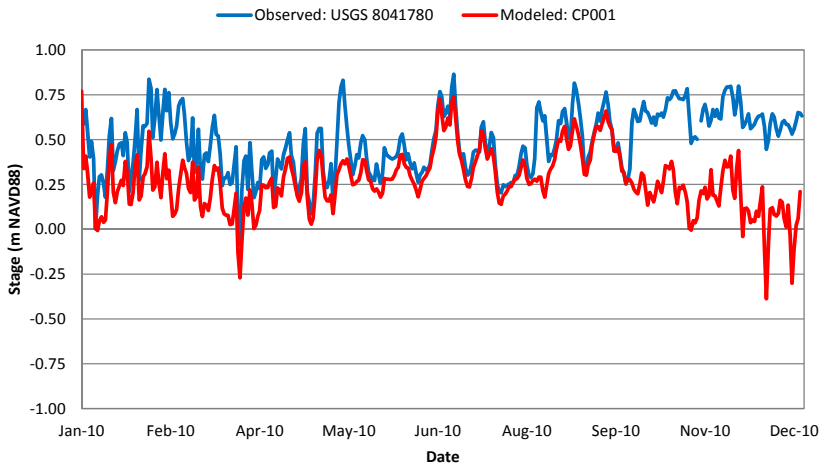

Figure 608 STG Validation Results for Neches River in the CP Model

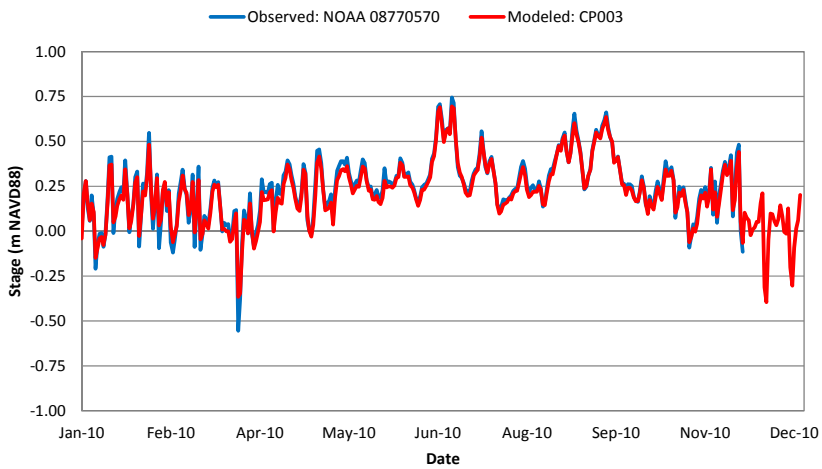

Figure 609 STG Validation Results for Sabine Pass in the CP Model

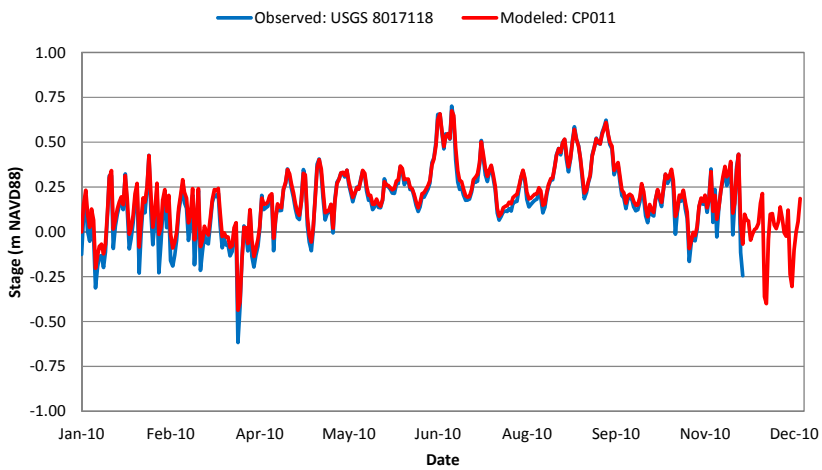

Figure 610 STG Validation Results for Calcasieu Pass in the CP Model

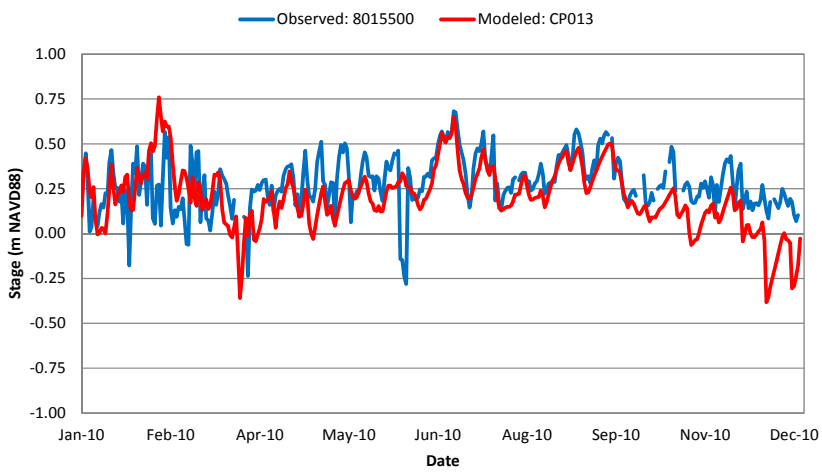

Figure 611 STG Validation Results for Upper Calcasieu River in the CP Model

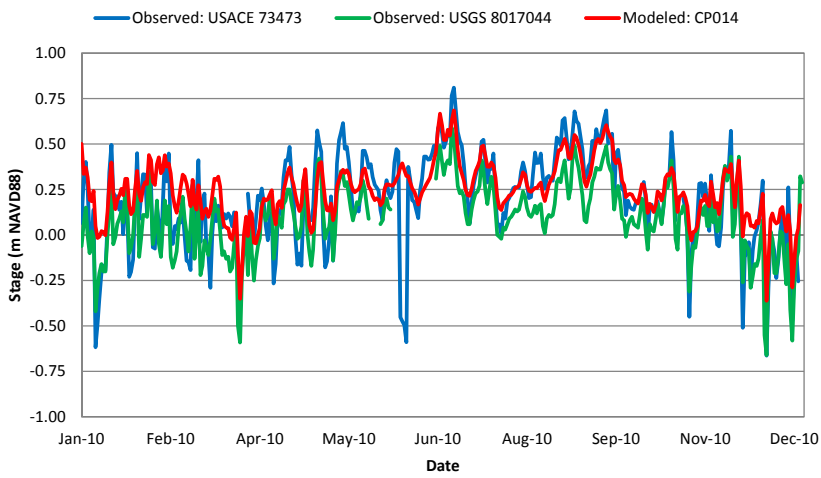

Figure 612 STG Validation Results for Lower Calcasieu River in the CP Model

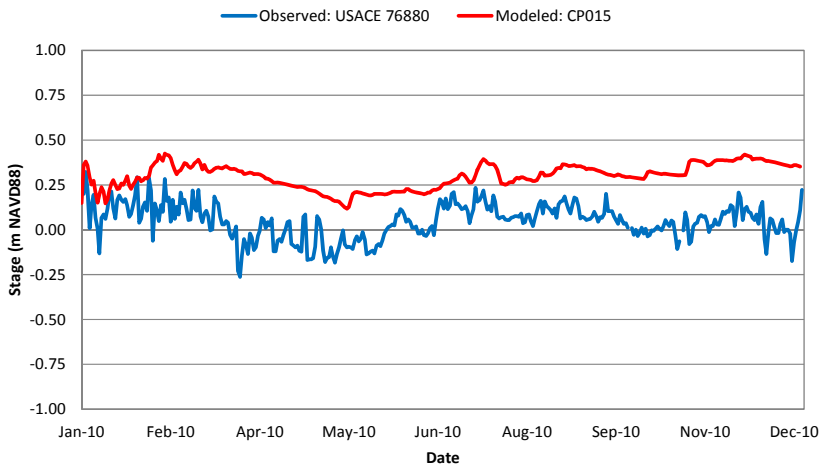

Figure 613 STG Validation Results for GIWW between Calcasieu River and Bayou Lacassine in the CP Model

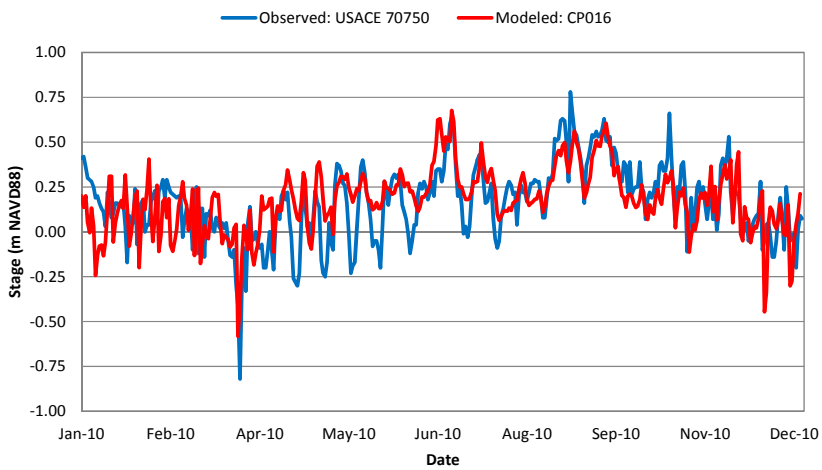

Figure 614 STG Validation Results for Lower Mermentau River in the CP Model

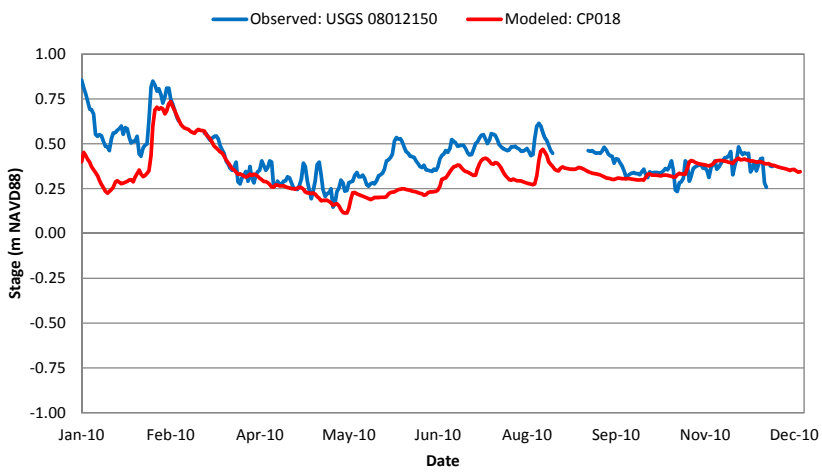

Figure 615 STG Validation Results for Mermentau River north of Grand Lake in the CP Model

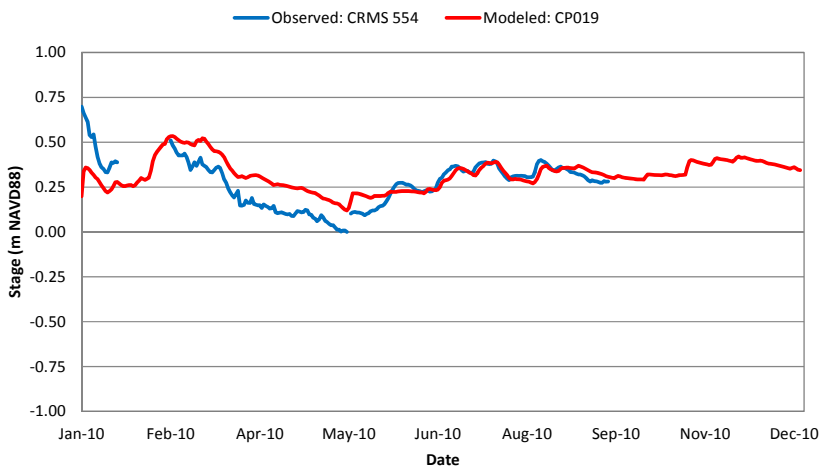

Figure 616 STG Validation Results for the Channel Connecting Grand Lake and White Lake in the CP Model

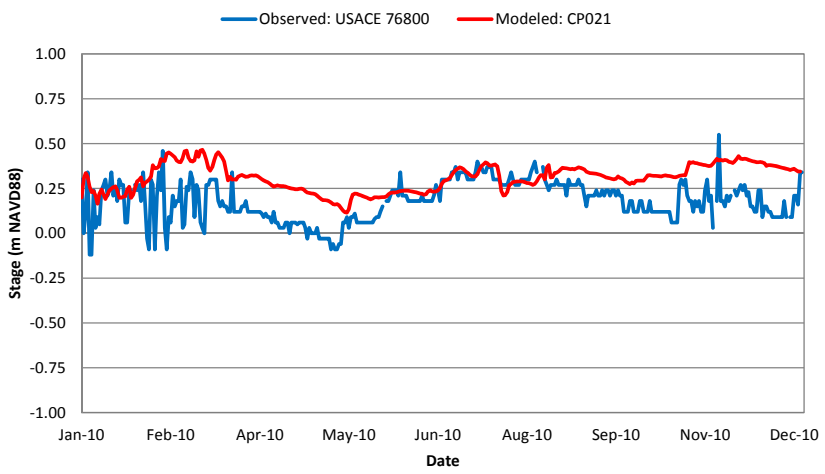

Figure 617 STG Validation Results for GIWW between Mermentau River and Vermilion River in the CP Model

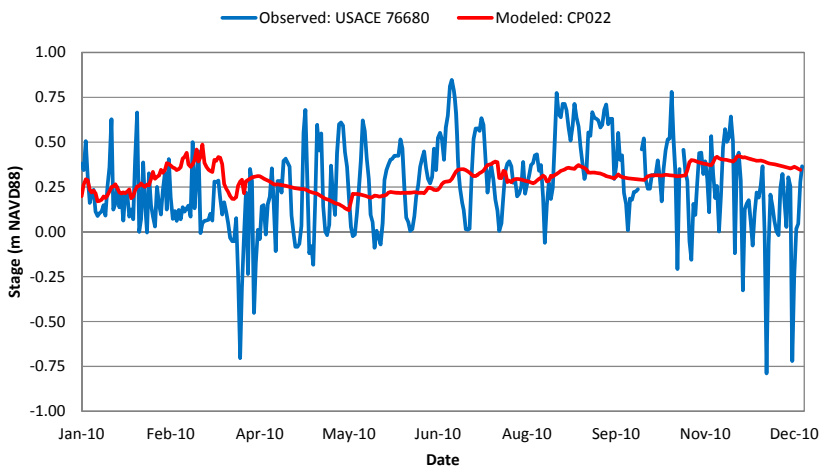

Figure 618 STG Validation Results for Schooner Bayou in the CP Model

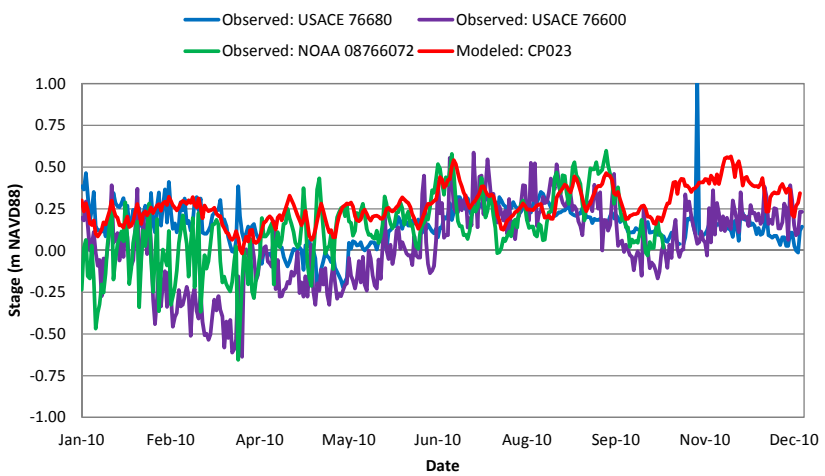

Figure 619 STG Validation Results for Freshwater Bayou in the CP Model

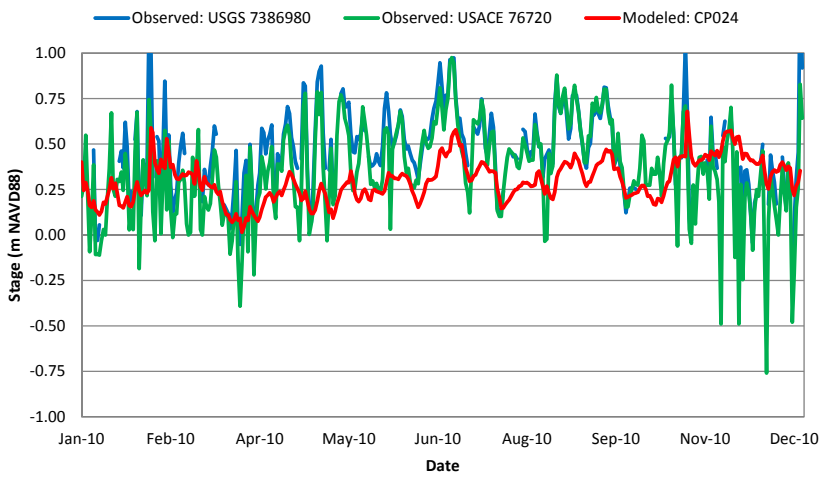

Figure 620 STG Validation Results for Vermilion River in the CP Model

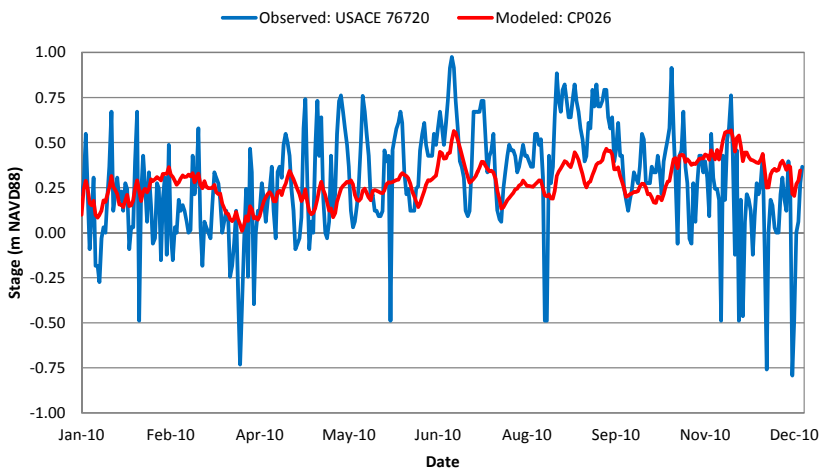

Figure 621 STG Validation Results for GIWW W of Vermilion River in the CP Model

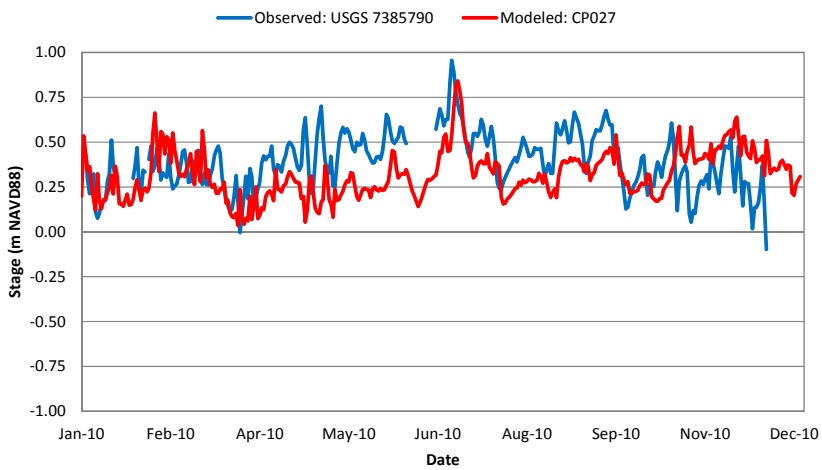

Figure 622 STG Validation Results for Charenton Drainage Canal in the CP Model

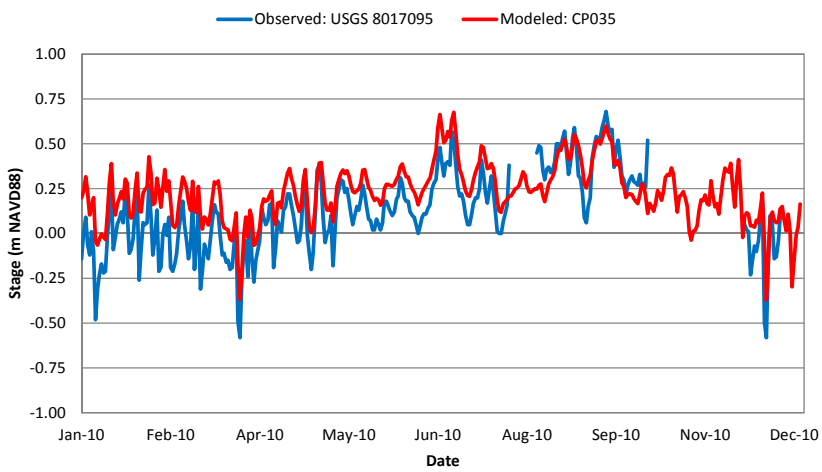

Figure 623 STG Validation Results for Calcasieu Lake in the CP Model

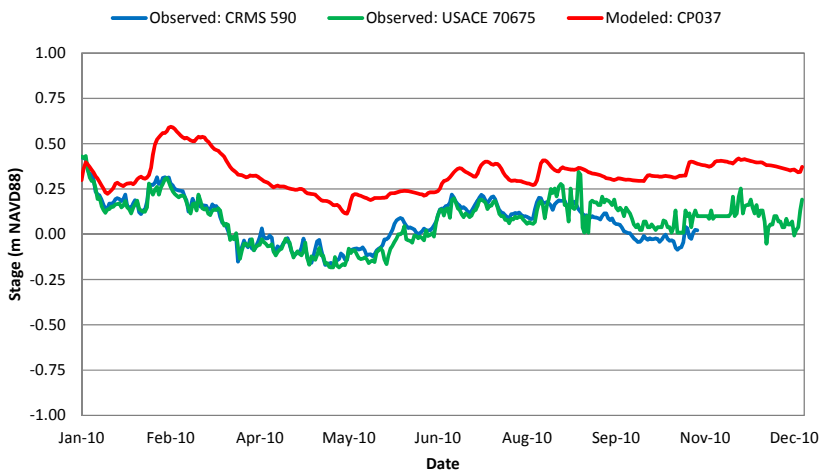

Figure 624 STG Validation Results for Grand Lake in the CP Model

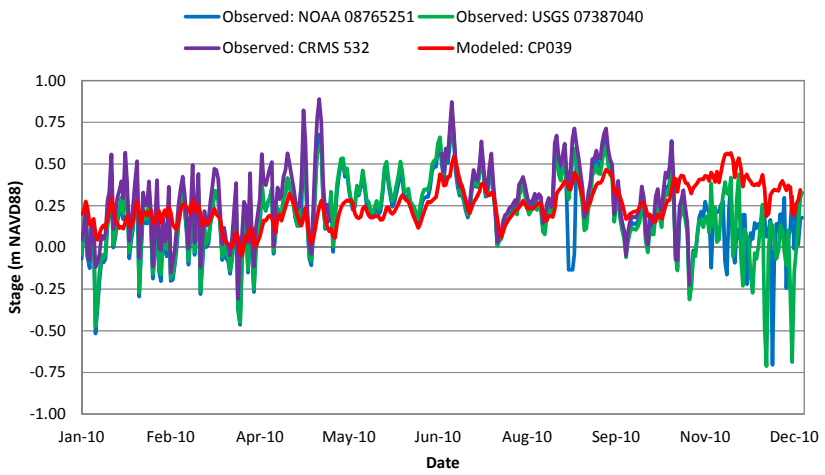

Figure 625 STG Validation Results for Vermilion Bay in the CP Model

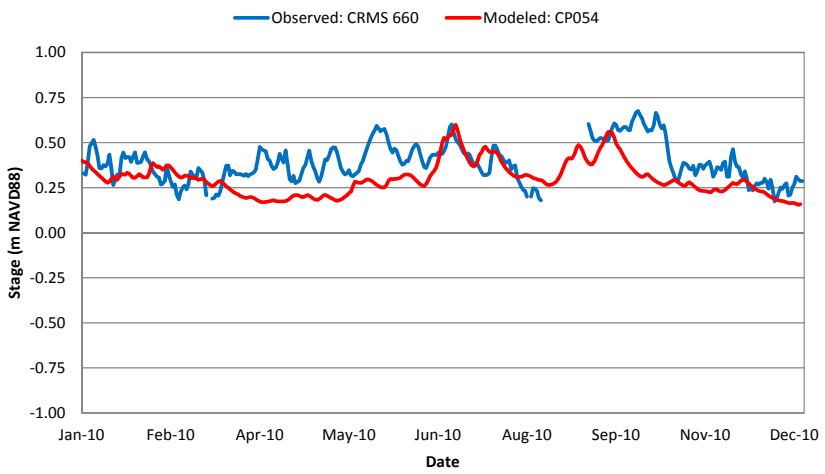

Figure 626 STG Validation Results for Greens Lake and Surrounding Marshes in the CP Model

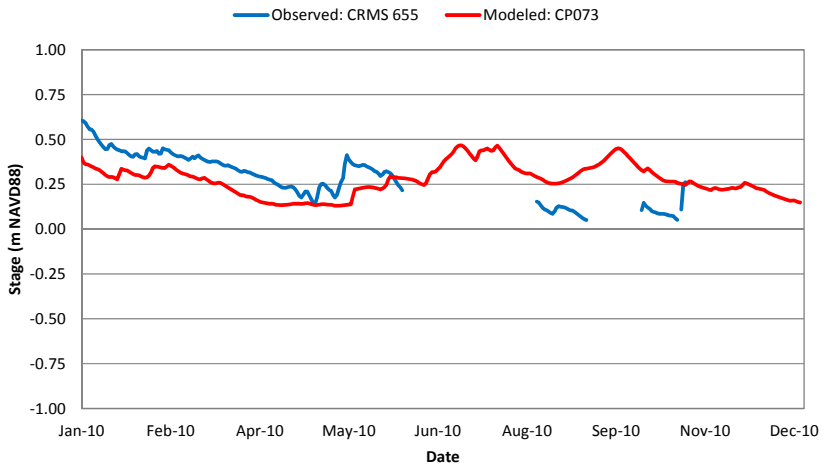

Figure 627 STG Validation Results for CP073 in the CP Model

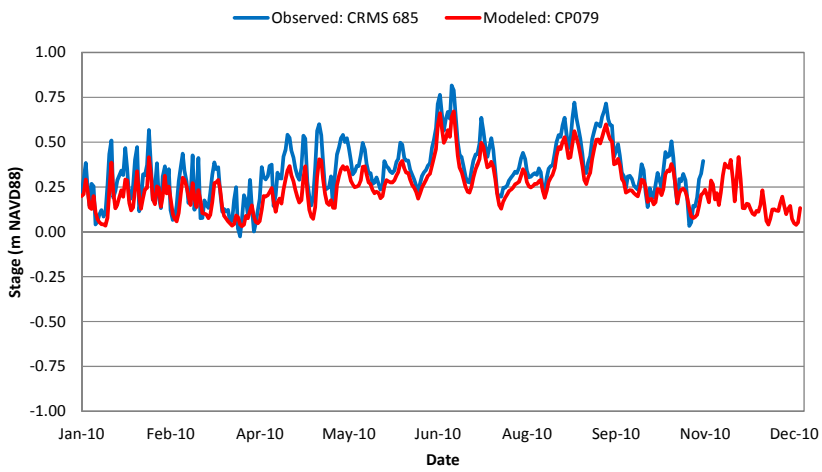

Figure 628 STG Validation Results for CP079 in the CP Model

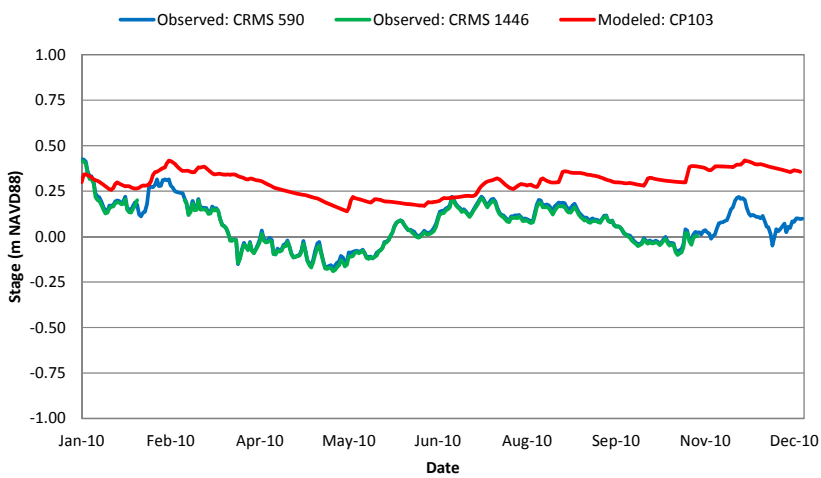

Figure 629 STG Validation Results for CP103 in the CP Model

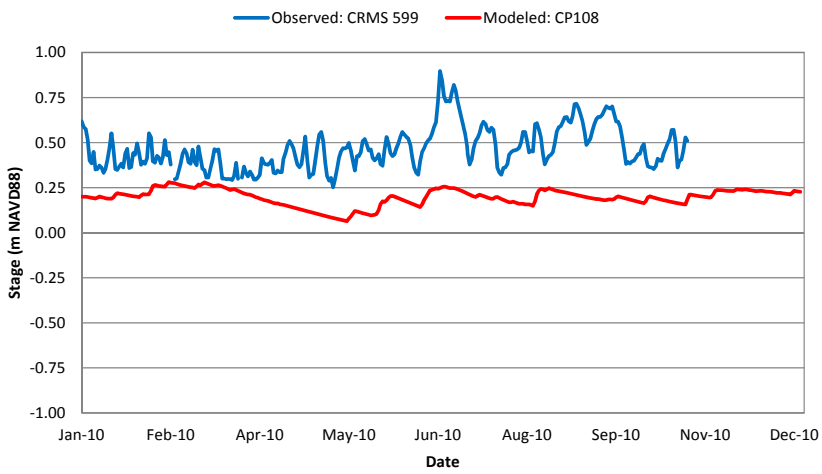

Figure 630 STG Validation Results for CP108 in the CP Model

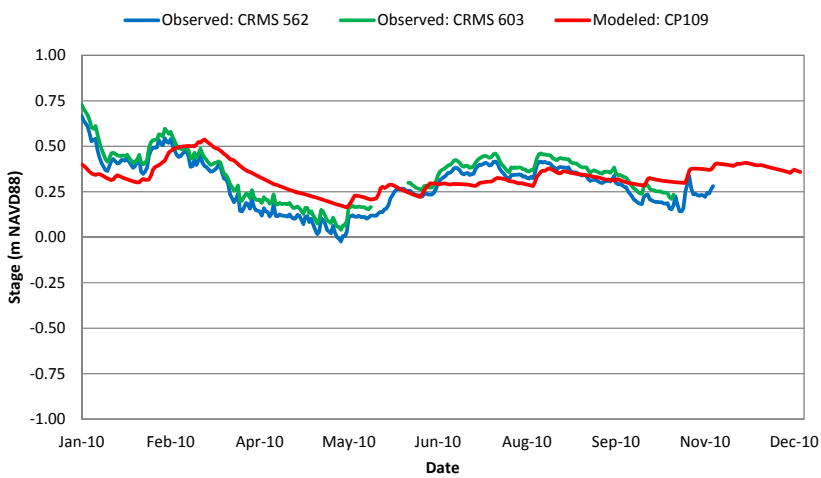

Figure 631 STG Validation Results for CP109 in the CP Model

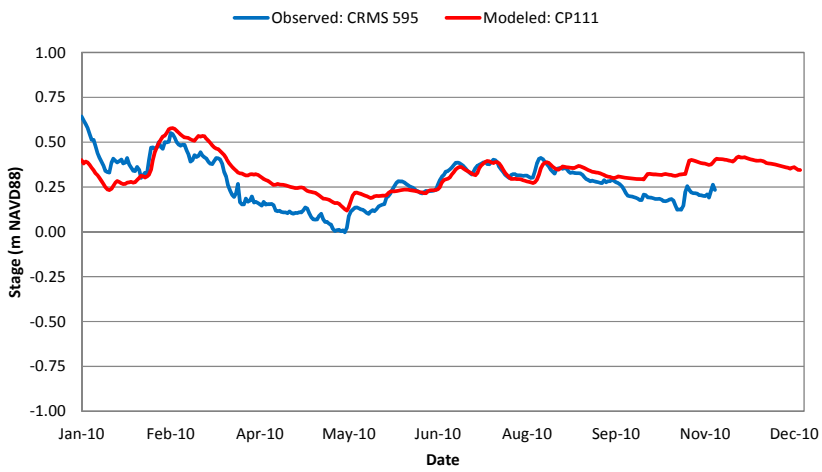

Figure 632 STG Validation Results for CP111 in the CP Model

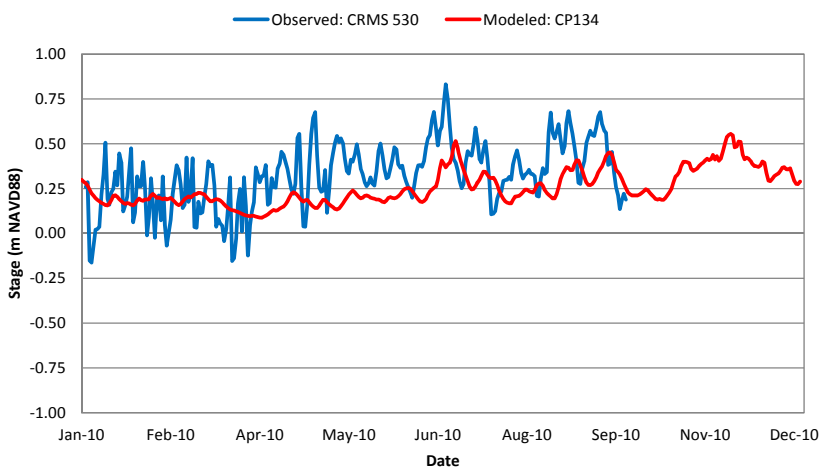

Figure 633 STG Validation Results for CP134 in the CP Model

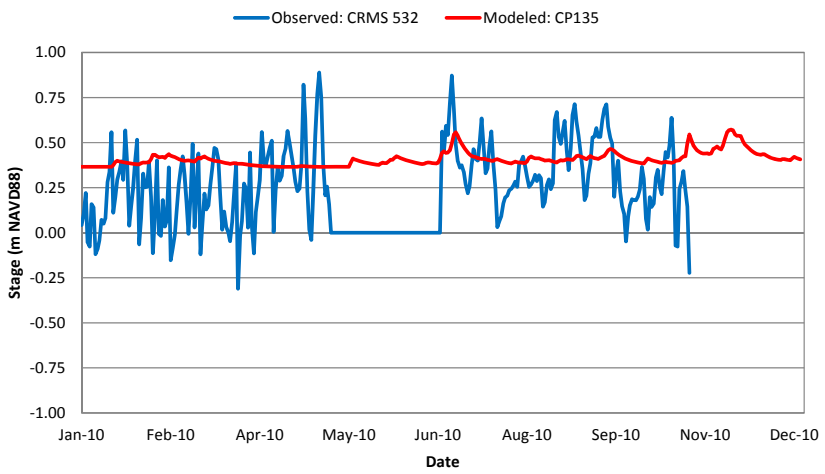

Figure 634 STG Validation Results for CP135 in the CP Model

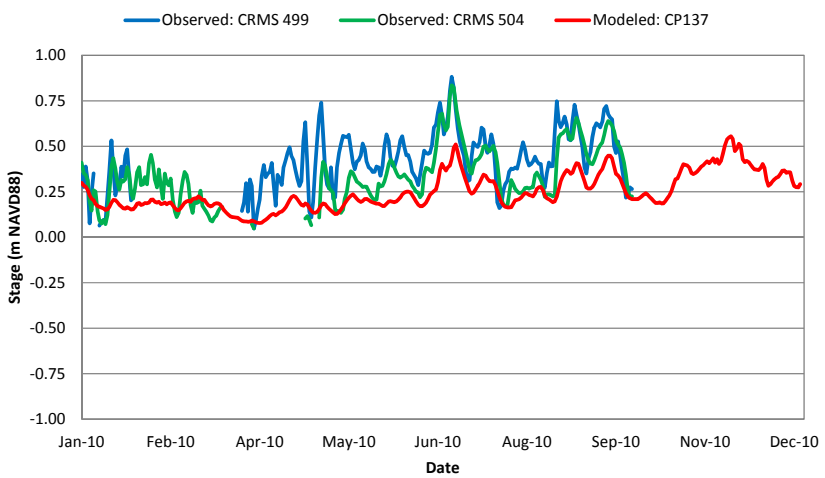

Figure 635 STG Validation Results for East Marsh Island in the CP Model

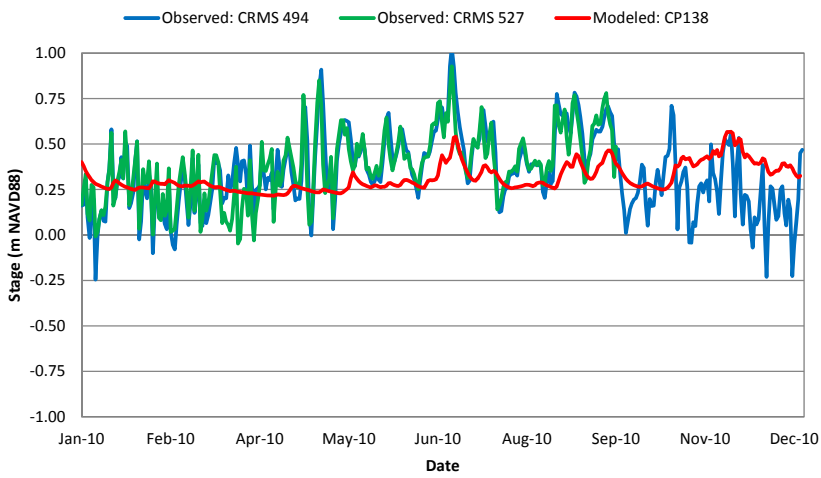

Figure 636 STG Validation Results for CP138 in the CP Model

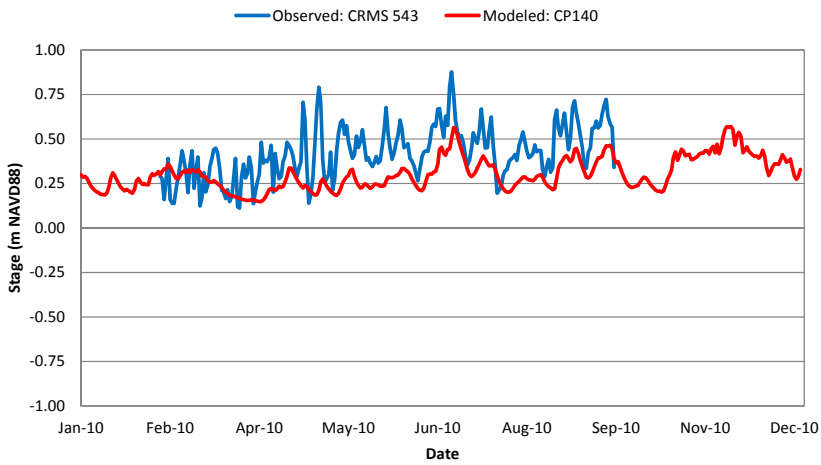

Figure 637 STG Validation Results for CP140 in the CP Model

Salinity (SAL)

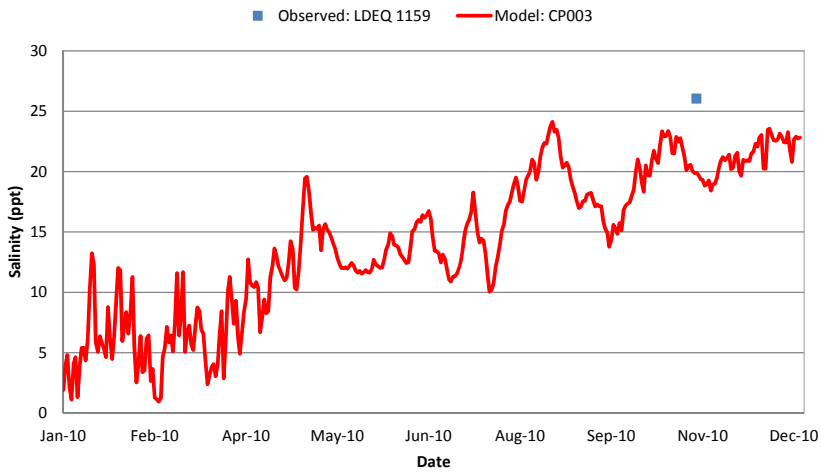

Figure 638 SAL Validation Results for Sabine Pass in the CP Model

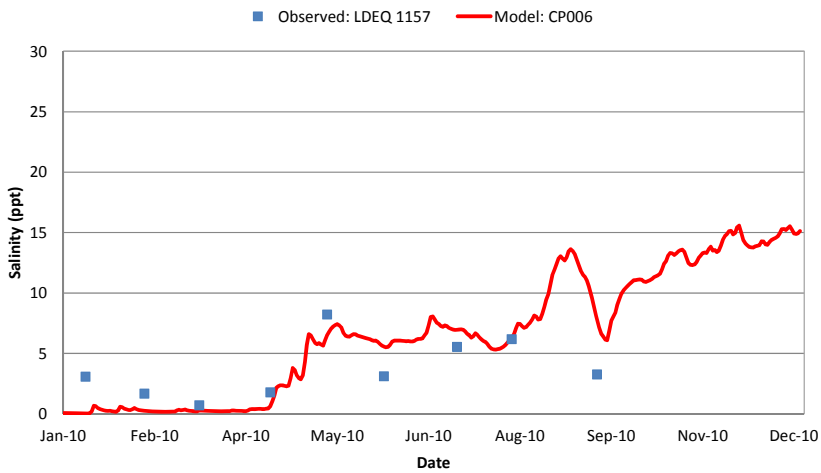

Figure 639 SAL Validation Results for Black Bayou in the CP Model

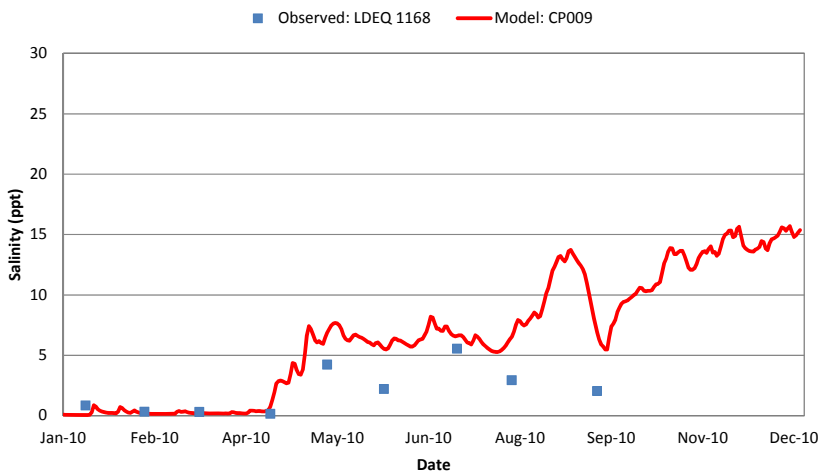

Figure 640 SAL Validation Results for the GIWW between Sabine and Calcasieu Rivers in the CP Model

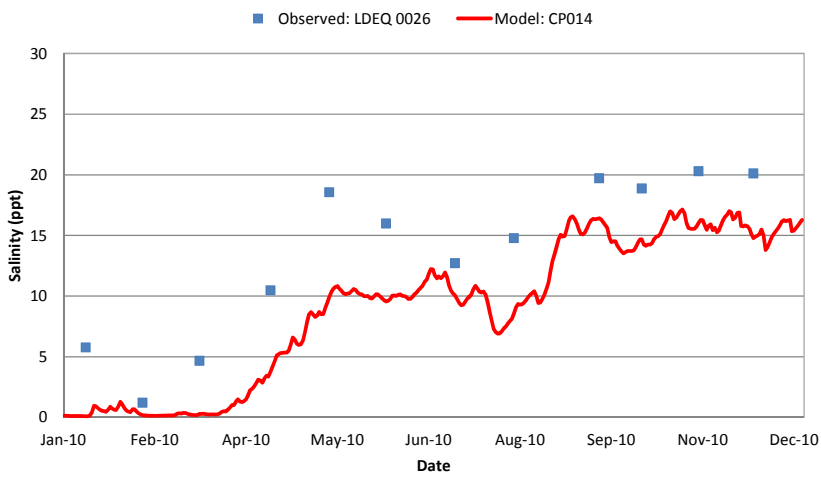

Figure 641 SAL Validation Results for Lower Calcasieu River in the CP Model

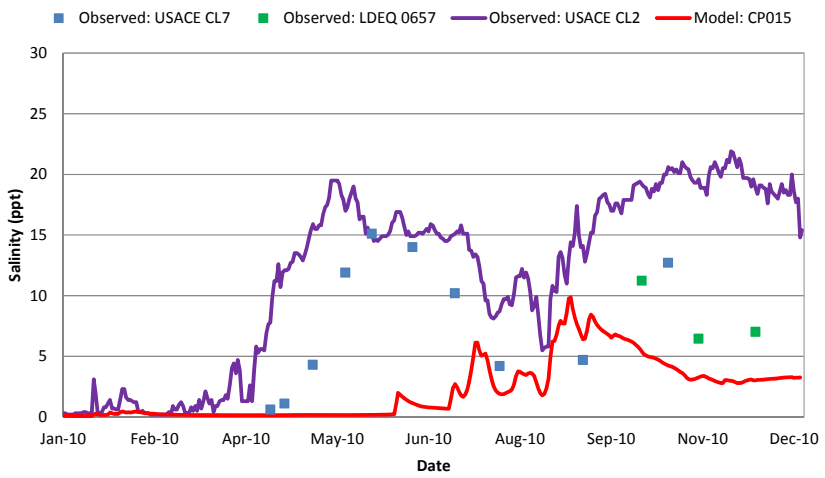

Figure 642 SAL Validation Results for GIWW between Calcasieu River and Bayou Lacassine in the CP Model

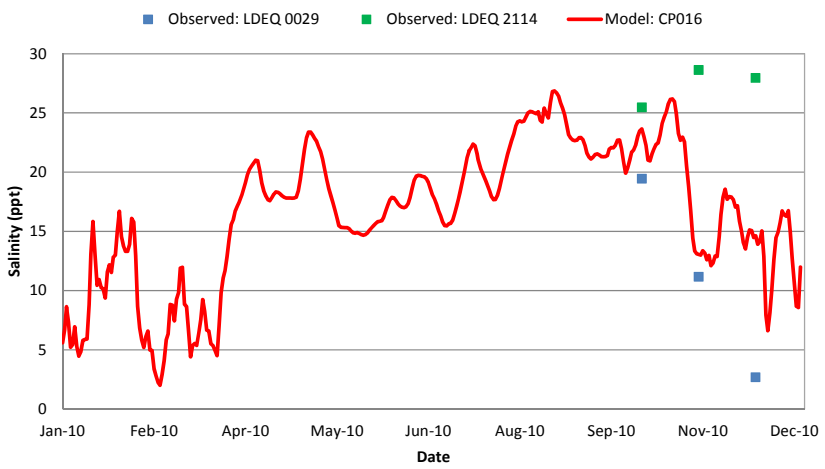

Figure 643 SAL Validation Results for Lower Mermentau River in the CP Model

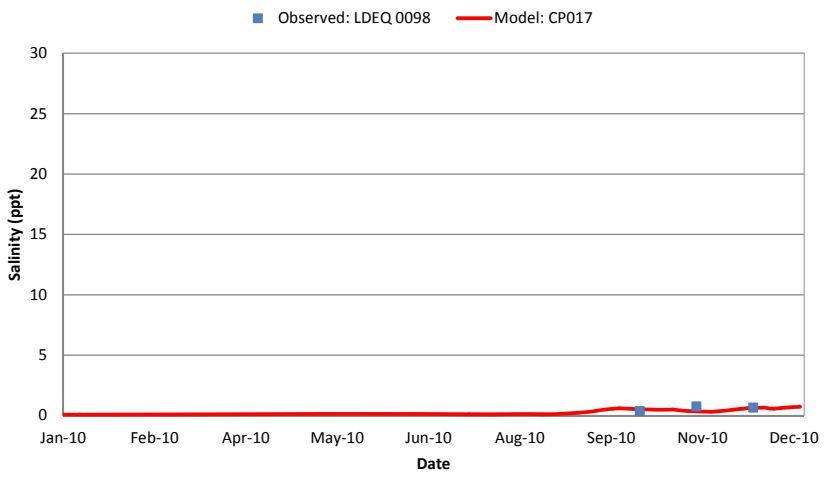

Figure 644 SAL Validation Results for Bayou Lacassine in the CP Model

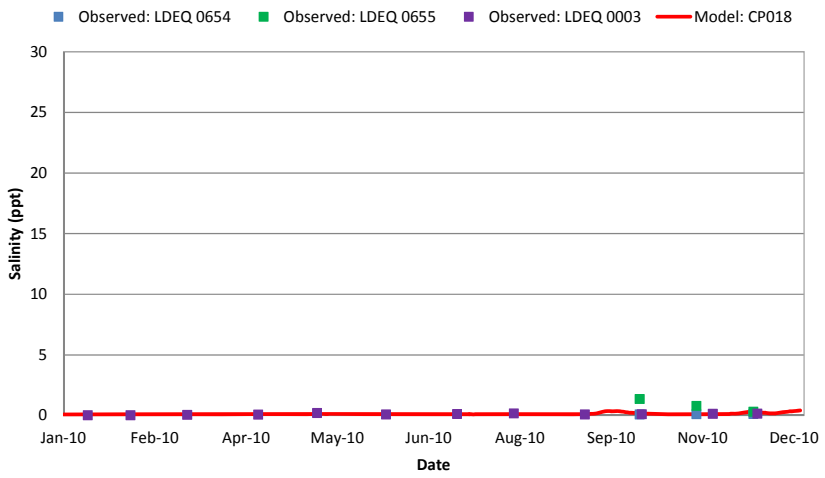

Figure 645 SAL Validation Results for Mermentau River in the CP Model

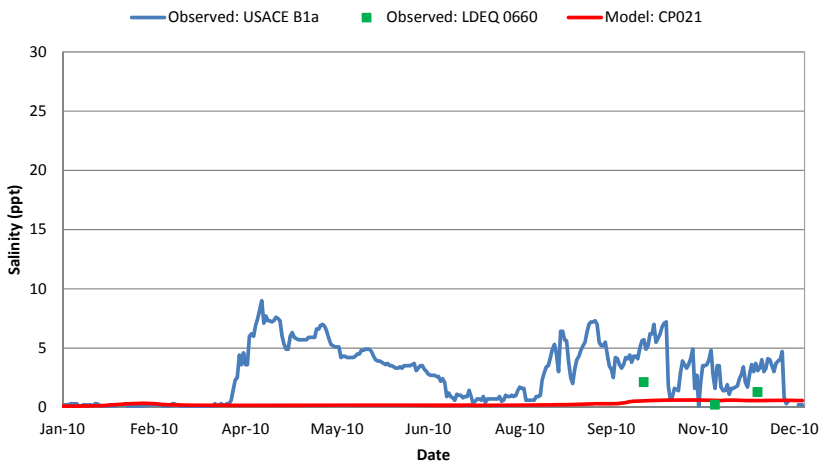

Figure 646 SAL Validation Results for GIWW between Mermentau River and Vermilion River in the CP Model

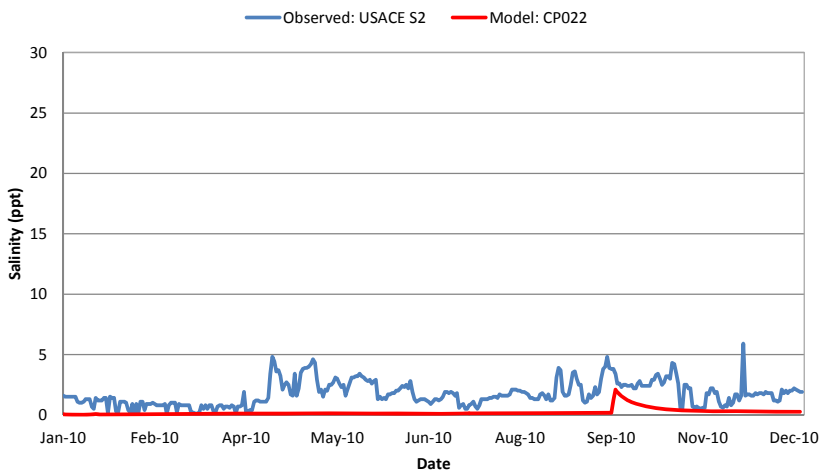

Figure 647 SAL Validation Results for Schooner Bayou in the CP Model

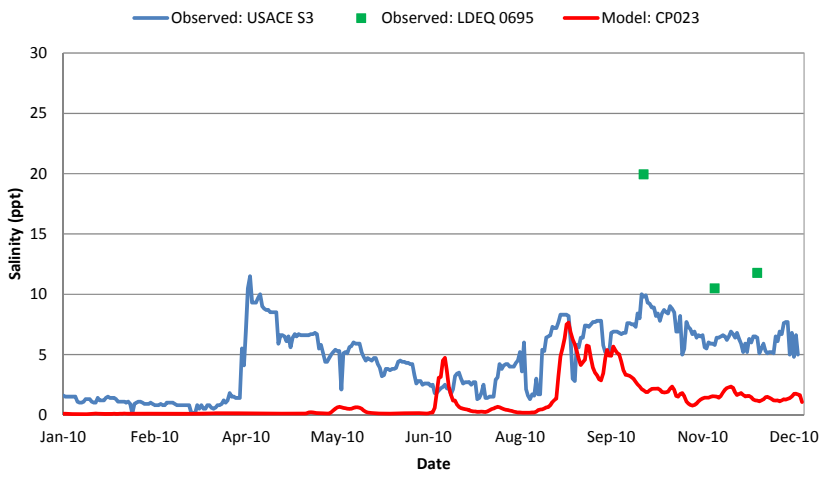

Figure 648 SAL Validation Results for Freshwater Bayou in the CP Model

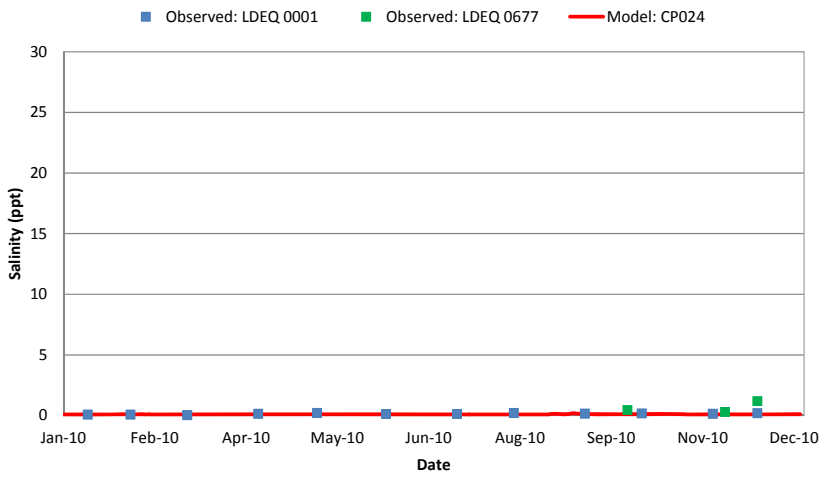

Figure 649 SAL Validation Results for Vermilion River in the CP Model

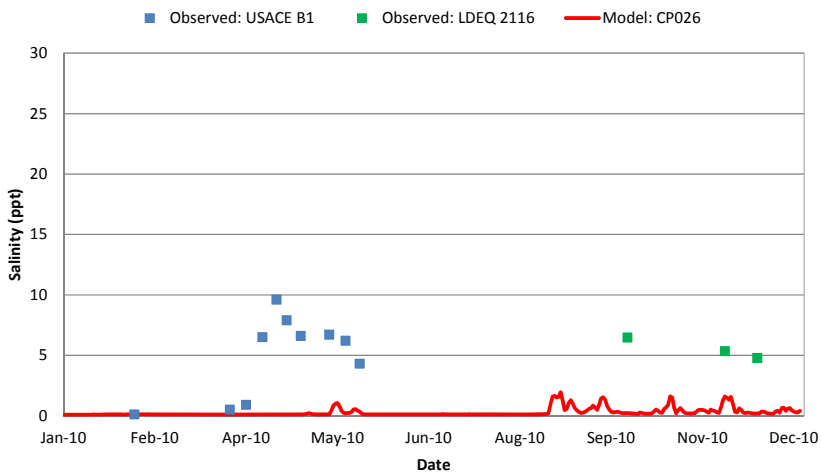

Figure 650 SAL Validation Results for GIWW W of Vermilion River in the CP Model

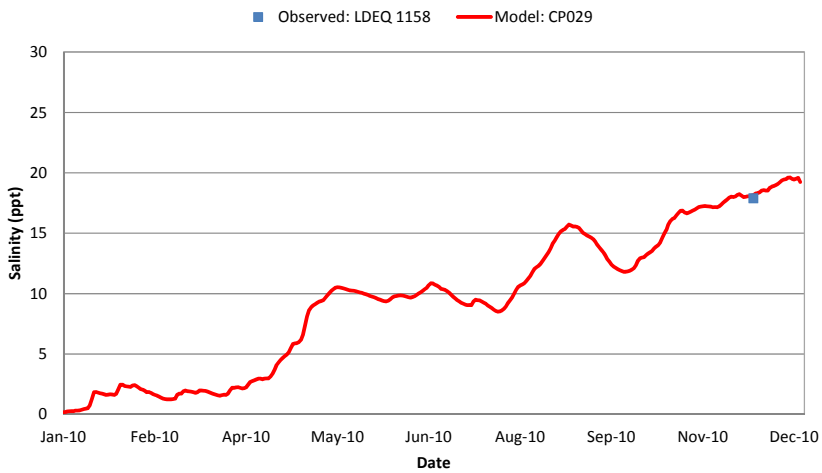

Figure 651 SAL Validation Results for Sabine Lake in the CP Model

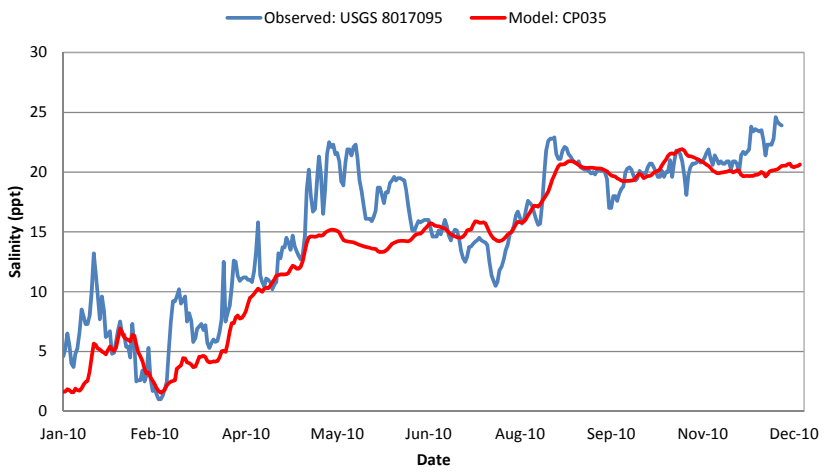

Figure 652 SAL Validation Results for Calcasieu Lake in the CP Model

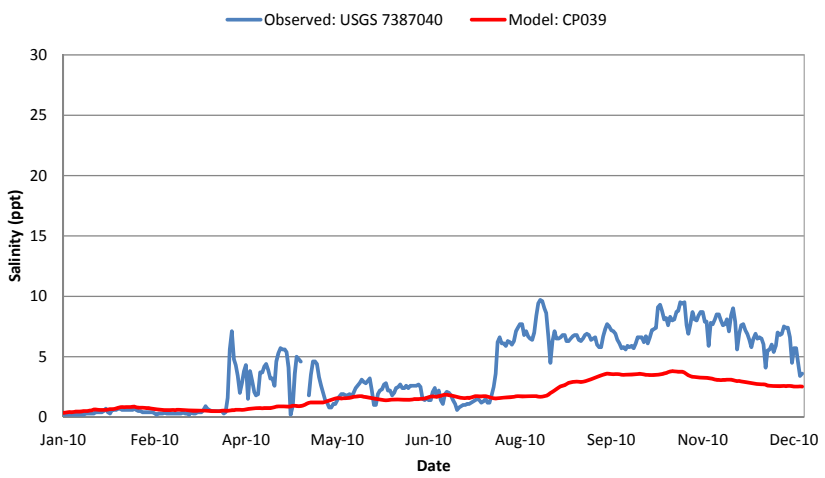

Figure 653 SAL Validation Results for Vermilion Bay in the CP Model

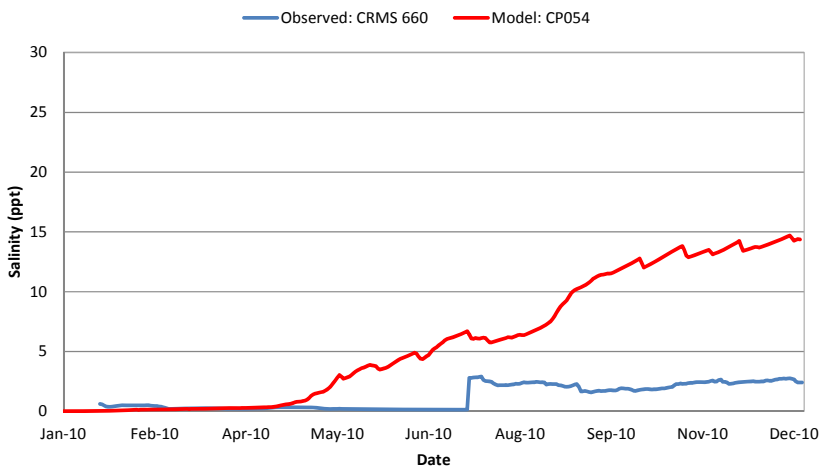

Figure 654 SAL Validation Results for Greens Lake and Surrounding Marshes in the CP Model

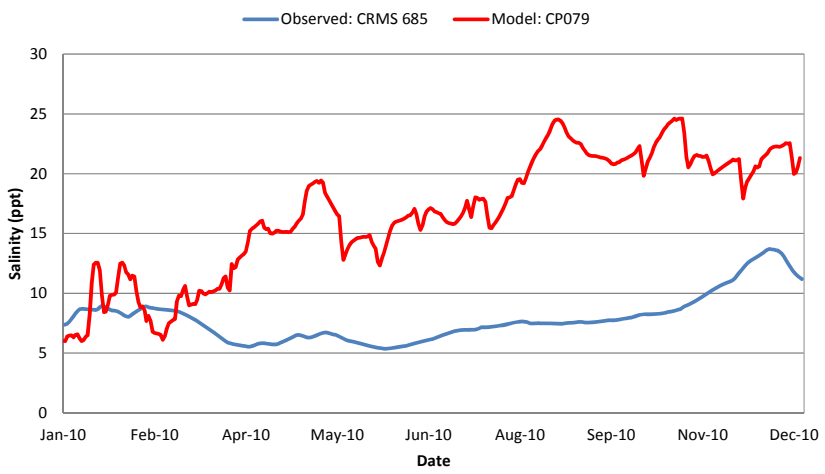

Figure 655 SAL Validation Results for CP079 in the CP Model

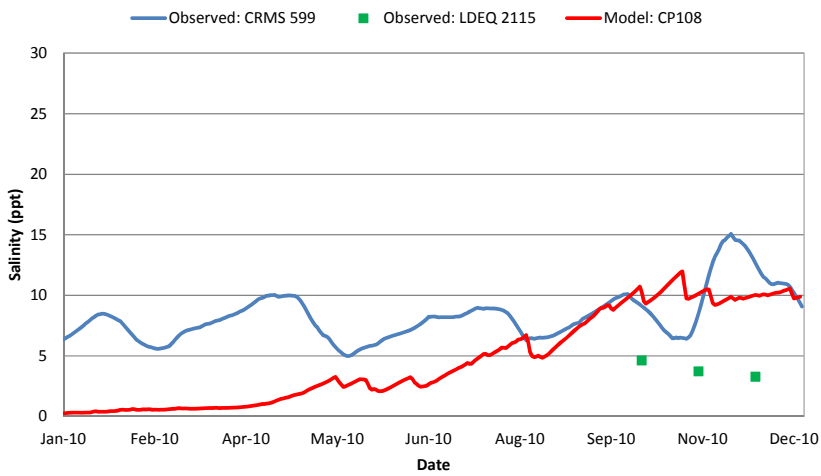

Figure 656 SAL Validation Results for CP108 in the CP Model

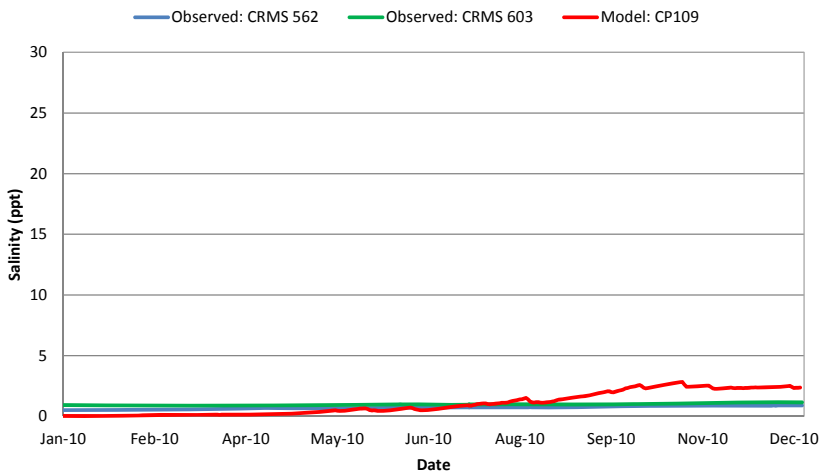

Figure 657 SAL Validation Results for CP109 in the CP Model

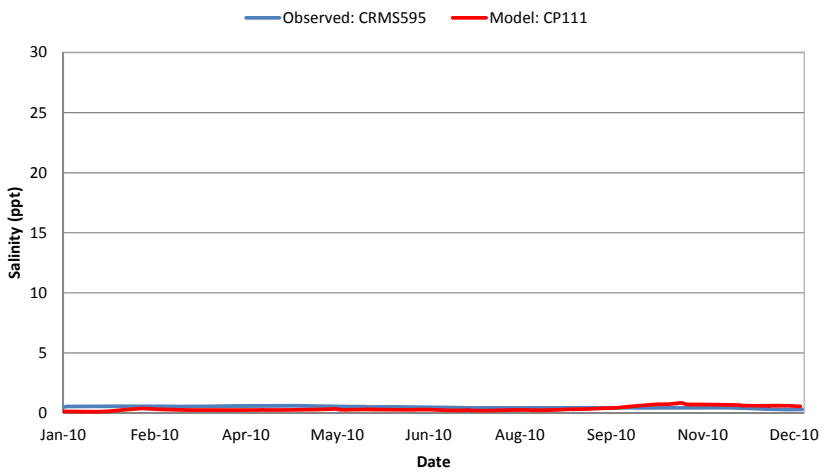

Figure 658 SAL Validation Results for CP111 in the CP Model

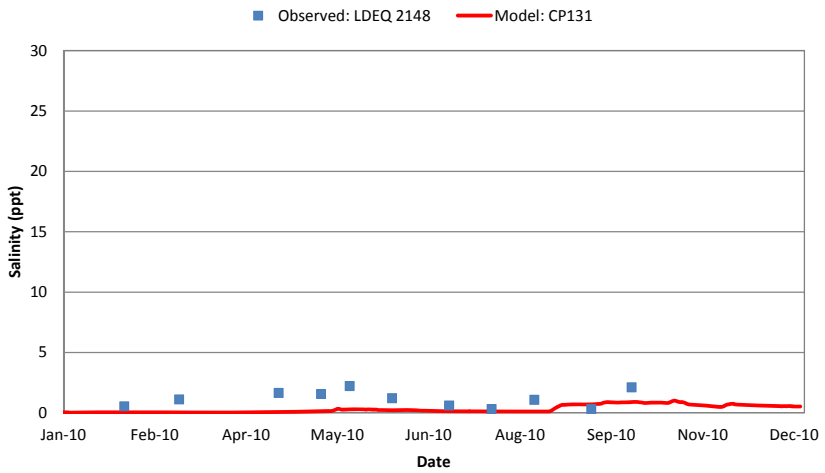

Figure 659 SAL Validation Results for CP131 in the CP Model

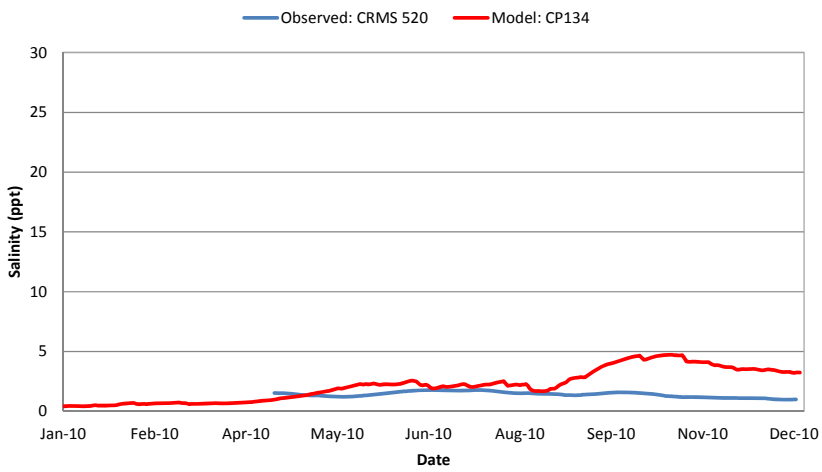

Figure 660 SAL Validation Results for CP134 in the CP Model

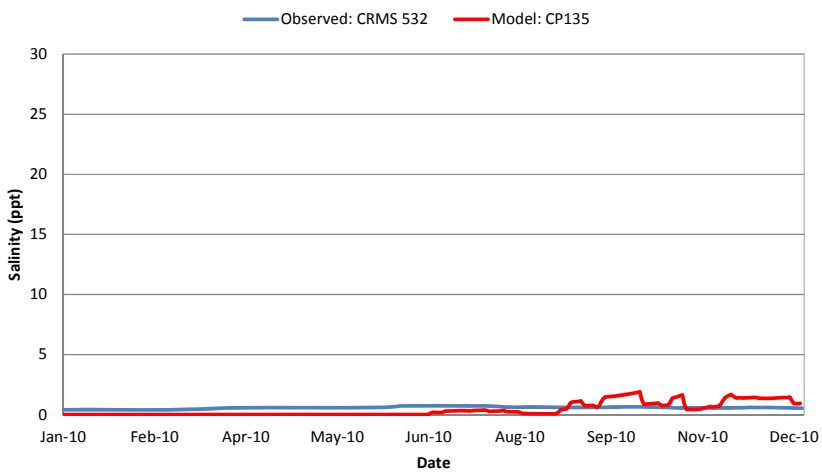

Figure 661 SAL Validation Results for CP135 in the CP Model

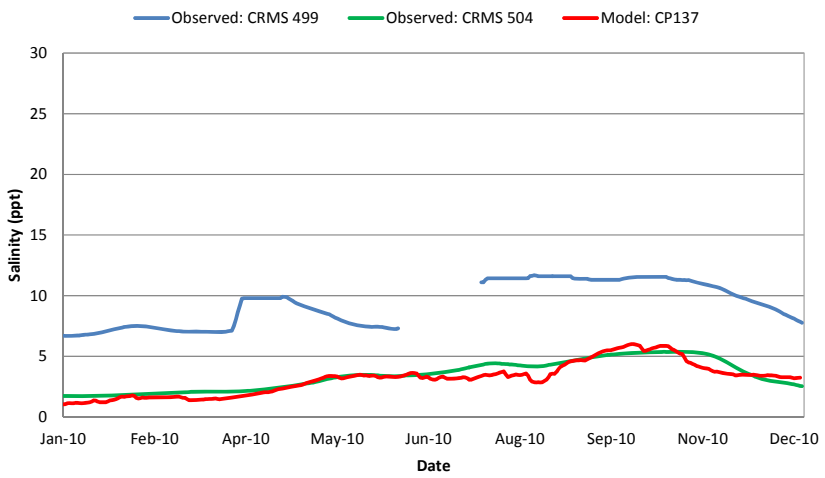

Figure 662 SAL Validation Results for East Marsh Island in the CP Model

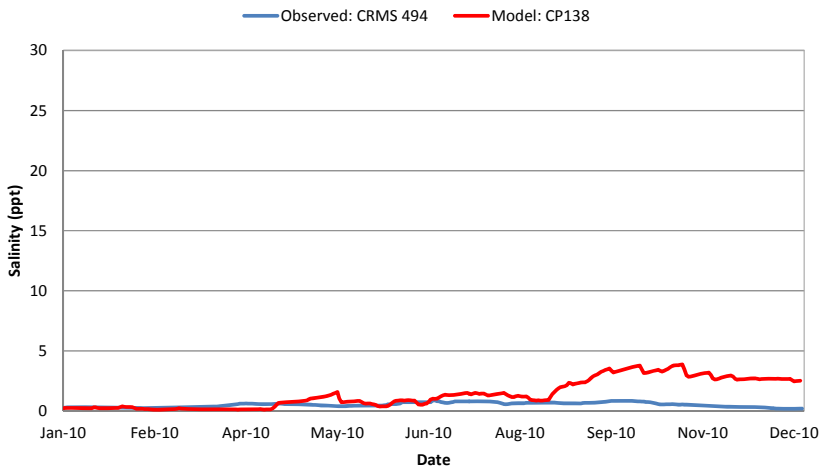

Figure 663 SAL Validation Results for CP138 in the CP Model

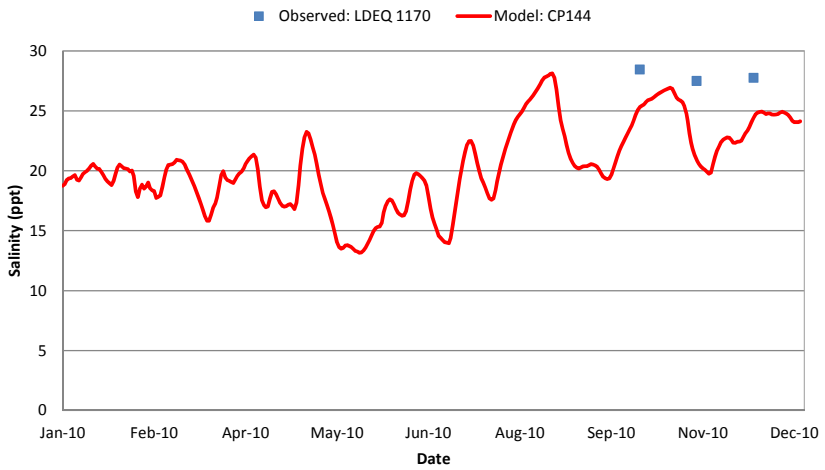

Figure 664 SAL Validation Results for CP144 in the CP Model

Temperature (TMP)

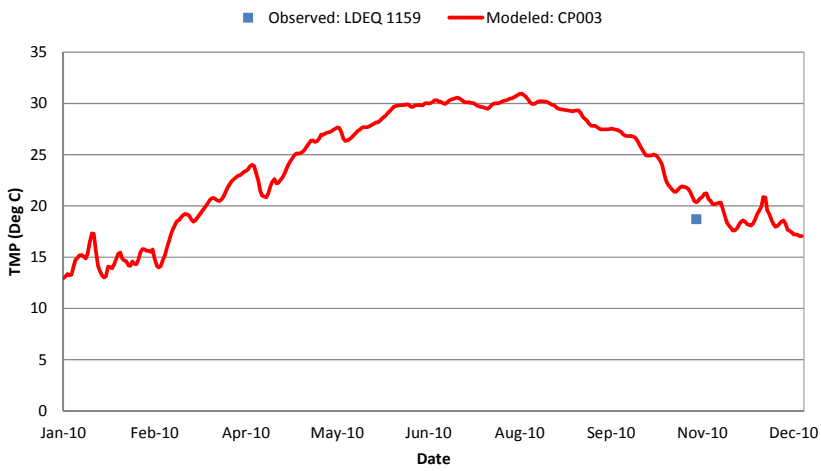

Figure 665 TMP Validation Results for Sabine Pass in the CP Model

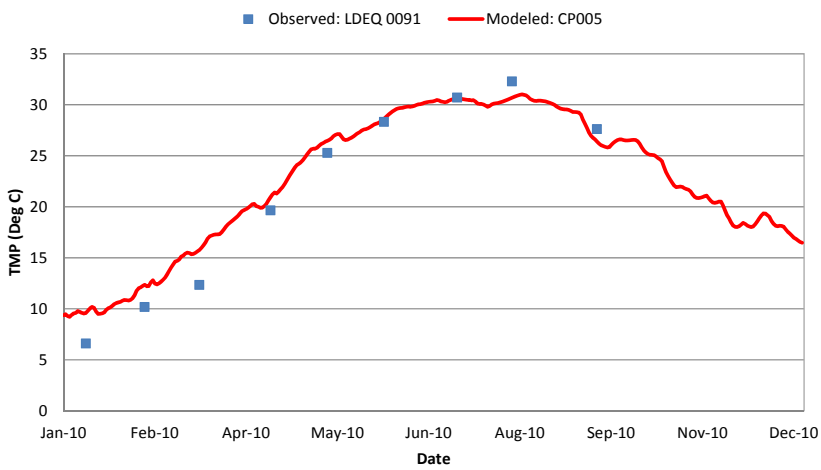

Figure 666 TMP Validation Results for Sabine River in the CP Model

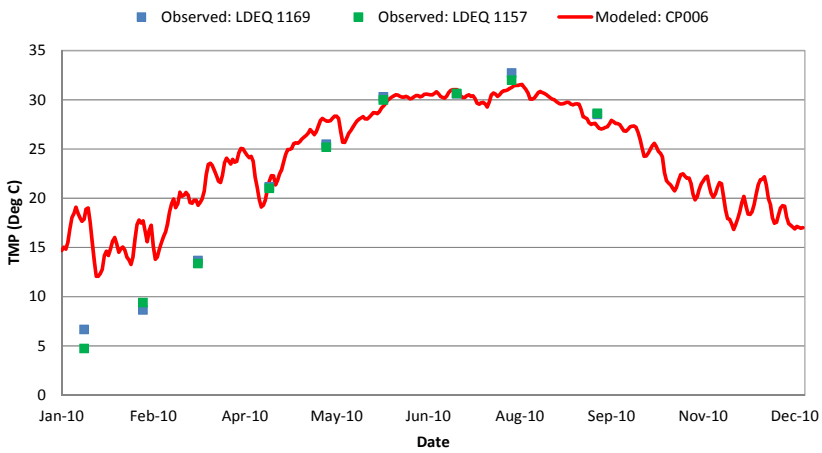

Figure 667 TMP Validation Results for Black Bayou in the CP Model

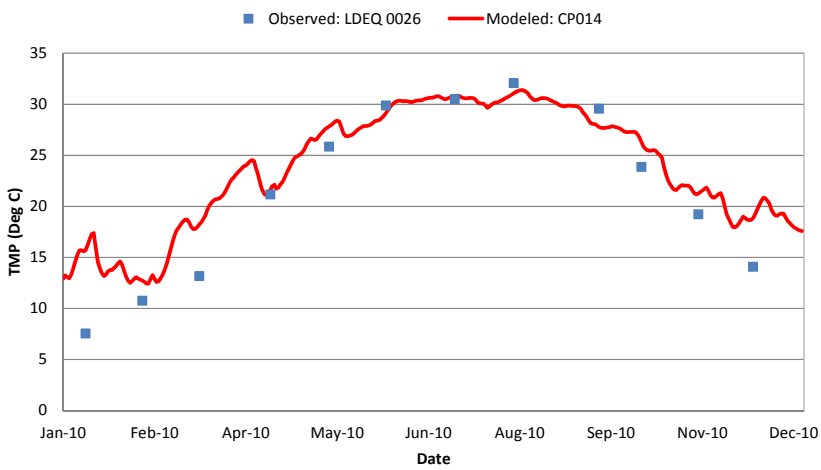

Figure 668 TMP Validation Results for Mermentau River in the CP Model

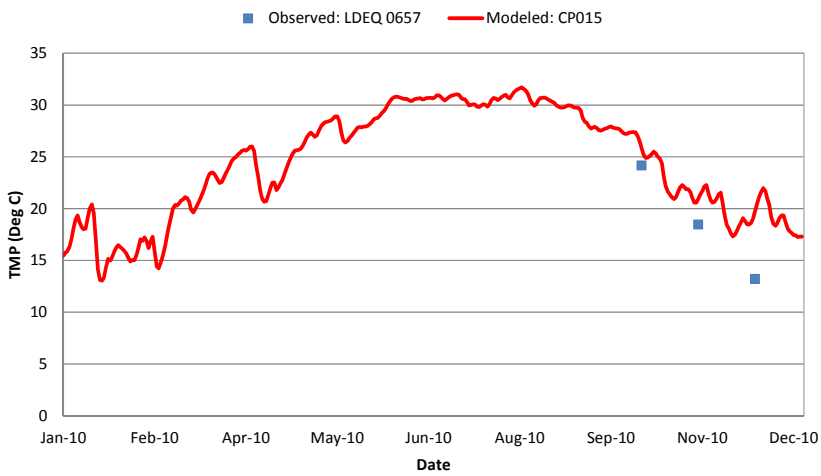

Figure 669 TMP Validation Results for GIWW between Calcasieu River and Bayou Lacassine in the CP Model

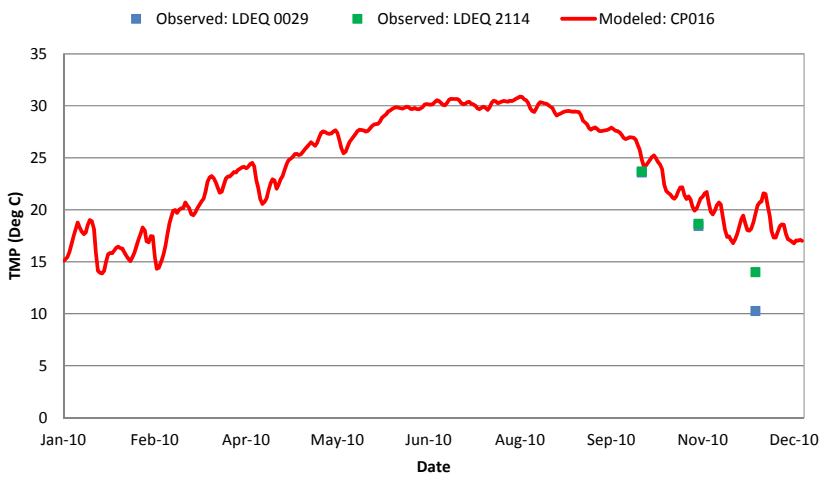

Figure 670 TMP Validation Results for Lower Mermentau River in the CP Model

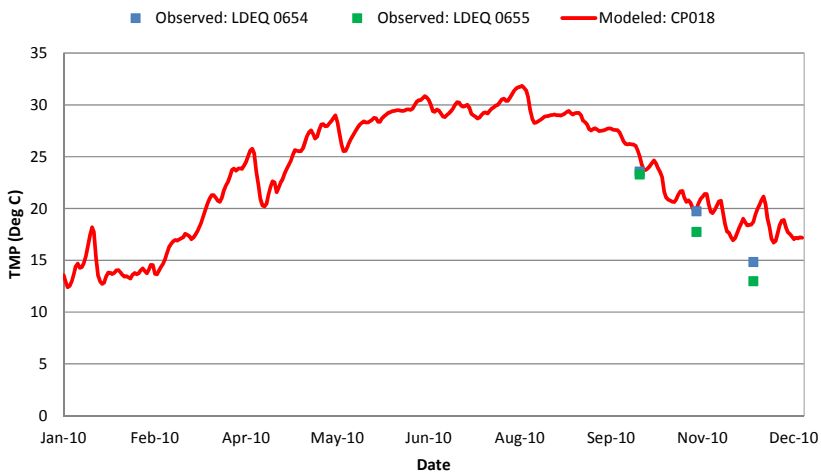

Figure 671 TMP Validation Results for Mermentau River in the CP Model

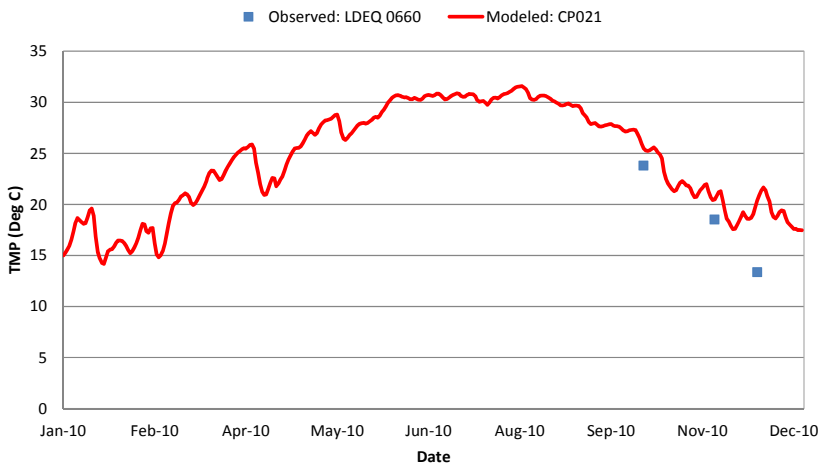

Figure 672 TMP Validation Results for GIWW between Mermentau River and Vermilion River in the CP Model

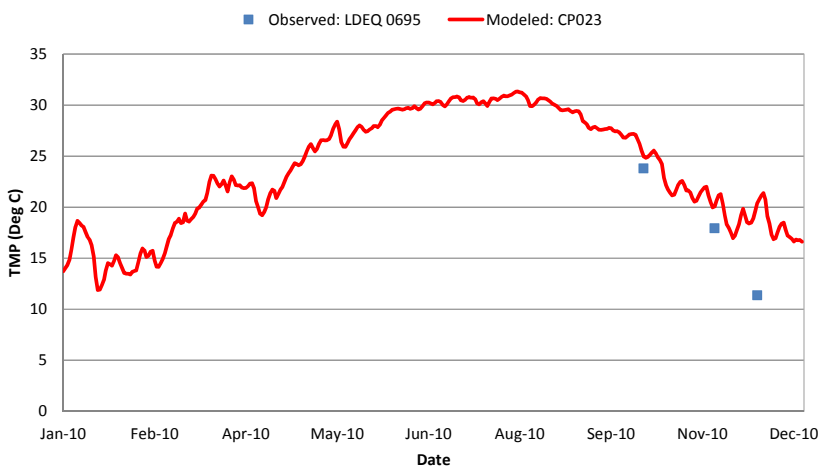

Figure 673 TMP Validation Results for Freshwater Bayou in the CP Model

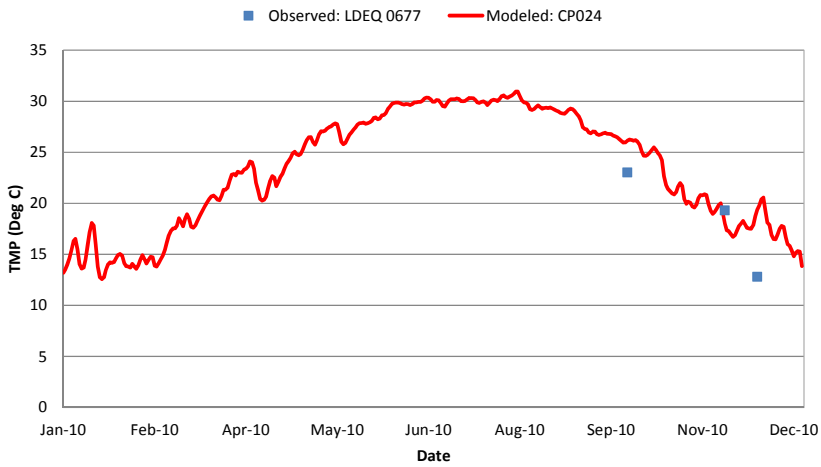

Figure 674 TMP Validation Results for Vermilion River in the CP Model

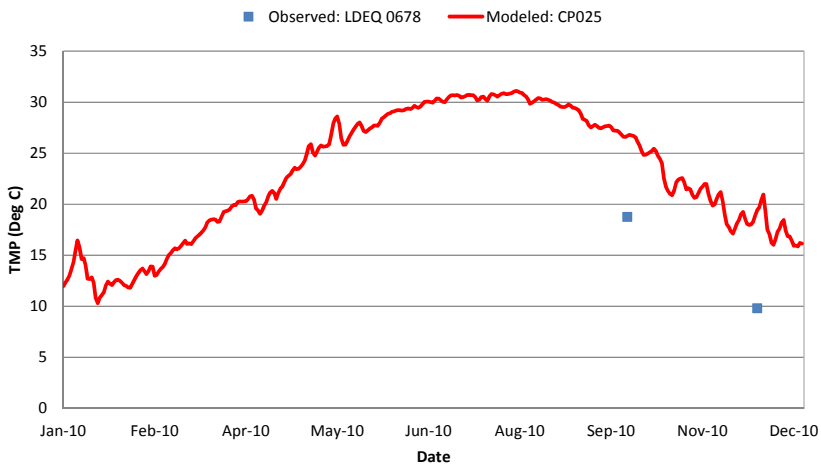

Figure 675 TMP Validation Results for CP025 in the CP Model

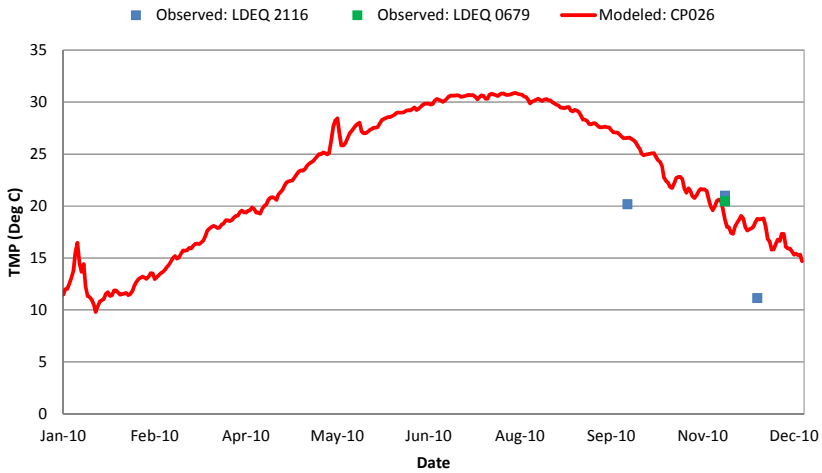

Figure 676 TMP Validation Results for GIWW East of Vermilion River in the CP Model

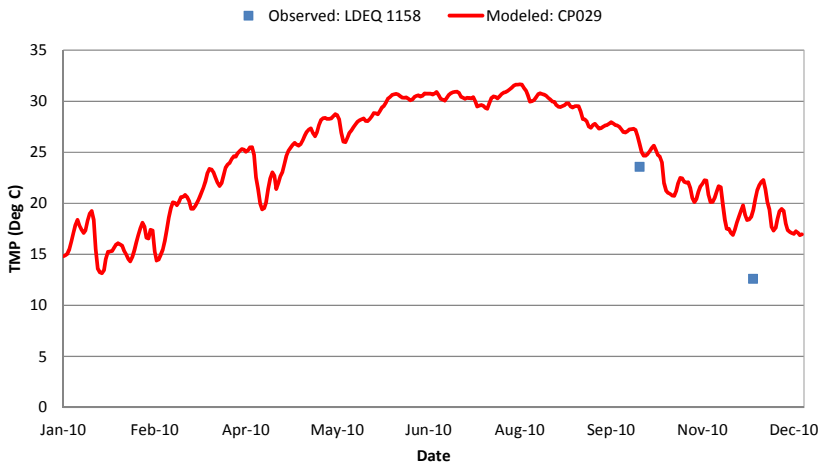

Figure 677 TMP Validation Results for Sabine Lake in the CP Model

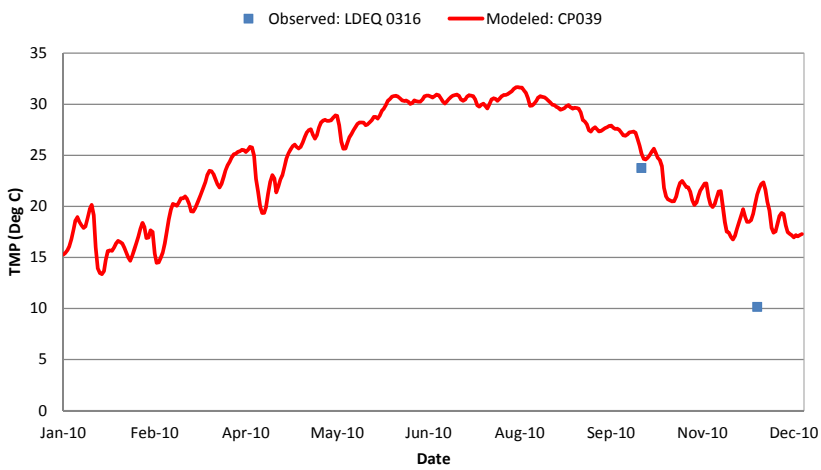

Figure 678 TMP Validation Results for Vermilion Bay in the CP Model

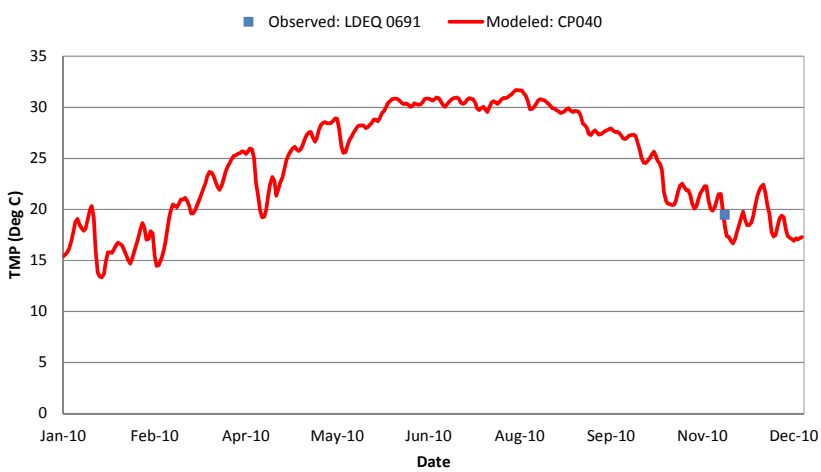

Figure 679 TMP Validation Results for West Cote Blanche Bay in the CP Model

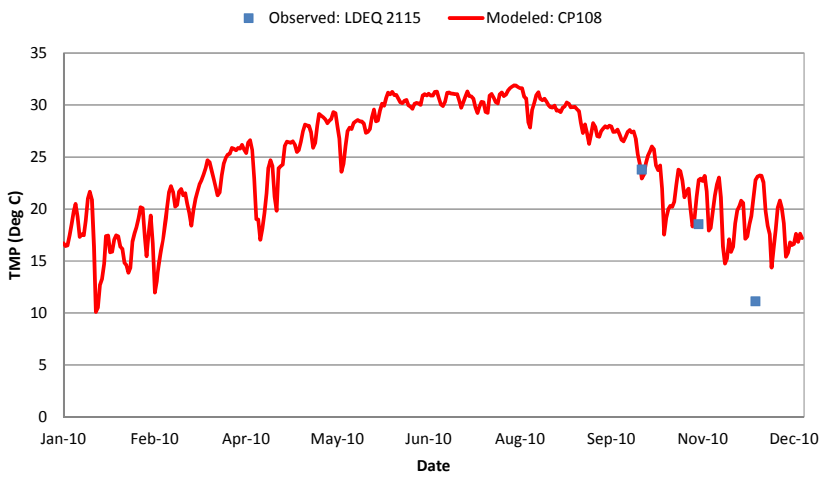

Figure 680 TMP Validation Results for CP108 in the CP Model

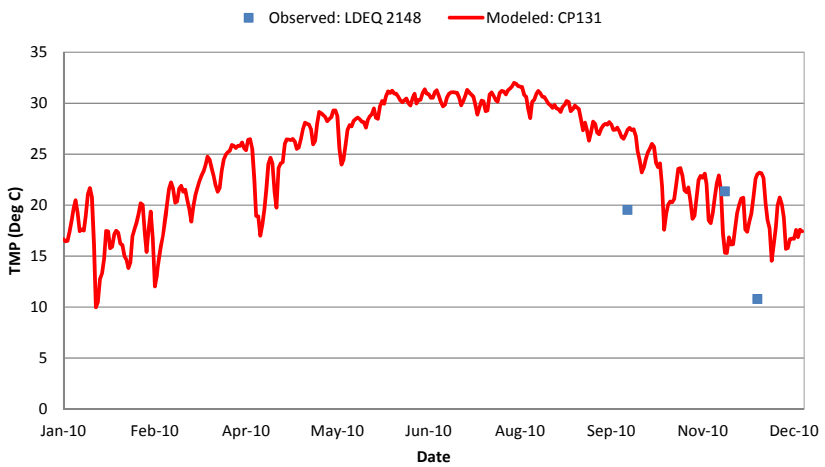

Figure 681 TMP Validation Results for NW of Vermilion Bay and N of GIWW in the CP Model

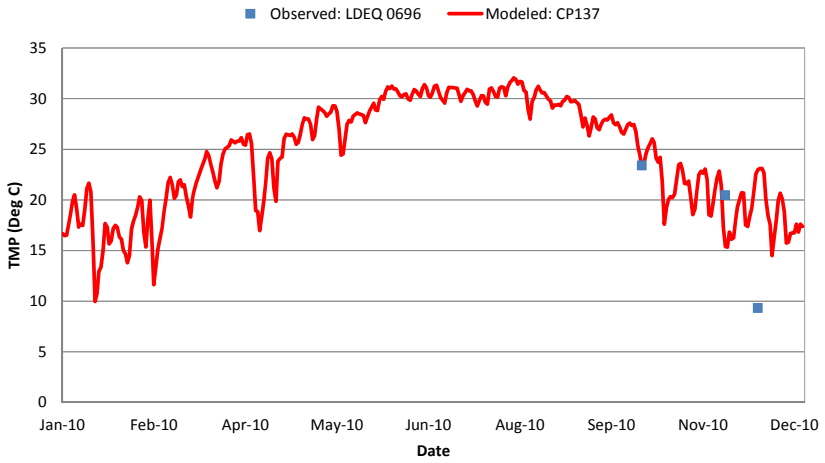

Figure 682 TMP Validation Results for East Marsh Island in the CP Model

Total Suspended Solids (TSS)

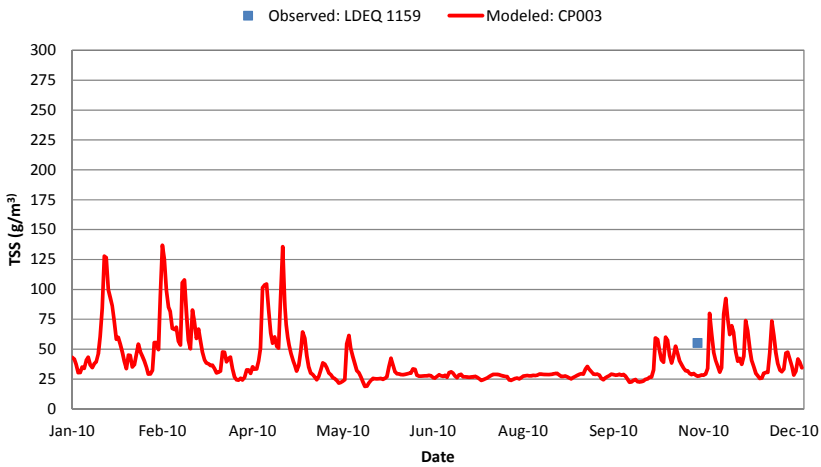

Figure 683 TSS Validation Results for Sabine Pass in the CP Model

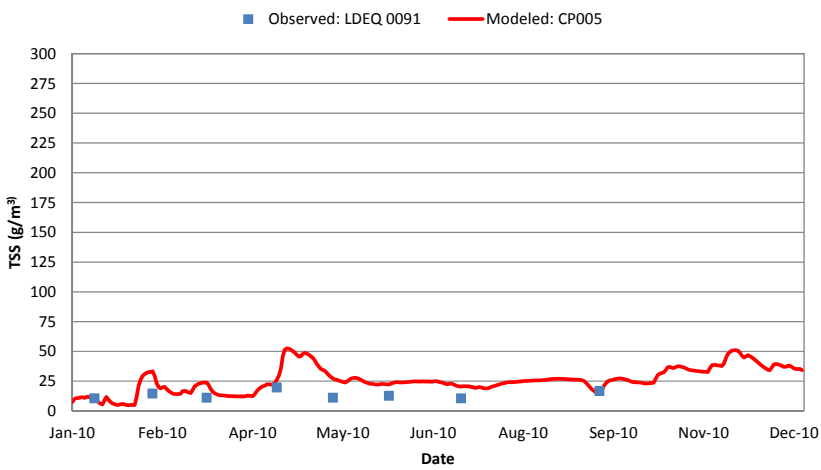

Figure 684 TSS Validation Results for Sabine River in the CP Model

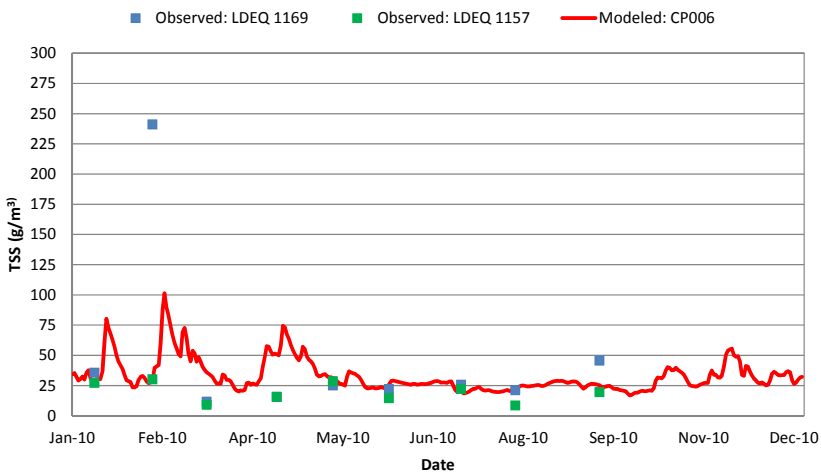

Figure 685 TSS Validation Results for Black Bayou in the CP Model

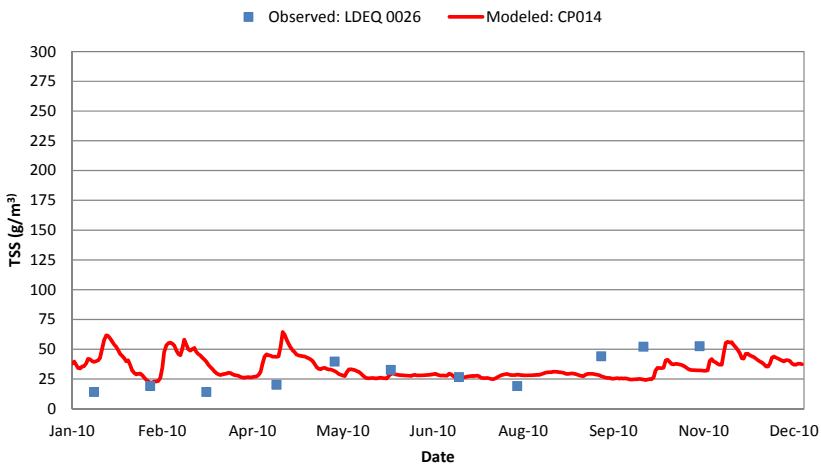

Figure 686 TSS Validation Results for Lower Calcasieu River in the CP Model

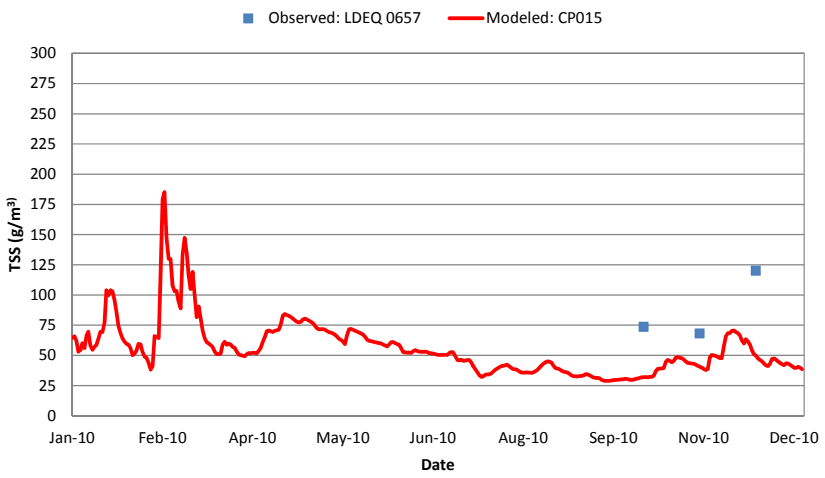

Figure 687 TSS Validation Results for GIWW between Calcasieu River and Bayou Lacassine in the CP Model

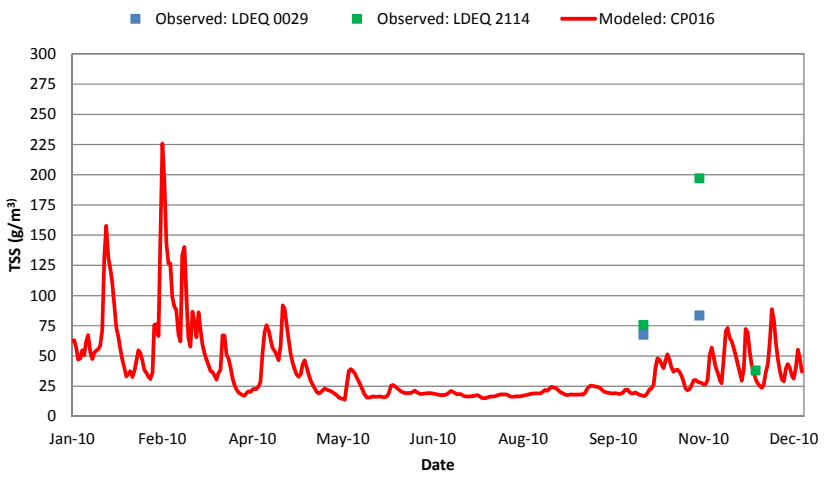

Figure 688 TSS Validation Results for Lower Mermentau River in the CP Model

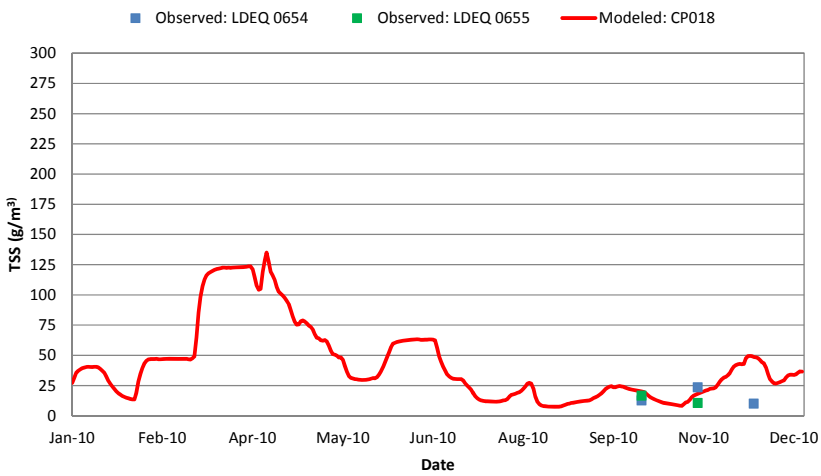

Figure 689 TSS Validation Results for Mermentau River in the CP Model

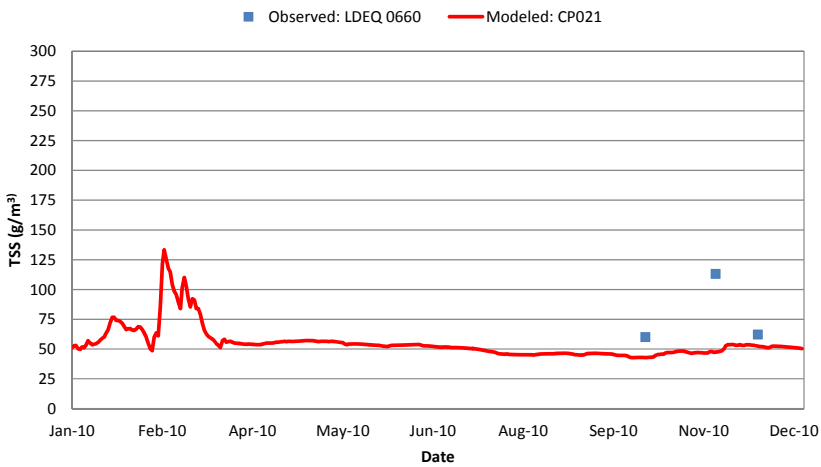

Figure 690 TSS Validation Results for GIWW between Mermentau River and Vermilion River in the CP Model

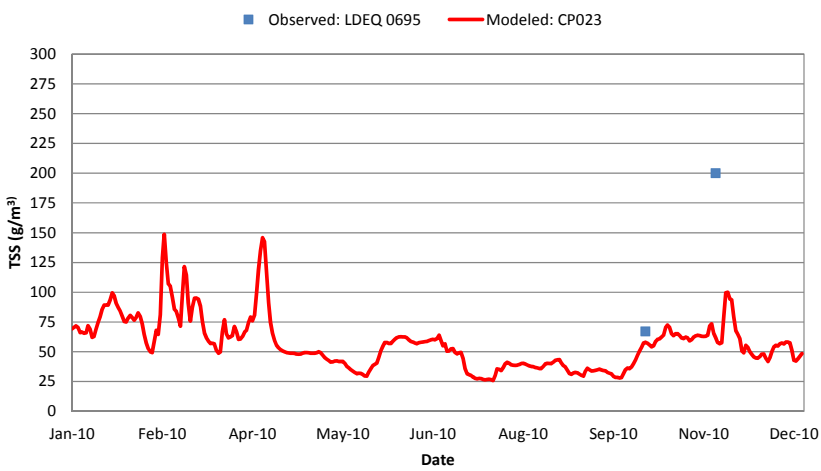

Figure 691 TSS Validation Results for Freshwater Bayou in the CP Model

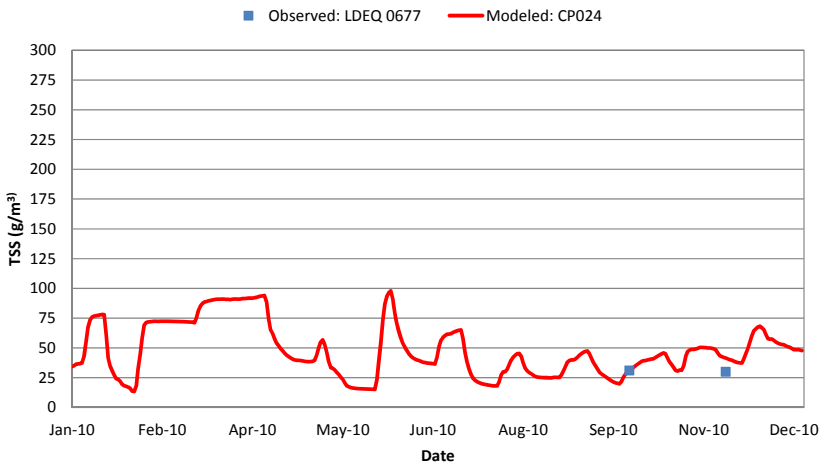

Figure 692 TSS Validation Results for Vermilion River in the CP Model

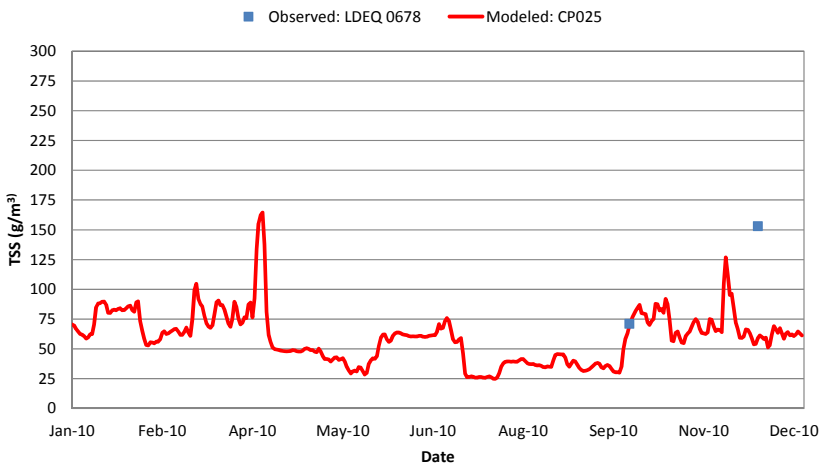

Figure 693 TSS Validation Results for CP025 in the CP Model

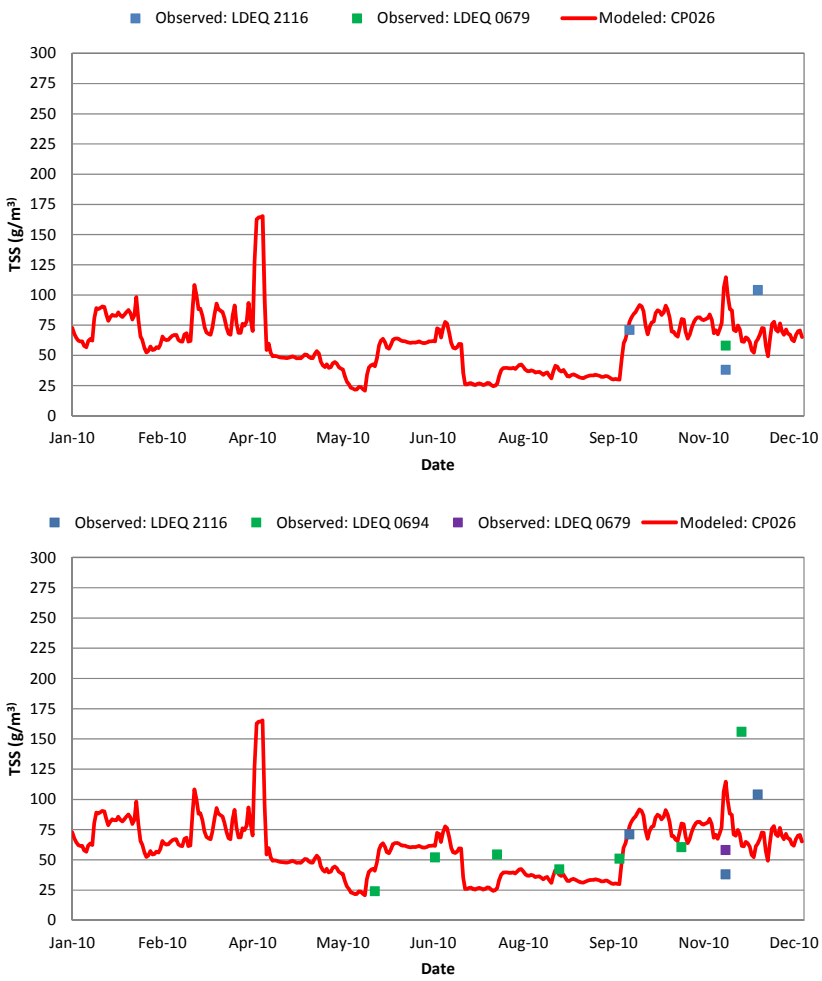

Figure 694 TSS Validation Results for GIWW East of Vermilion River in the CP Model

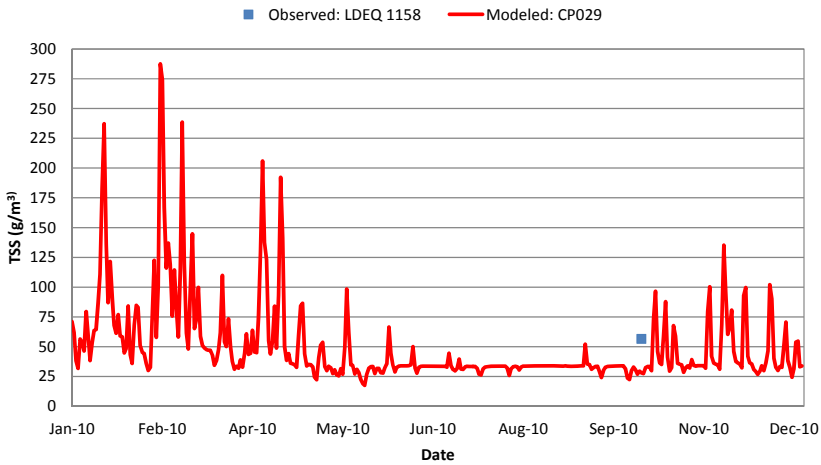

Figure 695 TSS Validation Results for Sabine Lake in the CP Model

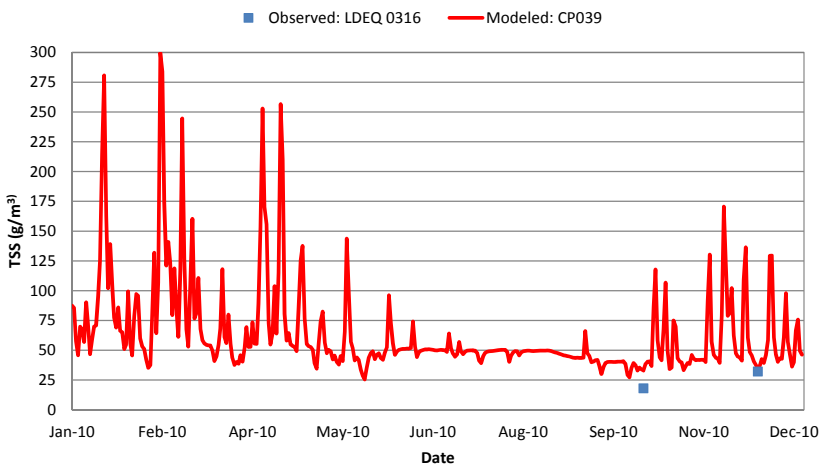

Figure 696 TSS Validation Results for Vermilion Bay in the CP Model

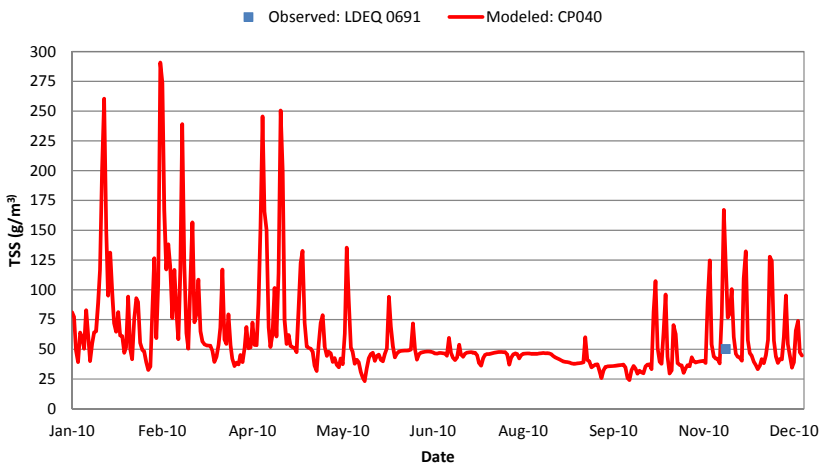

Figure 697 TSS Validation Results for West Cote Blanche Bay in the CP Model

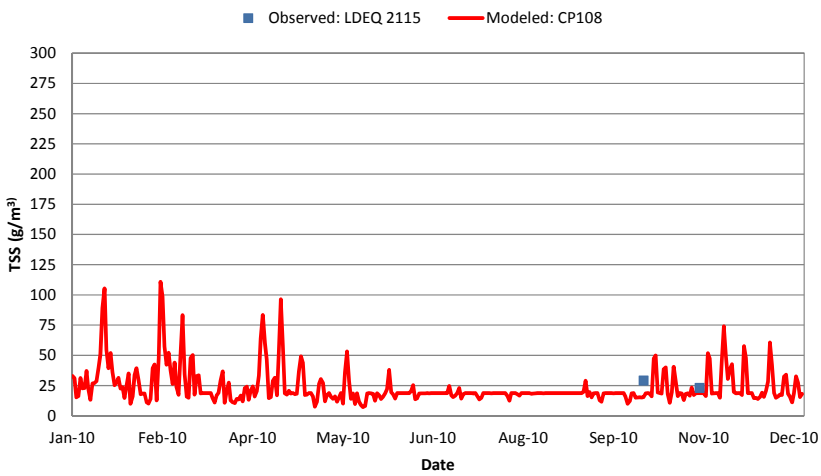

Figure 698 TSS Validation Results for CP108 in the CP Model

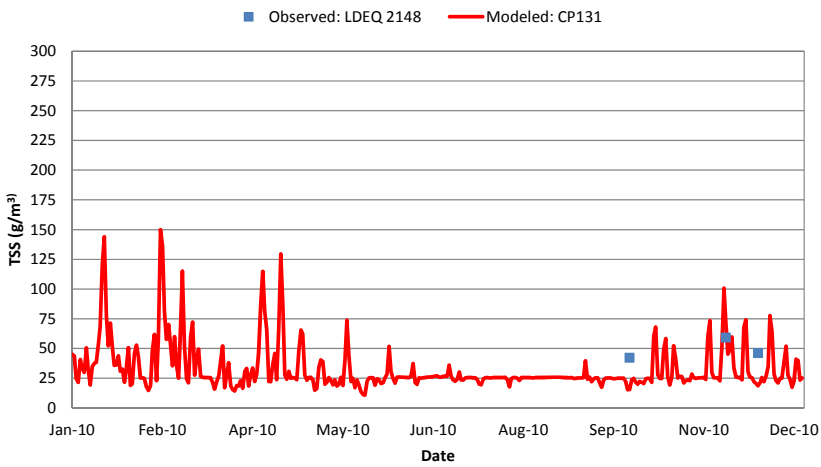

Figure 699 TSS Validation Results for Boston Canal in the CP Model

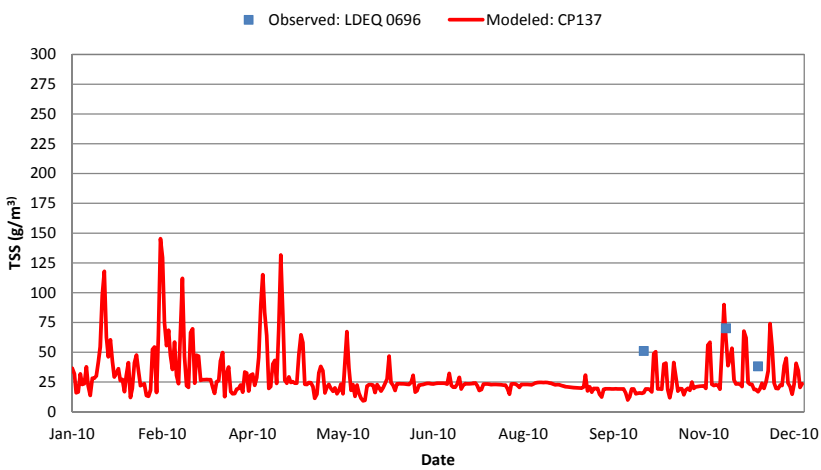

Figure 700 TSS Validation Results for East Marsh Island in the CP Model

Total Nitrogen (TN)

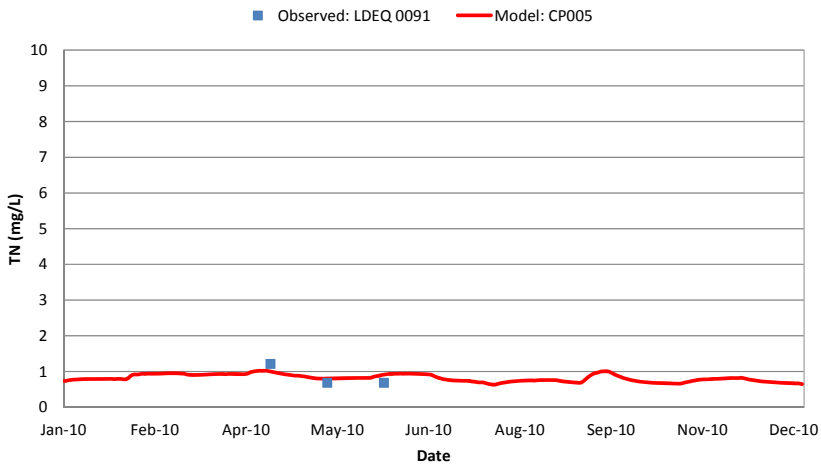

Figure 701 TN Validation Results for Sabine River in the CP Model

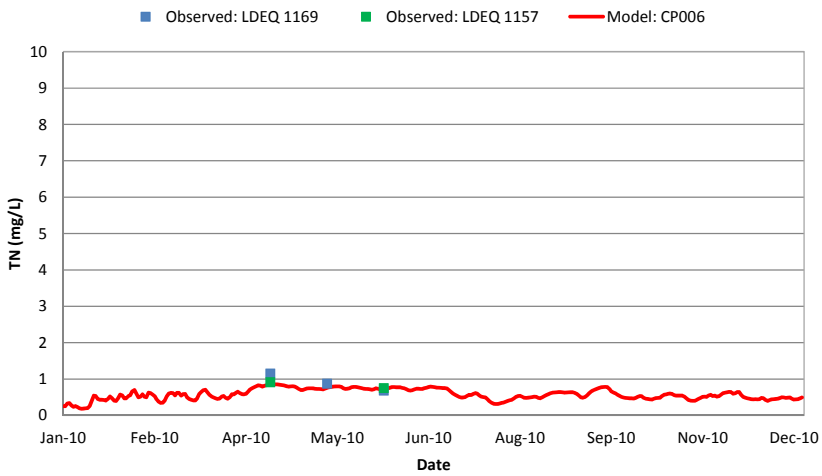

Figure 702 TN Validation Results for Black Bayou in the CP Model

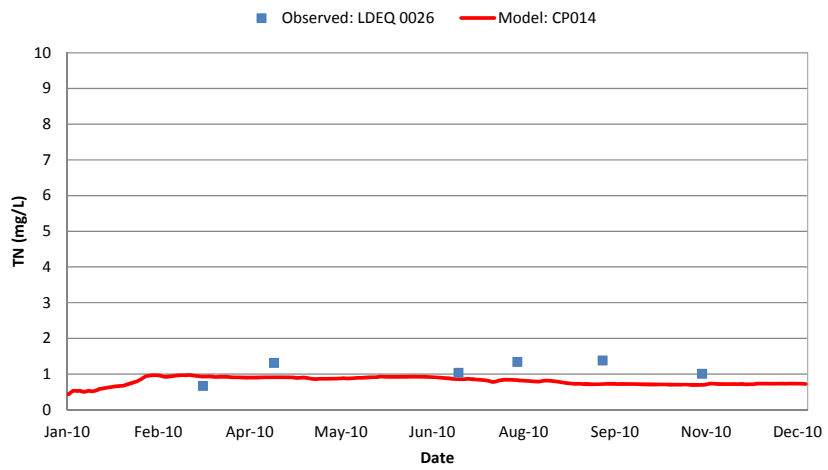

.

Figure 703 TN Validation Results for Lower Calcasieu River in the CP Model

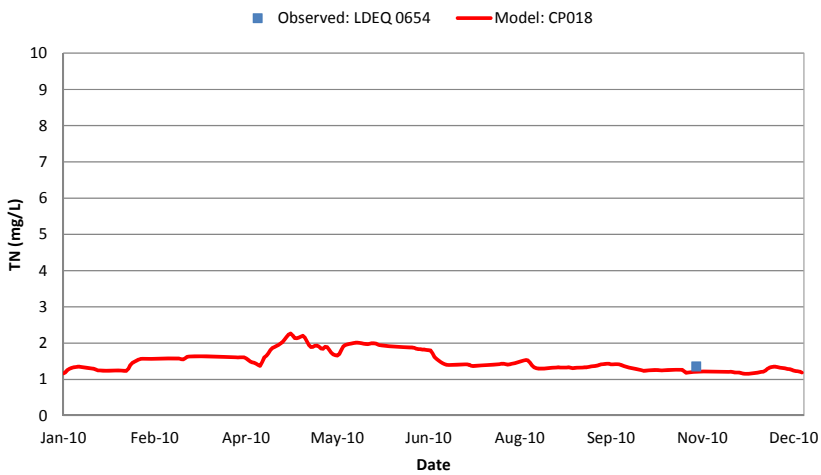

Figure 704 TN Validation Results for Mermentau River in the CP Model

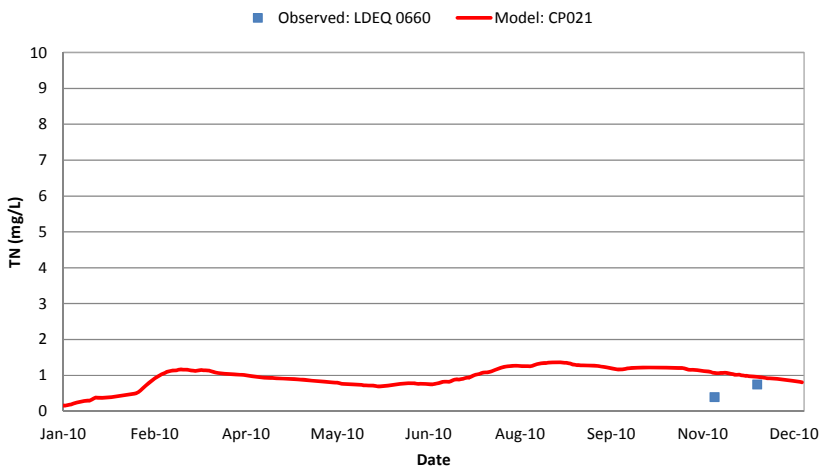

Figure 705 TN Validation Results for GIWW between Mermentau River and the Leland Bowman Lock in the CP Model

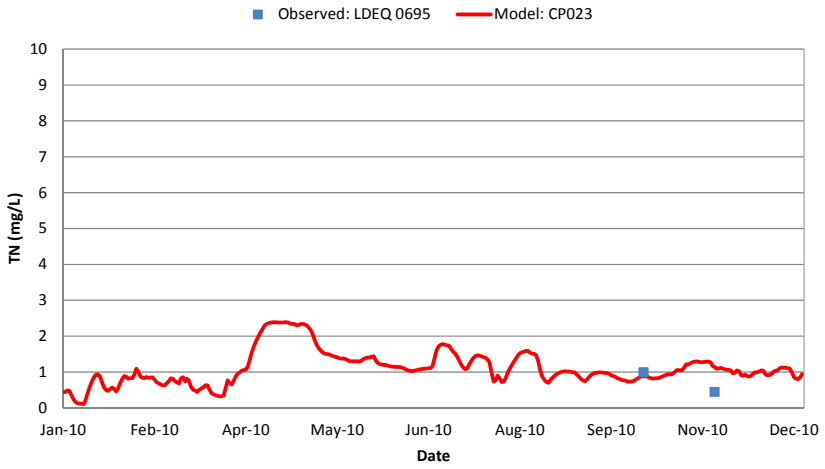

Figure 706 TN Validation Results for Freshwater Bayou in the CP Model

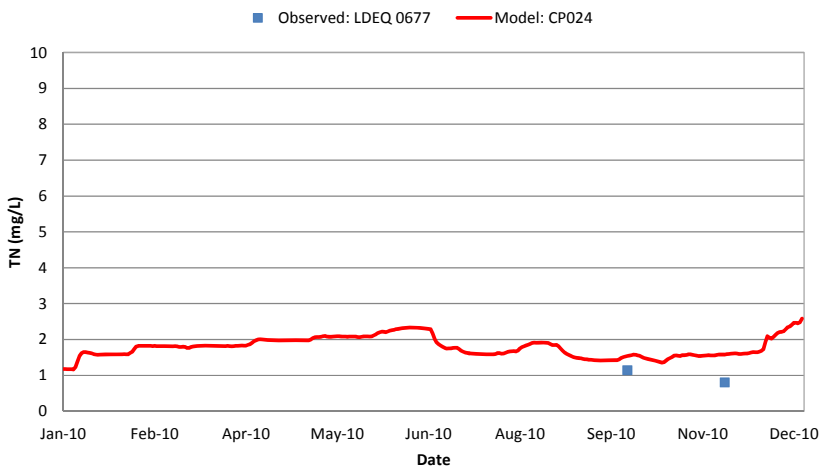

Figure 707 TN Validation Results for Vermilion River in the CP Model

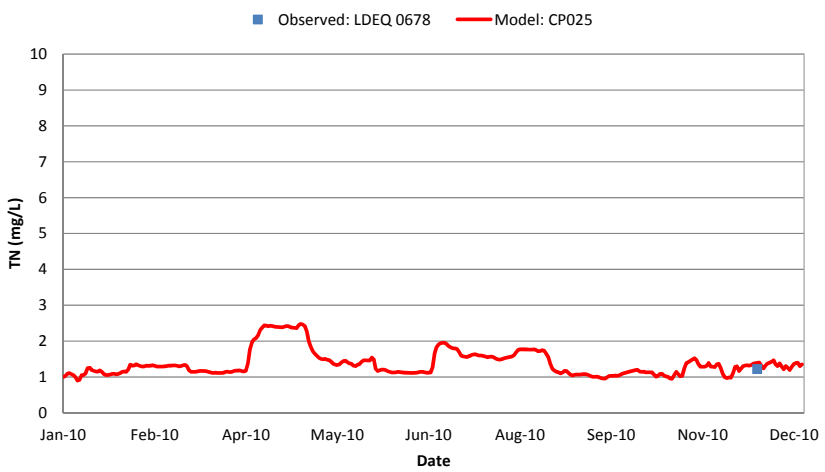

Figure 708 TN Validation Results for CP025 in the CP Model

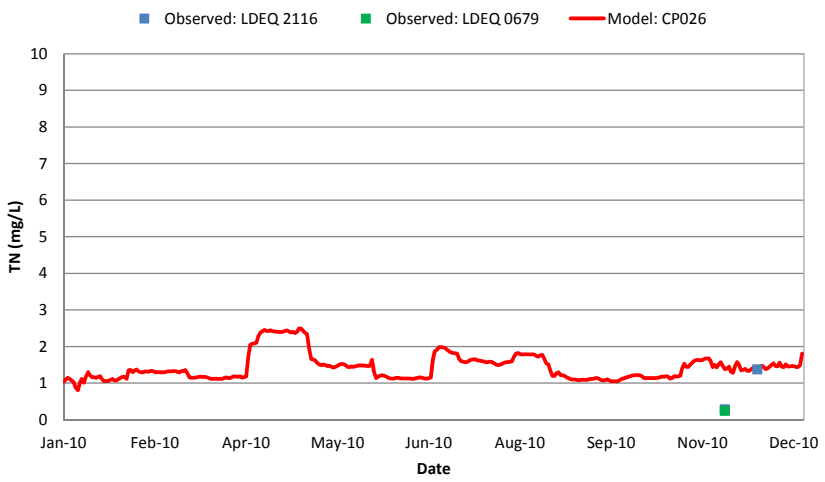

Figure 709 TN Validation Results for GIWW East of Vermilion River in the CP Model

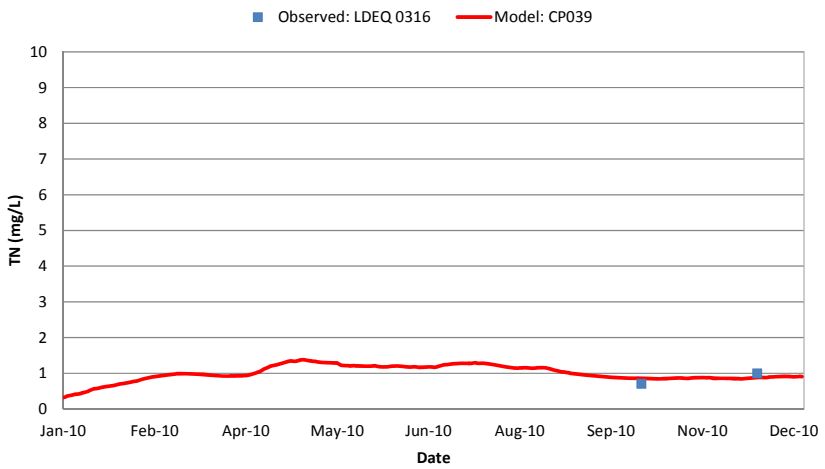

Figure 710 TN Validation Results for Vermilion Bay in the CP Model

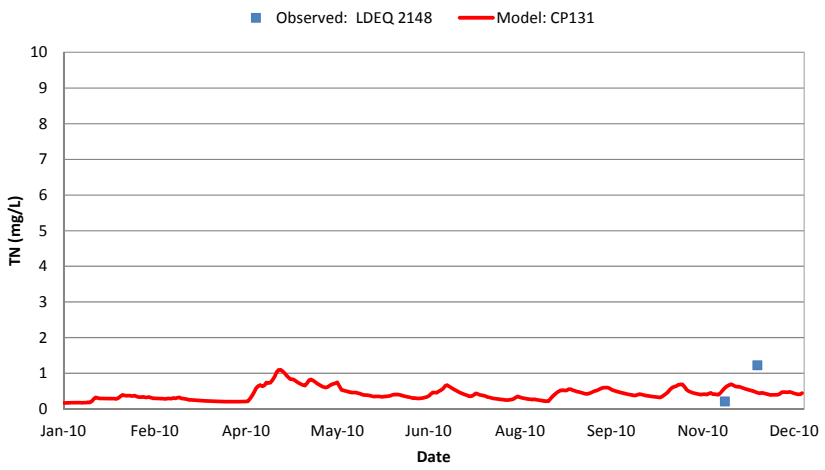

Figure 711 TN Validation Results for Boston Canal in the CP Model

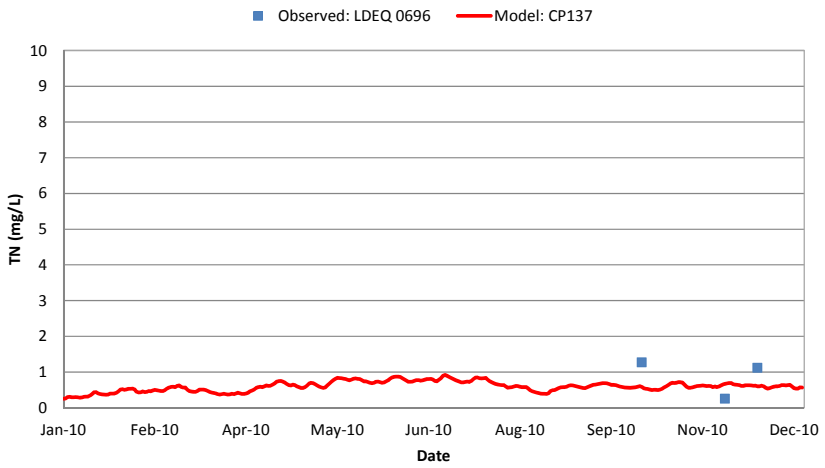

Figure 712 TN Validation Results for East Marsh Island in the CP Model

Total Phosphorus (TPH)

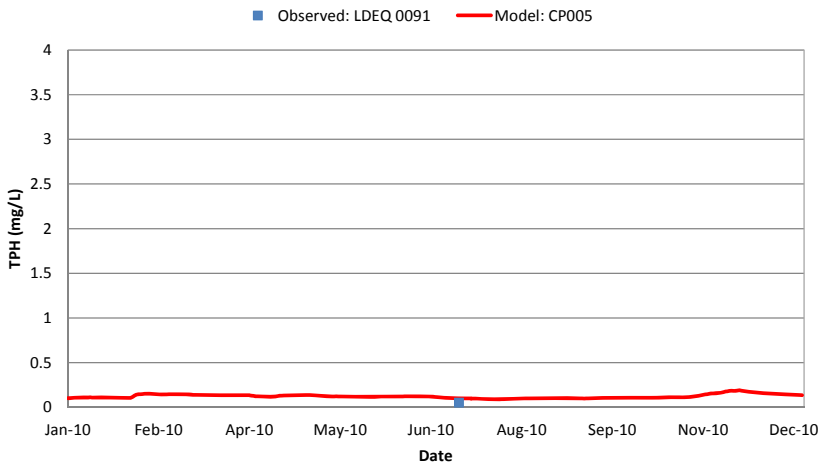

Figure 713 TPH Validation Results for Sabine River in the CP Model

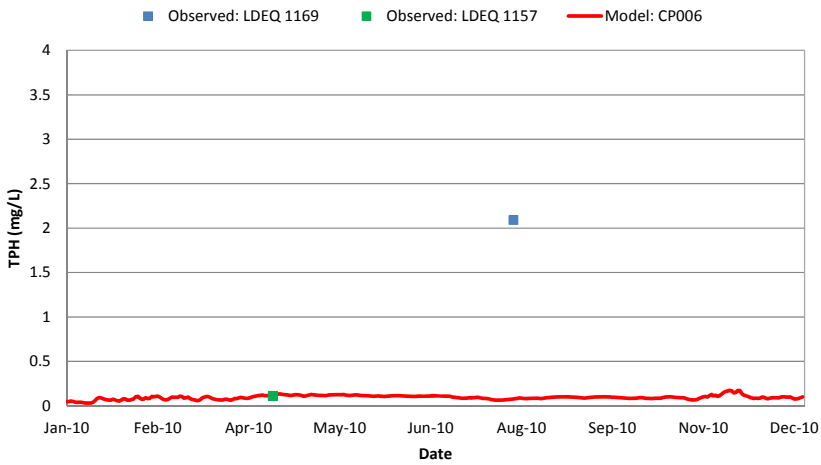

Figure 714 TPH Validation Results for Black Bayou in the CP Model

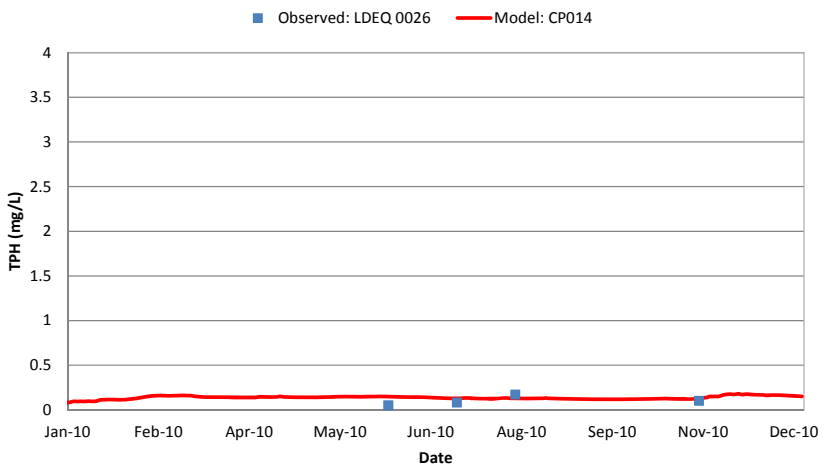

Figure 715 TPH Validation Results for Lower Calcasieu River in the CP Model

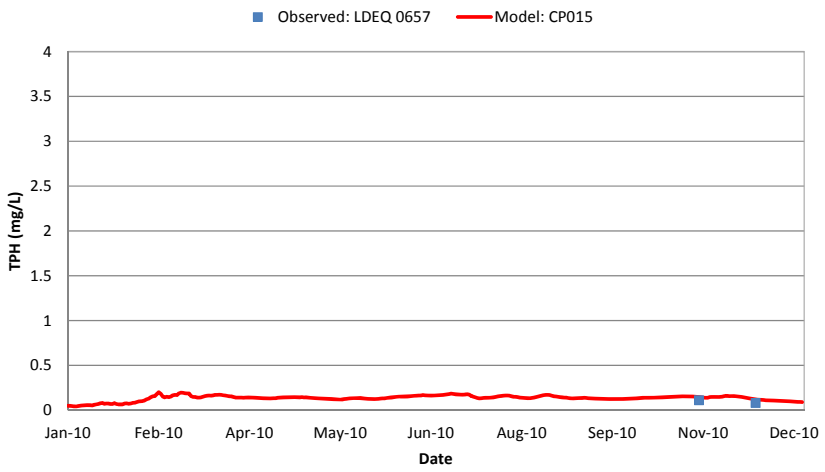

Figure 716 TPH Validation Results for GIWW between Calcasieu River and Bayou Lacassine in the CP Model

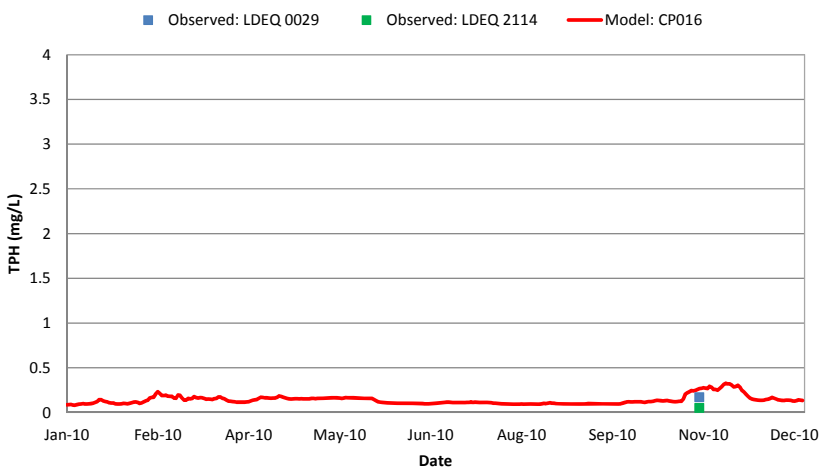

Figure 717 TPH Validation Results for Lower Mermentau River in the CP Model

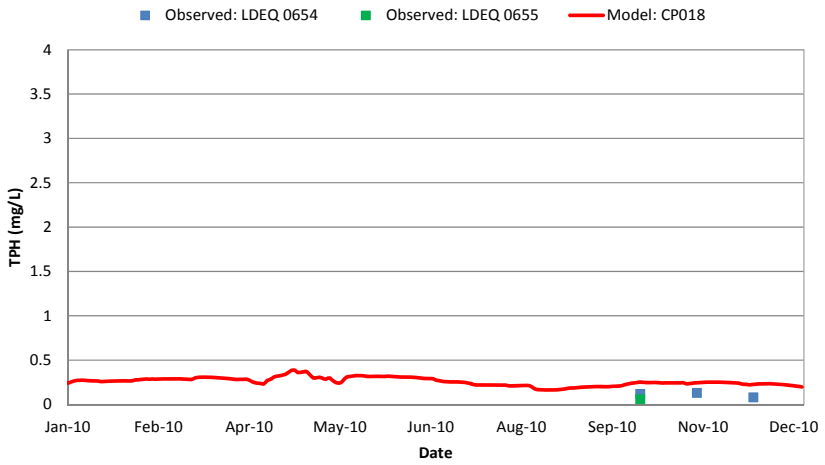

Figure 718 TPH Validation Results for Mermentau River in the CP Model

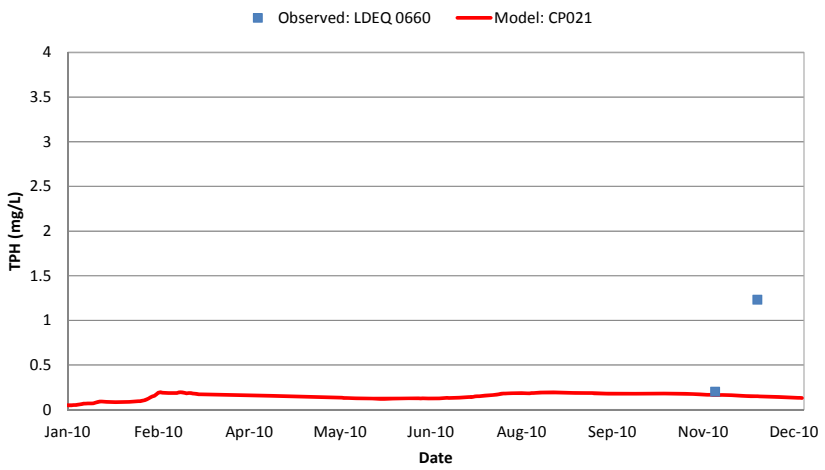

Figure 719 TPH Validation Results for GIWW between Mermentau River and Vermilion River in the CP Model

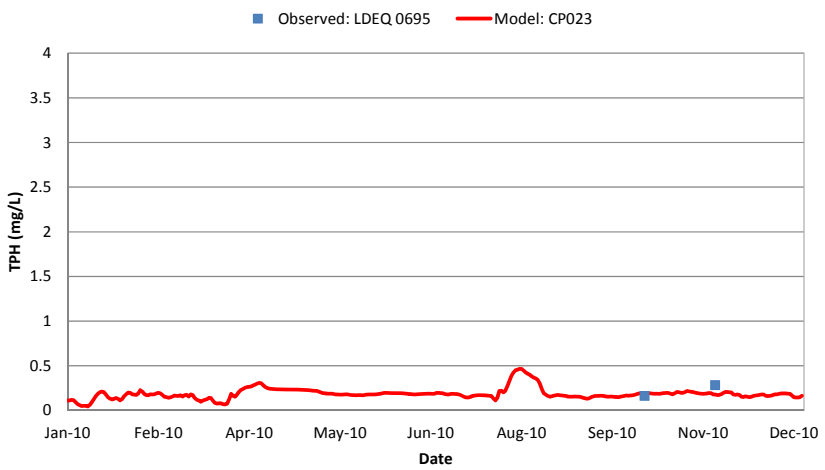

Figure 720 TPH Validation Results for Freshwater Bayou in the CP Model

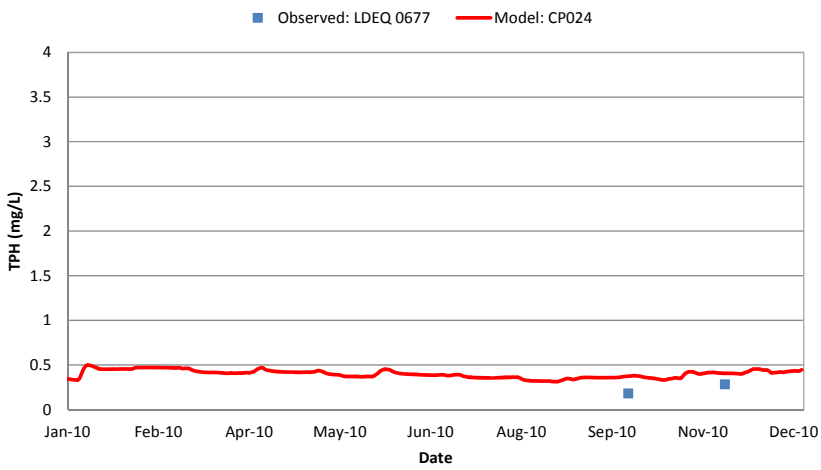

Figure 721 TPH Validation Results for Vermilion River in the CP Model

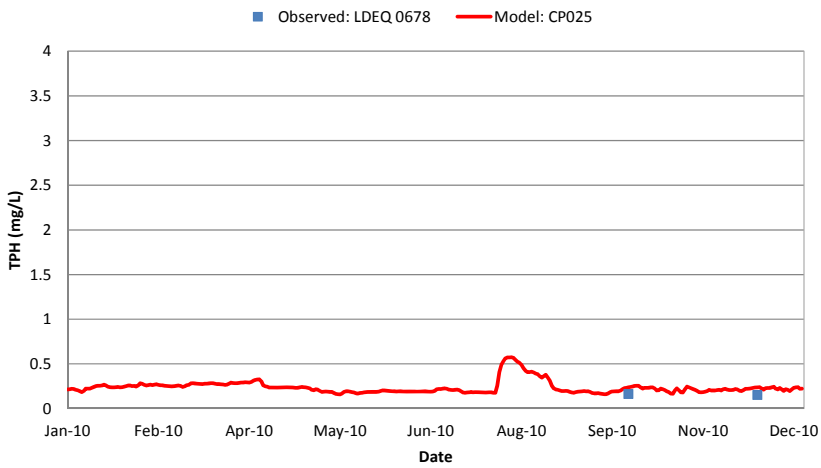

Figure 722 TPH Validation Results for CP025 in the CP Model

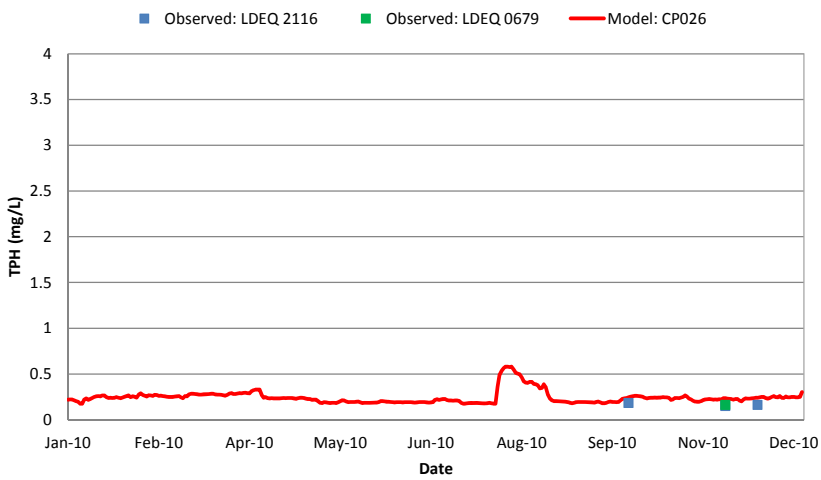

Figure 723 TPH Validation Results for GIWW East of Vermilion River in the CP Model

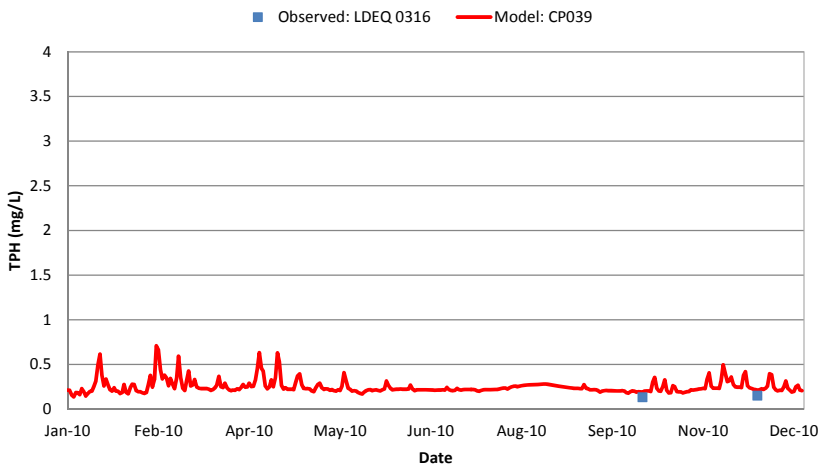

Figure 724 TPH Validation Results for Vermilion Bay in the CP Model

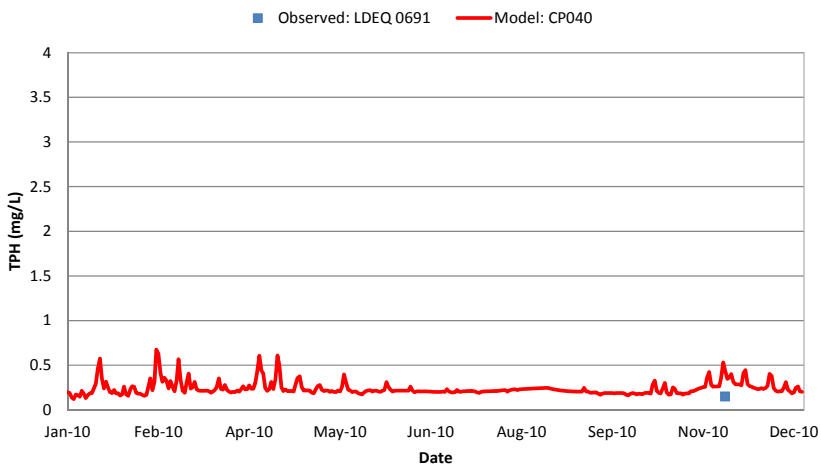

Figure 725 TPH Validation Results for West Cote Blanche Bay in the CP Model

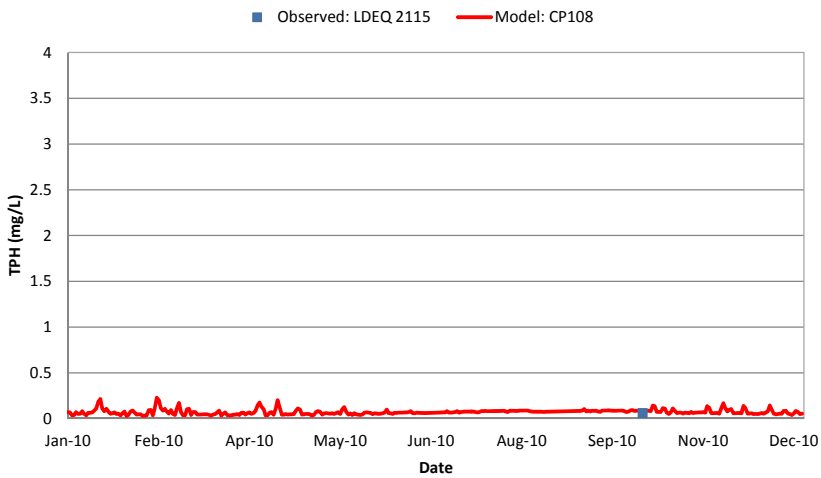

Figure 726 TPH Validation Results for CP108 in the CP Model

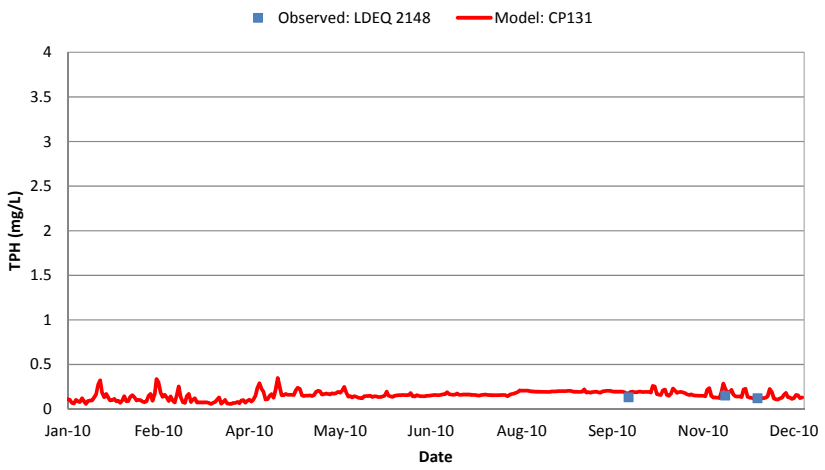

Figure 727 TPH Validation Results for Boston Canal in the CP Model

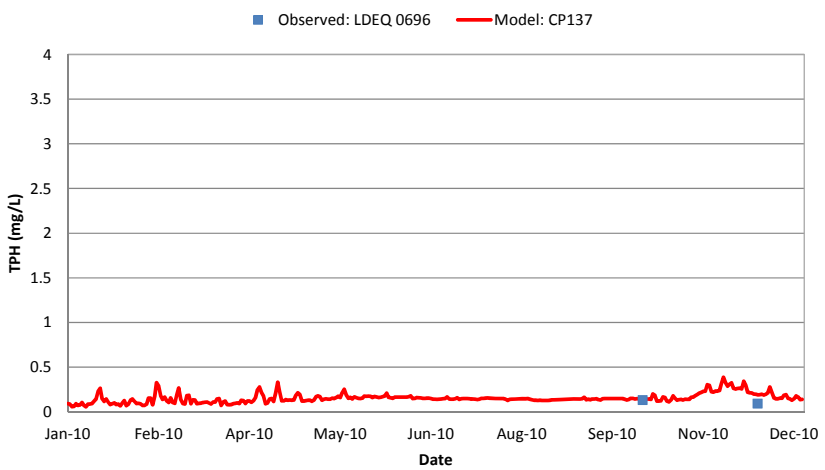

Figure 728 TPH Validation Results for East Marsh Island in the CP Model

Attachment C

AA	Atchafalaya Basin
ACC	Sediment Accretion
ADCIRC	Advanced Circulation Model
AGE	Water Age
ALG	Algae (Phytoplankton as Chlorophyll-a)
BOD	Biochemical Oxygen Demand
CLEAR	Coastal Louisiana Ecosystem Assessment & Restoration
CLIWS	Center for Louisiana Inland Water Studies
CP	Chenier Plain
CPRA	Coastal Protection and Restoration Authority
CPU	Central Processing Unit
CREST	Coastal Restoration Enhancement through Science and Technology
CRMS	Coastwide Reference Monitoring System Sites
CSC	Calcasieu Ship Channel
CSV	Comma Separated Value
DEM	Digital Elevation Model
DET	Detritus
DIN	Dissolved Inorganic Nitrogen
DIP	Dissolved Inorganic Phosphorus
DO	Dissolved Oxygen
DOC	Dissolved Organic Carbon
DON	Dissolved Organic Nitrogen
DOP	Dissolved Organic Phosphorus
EPA	Environmental Protection Agency
ESLR	Estimated Sea Level Rise
ET	Evapotranspiration
FAO	Food and Agriculture Organization
FWOA	Future Without Action
GIWW	Gulf Intracoastal Waterway
GOM	Gulf of Mexico
HAB	Harmful Algal Blooms
HNC	Houma Navigational Canal
ICWW	Intracoastal Waterway
IHNC	Inner Harbor Navigational Canal
IMU	Inertial Measurement Units
IWMI	International Water Management Institute
JCR	Journal of Coastal Research
JD	Julian Day
LA	Louisiana
LACES	Louisiana Applied Coastal Engineering and Science
LACPR	Louisiana Coastal Protection and Restoration
LDEQ	Louisiana Department of Environmental Quality
LDNR	Louisiana Department of Natural Resources
LiDAR	Light Detection and Ranging

LNW	Land and Water
LPBF	Lake Pontchartrain Basin Foundation
LSU	Louisiana State University
LUMCON	Louisiana Universities Marine Consortium
MGD	Million Gallons per Day
MP	Master Plan
MRGO	Mississippi River Gulf Outlet
MS	Mississippi
MSL	Mean Sea Level
NAD	North American Datum
NAVD	North American Vertical Datum
NCDC	National Climatic Data Center
NDBC	National Data Buoy Center
NEXRAD	Next Generation Radar
NGDC	National Geophysical Data Center
NGOM	Northern Gulf of Mexico
NGVD	National Geodetic Vertical Datum
NH4	Ammonium Nitrogen
NO3	Nitrate + Nitrite Nitrogen
NOAA	National Oceanic and Atmospheric Administration
NOD	New Orleans District
NODC	National Oceanographic Data Center
NOS	National Ocean Service
NRM	Nitrogen Removal
OCS	Office of Coast Survey
ORCS	Old River Control Structure
PAR	Photosynthetically Available Radiation
PB	Pontchartrain and Barataria Basin
PIP	Particulate Inorganic Phosphorus
POC	Particulate Organic Carbon
PON	Particulate Organic Nitrogen
POP	Particulate Organic Phosphorus
Q	Discharge
QA/QC	Quality Assurance/Quality Control
QR	Quality Review
RM	River Mile
SAL	Salinity
SHP	Shapefile
SLR	Sea Level Rise
SNWW	Sabine Navigation Waterway
SOD	Surface Data
SPH	Suspended Phosphorus
SSC	Suspended Sediment Concentration
STG	Water Stage
TCEQ	Texas Commission on Environmental Quality

TIP	Total Inorganic Phosphorus
TKN	Total Kjeldahl Nitrogen
TMP	Water Temperature
TN	Total Nitrogen
TOC	Total Organic Carbon
TON	Total Organic Nitrogen
TPH	Total Phosphorus
TRG	Tidal Range
TSS	Total Suspended Solids
TUR	Turbidity
TX	Texas
UNO	University of New Orleans
USACE	United States Army Corps of Engineers
USGS	United State Geological Survey
UTM	Universal Transverse Mercator
WAVCIS	Wave-Current-Surge Information System
WNAT	Western North Atlantic Tidal
WOA	World Ocean Atlas
WQ	Water Quality
WWTP	Wastewater Treatment Plant